# Nonlinear dynamics and interactions of tipping elements in the Earth system

## *Nichtlineare Dynamiken und Interaktionen von Kippelementen im Erdsystem*

**Kumulative Dissertation**

Vorgelegt von

**Nico Wunderling**

zur Erlangung des akademischen Grades
“doctor rerum naturalium” (Dr. rer. nat.)
in der Wissenschaftsdisziplin “Klimaphysik”


Potsdam-Institut für Klimafolgenforschung

eingereicht an der
Mathematisch-naturwissenschaftlichen Fakultät
Institut für Physik und Astronomie der Universität Potsdam
und dem
Potsdam-Institut für Klimafolgenforschung


Einreichung: Potsdam im Februar 2021
Ort und Tag der Disputation: Universität Potsdam (Golm), 15 Oktober 2021

Hauptbetreuerin: Prof. Dr. Ricarda Winkelmann
Betreuer: Dr. Jonathan F. Donges
Gutachter*innen: Prof. Dr. Ricarda Winkelmann, Dr. Jonathan F. Donges, Prof. Peter Ashwin, PhD

Published online on the
Publication Server of the University of Potsdam:
https://doi.org/10.25932/publishup-52514
https://nbn-resolving.org/urn:nbn:de:kobv:517-opus4-525140

Diese Arbeit ist bisher an keiner anderen Hochschule eingereicht worden. Sie wurde selbstständig verfasst und keine anderen als die angegebenen Quellen und Hilfsmittel wurden benutzt. Dies versichere ich hiermit an Eides statt.

[Ort], den [Datum] [Unterschrift]

Nico Wunderling
Research Department 1 (Erdsystemanalyse)
Potsdam-Institut für Klimafolgenforschung

# Abstract

With ongoing anthropogenic global warming, some of the most vulnerable components of the Earth system might become unstable and undergo a critical transition. These subsystems are the so-called *tipping elements*. They are believed to exhibit threshold behaviour and would, if triggered, result in severe consequences for the biosphere and human societies. Furthermore, it has been shown that climate tipping elements are not isolated entities, but interact across the entire Earth system. Therefore, this thesis aims at mapping out the potential for tipping events and feedbacks in the Earth system mainly by the use of complex dynamical systems and network science approaches, but partially also by more detailed process-based models of the Earth system.

In the first part of this thesis, the theoretical foundations are laid by the investigation of networks of interacting tipping elements. For this purpose, the conditions for the emergence of global cascades are analysed against the structure of paradigmatic network types such as Erdős-Rényi, Barabási-Albert, Watts-Strogatz and explicitly spatially embedded networks. Furthermore, micro-scale structures are detected that are decisive for the transition of local to global cascades. These so-called *motifs* link the micro- to the macro-scale in the network of tipping elements. Alongside a model description paper, all these results are entered into the Python software package PyCascades, which is publicly available on github.

In the second part of this dissertation, the tipping element framework is first applied to components of the Earth system such as the cryosphere and to parts of the biosphere. Afterwards it is applied to a set of interacting climate tipping elements on a global scale. Using the Earth system Model of Intermediate Complexity (EMIC) CLIMBER-2, the temperature feedbacks are quantified, which would arise if some of the large cryosphere elements disintegrate over a long span of time. The cryosphere components that are investigated are the Arctic summer sea ice, the mountain glaciers, the Greenland and the West Antarctic Ice Sheets. The committed temperature increase, in case the ice masses disintegrate, is on the order of an additional half a degree on a global average (0.39–0.46 °C), while local to regional additional temperature increases can exceed 5 °C. This means that, once tipping has begun, additional reinforcing feedbacks are able to increase global warming and with that the risk of further tipping events.

This is also the case in the Amazon rainforest, whose parts are dependent on each other via the so-called *moisture-recycling feedback*. In this thesis, the importance of drought-induced tipping events in the Amazon rainforest is investigated in detail. Despite the Amazon rainforest is assumed to be adapted to past environmental conditions, it is found that tipping events sharply increase if the drought conditions become too intense in a too short amount of time, outpacing the adaptive capacity of the Amazon rainforest. In these cases, the frequency of tipping cascades also increases to 50% (or above) of all tipping events. In the model that was developed in this study, the southeastern region of the Amazon basin is hit hardest by the simulated drought patterns. This is also the region that already nowadays suffers a lot from extensive human-induced changes due to large-scale deforestation, cattle ranching or infrastructure projects.

Moreover, on the larger Earth system wide scale, a network of conceptualised climate tipping ele-

ments is constructed in this dissertation making use of a large literature review, expert knowledge and topological properties of the tipping elements. In global warming scenarios, tipping cascades are detected even under modest scenarios of climate change, limiting global warming to 2 °C above pre-industrial levels. In addition, the structural roles of the climate tipping elements in the network are revealed. While the large ice sheets on Greenland and Antarctica are the initiators of tipping cascades, the Atlantic Meridional Overturning Circulation (AMOC) acts as the transmitter of cascades. Furthermore, in our conceptual climate tipping element model, it is found that the ice sheets are of particular importance for the stability of the entire system of investigated climate tipping elements.

In the last part of this thesis, the results from the temperature feedback study with the EMIC CLIMBER-2 are combined with the conceptual model of climate tipping elements. There, it is observed that the likelihood of further tipping events slightly increases due to the temperature feedbacks even if no further $CO_2$ would be added to the atmosphere.

Although the developed network model is of conceptual nature, it is possible with this work for the first time to quantify the risk of tipping events between interacting components of the Earth system under global warming scenarios, by allowing for dynamic temperature feedbacks at the same time.

# Zusammenfassung

Bei fortdauerndem anthropogenem Klimawandel, könnten einige der vulnerabelsten Komponenten des Erdsystem instabil werden und in einen anderen Zustand übergehen. Diese Komponenten des Erdsystems sind die sogenannten Kippelemente. Bei ihnen wird angenommen, dass sie einen Kipppunkt besitzen ab dem sie in einen qualitativ anderen Zustand übergehen können. Sollte das passieren, hätte das schwerwiegende Konsequenzen für die Biosphäre und menschliche Gesellschaften. Des Weiteren ist gezeigt worden, dass Kippelemente keine isolierte Reigionen oder Prozesse sind, sondern über das gesamte Erdsystem hinweg interagieren. Das Ziel dieser Arbeit ist es daher, die Wahrscheinlichkeit für Kippereignisse sowie deren Feedbacks im Erdsystem zu quantifizieren. Zu diesem Zweck kommen vor allem Frameworks aus der Wissenschaft komplexer Systeme und Netzwerke zum Einsatz. Für einige Teilaspekte dieser Arbeit wird aber auch ein detaillierteres und prozessbasierteres Erdsystemmodell verwendet.

Im ersten Teil dieser Arbeit werden die theoretischen Grundlagen gelegt, indem komplexe Netzwerke bestehend aus interagierenden Kippelementen untersucht werden. Hier werden Voraussetzungen für das Auftreten globaler Kippkaskaden anhand der Struktur paradigmatischer Netzwerktypen analysiert. Diese Typen sind Netzwerke wie Erdős-Rényi, Barabási-Albert, Watts-Strogatz Netzwerke oder auch explizit räumlich eingebettete Netzwerke. Darüber hinaus sind bestimmte Mikrostrukturen in Netzwerken dafür entscheidend, ob sich eine lokale Kaskaden auf das globale Netzwerk ausbreiten kann. Diese Strukturen sind das Bindeglied zwischen der Mikro- und der Makroebene des Netzwerks und werden *Motive* genannt. Zusammen mit einer Publikation zur Modellbeschreibung, werden alle diese Ergebnisse im Python-Softwarepaket PyCascades veröffentlicht, das auf github öffentlich verfügbar ist.

Im zweiten Teil dieser Dissertation wird das Kippelementframework zunächst auf Kompenenten des Erdsystems angewendet wie der Kryosphäre und Teilen der Biosphäre, und danach auf globaler Skala für interagierende Klimakippelemente. In einem ersten Schritt werden mit dem Erdsystemmodell mittlerer Komplexität CLIMBER-2 die Temperaturfeedbacks ermittelt, die entstehen würden, wenn große Gebiete der Kryosphäre auf lange Sicht eisfrei werden. In dieser Berechnung werden das arktische Sommermeereis, die Gebirgsgletscher, der grönländische und der westantarktische Eisschild berücksichtigt. Die quantifizierte Temperaturerhöhung liegt in der Größenordnung von einem halben Grad zusätzlicher globaler Erwärmung (0.39–0.46 °C). Lokale bis regionale Temperaturerhöhungen können allerdings 5 °C übersteigen. Wenn also das Kippen einiger Elemente begonnen hat, bedeutet dieses Ergebnis, dass Temperaturfeedbacks in der Lage sind, das Risiko weiterer Kippereignisse zu erhöhen.

Dies ist auch der Fall im Amazonasregenwald, dessen Unterregionen über den sogenannten *Feuchtigkeits-Recycling-Feedback* miteinander in Beziehung stehen und voneinander abhängen. In dieser Dissertation wird die Bedeutung von Kippereignissen im Detail untersucht, die aufgrund von Dürreperioden zustande kommen. Obwohl man davon ausgehen kann, dass der Regenwald sich an zurückliegende und gegenwärtige Klimabedingungen angepasst hat, kann festgestellt werden, dass die Häufigkeit von Kippereignissen stark zunimmt, wenn die jeweilige Trockenperiode eine gewisse Intensität übersteigt und damit die Anpassungsfähigkeit des Amazonasregenwalds überschritten wird. In

solchen Fällen steigt auch die Häufigkeit von Kippkaskaden unter allen Kippereignissen auf 50% (und mehr) an. In dem Modell, das in dieser Studie entwickelt wurde, zeigt sich, dass der Südosten des Amazonasbeckens am stärksten von den simulierten Trockenheitsmustern betroffen ist. Das ist gleichzeitig die Region, die bereits heute stark unter anthropogener Veränderung leidet, unter anderem aufgrund von großflächiger Abholzung, Viehzucht oder Infrastrukturprojekten.

Zudem wird in dieser Dissertation auf der größeren, erdsystemweiten Skala ein Netzwerk konzeptionalisierter Klimakippelemente aufgebaut. Zu diesem Zweck wird eine umfangreiche Literaturrecherche durchgeführt, die zusammen mit Expertenwissen und den topologischen Eigenschaften der Kippelemente in die Studien mit einfließt. In Klimawandelszenarien können dann Kippkaskaden beobachtet werden, selbst wenn die globale Erderwärmung auf 2 °C über dem vorindustriellen Niveau begrenzt werden kann. Außerdem werden die strukturellen Rollen der Klimakippelemente im Netzwerk ermittelt. Während die großen Eisschilde auf Grönland und der Westantarktis viele Kippkaskaden initiieren, ist die Atlantische Umwälzzirkulation für die Weitergabe vieler dieser Kaskaden verantwortlich. In unserem konzeptionellen Modell für Klimakippelemente wird darüber hinaus festgestellt, dass die Eisschilde von besonderer Bedeutung für die Stabilität des Gesamtsystems sind.

Im letzten Teil dieser Dissertation werden die Ergebnisse der Feedbackstudie (CLIMBER-2-Studie) zusammengebracht mit dem konzeptionellen Klimakippelementmodell. Dabei zeigt sich, dass die Wahrscheinlichkeit zusätzlicher Kippereignisse aufgrund der berücksichtigten Temperaturfeedbacks auch ohne das Zuführen eines zusätzlichen $CO_2$-Eintrags in die Atmosphäre leicht ansteigt.

Trotz der konzeptionellen Natur des entwickelten Netzwerkmodells, ist es mit dieser Arbeit erstmals möglich eine Risikoabschätzung über das Auftreten von Kippkaskaden im Erdsystem vorzunehmen. Darüber hinaus können, unter der Annahme globaler Erwärmungsszenarien, auch dynamische Temperaturfeedbacks berücksichtigt werden.

# Contents

# Chapter 1

# Introduction

*Look at the world around you. It may seem like an immovable implacable place. It is not. With the slightest push – in just the right place – it can be tipped.*

*Malcolm Gladwell*

## 1.1 The foundations of Earth system science

The Earth can be viewed as a complex system (Fan et al., 2020). It consists of a geosphere, biosphere and anthroposphere component (Steffen et al., 2020). On top of that it has been proposed that the living components themselves have a self-regulating and self-perpetuating nature by interacting with their environment such that they make the Earth itself to a more habitable place. This hypothesis is the so-called *GAIA* hypothesis that was formulated more than 40 years ago by James Lovelock and Lynn Margulis (Lovelock and Margulis, 1974). However, this self-organised life support may be threatened as the Earth has entered a time, where humans truly have become a geological force (Steffen et al., 2015; Zalasiewicz et al., 2019). During the Holocene in the last 11,700 years, unusually stable climatic conditions have enabled the rise of civilisations and provided home to more than 7 billion people. Meanwhile direct human impact has become measurable in many places around the world, for instance through a decline in biodiversity, an increase in extreme weather conditions or global warming (Rahmstorf and Coumou, 2011; Stocker et al., 2013; Brondizio et al., 2019). The human ability to significantly impact the Earth system in its entirety increases steadily and is nowadays seen as one of the dominant forces that drives the climate system, giving rise to a new age of time: the Anthropocene (Crutzen, 2002; Steffen et al., 2015; Zalasiewicz et al., 2019). To address one of the most fundamental threats that humanity is exposed to, the international community agreed in Paris 2015 to limit global warming to well below 2.0 °C above pre-industrial levels until 2100 (Paris Agreement, 2015).

Therefore, human forces have to be taken into account in contemporary Earth system analysis and could be represented by a dynamic and co-evolutionary relationship between anthropogenic and natural forces. More recently, the inherent co-evolution between the Anthroposphere and the climate system has been re-emphasised as a basis of state-of-the-art *Whole Earth system analysis* (Donges et al., 2017; Steffen et al., 2020). This kind of Earth system analysis was put forward more than 20 years ago as the *second Copernican revolution* (Schellnhuber, 1999). In contrast to the first Copernican revolution, the author argues that *macroscopes* instead of microscopes for Earth system scientists are required to be able to assess the Earth in a genuine and perceptually independent way. Thereby

three principles are distinguished: (i) The *'bird's eye'* principle: Measuring the Earth system from distance, as for instance with satellites, (ii) The *'Lilliput'* principle: Shrinking the Earth to an examinable size, as e.g. in small-scale models or experiments, and (iii) The *digital-mimikry* principle: Simulating the Earth by the use of mathematics, equations and process understanding.
More broadly spoken, there are three main methodologies to gain scientific knowledge, namely the triad of observation (measurement), experiment (laboratory) and simulation (modelling). In the Earth system sciences, observational data can be gained by satellites (e.g. the TRMM dataset; Huffman et al., 2007), instrumental data and reanalysis products (e.g. the NCEP-NCAR dataset; Kalnay et al., 1996). To look further back into the past than just a couple of decades, paleo climate archives can be investigated such as ice cores (e.g. Jouzel et al., 2007), speleothems (e.g. Cheng et al., 2016) or tree rings (e.g. Zhao et al., 2019). On the experimental side, classical laboratory experiments can be performed (such as the measurement of the ice flow law; Glen, 1958), but also experiments that take place in nature itself such as rainfall exclusion or fire experiments in tropical rainforests (Brando et al., 2008; Silvério et al., 2013). The third strategy to investigate the Earth system are computer simulations, i.e., modelling the Earth system. Since major parts of this thesis make use of models and develop them, the main focus will lie on those modelling perspectives.

### 1.1.1 Hierarchy of Earth system models

In principle, there are three different classes of model complexity in Earth system sciences that each serves a specific purpose (see Fig. 1.1). The first class of models are conceptual models whose dynamics are in many cases based on one or several equations or dynamical rules. There are many examples of conceptual models for the Earth system or components of it, but some well-known historical examples are ocean box-models, ice age oscillation models or energy-balance models (e.g. Stommel, 1961; Budyko, 1969; Sellers, 1969; Saltzman and Maasch, 1988).
At the other end of the spectrum of complexity is the Earth system model class of general circulation models (GCMs). GCM-type models solve the basic equations of motion (Navier-Stokes equation) for the oceans, the atmosphere and also posses model-dependent components for the land-surface and sea ice. Typically, GCMs are the models of highest complexity and are computationally expensive. However, some processes, e.g. for clouds or storm tracks, need to be parameterised additionally since their physical details are partially unknown or uncertain as of yet (Stocker et al., 2013). GCMs are the models that are used in coupled model intercomparison projects (CMIP) for the IPCC reports. They aim to simulate the response of global climate to increasing greenhouse gas emissions (Taylor et al., 2012; Stocker et al., 2013; Eyring et al., 2016).
In between these two model groups of very low and very high complexity are the Earth system models of intermediate complexity (EMICs). EMICs make use of particular simplifications to physical processes with an increased use of parametrisations and deliberate downscaling of the vertical and horizontal resolution of the climate system (Claussen et al., 2002; Weber, 2010; Flato, 2011).
In my thesis, I have made extensive use of EMICs and conceptual models. However, in light of the existence of more complex GCM-like models, the question can be raised as of why simplified modelling approaches are worth following at all.

### 1.1.2 Role of EMICs and conceptual models for Earth system science

Since EMICs are computationally less expensive than GCMs, they are the prime candidate for calculating long-term simulations, by at the same time being able to run larger ensembles of simulations. While GCMs are usually run for some hundreds of years, EMICs allow for climate simulations over

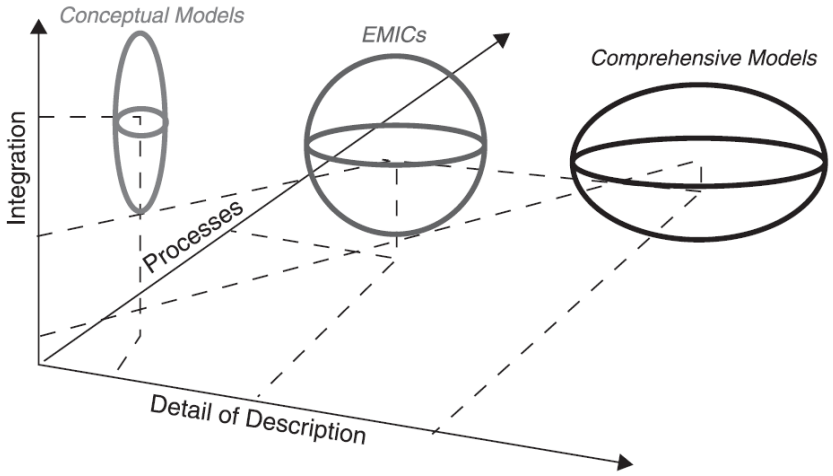


**Figure 1.1:** Model hierarchy of comprehensive models (GCMs), EMICs and conceptual models with respect to the number of interacting Earth system components (Integration), the number of processes explicitly modelled (Processes) and the detail of description of these processes. Figure taken from Claussen et al. (2000).

several thousands of years up to the simulation of glacial cycles for millions of years (e.g. Ganopolski et al., 2016; Willeit et al., 2019). As such they close the gap between the fully complex GCMs and purely conceptual models (Claussen et al., 2000, 2002), see Fig. 1.1. Nowadays, a range of powerful EMICs exists and is under further development (e.g. Petoukhov et al., 2005; Eby et al., 2013; Zickfeld et al., 2013). Further, EMICs are explicitly part of the IPCC-AR5 to assess the long-term climate change (Stocker et al., 2013). This illustrates the usefulness of EMICs (Weber, 2010) for various research questions on the Earth system, which include but are not limited to climate change (e.g. Eby et al., 2013; Zickfeld et al., 2013), human-Earth system interactions (e.g. Ganopolski et al., 2016) or instabilities of parts or the entire Earth system (e.g. Rahmstorf et al., 2005; Lucarini and Bódai, 2019).

Further, it is also debated whether Earth system models becoming more and more complex can always better represent the physical properties of the climate system in case the ensemble size has to be limited due to computational constraints at the same time. In contrast, it has been argued that simpler models such as EMICs or conceptual models could be advantageous if large and carefully chosen ensembles are employed (Stainforth et al., 2007; Daron and Stainforth, 2013).

Unlike EMICs, conceptual models aim to describe the essential properties of the modelled system with only one or a few components. A very typical approach are dynamic models based on differential equations. In my view, conceptual models can be viewed as the *macroscopes* among the three classes of Earth system models, putting particular spotlight on the modelled system. Especially, where knowledge is sparse and uncertainties are large, conceptual models can help creating some understanding about a particular system by focussing on its main and most important properties. One prominent example, where more complex approaches traditionally have difficulties or are just being developed, is the modelling of nonlinearities in the climate system, particularly concerning climate tipping elements. Therefore, conceptual models informed by complex systems are a promising strategy to help answering questions along nonlinear climate phenomena.

## 1.2 Climate tipping elements in the Anthropocene

As long as anthropogenic climate change has not come to a halt, the integrity of some of the most important regions and processes on Earth, which ensured our livelihood under the past very stable climate, are endangered (see Fig. 1.2). These vulnerable regions are the so-called *climate tipping elements* (Lenton et al., 2008). They comprise cryosphere components such as the large ice sheets on Greenland or Antarctica, circulation patterns such as monsoon systems or the Atlantic Meridional Overturning Circulation (AMOC) as well as biosphere components such as the Amazon rainforest or coral reefs. In the Anthropocene, humans are changing the world at an unprecedented speed (Steffen et al., 2015), putting the integrity of many tipping elements at risk since they can qualitatively alter their state within a small parameter change once they have been brought close to their critical threshold (*tipping point*). Their disintegration would have severe consequences for the biosphere and for human societies as a whole. The tipping elements are suspected to transgress their critical threshold at a certain level of warming (Schellnhuber et al., 2016).

With ongoing global warming, it has been proposed that the Earth system could potentially be forced over the boundary of the very stable current Holocene climate state from the last 11,700 years and transgress onto a trajectory towards a *hothouse* state with far higher temperatures than in the Holocene or during the last 1.2 million years (Steffen et al., 2018; Lenton et al., 2019). It is further suggested that some tipping elements already show early warning signs of a potential disintegration (Stocker et al., 2013; Lenton et al., 2019; Wang and Hausfather, 2020). For instance cryosphere components such as the West Antarctic Ice Sheet, the Greenland Ice Sheet, the Arctic summer sea ice and mountain glaciers show strongly declining trends in observations (Leclercq et al., 2011; Stroeve et al., 2012; Gardner et al., 2013; Shepherd et al., 2018; Rignot et al., 2019; Sasgen et al., 2020; Shepherd et al., 2020). At the same time, oceanic systems such as the overturning strength of the AMOC becomes weaker or biosphere components such as the Amazon rainforest are under increasing pressure from anthropogenic activities (Nobre et al., 2016; Caesar et al., 2018; Lovejoy and Nobre, 2019). Further, the climate tipping elements are not isolated but interact across scales in space and time (Kriegler et al., 2009; Rocha et al., 2018). This means, due to the interaction, positive internal feedbacks, and a potential irreversibility for some tipping elements, a possible tipping might be difficult to countermand once the individual thresholds of the tipping elements have been crossed.

## 1.3 Complex systems and network approaches to nonlinear climate science

Major parts of this dissertation exploit techniques from complex dynamical systems and network approaches to inform the conceptual modelling of the climate system. Complex networks are an extremely flexible tool, which has been applied successfully to many different fields in science ranging from biology, ecology, the energy system up to sociology (Albert and Barabási, 2002; Newman, 2003). They have been utilised in the synchronisation of nonlinear oscillators (Zou et al., 2013), neuroscience (Ashwin et al., 2016), food webs (Gross et al., 2009), climate dynamics (Donges et al., 2009) or in the description of social contagion phenomena such as opinion dynamics or disease propagation (Brockmann and Helbing, 2013; Wiedermann et al., 2020).

A typical way to model tipping elements in complex systems science is to view them as entities that possess multiple stable states with a potential to a state transition. Following Ashwin et al. (2012) and Halekotte and Feudel (2020), tipping of a system can be separated into four groups. (i) Bifurcation-induced tipping (*B tipping*), where a slow changing parameter induces a critical transition across a

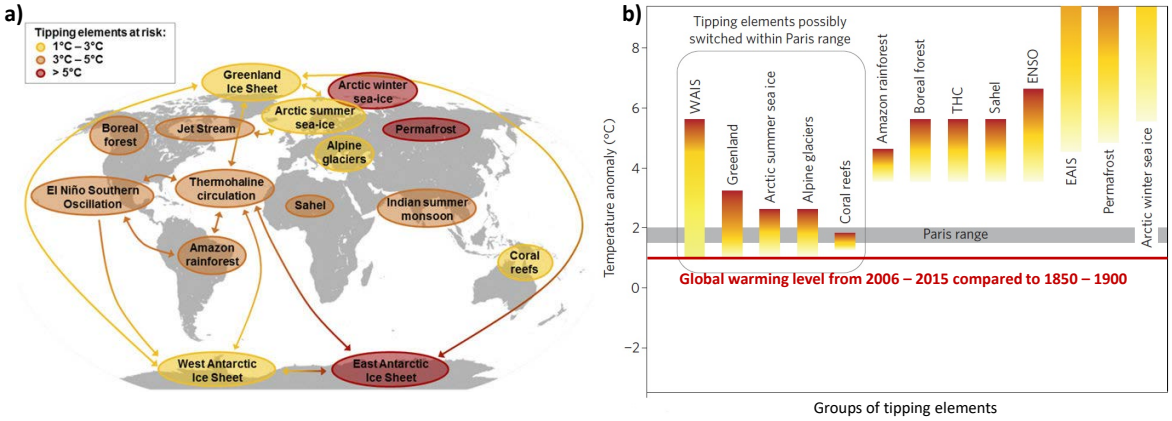


**Figure 1.2: a)** Tipping elements in the Earth system grouped along their potential tipping points with respect to global warming levels above pre-industrial. **b)** Range of critical levels of global warming in which tipping elements could be tipped. In red, the Anthropogenic global warming is shown comparing 1850–1900 with 2006–2015. This value lies at 0.9 °C above pre-industrial levels (Masson-Delmotte et al., 2018). Following recent developments, abrupt and irreversible changes in the climate system might start at lower temperature thresholds than previously thought (Lenton et al., 2019). Figure adapted from Steffen et al. (2018) for panel (a) and Schellnhuber et al. (2016) for panel (b).

bifurcation point, i.e., tipping point (Examples: Cessi, 1994; van Nes et al., 2014). (ii) Noise-induced tipping (*N tipping*), where random fluctuations lead to leaving the attractor (Examples: Thompson and Sieber, 2011; Ritchie and Sieber, 2017). (iii) Rate-induced tipping (*R tipping*), where the system cannot keep track of the slow changing attractor due to rapid changes in the forcing (Examples: Ashwin et al., 2017; Alkhayuon and Ashwin, 2018). (iv) Shock-induced tipping (*S tipping*), where a sufficiently large perturbation kicks the system out of its basin of attraction (Halekotte and Feudel, 2020).

In my dissertation, I focus on bifurcation-induced tipping apart from two minor examples in [P1] and [AP1] (see Sects. 2.1 and 5.1) where noise-induced tipping events play a role. A bifurcation is a qualitative state change in response to a (small) change of a critical parameter $c$ over its tipping point $c_{\text{critical}}$. An example for a fold-bifurcation with the critical parameter $c$ and the tipping point $c_{\text{critical}}$ is shown in Fig. 1.3a. Along these lines, the notion of interacting tipping elements in complex networks has gained increasing attention (Eom, 2018), where the dynamical structures are represented by certain entities as nodes and their interactions as edges in the network (Fig. 1.3b). The respective dynamical equation representing this behaviour can be written as

$$f_{\text{Cusp, i}}(x) = dx_i = \left[ -a_i \left(x_i - x_{0,i}\right)^3 + b_i \left(x_i - x_{0,i}\right) + c_i + d \sum_{j=1}^{N} A_{ij} x_j \right] dt + \sigma dW. \qquad (1.1)$$

The state of a tipping element $i$ is denoted by $x_i$. $a_i$, $b_i$ and $x_{0,i}$ are parameters. $c_i$ is the critical parameter that invokes a state transition as soon as its critical value $c_{\text{critical}}$ is surpassed (see Fig. 1.3a). The last term in brackets denotes the coupling to other tipping elements. In this case, a linear form is chosen with a given strength $d$ and the adjacency matrix $A_{ij}$ (see Fig. 1.3b). $A_{ij} = 0$ if there is no connection between node $i$ and $j$, and $A_{ij} = 1$ if there is a connection. The last term in Eq. 1.1 represents the noise, where $\sigma$ stands for the level of the noise and $W$ describes the Wiener process.

Overall, tipping elements, whether interacting or not, are not restricted to tipping processes in the climate sense (Lenton et al., 2008; Kriegler et al., 2009), but they also appear in various other contexts such as ecology, finance, or politics (Scheffer et al., 2001; May et al., 2008; Brummitt et al.,

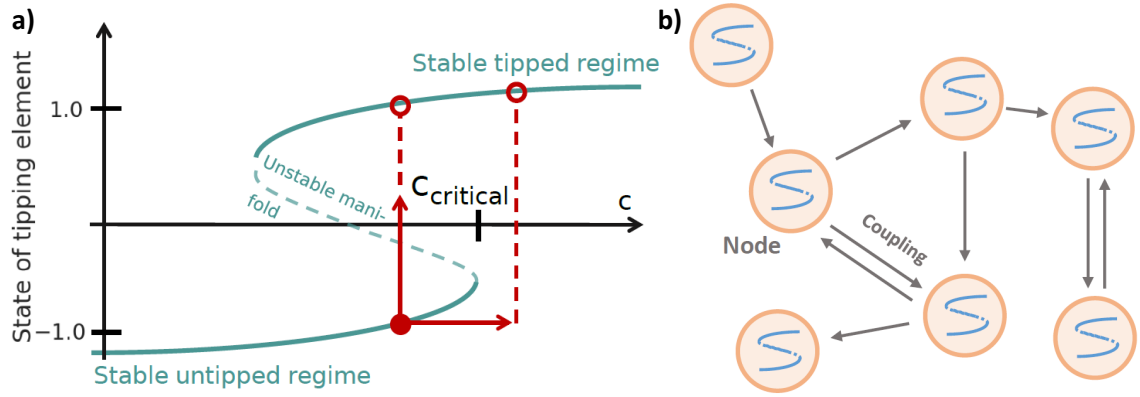


**Figure 1.3: a)** (Fold-)Bifurcation diagram of an exemplary tipping element with two stable states, in this case exhibiting a fold-bifurcation once the critical parameter $c$ surpassed its critical value $c_{\text{critical}}$. **b)** Network of nodes, where the nodes represent individual tipping elements and the edges represent interactions between them. This figure is adapted and extended from [P6] (see Sect. 2.6).

2015). However, in the climate system, nonlinear (tipping) dynamics have been applied as threshold or binary models to the entire Earth system as well as to specific subsystems, e.g. to the Amazon rainforest (Gaucherel and Moron, 2017; Zemp et al., 2017). For the climate system much progress has been made in more comprehensive Earth system modelling during the last decades, but nevertheless they cannot yet comprehensively propagate all uncertainties in the climate tipping elements due to computational limitations (e.g. Wood et al., 2019). Although there exist conceptual models of two interacting tipping elements (Dekker et al., 2018), there is no general framework or model of interacting tipping elements available as of now. A reason might be that parts of the interaction structure is not yet fully understood and partially explicitly based on expertise from respective specialists (e.g. Kriegler et al., 2009).
Out of all these reasons, it is crucial to understand the dynamics of interacting tipping elements as well as their potential to undergo dangerous tipping events, for instance in triggering tipping cascades. This dissertation is dedicated to elaborate on specific questions along these lines (see Sect. 1.4). According to that, this dissertation contributes to some of the *Hilbertian* questions (Schellnhuber et al., 2004, page 9) posed for Earth system sciences with respect to nonlinear climate phenomena (see also Sect. 4).

## 1.4 Research questions and scope of this thesis

Tipping elements can be decisive for the determination of stability in complex systems. Furthermore, network interactions between tipping elements can lead to nonlinear and potentially dangerous tipping events among certain subsystems, even before their actual tipping point is reached. Therefore, the following set of guiding questions arises:

**RQ1:** What are the conditions under which tipping cascades can emerge in interacting complex systems? What are the implications for the stability of that system?

Following this question, this can be specified for the Earth's climate system. In many cases, tipping elements possess reinforcing feedbacks once they commence tipping. This applies to climate system

components such as the large ice sheets on Greenland and Antarctica via the melt-elevation feedback and marine ice sheet instabilities (Schoof, 2007; Levermann and Winkelmann, 2016). Further, the tipping elements also exert feedbacks directly on the global mean temperature via fast-climate feedbacks such as albedo, water vapour, lapse rate and clouds feedbacks. These fast climate feedbacks are especially important for the cryosphere components since their albedo would change drastically in case they become ice-free. This leads to the following question:

**RQ2:** How large are the temperature feedbacks of the large cryosphere components on a regional and global level?

Feedbacks are also internally important for other sub-components of the Earth system such as the Amazon rainforest via the moisture-recycling feedback (Aragão, 2012). At this point, it could be asked for the Amazon rainforest:

**RQ3:** Under which conditions can tipping events occur in the Amazon rainforest and in a set of tipping elements in the Earth system? Which role do tipping cascades play in that regard? How strongly do feedbacks affect the occurrence of tipping events of further tipping elements?

This is not only an important question for the Amazon rainforest as a particular tipping element in the climate system, but also for a larger set of interacting climate tipping elements. For them, the question as of how temperature feedbacks would increase the likelihood for tipping, combines RQ2 with RQ3.

In order to answer these research questions, I employed different methodologies ranging from complex systems science to Earth system modelling with an EMIC. Therefore, this work is separated into two different parts (see Fig. 1.4). In the **first major part of my thesis (Theory & Methodologies)**, a generic model is developed (PyCascades), which is able to simulate tipping elements on different network interaction structures [P1]. With this generic model, fundamental properties of deterministic and stochastic tipping elements are investigated on several generic and spatially embedded network [P2, P3]. Building on these methodological advances, the **second major part of my thesis (Climate tipping elements)** deals with applications to the Earth's climate tipping elements. First, selected components in the Earth system are investigated such as cryosphere elements [P4] and the Amazon rainforest [P5], and after that, a set of climate tipping elements [P6, P7]. In [P4], the Earth system Model of Intermediate Complexity (EMIC) CLIMBER-2 (Petoukhov et al., 2000; Ganopolski et al., 2001) has been used to determine the global mean temperature feedback. To investigate the potential for tipping events and cascades, the conceptual network model PyCascades (developed in [P1–P3]) is first applied to the Amazon rainforest [P5] and then to interacting climate tipping elements [P6, P7], Lastly, the temperature feedback values from [P4] are applied to the conceptual Earth system model developed in [P6, P7] to determine as to whether the tipping events significantly change under these additional temperature increases (see chapter 3).

The structure of my dissertation is depicted in Fig. 1.4. The following chapter 2 constitutes the main body of my dissertation and is built around these seven aforementioned articles. Before the original manuscripts of the respective publications, I will give a short summary of the content, the authors, journal and author contributions for each article. The original bodies of the seven publications are deposited in the main part of this dissertation, comprising my most substantial contributions to this dissertation. In chapter 3, the main results composed of all publications of this dissertation will be summarised and the research questions posed above will be answered. In the discussion (chapter 4), I will put my findings into the larger research context, name limitations and provide an outlook on

potential future lines of research.

Lastly, four further contributions to publications are deposited in the Appendix (see chapter 5 and Fig. 5.1), elaborating further on the *Theory & Methodologies* and *(Climate) tipping elements* parts. The first contribution deals with the high connectivity limit of conceptualised tipping elements. There, it has been observed that cooperativity emerges under a sufficiently large connectivity of single tipping elements. They can then be aggregated to one large overarching tipping element [AP1] (see Sect. 5.1). Upon all theoretical and methodological thoughts from this dissertation [P1-P3, AP1], there is a discussion on what is meant by a 'tipping cascade' since the concept of tipping cascades is understood differently by different research communities [AP2] (see Sect. 5.2). Furthermore, another study with a smaller contribution of mine deals with an observed hysteresis of the Amazon rainforest, as has been found in a global vegetation model [AP3] (see Sect. 5.3). The last small contribution concerns the structure and dynamics of social tipping processes, also in contrast to natural tipping elements [AP4] (see Sect. 5.4). This part also represents an outlook of this thesis in the way that tipping elements are not limited or restricted to certain natural systems, but reach far beyond.

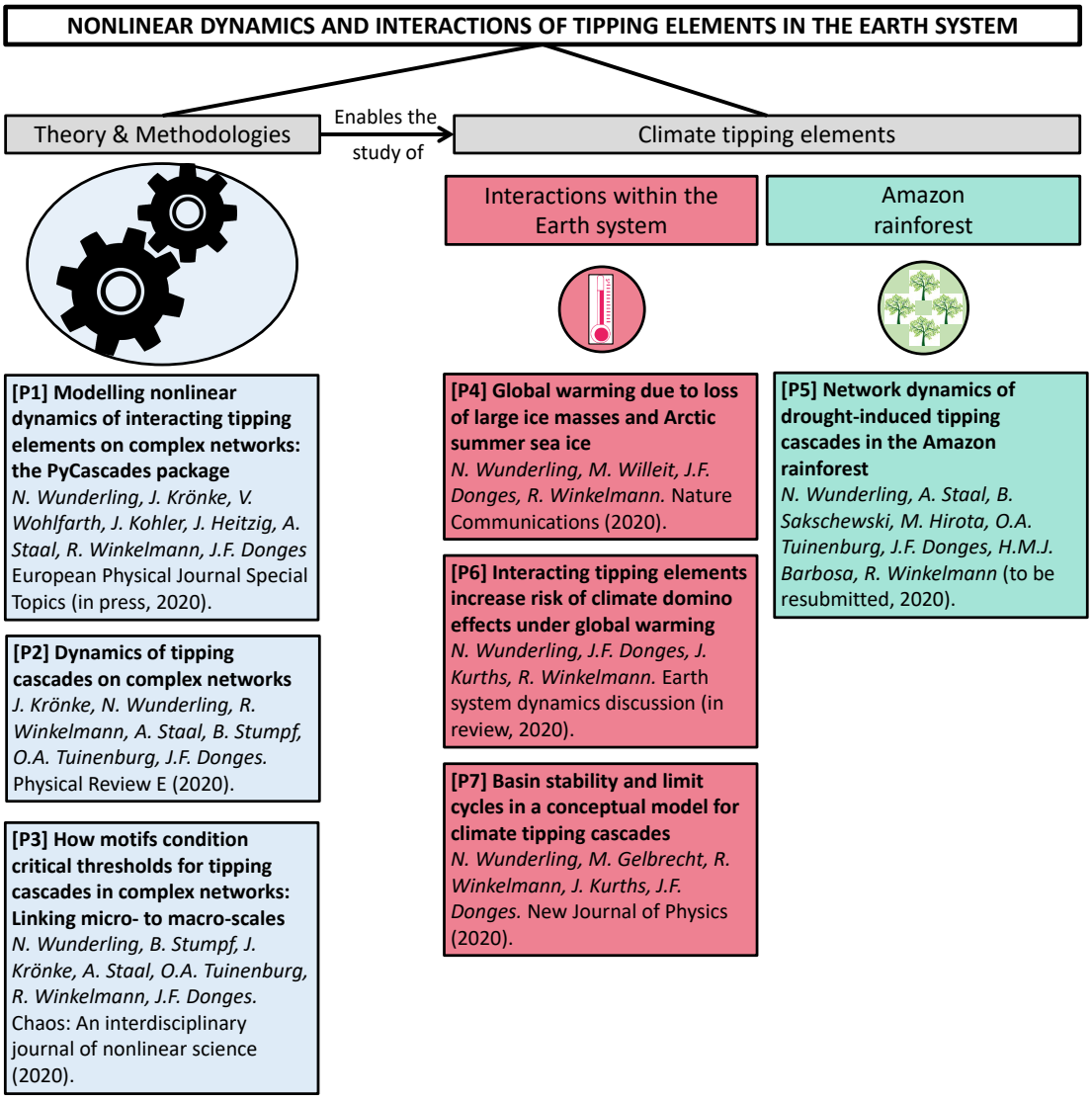


**Figure 1.4:** Overview of the sub-projects in my dissertation divided into *Theory & Methodologies* and *Climate tipping elements* (divided into *Interactions within the Earth system* and *Amazon rainforest*).

# Chapter 2

# Original manuscripts

*I now believe that this theory tells us something quite general about the way complex systems, not just ecological systems, change over time. And collapse is usually part of the story.*

*Crawford Stanley (Buzz) Holling*

The main part of this thesis is based on seven articles. Four articles are published, one is accepted, another is in review, and one is to be resubmitted. Each article is a stand-alone contribution with an introduction, results, methods and conclusions as well as references. In this chapter, I give an overview of these individual articles together with a short summary of its contents, authors, journal and author contributions. If applicable, the supplementary information of the articles can be found directly after the respective manuscript.

# 2.1 Modelling nonlinear dynamics of interacting tipping elements on complex networks: the PyCascades package [P1]

**Authors**
Nico Wunderling, Jonathan Krönke, Valentin Wohlfarth, Jan Kohler, Jobst Heitzig, Arie Staal, Sven Willner, Ricarda Winkelmann, Jonathan F. Donges

**Status**
Accepted at *European Physical Journal Special Topics* (January 2021). Pre-print available in the arXiv under: arXiv:2011.02031

**Short summary**
With this manuscript, the open source software package *PyCascades* is introduced (available under the doi: 10.5281/zenodo.4153102). PyCascades is written in Python and is able to simulate networks of paradigmatic tipping elements, e.g., tipping elements that have a fold-bifurcation or a Hopf-bifurcation. Tipping cascades can be simulated on various standardised network types such as, among others, Erdős-Rényi, Barabási-Albert or Watts-Strogatz networks. Furthermore, PyCascades hosts the possibility to be coupled to the software package *sdeint*, which also is a Python-written open source software tool. In this combination, different types of tipping elements with noise are implemented and can be used with PyCascades. The types of noise that are supplied are Gaussian, Lévy and Cauchy noise. Additionally, it is shown how PyCascades can be applied to various spatially explicit networks of tipping elements, for instance to an atmospheric moisture-recycling network of the Amazon rainforest, to a network of four climate tipping elements and to the global trade network. In these examples, two important features of PyCascades are demonstrated: (i) The use of another differential equation (other than the two predefined differential equation types) and (ii) The combination with a large-scale Monte Carlo ensemble approach to propagate uncertainties that are present in the desired application.

**Author contributions**
Nico Wunderling designed the study together with Ricarda Winkelmann and Jonathan Donges. Nico Wunderling performed the simulations and prepared the figures for this work with contributions from Jonathan Krönke (in the section: Structure of the core of PyCascades) and Valentin Wohlfarth (in the section: International Trade Network). Nico Wunderling led the writing of this work with inputs from all authors. Jonathan Krönke developed the software package PyCascades with inputs and extensions from Jan Kohler, Valentin Wohlfarth and Nico Wunderling. Jonathan Donges supervised this study.

**EPJ manuscript No.**
(will be inserted by the editor)

# Modelling nonlinear dynamics of interacting tipping elements on complex networks: the *PyCascades* package

Nico Wunderling[1,2,3,a], Jonathan Krönke[1,2], Valentin Wohlfarth[1,3], Jan Kohler[1,4], Jobst Heitzig[5], Arie Staal[6,7], Sven Willner[5], Ricarda Winkelmann[1,2], and Jonathan F. Donges[1,7,a]

[1] Earth System Analysis, Potsdam Institute for Climate Impact Research (PIK), Member of the Leibniz Association, 14473 Potsdam, Germany
[2] Institute of Physics and Astronomy, University of Potsdam, 14476 Potsdam, Germany
[3] Department of Physics, Humboldt University of Berlin, 12489 Berlin, Germany
[4] Institute for Theoretical Physics, University of Leipzig, 04103 Leipzig, Germany
[5] Complexity Science, Potsdam Institute for Climate Impact Research (PIK), Member of the Leibniz Association, 14473 Potsdam, Germany
[6] Department of Environmental Sciences, Copernicus Institute of Sustainable Development, Utrecht University, Utrecht, 3584 CB, The Netherlands
[7] Stockholm Resilience Centre, Stockholm University, Stockholm, SE-10691, Sweden



**Abstract.** Tipping elements occur in various systems such as in socio-economics, ecology and the climate system. In many cases, the individual tipping elements are not independent from each other, but they interact across scales in time and space. To model systems of interacting tipping elements, we here introduce the *PyCascades* open source software package for studying interacting tipping elements (doi: 10.5281/zenodo.4153102). *PyCascades* is an object-oriented and easily extendable package written in the programming language Python. It allows for investigating under which conditions potentially dangerous cascades can emerge between interacting dynamical systems, with a focus on tipping elements. With *PyCascades* it is possible to use different types of tipping elements such as double-fold and Hopf types and interactions between them. *PyCascades* can be applied to arbitrary complex network structures and has recently been extended to stochastic dynamical systems. This paper provides an overview of the functionality of *PyCascades* by introducing the basic concepts and the methodology behind it. In the end, three examples are discussed, showing three different applications of the software package. First, the moisture recycling network of the Amazon rainforest is investigated. Second, a model of interacting Earth system tipping elements is discussed. And third, the *PyCascades* modelling framework is applied to a global trade network.

[a] Correspondences should be addressed to nico.wunderling@pik-potsdam.de or donges@pik-potsdam.de

## 1 Introduction

In the recent years complex systems research has increasingly focused on the matter of tipping points [1, 2, 3] since they occur in many different systems including ecosystems, over economics, the Earth's climate system and social systems [4, 5, 6, 7, 8, 9, 10]. Tipping points are the critical thresholds of tipping elements, where a small perturbation can be sufficient to invoke a qualitative change of the whole system. Whether such qualitative changes can be seen as something desirable or undesirable depends a lot on the context: for instance, a potential transition of climate tipping elements towards a potential "hothouse" state might be dangerous for humanity [11, 12], while a rapid transition towards a sustainable future lies well within the scope of desired tipping events [13]. However, oftentimes tipping elements do not exist in isolation, but interact across scales in time and space [14, 15] such as connected lakes in ecology [16, 17], in the adoption of new technologies in the economy [18] or the climate tipping elements in the Earth system [19]. Since several decades, networks are an established tool for the description of complex systems [e.g., 20, 21]. Complex networks are structures that represent certain entities as their nodes and their interaction as their edges. They have been used, for example, to model oscillators in power grids [22], food webs [23], interactions of climate system components [24] and the collaboration network of scientists [25]. Critical behaviour has also been revealed on the network level. For instance, it has been shown that the likelihood of developing diabetes depends of the criticality of excitable tissue in the Langerhans Isles of the pancreas [26].

Since there is increasing interest in modelling interacting tipping elements within the context of complex systems [27, 28, 29], we bring these two strands of research together since tipping elements on networks can not only tip themselves but also imply tipping of neighbouring systems or even the network as a whole. Building upon recent developments in studying interacting nonlinear dynamics on complex networks [30, 31, 32, 33, 34], we here introduce the unified Python package *PyCascades*.

In Chapt. 2, we describe how *PyCascades* can be installed and what the package contains (Sect. 2.1). Further, we describe the general structure of our package (Sect. 2.2), the building blocks of nonlinear dynamical systems, namely the tipping elements and their interaction structure (Sect. 2.3) as well as the network types natively included in the package (Sect. 2.4) and lastly, the extension to several types of stochastic tipping elements (Sect. 2.5). Thereafter, we apply our modelling framework to three different examples (Chapt. 3). First, we use our model to simulate tipping cascades in the Amazon rainforest, which is connected by a network of atmospheric moisture flows (Sect. 3.1). Second, we show how *PyCascades* can be extended to large scale Monte Carlo ensemble studies such that many uncertainties can be propagated (Sect. 3.2). Third, we exchange the fundamental differential equation that has been used in the two earlier examples to model tipping cascades in an economic example of a global trade network (Sect. 3.3). Lastly in Chapt. 4, we shortly summarise the functionalities of *PyCascades*.

## 2 Methods

This chapter describes the basic features that are supplied by *PyCascades* from the installation and the structure of the package to the fundamental features that have been developed. Here, a tutorial can be found that guides the interested reader through the most important first steps to simulate tipping cascades on interacting tipping elements (doi: 10.5281/zenodo.4153102). Furthermore, the code for each of the following fundamental features and the three applications is provided there.

### 2.1 Installation and package structure

*PyCascades* can be installed via the command line using the pip-command

`pip install pycascades==1.0.1`[1].

Alternatively, the package can directly be downloaded via the website following the zenodo-doi: 10.-5281/zenodo.4153102. The layout of the file structure of *PyCascades* can be found in Tab. 1. Important files, which led to the outcomes of this work, are listed and described there. A dedicated tutorial has been developed, guiding the interested reader through some important first steps and features of the software package. For the Amazon rainforest application and the climate tipping elements application, further readme-files have been added in the respective directory. There, it is explained how the respective simulations can be started and evaluated. Additionally, the plot scripts for these two applications are deposited.

[1] The current version of *PyCascades* is stored at https://pypi.org/project/pycascades/.

**Table 1.** File structure of *PyCascades*. Only important files are described below. Separate plot-files and extended readme-files for the Amazon rainforest and the climate tipping cascades are also supplied in the corresponding directory to facilitate the usage of *PyCascades*.

| Directory | Important File(s) | Purpose |
|---|---|---|
| pycascades/examples | tutorial.py | Introduction to basic features |
| pycascades/examples | example_cusp_hopf.py | Timelines of tipping events (Fig. 2) |
| pycascades/examples | network_types_plot.py | Network plots (Fig. 3) |
| pycascades/examples | network_tipping_cascade_plot.py | Network of tipping cascades (Fig. 3) |
| pycascades/examples | example_cusp_noise.py | Different types of noise (Fig. 4) |
| pycascades/examples | economic_cascade.py | Economic cascades |
| pycascades/modules | core/gen/utils | Core of *PyCascades* (Sect. 2.2) |
| pycascades/amazon_rainforest | r_crit_unstable_amazon.py | Start Amazon rainforest simulations |
| pycascades/earth_system | Main_earth_system.py | Start climate tipping events simulations |
| pycascades/sdeint | readme_sdeint.txt | How to implement tipping elements with noise and *sdeint* |

### 2.2 Structure of the core of *PyCascades*

*PyCascades* provides a convenient framework to solve differential equations on complex networks, i.e., it describes the dynamics of states of nodes in such a network as well as their interactions. The basic assumption is that the dynamics of tipping elements can be separated into one part for the isolated dynamics of the tipping element and another part representing the interaction terms (see Sect. 2.3 for more details). For that, it builds on *SciPy* differential equation solvers [35] for the dynamics and on *NetworkX* [36] to generate the underlying network.

The core of *PyCascades* is structured as follows (see Fig. 1). It provides the two classes `tipping_element` and `coupling` that implement the two described types of dynamics. From these classes that can be viewed as references, concrete classes for tipping elements and interactions can be derived. Currently, *PyCascades* provides the classes `cusp` and `hopf` derived from `tipping_element` and `linear_coupling` derived from `coupling`. Other types of tipping elements or couplings can be implemented in an analogous way. The class `tipping_network` which is derived from the `DiGraph` class of *NetworkX* is used to combine different `tipping_element` and `coupling` objects into a network and identify each `tipping_element` object with a node and each `coupling` object with a link. Finally, an `evolve` class is provided with methods to integrate the resulting ODE system or to trigger tipping events.

### 2.3 Different types of tipping elements and interactions

Through the `tipping_element` class in *PyCascades* different types of tipping elements can be defined and coupled together. Each tipping element can be described by its individual dynamics $f_i$ and the interaction term $g_i$, i.e., the coupling to other tipping elements. This yields

$$\tau_i \frac{dx_i}{dt} = f_i(x_i) + g_i(x), \tag{1}$$

where $x_i$ represents the state of the respective tipping element. $\tau_i$ stands for a typical timescale of tipping. The direct interaction term $g_i(x)$ is assumed to be separable into the summands

$$g_i(x) = \sum_j g_{ij}(x_i, x_j), \tag{2}$$

linking the tipping elements $i$ and $j$.

In principle, any kind of tipping element can be supplied in the `tipping_element` class of *PyCascades*, but as of now, there are two kinds of tipping elements predefined that are ready to be used and implemented. These two tipping elements are elements that possess a Cusp-bifurcation or a Hopf-bifurcation [37]. The first preimplemented tipping element is the Cusp-differential equation, which has been used in many contexts before to model nonlinear transitions between two alternative stable states [15, 38]. The normal form of its differential can be written as

$$f_{\mathrm{Cusp}}(x) = \frac{dx}{dt} = -a\,(x - x_0)^3 + b\,(x - x_0) + c. \tag{3}$$

Here, $a, b > 0$ and $x_0$ represents a shift on the x-axis. The parameter $c$ is the critical parameter, which invokes a shift from a lower stable state to an upper stable state as soon as the critical value $c_{\mathrm{crit,\ high}}$ is surpassed. The other way round, when $c$

is diminished, a state transition from the upper to the lower stable state occurs at $c_{\text{crit, low}}$. Eq. 3 has the normal form of a fold-bifurcation and has, as a paradigmatic model, been applied in many different areas such as systems in ecology, climate science and economics [15, 29, 31, 39, 40]. For the special case that $a = 4, b = 1$ and $x_0 = 0.5$, the two stable states are located at $x_1 = 0$ and $x_2 = 1$ for $c = 0$. The critical parameter lies at $c_{\text{crit, high}} = -c_{\text{crit, low}} = \sqrt{(4b^3)/(27a)} = \sqrt{4/(27 \cdot 4)} \approx 0.19$. The bifurcation diagram of this equation is shown in Fig. 2a.

The second tipping element that is provided by *PyCascades* is a Hopf-bifurcation. The normal form in polar coordinates of this bifurcation can be written as

$$\begin{aligned} f_{\text{Hopf, r}}(r) &= \frac{dr}{dt} = \left(\mu - r^2\right) \cdot ra \\ f_{\text{Hopf, }\phi}(\phi) &= \frac{d\phi}{dt} = b \end{aligned} \tag{4}$$

with the parameters $a$ and $b$. Here, the Hopf-bifurcation is given in polar coordinates with the radius $r$ and the angle $\phi$. Importantly, $\mu$ is the critical parameter and a bifurcation from a stable fixed point to a stable limit and an unstable fixed point occurs when $\mu$ crosses zero from below. The bifurcation diagram is shown in Fig. 2b. Applications of Hopf-bifurcations have been found, for instance, in predator-prey cycles in Lotka-Volterra systems or in the Hodgkin-Huxley model of neurons [41, 42]. In the climate system, there exist conceptual models that represent the El-Niño Southern Oscillation as a Hopf bifurcation [43, 44] based on a model by Zebiak & Cane (1987) [45].

Next, for the interactions, any type of coupling can in principle be used and implemented in *PyCascades*. However, for the moment only linear interactions are considered

$$g_i(x) = \sum_{j=1}^{N} A_{ij} x_j. \tag{5}$$

If there is a connection between tipping element $i$ and $j$, then $A_{ij} \neq 0$, otherwise $A_{ij} = 0$. In Fig. 2c-f, we show an example how tipping cascades can emerge from the coupling between two tipping elements for the case of two cusp-differential and for the case of one cusp coupled to the normal form of a Hopf-bifurcation.

### 2.4 Paradigmatic network types of interacting tipping elements

With *PyCascades* it is possible to investigate the dynamics of tipping and tipping cascades in larger directed networks. These types of networks can either be explicitly spatially embedded (see Chapt. 3) or well-known predefined network models such as the Erdős-Rényi model, the Barabási-Albert model or the Watts-Strogatz model [46, 47, 48]. Originally, the network models that are inbuilt in python's network package *NetworkX* are undirected for Watts-Strogatz networks and Barabási-Albert networks, while we require directed networks. Additionally, it might also be helpful or necessary to be able to determine a certain average degree. Therefore, a generalisation of these two networks types has been developed. (i) Watts-Strogatz network: A regular network is created where each node $i$ is connected to its $m$ closest neighbours in both directions. $m$ must be an even integer and the average degree $\langle k \rangle = m$. $m$ is chosen in such a way that the average degree of the resulting network is larger than the desired average degree. Then, links are randomly deleted until the desired average degree is reached. Lastly, each of the remaining links is rewired with the desired rewiring probability as in the usual Watts-Strogatz model. (ii) Barabási-Albert model: First, two

nodes are bidirectionally coupled. Each further node is, again, bidirectionally coupled to one already existing node $i$ with the probability $p = (k_i^{\text{in}} + k_i^{\text{out}})/(\sum_{mn} a_{mn})$, where $k_i^{\text{in}}$ is the in-degree and $k_i^{\text{out}}$ is the out-degree of node $i$. With $a_{mn}$, the sum of all edges in the network is denoted. In the end, the average degree $\langle k \rangle$ depends on the stochastic network. Therefore, it can happen that the actual average degree $\langle k \rangle$ of the network exceeds or falls below the desired average degree $k_{\text{des}}$. While $\langle k \rangle < k_{\text{des}}$, another link is added between two randomly selected nodes $i$ and $j$. While $\langle k \rangle > k_{\text{des}}$, a link between two randomly selected nodes $i$ and $j$ is deleted. For comparison of the construction of these network models, see also Krönke et al.(2020) [30]. Examples for a realisation of these three network types and an exemplary tipping cascade in those can be found in Fig. 3.

### 2.5 Stochasticity in tipping elements

In the real-world, systems often underlie fluctuations, which under certain circumstances can cause critical transitions, called *noise-induced tipping*. Numerous prominent examples can be found in dynamical systems such as in electronics, optics or neurons, but also in ecology and in the Earth's climate system [49, 50, 51, 52, 53]. Therefore, we decided to create a class for a stochastic version of the cusp tipping element (Eq. 3) for additive noise

$$f_{\text{Cusp, stoch.}} = dx = \Big[-a\,(x - x_0)^3 + b\,(x - x_0) + c\Big]\,dt + \sigma dW. \tag{6}$$

Here, $\sigma$ denotes the noise level and $dW/dt$ describes the Wiener process or Brownian motion. In the case of random white noise (Gaussian white noise) as used here, $W$ is sampled from a Gaussian distribution. To implement stochastic differential equations, python's SciPy function `odeint` has been replaced by `sdeint` [54]. `sdeint` has several algorithms implemented, which are able to solve stochastic differential equations. Here, and in the provided version of *PyCascades*, an order 1.0 strong stochastic Runge-Kutta algorithm is employed [55].

Furthermore, Gaussian noise distributions are not necessarily able to describe all types of fluctuations in real-world systems since in reality noise might be correlated or not be standard normally distributed. Besides Gaussian noise, *PyCascades* allows to compute systems with Lévy and Cauchy noise (see Fig. 4). These types of noise (Lévy, Cauchy) may be more suitable for describing extreme events than Gaussian noise, however, in the implemented form they still remain uncorrelated. It has been found that the probability of jumping between the two stable states in a double-well potential is impacted by single strong extreme events from those $\alpha$-stable noise distributions [56]. For instance, it has been proposed that this might have been of relevance for climate system states on a millennial time scale during the last glacial period as was observed in ice-cores [57]. Also, transitions triggered by extreme events emerging from Lévy-distributions in other nonlinear climate system components such as the Amazon rainforest or the thermohaline circulation have been investigated, as well as transitions in gene expression processes in molecular biology [58, 59, 60].

The distributions for Gaussian, Lévy and Cauchy noise in *PyCascades* are taken from python's SciPy libraries

$$\begin{aligned} p_{\text{Gauss}}(x) &= \frac{1}{\sqrt{2\pi\sigma^2}} \cdot \exp\left(-\frac{x^2}{2\sigma^2}\right) \\ p_{\text{Lévy}}(x) &= 0.5 \cdot p_{\text{Lévy, pos.}} + 0.5 \cdot p_{\text{Lévy, neg.}} = \\ &= 0.5 \cdot \sqrt{\frac{\sigma}{2\pi x^3}} \cdot \exp\left(-\frac{\sigma}{2x}\right) + 0.5 \cdot \sqrt{\frac{\sigma}{2\pi\,|x|^3}} \cdot \exp\left(-\frac{\sigma}{2\,|x|}\right) \\ p_{\text{Cauchy}}(x) &= \frac{1}{\sigma\pi} \cdot \frac{\sigma^2}{\sigma^2 + x^2}, \end{aligned} \tag{7}$$

where $\sigma$ is the standard deviation and the mean value $\mu \equiv 0$.

## 3 Applications

In this section, we show three examples of how *PyCascades* can be applied to real-world systems. The first application is the moisture-recycling network of the Amazon rainforest, where we introduce *PyCascades* on a spatially embedded network. In the second application in a subset of interacting climate tipping elements, we combine the *PyCascades* modelling framework with a large-scale setup of Monte Carlo simulation to show how numerous uncertainties in parameters can be propagated systematically. The third application, a global trade network of more than 5 000 nodes and 400 000 links, complements our analysis by simulating tipping cascades with a modernised, economically motivated differential equation (see Eq. 10) replacing the Cusp-differential equation (see Eq. 3).

### 3.1 The Amazon rainforest

It is suspected that the Amazon rainforest is a tipping element in the Earth's climate system [4], which might approach a tipping point due to various anthropogenic pressures including climate change, fires and land-use change [61, 62, 63]. The Amazon rainforest might exhibit multistability at certain rainfall levels, as suggested by conceptual models and observational data [64, 65, 66, 67, 68]. This implies that rainforest patches may transition to a savannah-like state when the rainfall drops below a certain critical level. These rainforest patches depend on each other, as rain is re-evaporated by the trees and thus preserved in the system through atmospheric moisture recycling [69, 70] (see Fig. 5a). This means that the Amazon rainforest is an excellent example of how tipping cascades can travel through a system, which can be modelled with *PyCascades*. We divide the Amazon into $0.5{\times}0.5^\circ$ (appr. 50 km) grid cells and assume that each is an interacting tipping element that can be described by the Eqs. 3 and 5. For simplicity, we chose $a_i = b_i = 1$ and $x_{0,i} = 0$ for all tipping elements and further assume that the critical parameter is only dependent on the rainfall a rainforest cell receives, which tips in case the received rainfall is less than the critical rainfall. Then, the critical parameter $c_i$ and the coupling $g_i(x)$ can be denoted as

$$\begin{aligned} c_i &= c_0 \cdot \frac{R_i - \langle R \rangle}{R_{\text{crit}} - \langle R \rangle} \\ g_i(x) &= \frac{1}{2} \frac{c_0}{R_{\text{crit}} - \langle R \rangle} \sum_{j=1}^{N} \delta_{ij}^{\text{Rain}}. \end{aligned} \tag{8}$$

Here, $R_i$ is the rainfall in cell $i$, $\langle R \rangle$ is the average rainfall over the whole Amazon basin and $R_{\text{crit}}$ is the critical rainfall. Further, $c_0 = \sqrt{4/27}$ if $a = b = 1$ and $x_0 = 0$. Lastly, $\delta_{ij}^{\text{Rain}}$ is the moisture transport in mm/yr from cell $j$ to cell $i$. Since the distance between the two stable states is 2, a prefactor of $1/2$ is required to re-normalise the coupling. We choose the critical rainfall $R_{\text{crit}}$ to be 1700 mm/yr for all cells, which is approximately the value below which the alternative savannah state becomes more resilient than the rainforest state [71]. The atmospheric moisture recycling simulations used in this work were performed by Staal et al. (2018) [72] for the years 2003–2014 and assembled into a network by Krönke et al. (2020) [30]. In this simplified example, we assume that if a forested grid cell tips, moisture recycling via that cell stops. We performed a tipping experiment for each year between 2003 and 2014 and averaged the results over this period. We find tipping events in several parts of the Amazon basin which cascade to other forest patches (Fig. 5b–d). This analysis illustrates how *PyCascades* can be applied to simulate tipping events and cascades in a real-world network of interacting tipping elements.

### 3.2 Climate tipping elements

Apart from the Amazon rainforest, there exists a range of processes and systems in the Earth's climate system that exhibit threshold behaviour [4]. These tipping elements contain biosphere components (e.g. Amazon rainforest, coral reefs), large-circulation patterns (e.g. Atlantic Meridional Overturning Circulation, monsoon systems) or cryosphere components (e.g. Greenland Ice Sheet, West Antarctic Ice Sheet). Under ongoing global warming, many of them are at risk of transitioning into an alternative, tipped state at lower levels of global warming than previously though [12, 73]. Such transitions would have dangerous consequences for humanity and biosphere integrity in the Earth system [11, 12]. There is an additional risk that tipping elements are strengthened by reinforcing, positive feedbacks within the climate system such that cascades might be triggered, potentially up to a planetary-scale tipping cascade that could push the Earth towards a "hothouse" state [11]. Moreover, the tipping elements in the climate system are interacting and there is a subset of five tipping elements where the interaction structure has been made explicit by an expert elicitation [19]. This network and their interactions have been used by some studies to investigate the risk of tipping cascades in the climate system, but also to quantify economic damages exerted by interacting tipping elements [27, 33, 74].

Here, we show how *PyCascades* can be used to simulate tipping events in four of the five aforementioned tipping elements: the Greenland Ice Sheet (GIS), the West Antarctic Ice Sheet (WAIS), the Atlantic Meridional Overturning Circulation (AMOC) and the Amazon Rainforest (AR). For these four tipping elements, there exist conceptual models of their nonlinear behaviour with respect to a forcing parameter [64, 66, 75, 76, 77], which can be traced back to increases in levels of global warming above pre-industrial [73]. Therefore, we can arguably model these four elements by

$$\frac{dx_i}{dt} = \left[ \underbrace{-x_i^3 + x_i + \frac{\sqrt{4/27}}{T_{\text{crit, i}}} \cdot \Delta\text{GMT}}_{\text{Individual dynamics term}} + \underbrace{\sum_{\substack{j \\ j \neq i}} \frac{s_{ij}}{4} (x_j + 1)}_{\text{Interaction term}} \right] \frac{1}{\tau_i} \tag{9}$$

with $i = \{\text{GIS, WAIS, AMOC, AR}\}$.

Here, $\Delta$GMT is the increase of the global mean temperature, $T_{\mathrm{crit,\,i}}$ the critical temperature at which a certain tipping element transgresses its baseline state, $s_{ij}$ the interaction strength between the tipping elements and $\tau_i$ the time a certain tipping event needs. Each $s_{ij}$ has a certain physical meaning, for instance, the freshwater entry from the GIS weakens the AMOC, while a weaker AMOC cools the northern hemisphere at the same time [e.g. 78]. The typical tipping time scales $\tau_i$ are chosen to be 4900, 2400, 300 and 50 years at 4 °C above pre-industrial levels of global warming for GIS, WAIS, AMOC and AR, respectively. For more details, see Fig. 6 and please be referred to Wunderling et al. (2020) [31]. The parameter uncertainties and a potential interaction structure are shown in Figs. 6 and 7. In Eq. 9, there are many parameters with uncertainties, for instance at which temperature $T_{\mathrm{crit,\,i}}$ a critical transition occurs or how strong the interactions $s_{ij}$ are. While upper and lower limits are given in the literature [19, 73], their uncertainty need to be propagated thoroughly. For this purpose, we use a large scale Monte-Carlo ensemble based on the latin hypercube sampling (LHS) method *pyDOE* [79]. The LHS is a sampling method that generates initial conditions that can be used in a Monte Carlo ensemble. They cover the state space of all uncertain parameters to a higher degree than random sample generation and are therefore better suited to create Monte Carlo ensembles in higher-dimensional systems. In Figs. 6 and 7, we demonstrate that constructing a large-scale Monte Carlo ensemble can be combined with simulating tipping cascades with *PyCascades*. In the critical temperatures $T_{\mathrm{crit,\,i}}$ and the interaction strengths $s_{ij}$ are 11 parameters with uncertainties (see Fig. 6). Upon that, we construct an ensemble of 1000 initial conditions.

In Eq. 9, we assume that the interaction term is 25% as important as the individual dynamics term. Thus, the interaction strength $s_{ij}$ is divided by 4 in Eq. 9. While this poses a hypothetical scenario, it allows us to estimate the likelihood of tipping of certain element at a certain increase of the global mean temperature $\Delta$GMT. For 2 °C, we find that the likelihood of tipping is around 50% for the GIS and WAIS, while it is significantly lower for the AMOC (around 25%) and the AR (less than 5%). There is a relatively high likelihood that GIS and WAIS tip since their critical temperature is lowest and there is a strong interaction link from GIS to WAIS. Therefore, the likelihood of tipping is lower for the AMOC, but the uncertainty is higher due to the strong negative feedback loop with GIS. Lastly, the AR has a very low likelihood of tipping since it is only connected to the other tipping elements via one uncertain link from AMOC.

### 3.3 International Trade Network

In the third example, we apply the *PyCascades* framework of interacting tipping elements to the *International Trade Network*. We construct the network from the EORA multi-regional input-output (MRIO) database [80] as also done in other studies [81, 82]. The database, which has also been subject to static analyses [83], consists of 188 countries with 27 economic sectors each, and includes the annual monetary flows between these sectors and regions. We interpret the individual sectors in each country as nodes of a network, and the flow $f_{ij}$ in the MRIO table as the weight for each directed link from node $j$ to $i$. In our analysis, we use the data for the year 2012. Following previous analyses [81, 82, 84], we also use a threshold of $10^6$ US-$ such that we exclude unrealistically small flows.

Propagation of economic losses on the trade network has previously been studied, for instance, with the *Acclimate* model [84]. This model interprets the economic sectors in each country as *firms* producing a *commodity* specific for the respective sector. Each firm does so using other commodities as inputs with specific, fixed

proportions according to a *Leontief* production function [85] as also used in simpler input-output models. These fixed proportions are taken from the multi-regional input-output (MRIO) table underlying the construction of the trade network, which constitute the *baseline state* (untipped state) of the model. If, for instance, the transportation sector in a country receives an input of ten billion US-$ from the oil sector and 90 billion US-$ from the machinery sector, it might have an output of 110 billion US-$ according to the MRIO table such that the created surplus would be 10 billion US-$. However, the according sector always produces according to these proportions using nine times as much "machinery commodity" as "oil commodity", and produces ten percent more "transportation commodity" than the sum of its inputs. If a firm receives only a certain fraction of the baseline state of a commodity due to some perturbation, the firm's output is limited to the same fraction of the baseline output. However, in the Acclimate model firms have idle capacities, i.e. the ability to temporarily produce more than their baseline output, if they have the necessary inputs and demand is high. The dynamics of this *anomaly model* are focused on perturbations around the baseline state with each agent aiming for maximum profit and minimum costs under local circumstances. After a shock or perturbation ceases the model returns back to the baseline state, which constitutes an equilibrium of the model's dynamics.

Tipping is not at the centre of the Acclimate model whose scope, as an anomaly model, vanishes for very large perturbations such as bankruptcies. We here, thus, define a simple dynamic for tipping on the trade network while keeping the linear Leontief production assumption for small perturbations, whereas nonlinear dynamics are assumed for larger perturbations. Nonlinear behaviour and tipping is common in economic networks, for instance in the banking sector [86, 87]. The nodes in the trade network are only to be perceived as representative firms, i.e., aggregates of national sectors, which consist of a variety of connected actors – so each node represents a network itself and might show nonlinear as well as tipping behaviour. The standard form of a tipping element defined by the Cusp-differential equation (see Eq. 3) is not well suited for this purpose. Instead, we are here looking for a new differential equation with the following properties:

1) The state $x_i$ of a node $i$ should represent its productivity that is between 0 (no production) to 1 (full production).
2) The element should react almost linearly to small perturbations as in the Acclimate model.
3) For large perturbations there should be a collapse of the productivity, including tipping and hysteresis.

To meet these criteria, we propose the differential equation

$$\frac{dx_i}{dt} = r_i - x_i - a\sqrt{x} \cdot \exp\left(-bx_i\right) + w_{\log} x_i \cdot \left(1 - x_i\right), \tag{10}$$

where $a$ and $b$ are parameters and $r_i$ is the limiting relative input as in the Leontief production function. The bifurcation diagram is given in Fig. 8a. The first two terms in equation 10 represent a linear response to perturbations, similar to the Acclimate model (see the dotted line in Fig. 8a). The third term is responsible for the nonlinear behaviour, causing tipping and hysteresis (see the dashed line in Fig. 8a). However, an economic tipping element defined by these three terms would be inherently unstable. Even small perturbations would finally lead to a collapse of the node since perturbations are almost always growing due to the structure of the network. However, we know that the trade network is not that fragile. Therefore, we add a logistic growth term to the differential equation to stabilise the network on the individual node level with the weight $w_{\log}$. Here, we argue that a certain flexibility in substituting inputs

exists. Within limits, it is therefore possible to return to the original production due to the logistic growth term. To illustrate an example, we choose $a = 4, b = 10$ for the parameters in Eq. 10. Therefore, the two bifurcation points lie at $r_1 = 0.4$ and $r_2 = 0.6$. The strength of the logistic growth term is chosen as $w_{\log} = 0.2$ (see the blue line in Fig. 8a).

In order to calculate the input term represented by $r_i$, every flow is normalised to the sum of flows from nodes of that sector to the target node. So the new weight $w_{c,s\to i}$ of a link from sector $s$ in country $c$ to node $i$ is given as

$$w_{c,s\to i} = \frac{f_{c,s\to i}}{\sum_k f_{k,s\to i}}. \tag{11}$$

With this, we can write the coupling term for the differential equation as

$$r_i = \min_{s \text{ in sectors}} \left\{ \sum_{c \text{ in countries}} w_{c,s\to i} \cdot x_{c,s} \right\}. \tag{12}$$

To simulate cascades, we start with all nodes in the untipped state, here $x_i = 1$ for all nodes $i$. We select a random starting node and tip it by setting its productivity to zero and then evolve the system with *PyCascades*. We exemplify this for a cascade between three countries, where one node has been tipped artificially (see Fig. 8b). The graph illustrates how the cascade propagates within and across the different countries forming densely connected network communities. Once the cascade reaches a country, most of that country's nodes tip almost at the same time. However, this gradual and sequential propagation of a tipping event is only one pattern of cascading behaviour observed. In Fig. 9, we show cascades for 30 different start nodes, chosen such that a wide range of different tipping cascades can be observed. Fig. 9a shows the number of tipped nodes, and Fig. 9b the average node state $\langle x \rangle = \frac{1}{N}\sum_i^N x_i$.

## 4 Conclusion

In this work, we have outlined the software package *PyCascades*, which is designed for simulating nonlinear dynamics, in particular tipping behaviour of interacting systems. For that purpose, two different types of tipping elements (Cusp and Hopf-bifurcation type models) are provided in *PyCascades* as well as different paradigmatic complex network types (Erdős-Rényi, Barabási-Albert, Watts-Strogatz networks) and a stochastic version of the tipping elements supplying Gaussian, Lévy and Cauchy noise. *PyCascades* is written in the programming language Python and is written with an object-oriented architecture such that it remains flexible and can easily be adapted or extended to further applications or theoretical problems.

However, a distinct limitation is, as of now, that only systems can be investigated, where the individual dynamics part can be separated from the interaction part. We also suspect that there is considerable potential for improvement in some technical details. For instance, more interaction types or multiplicative noise could be implemented. Another distinct constraint of *PyCascades* is that only paradigmatic dynamics of tipping elements are implemented. In particular, it would be highly desirable to develop process-based tipping elements depending on the respective application.

All in all, due to modular setup, *PyCascades* has the potential to contribute to relevant questions about the emergence of tipping cascades in various contexts, ranging from economics, ecology, climate science and beyond.

## 5 Acknowledgements

We thank Dorothea Kistinger for her work implementing the Hopf-bifurcation equation into *PyCascades* and Benedikt Stumpf for many fruitful discussions during the development of *PyCascades*. This work has been carried out within the framework of the IRTG 1740/TRP 2015/50-122-0 project funded by DFG and FAPESP. N.W. and R.W. acknowledge their financial support. This work is also part of PIK's FutureLab on Earth Resilience in the Anthropocene. N.W. is grateful for a scholarship from the Studienstiftung des deutschen Volkes. N.W., J.F.D., J.H. and R.W. are thankful for financial support by the Leibniz Association (project DominoES). A.S. and J.F.D. acknowledge support from the European Research Council Advanced Grant project ERA (Earth Resilience in the Anthropocene, ERC-2016-ADG-743080). J.F.D. is grateful for financial support by the Stordalen Foundation via the Planetary Boundary Research Network (PB.net) and the Earth League's EarthDoc program, and S.W. acknowledges support by the German Federal Ministry of Education and Research (BMBF) under the research project CLIC (FKZ: 01LA1817C). The authors gratefully acknowledge the European Regional Development Fund (ERDF), the German Federal Ministry of Education and Research and the Land Brandenburg for supporting this project by providing resources on the high performance computer system at the Potsdam Institute for Climate Impact Research.

## 6 Author contribution statement

N.W. designed the study together with R.W. and J.F.D.. N.W. performed the simulations and prepared the figures for this work with contributions from J.Kr. (in the section: Structure of the core of PyCascades) and V.W. (in the section: International Trade Network). N.W. led the writing of this work with inputs from all authors. J.Kr. developed the software package PyCascades with inputs and extensions from J.Ko., V.W. and N.W.. J.F.D. supervised this study.

## 7 Code and data availability

The code of this work has been provided as the open source software package *PyCascades* written in the programming language Python. It is freely available on github under the doi: 10.5281/zenodo.4153102. To be used, *PyCascades* is supplied with a 3-clause BSD license. In this repository, you can also find the code and data for the examples and applications that are discussed in this work. In case questions arise, please contact the corresponding authors of this study.

## References

1. Gladwell, M. *The tipping point: How little things can make a big difference* (Little, Brown, 2006).
2. van Nes, E. H. *et al.* What do you mean,'tipping point'? *Trends in Ecology & Evolution* **31**, 902–904 (2016).
3. Milkoreit, M. *et al.* Defining tipping points for social-ecological systems scholarship—an interdisciplinary literature review. *Environmental Research Letters* **13**, 033005 (2018).

4. Lenton, T. M. *et al.* Tipping elements in the earth's climate system. *Proceedings of the National Academy of Sciences* **105**, 1786–1793 (2008).
5. May, R. M., Levin, S. A. & Sugihara, G. Ecology for bankers. *Nature* **451**, 893–894 (2008).
6. Helbing, D. *et al.* Saving human lives: What complexity science and information systems can contribute. *Journal of Statistical Physics* **158**, 735–781 (2015).
7. Kopp, R. E., Shwom, R. L., Wagner, G. & Yuan, J. Tipping elements and climate–economic shocks: Pathways toward integrated assessment. *Earth's Future* **4**, 346–372 (2016).
8. Tàbara, J. D. *et al.* Positive tipping points in a rapidly warming world. *Current Opinion in Environmental Sustainability* **31**, 120–129 (2018).
9. Otto, I. M. *et al.* Social tipping dynamics for stabilizing earth's climate by 2050. *Proceedings of the National Academy of Sciences* **117**, 2354–2365 (2020).
10. Winkelmann, R. *et al.* Social tipping processes for sustainability: An analytical framework. *arXiv preprint arXiv:2010.04488* (2020).
11. Steffen, W. *et al.* Trajectories of the Earth System in the Anthropocene. *Proceedings of the National Academy of Sciences* **115**, 8252–8259 (2018).
12. Lenton, T. M. *et al.* Climate tipping points—too risky to bet against. *Nature* **575**, 592–595 (2019).
13. Lenton, T. M. Tipping positive change. *Philosophical Transactions of the Royal Society B* **375**, 20190123 (2020).
14. Rocha, J. C., Peterson, G., Bodin, Ö. & Levin, S. Cascading regime shifts within and across scales. *Science* **362**, 1379–1383 (2018).
15. Brummitt, C. D., Barnett, G. & D'Souza, R. M. Coupled catastrophes: sudden shifts cascade and hop among interdependent systems. *Journal of The Royal Society Interface* **12**, 20150712 (2015).
16. Van Gerven, L. P. *et al.* How regime shifts in connected aquatic ecosystems are affected by the typical downstream increase of water flow. *Ecosystems* **20**, 733–744 (2017).
17. Scheffer, M., Carpenter, S., Foley, J. A., Folke, C. & Walker, B. Catastrophic shifts in ecosystems. *Nature* **413**, 591 (2001).
18. Comin, D. & Hobijn, B. Cross-country technology adoption: making the theories face the facts. *Journal of Monetary Economics* **51**, 39–83 (2004).
19. Kriegler, E., Hall, J. W., Held, H., Dawson, R. & Schellnhuber, H. J. Imprecise probability assessment of tipping points in the climate system. *Proceedings of the National Academy of Sciences* **106**, 5041–5046 (2009).
20. Newman, M. E. The structure and function of complex networks. *SIAM Review* **45**, 167–256 (2003).
21. Albert, R. & Barabási, A.-L. Statistical mechanics of complex networks. *Reviews of Modern Physics* **74**, 47 (2002).
22. Zou, W., Senthilkumar, D., Zhan, M. & Kurths, J. Reviving oscillations in coupled nonlinear oscillators. *Physical Review Letters* **111**, 014101 (2013).
23. Gross, T., Rudolf, L., Levin, S. A. & Dieckmann, U. Generalized models reveal stabilizing factors in food webs. *Science* **325**, 747–750 (2009).
24. Donges, J. F., Zou, Y., Marwan, N. & Kurths, J. The backbone of the climate network. *EPL (Europhysics Letters)* **87**, 48007 (2009).
25. Newman, M. E. The structure of scientific collaboration networks. *Proceedings of the National Academy of Sciences* **98**, 404–409 (2001).
26. Stožer, A. *et al.* Heterogeneity and delayed activation as hallmarks of self-organization and criticality in excitable tissue. *Frontiers in Physiology* **10**, 869 (2019).
27. Gaucherel, C. & Moron, V. Potential stabilizing points to mitigate tipping point interactions in earth's climate. *International Journal of Climatology* **37**, 399–408

(2017).
28. Eom, Y.-H. Resilience of networks to environmental stress: From regular to random networks. *Physical Review E* **97**, 042313 (2018).
29. Klose, A. K., Karle, V., Winkelmann, R. & Donges, J. F. Emergence of cascading dynamics in interacting tipping elements of ecology and climate. *Royal Society Open Science* **7**, 200599 (2020).
30. Krönke, J. *et al.* Dynamics of tipping cascades on complex networks. *Physical Review E* **101**, 042311 (2020).
31. Wunderling, N., Donges, F. J., Kurths, J. & Winkelmann, R. Interacting tipping elements increase risk of climate domino effects under global warming. *Earth System Dynamics Discussions (in review, doi: 10.5194/esd-2020-18)* (2020).
32. Wunderling, N. *et al.* How motifs condition critical thresholds for tipping cascades in complex networks: Linking micro-to macro-scales. *Chaos: An Interdisciplinary Journal of Nonlinear Science* **30**, 043129 (2020).
33. Wunderling, N., Gelbrecht, M., Winkelmann, R., Kurths, J. & Donges, J. F. Basin stability and limit cycles in a conceptual model for climate tipping cascades. *New Journal of Physics* (2020).
34. Wunderling, N. *et al.* Network dynamics of drought-induced tipping cascades in the Amazon rainforest. *(in review, doi: 10.21203/rs.3.rs-71039/v1)* (2020).
35. Virtanen, P. *et al.* SciPy 1.0: Fundamental Algorithms for Scientific Computing in Python. *Nature Methods* **17**, 261–272 (2020).
36. Hagberg, A., Swart, P. & S Chult, D. Exploring network structure, dynamics, and function using networkx. Tech. Rep., Los Alamos National Lab.(LANL), Los Alamos, NM (United States) (2008).
37. Kuznetsov, Y. A. *Elements of applied bifurcation theory*, vol. 112 (Springer Science & Business Media, 2013).
38. Abraham, R., Keith, A., Koebbe, M. & Mayer-Kress, G. Computational unfolding of double-cusp models of opinion formation. *International Journal of Bifurcation and Chaos* **1**, 417–430 (1991).
39. van Nes, E. H., Rip, W. J. & Scheffer, M. A theory for cyclic shifts between alternative states in shallow lakes. *Ecosystems* **10**, 17 (2007).
40. Scheffer, M. & Jeppesen, E. Regime shifts in shallow lakes. *Ecosystems* **10**, 1–3 (2007).
41. Gardini, L., Lupini, R. & Messia, M. Hopf bifurcation and transition to chaos in lotka-volterra equation. *Journal of Mathematical Biology* **27**, 259–272 (1989).
42. Guckenheimer, J. & Labouriau, J. Bifurcation of the hodgkin and huxley equations: a new twist. *Bulletin of Mathematical Biology* **55**, 937 (1993).
43. Timmermann, A., Jin, F.-F. & Abshagen, J. A nonlinear theory for el niño bursting. *Journal of the atmospheric sciences* **60**, 152–165 (2003).
44. Dekker, M. M., Heydt, A. S. & Dijkstra, H. A. Cascading transitions in the climate system. *Earth System Dynamics* **9**, 1243–1260 (2018).
45. Zebiak, S. E. & Cane, M. A. A model el niñ–southern oscillation. *Monthly Weather Review* **115**, 2262–2278 (1987).
46. Erdös, P. & Rényi, A. On random graphs, i. *Publicationes Mathematicae (Debrecen)* **6**, 290–297 (1959).
47. Barabási, A.-L. & Albert, R. Emergence of scaling in random networks. *Science* **286**, 509–512 (1999).
48. Watts, D. J. & Strogatz, S. H. Collective dynamics of 'small-world'networks. *Nature* **393**, 440–442 (1998).
49. Kondepudi, D., Moss, F. & McClintock, P. V. Observation of symmetry breaking, state selection and sensitivity in a noisy electronic system. *Physica D: Nonlinear Phenomena* **21**, 296–306 (1986).

50. Gammaitoni, L., Hänggi, P., Jung, P. & Marchesoni, F. Stochastic resonance. *Reviews of Modern Physics* **70**, 223 (1998).
51. Scheffer, M. *et al.* Early-warning signals for critical transitions. *Nature* **461**, 53–59 (2009).
52. Thompson, J. M. T. & Sieber, J. Predicting climate tipping as a noisy bifurcation: a review. *International Journal of Bifurcation and Chaos* **21**, 399–423 (2011).
53. Ashwin, P., Wieczorek, S., Vitolo, R. & Cox, P. Tipping points in open systems: bifurcation, noise-induced and rate-dependent examples in the climate system. *Philosophical Transactions of the Royal Society A: Mathematical, Physical and Engineering Sciences* **370**, 1166–1184 (2012).
54. Aburn, M. J. & Ram, Y. Numerical integration of stochastic differential equations (SDEs) (2017). URL `https://github.com/mattja/sdeint/`. Accessed Sep. 23, 2020.
55. Rößler, A. Runge–kutta methods for the strong approximation of solutions of stochastic differential equations. *SIAM Journal on Numerical Analysis* **48**, 922–952 (2010).
56. Ditlevsen, P. D. Anomalous jumping in a double-well potential. *Physical Review E* **60**, 172 (1999).
57. Ditlevsen, P. D. Observation of $\alpha$-stable noise induced millennial climate changes from an ice-core record. *Geophysical Research Letters* **26**, 1441–1444 (1999).
58. Tesfay, D. *et al.* Influence of extreme events modeled by lévy flight on global thermohaline circulation stability. *Nonlinear Processes in Geophysics Discussions* 1–16 (2020).
59. Serdukova, L., Zheng, Y., Duan, J. & Kurths, J. Metastability for discontinuous dynamical systems under lévy noise: Case study on Amazonian vegetation. *Scientific Reports* **7**, 1–13 (2017).
60. Zheng, Y., Serdukova, L., Duan, J. & Kurths, J. Transitions in a genetic transcriptional regulatory system under lévy motion. *Scientific Reports* **6**, 29274 (2016).
61. Nobre, C. A. *et al.* Land-use and climate change risks in the Amazon and the need of a novel sustainable development paradigm. *Proceedings of the National Academy of Sciences* **113**, 10759–10768 (2016).
62. Davidson, E. A. *et al.* The Amazon basin in transition. *Nature* **481**, 321–328 (2012).
63. Cox, P. M. *et al.* Increasing risk of Amazonian drought due to decreasing aerosol pollution. *Nature* **453**, 212–215 (2008).
64. Zemp, D. C. *et al.* Self-amplified Amazon forest loss due to vegetation-atmosphere feedbacks. *Nature Communications* **8**, 1–10 (2017).
65. Staal, A., Dekker, S. C., Hirota, M. & van Nes, E. H. Synergistic effects of drought and deforestation on the resilience of the south-eastern Amazon rainforest. *Ecological Complexity* **22**, 65–75 (2015).
66. van Nes, E. H., Hirota, M., Holmgren, M. & Scheffer, M. Tipping points in tropical tree cover: linking theory to data. *Global Change Biology* **20**, 1016–1021 (2014).
67. Hirota, M., Holmgren, M., Van Nes, E. H. & Scheffer, M. Global resilience of tropical forest and savanna to critical transitions. *Science* **334**, 232–235 (2011).
68. Staver, A. C., Archibald, S. & Levin, S. A. The global extent and determinants of savanna and forest as alternative biome states. *Science* **334**, 230–232 (2011).
69. Aragão, L. E. Environmental science: The rainforest's water pump. *Nature* **489**, 217–218 (2012).
70. Eltahir, E. A. & Bras, R. L. Precipitation recycling in the Amazon basin. *Quarterly Journal of the Royal Meteorological Society* **120**, 861–880 (1994).

71. Staal, A., Dekker, S. C., Xu, C. & van Nes, E. H. Bistability, spatial interaction, and the distribution of tropical forests and savannas. *Ecosystems* **19**, 1080–1091 (2016).
72. Staal, A. *et al.* Forest-rainfall cascades buffer against drought across the Amazon. *Nature Climate Change* **8**, 539–543 (2018).
73. Schellnhuber, H. J., Rahmstorf, S. & Winkelmann, R. Why the right climate target was agreed in paris. *Nature Climate Change* **6**, 649–653 (2016).
74. Cai, Y., Lenton, T. M. & Lontzek, T. S. Risk of multiple interacting tipping points should encourage rapid CO2 emission reduction. *Nature Climate Change* **6**, 520–525 (2016).
75. Levermann, A. & Winkelmann, R. A simple equation for the melt elevation feedback of ice sheets. *The Cryosphere* **10**, 1799–1807 (2016).
76. Wood, R. A., Rodríguez, J. M., Smith, R. S., Jackson, L. C. & Hawkins, E. Observable, low-order dynamical controls on thresholds of the atlantic meridional overturning circulation. *Climate Dynamics* **53**, 6815–6834 (2019).
77. Stommel, H. Thermohaline convection with two stable regimes of flow. *Tellus* **13**, 224–230 (1961).
78. Caesar, L., Rahmstorf, S., Robinson, A., Feulner, G. & Saba, V. Observed fingerprint of a weakening atlantic ocean overturning circulation. *Nature* **556**, 191–196 (2018).
79. Baudin, M. pydoe: The experimental design package for python, sofware available under the bsd license (3-clause). `https://pythonhosted.org/pyDOE/index.html` (2013). Accessed: 2020-09-25.
80. Lenzen, M., Kanemoto, K., Moran, D. & Geschke, A. Mapping the structure of the world economy. *Environmental Science & Technology* **46**, 8374–8381 (2012).
81. Bierkandt, R., Wenz, L., Willner, S. N. & Levermann, A. Acclimate—a model for economic damage propagation. part 1: basic formulation of damage transfer within a global supply network and damage conserving dynamics. *Environment Systems and Decisions* **34**, 507–524 (2014).
82. Wenz, L., Willner, S. N., Bierkandt, R. & Levermann, A. Acclimate—a model for economic damage propagation. part ii: a dynamic formulation of the backward effects of disaster-induced production failures in the global supply network. *Environment Systems and Decisions* **34**, 525–539 (2014).
83. Maluck, J. & Donner, R. V. A network of networks perspective on global trade. *PLOS ONE* **10**, 1–24 (2015). URL `https://doi.org/10.1371/journal.pone.0133310`.
84. Otto, C., Willner, S. N., Wenz, L., Frieler, K. & Levermann, A. Modeling loss-propagation in the global supply network: The dynamic agent-based model acclimate. *Journal of Economic Dynamics and Control* **83**, 232–269 (2017). URL `http://www.sciencedirect.com/science/article/pii/S0165188917301744`.
85. Fandel, G. *Limitational Production Functions*, 111–146 (Springer, Berlin, Heidelberg, 1991).
86. May, R. M., Levin, S. A. & Sugihara, G. Ecology for bankers. *Nature* **451**, 893–894 (2008).
87. Haldane, A. G. & May, R. M. Systemic risk in banking ecosystems. *Nature* **469**, 351–355 (2011).

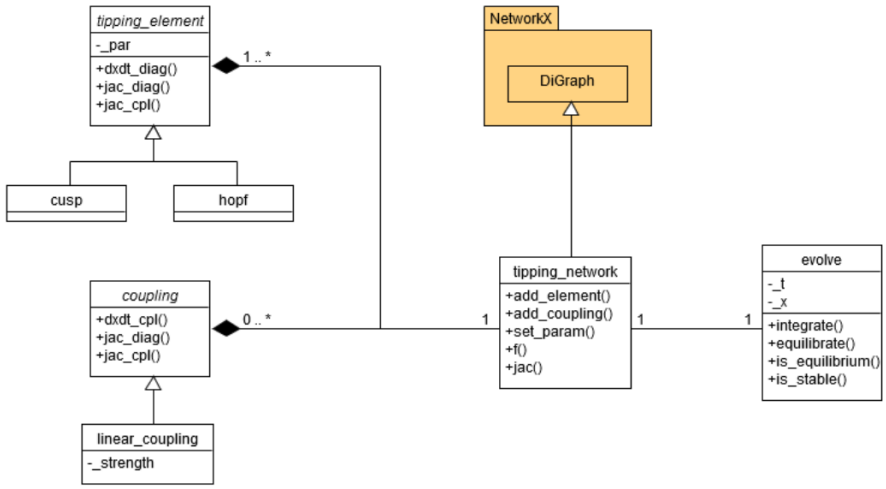


**Fig. 1.** UML class diagram of the core of *PyCascades* that depicts structure and dependencies of *PyCascades'* functionalities separated in the different python classes. The class `tipping_network` is derived from the `DiGraph` class of the *NetworkX* package [36]. It aggregates instances of the general classes `tipping_element` and `coupling`. The `evolve` class is associated with one instance of the `tipping_network` class and simulates the evolution of the complex dynamical system which is implemented by the concrete `tipping_element` and `coupling` objects with their specific parameters. For simplicity, only classes and class members important to the understanding of the *PyCascades* core are shown.

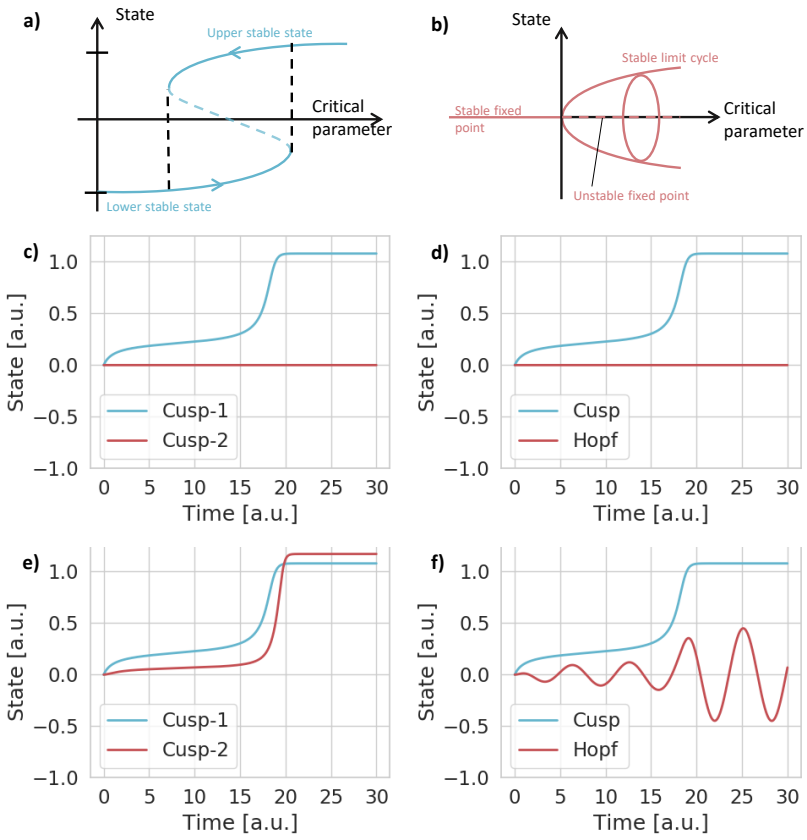


**Fig. 2.** The bifurcation diagrams of the pre-implemented tipping elements are shown, which possess a Cusp- or a Hopf-bifurcation, respectively (panels a) and b)). Further, two examples of tipping events are shown, once for the case where no tipping cascade emerges (panels c) and d)), and once where a tipping cascade emerges (panels e) and f) ). **a)** Bifurcation diagram of a fold-bifurcation (see Eq. 3). **b)** Bifurcation diagram of a (supercritical) Hopf-bifurcation (see Eq. 4). **c)** Two cusp differential equations with the parameters $a_1 = a_2 = 4$, $b_1 = b_2 = 1$, $x_{0,\,1} = x_{0,\,2} = 0.5$ and $c_1 = 0.2$, $c_2 = 0$. Thus, the first tipping element is slightly pushed over its upper critical value and a state transition occurs. **d)** One cusp, initialised as in panel c), and one tipping element that possibly could undergo a Hopf-bifurcation ($a = 1$, $\mu = -1$). In the panels c) and d), there is no interaction between the tipping elements, i.e., $A_{ij} = 0\ \forall i, j$. **e) and f)** Same as in panel c) and d), but with $A_{21} = 0.5$ such that the second tipping element (Cusp-2, Hopf) is coupled to the state of the first element (Cusp-1, Cusp). Therefore, in the lower panels a tipping cascade of two fold-bifurcations or, respectively, a tipping cascade of one fold- and one Hopf-bifurcation can be observed.

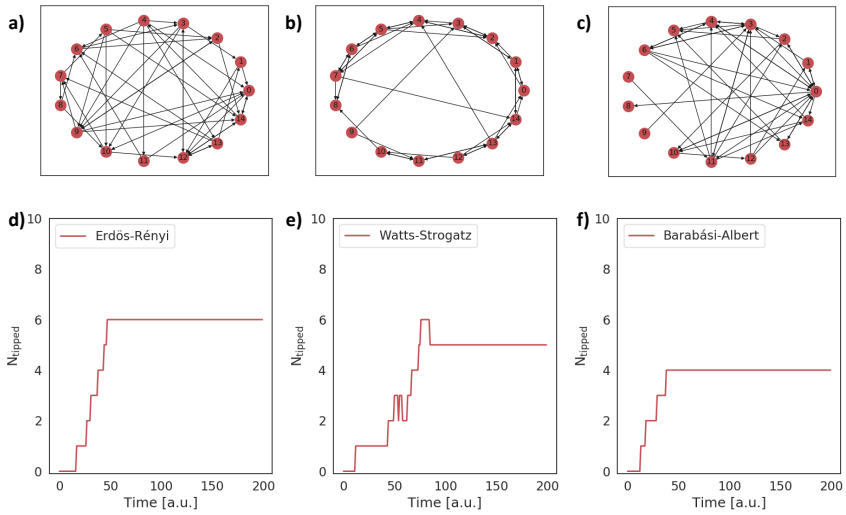


**Fig. 3.** The three paradigmatic and pre-implemented network types are shown together with an example of a tipping cascade in this network. Exemplary network structure with 15 nodes and an average degree of 3 for **a)** an Erdős-Rényi network, **b)** a Watts-Strogatz network (rewiring probability: 0.15) and **c)** a Barabási-Albert network. Exemplary tipping cascades for a network of 15 nodes, an average degree of 3, where each node is represented by a Cusp-tipping element (see Eq. 3) with $a = 4$, $b = -1$, $x_0 = 0.5$ for all nodes. The couplings between the nodes are alternately set to 0.2 and $-0.4$ for interaction 1, 2, 3, etc.. Then, at $t = 0$ one randomly chosen node $i$ is set to the upper state by choosing $c_i = 0.2$ such that tipping cascades can emerge. The number of tipped elements are shown for **d)** an Erdős-Rényi network, **e)** a Watts-Strogatz network (rewiring probability: 0.15) and **f)** a Barabási-Albert network.

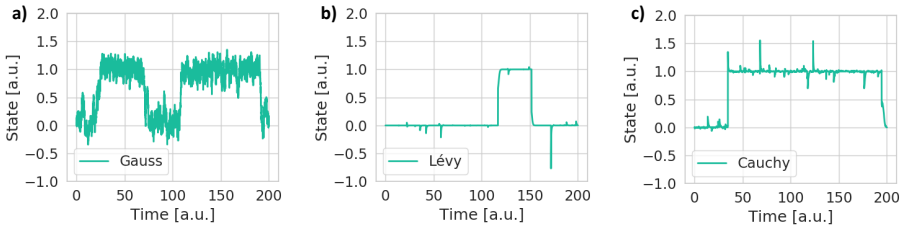


**Fig. 4.** Noise-induced tipping events with respect to different types of noise (Gauss, Lévy, Cauchy) that are available in *PyCascades*. Simulation of one Cusp-tipping ($a = 4$, $b = 1$, $c = x_0 = 0$) element with stochastic noise (see Eq. 6) of the following type: **a)** Gaussian noise ($\sigma = 0.25$, see Eq. 7), **b)** Lévy noise ($\sigma = 1.0$, see Eq. 7) and **c)** Cauchy noise ($\sigma = 1.0$, see Eq. 7).

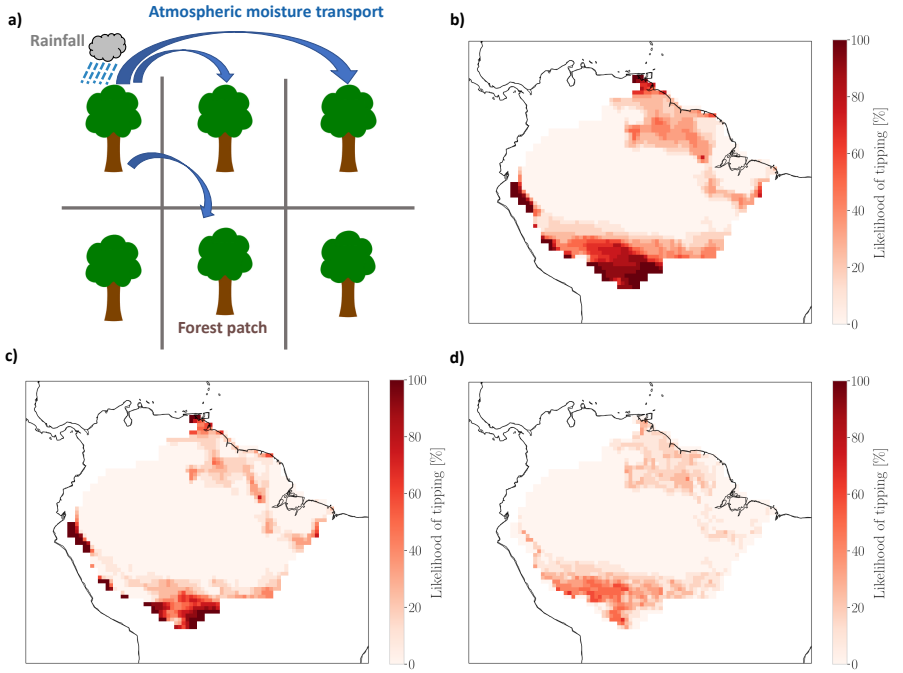


**Fig. 5.** Tipping cascades in a conceptual model of the Amazon rainforest connected via an atmospheric moisture recycling network. **a)** Sketch of the network of interacting rainforest patches in the Amazon rainforest. Precipitation rains down over some parts of the rainforest and parts of it are re-evapotranspirated and transported further by the wind (atmospheric moisture transport). **b)–d)** Exemplary tipping experiment on a $0.5\times0.5^\circ$ grid, where each grid cell represents one rainforest patch. The colourbar represents the likelihood of tipping averaged over the years 2003–2014. We show a comparison between **b)** coupling switched on (see Eq. 8), **c)** coupling switched off (see Eq. 8 with $g_i(x) \equiv 0\ \forall i$) and **d)** the difference between the panels b) and c). For each year in the study period (2003-2014), we performed one such tipping experiment, and the results shown are an average over this period.

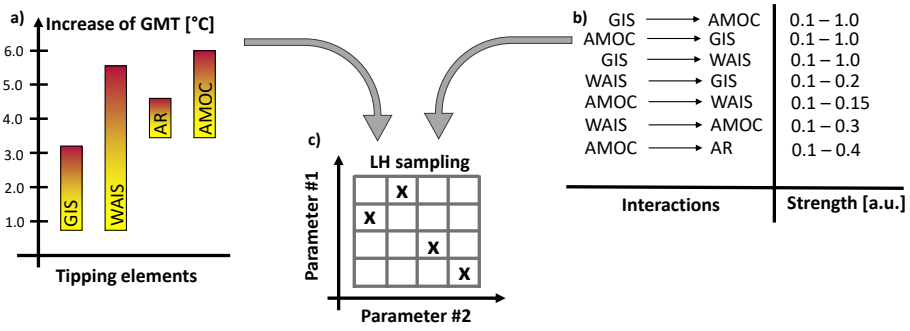


**Fig. 6.** Construction of the simulation ensemble to cover a large part of the phase space. **a)** Uncertainties in the critical temperatures [73] and **b)** interaction strengths [19] are put into a latin hypercube sampling algorithm [79] to construct suitable initial conditions (**c)**) that cover a larger part of the state space than normal random sampling would.

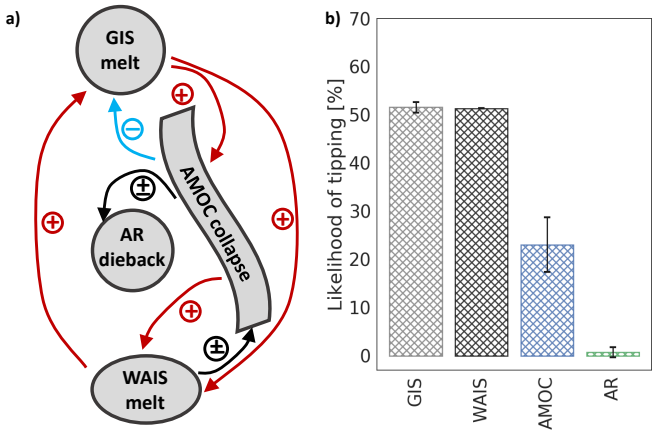


**Fig. 7.** Tipping cascades in a conceptual model of climate tipping elements. **a)** Interaction structure of four tipping elements (Greenland Ice Sheet: GIS, West Antarctic Ice Sheet: WAIS, Atlantic Meridional Overturning Circulation: AMOC, AR: Amazon rainforest). Destabilising interactions are depicted in red, stabilising interactions are depicted in light blue and uncertain interactions are shown in black. **b)** Likelihood for the respective tipping element to transgress its stable branch computed by running Eq. 9 into equilibrium. The error bar shows the standard deviation arising from the nine different possibilities of constructing the network. There are two uncertain links since their direction of interaction is unclear, meaning they could be stabilising, destabilising or zero, i.e., $[-, 0, +]$. Permuting these three options, gives nine different network structures and for each of them, we simulate 1000 ensemble members. We chose a scenario, where $\Delta$GMT = 2 °C above pre-industrial levels.

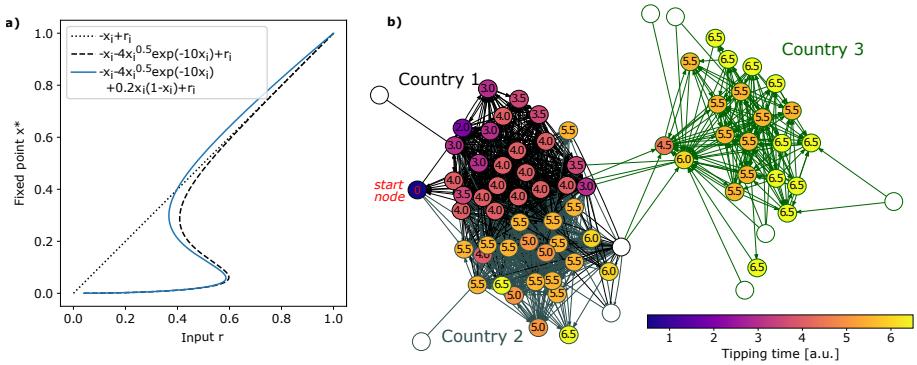


**Fig. 8.** Tipping cascades in a conceptual model of interacting countries in the *International Trade Network*. **a)** Bifurcation diagram for the proposed economic tipping element defined by equation 10. **b)** Tipping cascade between three different countries starting at the red *start node* at $t = 0$. The colour of the nodes represents the time at which a certain sector in that country tips and the colour of the arrows indicate the targeted country.

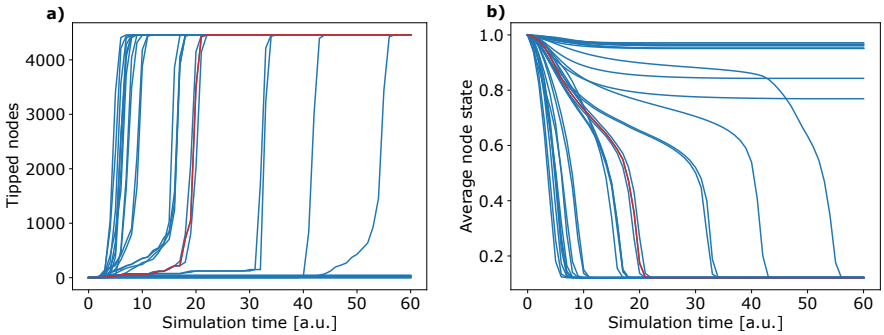


**Fig. 9.** Tipping cascades with the economic tipping element defined by equation 10 on the normalised trade network. The cascade depicted in Fig. 8 is plotted in red. **a)** Number of tipped nodes over the course of the simulation time. Cascades either lead to tipping of almost all nodes (global tipping) or the dynamics of the tipping cascade stops growing after very few nodes are tipped. **b)** Average node state $\langle x \rangle$ over the course of the simulation time. At the onset of the tipping cascade, the average stage shows a sharp decline. Since a decline in the average state does not automatically mean that nodes were tipped, some average state time series stabilise while others show a global cascade.

## 2.2 Dynamics of tipping cascades on complex networks [P2]

**Authors**
Jonathan Krönke, Nico Wunderling, Ricarda Winkelmann, Arie Staal, Benedikt Stumpf, Obbe A. Tuinenburg, Jonathan F. Donges

**Status**
Published in *Physical Review E* (April 2020; ©American Physical Society (United States)), doi: 10.1103/PhysRevE.101.042311

**Short summary**
In this work, it is examined in detail under which conditions tipping cascades can emerge for various different network topologies such as Erdős-Rényi, Barabási-Albert or Watts-Strogatz networks. With the use of PyCascades, the dependence of tipping cascades on the network size, the average network degree, clustering and reciprocity is shown. In addition, a spatially explicit network is constructed using atmospheric moisture recycling data within the Amazon rainforest. It is found that the onset of tipping cascades is shifted towards lower coupling strengths between the individual tipping elements compared to an Erdős-Rényi network. In order to understand the network structures that lead to this decrease of the coupling strength, tipping cascades in a network from a stochastic block model and from a configuration model are compared to tipping cascades in the Amazon rainforest network. With these models, it is confirmed that spatial organisation and clustering contributes significantly to an increased network vulnerability.

**Author contributions**
Jonathan Krönke, Nico Wunderling and Jonathan Donges designed this study. Jonathan Krönke performed the simulations and prepared the figures for this manuscript. Jonathan Krönke has written this paper with inputs from all authors. The part about the Amazon rainforest has been written by Jonathan Krönke, Nico Wunderling and Arie Staal. Arie Staal and Obbe Tuinenburg developed the moisture recycling dataset of the Amazon rainforest. This paper is an outcome of the master thesis of Jonathan Krönke, who was (co-)supervised by Nico Wunderling.

PHYSICAL REVIEW E **101**, 042311 (2020)

# Dynamics of tipping cascades on complex networks

Jonathan Krönke,[1,2,*] Nico Wunderling,[1,2,3,†] Ricarda Winkelmann,[1,2] Arie Staal,[4] Benedikt Stumpf,[1,5] Obbe A. Tuinenburg,[4,6] and Jonathan F. Donges[1,4,‡]

[1]*Earth System Analysis, Potsdam Institute for Climate Impact Research, Member of the Leibniz Association, 14473 Potsdam, Germany*

[2]*Institute of Physics and Astronomy, University of Potsdam, 14476 Potsdam, Germany*

[3]*Department of Physics, Humboldt University of Berlin, 12489 Berlin, Germany*

[4]*Stockholm Resilience Centre, Stockholm University, 10691 Stockholm, Sweden*

[5]*Department of Physics, Free University Berlin, 14195 Berlin, Germany*

[6]*Copernicus Institute, Faculty of Geosciences, Utrecht University, 3584 CB Utrecht, The Netherlands*

(Received 9 May 2019; revised manuscript received 15 January 2020; accepted 18 March 2020; published 29 April 2020)

Tipping points occur in diverse systems in various disciplines such as ecology, climate science, economy, and engineering. Tipping points are critical thresholds in system parameters or state variables at which a tiny perturbation can lead to a qualitative change of the system. Many systems with tipping points can be modeled as networks of coupled multistable subsystems, e.g., coupled patches of vegetation, connected lakes, interacting climate tipping elements, and multiscale infrastructure systems. In such networks, tipping events in one subsystem are able to induce tipping cascades via domino effects. Here, we investigate the effects of network topology on the occurrence of such cascades. Numerical cascade simulations with a conceptual dynamical model for tipping points are conducted on Erdős-Rényi, Watts-Strogatz, and Barabási-Albert networks. Additionally, we generate more realistic networks using data from moisture-recycling simulations of the Amazon rainforest and compare the results to those obtained for the model networks. We furthermore use a directed configuration model and a stochastic block model which preserve certain topological properties of the Amazon network to understand which of these properties are responsible for its increased vulnerability. We find that clustering and spatial organization increase the vulnerability of networks and can lead to tipping of the whole network. These results could be useful to evaluate which systems are vulnerable or robust due to their network topology and might help us to design or manage systems accordingly.

DOI: 10.1103/PhysRevE.101.042311

## I. INTRODUCTION

In the last decades the study of tipping elements has become a major topic of interest in climate science. Tipping elements are subsystems of the Earth system that may pass a critical threshold (tipping point) at which a tiny perturbation can qualitatively alter the state or development of the subsystem [1]. However, tipping points also occur in various complex systems such as systemic market crashes in financial markets [2], technological innovations [3], or shallow lakes [4] and other ecosystems [5]. Understanding their dynamics is thus crucial not only for climate science but also for other disciplines that use complex systems approaches.

Many tipping elements are not independent of each other [6]. In such cases, if one tipping element passes its tipping point, the probability of tipping of a second tipping element is often increased [7], yielding the potential of tipping cascades [8] via domino effects with significant potential impacts on human societies in the case of climate tipping elements [9]. In this study, we investigate the dynamics of complex networks of interacting tipping elements. A tipping element is described by a differential equation based on the normal form of the cusp catastrophe, which exhibits fold bifurcations and hysteresis properties. The interactions are accounted for by linear coupling terms. Many environmental tipping points can be described as fold bifurcations [10] and prototypical conceptual models that exhibit fold bifurcations have been developed for the thermohaline circulation [11], the Greenland ice sheet [12], and tropical rainforests [13] among others. Coupled cusp catastrophes have been studied in detail for two or three subsystems [6,14,15] or in combination with Hopf bifurcations [16]. On the other hand, threshold models for global cascades on large random networks have been investigated [17].

Here, we study cascades in complex systems with continuous state space that are moderate in size yet large enough for statistical properties of the complex interaction networks to become relevant. Cascades in complex systems with continuous state space have been investigated, for example, for power grids [18,19]. We use a paradigmatic coupled hysteresis model based on the normal form of the cusp catastrophe. Employing different network topologies such as Erdős-Rényi (ER), Watts-Strogatz (WS), and Barabási-Albert (BA) networks as

*kroenke@pik-potsdam.de

†Author to whom correspondence should be addressed: wunderling@pik-potsdam.de

‡Author to whom correspondence should be addressed: donges@pik-potsdam.de



2470-0045/2020/101(4)/042311(9)  

well as networks generated from moisture-flow data on the Amazon rainforest, we investigate the effect of topological properties of the network. We find that networks with a large average clustering coefficient are more vulnerable to cascading tipping and discuss how this is connected to the occurrence of small-scale motifs such as direct feedback and feed-forward loops. We consistently observe that networks with spatial organization like the small-world and Amazon networks are more vulnerable than strongly disordered networks.

## II. THE MODEL

### A. System

In our conceptual model, a tipping element is represented by a (real) time-dependent quantity $x(t)$ that evolves according to the autonomous ordinary differential equation

$$\frac{dx}{dt} = -a(x - x_0)^3 + b(x - x_0) + r, \tag{1}$$

where $r$ is the control parameter and $a, b > 0$. The parameters $a$ and $b$ control the strength of these effects, respectively, and $x_0$ controls the position of the system on the $x$ axis. The equation thus has one stable equilibrium for $|r| > r_{\text{crit}}$ and a bistable region for $-r_{\text{crit}} < r < r_{\text{crit}}$ (see the bifurcation diagram depicted in the box in Fig. 1).

We describe the characteristic behavior of Eq. (1): If the system state is initially in the lower stable equilibrium ($x \approx 0$) and $r$ is slowly increased, eventually at $r = r_{\text{crit}}$ a tipping point is reached and a critical transition to the upper stable equilibrium ($x \approx 1$) occurs. If $r$ is afterwards decreased, the system state stays on the upper branch and, only at $r = -r_{\text{crit}}$, tips down to the lower branch again. Equation (1) is a minimal model for ecosystems with alternative stable states and hysteresis [5] but can also be used to conceptualize other systems with similar properties such as the thermohaline circulation and ice sheets [12,20].

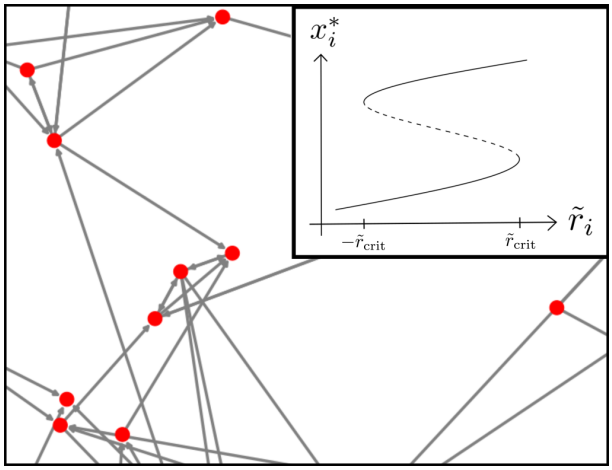


FIG. 1. Illustration of a tipping network. Each node represents a tipping element with a corresponding state variable $x_i$. A directed link corresponds to a positive linear coupling with strength $d$. The effective control parameter $\tilde{r}_i$ of a node depends on the state of the nodes it is coupled to. The equilibria with respect to the effective control parameter are qualitatively illustrated in the box.

Next, we consider a directed network of $N$ interacting tipping elements as a linearly coupled system of ordinary differential equations,

$$\frac{dx_i}{dt} = -a(x_i - x_0)^3 + b(x_i - x_0) + \underbrace{r_i + d\sum_{j=1, j\neq i}^{N} a_{ij}x_j}_{\tilde{r}_i(x_1, x_2, \ldots, x_N)}, \tag{2}$$

where $d > 0$ is the coupling strength and

$$a_{ij} = \begin{cases} 1 & \text{if there is a directed link from element } j \text{ to element } i, \\ 0 & \text{otherwise.} \end{cases} \tag{3}$$

For simplicity, we use the same parameters $a$ and $b$ for all tipping elements in the network. An illustration of such a system with several tipping elements is depicted in Fig. 1. Similar systems have been studied with diffusive coupling focusing on hysteresis effects [21].

We briefly review the behavior of two tipping elements with unidirectional coupling ($X_1 \to X_2$) [6]. The elements of the adjacency matrix are $a_{21} = 1$ and $a_{12} = 0$, which means that element 1 has an effect on element 2 but there is no effect in the other direction. As $r_1$ is slowly increased, it approaches its tipping point at $r_{\text{crit}}$ and eventually tips from $x_-$ to $x_+$. The effective control parameter $\tilde{r}_2$ is thus increased by $\Delta\tilde{r} = d(x_+ - x_-)$. For $r_2 = 0$, a tipping event in the second element is induced if $\Delta\tilde{r} > r_{\text{crit}}$ and therefore if the coupling strength exceeds a critical threshold of $d_c = \frac{r_{\text{crit}}}{x_+ - x_-}$.

### B. Network models

To investigate the effect of the network topology on tipping cascades we use different network models: We use three well-known models, the Erdős-Rényi model [22], the Watts-Strogatz model [23], and the Barabási-Albert model [24]. We slightly extend the latter two models such that we are able to generate and compare directed networks with a controllable average degree $\langle k \rangle = \langle k_{\text{in}} + k_{\text{out}} \rangle$. Furthermore, we use models to control the reciprocity and average clustering coefficient as well as a directed configuration model and a stochastic block model. All network models are briefly discussed in the following paragraphs.

(i) The ER model is a simple random network model, where a directed link between two elements $i$ and $j$ is added with probability $p$. The resulting average degree is $\langle k \rangle \approx p(N - 1)$.

(ii) The WS model is usually used to generate networks with large clustering coefficients but small average path lengths to resemble the small-world phenomenon [25]. We implement a directed WS model as follows: Initially, a regular network is generated where each node $i$ is connected in both directions to its $m$ nearest neighbors, e.g., nodes $i+1,\ i-1,\ldots,i+\frac{m}{2},\ i-\frac{m}{2}$. Therefore, $m$ has to be an even integer and the average degree of the resulting regular network is equal to $m$. In order to generate networks with arbitrary average degree, $m$ is chosen such that the average degree of the resulting regular network is larger than the desired average degree. Then, until the average degree of the network matches the desired average degree, links are randomly deleted. Finally, each of the remaining links is rewired with probability $\beta$, similar to the usual WS model [23]. With increasing rewiring probability $\beta$ the generated network becomes more and more random.

(iii) The BA model is used to generate scale-free networks, i.e., networks with a power-law degree distribution. We implement a directed BA model as follows: We start with two bidirectionally coupled nodes. Every additional node is in both directions connected to an already existing node $i$ with probability $p=\frac{k_i^{\text{in}}+k_i^{\text{out}}}{\sum_{m,n}a_{mn}}$. When the specified network size $N$ is reached, the average degree $\langle k\rangle\approx\frac{\sum_{m,n}a_{mn}}{N}$ is compared to the desired average degree. If the average degree is smaller than the desired average degree, links between randomly selected nodes $i$ and $j$ are added with probability $p=\frac{k_i^{\text{in}}+k_i^{\text{out}}+k_j^{\text{in}}+k_j^{\text{out}}}{2\sum_{m,n}a_{mn}}$ until the average degree matches the desired average degree. Otherwise, if the average degree is greater than the desired average degree, links are randomly deleted as in the WS model.

(iv) To generate networks with arbitrary reciprocity $R$, we initially generate an ER network where all links are reciprocal ($R=1$). Afterwards, links are randomly chosen and rewired until the desired reciprocity is achieved.

(v) The procedure to generate networks with arbitrary average clustering coefficent $\mathcal{C}$ is similar. Initially a network with only reciprocal triangles between three randomly chosen nodes is generated. Afterwards links are randomly chosen and rewired again until the desired average clustering coefficient is achieved. That way, we are able to generate networks with an average clustering coefficient between $\mathcal{C}=0.05$ and $\mathcal{C}=0.35$. Note that the reciprocity is also large for networks with a large average clustering coefficient.

(vi) A directed configuration model can be used to generate networks with arbitrary average in and out degree. Links are randomly assigned to node pairs where the corresponding in and out degree has not been reached before [26].

(vii) Finally, stochastic block models (SBMs) are used to generate networks with community structures. For each (directed) combination of communities there is a separate link probability, which is usually high within the community and low between two communities [27].

### C. Simulation procedure

We use the system given in Eq. (2) and conduct cascade simulations on different network topologies. The parameters of the equation are chosen such that $r_{\text{crit}}=0.183$ and for $r=0$ the two stable equilibria are $x_-=0$ and $x_+=1$ for all elements. The resulting parameters are $a=4$, $b=1$, and $x_0=0.5$. Consider a network with $N$ tipping elements and a topology that is described by the adjacency matrix $A=(a_{ij})$. Initially, $r_i=0$ and $x_i=0$ for all $i=1,\ldots,N$. The algorithm of a cascade simulation is the following:

(1) Choose a random starting node $m$ of the network.

(2) Slowly increase $r_m$ ($r_m\to r_m+\Delta r$).

(3) Let the system equilibrate, e.g., integrate the ODE system until $\dot{x}_i<\varepsilon$ for all $i=1,\ldots,N$.

(4) Check whether at least one element tipped. If not, jump back to step 2. Otherwise, count the total number of tipped elements.

The algorithm stops when the starting node $m$ tips, which is always the case. We normalize the total number of tipped elements (minus 1 for the starting node) by the number of nodes that can be reached on a directed path from the starting node (the size of the out component). We call the resulting number cascade size $L$. Note that due to the normalization a small disconnected component where all elements tip is also considered as a cascade with size $L=1$ even though only a small number of elements was tipped. The ODE system was integrated with the function `scipy.integrate.odeint` from the SCIPY python package [28]. In all simulations, $\Delta r=0.01$ and $\varepsilon=0.005$ were used. Examples of tipping cascades with size $L=1$ are shown in Fig. 2 for ER networks with different-sized $N$.

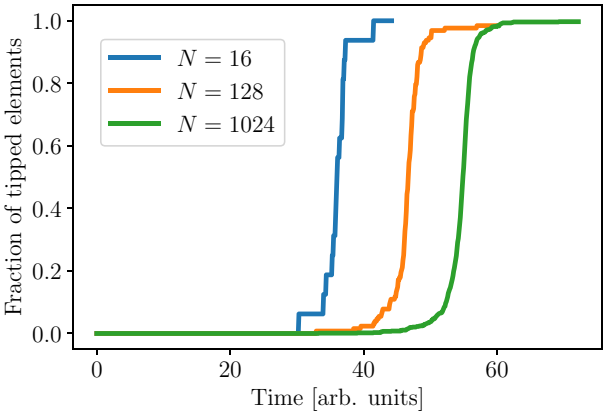


FIG. 2. Cascade simulations on ER networks of different sizes, an average degree of $\langle k\rangle\approx 5$, and a coupling strength of $d=0.2$. The time evolution of the fraction of tipped elements is shown.

## III. RESULTS AND DISCUSSION

### A. Cascades on generic network topologies

We start with cascade simulations on networks generated with the ER model. For any parameter combination we generate 100 different networks and simulate one cascade on each network. We use the average cascade size from these simulations as a measure of the vulnerability of the corresponding network structure, ranging from robust ($\langle L\rangle=0$) to highly vulnerable ($\langle L\rangle=1$) networks. The dependence of the average cascade size with respect to the coupling strength is shown in the upper panel in Fig. 3 for random networks with

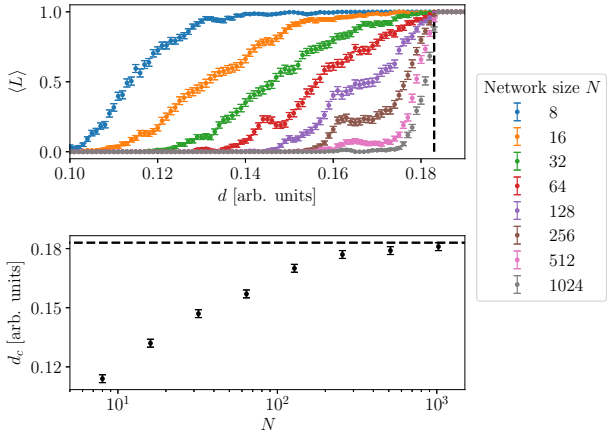


FIG. 3. Network size dependency of critical coupling strength in ER networks with $\langle k \rangle \approx 5$. Upper panel: Average cascade size with respect to the coupling strength in the transition region. Each average is calculated from 100 cascade simulations on different randomly generated networks with $N = 100$. Error bars indicate the standard error. Lower panel: Approximate critical coupling strength (coupling strength where $\langle L \rangle \approx 0.5$) with respect to the network size $N$. The dashed line indicates the critical coupling strength $d_c \approx r_{\text{crit}} = 0.183$ for a simple unidirectional coupling of two elements.

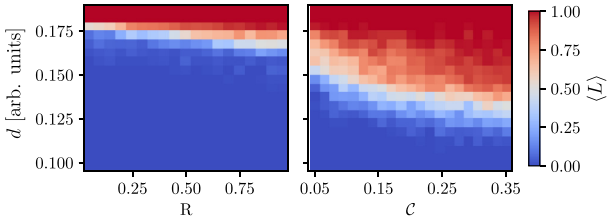


FIG. 4. Dependence of the transition region on the reciprocity $R$ (left panel) and on the clustering coefficient $C$ (right panel). Each average is calculated from 100 cascade simulations on different randomly generated networks with $N = 100$.

a fixed average degree $\langle k \rangle \approx 5$. For low coupling strengths ($d \lesssim 0.1$) the network is not affected by the externally induced tipping of one element and the average cascade size remains 0. With increasing coupling strength, a transition from robust to vulnerable networks is observed. From the analysis of the unidirectional system, a sharp transition at $d \approx r_{\text{crit}}$ would be expected for all networks. However, only for $N \to \infty$ does the transition become more and more steep and approximately approach $r_{\text{crit}}$. For networks of finite size, the onset of the transition is shifted to lower coupling strengths with decreasing network size. We hypothesize that the reason for this is two effects: The first effect is the destabilization of the system by feedback loops ($X_1 \leftrightarrows X_2$), which can lead to a decrease in the tipping point $r_{\text{crit}}$ of certain nodes. The second effect is due to the gradual change in the state of a tipping element $X_3$ that is coupled to another element ($X_1 \to X_3$). When the element $X_1$ tips, the state of the element $X_3$ will be slightly altered even if it does not tip. If it is coupled to another element $X_2$, however ($X_2 \to X_3$), the effective control parameter of element $X_3$ will be slightly increased, by an increment of the order $\Delta\tilde{r} \sim d^2$. Therefore an additional indirect coupling with one intermediate node, called a feed-forward loop, will decrease the critical coupling strength $d_c$ of the target node. But how can the size dependence of the critical coupling strength be explained? The reason for this is the following: With increasing network size while fixing the average degree, the relative density of the motifs decreases, and thus, for $N \to \infty$, the destabilizing effect of the motifs vanishes. Therefore, the critical coupling strength $d_c$ approaches the critical coupling strength of a unidirectionally coupled system. If, in contrast, we fixed the link density, the relative density of motifs would increase and thus the critical coupling strength would probably decrease with increasing network size.

To test this hypothesis, cascade simulations on networks with different reciprocities and average clustering coefficients are conducted. The reciprocity is the number of reciprocated links ($a_{ij} = a_{ji} = 1$) divided by the total number of links in the network. Thus, the reciprocity measures the relative amount of feedback loops in the tipping network. The average clustering coefficient is the number of triangles a node is part of divided by the potential number of triangles averaged over all nodes [29]. Therefore, the average clustering coefficient is strongly related to the number of feed-forward loops. Simulation results for different reciprocities $R$ can be seen in the left panel in Fig. 4. As expected, for networks with a high reciprocity, the transition region is shifted to lower coupling strengths. As can be seen, however, the dependence on the reciprocity is rather weak. Simulation results for networks with different average clustering coefficient $C$ are shown in the right panel in Fig. 4. It can be clearly seen that the vulnerability to tipping cascades is significantly increased for high average clustering coefficients. There are eight motifs that contribute to the average clustering coefficient in a directed network, two (indirect) feedback loops and six feed-forward loops [30]. We suspect that the effect of indirect feedback loops is smaller than the effect of direct feedback loops for $d < 1$. Therefore, we conclude that feed-forward loops are mainly responsible for the increased vulnerability of networks with large average clustering (see Fig. 4).

We also observe a transition of the average cascade size when the coupling strength is held constant at $d = 0.15$ and the average degree is varied (Fig. 5). In this case the transition is shifted to higher average degrees when the network size increases, because a higher average degree is necessary to yield the same relative density of destabilizing motifs.

Cascade distributions for $\langle k \rangle \approx 5$ and selected coupling strengths at the onset, in the center, and at the end of the respective transition region are shown in Fig. 6. We find a bimodal distribution of very small cascades ($L \approx 0$) and very large cascades ($L \approx 1$). For networks with small-world and scale-free topology generated with the WS model with $\beta = 0.1$ and the BA model, respectively, we observe similar transitions of the average cascade size. For the scale-free topology, the large cascades are distributed around an average size $\langle L \rangle < 1$. This can be explained by the preferential attachment mechanism. Through this mechanism a large number of weakly connected elements develop which can only be tipped when the coupling strength is very high ($d \gtrsim r_{\text{crit}}$).

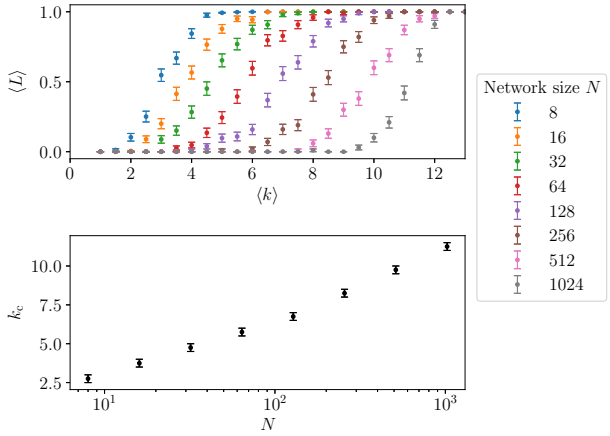


FIG. 5. Network size dependency of the critical average degree $k_c$ in ER networks with $d = 0.15$. Upper panel: Average cascade size with respect to the average degree in the transition region. Each average is calculated from 100 cascade simulations on different randomly generated networks with $N = 100$. Error bars indicate the standard error in both panels. Lower panel: Approximate critical average degree (average degree where $\langle L \rangle \approx 0.5$) with respect to the network size $N$.

Now we focus on the effect of the network topology. For all network models, the transition from robust to vulnerable networks is shifted to lower coupling strengths when the average degree is increased (Fig. 7). The topology of the network

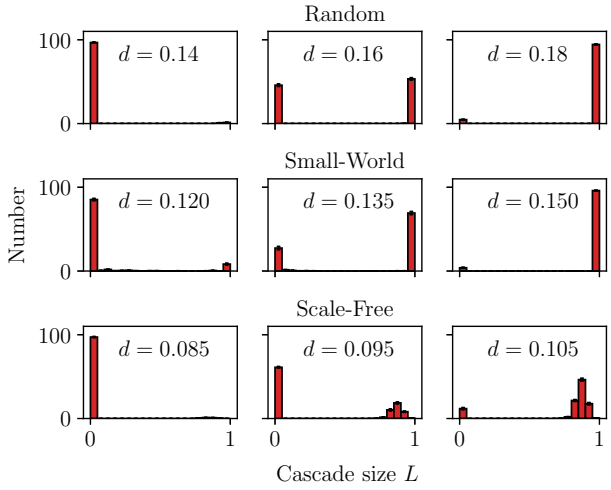


FIG. 6. Distributions of cascade sizes $L$ for different network topologies. A random topology generated with the ER model (first row), a small-world topology generated with the WS model and $\beta = 0.1$ (second row), and a scale-free topology generated with the BA model (third row). Each distribution is an average of 10 distributions with 100 cascade simulations on different networks with $N = 100$ and $\langle k \rangle \approx 5$. The (almost-invisible) error bars indicate the standard error across the 10 distributions. Three coupling strengths for each network topology are shown: one where almost no cascades occur; one where in about half of the simulations cascades are triggered; and one where in almost all simulations cascades are triggered.

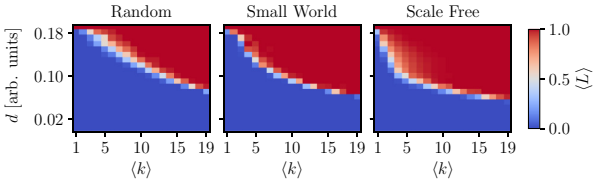


FIG. 7. Average cascade size $\langle L \rangle$ with respect to average degree $\langle k \rangle$ and coupling strength $d$ for three network topologies. Random networks generated with the ER model (left), small-world topology networks generated with the WS model and $\beta = 0.1$ (center), and scale-free networks generated with the BA model (right). Each average is calculated from 100 cascade simulations on different randomly generated networks with $N = 100$.

has a significant effect on this shift of the transition region for sparse networks ($\langle k \rangle \approx 5$). For networks with small-world and scale-free topology, the transition is shifted to lower coupling strengths compared to the simple random topology generated with the ER model. For the scale-free topology the transition width is also significantly increased for $\langle k \rangle \approx 5$. For denser networks ($\langle k \rangle \gtrsim 19$), the differences between the network topologies are less pronounced.

We further investigate in which way the rewiring in the WS model decreases the vulnerability of the network. In Fig. 8 the shift of the transition region to higher coupling strengths with respect to the rewiring probability $\beta$ can be clearly seen. The increase in the critical coupling strength mainly occurs between $\beta = 0.1$ and $\beta = 1$. The lower panel in the figure again demonstrates how this corresponds to the decay of the average clustering coefficient $\mathcal{C}$. Thus, we again conclude that tipping networks with an increased average clustering coefficient such as small-world networks (but also spatially

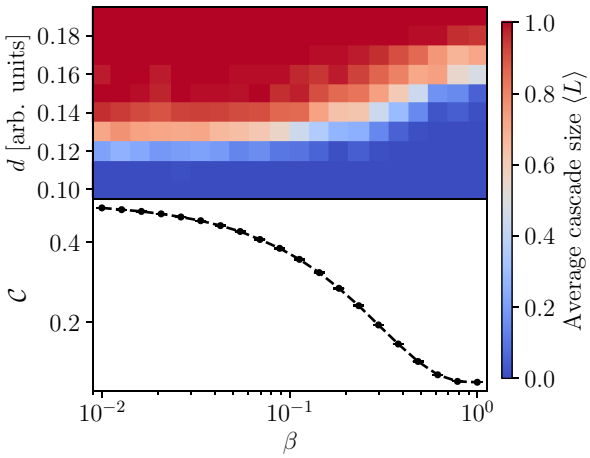


FIG. 8. Shift of the transition (upper panel) and average clustering coefficient $\mathcal{C}$ (lower panel) with increasing rewiring probability $\beta$ for WS networks with $N = 100$ and $\langle k \rangle \approx 5$. The shift of the transition towards higher coupling strengths for high rewiring probabilities corresponds to the decrease in the average clustering coefficient. The extent of the small black circles in the lower panel exceeds the standard error, which is therefore not visible.

structured networks [31]; see Sec. III B) are especially vulnerable to cascades and that the average clustering coefficient is a good indicator of the vulnerability of a network topology.

### B. Cascades on spatial network topologies from moisture-flow data

To investigate the effects of spatial organization of the network on vulnerability with respect to tipping cascades, we apply our model to network topologies generated from data of atmospheric moisture flows between different forest cells in the Amazon. On a local scale, the Amazon may exhibit alternative stable states between rainforest and savanna, with tipping points between them depending on rainfall levels [32–35]. Models that capture the basic mechanisms also reveal a bifurcation structure with hysteresis and saddle-node bifurcations with rainfall level as the control parameter, comparable to our conceptual model [36]. On a regional scale, the forest enhances rainfall through the "transpiration" of groundwater to the atmosphere; local-scale tipping may thus increase the vulnerability of remote forest patches by allowing less local precipitation to be passed on to other patches because the transpiration capacity of savanna is lower than that of forest. Therefore, the Amazon can be thought of as a spatial network of local-scale tipping elements. Note that the Amazon as a whole is often viewed as a tipping element [37]. In our framework, vulnerable regimes where tipping of single cells induces large cascades correspond to such threshold behavior of the large-scale Amazon system. Complex-network approaches such as a cascade model inspired by the Watts model [17] have been applied to observation-based data on Amazon forest patches [38]. Here we analyze the effect of the network structure of transpired-moisture flows for the Amazon that were calculated by Staal *et al.* [39], aggregated to a single year (2014) on 1° spatial resolution.

As our analysis is focused on the effect of the network topology, we neglect the actual moisture-flow values and use a homogeneous coupling strength analogous to the above simulations. This makes the simulation results less realistic and applicable, however, we do not aim to draw conclusions about the Amazon system. Rather, we want to compare the network topology to common random networks and identify topological effects on the vulnerability of tipping networks with respect to tipping cascades.

To generate and compare networks with arbitrary average degree, similar to the random network topologies above, we calculate a moisture-flow threshold from a specified average degree. Only when the moisture flow between two cells exceeds the threshold are these cells connected with a link in the corresponding direction. If a large average degree is specified, the threshold becomes small and the resulting network will be dense. That way we are able to generate networks with an arbitrary average degree from the data. An example network with $\langle k \rangle = 5$ is depicted in Fig. 9.

The average cascade size is calculated by conducting one cascade simulation with each node of the generated network as the starting node and averaging over the cascade size. We generate networks from data with a $1 \times 1^\circ$ grid ($N = 567$) and with a $2 \times 2^\circ$ grid ($N = 160$) and $\langle k \rangle = 5$. The average cascade size of ER networks with the same size is shown for comparison (upper panel in Fig. 10). For the Amazon network, the onset of the transition from robust to vulnerable networks is shifted to the lower coupling strength of $d \approx 0.08$ compared to the ER network. In contrast to the ER networks there is no strong size dependency. However, a small shift to lower coupling strengths is observed.

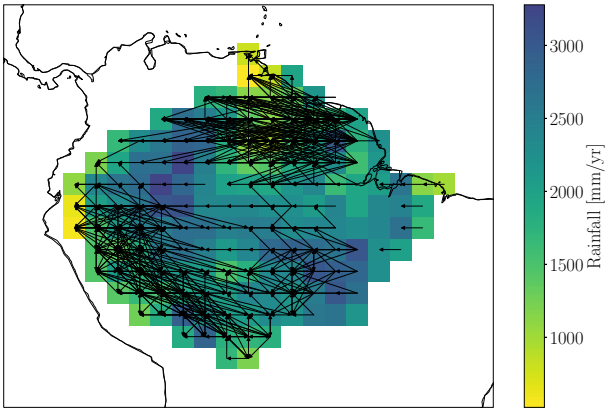


FIG. 9. Spatially organized network generated from atmospheric moisture-flow data ($2 \times 2^\circ$-grid resolution) of the Amazon rainforest. The threshold is chosen such that $\langle k \rangle = 5$. Total rainfall values for each node in 2014 are shown in the background.

Additionally to the Amazon moisture-flow network obtained by thresholding, we generate networks with a directed configuration model [26] and a stochastic block model [27] to isolate the effects of the degree sequence and the community

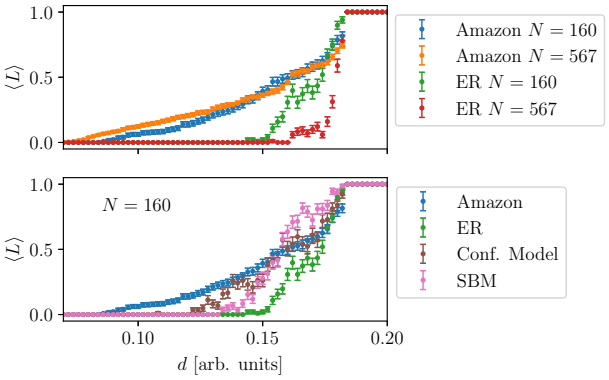


FIG. 10. Average cascade size $\langle L \rangle$ with respect to coupling strength for different networks with an average degree of $\langle k \rangle = 5$. Upper panel: Results for the networks generated from the moisture-flow data with $1 \times 1^\circ$-grid resolution (567 nodes) and $2 \times 2^\circ$-grid resolution (160 nodes). For comparison, simulation results for ER networks with the same network sizes are shown. Lower panel: Simulation results for a directed configuration model and a stochastic block model are compared with the results of the Amazon network and the ER networks with $N = 160$ for all networks. Error bars indicate the standard error. Note that the standard errors for the original moisture-flow networks are smaller than for the other network types. The reason is that all moisture-flow simulation results are based on the same network, whereas the other results are based on different randomly generated networks.

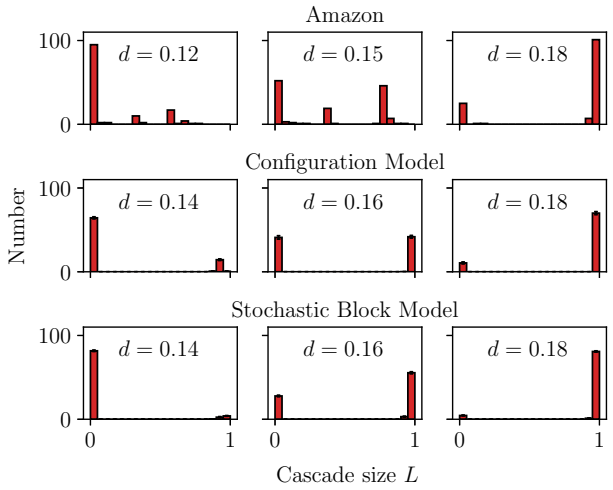


FIG. 11. Distribution of cascade sizes analogous to the above distributions for different networks generated from moisture-flow simulations of the Amazon rainforest ($N = 160$). Note that there is no standard error indicated (error bars) for the original moisture-flow networks, as there is only one distribution due to the deterministic network generation procedure.

structure of the network, respectively. For the directed configuration model, we specify the joint degree sequence of the Amazon network. For the SBM, we apply a Girvan-Newman algorithm to the original Amazon network [40]. The algorithm progressively removes edges with the highest edge betweenness, i.e., those rare links that connect separate communities. When the network breaks into two components, we calculate the elements of the probability matrix (fraction of links over possible links for the corresponding combination of components). With the probability matrix and the component sizes, we then generate a random network with the SBM.

In the lower panel in Fig. 10, the transition of the configuration model and the SBM is compared to the original Amazon network and the ER network with $N = 160$. Although the vulnerability of the network is increased in both cases compared to the ER model, neither of the topological properties alone, degree sequence or community structure, sufficiently explains the early onset of the transition in the original Amazon network.

Cascade distributions for the coarse resolution ($2 \times 2^\circ$ grid) are depicted in Fig. 11. They show that already for values of $d \approx 0.1$, cascades with two typical cascade sizes occur for the original Amazon network. With increasing coupling strength the frequency of these cascades increases and the cascade size is shifted to higher values. Comparing this observation to the network in Fig. 9 suggests that these cascades correspond to the two subclusters in the north and southwest regions of the Amazon rainforest. These subregions form clusters that are much more strongly connected than the rest of the network and are thus much more vulnerable to tipping cascades. Interestingly, separate tipping of subclusters is not observed for the networks generated with the SBM, implying that some relevant topological property of the spatially structured Amazon network, for example, the

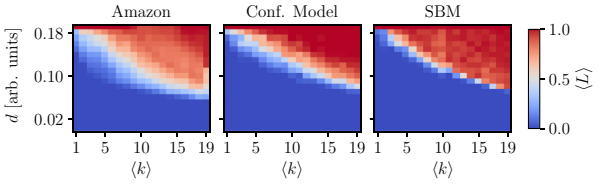


FIG. 12. Average cascade size $\langle L \rangle$ with respect to average degree and coupling strength for different networks generated with moisture-flow simulations of the Amazon rainforest ($N = 160$).

anisotropy of the link direction due to atmospheric wind patterns, might still be missing. The robust and vulnerable regimes of the networks are shown in Fig. 12. Consistent with the above results, we observe a shift of the transition to lower coupling strengths with increasing average degree $\langle k \rangle$ where the transition is smooth for the Amazon network and steep for the configuration model and the SBM. Similarly to the random network topologies, the differences are only relevant for the sparse regime below $\langle k \rangle \lesssim 19$.

## IV. CONCLUSION

The aim of our study was to assess the effect of the network topology on the vulnerability of tipping networks to cascades. This is not only important for understanding the effect that the tipping of potential tipping elements in the climate system might have on the complete Earth system, but also of high relevance for other fields that use complex system approaches. We found that networks with large average clustering coefficients and spatially structured networks are more vulnerable to tipping cascades than more disordered network topologies. This implies that the risk of a cascade's being triggered could be surprisingly high for real-world networks where large clustering is common. Furthermore, we found that the effect of the network topology is relevant only for relatively sparsely connected networks. The analysis of the Amazon network suggests that the structure of the forest-climate system in the Amazon might yield subregions that are especially vulnerable to tipping cascades. A detailed study using actual moisture flows could investigate the question whether the Amazon rainforest consists of separate subregional-scale tipping elements. Generally, heterogeneity in the parameters, for example, the temporal and spatial scales or the coupling strengths of the ODE system stated in Eq. (2), could have a further influence on the results [41].

## ACKNOWLEDGMENTS

The authors thank M. Wiedermann and J. Heitzig for fruitful discussions. N.W. acknowledges support from IRTG 1740/TRP 2015/50122-0 funded by the DFG and FAPESP. N.W. is grateful for support through a scholarship from the Studienstiftung des deutschen Volkes. R.W. and J.F.D. are thankful for support from the Leibniz Association (project DominoES). A.S. and J.F.D. acknowledge support from the European Research Council project Earth Resilience in the Anthropocene (743080 ERA). A.S. and O.A.T. thank the Bolin Centre for Climate Research for support. O.A.T. acknowledges funding from the Netherlands Organization for

Scientific Research Innovational Research Incentive Schemes VENI (No. 016.171.019). J.F.D. thanks the Stordalen Foundation (via the Planetary Boundaries Research Network PB.net) and the Earth League's EarthDoc program for financial support. The authors gratefully acknowledge the European Regional Development Fund (ERDF), the German Federal Ministry of Education and Research, and the Land Brandenburg for supporting this project by providing resources on the high-performance computer system at the Potsdam Institute for Climate Impact Research.

[1] T. M. Lenton, H. Held, E. Kriegler, J. W. Hall, W. Lucht, S. Rahmstorf, and H. J. Schellnhuber, Tipping elements in the earth's climate system, Proc. Natl. Acad. Sci. USA **105**, 1786 (2008).

[2] R. M. May, S. A. Levin, and G. Sugihara, Ecology for bankers, Nature **451**, 893 (2008).

[3] P. A. Herbig, A cusp catastrophe model of the adoption of an industrial innovation, J. Prod. Innov. Manage. **8**, 127 (1991).

[4] M. Scheffer and E. H. van Nes, Shallow lakes theory revisited: Various alternative regimes driven by climate, nutrients, depth and lake size, Hydrobiologia **584**, 455 (2007).

[5] M. Scheffer, S. Carpenter, J. A. Foley, C. Folke, and B. Walker, Catastrophic shifts in ecosystems, Nature **413**, 591 (2001).

[6] C. D. Brummitt, G. Barnett, and R. M. D'Souza, Coupled catastrophes: Sudden shifts cascade and hop among interdependent systems, J. R. Soc., Interface **12**, 20150712 (2015).

[7] E. Kriegler, J. W. Hall, H. Held, R. Dawson, and H. J. Schellnhuber, Imprecise probability assessment of tipping points in the climate system, Proc. Natl. Acad. Sci. USA **106**, 5041 (2009).

[8] W. Steffen, J. Rockström, K. Richardson, T. M. Lenton, C. Folke, D. Liverman, C. P. Summerhayes, A. D. Barnosky, S. E. Cornell, M. Crucifix, J. F. Donges, I. Fetzer, S. J. Lade, M. Scheffer, R. Winkelmann, and H. J. Schellnhuber, Trajectories of the earth system in the anthropocene, Proc. Natl. Acad. Sci. USA **115**, 8252 (2018).

[9] Y. Cai, T. M. Lenton, and T. S. Lontzek, Risk of multiple interacting tipping points should encourage rapid $CO_2$ emission reduction, Nat. Clim. Chang. **6**, 520 (2016).

[10] T. M. Lenton, Environmental tipping points, Annu. Rev. Environ. Resour. **38**, 1 (2013).

[11] D. G. Wright and T. F. Stocker, A zonally averaged ocean model for the thermohaline circulation. I: Model development and flow dynamics, J. Phys. Oceanogr. **21**, 1713 (1991).

[12] A. Levermann and R. Winkelmann, A simple equation for the melt elevation feedback of ice sheets, Cryosphere **10**, 1799 (2016).

[13] A. Staal, E. H. van Nes, S. Hantson, M. Holmgren, S. C. Dekker, S. Pueyo, C. Xu, and M. Scheffer, Resilience of tropical tree cover: The roles of climate, fire, and herbivory, Glob. Chang. Biol. **24**, 5096 (2018).

[14] R. Abraham, A. Keith, M. Koebbe, and G. Mayer-Kress, Computational unfolding of double-cusp models of opinion formation, Int. J. Bifurc. Chaos **01**, 417 (1991).

[15] A. K. Klose, V. Karle, R. Winkelmann, and J. F. Donges, Dynamic emergence of domino effects in systems of interacting tipping elements in ecology and climate, arXiv:1910.12042.

[16] M. M. Dekker, A. S. von der Heydt, and H. A. Dijkstra, Cascading transitions in the climate system, Earth Syst. Dynam. **9**, 1243 (2018).

[17] D. J. Watts, A simple model of global cascades on random networks, Proc. Natl. Acad. Sci. USA **99**, 5766 (2002).

[18] Y. Yang, T. Nishikawa, and A. E. Motter, Small vulnerable sets determine large network cascades in power grids, Science **358**, eaan3184 (2017).

[19] B. Schäfer, D. Witthaut, M. Timme, and V. Latora, Dynamically induced cascading failures in power grids, Nat. Commun. **9**, 1975 (2018).

[20] H. Stommel, Thermohaline convection with two stable regimes of flow, Tellus A **13**, 224 (1961).

[21] Y.-H. Eom, Resilience of networks to environmental stress: From regular to random networks, Phys. Rev. E **97**, 042313 (2018).

[22] B. Bollobas, in *Random Graphs*, edited by W. Fulton, A. Katok, F. Kirwan, P. Sarnak, B. Simon, and B. Totaro (Cambridge University Press, Cambridge, UK, 2001).

[23] D. J. Watts and S. H. Strogatz, Collective dynamics of small-world networks, Nature **393**, 440 (1998).

[24] A. Barabási and R. Albert, Emergence of scaling in random networks, Science **286**, 509 (1999).

[25] S. Milgram, The small-world problem, Psychol. Today **2**, 60 (1967).

[26] M. E. J. Newman, S. H. Strogatz, and D. J. Watts, Random graphs with arbitrary degree distributions and their applications, Phys. Rev. E **64**, 026118 (2001).

[27] P. W. Holland, K. B. Laskey, and S. Leinhardt, Stochastic block models: First steps, Soc. Networks **5**, 109 (1983).

[28] T. E. Oliphant, Python for scientific computing, Comput. Sci. Eng. **9**, 10 (2007).

[29] G. Fagiolo, Clustering in complex directed networks, Phys. Rev. E **76**, 026107 (2007).

[30] R. Milo, S. Shen-Orr, S. Itzkovitz, N. Kashtan, D. Chklovskii, and U. Alon, Network motifs: Simple building blocks of complex networks, Science **298**, 824 (2002).

[31] M. Wiedermann, J. F. Donges, J. Kurths, and R. V. Donner, Spatial network surrogates for disentangling complex system structure from spatial embedding of nodes, Phys. Rev. E **93**, 042308 (2016).

[32] M. Hirota, M. Holmgren, E. H van Nes, and M. Scheffer, Global resilience of tropical forest and savanna to critical transitions, Science **334**, 232 (2011).

[33] A. C. Staver, S. Archibald, and S. A. Levin, The global extent and determinants of savanna and forest as alternative biome states, Science **334**, 230 (2011).

[34] C. Xu, S. Hantson, M. Holmgren, E. H. van Nes, A. Staal, and M. Scheffer, Remotely sensed canopy height reveals three pantropical ecosystem states, Ecology **97**, 2518 (2016).

[35] C. Ciemer, N. Boers, M. Hirota, J. Kurths, F. Müller-Hansen, R. S. Oliveira, and R. Winkelmann, Higher resilience to climatic disturbances in tropical vegetation exposed to more variable rainfall, Nat. Geosci. **12**, 174 (2019).

[36] E. H. van Nes, M. Hirota, M. Holmgren, and M. Scheffer, Tipping points in tropical tree cover: Linking theory to data, Glob. Chang. Biol. **20**, 1016 (2014).

[37] P. M. Cox, R. A. Betts, M. Collins, P. P. Harris, C. Huntingford, and C. D. Jones, Amazonian forest dieback under climate-carbon cycle projections for the 21st century, Theor. Appl. Climatol. **78**, 137 (2004).

[38] D. C. Zemp, H. M. J. Schleussner, Barbosa, M. Hirota, V. Montade, G. Sampaio, A. Staal, L. Wang-Erlandsson, and A. Rammig, Self-amplified amazon forest loss due to vegetation-atmosphere feedbacks, Nat. Commun. **8**, 14681 (2017).

[39] A. Staal, O. A. Tuinenburg, J. H. C. Bosmans, M. Holmgren, E. H. van Nes, M. Scheffer, D. C. Zemp, and S. C. Dekker, Forest-rainfall cascades buffer against drought across the Amazon, Nat. Clim. Chang. **8**, 539 (2018).

[40] M. Girvan and M. E. J. Newman, Community structure in social and biological networks, Proc. Natl. Acad. Sci. USA **99**, 7821 (2002).

[41] J. C. Rocha, G. Peterson, Ö. Bodin, and S. Levin, Cascading regime shifts within and across scales, Science **362**, 1379 (2018).

# 2.3 How motifs condition critical thresholds for tipping cascades in complex networks: Linking micro-to macro-scales [P3]

**Authors**
Nico Wunderling, Benedikt Stumpf, Jonathan Krönke, Arie Staal, Obbe A. Tuinenburg, Ricarda Winkelmann, Jonathan F. Donges

**Status**
Published in *Chaos: An interdisciplinary journal of nonlinear science* (April 2020, ©American Institute of Physics (AIP)), doi: 10.1063/1.51428271

**Short summary**
In this work, vulnerable structures in networks of tipping elements are identified, the so-called *motifs*. Motifs are micro-scale substructures in networks that can, under certain circumstances, reduce the robustness of the network of tipping elements: this links micro-scale tipping events to macro-scale tipping cascades of the whole network. The strongest motif is the *feed forward loop* motif, which connects three interacting tipping elements in a triangular network structure such that the effect of one tipped element is transferred to two further elements by a direct and an indirect pathway. The occurrence of motifs in Erdős-Rényi networks is compared to the occurrence of motifs in the moisture recycling network of the Amazon rainforest. It is found that the occurrence of motifs is one order of magnitude higher in the latter case indicating why the real world network of the Amazon rainforest is more vulnerable than an Erdős-Rényi network. This underlines the importance of local-scale interaction structures for the robustness of the entire network.

**Author contributions**
Nico Wunderling and Benedikt Stumpf have contributed equally to this study. Nico Wunderling, Benedikt Stumpf and Jonathan Donges designed the study. Benedikt Stumpf conducted the model simulation runs for the random network, Nico Wunderling for the moisture recycling network. Nico Wunderling and Benedikt Stumpf prepared the figures. Jonathan Krönke has developed the nonlinear dynamical systems model PyCascades used in this work. Arie Staal and Obbe Tuinenburg developed the moisture recycling dataset of the Amazon rainforest. Nico Wunderling wrote the manuscript. All authors discussed the results and edited the manuscript. This paper is the partially based on the results of the master thesis of Benedikt Stumpf, who was (co-)supervised by Nico Wunderling.

Chaos

# How motifs condition critical thresholds for tipping cascades in complex networks: Linking micro- to macro-scales

Cite as: Chaos **30**, 043129 (2020); https://doi.org/10.1063/1.5142827
Submitted: 17 December 2019 . Accepted: 02 April 2020 . Published Online: 24 April 2020

Nico Wunderling, Benedikt Stumpf, Jonathan Krönke, Arie Staal, Obbe A. Tuinenburg, Ricarda Winkelmann, and Jonathan F. Donges

Chaos ARTICLE scitation.org/journal/cha

# How motifs condition critical thresholds for tipping cascades in complex networks: Linking micro- to macro-scales

Cite as: Chaos **30**, 0431 29 (2020); doi: 1 0.1 063/1 .51 42827
Submitted: 1 7 December 201 9 · Accepted: 2 April 2020 ·
Published Online: 24 April 2020



Nico Wunderling,[1,2,3,a] Benedikt Stumpf,[1,4] Jonathan Krönke,[1,2] Arie Staal,[5] Obbe A. Tuinenburg,[5,6] Ricarda Winkelmann,[1,2] and Jonathan F. Donges[1,5]

AFFILIATIONS

[1] Earth System Analysis, Potsdam Institute for Climate Impact Research (PIK), Member of the Leibniz Association, 14473 Potsdam, Germany
[2] Institute of Physics and Astronomy, University of Potsdam, 14476 Potsdam, Germany
[3] Department of Physics, Humboldt University of Berlin, 12489 Berlin, Germany
[4] Department of Physics, Free University of Berlin, 14195 Berlin, Germany
[5] Stockholm Resilience Centre, Stockholm University, Stockholm SE-10691, Sweden
[6] Copernicus Institute, Faculty of Geosciences, Utrecht University, 3584 CB Utrecht, The Netherlands

[a] **Author to whom correspondence should be addressed:** nico.wunderling@pik-potsdam.de

ABSTRACT

In this study, we investigate how specific micro-interaction structures (motifs) affect the occurrence of tipping cascades on networks of stylized tipping elements. We compare the properties of cascades in Erdős–Rényi networks and an exemplary moisture recycling network of the Amazon rainforest. Within these networks, decisive small-scale motifs are the feed forward loop, the secondary feed forward loop, the zero loop, and the neighboring loop. Of all motifs, the feed forward loop motif stands out in tipping cascades since it decreases the critical coupling strength necessary to initiate a cascade more than the other motifs. We find that for this motif, the reduction of critical coupling strength is 11% less than the critical coupling of a pair of tipping elements. For highly connected networks, our analysis reveals that coupled feed forward loops coincide with a strong 90% decrease in the critical coupling strength. For the highly clustered moisture recycling network in the Amazon, we observe regions of a very high motif occurrence for each of the four investigated motifs, suggesting that these regions are more vulnerable. The occurrence of motifs is found to be one order of magnitude higher than in a random Erdős–Rényi network. This emphasizes the importance of local interaction structures for the emergence of global cascades and the stability of the network as a whole.



**Tipping elements are nonlinear systems, where a small perturbation can be sufficient to induce a qualitative change in the whole system as soon as a critical threshold (tipping point) is crossed. Coupled tipping elements exist, for instance, in connected lake systems, in the Earth's climate system, or in social systems. Here, we investigate networks of interacting tipping elements, where each node consists of a stylized tipping element and explore important interaction structures on the microscale of the network, the so-called *motifs*. Such motifs in complex networks have been found in multiple systems such as cell metabolism, food webs, or neural networks and are known to be significantly overexpressed in real-world compared to random networks. However, motifs have not yet been studied extensively in complex networks, where nodes have their own dynamics. In our study, we find that tipping cascades occur more often at locations with a high motif frequency revealing locations (nodes) of decreased robustness.**

## I. INTRODUCTION

Methodologies from complex networks science have gained increasing attention since they have successfully been applied to a broad range of different fields ranging from physical sciences, biology, or ecology to information transfer, energy systems, and sociology.[1] In many cases, network nodes are reasonably represented by continuous, nonlinear dynamical systems as, for instance,

Chaos ARTICLE scitation.org/journal/cha

in oscillators in power grids, population dynamics in food webs, or synchronization of nonlinear oscillators.[2–4] More recently, one focus of research shifted to the investigation of interacting tipping elements. Tipping elements are systems in which a small perturbation can lead to a qualitative change in the system in case a critical value (*tipping point*) is surpassed. Tipping elements have been identified in the Earth's climate system[5] and also in various other contexts such as finance, politics, ecology, or climate.[6–9] In the Earth's system, tipping elements can interact across scales in time and space,[9–11] which could, in principle, lead to feedbacks, domino effects,[12] and ultimately to a hothouse state.[13]

Lately, these two approaches, complex networks and tipping elements, have been linked together in a conceptual approach to study cascading failures on networks.[14,15] Here, each node of such a network is a tipping element and has its own dynamics compared to other studies where the cascading failure has been studied with discrete states of network nodes and a fixed threshold beyond which the failure of the respective node is induced.[16,17] The links of the network then consist of any arbitrary positive or negative coupling, potentially with different weights, between the network nodes. This procedure yields a set of connected differential equations that can be described well by a network approach. If the network nodes are indeed tipping elements, the occurrence of tipping cascades, the failure of at least two nodes together, can be investigated. The dependence of cascades based on different interaction structures resembling the structure of paradigmatic network types such as Erdős–Rényi, small-world, or scale-free networks has been assessed.[14] However, as we find here, in a certain regime of coupling strengths between the nodes, the dynamics of the whole network are dominated by local structures within the network. These sub-structures are the so-called *motifs*.

Contrasting other recent publications reflecting the influence of the general network topology of cascading failures in complex networks[18–21] and how local interaction patterns determine the dynamics of their larger parent networks,[22–24] this work aims to reveal how these local, small-scale structures condition tipping cascades within the whole system.

The notion of motifs has been introduced by Milo *et al.*[25] as the basic building blocks of complex networks. It has been shown that motifs can be identified, for instance, in food webs,[26] authorship attribution[27] up to transcriptional networks that control the expression of genes,[28] e.g., in tumor suppressors or *E. coli*.[29–32] The so-called *feed forward loop* is an essential motif in such networks since it is significantly overexpressed in these real-world networks compared to typical random graphs.[25] Furthermore, the feed forward loop motif has been used to identify functionally important nodes in various real-world networks through the aggregation of several such motifs into clusters. This has been investigated, among others, in transcription networks of *E. coli*, online Wikipedia networks, or air-traffic[33] and hints at a special role of this motif as it efficiently passes system dependent information forward.

Here, we examine how selected microstructures within an Erdős–Rényi network of tipping elements significantly alter the occurrence of tipping cascades and with that the stability of the whole network (Fig. 1). We investigate these features on Erdős–Rényi networks since their properties are controllable and reproducible. Furthermore, we look at the scaling behavior of the motif occurrence, and we are able to predict critical couplings in dense Erdős–Rényi networks, which can be traced back to coupled feed forward loops. Additionally, we compare our results for this to a real-world example, the moisture recycling network structure of the Amazon rainforest, and point out important differences.

## II. METHODS

### A. System of differential equations

In this study, the dynamics of each of the nodes in the network follows the autonomous ordinary differential equation,

$$\frac{dx}{dt} = -a(x - x_0)^3 + b(x - x_0) + c, \tag{1}$$

when interactions are ignored. Here, $c$ is the critical individual forcing parameter, $a, b > 0$, and $x_0$ represents a shift in the x axis.[12,14] This equation is unistable below a certain critical parameter $c_{\mathrm{crit,low}}$ and above $c_{\mathrm{crit,high}}$. In between, the system is bistable, and state transitions occur via a saddle-node bifurcation at $c_{\mathrm{crit,low}}$ and $c_{\mathrm{crit,high}}$. Equation (1) is a minimal example for continuous dynamical systems that possess two distinct stable states. Hence, this model can act as a paradigmatic model and has been applied to ecosystems such as shallow lakes but also ice sheets or the thermohaline circulation.[6,34–36] The bifurcation diagram of one of these tipping elements is shown in Fig. 1(a).

We connect these tipping elements via a linear coupling term such that Eq. (1) becomes

$$\frac{dx_i}{dt} = -a(x_i - x_0)^3 + b(x_i - x_0) + c_i + r\sum_{j=1, j\neq i}^{N} A_{ij}x_j, \tag{2}$$

where $r > 0$ is the global *coupling strength* between the elements and $A_{ij}$ is one if there exists a link from node $j$ to $i$ and it is zero otherwise. Thus, the networks considered here are directed; however, couplings of the node to itself are not considered. In our network, we use $a = 4$, $b = 1$, and $x_0 = 0.5$ for all nodes (i.e., tipping elements) such that the stable states $x_i$ are at 0 or 1, respectively, if $c_i = 0$. If not stated otherwise, we simulate all our results on Erdős–Rényi networks[37] of size 100. This means that our work here is based on the network framework developed by Krönke *et al.*[14] However, Krönke *et al.*[14] touch on important global features of the model, whereas this work emphasizes how small-scale structures change the behavior of the entire network. Furthermore, the system is assumed to be in equilibrium as soon as the change in the state of no tipping element exceeds 0.005 per time step.

### B. Definition of a tipping cascade

In the investigated networks, we define a tipping cascade as the joint transgression of at least two tipping elements in the network. To check if a tipping cascade can occur at a certain coupling strength $r$, a randomly chosen *source node* $i$ is tipped by shifting its individual forcing parameter $c_i$ above its threshold of $c_{\mathrm{crit,high}} = \sqrt{\frac{4}{27}\cdot\frac{b^3}{a}} \approx 0.193$. The individual forcing parameter of all other nodes $c_j$ is kept at zero such that a cascade can only be caused

Chaos ARTICLE scitation.org/journal/cha

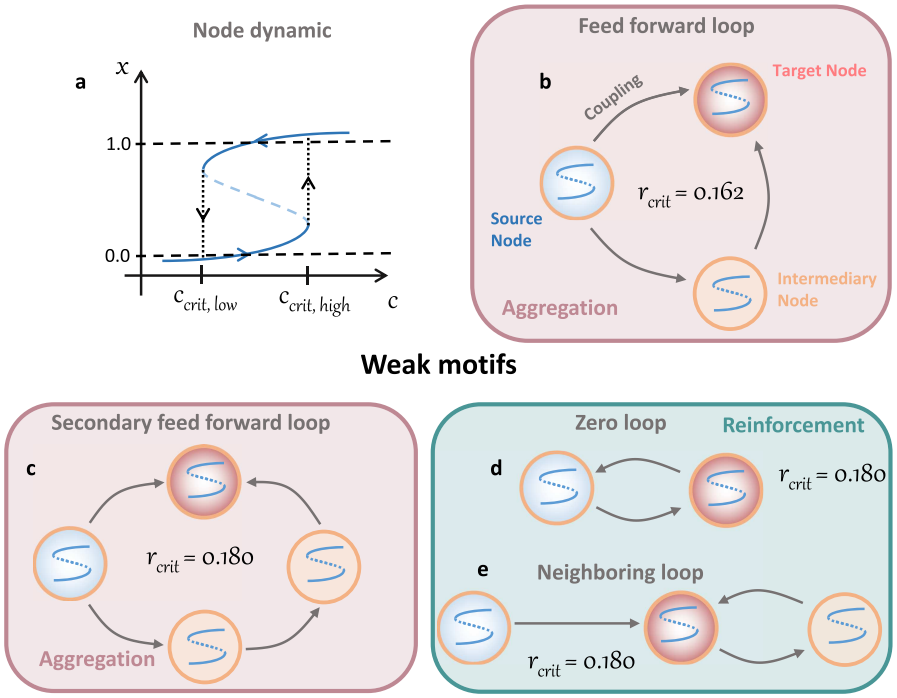


**FIG. 1.** (a) Bifurcation diagram of a single node (tipping element) in the network. If not stated otherwise, the network size is 100 nodes. Each of these nodes has two stable states, where the stable state is dependent upon the critical parameter $r$. If the critical parameter is increased over a threshold, a saddle-node bifurcation occurs. (b)–(e) Motifs that reduce the minimal necessary critical coupling strength within the network and lead to tipping cascades. In case the source node (light blue) is tipped, the target node (light red) will tip earlier due to the specific local network structure and the additional coupling from the intermediary node(s) and thus triggers a cascade at lower coupling constants than it would be the case if we would only consider a pair of source nodes and target nodes. (b) Feed forward loop: This motif is a strong motif that reduces the critical coupling strength significantly to 0.162 (from 0.183; see Fig. 2). (c)–(e) Weaker motifs (secondary feed forward loop, zero loop, and neighboring loop) that reduce the minimal necessary coupling strength only slightly to around 0.180, where each of the three weaker motifs individually reduces the critical coupling strength to 0.180. The feed forward and the secondary feed forward loop function over *aggregation* effects of coupling, while the zero loop and the neighboring loop function over *reinforcement* feedbacks shown as light red and green colored boxes.

by the coupling of the tipped node to other nodes in the network. With this setting, the cascade simulations in this work are conducted as follows: First, the critical value $c_i$ of source node $i$ is slowly increased (in steps of 0.01) until 0.193 is surpassed such that this node tips. Then, the simulation is integrated forward in time using python's *scipy.integrate.odeint* until an equilibrium is reached. The equilibrium condition is that $\Delta x_i < 0.005$ in two consecutive time steps for each node $i = 1, \ldots, N$ in the network. Thus, the cascade simulations are conducted as in Krönke *et al.*[14]

Note that if node $i$ tips at $c_{\mathrm{crit,\,high},\,i} \approx 0.193$, its stable state in the upper branch is approximately at $x_{\mathrm{crit,\,high},\,i} \approx 1.05$, slightly higher than 1.0 [see Fig. 1(a)]. If then node $i$ is coupled to another node $k$ (and no other connections are considered for the moment), the coupling term of Eq. (2) pointing to node $k$ would be $\mathrm{Cpl}_k = r \sum_{j=1, j\neq k}^{N} A_{kj} x_j = r \cdot x_{\mathrm{crit,\,high},\,i} \approx r \cdot 1.05$. $\mathrm{Cpl}_k$ surpasses the critical value of 0.193 such that node $k$ would tip as soon as the coupling strength $r$ is larger than $r = r_{\mathrm{crit}} \approx 0.183$ [see Fig. 1(a) and Eq. (2)].

## C. Network motifs

Some of the most important features in networks are small-scale motifs,[25,33] where a tipped node (*source node*) has a primary direct impact on a *target node* but also a secondary, indirect impact over *intermediary nodes*. The number of nodes in between a source and a target node over intermediary nodes is called a *secondary impact path length*. Thus, a connection of a source node over one intermediary node to a target node would have a secondary impact path length of two. In Figs. 1(b)–1(e), we show all motifs that have a secondary impact path length of two (*feed forward loop*) and three (*secondary feed forward loop*, *zero loop*, and *neighboring loop*). In the case of the zero loop, the intermediary node is also the source node. The critical coupling strength of the feed forward loop to tip the target node is reduced from 0.183 to 0.162; for the weaker motifs, it is reduced to 0.180 for each of the motifs individually, as we found by simulations. The two types of feed forward loops reduce the critical coupling strength over aggregation effects toward the target node, while the zero loop and the neighboring loop do this via

Chaos ARTICLE scitation.org/journal/cha

reinforcement loops. The underlying dynamical mechanism is that feed forward loops decrease the critical coupling strength more than weaker motifs. They also contribute more to the average clustering coefficient, which is linked to a decrease in the critical coupling strength.[14] Hence, on a macro-scale, if there are more feed forward loops, the critical coupling strength decreases, while the clustering increases. This is more of a correlation, not a causation.

### D. Real-world application: The Amazon rainforest network

The Amazon moisture recycling network is a network of atmospheric water flows within the Amazon rainforest. The Amazon can be seen as a network of tipping elements[14,38] where forests may locally tip to a state of low tree cover, depending on rainfall levels.[39] If an area contains a forest, evaporation is higher than without a forest, as trees can access deep groundwater that they release to the atmosphere in a process called transpiration. Because this atmospheric water rains down over other parts of the forest, forest transpiration is a mechanism by which tipping elements are connected. This cycling of forest transpiration to rainfall was simulated by Staal *et al.*[40] and analyzed as a network.[14,38] Our nodes are the forests within areas of a size of $2^\circ \times 2^\circ$. We use the simulated transpiration flows between these nodes for the year 2014. For further details on the methods behind the simulations, we refer to Staal *et al.*[40]

## III. RESULTS

### A. Motifs in sparse networks

We find that particularly in Erdős–Rényi networks, motifs can significantly reduce the critical coupling strength that is necessary to start a cascade. In Fig. 2, the occurrence of cascades $\sigma$ is shown vs the coupling strength $r$, where vertical lines indicate the coupling strength where a tipping cascade is expected for the respective motif or motif group. The actual fingerprint of the respective motif can be observed in step-like features in cascade occurrences $\sigma$ toward higher coupling strengths. If the network has an average degree of one, two, or three, these reductions can be seen clearly for the feed forward loop as well as for the weak motifs [the secondary feed forward loop, the zero loop, and the neighboring loop; see Figs. 2(a)–2(c)]. Toward higher average degrees, two things can be found: first, cascade occurrence increases, and second, the coupling strength $r$ at which cascade occurrences are different from zero decreases. For instance, at an average degree of eight, cascades can already be found for a coupling strength around 0.12, whereas for an average degree of two, this coupling strength is around 0.16 [see Figs. 2(b) and 2(h)]. This might be due to the fact that combinations of different or the same motifs point to the same target node (see, for instance, Fig. S3 in the supplementary material). Since the reduction of the critical coupling strength for the feed forward loop is larger than for the weaker motifs, it remains visible up to higher average degrees ($\langle k\rangle = 7$; see Fig. 2). With increasing average degree, the networks show an increasing likelihood of cascade occurrences and size of the cascade (Fig. S1 in the supplementary material). The frequency of cascades does not reach 100% for average degree one (around 60%), two (about 90%), and three (about 99%) even if the coupling is above 0.183, the coupling value at which a pair of two tipping elements tip (*single coupling* in Fig. 2). The reason is that for low average degrees, the Erdős–Rényi network is not in the connected regime, meaning not all nodes are part of the giant component. Consequently, for low average degrees, some nodes cannot be involved in the tipping cascade as they do not hold any couplings, i.e., their in-degree is zero.

How often are motifs expected in random networks? The proportion of networks with the respective motif depending on the average degree is sharply ascending [Fig. 3(a)]. Here, we compare the simulation (points and error bars) to the theory (dashed lines) and obtain a good match. In the simulation, the occurrence is the probability to find the respective motif at an arbitrarily chosen node.

The theoretically derived values can be obtained with the following considerations: for an Erdős–Rényi network with an average degree $\langle k\rangle$, each node is expected to have $\langle k\rangle$ neighbors that it is linked to. Thus, the number of possible pairs between any two neighbor nodes is given by $\binom{\langle k\rangle}{2} = \frac{\langle k\rangle\cdot(\langle k\rangle-1)}{2}$. In a directed network, this number needs to be multiplied by 2 such that the number of possible links is given by $N_{\text{possible links}} = \langle k\rangle\left(\langle k\rangle - 1\right)$. The probability that at least one event $A_i$ occurs out of $\mathcal{N}$ independent events is given by

$$\mathcal{P}\left(\bigcup_{i=1}^{\mathcal{N}} A_i\right) = 1 - (1-p)^{\mathcal{N}} \tag{3}$$

for a fixed probability $p$ that one independent event occurs. In an Erdős–Rényi network, $p = \frac{\langle k\rangle}{N-1}$, where $N$ is the size of the network. This leads to

$$\begin{aligned}\mathscr{P}_{\text{feed forward loop}} &= 1 - (1-p)^{N_{\text{possible links}}} \\ &= 1 - \left(1 - \frac{\langle k\rangle}{N-1}\right)^{\langle k\rangle(\langle k\rangle-1)}\end{aligned} \tag{4}$$

to have at least one feed forward loop at any node of the network. Similarly, this approach can be used for the neighboring loop. There are, on average, $\langle k\rangle\left(\langle k\rangle - 1\right)$ possibilities that neighbor to neighbor nodes form a feedback such that it results in a neighboring loop. Accordingly, we have

$$\mathscr{P}_{\text{neighboring loop}} = \mathscr{P}_{\text{feed forward loop}} = 1 - \left(1 - \frac{\langle k\rangle}{N-1}\right)^{\langle k\rangle(\langle k\rangle-1)}. \tag{5}$$

For the zero loop $\langle k\rangle$ possible links that need to be considered for reconnecting any neighbor node back to the source node such that the probability of at least one occurrence is given by

$$\mathscr{P}_{\text{zero loop}} = 1 - \left(1 - \frac{\langle k\rangle}{N-1}\right)^{\langle k\rangle}. \tag{6}$$

Finally, we compute the probability for the secondary feed forward loop. We know that the number of neighbors-of-neighbors is $\langle k\rangle\left(\langle k\rangle - 1\right)$ excluding the source node as a neighbor. Each of these neighbors-of-neighbors has $\left(\langle k\rangle - 1\right)$ possibilities to link to a specific

Chaos ARTICLE scitation.org/journal/cha

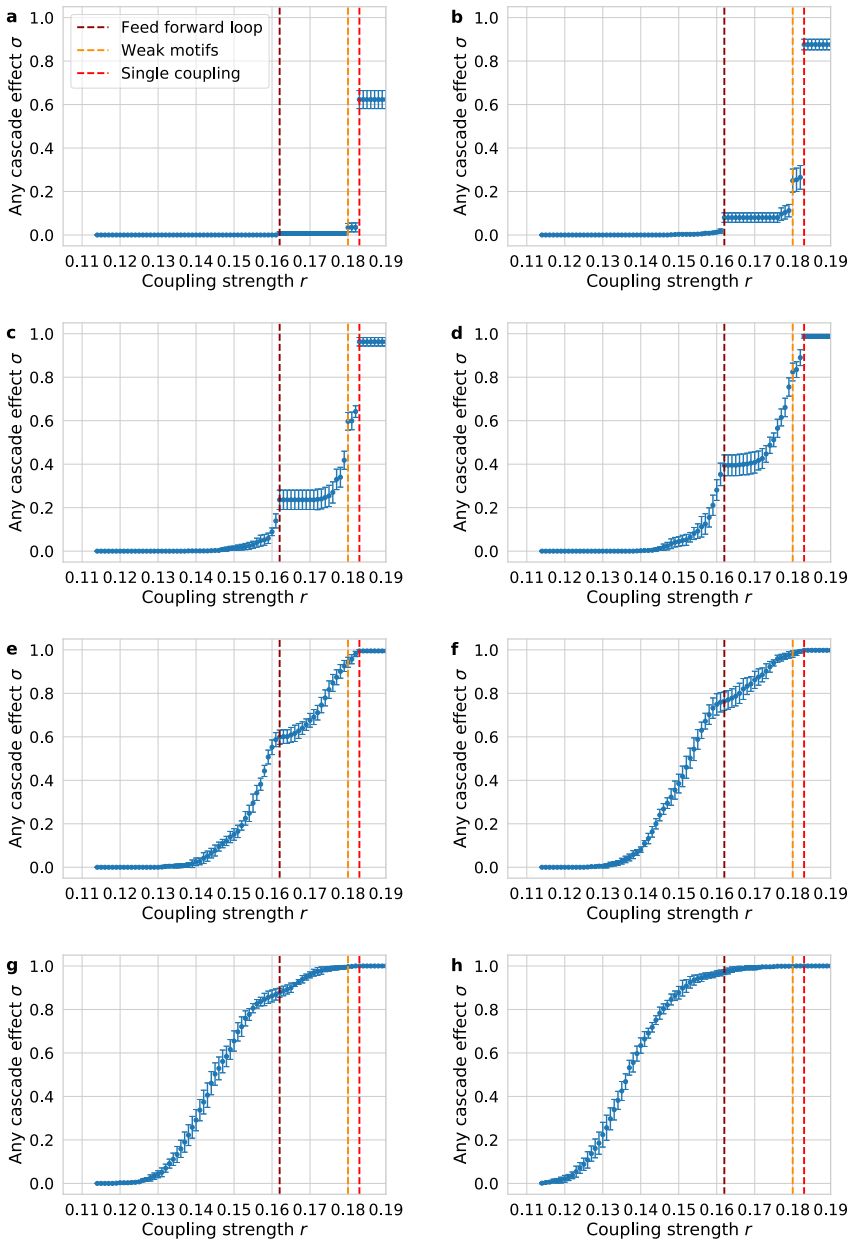


**FIG. 2.** The effect of the coupling strength on the proportion of networks that show any cascading effect. The critical coupling strength to start a cascade for the feed forward loop is 0.162, for the three weaker motifs is 0.180, and for the single coupling is 0.183. Since each of the weaker motifs reduces the critical coupling strength to 0.180, it is not possible to separate these three motifs from its tipping cascade pattern. The error bars show the standard deviation of 10 simulations and 100 simulated networks. In total, 1000 runs with Erds–Rényi networks of size 100 were computed. (a) Has average degree 1, (b) has average degree 2, (c) has average degree 3, (d) has average degree 4, (e) has average degree 5, (f) has average degree 6, (g) has average degree 7, and (h) has average degree 8.

target node such that we get

$$\mathscr{P}_{\text{secondary feed forward loop}} = 1 - \left(1 - \frac{\langle k\rangle}{N-1}\right)^{\langle k\rangle(\langle k\rangle-1)^2}. \quad (7)$$

This is the probability of obtaining at least one secondary feed forward loop at any given node in the network.

The occurrences of the feed forward loop, the neighboring loop, and the secondary feed forward loop increase sharper than the occurrence of the zero loop with an increasing average degree such that at an average degree of 9, the first three motifs occur in practically every Erdős–Rényi network of size 100 [Fig. 3(a)].

The simulated occurrences of the motifs match reasonably well with the theory. However, for the feed forward loop and the

Chaos ARTICLE scitation.org/journal/cha

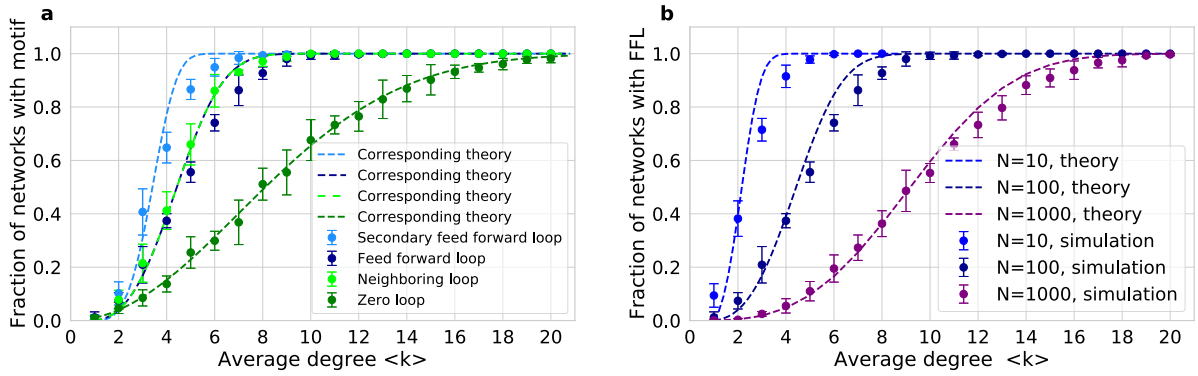


**FIG. 3.** (a) Motif occurrence in a random network of size 100 together with their theoretically expected values (dashed lines). The theoretical formulas are found in Eqs. (4)–(7). (b) Scaling of the occurrence of the feed forward loop for networks of size 10, 100, and 1000. Theory from Eq. (4). The other motifs' scaling behavior can be found in Fig. S2 of the supplementary material. Error bars in both panels show the error in the occurrence in 1000 realizations grouped as 10 × 100 samples.

secondary feed forward loop, our theory slightly overestimates the occurrence of these motifs for an intermediate occurrence probability. This is probably due to the fact that out-degrees smaller or equal to 1 at a certain node are neglected in the respective equations [i.e., in Eqs. (4) and (7)]. However, in fact, the source node of both motifs, the feed forward loop and the secondary feed forward loop, requires an out-degree of at least two. Otherwise, these motifs cannot exist.

The scaling of the frequency of the feed forward loop for networks of size 10, 100, and 1000 shows that for larger networks, the occurrence of motifs requires higher average degrees, for theory and simulations [Fig. 3(b); for other motifs, see Fig. S2 in the supplementary material]. The scaling behavior of the other three motifs (the zero loop, the neighboring loop, and the secondary feed forward loop) can be found in Fig. 2 of the supplementary material. The observed scaling dependency of the motif occurrence in Erdős–Rényi networks can also be interpreted as a dependency on the clustering coefficient $\mathscr{C}$ of the networks since $\mathscr{C} = \frac{\langle k \rangle}{N-1}$ in Erdős–Rényi networks, since the clustering coefficient is inversely proportional to the network size $N$.

## B. Motifs in dense networks

The occurrence of single motifs plays a crucial role for the occurrence of tipping cascades in sparse networks. For an Erdős–Rényi network of size 100, this is the case for average degrees of 6 or below (see Fig. 2). However, single motifs cannot explain the drop in the critical coupling strength for denser networks. The critical coupling strength for the initiation of cascades lies well below 0.050 in dense networks, which is way below the critical coupling strength of a feed forward loop ($r_{\text{crit feed forward loop}} = 0.162$; see the transition zone in Fig. 4). Above the *transition zone*, more than 90% of all networks show tipping cascades and below it, less than 10% show cascades. To explore the strength of the effect of multiple motifs, construction rules for N-fold feed forward loops and N-fold *coupled* feed forward loops were designed (see Fig. 3 in the supplementary material). Subsequently, numerical simulations of isolated multiple motifs were conducted to assess the critical coupling thresholds (triangles in Fig. 4). The isolated, multiple motifs exhibit significantly reduced critical coupling strengths, and it can, therefore, be expected that, in turn, their occurrence in Erdős–Rényi networks decreases the critical coupling strength for tipping cascades.

The critical coupling strength of a 98-fold coupled feed forward loop ($r_{\text{98-fold coupled feed forward loop}} = 0.016$) matches the critical coupling strength of the transition zone of a fully connected network. This means that the critical coupling compared with the single critical coupling strength of two nodes ($r_{\text{crit}} = 0.183$) drops by 91%. It has to be remarked that the critical coupling values of manifold motifs are shown against their multiplicity (the lower x axis in Fig. 4), while

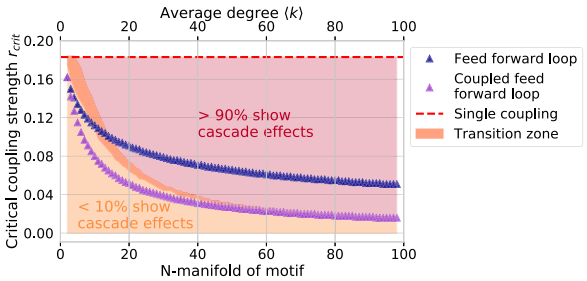


**FIG. 4.** The critical coupling strength vs the N-foldness of motifs. The critical coupling strengths are shown as colored triangles for the feed forward loop and the coupled feed forward loop (the lower x axis). The transition zone is the zone where between 10% and 90% of all networks show a cascading effect (orange shading). Above the transition zone, more than 90% of all networks show cascading effects (red shading) and below less than 10% (yellow shading). These measures are shown with respect to the average degree of the network (the upper x axis). For dense Erds–Rényi networks, the match between the transition zone and the N-fold coupled feed forward loop is high. This means that the coupled feed forward loop seems to be a good explanation for the drop in the critical coupling strength for densely connected random networks.

Chaos ARTICLE scitation.org/journal/cha

the critical values corresponding to the transition zone are plotted in relation to the average degree (the upper x axis in Fig. 4). Thus, this does not provide direct information which N-fold motif occurs at what average degree, but the comparison between the critical value of the N-fold coupled feed forward loop and the observed critical coupling strength in the Erdős–Rényi shows a very good match for networks with high densities of $\langle k \rangle > 50$ and is as such a very likely explanation for the observed drop in the critical coupling strength.

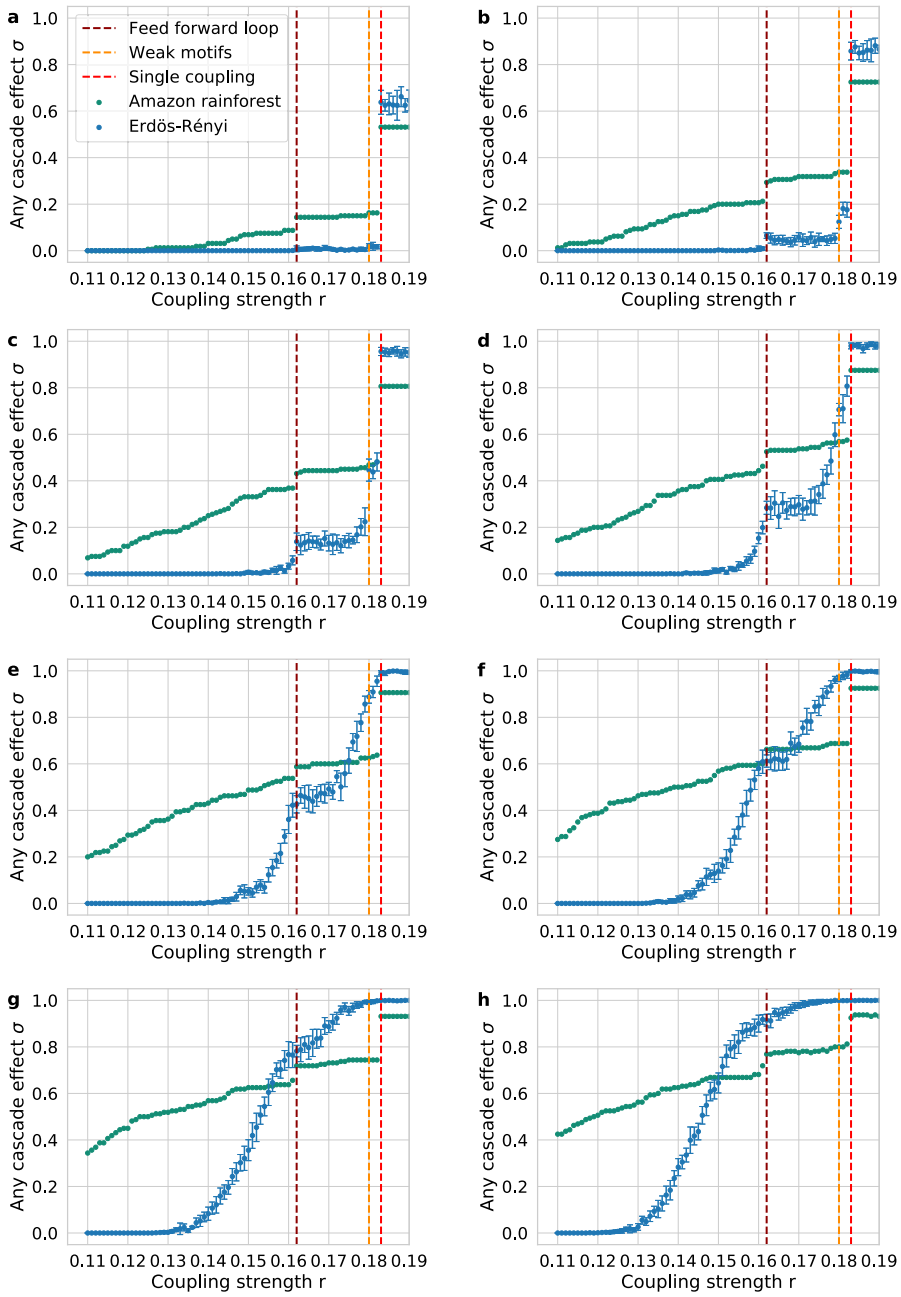


**FIG. 5.** Comparison between tipping cascades in Erds–Rényi networks (blue) and in the Amazon rainforest (green) depending on the coupling strength $r$ for (a)–(h) average degrees from 1 to 8. For both network types, the size is 160 nodes. The error for the Erds–Rényi networks is the standard deviation of 10 bundles of simulations, where each bundle consists of 100 tipping cascade experiments (compare to Fig. 2). For the moisture recycling network, we simulate cascades for each of the 160 nodes and compute the average number of experiments, where a cascade is observed.

Chaos ARTICLE scitation.org/journal/cha

### C. Motifs in a real-world application: The Amazon rainforest

Motifs also foster connectivity in real-world networks, for instance, in medicine, food webs, or the world wide web, carrying information forward.[26–29] Basically, each network consists of certain motif structures that might be essential for the dynamics of the whole graph. One such example could be the moisture recycling network of the Amazon rainforest. It has been proposed that the Amazon rainforest is a tipping element with respect to the local precipitation,[5,41] which is suggested by conceptual models[42] and data suggesting multistability of the rainforest,[39,40,43] also on the regional scale.

Here, we construct a moisture recycling network in the Amazon rainforest and use the moisture flow data from tree transpiration on a $2^\circ \times 2^\circ$ resolution over the Amazon basin for the year 2014. The data have been created in Staal *et al.*[40] Each node represents a $2^\circ \times 2^\circ$ patch of the rainforest, and each link represents the atmospheric moisture transport from forest transpiration from one cell to another. To be able to compare the moisture recycling network with random networks, we construct the network in such a way that the average degree is the same as for the Erdős–Rényi case. For instance, if we aim for an average degree of 5 in the network, we only set the $160 \times 5 = 800$ strongest moisture transport links. Since this procedure favors strong connections, some weaker teleconnections between grid cells that are further away are lost. However, the dominant links remain such that the main network topology is preserved.

The coupling strength of these links is then set to the same value, and the remaining connections are set to zero. Other effects are also neglected in this network since the aim is here to focus on the local and regional microstructures of the moisture recycling network and making it comparable to random networks. With these simplifications, we intend to investigate the structure and the possible implications it could have, instead of realistically modeling the

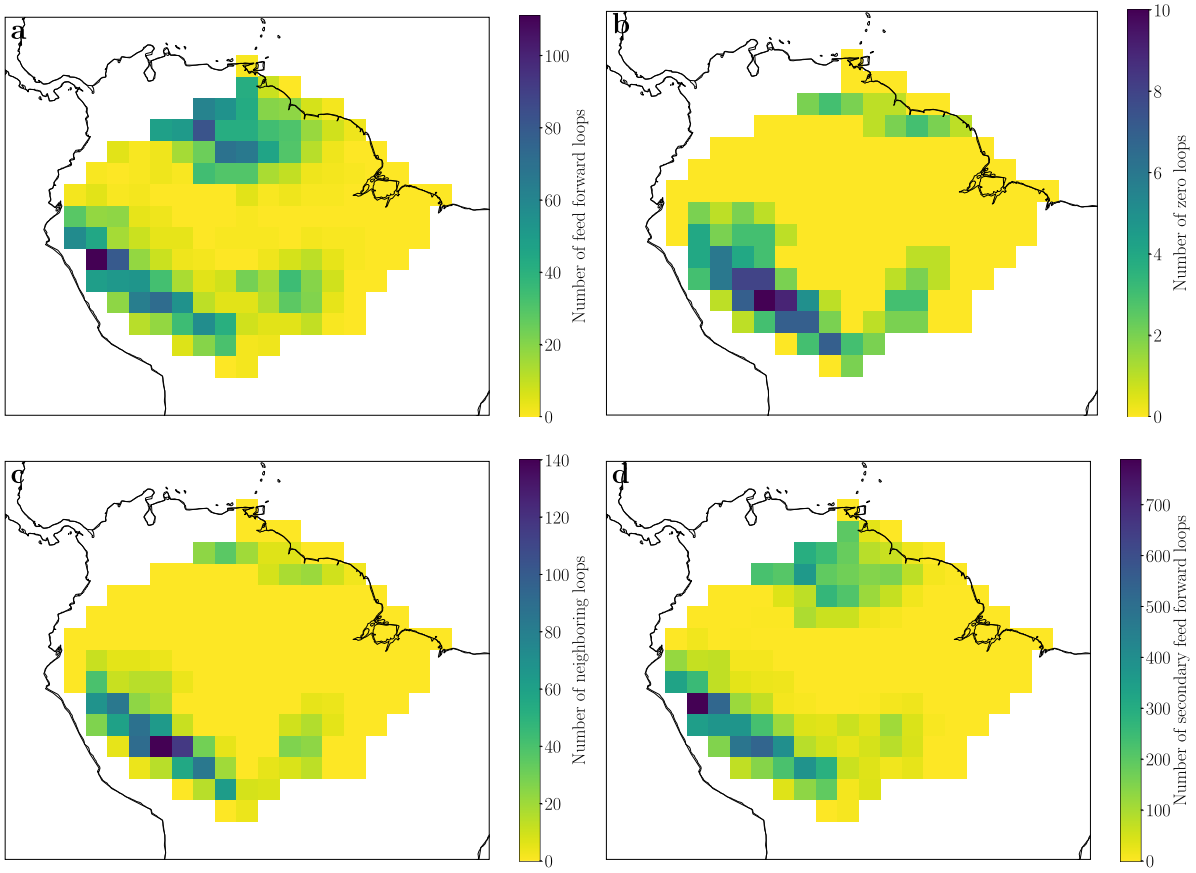


**FIG. 6.** Number of motifs that point to a certain location in the $2^\circ \times 2^\circ$ grid. Two regions with different vulnerability regimes can clearly be distinguished for all four investigated motifs. (a) Feed forward loop, (b) zero loop, (c) neighboring loop, and (d) secondary feed forward loop. The average degree is 5 and the number of nodes is 160. Note the different colorbar scales between the sub-plots.

Chaos ARTICLE scitation.org/journal/cha

tipping behavior of the Amazon rainforest. Similar approaches on viewing the Amazon rainforest as a complex network have been used earlier in literature studies.[38,44] In these studies, it is shown that forest loss might be self-amplified in the Amazon basin if moisture recycling in the network is reduced, e.g., due to deforestation, and might lead to adverse cascading effects.

We evaluate the critical coupling that is necessary to start a cascade comparing the occurrence of tipping cascades between random networks and the moisture recycling network in the Amazon rainforest depending on the coupling strength (Fig. 5; compare with Fig. 2). We reveal jumps in the occurrence of cascade effects in the moisture recycling network when the coupling exceeds the critical strength of the feed forward loop. This is already the case for very sparse networks at low average degrees, which hints at a highly clustered network with very localized motif structures (see also Fig. 6). Due to this structure, the moisture recycling network shows significantly more cascade effects at coupling strengths below 0.183 (single coupling) for low average degrees. For the other, weaker motifs, a step-like structure in the tipping cascades of the Amazon rainforest can hardly be noticed. Thus, these motifs only play a minor role in comparison with those in Erdős–Rényi networks. The highly clustered moisture recycling network facilitates the likelihood for combinations of micro-motifs that significantly elevate tipping cascades at lower couplings than in random networks. Hence, our results provide additional evidence that the Amazon network is more vulnerable than random networks following up on other aspects investigated in an earlier study.[14] For the same reason, more cascades occur in random networks than in the moisture recycling network for high coupling strengths (greater than 0.183) at the same average degree, since some parts of the Amazon rainforest network remain unconnected, because links between the closely connected clusters of highly connected areas are rare.

In the remainder of this section, we show results for an average degree of 5, but the results are robust against other average degrees (see Fig. S4 in the supplementary material). Basic motifs in the Amazon rainforest occur approximately ten times more often than in the random network (Table I). This is due to the high connectivity in the Amazon rainforest in some regions of the network, while others are barely connected at all (Fig. 6). The clustering coefficient also hints at this network property of the Amazon network since it is one magnitude higher than in the Erdős–Rényi network (0.297 vs $0.031 \pm 0.001$). An overexpression, especially of the feed forward loop, has also been found in other real-world networks in biology or technology,[25] suggesting an enhanced information or material flow through this network structure.

**TABLE I.** Comparison of the occurrence of a motif between the Amazon rainforest network with an average degree of 5 (and network size 160) with the respective Erds–Rényi networks, both with a network size of 160 and an average degree of 5. The clustering coefficient of the Erds–Rényi network is $0.031 \pm 0.001$ and 0.297 for the Amazon network.

| Number of motif occurrence | Amazon rainforest | Erdős–Rényi |
|---|---|---|
| Feed forward loop | 2 378 | $123 \pm 2$ |
| Zero loop | 168 | $25 \pm 1$ |
| Neighboring loop | 1 499 | $149 \pm 6$ |
| Secondary feed forward loop | 11 831 | $723 \pm 13$ |

In Fig. 6, the occurrence of the four motifs is mapped. There are two major regions where motifs occur more frequently than others. The first major region is located in the north of the rainforest and the second in the south-west. These regions with a high occurrence of motifs, most importantly the feed forward loop, rely more on tree transpiration than other parts of the rainforest. However, even though the moisture transport link strength varies from connection to connection in our network (from 10 to a bit more than 100 mm per year), the number of motifs, especially for the feed forward loop, indicates a reduced stability against tipping cascades. Thus, it can be expected that these regions are more vulnerable than others in terms of changing rainfall conditions such that potential cascades could emerge faster.

## IV. DISCUSSION AND CONCLUSION

In this study, we found that network motifs are able to disseminate critical transitions of tipping elements to further network nodes and can thus foster the emergence of tipping cascades. We worked out how motifs decrease the critical coupling strength that is necessary to start a cascade and quantified the occurrence of simple but decisive microstructures. We detected that feed forward loops, the strongest three-node motif in our study, occur in sparse networks, thus suggesting the existence of important hub nodes that tend to be more vulnerable than others and are prone to start a cascade. This seems to be of special importance also for real-world networks since feed forward loops are often significantly overexpressed, which has been found in the Amazon moisture recycling network example here. Similar findings have been made in other systems reported in the literature.[25] It is also stated in the literature that six types of feed forward loops exist, which are combinations of the motifs described in this paper, i.e., one or more zero loops on top of a feed forward loop. These specific combinations could be interesting to be investigated in future research in more detail due to the importance of the feed forward loop motif. However, we restricted our analysis to the four fundamental motifs since it is their fingerprint that is observed in the tipping cascade experiments (see Fig. 2). Additionally, we find in our experiments that the critical coupling strength in densely connected Erdős–Rényi networks is more than 90% lower compared to the single coupling of two tipping elements due to coupled feed forward loops. Thus, we are able to understand the occurrence of tipping cascades in sparse and dense random networks.

In the Amazon rainforest application, the location of motifs is highly clustered in distinct areas of the rainforest, thus indicating increased vulnerability in these locations. There, tipping cascades can emerge there at lower couplings than they could for Erdős–Rényi networks. In turn, this would also imply that reforestation in these regions is more effective.

However, this conclusion is limited by the simplified nature of the Amazon network realization in this study and could be examined further by the usage of the actual moisture recycling values in a more in-depth study. Since the model employed here is simplified and conceptual, the question remains if the role of motifs would change under more realistic model realizations or other dynamics on the nodes themselves.

Chaos ARTICLE scitation.org/journal/cha

In turn, it might be insightful to investigate the role of motifs on other fully dynamic systems that are connected via a network structure, for instance, in food webs, transcriptional networks, or Earth system components.

## SUPPLEMENTARY MATERIAL

See the supplementary material for more details on the scaling for the weaker motifs (the zero loop, the neighboring loop, and the secondary feed forward loop) in parallel to the feed forward loop [Fig. 3(b)]. Furthermore, details on multiple motifs and the degree dependency of the feed forward loop in the moisture recycling network are shown.

## AUTHOR'S CONTRIBUTIONS

N.W. and B.S. have contributed equally to this study.

## ACKNOWLEDGMENTS

This work has been carried out within the framework of the PIK FutureLab on Earth Resilience in the Anthropocene. N.W. and R.W. acknowledge the financial support of the IRTG 1740/TRP 2015/50122-0 project funded by Deutsche Forschungsgemeinschaft (DFG) and FAPESP. N.W. is grateful for a scholarship from the Studienstiftung des deutschen Volkes. A.S. and J.F.D. acknowledge support from the European Research Council project Earth Resilience in the Anthropocene (No. 743080 ERA). A.S. and O.A.T. acknowledge support from the Bolin Centre for Climate Research. O.A.T. acknowledges funding from the Netherlands Organization for Scientific Research Innovational Research Incentive Schemes VENI (No. 016.171.019). J.F.D. is grateful for financial support by the Stordalen Foundation via the Planetary Boundary Research Network (PB.net) and the Earth League's EarthDoc program. The authors acknowledge financial support from the Leibniz Association (Project DominoES). The authors gratefully acknowledge the European Regional Development Fund (ERDF), the German Federal Ministry of Education and Research, and the Land Brandenburg for supporting this project by providing resources on the high performance computer system at the Potsdam Institute for Climate Impact Research. The authors also gratefully acknowledge discussions with Ann-Kristin Klose, Marc Wiedermann, and Jobst Heitzig. The authors declare no competing financial interest. The data that were used in this study are available from the corresponding author upon reasonable request.

## REFERENCES

[1] M. E. Newman, "The structure and function of complex networks," SIAM Rev. **45**, 167–256 (2003).
[2] W. Zou, D. Senthilkumar, M. Zhan, and J. Kurths, "Reviving oscillations in coupled nonlinear oscillators," Phys. Rev. Lett. **111**, 014101 (2013).
[3] T. Gross, L. Rudolf, S. A. Levin, and U. Dieckmann, "Generalized models reveal stabilizing factors in food webs," Science **325**, 747–750 (2009).
[4] J. Nitzbon, P. Schultz, J. Heitzig, J. Kurths, and F. Hellmann, "Deciphering the imprint of topology on nonlinear dynamical network stability," New J. Phys. **19**, 033029 (2017).
[5] T. M. Lenton, H. Held, E. Kriegler, J. W. Hall, W. Lucht, S. Rahmstorf, and H. J. Schellnhuber, "Tipping elements in the Earth's climate system," Proc. Natl. Acad. Sci. U.S.A. **105**, 1786–1793 (2008).
[6] C. D. Brummitt, G. Barnett, and R. M. D'Souza, "Coupled catastrophes: Sudden shifts cascade and hop among interdependent systems," J. R. Soc. Interface **12**, 20150712 (2015).
[7] E. Kriegler, J. W. Hall, H. Held, R. Dawson, and H. J. Schellnhuber, "Imprecise probability assessment of tipping points in the climate system," Proc. Natl. Acad. Sci. U.S.A. **106**, 5041–5046 (2009).
[8] Y. Cai, T. M. Lenton, and T. S. Lontzek, "Risk of multiple interacting tipping points should encourage rapid $CO_2$ emission reduction," Nat. Clim. Change **6**, 520–525 (2016).
[9] J. C. Rocha, G. Peterson, Ö. Bodin, and S. Levin, "Cascading regime shifts within and across scales," Science **362**, 1379–1383 (2018).
[10] C. Gaucherel and V. Moron, "Potential stabilizing points to mitigate tipping point interactions in Earth's climate," Int. J. Climatol. **37**, 399–408 (2017).
[11] M. M. Dekker, A. S. Heydt, and H. A. Dijkstra, "Cascading transitions in the climate system," Earth Syst. Dyn. **9**, 1243–1260 (2018).
[12] A. K. Klose, V. Karle, R. Winkelmann, and J. F. Donges, "Dynamic emergence of domino effects in systems of interacting tipping elements in ecology and climate," arXiv:1910.12042 (2019).
[13] W. Steffen, J. Rockström, K. Richardson, T. M. Lenton, C. Folke, D. Liverman, C. P. Summerhayes, A. D. Barnosky, S. E. Cornell, M. Crucifix *et al.*, "Trajectories of the Earth System in the Anthropocene," Proc. Natl. Acad. Sci. U.S.A. **115**, 8252–8259 (2018).
[14] J. Krönke, N. Wunderling, R. Winkelmann, A. Staal, B. Stumpf, O. A. Tuinenburg, and J. F. Donges, "Dynamics of tipping cascades on complex networks," Phys. Rev. E (to be published).
[15] Y.-H. Eom, "Resilience of networks to environmental stress: From regular to random networks," Phys. Rev. E **97**, 042313 (2018).
[16] D. J. Watts, "A simple model of global cascades on random networks," Proc. Natl. Acad. Sci. U.S.A. **99**, 5766–5771 (2002).
[17] S. V. Buldyrev, R. Parshani, G. Paul, H. E. Stanley, and S. Havlin, "Catastrophic cascade of failures in interdependent networks," Nature **464**, 1025 (2010).
[18] M. Turalska, K. Burghardt, M. Rohden, A. Swami, and R. M. D'Souza, "Cascading failures in scale-free interdependent networks," Phys. Rev. E **99**, 032308 (2019).
[19] A. Loppini, S. Filippi, and H. E. Stanley, "Critical transitions in heterogeneous networks: Loss of low-degree nodes as an early warning signal," Phys. Rev. E **99**, 040301 (2019).
[20] X.-Z. Wu, P. G. Fennell, A. G. Percus, K. Lerman *et al.*, "Degree correlations amplify the growth of cascades in networks," Phys. Rev. E **98**, 022321 (2018).
[21] X. Liu, L. Pan, H. E. Stanley, and J. Gao, "Multiple phase transitions in networks of directed networks," Phys. Rev. E **99**, 012312 (2019).
[22] S. Krishnagopal, J. Lehnert, W. Poel, A. Zakharova, and E. Schöll, "Synchronization patterns: From network motifs to hierarchical networks," Philos. Trans. R. Soc. A **375**, 20160216 (2017).
[23] O. D'Huys, R. Vicente, T. Erneux, J. Danckaert, and I. Fischer, "Synchronization properties of network motifs: Influence of coupling delay and symmetry," Chaos **18**, 037116 (2008).
[24] L. V. Gambuzza, J. Gómez-Gardeñes, and M. Frasca, "Amplitude dynamics favors synchronization in complex networks," Sci. Rep. **6**, 24915 (2016).
[25] R. Milo, S. Shen-Orr, S. Itzkovitz, N. Kashtan, D. Chklovskii, and U. Alon, "Network motifs: Simple building blocks of complex networks," Science **298**, 824–827 (2002).
[26] D. B. Stouffer, M. Sales-Pardo, M. I. Sirer, and J. Bascompte, "Evolutionary conservation of species' roles in food webs," Science **335**, 1489–1492 (2012).
[27] V. Q. Marinho, G. Hirst, and D. R. Amancio, "Authorship attribution via network motifs identification," in *2016 5th Brazilian Conference on Intelligent Systems (BRACIS)* (IEEE, 2016), pp. 355–360.
[28] U. Alon, "Network motifs: Theory and experimental approaches," Nat. Rev. Genet. **8**, 450 (2007).
[29] G. Lahav, N. Rosenfeld, A. Sigal, N. Geva-Zatorsky, A. J. Levine, M. B. Elowitz, and U. Alon, "Dynamics of the p53-Mdm2 feedback loop in individual cells," Nat. Genet. **36**, 147 (2004).
[30] E. Anastasiadou, L. S. Jacob, and F. J. Slack, "Non-coding RNA networks in cancer," Nat. Rev. Cancer **18**, 5 (2018).
[31] S. S. Shen-Orr, R. Milo, S. Mangan, and U. Alon, "Network motifs in the transcriptional regulation network of *Escherichia coli*," Nat. Genet. **31**, 64 (2002).

[32]S. Mangan, S. Itzkovitz, A. Zaslaver, and U. Alon, "The incoherent feed-forward loop accelerates the response-time of the *gal* system of *Escherichia coli*," J. Mol. Biol. **356**, 1073–1081 (2006).
[33]T. E. Gorochowski, C. S. Grierson, and M. di Bernardo, "Organization of feed-forward loop motifs reveals architectural principles in natural and engineered networks," Sci. Adv. **4**, eaap9751 (2018).
[34]E. H. van Nes, W. J. Rip, and M. Scheffer, "A theory for cyclic shifts between alternative states in shallow lakes," Ecosystems **10**, 17 (2007).
[35]M. Scheffer and E. Jeppesen, "Regime shifts in shallow lakes," Ecosystems **10**, 1–3 (2007).
[36]M. Scheffer, S. Carpenter, J. A. Foley, C. Folke, and B. Walker, "Catastrophic shifts in ecosystems," Nature **413**, 591 (2001).
[37]P. Erdös and A. Rényi, "On random graphs, I," Publ. Math. **6**, 290–297 (1959).
[38]D. C. Zemp, C.-F. Schleussner, H. M. Barbosa, M. Hirota, V. Montade, G. Sampaio, A. Staal, L. Wang-Erlandsson, and A. Rammig, "Self-amplified Amazon forest loss due to vegetation-atmosphere feedbacks," Nat. Commun. **8**, 14681 (2017).
[39]M. Hirota, M. Holmgren, E. H. van Nes, and M. Scheffer, "Global resilience of tropical forest and savanna to critical transitions," Science **334**, 232–235 (2011).
[40]A. Staal, O. A. Tuinenburg, J. H. Bosmans, M. Holmgren, E. H. van Nes, M. Scheffer, D. C. Zemp, and S. C. Dekker, "Forest-rainfall cascades buffer against drought across the Amazon," Nat. Clim. Change **8**, 539–543 (2018).
[41] C. A. Nobre, G. Sampaio, L. S. Borma, J. C. Castilla-Rubio, J. S. Silva, and M. Cardoso, "Land-use and climate change risks in the Amazon and the need of a novel sustainable development paradigm," Proc. Natl. Acad. Sci. U.S.A. **113**, 10759–10768 (2016).
[42]E. H. van Nes, M. Hirota, M. Holmgren, and M. Scheffer, "Tipping points in tropical tree cover: Linking theory to data," Global Change Biol. **20**, 1016–1021 (2014).
[43]A. Staal, S. C. Dekker, M. Hirota, and E. H. van Nes, "Synergistic effects of drought and deforestation on the resilience of the south-eastern Amazon rainforest," Ecol. Complex. **22**, 65–75 (2015).
[44]D. C. Zemp, C.-F. Schleussner, H. Barbosa, R. Van der Ent, J. F. Donges, J. Heinke, G. Sampaio, and A. Rammig, "On the importance of cascading moisture recycling in South America," Atmos. Chem. Phys. **14**, 13337–13359 (2014).

# Supplementary material of

# How motifs condition critical thresholds for tipping cascades in complex networks: Linking Micro- to Macro-scales

Nico Wunderling,[1,2,3,a)] Benedikt Stumpf,[1,4,a)] Jonathan Krönke,[1,2] Arie Staal,[5] Obbe A. Tuinenburg,[5,6] Ricarda Winkelmann[1,2] & Jonathan F. Donges[1,5]

[1]Earth System Analysis, Potsdam Institute for Climate Impact Research (PIK), Member of the Leibniz Association, 14473 Potsdam, Germany
[2]Institute of Physics and Astronomy, University of Potsdam, 14476 Potsdam, Germany
[3]Department of Physics, Humboldt University of Berlin, 12489 Berlin, Germany
[4]Department of Physics, Free University of Berlin, 14195 Berlin, Germany
[5]Stockholm Resilience Centre, Stockholm University, Stockholm, SE-10691, Sweden
[6]Copernicus Institute, Faculty of Geosciences, Utrecht University, 3584 CB Utrecht, Netherlands

a) These authors equally contributed to this study.
Correspondences should be addressed to: nico.wunderling@pik-potsdam.de

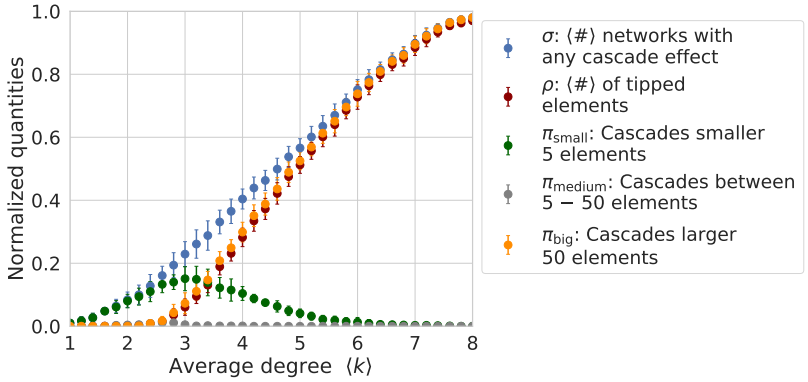


**Figure S. 1** Share of networks with any cascade effect $\sigma$ against average degree with a constant coupling constant of 0.162 (equal to the critical coupling constant of the feed forward loop). $\rho$ denotes the average number of tipped elements. Small $\pi_{\text{small}}$, medium $\pi_{\text{medium}}$ and big cascades $\pi_{\text{big}}$ cascade occurrences are shown, where small cascades involve at most 5 tipped nodes, medium cascades $5-50$ nodes and big cascades more than 50 tipped nodes. Each point was evaluated from 1000 Erdős-Rényi networks with N = 100 and the standard deviation of occurrence are shown as error bars.

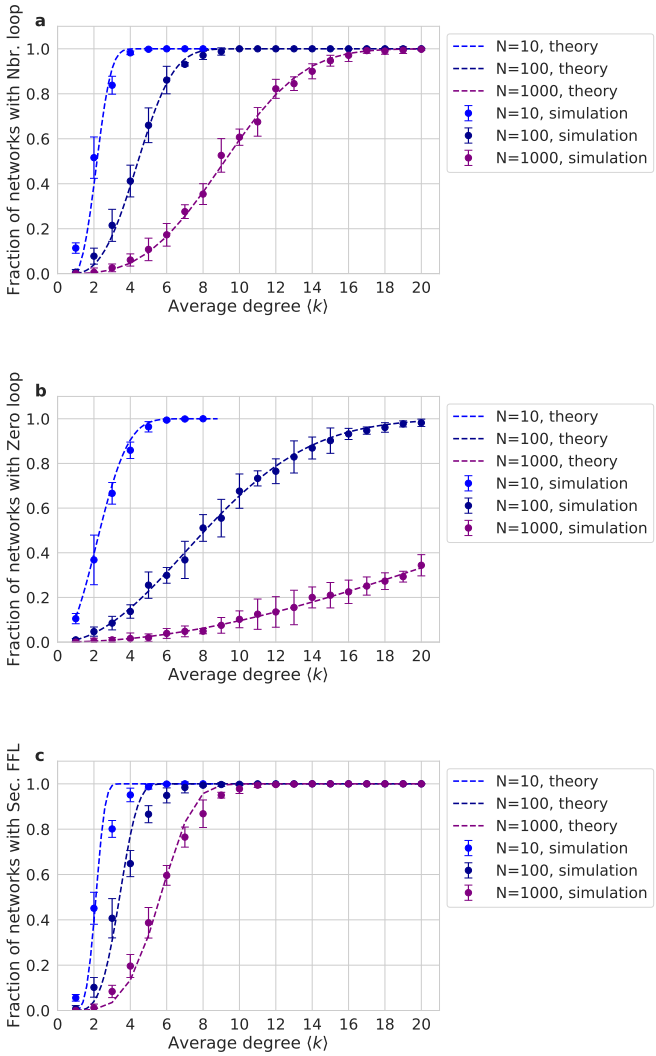


**Figure S. 2** Scaling of the occurrence of the **a)** neighboring loop (theory from equation 5), **b)** zero loop (theory from equation 6) and **c)** the secondary feed forward loop (theory from equation 7) for networks of size 10, 100 and 1000. Error bars in both panels show the error in occurrence in 1000 realisations grouped as $10 \times 100$ samples.

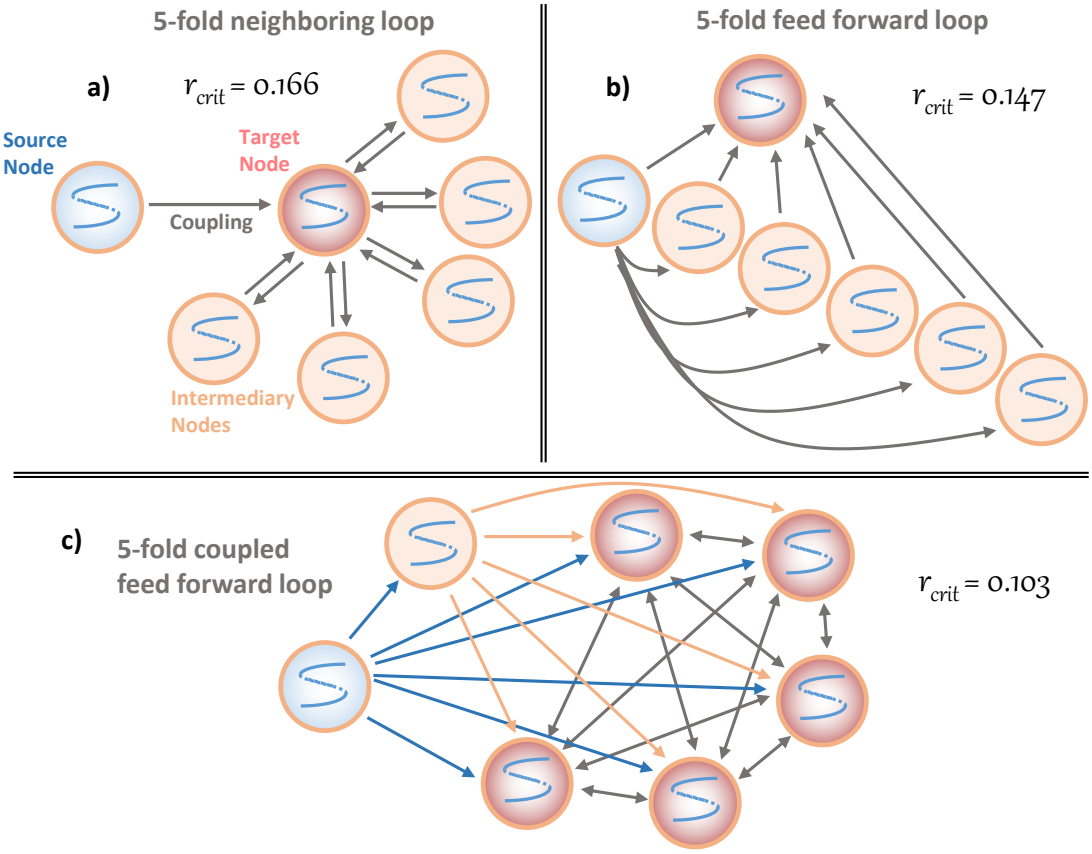


**Figure S. 3** Examples for five fold coupled motifs as evaluated in Fig. 4 in the main manuscript. **a)** 5-fold neighboring loop, **b)** 5-fold feed forward loop and **c)** 5-fold coupled feed forward loop. The target nodes are fully connected between each other. For better visibility, the couplings from the source node are blue and the orange from the intermediary node and feedback loops are shown by a double headed arrow. All arrows have the same coupling strength. Furthermore, there are five target nodes since this motif is symmetric towards these nodes.

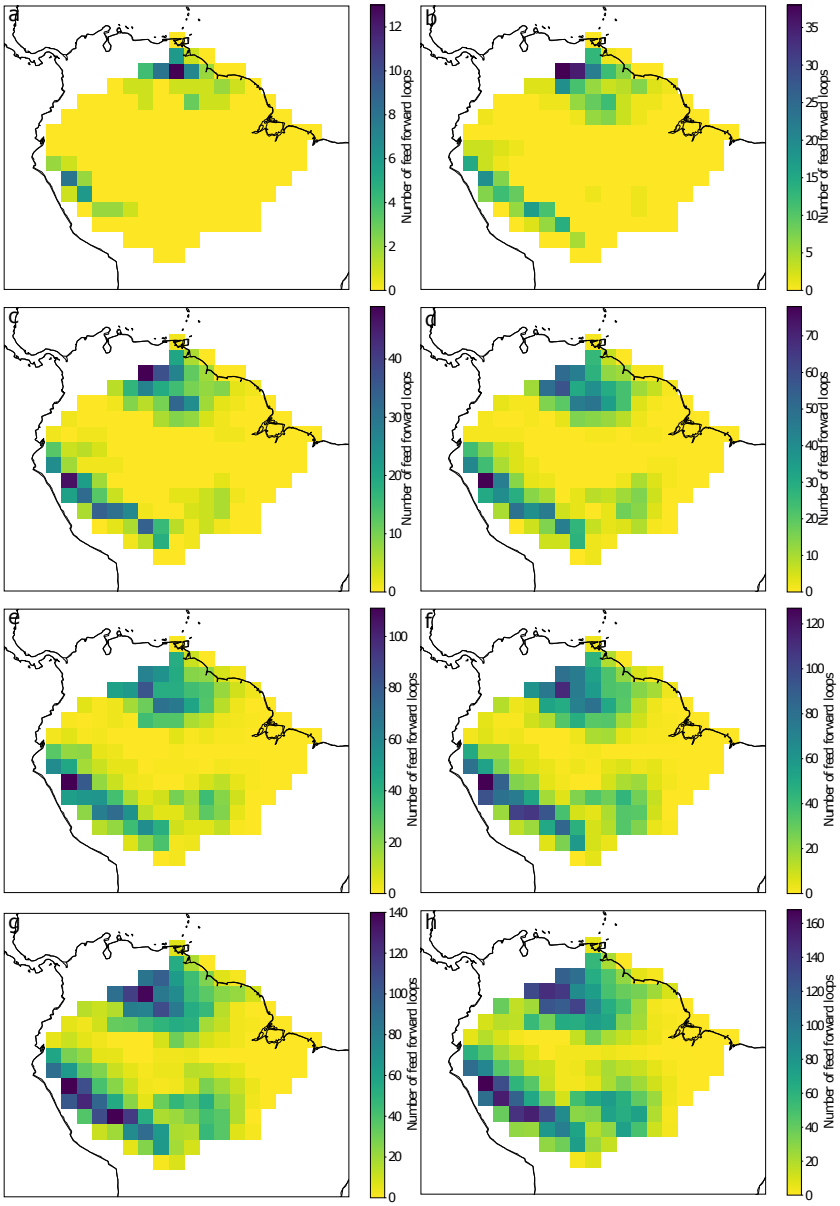


**Figure S. 4** Number of motifs that point to a certain cell in the $2 \times 2$ ° grid for the feed forward loop motif (similar for other motif types: zero loop, neighboring loop and secondary feed forward loop; not shown) for average degrees from **a)** $-$ **h)** $1 - 8$.

# 2.4 Global warming due to loss of large ice masses and Arctic summer sea ice [P4]

**Authors**
Nico Wunderling, Matteo Willeit, Jonathan F. Donges, Ricarda Winkelmann

**Status**
Published at *Nature Communications* (October, 2020), doi: 10.1038/s41467-020-18934-3

**Short summary**
Under ongoing global warming, feedbacks on the global mean temperature have to be expected from the disintegration of large cryosphere components. In this study, the temperature increase by the collapse of the Greenland and the West Antarctic Ice Sheet as well as the Arctic summer sea ice and the mountain glaciers is quantified. It is found that their disintegration would exert a warming of 0.43 °C (interquartile range: 0.39–0.46 °C) on top of the warming from the emission of $CO_2$. Furthermore, a separation of this additional warming into the fast climate feedbacks (albedo, water vapour, lapse rate and clouds) has been performed. It was found that most of these feedbacks (55%) are due to albedo changes, 30% due to changes in the lapse rate and the water vapour, and 15% due to the clouds feedback. Apart from the Arctic summer sea ice, the disappearance of these large cryosphere elements and, as such, the realisation of the temperature feedbacks lies hundreds up to thousands of years in the future. However, the commitment to such integral changes of the climate system is in the hands of the current and next generation.

**Author contributions**
Ricarda Winkelmann conceived the study. All authors designed the study and wrote the text including revisions, upon a first version drafted by Nico Wunderling. Nico Wunderling prepared the data, conducted the model simulation runs and prepared the figures. Matteo Willeit designed the model calibration and prepared CLIMBER-2 for simulations.

nature COMMUNICATIONS

ARTICLE

https://doi.org/10.1038/s41467-020-18934-3 OPEN

# Global warming due to loss of large ice masses and Arctic summer sea ice

Nico Wunderling [1,2,3]✉, Matteo Willeit[1], Jonathan F. Donges [1,4] & Ricarda Winkelmann [1,2]✉

Several large-scale cryosphere elements such as the Arctic summer sea ice, the mountain glaciers, the Greenland and West Antarctic Ice Sheet have changed substantially during the last century due to anthropogenic global warming. However, the impacts of their possible future disintegration on global mean temperature (GMT) and climate feedbacks have not yet been comprehensively evaluated. Here, we quantify this response using an Earth system model of intermediate complexity. Overall, we find a median additional global warming of 0.43 °C (interquartile range: 0.39−0.46 °C) at a $CO_2$ concentration of 400 ppm. Most of this response (55%) is caused by albedo changes, but lapse rate together with water vapour (30%) and cloud feedbacks (15%) also contribute significantly. While a decay of the ice sheets would occur on centennial to millennial time scales, the Arctic might become ice-free during summer within the 21st century. Our findings imply an additional increase of the GMT on intermediate to long time scales.

[1] Earth System Analysis, Potsdam Institute for Climate Impact Research (PIK), Member of the Leibniz Association, Potsdam D-14473, Germany. [2] Institute of Physics and Astronomy, University of Potsdam, Potsdam D-14476, Germany. [3] Department of Physics, Humboldt University of Berlin, Berlin D-12489, Germany. [4] Stockholm Resilience Centre, Stockholm University, Stockholm, SE 10691, Sweden. ✉email: nico.wunderling@pik-potsdam.de; ricarda.winkelmann@pik-potsdam.de

Extensive changes have been observed in large-scale cryosphere elements during the last decades such as the Arctic summer sea ice, mountain glaciers, the Greenland and West Antarctic Ice Sheet[1–5].

From the late 1970s to the mid-2000s, the Arctic summer sea ice area has declined by more than 10% per decade, as satellite measurements reveal[1]. If this trend continues, the Arctic could become ice-free in summer for the first time within the 21st century. Projections with CMIP-5[6] (Coupled Model Intercomparison Project Phase 5) models show that this could be the case as early as 2030 to 2050 for higher emission scenarios such as RCP8.5 (Representative Concentration Pathway)[7]. Some GCMs (global circulation models) show an ice-free Arctic for the first time within this century also for the moderate emission scenarios at a warming of 1.7 °C above pre-industrial[8,9]. Furthermore, observations reveal that the Arctic summer sea ice declines faster than expected in experiments from GCMs[1].

At the same time, mountain-glaciers world-wide have retreated, with an average weight equivalent ice loss of approximately 250 ± 30 Gt per year between 1901 and 2009[2,10]. This translates, in the same time span, into a loss of 21% of the glaciated volume of mountain glaciers worldwide, excluding (Sub-) Antarctic peripheral glaciers, as found in model simulations[11]. During this time, it is estimated that approximately 600 glaciers have disappeared and many more are likely to follow in the future (IPCC-AR5, Chapter 4[6]). 36 ± 8% of today's glacier mass is already committed to be lost in response to past greenhouse gas emissions[12] and it has been found that many mountain glaciers are currently in disequilibrium and will be subject to further ice loss[13].

Moreover, both the West Antarctic and the Greenland Ice Sheet have lost mass at an accelerating pace in the past decades[3–5]. With progressing global warming, ice loss from the polar ice sheets and subsequent sea-level rise is expected to further increase[14,15]. Beyond a critical temperature threshold, large parts of the Greenland Ice Sheet might melt, accelerated by positive feedbacks such as the ice-albedo and melt-elevation feedbacks[16,17]. From model simulations, this threshold temperature is suggested to range between 0.8 and 3.2 °C above pre-industrial levels[18].

Parts of the West Antarctic Ice Sheet might already have crossed a point of instability: the grounding lines of several glaciers in the Amundsen basin are rapidly retreating and have likely become unstable, causing sustained ice discharge from the entire basin which could lead to more than 1 m of global sea-level rise[19]. Similar dynamics might be induced in other parts of the Antarctic Ice Sheet and could eventually lead to its complete disintegration under unmitigated climate change[20].

Anthropogenic climate change has already caused a rise in global mean temperature (GMT) by 0.9 °C comparing 1850–1900 to 2006–2015[21], with observable impacts on the cryosphere elements mentioned above[6]. It has also been suggested that these regions are likely to change dramatically with ongoing climate warming and some of these changes are suspected to possess some degree of irreversibility[22,23].

Following these recent developments of the cryosphere components, it seems possible that they might be lost at lower temperatures than commonly thought, potentially as low as 1.5 °C above pre-industrial levels[23]. The disintegration of these elements is associated with feedbacks that impact back on GMT, for instance via a change in albedo, clouds or lapse rate, among others, which has not been quantified comprehensively so far. Therefore, we assess the additional global warming caused by disintegration of the Greenland Ice Sheet, the West Antarctic Ice Sheet, the mountain glaciers and the Arctic summer sea ice. Although the Arctic summer sea ice is implemented in more complex Earth system models and its loss part of their simulation results (e.g. in CMIP-5), it is one of the fastest changing cryosphere elements whose additional contribution to global warming is important to be considered. Therefore, we compute and separate its contribution to GMT increase. On the other side, the temperature feedbacks of ice sheets like Greenland, West Antarctica and mountain glaciers are not yet fully integrated in assessments such as CMIP-5.

We base our simulations on the Earth system model of intermediate complexity, CLIMBER-2[24,25] because it is computationally efficient and allows a systematic analysis of the decay of the cryosphere components. CLIMBER-2 includes atmosphere, ocean, sea ice, vegetation and land-ice model components and has been applied extensively to understand past and future climate changes[26,27].

In large ensembles of equilibrium model simulations, constrained by fast climate feedbacks strength from global circulation models[28] (see "Methods"), we compare the long-term GMT change in idealised scenarios, where the cryosphere elements are removed, to scenarios where they remain intact. The uncertainty in the additional warming in our simulations is constrained by the uncertainty of the feedback strength in the GCM simulations which we used to mimic the more complex behaviour of GCMs[28] (Supplementary Fig. 1). To change the feedback strengths, we alter CLIMBER-2 model parameters that act on the strength of the feedbacks themselves, particularly in the structure of the troposphere and the clouds (atmospheric changes) as well as in the snow albedo (see Supplementary Table 1). With reasonably altered parameters in CLIMBER-2, we arrive at an equilibrium climate sensitivity of 2.0–3.75 °C for our ensemble leading to smaller temperature responses than the full range from CMIP-5 (2.0–4.7 °C) or CMIP-6 (1.8–5.6 °C) would[29]. Details on the calibration process are given in the methods section: uncertainty estimates.

In our experiments the state of the Greenland Ice Sheet, the West Antarctic Ice Sheet and mountain glaciers is simply prescribed in the model and affects both, ice cover and topography. In our simulations for the Arctic summer sea ice, the albedo during the summer months (June, July, August) is lowered to average values for open ocean waters instantaneously similar to Blackport and Kushner[30], while keeping the computation of ice-covered areas dynamic, such that the experiment does not violate energy and water conservation.

In this study, we find that global warming is amplified by the decay of the Earth's cryosphere as expected from theory and quantify the contribution of each of the four cryosphere components. We further separate the GMT response into contributions from albedo, lapse rate, water vapour and clouds in terms of perturbation of the net radiation at the top of the atmosphere[31]. Here, we focus on the purely radiative effects and neglect freshwater contributions to feedbacks and warming. Thus, our estimates are long-term equilibrium responses when the large ice masses are disintegrated. However, transient warming responses would be reduced due to freshwater input from the West Antarctic and Greenland Ice Sheet on centennial time-scales[32–35].

## Results

**Additional global and regional warming**. We consider several different climate scenarios, with atmospheric $CO_2$ concentrations ranging from the pre-industrial 280 ppm up to 700 ppm and run the model forward until it reaches equilibrium. If not stated otherwise, our findings are shown for a reference simulation at a fixed $CO_2$ concentration of 400 ppm in equilibrium after 10,000 years. 400 ppm corresponds to an equilibrium GMT increase of 1.5 °C above pre-industrial in CLIMBER-2 simulations. Upon this, we evaluate the additional regional and global warming

caused by the large-scale loss of the Arctic sea ice during summer, mountain glaciers, and the polar ice sheets. While this ad-hoc loss of the ice masses poses a hypothetical scenario, it allows us to separate the additional warming through the ice-climate feedbacks from other effects. In our experiments, we report the median value of the ensemble and the brackets represent the interquartile range unless stated otherwise.

In our simulations, we find that global warming is increased by the decay of the Earth's cryosphere. The disintegration of the Arctic summer sea ice and the retreat of mountain glaciers, the Greenland and the West Antarctic Ice Sheets together cause an additional GMT increase of 0.43 °C (0.39–0.46 °C) for a baseline-scenario of 1.5 °C warming above pre-industrial levels, which translates into an additional warming of 29% (26–31%).

Locally, the loss of each element induces a very strong warming signal, which is consistent with previous studies on polar and Arctic amplification[36,37]. Local warming around the cryosphere components is up to 5 °C stronger, particularly around Greenland and West Antarctica (Fig. 1a). However, the ice loss causes significant warming also in lower latitudes, with values of 0.2 °C around the equator.

The warming results from our simulations are consistent in magnitude and polar amplification with past warm periods, particularly the Mid-Pliocene Warm Period, during which the large ice sheets were at least partially disintegrated[38,39]. Still, the distribution among the feedback processes in these paleoclimate states remains uncertain.

Under ongoing global warming, further ice loss is to be expected for all of the four cryosphere components considered here; however, the corresponding time scales differ by several orders of magnitude. While substantial ice loss from Greenland or Antarctica might be triggered by anthropogenic climate change within the current century, these changes would manifest over several centuries to millennia[15]. Ice-free Arctic summers on the other side might already occur in the next decades[1,7,9]. Therefore, we also consider the regional warming caused solely by the loss of the Arctic summer sea ice (Fig. 1b). The additional warming in the Arctic region on a yearly average accounts for more than 1.5 °C regionally and for 0.19 °C globally. The meltdown of the Arctic sea ice and its regional warming effect is also simulated by CMIP-5 runs dependent on the future anthropogenic $CO_2$ forcing scenarios, the RCP scenarios[6,9].

With CLIMBER-2, we are able to distinguish between the respective cryosphere elements and can compute the additional warming resulting from each of these (Fig. 2). The additional warmings are 0.19 °C (0.16–0.21 °C) for the Arctic summer sea ice, 0.13 °C (0.12–0.14 °C) for GIS, 0.08 °C (0.07–0.09 °C) for mountain glaciers and 0.05 °C (0.04–0.06 °C) for WAIS, where the values in brackets indicate the interquartile range and the main value represents the median. If all four elements would disintegrate, the additional warming is the sum of all four individual warmings resulting in 0.43 °C (0.39–0.46 °C) (thick dark red line in the Fig. 2). Our results regarding the amount of warming are of comparable magnitude to previous efforts computed for late Pliocene realisations (PRISM) of the ice sheets[40,41]. Both studies show a pronounced warming in the proximity of the locations where ice is removed, which is in good agreement with our results (see Fig. 1 and Supplementary Fig. 2).

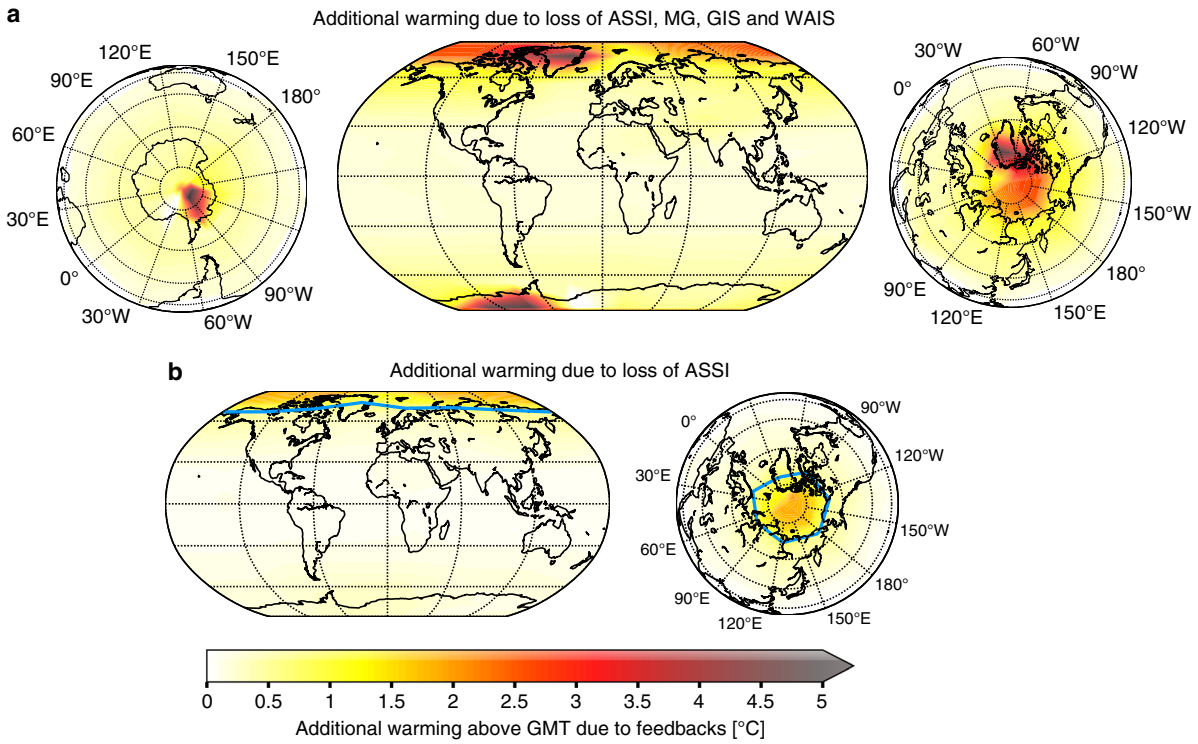


**Fig. 1 Regional warming due to feedbacks. a** Regional warming for the whole Earth if Arctic summer sea ice (ASSI) in June, July and August, mountain glaciers (MG), Greenland Ice Sheet (GIS) and West Antarctic Ice Sheet (WAIS) vanish at a global mean temperature of 1.5 °C above pre-industrial. **b** Same as in (**a**) with an additional zoom-in of the Arctic region if only the Arctic summer sea ice vanishes, which might happen until the end of the century. The light blue line indicates the region of removed Arctic summer sea ice extent, where its concentration in CLIMBER-2 is 15% or higher. In all panels, the average additional warming on top of 1.5 °C is shown in absolute degree.

The disintegration of all elements at the same time can very closely be approximated by the sum of single elements disintegrated indicating that their effects on GMT add up linearly. This can be found in Fig. 3, where we also show the warming for $CO_2$ concentrations from 280 to 700 ppm. Fig. 2 highlights the additional warming of 1.5 °C above pre-industrial.

**Warming from the Arctic summer sea ice**. We obtain that the warming results are independent from the $CO_2$ concentration forcing between 280 and 700 ppm apart from the Arctic summer sea ice (see Fig. 3a), which shows a decreasing additional warming for higher $CO_2$ concentrations (Fig 4). This can, in turn, be explained: In CLIMBER-2 simulations we find, with increasing prescribed $CO_2$ concentrations corresponding to increasing GMT, that the Arctic summer sea ice area declines in a linear way, which was also found in observational records[42] and in GCM simulations[9]. For a $CO_2$ concentration of 400 ppm corresponding to 1.5 °C in CLIMBER-2 above pre-industrial GMT levels, the additional warming is 0.19 °C (0.16–0.21 °C). The actual minimal sea ice cover observed by NERSC (Nansen Environmental & Remote Sensing Center) as an average area from 1979 to 2006 is on the order of 5.5–6.5 × $10^6$ $km^2$ which would correspond to a warming of approximately 0.15 °C in our simulations (see Fig. 4). In Supplementary Fig. 3, we show the sea ice area over the course of 1 year for the control and the perturbed run.

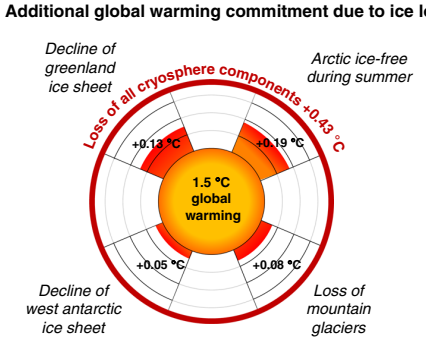


**Fig. 2 GMT increase through disappearance of cryosphere elements.** The additional warming for the cryosphere components is shown for a scenario consistent with global warming levels of 1.5 °C. Radially outward, the temperature anomaly is displayed which arises from the disappearance of the cryosphere elements. The thick dark red line indicates the maximum effect of additional warming in case all cryosphere elements lose stability. All values are the medians of the ensemble.

**Radiative perturbations at the top of the atmosphere**. For each cryosphere element, we are able to deconvolve the net change of radiative perturbations at the top of the atmosphere into several components that affect the radiative balance of the Earth: water vapour, clouds, lapse rate and albedo. These factors can be quantified in CLIMBER-2 (Table 1).

The values for water vapour, lapse rate and clouds in Table 1 can to a very good approximation directly be interpreted as feedback factors once they are divided by the respective warming, e.g., by 0.43 °C in case all investigated cryosphere elements are removed. However, it is important to note that the perturbation arising from albedo changes is both, a forcing and a feedback. The forcing component originates from the prescribed removal of the cryosphere elements. On the other side, the feedback component

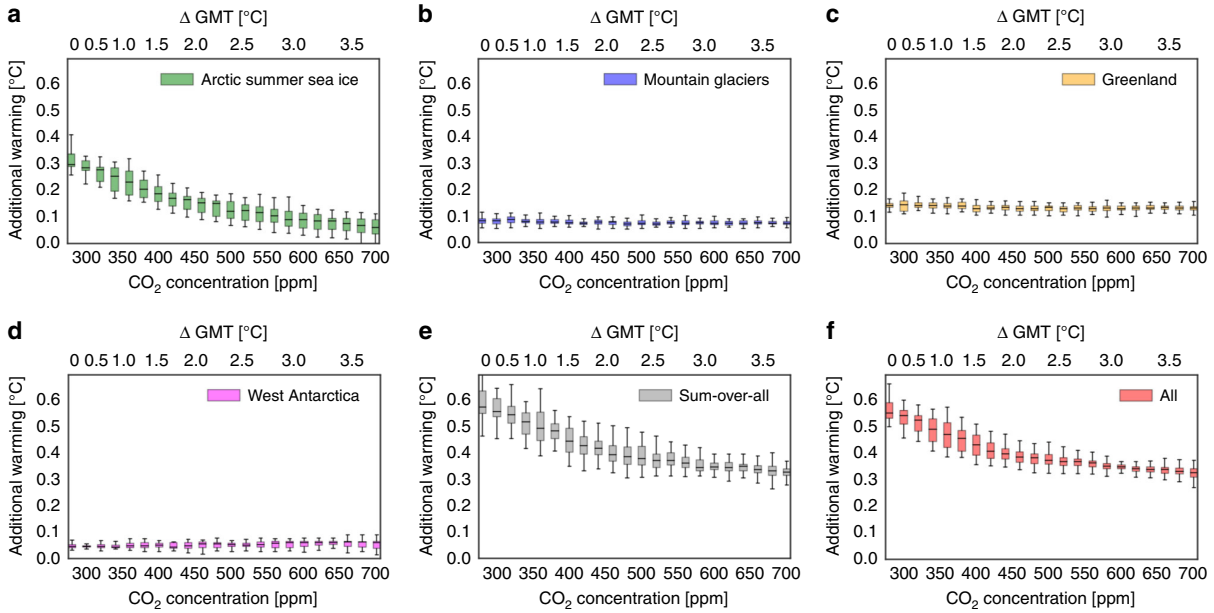


**Fig. 3 Linearity of additional warming due to disintegration of cryosphere elements.** Additional warming plotted against $CO_2$ concentration. Disintegration of of cryosphere components separately for (**a**) the Arctic summer sea ice, (**b**) the mountain glaciers, (**c**) the Greenland Ice Sheet, (**d**) the West Antarctic Ice Sheet, (**e**) the sum of all additional warmings from the separately disintegrated cryosphere elements and (**f**) the disintegration of all four elements at the same time. The grey bars match the red bars within their errors which means, according to CLIMBER-2, that the warming effect of singular disintegrated cryosphere elements can linearly be added up to the effect of all four elements disintegrated at the same time. Here we show median, interquartile range and full ensemble spread for each $CO_2$ concentration. The upper horizontal axis shows the temperature increase above pre-industrial, where a least-square fit converting $CO_2$ concentration to temperature with python's function scipy.optimize.curve_fit was used. The respective fitted temperatures arise from full ensemble simulations at prescribed $CO_2$ concentrations, but without removed cryosphere elements.

derives from responses of the surface albedo to the additional warming as for instance through changes in the extent of snow covered area or changes in vegetation cover. Thus both, the feedback and the forcing contribute to the measured radiative perturbation quantified in Table 1.

Change in surface albedo is the dominant additional radiative perturbation for each considered cryosphere element. It is mainly caused by the albedo change of large ice-covered areas from ice to other non ice-covered surface types, but also by other land cover changes. In total around 55% of the radiative perturbations can be attributed to the change of the albedo.

Two more additional radiative perturbations which are evaluated together as they are anti-correlated are the lapse rate and the water vapour fast climate feedback[28,31]. The lapse rate change arises from non-uniform temperature changes in the vertical atmospheric column and subsequent changes in outgoing longwave radiation. The water vapour change describes the capacity of the air to sustain water vapour in the air. The capacity to sustain water vapour is increased by 7% per degree of warming as can be computed using the Clausius–Clapeyron equation. Since the GMT is increasing through the removal of the cryosphere elements, the air can sustain more water vapour which then in turn leads to an additional warming. Together, the additional radiative perturbation of water vapour and lapse rate combine for approximately 30% of the complete radiative perturbation.

For the cloud feedbacks, the IPCC AR5 and newer studies hypothesised that the feedback from clouds is likely positive[6,43] as we also find here. It is responsible for 15% of the total radiative perturbation.

Within our experimental setting, it can be expected that the radiative perturbation from albedo changes is very high due to the prescribed removal of the respective cryosphere element. However, the radiative perturbation related to different fast climate feedbacks such as water vapour, lapse rate and clouds also play an important role as drivers of additional warming. Together they account for more than 40% of the total radiative perturbation on average.

Similar investigations on the additional radiative perturbation from albedo changes have been performed for the removal of Arctic sea ice. For a removal of one month during summer an additional radiative perturbation of 0.3 W/m$^2$ is reported[44] which is in good agreement with Flanner et al. (2011)[45]. We find a slightly higher value of 0.49 W/m$^2$ for albedo plus clouds value when the Arctic summer sea ice is removed (Table 1). This value probably is higher since we have low sea ice for approximately five months (Supplementary Fig. 3) in our perturbed experiments instead of one as in Hudson[44], but parts of the deviation might also be due to the slightly different experimental setup.

In Supplementary Fig. 4a, we show the latitudinal distribution of the additional radiative perturbation at the top of the atmosphere. The contribution from albedo as well as from lapse rate and water vapour are higher in polar regions and thus contribute to polar amplification which is also apparent in the corresponding zonal mean surface warming (see Supplementary Fig. 4b). On the other hand, the additional cloud feedback does not strongly contribute to polar amplification in our simulations. These trends for clouds and albedo have also been found by other studies[36,46]. Further studies mention that the lapse rate feedback plays a major role in polar amplification[47]. This seems to be the case here as well (see Supplementary Fig. 4a), but we can only make this statement for the combined feedbacks of lapse rate and water vapour since we do not separate them in our analysis.

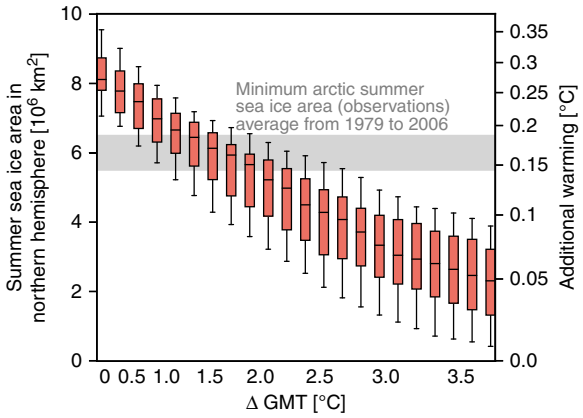


**Fig. 4 Additional warming due to meltdown of Arctic summer sea ice.** Box whiskers plot of global mean temperature (ΔGMT) versus Arctic summer sea ice area with error boxes (error bars) representing the interquartile range (full spread) of the ensemble at the according GMT over the CLIMBER-2 ensemble runs. The additional warming when the Arctic summer sea ice disappears is represented by a second y-axis computed via a least-square fit from the corresponding summer sea ice area. The relationship between summer sea ice area and additional warming is slightly nonlinear. This means that a doubling of the ice area does not quite translate into a doubling of the additional warming. The x-axis shows ΔGMT above pre-industrial computed via a GMT-$CO_2$ concentration least-square fit. The shaded area shows the mean Arctic sea ice area as observed by NERSC (Nansen Environmental & Remote Sensing Center) from 1979 to 2006, where the uncertainty indicates one standard deviation: 6.0 ± 0.5 × 10$^6$ km$^2$.

## Discussion

Our results concern short and long term effects on GMT due to the disintegration of cryosphere elements which experienced significant changes within the last decades and are likely to also change strongly in the future due to global warming.

**Table 1 Drivers of warming as seen from the top of the atmosphere.**

| Cryosphere element | LR + WV [W/m$^2$] | Clouds [W/m$^2$] | Albedo [W/m$^2$] | All changes [W/m$^2$] |
|---|---|---|---|---|
| ASSI | 0.20 (0.17–0.23) | 0.08 (0.07–0.09) | 0.41 (0.35–0.47) | 0.69 (0.59–0.79) |
| GIS | 0.14 (0.13–0.16) | 0.06 (0.05–0.07) | 0.22 (0.20–0.25) | 0.43 (0.39–0.47) |
| WAIS | 0.05 (0.04–0.05) | 0.04 (0.03–0.05) | 0.10 (0.08–0.11) | 0.18 (0.16–0.21) |
| MG | 0.09 (0.08–0.10) | 0.04 (0.03–0.05) | 0.16 (0.14–0.17) | 0.28 (0.26–0.32) |
| All | 0.45 (0.41–0.49) | 0.17 (0.16–0.19) | 0.72 (0.66–0.78) | 1.35 (1.22–1.46) |

*ASSI* Arctic summer sea ice, *GIS* Greenland Ice Sheet, *WAIS* West Antarctic Ice Sheet, *MG* Mountain glaciers.
The additional radiative perturbation for the fast climate feedbacks as evaluated in CLIMBER-2 at a global warming of 1.5 °C above pre-industrial for disintegration of the respective element given as changes in W/m$^2$. The values are given as median and interquartile range (in brackets) of the ensemble. The "LR + WV" column represents the lapse rate and water vapour additional radiative perturbation column together as they are anti-correlated and thus not independent[57]. Note that the albedo forcing values refer to both, a forcing and a feedback. The forcing part is the removal of the cryosphere components and the feedback part comprises changes in vegetation and snow cover in response to the additional warming.

On shorter time scales, the decay of the Arctic summer sea ice would exert an additional warming of 0.19 °C (0.16–0.21 °C) at a uniform background warming of 1.5 °C (=400 ppm) above pre-industrial. On longer time scales, which can typically not be considered in CMIP projections, the loss of Greenland and West Antarctica, mountain glaciers and the Arctic summer sea ice together can cause additional GMT warming of 0.43 °C (0.39–0.46 °C). This effect is robust for a whole range of $CO_2$ emission scenarios up to 700 pm and corresponds to 29% extra warming relative to a 1.5 °C scenario.

In fact, some feedbacks will also be at play before the complete disintegration of the large ice sheets, for instance due to increased ice-drainage from the Amundsen region in West Antarctica[19,48,49]. Furthermore, it has been shown for WAIS and GIS that transgressing their critical thresholds is likely not reversible due to hysteresis effects[18,50,51].

The additional commitment to global warming that we study here represents a long-term, mean-field effect which is separated from possible direct interactions between the elements such as the freshwater input into the thermohaline circulation from the large ice sheets. In other words, the disintegration of the ice sheets has a direct increasing temperature impact on the GMT via the feedbacks quantified here.

## Methods

**Earth system model**. For our analysis, we use the Earth system model of intermediate complexity (EMIC) CLIMBER-2[24,25] on a coarse spatial resolution of 10 × 52° (lat × lon) resolution. CLIMBER-2 includes a 2.5-D dynamical-statistical atmosphere and a multi-basin, zonally averaged ocean model including sea ice as well as a dynamic model of the terrestrial biosphere. CLIMBER-2 also includes a model for ice sheets, a global carbon cycle model and an atmosphere surface interaction coupler, which are not used in this study since ice sheets and atmospheric $CO_2$ are prescribed in our experiments. In CLIMBER-2, changes in the cloud fraction are possible. Apart from that, cloud top height can change following changes in the height of the tropopause. The cloud optical thickness parameterisation includes a dependence on the cumulus cloud fraction in addition to a prescribed increase of optical thickness with latitude. With this representation of clouds, CLIMBER-2 is able to reproduce the planetary albedo as observed from CERES (see Supplementary Fig. 5)[52]. We benefit from the use of an EMIC as it is highly computationally efficient and allows for a systematic analysis of the impact of disintegration of the cryosphere elements on GMT. With CLIMBER-2 we are able to distinguish different feedbacks and are able to run a robustness analysis using systematic parameter studies. CLIMBER-2 is a good representative of other EMICs[53].

**Model initialisation**. In preparation of the model runs, we set up the ice sheets inbuilt in CLIMBER-2. For distinguishing the West and East Antarctic Ice Sheet, we created a mask based on the Antarctic drainage basins[54]. We also included a mountain glacier mask with data from the Randolph glacier inventory[55]. Since we are interested in the climatological behaviour of the disintegration of one or more of the cryosphere elements, we artificially change the setup of CLIMBER-2 depending on which element we remove: In case of WAIS and GIS, the topography of the ice sheet itself is removed together with the ice sheet as the height of the ice sheet is several thousand metres thick and thus might play an important role on the feedbacks. The albedo is replaced by the albedo of bare land or ocean (where appropriate) at first, but can then change freely into any kind of vegetation or snow cover during the simulation run. For our simulations, isostatic rebound is neglected.

For the Arctic summer sea ice and the mountain glaciers, the topography is not taken into account as either the height of the ice or the spacial extent of high thickness regions is very low. To remove the Arctic summer sea ice during the summer months (June, July and August: JJA), the surface covered by sea ice is darkened and the albedo in this region is replaced by the ocean albedo. With this procedure the energy conservation law is not violated since the ice is not just removed and still retains its function as boundary layer between ocean and atmosphere. Thus we are able to compute the effect of summer sea ice in an energetically self-consistent manner. Note that CLIMBER-2 is mass conserving. Our procedure is similar to the experimental setup of Blackport and Kushner[30], who also reduce albedo values of the sea ice instantaneously. They do this for the whole year and all sea ice compared to our setup, where the albedo is changed only in the northern hemisphere in the summer months.

**Model calibration**. To emulate the behaviour of more complex general circulation models (GCMs) we created a model ensemble by perturbing several parameters with the target to cover the range of strength of the fast climate feedbacks found by Soden and Held[28] using an ensemble of GCMs. Equally, this could have been done with the feedbacks stated in the IPCC assessment report 5 (AR5), but changes in the reported feedback strengths are small except for the cloud feedback which is less well constrained in AR5 (see IPCC on page 819 for a direct comparison between AR5 values and the values given in Soden and Held[28]). Thus, our ensemble and our results can be expected to stay the same. The fast climate feedbacks include the water vapour, the lapse rate, the cloud and the albedo feedback. Each of our 39 ensemble members, that we end up with, is constructed from a pair of simulations: one control run at 280 ppm and one perturbed run at a $CO_2$ doubling of 560 ppm. We then compute the magnitude of the fast climate feedbacks between these pairs of runs (see Supplementary Fig. 1a). Here, we evaluate the feedbacks using the partial radiation perturbation method[31,56]. In this method partial derivatives of model top of the atmosphere radiation with respect to changes in model parameters (such as water vapour, lapse rate and clouds) are determined by diagnostically rerunning of the model radiation code.

The water vapour feedback added to the lapse rate feedback is supposed to lie in the range of 0.8–1.2 W/m$^2$/K. These two feedbacks are evaluated together as they are correlated negatively[28,57]. The cloud feedback is supposed to range between 0.3 and 1.1 W/m$^2$/K and the albedo feedback between 0.2 and 0.45 W/m$^2$/K. Furthermore, we put a constraint on the minimal summer sea ice cover in the northern hemisphere to 1.5–6.5 km$^2$ (see Supplementary Fig. 1d). In Soden and Held[28], the albedo value is constraint to values between 0.2 and 0.4 W/m$^2$/K, but in our calibration run, it is necessary to increase the upper limit to 0.45 W/m$^2$/K since vegetation shifts are considered and otherwise the ensemble gets distorted to small summer sea ice values in the control run.

On top of the fast climate feedbacks, we require each ensemble member (each pair of runs) to possess an equilibrium climate sensitivity above 1.5 and below 4.5 °C, where the equilibrium climate sensitivity is the global warming per doubling of atmospheric $CO_2$ concentration (see Supplementary Fig. 1b). It is important to note that our ensemble members span the range from 2.0 to 3.75 °C. This leads to smaller temperature response ranges than the full range from 1.5 to 4.5 °C would. Furthermore, a last constraint is applied at a $CO_2$ concentration of 280 ppm. The temperature difference between the runs with perturbed parameters and the reference run with unperturbed parameters (brackets in Supplementary Table 1) should be less or equal than ±1.0 °C (see Supplementary. Fig. 1c). After the application of all these constraints, we find 39 pairs of runs that match our restrictions.

For covering the uncertainty ranges of the feedbacks we perturb parameters (within their experimental uncertainty range) influencing lapse rate together with the water vapour, cloud and albedo feedbacks similarly to Deimling et al.[57] (Supplementary Table 1). With this procedure, we are able to reconstruct the uncertainty ranges of the four fast climate feedbacks stated in Soden and Held[28] fairly well.

**Uncertainty estimates**. We used these 39 calibrated runs, which also represent the uncertainty of our results, as initialisation for our large-scale ensemble simulations. For each of the cryosphere elements, i.e., WAIS, GIS, Arctic summer sea ice and mountain glaciers, as well as all together, we performed the following experiments: (i) Control runs: the respective cryosphere element(s) is/are kept and (ii) experiment runs: removed cryosphere element(s).

We performed the experiments in (i) and (ii) for different atmospheric $CO_2$ concentrations as external forcing. We chose the $CO_2$ concentration parameter since it is the one which is most probably increasing in future climate change scenarios. Each of the experiments is performed as a long term equilibrium run for 10,000 simulation years with today's boundary conditions, i.e., astrophysical parameters like eccentricity and obliquity, and fixed $CO_2$ concentration. The results are taken as the mean over the last 4000 simulated years since this cancels out minor fluctuations in the equilibrium state. In the end we subtract the experimental run (ii) from the control run (i) to retrieve the temperature difference. Since we are reporting these differences between perturbed (experimental) and control run throughout the main manuscript, the uncertainties given as interquartile ranges are small, also compared to the calibration (see Supplementary Fig. 1). This means that our CLIMBER-2 ensemble is robust against the same perturbations in the cryosphere components. We constructed our ensemble aiming at covering a range of sensitivities and different strengths of the feedbacks by the variation of the parameters in Supplementary Table 1.

## Data availability

The data that support the findings of this study are available from the corresponding author upon reasonable request.

## Code availability

There is no comprehensively documented code for the Earth system model CLIMBER-2 available owing to a lack of comprehensive technical description, but the code is available upon request from M.W.

Received: 22 January 2019; Accepted: 17 September 2020;
Published online: 27 October 2020

## References


1. Stroeve, J. C. et al. The arctic's rapidly shrinking sea ice cover: a research synthesis. *Clim. Change* **110**, 1005–1027 (2012).
2. Gardner, A. S. et al. A reconciled estimate of glacier contributions to sea level rise: 2003 to 2009. *Science* **340**, 852–857 (2013).
3. Zwally, H. J. et al. Greenland ice sheet mass balance: distribution of increased mass loss with climate warming; 2003–07 versus 1992–2002. *J. Glaciol.* **57**, 88–102 (2011).
4. Khan, S. A. et al. Sustained mass loss of the northeast greenland ice sheet triggered by regional warming. *Nat. Clim. Change* **4**, 292–299 (2014).
5. Shepherd, A. et al. Mass balance of the antarctic ice sheet from 1992 to 2017. *Nature* **558**, 219–222 (2018).
6. Stocker, T. F. et al. *Climate change 2013: The Physical Science Basis. Contribution of Working Group I to the Fifth Assessment Report of the Intergovernmental Panel on Climate Change* 1535 (Cambridge University Press, 2013).
7. Overland, J. E. & Wang, M. When will the summer arctic be nearly sea ice free? *Geophys. Res. Lett.* **40**, 2097–2101 (2013).
8. Niederdrenk, A. L. & Notz, D. Arctic sea ice in a 1.5 c warmer world. *Geophys. Res. Lett.* **45**, 1963–1971 (2018).
9. Notz, D., Haumann, F. A., Haak, H., Jungclaus, J. H. & Marotzke, J. Arctic sea-ice evolution as modeled by max planck institute for meteorology's earth system model. *J. Adv. Modeling Earth Syst.* **5**, 173–194 (2013).
10. Leclercq, P. W., Oerlemans, J. & Cogley, J. G. Estimating the glacier contribution to sea-level rise for the period 1800–2005. *Surv. Geophys.* **32**, 519 (2011).
11. Marzeion, B., Jarosch, A. & Hofer, M. Past and future sea-level change from the surface mass balance of glaciers. *Cryosphere* **6**, 1295 (2012).
12. Marzeion, B., Kaser, G., Maussion, F. & Champollion, N. Limited influence of climate change mitigation on short-term glacier mass loss. *Nat. Clim. Change* **8**, 305–308 (2018).
13. Christian, J. E., Koutnik, M. & Roe, G. Committed retreat: controls on glacier disequilibrium in a warming climate. *J. Glaciol.* **64**, 675–688 (2018).
14. Steffen, W. et al. Trajectories of the earth system in the anthropocene. *Proc. Natl Acad. Sci.* **115**, 8252–8259 (2018).
15. Clark, P. U. et al. Consequences of twenty-first-century policy for multi-millennial climate and sea-level change. *Nat. Clim. Change* **6**, 360–369 (2016).
16. Levermann, A. & Winkelmann, R. A simple equation for the melt elevation feedback of ice sheets. *Cryosphere* **10**, 1799–1807 (2016).
17. Box, J. et al. Greenland ice sheet albedo feedback: thermodynamics and atmospheric drivers. *Cryosphere* **6**, 821–839 (2012).
18. Robinson, A., Calov, R. & Ganopolski, A. Multistability and critical thresholds of the greenland ice sheet. *Nat. Clim. Change* **2**, 429–432 (2012).
19. Favier, L. et al. Retreat of pine island glacier controlled by marine ice-sheet instability. *Nat. Clim. Change* **4**, 117–121 (2014).
20. Winkelmann, R., Levermann, A., Ridgwell, A. & Caldeira, K. Combustion of available fossil fuel resources sufficient to eliminate the antarctic ice sheet. *Sci. Adv.* **1**, e1500589 (2015).
21. Masson-Delmotte, V. et al. *Global Warming of 1.5 °C: An IPCC Special Report on the Impacts of Global Warming of 1.5 °C Above Pre-industrial Levels and Related Global Greenhouse Gas Emission Pathways, in the Context of Strengthening the Global Response to the Threat of Climate Change, Sustainable Development, and Efforts to Eradicate Poverty* (World Meteorological Organization Geneva, Switzerland, 2018).
22. Lenton, T. M. et al. Tipping elements in the earth's climate system. *Proc. Natl Acad. Sci.* **105**, 1786–1793 (2008).
23. Schellnhuber, H. J., Rahmstorf, S. & Winkelmann, R. Why the right climate target was agreed in paris. *Nat. Clim. Change* **6**, 649 (2016).
24. Petoukhov, V. et al. Climber-2: a climate system model of intermediate complexity. part i: model description and performance for present climate. *Clim. Dyn.* **16**, 1–17 (2000).
25. Ganopolski, A. et al. Climber-2: a climate system model of intermediate complexity. part ii: model sensitivity. *Clim. Dyn.* **17**, 735–751 (2001).
26. Ganopolski, A. & Brovkin, V. Simulation of climate, ice sheets and co2 evolution during the last four glacial cycles with an earth system model of intermediate complexity. *Climate* **13**, 1695–1716 (2017).
27. Ganopolski, A., Winkelmann, R. & Schellnhuber, H. J. Critical insolation–$CO_2$ relation for diagnosing past and future glacial inception. *Nature* **529**, 200–203 (2016).
28. Soden, B. J. & Held, I. M. An assessment of climate feedbacks in coupled ocean–atmosphere models. *J. Clim.* **19**, 3354–3360 (2006).
29. Meehl, G. A. et al. Context for interpreting equilibrium climate sensitivity and transient climate response from the cmip6 earth system models. *Sci. Adv.* **6**, eaba1981 (2020).
30. Blackport, R. & Kushner, P. J. The transient and equilibrium climate response to rapid summertime sea ice loss in ccsm4. *J. Clim.* **29**, 401–417 (2016).
31. Bony, S. et al. How well do we understand and evaluate climate change feedback processes? *J. Clim.* **19**, 3445–3482 (2006).
32. Golledge, N. R. et al. Global environmental consequences of twenty-first-century ice-sheet melt. *Nature* **566**, 65–72 (2019).
33. Bronselaer, B. et al. Change in future climate due to antarctic meltwater. *Nature* **564**, 53–58 (2018).
34. Swingedouw, D. et al. Antarctic ice-sheet melting provides negative feedbacks on future climate warming. *Geophys. Res. Lett.* **35** https://doi.org/10.1029/2008GL034410 (2008).
35. Fichefet, T. et al. Implications of changes in freshwater flux from the greenland ice sheet for the climate of the 21st century. *Geophys. Res. Lett.* **30**, https://doi.org/10.1029/2003GL017826 (2003).
36. Pithan, F. & Mauritsen, T. Arctic amplification dominated by temperature feedbacks in contemporary climate models. *Nat. Geosci.* **7**, 181–184 (2014).
37. Screen, J. A. & Simmonds, I. The central role of diminishing sea ice in recent arctic temperature amplification. *Nature* **464**, 1334–1337 (2010).
38. Fischer, H. et al. Palaeoclimate constraints on the impact of 2 c anthropogenic warming and beyond. *Nat. Geosci.* **11**, 474 (2018).
39. Dutton, A. et al. Sea-level rise due to polar ice-sheet mass loss during past warm periods. *Science* **349**, aaa4019 (2015).
40. Lord, N. S. et al. Emulation of long-term changes in global climate: application to the late pliocene and future. *Climate* **13**, 1539–1571 (2017).
41. Lunt, D. J. et al. On the causes of mid-pliocene warmth and polar amplification. *Earth Planet. Sci. Lett.* **321**, 128–138 (2012).
42. Notz, D. & Stroeve, J. Observed arctic sea-ice loss directly follows anthropogenic $CO_2$ emission. *Science* **354**, 747–750 (2016).
43. Zelinka, M. D., Randall, D. A., Webb, M. J. & Klein, S. A. Clearing clouds of uncertainty. *Nat. Clim. Change* **7**, 674–678 (2017).
44. Hudson, S. R. Estimating the global radiative impact of the sea ice–albedo feedback in the arctic. *J. Geophys. Res.: Atmos.* **116**, https://doi.org/10.1029/2011JD015804 (2011).
45. Flanner, M. G., Shell, K. M., Barlage, M., Perovich, D. K. & Tschudi, M. Radiative forcing and albedo feedback from the northern hemisphere cryosphere between 1979 and 2008. *Nat. Geosci.* **4**, 151–155 (2011).
46. Goosse, H. et al. Quantifying climate feedbacks in polar regions. *Nat. Commun.* **9**, 1–13 (2018).
47. Stuecker, M. F. et al. Polar amplification dominated by local forcing and feedbacks. *Nat. Clim. Change* **8**, 1076–1081 (2018).
48. Joughin, I. & Alley, R. B. Stability of the west antarctic ice sheet in a warming world. *Nat. Geosci.* **4**, 506–513 (2011).
49. Joughin, I., Smith, B. E. & Medley, B. Marine ice sheet collapse potentially under way for the thwaites glacier basin, west antarctica. *Science* **344**, 735–738 (2014).
50. Pollard, D. & DeConto, R. M. Modelling west antarctic ice sheet growth and collapse through the past five million years. *Nature* **458**, 329–332 (2009).
51. Pollard, D. & DeConto, R. M. Hysteresis in cenozoic antarctic ice-sheet variations. *Glob. Planet. Change* **45**, 9–21 (2005).
52. Wielicki, B. A. et al. Clouds and the earth's radiant energy system (ceres): An earth observing system experiment. *Bull. Am. Meteorol. Soc.* **77**, 853–868 (1996).
53. Petoukhov, V. et al. EMIC Intercomparison Project (EMIP-$CO_2$): comparative analysis of emic simulations of climate, and of equilibrium and transient responses to atmospheric $CO_2$ doubling. *Clim. Dyn.* **25**, 363–385 (2005).
54. Zwally, H. J., Giovinetto, M. B., Beckley, M. A. & Saba, J. L. *Antarctic and Greenland Drainage Systems* (GSFC Cryospheric Sciences Laboratory, 2012).
55. RGI Consortium. Randolph Glacier Inventory—A Dataset of Global Glacier Outlines, Version 6.0: Technical Report, *Global Land Ice Measurements from Space*, Colorado, USA. Digital Media. https://doi.org/10.7265/N5-RGI-60 (2017).
56. Wetherald, R. & Manabe, S. Cloud feedback processes in a general circulation model. *J. Atmos. Sci.* **45**, 1397–1416 (1988).
57. von Deimling, T. S., Held, H., Ganopolski, A. & Rahmstorf, S. Climate sensitivity estimated from ensemble simulations of glacial climate. *Clim. Dyn.* **27**, 149–163 (2006).


## Acknowledgements

This work has been carried out within the framework of the IRTG 1740/TRP 2015/50122-0 funded by DFG and FAPESP. N.W. and R.W. acknowledge their support. M.W. acknowledges support from the BMBF through the project PalMod. J.F.D. is grateful for financial support by the Stordalen Foundation via the Planetary Boundary Research Network (PB.net), the Earth League's EarthDoc programme, and the European Research Council Advanced Grant project ERA (Earth Resilience in the Anthropocene; grant ERC-

2016-ADG-743080). We are thankful for support by the Leibniz Association (project DominoES). The authors gratefully acknowledge the European Regional Development Fund (ERDF), the German Federal Ministry of Education and Research and the Land Brandenburg for supporting this project by providing resources on the high performance computer system at the Potsdam Institute for Climate Impact Research.

## Author contributions

N.W., M.W., J.F.D. and R.W. designed the study and wrote the text including revisions. N.W. conducted the model simulation runs and prepared the figures. M.W. designed the model calibration and prepared CLIMBER-2 for simulations.

## Funding

Open Access funding enabled and organized by Projekt DEAL.

## Competing interests

The authors declare no competing interests.

## Additional information

**Supplementary information** is available for this paper at https://doi.org/10.1038/s41467-020-18934-3.

**Correspondence** and requests for materials should be addressed to N.W. or R.W.

**Peer review information** *Nature Communications* thanks Jan Sieber and the other, anonymous, reviewer(s) for their contribution to the peer review of this work. Peer reviewer reports are available.

# Supplementary Information

## Global warming due to loss of large ice masses and Arctic summer sea ice

Wunderling et al.

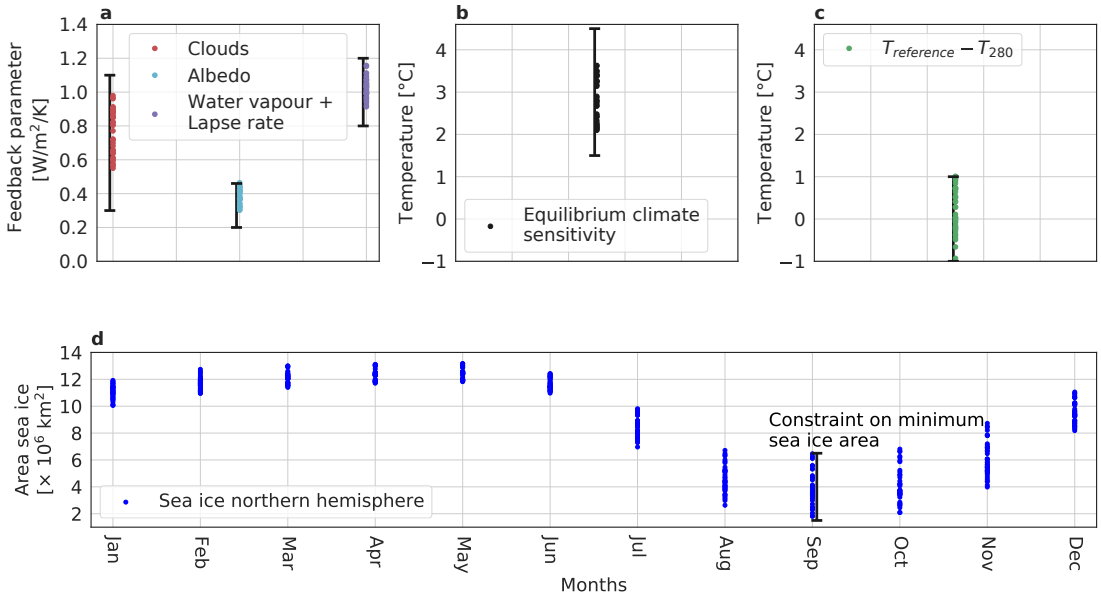


**Supplementary Figure 1 | CLIMBER-2-GCM calibration.** **a**, Calibration measurements for the cloud (red), the albedo (cyan) and the water vapour together with the lapse rate feedback (purple) constrained using the GCMs from Soden & Held(2006)[1]. The exact values that we constrained for are 0.8 – 1.2 W/m$^2$/K for the water vapour together with the lapse rate feedback, 0.3 – 1.1 W/m$^2$/K for the cloud feedback and 0.2 – 0.45 W/m$^2$/K for the albedo feedback. Note that not all climate feedbacks cover the whole range of possible limits shown as black errorbars[1,2]. **b**, An additional constraint due to the equilibrium climate sensitivity when $CO_2$ concentration is doubled (black) is applied. The equilibrium climate sensitivity is restricted to 1.5–4.5 °C. **c**, Another constraint (green) is applied for a reference run at a concentration of $p(CO_2) = 280$ ppm compared with a perturbed parameter run at the same $CO_2$ concentration. This results in: $|T_{\text{reference}} - T_{280}| \leqslant 1,0°\text{C}$. **d**, A final constraint is applied to the minimum sea ice area in the northern hemisphere which is supposed to be between $1.5{-}6.5{\times}10^6$ km$^2$. This constraint is applied to prevent too low sea ice areas at a $CO_2$ concentration of 280 ppm. For all the calibration runs, the parameters from supplementary Table 1 were varied.

| Parameter | Varied range (Mean) | Source |
|---|---|---|
| $\Gamma_0$: Temp. lapse rate parameter | $4.7 - 5.2$ (5.0) $\cdot 10^{-3}$ | Eq. 2[3] |
| $\Gamma_1$: Temp. lapse rate parameter | $3.6 - 4.4$ (4.0) $\cdot 10^{-5}$ | Eq. 2[3] |
| $\Gamma_2$: Temp. lapse rate parameter | $0.7 - 1.3$ (1.0) $\cdot 10^{-3}$ | Eq. 2[3] |
| $OD_1$: Cloud optical depth parameter | $9.5 - 10.5$ (10.0) | App. 7.3[4] |
| $OD_2$: Cloud optical depth parameter | $7.5 - 8.5$ (8.0) | App. 7.3[4] |
| $D(A_{CO21})$: Integral transmission of atm. | $0.3 - 0.65$ (0.5) | Eq. 3[3] |
| $c_1$: Cloudiness height parameter | $0.178 - 0.188$ (0.183) | Eq. 34[3] |
| $\alpha_{\text{snow}}$: Diffusive new snow albedo | $0.85 - 1.0$ (0.95) | Fig. 2[5] |

**Supplementary Table 1 | Parameters for calibration of CLIMBER-2.** Varied parameters in CLIMBER-2 in order to reconstruct GCM-uncertainty ranges of feedbacks[1]. Procedure of varying parameters similar to Deimling et al.(2006)[4].

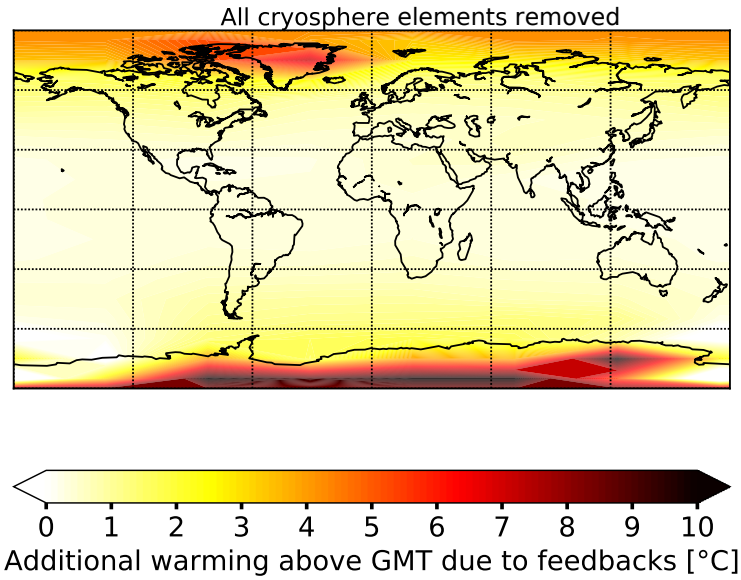


**Supplementary Figure 2 | Warming including the Antarctic Ice Sheet.** For a better comparability to literature[6,7], we ran a simulation, where we removed all the cryosphere elements: West Antarctica, Greenland, Arctic summer sea ice, mountain glaciers and East Antarctica. We find a strong warming in the proximity of the locations where ice is removed, which is in good agreement with literature, see also Fig. 4e in Lunt et al. (2012)[7]. However, both studies from the literature used an ice sheet reconstruction for the late Pliocene (PRISM), which includes the loss of most of Greenland and West Antarctica, but also of substantial parts of East Antarctica. With these prescribed ice sheets Lunt et al. (2012)[7] found a global warming of 0.7 °C, where we find 0.2 °C, but the discrepancy comes mainly from East Antarctica, which is still intact in our simulations in the main manuscript (see Fig. 1). With the additional removal of the East Antarctic Ice Sheet at a $CO_2$ concentration of 280 ppm, we find an additional warming of 0.82 °C.

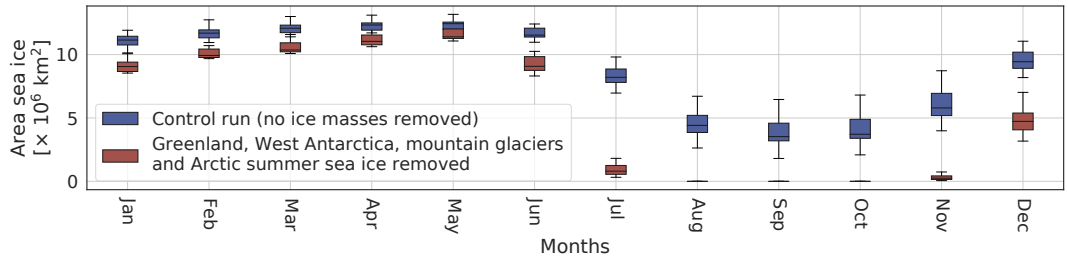


**Supplementary Figure 3 | Sea ice area in the northern hemisphere.** Loss of sea ice in the control (intact cryosphere components) and perturbed run for a $CO_2$ concentration of 280 ppm over the course of one year. In the perturbed run Greenland, West Antarctica, the mountain glaciers were removed and the albedo area of the Arctic summer sea ice was replaced by the ocean albedo during June, July and August. The main values indicate the median of the ensemble, the boxes show the interquartile range and the error bars depict the full ensemble spread.

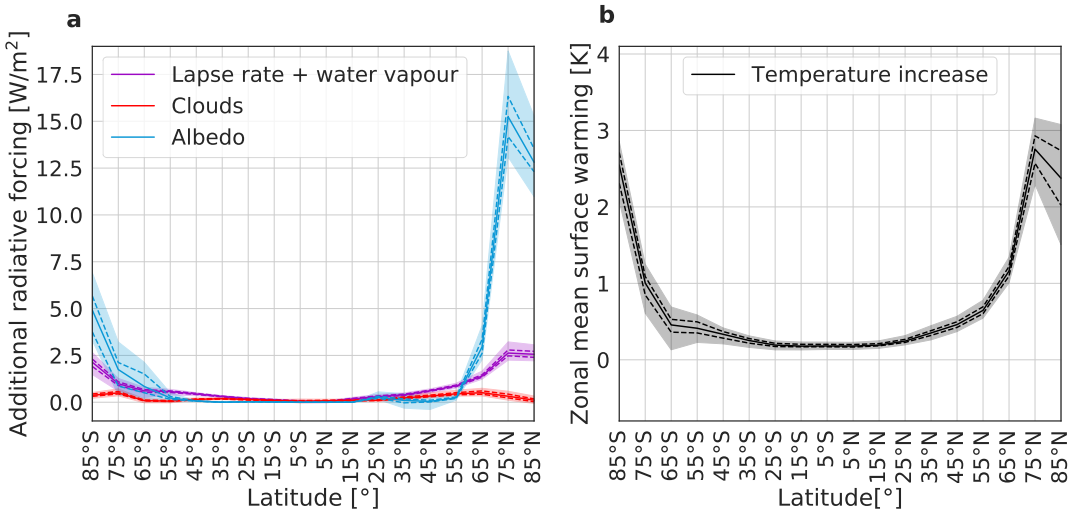


**Supplementary Figure 4 | Zonal distribution of additional radiative perturbation and surface warming. a**, Contributions from different causes of additional radiative perturbation, where we compare the perturbed run (without cryosphere elements) with the control run (with cryosphere elements) for all 39 runs at a $CO_2$ concentration of 400 ppm. The additional radiative perturbation is strongest in the polar regions. **b**, Zonal mean surface warming over latitude with a strong warming in polar regions. The errors are given as the full ensemble spread in shaded colours, the straight line denotes the median of the ensemble and the dashed lines show the interquartile range.

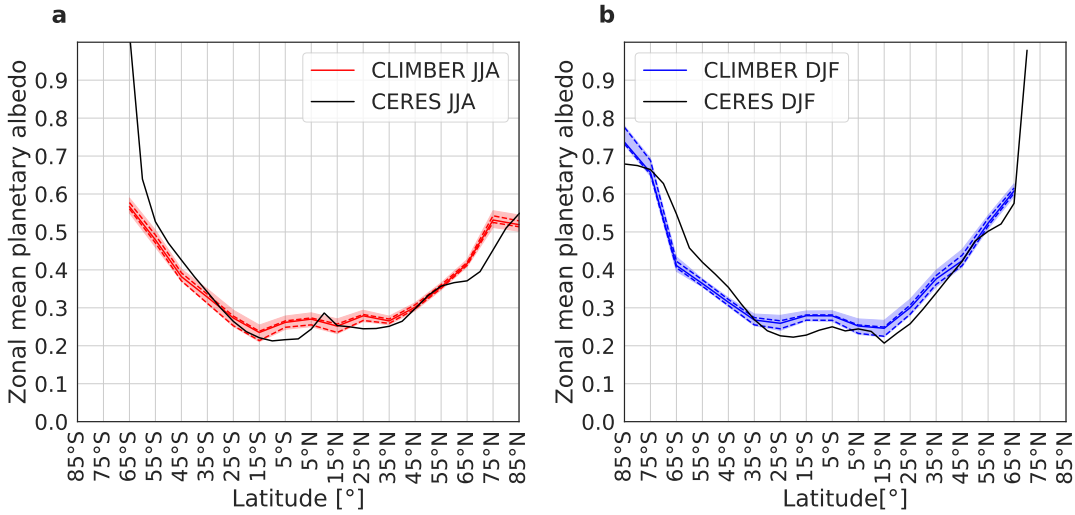


**Supplementary Figure 5 | Comparison of zonal mean of planetary albedo between CERES and CLIMBER-2.** Planetary albedo in CLIMBER-2 and CERES data[8] are in good agreement, **a,** for the months JJA and **b,** for the months DJF. The CLIMBER-2 data is shown as the full ensemble spread, where the straight line indicates the median of the ensemble, the dashed line the interquartile range and the shaded area the full ensemble spread. The data is cut at 65 °S during JJA since no planetary albedo values are available at this time due to the Antarctic night. The CERES data deviates at this edge from the CLIMBER data due to the observational sparse data close to the Antarctic night region. For the same reason, the data is cut due to the Arctic night in panel **b**.

## Supplementary References


1. Soden, B. J. & Held, I. M. An assessment of climate feedbacks in coupled ocean–atmosphere models. *Journal of climate* **19**, 3354–3360 (2006).

2. Stocker, T. F. *et al.* Climate change 2013: The physical science basis. *Contribution of working group I to the fifth assessment report of the intergovernmental panel on climate change* **1535** (2013).

3. Petoukhov, V. *et al.* Climber-2: a climate system model of intermediate complexity. part i: model description and performance for present climate. *Climate dynamics* **16**, 1–17 (2000).

4. von Deimling, T. S., Held, H., Ganopolski, A. & Rahmstorf, S. Climate sensitivity estimated from ensemble simulations of glacial climate. *Climate Dynamics* **27**, 149–163 (2006).

5. Rösel, A., Kaleschke, L. & Birnbaum, G. Melt ponds on arctic sea ice determined from modis satellite data using an artificial neural network. *The cryosphere* **6**, 431–446 (2012).

6. Lord, N. S. *et al.* Emulation of long-term changes in global climate: application to the late pliocene and future. *Climate of the Past* **13**, 1539–1571 (2017).

7. Lunt, D. J. *et al.* On the causes of mid-pliocene warmth and polar amplification. *Earth and Planetary Science Letters* **321**, 128–138 (2012).

8. Wielicki, B. A. *et al.* Clouds and the earth's radiant energy system (ceres): An earth observing system experiment. *Bulletin of the American Meteorological Society* **77**, 853–868 (1996).

# 2.5 Network dynamics of drought-induced tipping cascades in the Amazon rainforest [P5]

**Authors**
Nico Wunderling, Arie Staal, Boris Sakschewski, Marina Hirota, Obbe A. Tuinenburg, Jonathan F. Donges, Henrique M.J. Barbosa, Ricarda Winkelmann

**Status**
To be Resubmitted (December 2020), pre-print available under the doi: 10.21203/rs.3.rs-71039/v1

**Short summary**
This work deals with the vulnerabilities of the Amazon rainforest to tipping and subsequent cascading failure. It is assessed how future extreme climates might impact the stability of the Amazon rainforest with respect to the mean annual precipitation and the mean cumulative water deficit as critical parameters and an Amazon rainforest that is adapted to its past climatic conditions. Despite this adaptation, it has been observed that increased patterns of tipping have to be expected at high drought severities, representing a scenario where the adaptive capacity would be outpaced by the speed of climatic change. At the same time, additional effects from cascading transitions through the atmospheric moisture recycling network adversely affect the rainforest under such harsh drought conditions. The most vulnerable region lies in the south-east Amazon basin. This is a region that already nowadays suffers most from anthropogenic land-use change such as deforestation, extensive agricultural use and infrastructure projects.

**Author contributions**
Nico Wunderling, Jonathan Donges, Henrique Barbosa and Ricarda Winkelmann designed the study. Nico Wunderling conducted the model simulation runs and prepared the figures. Nico Wunderling and Arie Staal led the writing of the manuscript with input from all authors. Arie Staal and Obbe Tuinenburg developed the moisture recycling dataset of the Amazon rainforest. Henrique Barbosa and Ricarda Winkelmann jointly supervised this study.

# Network dynamics of drought-induced tipping cascades in the Amazon rainforest

Nico Wunderling,[1,2,3*] Arie Staal,[4,5] Boris Sakschewski,[1]
Marina Hirota,[6,7] Obbe A. Tuinenburg,[4,5] Jonathan F. Donges[1,4],
Henrique M. J. Barbosa[8,9*†] & Ricarda Winkelmann[1,2*†]

[1]Earth System Analysis, Potsdam Institute for Climate Impact Research (PIK), Member of the Leibniz Association, 14473 Potsdam, Germany
[2]Institute of Physics and Astronomy, University of Potsdam, 14476 Potsdam, Germany
[3]Department of Physics, Humboldt University of Berlin, 12489 Berlin, Germany
[4]Stockholm Resilience Centre, Stockholm University, Stockholm, SE-10691, Sweden
[5]Department of Environmental Science, Copernicus Institute of Sustainable Development, Utrecht University, Utrecht, 3512 JE, The Netherlands
[6]Department of Physics, Federal University of Santa Catarina, Florianópolis, 88040-900-SC, Brazil
[7]Department of Plant Biology, University of Campinas, Campinas, 13083-970-SP, Brazil
[8]Instituto de Física, Universidade de São Paulo, São Paulo, 05508-090-SP, Brazil
[9]Physics Department, University of Maryland Baltimore County, Baltimore, MD 21250, USA

*Correspondences should be addressed to: nico.wunderling@pik-potsdam.de, hbarbosa@if.usp.br or ricarda.winkelmann@pik-potsdam.de
†These authors jointly supervised this study.

**Tipping elements are nonlinear subsystems of the Earth system that can potentially abruptly and irreversibly shift if environmental change occurs. Among these tipping elements is the Amazon rainforest, which is threatened by anthropogenic activities and increasingly frequent droughts. Here, we assess how extreme deviations from climatological rainfall regimes may cause local forest-savanna transitions that cascade through the coupled forest-climate system. We develop a dynamical network model to uncover the role of atmospheric moisture recycling in such tipping cascades. We account for the heterogeneity in critical thresholds of the forest caused by adaptation to local climatic conditions. Our results reveal that, despite this adaptation, increased dry-season intensity may trigger tipping events particularly in the southeastern Amazon. Moisture recycling is responsible for one-fourth of the tipping events. If the rate of climate change exceeds the adaptive capacity of some parts of the forest, secondary effects through moisture recycling may exceed this capacity in other regions, increasing the overall risk of tipping across the Amazon rainforest.**

The Amazon rainforest is the most biodiverse terrestrial ecosystem and plays a fundamental role in regulating the global climate[1,2,3]. However, human-induced impacts and climatic extremes are increasingly threatening the forest's integrity and the services it provides[4,5,6]. Furthermore, changes might not be gradual, but could be rather abrupt due to nonlinear interactions, as suggested by simulation studies[7,8], data-based approaches[9,10], conceptual models[11,12] and long-term experiments[13]. Parts of the Amazon rainforest may be bistable, meaning that they could tip to an alternative state of low tree cover[9,10]. Indeed, the Amazon has been suggested to be a tipping element in the Earth system[14] and might be at risk of approaching or exceeding its tipping point[4,15,16]. This tipping point can be crossed when the conditions become too dry. Potentially, this could occur due to declining average precipitation levels or with increasing dry spells and severity of extreme droughts[17,18,19,20]. Changes in precipitation regimes are already occurring over southern Amazonian regions where the length of the dry season has been increasing by 1 month since the middle of the 1970's[19,21]. A lengthening and strengthening of the dry season in southern Amazonia has also been confirmed by other model studies from CMIP5 simulations as well as empirical precipitation models[22,23]. In regions where dry periods last longer than four months, this would severely impact vital functions of the Amazon rainforest[4,22].

The Amazon is not a uniform forest as trees can adapt to local climatic conditions, for instance through variable rooting strategies[24,25]. This can lead to different absolute forest mortality thresholds with respect to precipitation and drought conditions on local to regional scales. Forest adaptation can therefore ensure that plants will operate close to their physiological maximum, but this creates vulnerabilities when the climate changes faster than the ecosystem can respond to[26]. In case of this inadequate response, regional climatic changes can be accelerated by the forest itself, because trees contribute to precipitation regionally.

Trees recycle part of the precipitated moisture through continental moisture recycling[27,28]. They do so by extracting water from deeper soil levels and releasing it through their leaves (transpiration) and by directly re-evaporating precipitation from their leaves (interception evaporation). The total amount of moisture recycling accounts for up to half of the precipitation over the Amazon basin and moisture is recycled up to six times[28,29,30,31]. Thus, the rainforest depends on itself, and precipitation and evapotranspiration cycles promote cascading forest growth[29]. The positive interplay between the forest and regional precipitation implies that local perturbations can propagate through the system via reduced moisture recycling. In other words, the Amazon rainforest can be considered a network of local tipping elements that are connected via moisture recycling.

The loss of the moisture flows among different parts of the Amazon as a result of state transitions can increase vulnerabilities remotely and exacerbate tipping events since the forest would then no longer be adapted to the prevailing conditions[32,33]. Recent severe droughts such as in 2005 and 2010 already impacted the rainforest[34,35], but without causing major state transitions of vegetation cover. While the rainforest might be able to withstand incidental droughts, the adaptations may become insufficient when such droughts become the new climate normal. Indeed, it has been projected that the major drought event of 2005 might occur more frequently, up to nine out of ten years by 2060[36,37]. By reconstructing the dynamical moisture recycling networks from the recent past, we can study how climate change may exceed the adaptation capacity of the forest and subsequently trigger tipping points that cascade through the Amazon rainforest system.

Here, we integrate for the first time in a dynamical network model the tipping behaviour of

the Amazon forest, atmospheric moisture flows from evapotranspiration to precipitation and the adaptation of the forest to annual precipitation and droughts (Fig. 1). Specifically, we combine a dynamical system model to represent empirically obtained forest tipping points with regard to mean annual precipitation (MAP) and drought intensity (MCWD: Maximum Cumulative Water Deficit). We assume that the forest is adapted to its local values of MAP and MCWD over 30 years. To account for possible spatial variability in the adaptation levels, we construct an ensemble of size 100 for each investigated year. We construct this moisture recycling network using output from Lagrangian atmospheric moisture tracking simulations and a global hydrological model (see methods)[29,30,38].

We simulate a range of different future conditions, imposing average climatic conditions that resemble the conditions observed in each year from 2004 to 2014, during which the Amazon experienced two "droughts of a century" (2005 & 2010)[39]. We analyse Amazon rainforest cells as local-scale tipping elements of the moisture recycling network on a resolution of $1^{\circ}$x$1^{\circ}$ to assess their impact on the Amazon-wide system stability. Using this approach, we provide a bottom-up quantification of Amazon system stability, aiming to reveal where cascading effects of moisture recycling have the potential to induce domino effects in forest cover loss.

## Results

**Tipping due to drier conditions.** To investigate a range of drought intensities and precipitation anomalies, we study the extent of the tipped area with respect to $\mathcal{Z}$-scores, which represent how many standard deviations the conditions are away from the mean across 1974-2003. We find a close correlation between $\mathcal{Z}_{\mathrm{MCWD}}$ and the tipped area, where a higher index reflects a larger tipped area (see Fig. 2a). The years 2005, 2007 and 2010, which are the years with the largest ENSO ONI indices[40], show the largest tipped area. Overall, we find that the number of tipped

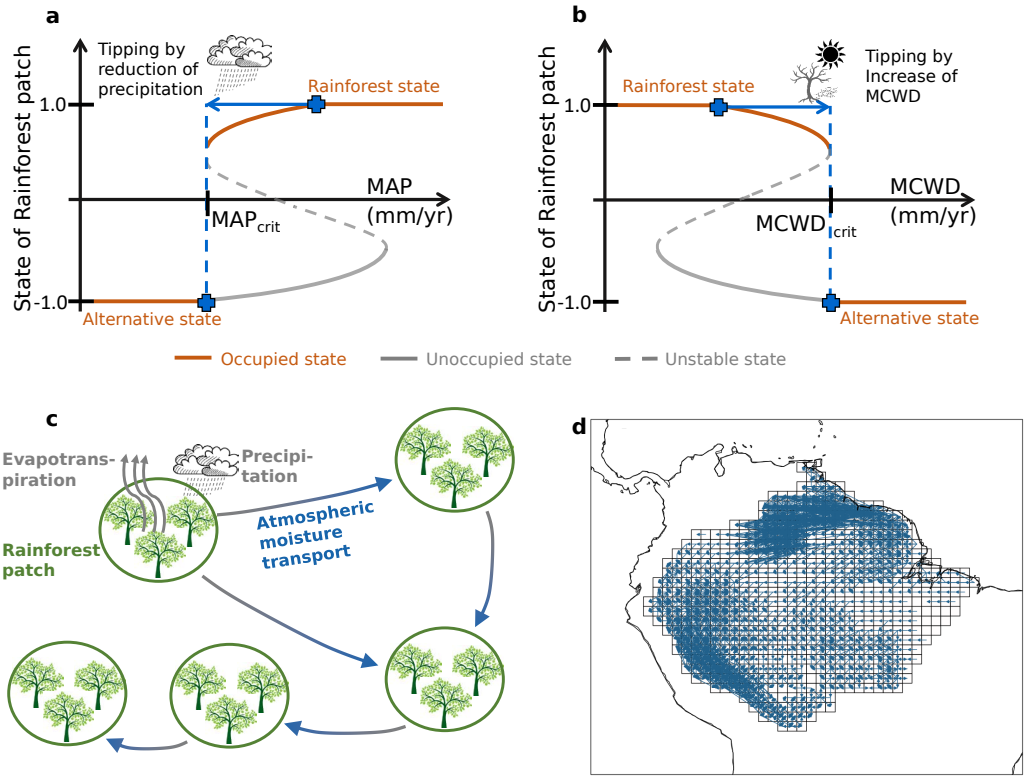


**Figure 1 | Nonlinear effects and moisture recycling network in the Amazon rainforest. a,** Dynamical property of each 1°x1° cell of the rainforest depicted as state of rainforest cell (forest cover) versus MAP value. The state of the rainforest is limited by full forest cover (1.0) and no forest cover (-1.0). Between these two stable states, there is a tipping process as soon as the MAP value has fallen below its adaptation specific $MAP_{crit}$ value. Since we are focussing on drought triggered tipping events from forest to non-forest states in this study, each cell can only exist on the occupied states (brown), but not on the unoccupied states (grey). The blue arrow depicts a potential reduction in precipitation that is sufficient to trigger a tipping event in this specific cell. **b,** Same as in **a** for MCWD. **c,** Exemplary moisture recycling network: the rainforest cells are interconnected via a moisture recycling network due to precipitation and evapotranspiration. Through this mechanism effects of reduced tree cover can be promoted and tipping cascades are possible. **d,** Moisture recycling network for the hydrological year 2014 thresholded for links above 10 mm/yr to remain visibility. In the simulation results, links above 1 mm/yr are used. The dominant flow direction comes from the Atlantic ocean through easterly winds, reaches the Andes, and is then bend southward along the Andes. Moisture recycling links based on separate months can be found in Supplementary Figs. 1 and 2 comparing the year 2014 with the extreme drought year 2010.

cells is significantly higher for the years 2005 and 2010 than for the other years (see Fig. 2a). Both droughts have been termed a "once in a century drought"[41]. 2010 shows the highest vulnerability pattern, despite a lower $\mathcal{Z}_{\mathrm{MCWD}}$ index than for 2005. The reason might be that the 2010 drought was spatially more extensive than the one in 2005. In 2010, $3.0\times10^6$ km$^2$ versus $1.9\times10^6$ km$^2$ in 2005 showed rainfall anomalies of one standard deviation less than during the decadal climatological mean[35]. From a tipping point of view, 2010 causes the highest vulnerabilities, whereas 2005 is the most extreme year from a rainfall (from oceanic background) perspective within our study period[29]. This suggests that the drought anomaly pattern is more important for the stability of the rainforest than the extremity of moisture inflow itself.

We separate tipping events into primarily induced tipping events from MAP or MCWD and secondary events from network effects (tipping cascades). Our model shows that between 10% and 60% of the tipping is due to the cascading effects from the moisture recycling network depending on the drought strength (see network effects in Fig. 2b). The cascading effect is especially strong for the years that show the strongest drought signatures (2005, 2007 & 2010). This is probably due to the fact that many cells are shifted towards their tipping point and some of them over it. Then, in succession of this tipping and the subsequent further reduction of the moisture transport, many more cells in these years transgress their calculated threshold. In turn, if droughts intensify in the future, cascading tipping may increase disproportionally.

We also compared these results with the results of an only MAP-based normalised drought index $\mathcal{Z}_{\mathrm{MAP}}$ analogous to Eq. 2, but find no correlation between the tipped area and the MAP based index (see Supplementary Fig. 3).

**Vulnerability maps.** Over the course of the evaluated time span from 2004−2014, one region

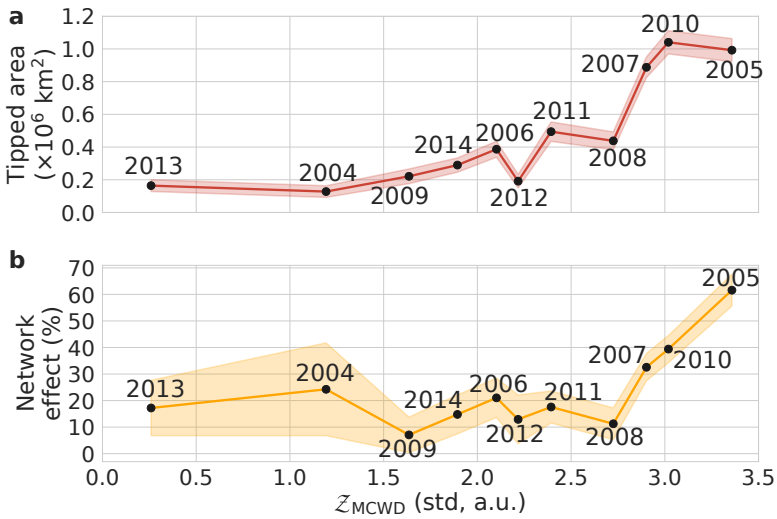


**Figure 2 | Vulnerability of the rainforest against MCWD-based drought intensity. a,** The total tipped area is shown over the course of the normalised drought index based on the MCWD $\mathcal{Z}$-score. The tipped area represents the number of tipped cells in the model where each $1^{\circ}$x$1^{\circ}$ cell has an area of approximately $\left(111\ \mathrm{km}^2\right)$. **b,** The additional tipped area due to network effects for each year is shown in percentage of the tipped area in panel **a**. This shows the effects of cascading transitions which are on the order of 10% to 60% depending on the evaluated hydrological year. The same analysis has been performed for a MAP based index, but no correlation was found (see Supplementary Fig. 3).

shows increased patterns of vulnerability (see likelihood of vulnerability in Fig. 3a). This region is located in the southeastern Amazon, and caused by the combination of MCWD anomalies and network effects. As expected from Fig 2, the likelihood of the vulnerability patterns varies strongly from year to year (see Supplementary Fig. 4), but the vulnerable region in the southeast is a recurrent phenomenon across all years.

We investigate the vulnerable regions in detail since, in our model, small changes in the state already have an impact on the moisture recycling network, even though the respective cell does not tip. This can be realised if the environmental conditions shift a rainforest cell in our model close, but not over, its tipping point. Therefore, we define a shift towards the tipping point without an actual tipping event as the *closeness to tipping*. We find that this closeness to tipping is high in the southeast of the Amazon basin and in the subsequent dominant downwind direction towards the Andes. The largest average shifts towards the tipping point are located around and close to the most endangered region in the southeast (see Fig. 3). The reason is that these cells are already tipped in most cases and do not contribute to the average closeness to tipping (see Fig. 4a), but that is expressed by the high variability among the ensemble members (see southeastern region in Fig. 4b).

Although tipping points are thresholds by definition, the effects on the Amazon forest-rainfall system already occur before MCWD or MAP reaches that point. Droughts, even if these do not cause tipping of the forest, can have significant impacts on photosynthesis and evapotranspiration that may last for years[42,43]. A threshold-only model cannot account for these effects. In our model, however, evapotranspiration scales with distance to the tipping point. In other words, when a forest becomes drier it generates less evapotranspiration, an effect that may cascade through the system. Thus, even though our approach is conceptual, it allows us to identify which areas are most vulnerable to the *invisible* effect of the moisture recycling network. The magnitude of this effect is on the order of 20% for many regions apart from the central Amazon

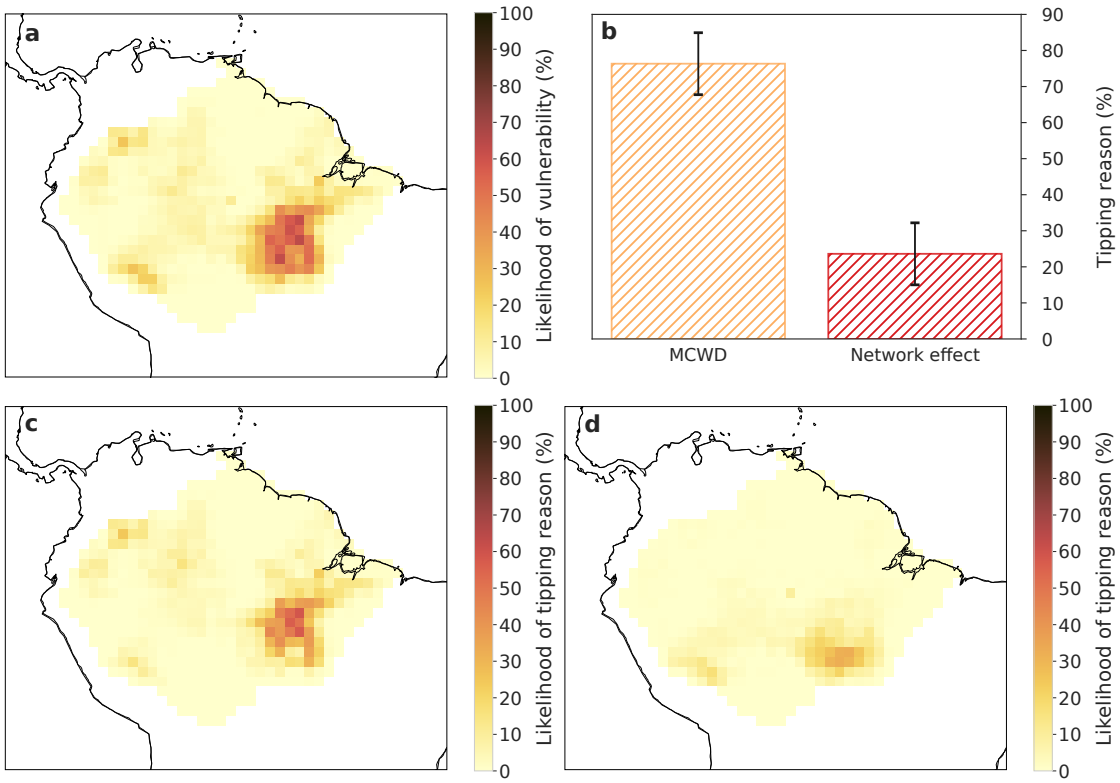


**Figure 3 | Vulnerable regions and tipping reason. a,** The likelihood of tipping as an average over all ensemble members and all evaluated years from the hydrological years 2004 to 2014. The southeastern region is more vulnerable than other regions. In Supplementary Fig. 4, the yearly resolution results? can be found. **b,** Overall tipping reason averaged over the entire Amazon basin with error bars as the standard deviation over all years and all 100 ensemble members. A version separated into the future drought conditions from 2004 to 2014 can be found in Supplementary Fig. 5 for all these potential future drought scenarios. MAP does not contribute to tipping events (probability is less than 0.1%) and is thus omitted from this figure. **c,** Tipping reason map: MCWD, **d,** Tipping reason map: Network (Cascading effects of the moisture recycling network). Note that panel **a** is the sum of the panels **c** and **d**.

and a small region in the very south of the Amazon. This represents an average evapotranspiration decrease of approximately 10% due to a shift towards the tipping point in the southeastern Amazon region (see Fig. 4a).

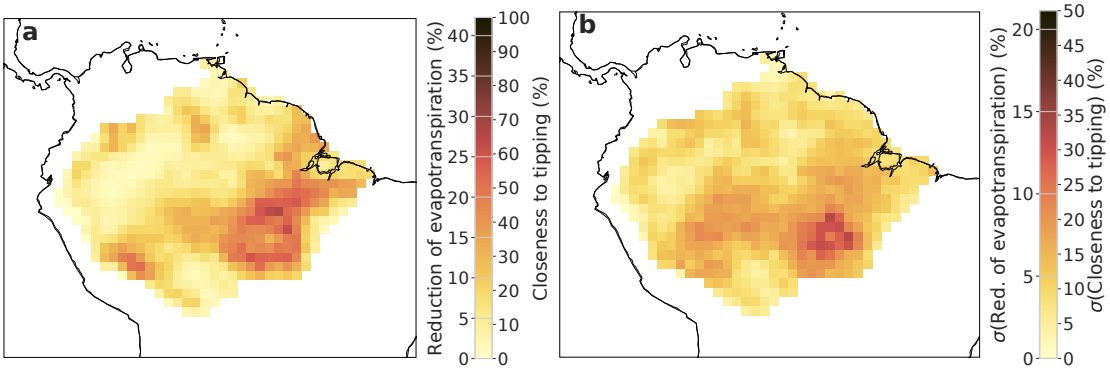


**Figure 4 | Average shift towards the tipping point (*Closeness to tipping*). a,** Mean shift to the tipping point as an average over all ensemble members. It can be seen that the shift is larger southern part of the Amazon rainforest such that these regions are the most vulnerable ones. **b,** Standard deviation of **a** over all ensemble members. Note that cells are only accounted for if and only if the cell is not in the tipped regime in the respective simulation run. A second colour bar indicates the reduction of evapotranspiration due to changes in the state on average (panel **a**) together with its standard deviation (panel **b**). A version separated into the future conditions from 2004-2014 can be found in Supplementary Fig. 6.

**The tipping reason and cascading effects.** We reveal that, over the whole set of drought conditions, the direct effect of MCWD-induced tipping is prevalent (76.3±8.5%) over the 23.6±8.5% that are due to cascading failure (see Fig. 3b). Moreover, transitions of the forest due to MAP as a primary reason are nearly completely negligible, they are responsible for less than 0.1% of all tipping events. On the other hand, the effect of cascading failure is considerably affecting the Amazon of up to a one-fourth of cells that tip additionally, on average, with large spread from year to year over the study period (see Supplementary Fig. 5).

The network effects are especially strong close to the region of direct MCWD-induced tipping

and downwind from that (Fig. 3c, d). MCWD is the most important reason for tipping events in the southeast, whereas MAP is not responsible for many tipping events (see Fig. 3a, b). Overall, the region in the southeast is vulnerable with respect to MCWD since this region has a relatively low interannual variability (standard deviation) of MCWD, while the intra-annual variability (mean) MCWD value is high (see Supplementary Fig. 7c, d).

## Discussion

We estimate that tipping cascades may be responsible for around a one-fourth (23.6±8.5%) of the tipping events in the Amazon rainforest following droughts. These cascades occur even when the forest is adapted to local climatic conditions. The reason is that drying is amplified by the moisture losses that result from such tipping. Loss of forest cover causes a reduction in evapotranspiration, which affects precipitation levels regionally. By constructing a dynamical network of forest cells connected by forest-induced moisture flows estimated from detailed atmospheric moisture flow simulations, we reveal how and where the Amazon is vulnerable to tipping cascade effects. Tipping due to fluctuating dry-season intensity (as measured by MCWD) is the dominant primary tipping reason (76.3±8.5%) compared to fluctuations in annual rainfall. With a potential increase of future extreme drought events[36,37,44], the average regional climate will be drier and some parts of the rainforest might thus be set under imminent risk of instability and could transgress into a less or non forest-covered state. We uncover that tipping events occur most frequently in southeastern Amazon (Fig. 3). This is also the region that is affected by three other factors. First, extended tipping cascades can be expected due to local interaction structures and reduced downwind moisture transport (Figs. 3 and 4). Second, it is also one of the regions located along the "arc of deforestation" and therefore already suffers from the pressure of human-induced activities, such as deforestation, ranching and extensive agriculture[45,46]. And third, this region as well as the whole Amazon rainforest is threatened by

road infrastructure projects[47,48,49] and lack of environmental policies[50,51].

In our study, we also find that potential future extreme drought conditions with a higher MCWD anomalies show a considerably larger tipped area. Cascading tipping events are more pronounced under these circumstances (Fig. 2). These are the drought conditions that can be expected from mid-century onwards if climate change progresses in a business-as-usual scenario[37]. The highest tipping signal in our model coincides with the strongest El-Niño ONI indices during the period 2004-2014[41]. It is known from the literature that El-Niño related droughts and other variability patterns affect the stability of the rainforest and tropical vegetation[18,52,53]. If the anomalies associated El-Niño events intensify as projected by CMIP (Coupled Model Intercomparison Project) simulations and perturbed physics models[54,55,56], this would endanger substantial portions of the Amazon basin[57]. However, uncertainties remain whether strong El-Niño events might become more frequent in the future climate[58].

Further human-induced changes such as deforestation also affect the evapotranspiration negatively which might then increase the frequency and severity of droughts together with ongoing climate change[30,33,59,60]. Overall, our results emphasise the relevance of the atmospheric moisture recycling network as an ecosystem service whose (partial) breakdown, combined with an increased number of climate-change induced extreme droughts, could trigger substantial changes across the Amazon basin.

Furthermore, moisture export supplies systems that are thousands of kilometres away, implying that forest-induced moisture export is an ecological service for regions beyond the Amazon rainforest itself. Altogether, preserving the Amazon and its ecological services are of utmost importance for local, regional and global climate stability.

## Methods

**Data.** The network was constructed using atmospheric moisture tracking simulations by Staal et al. (2018)[29]. In that study, tree transpiration across South America during 2003-2014 was estimated and its atmospheric trajectories subsequently simulated using a Lagrangian atmospheric moisture tracking model with simulation time steps of 0.25 hours. The model output is on a monthly basis on 0.25° resolution. Here, we reconstructed those simulation results by taking the moisture recycling ratios between 0.25° grid cells, building monthly networks of moisture flows between each pair of cells of a certain resolution for the Amazon region and aggregating them to $1^\circ \times 1^\circ$ grid cells. In addition to tree transpiration, we also included interception evaporation from tree canopies, taken from Staal et al. (2020)[30]. We thus obtained temporally varying monthly networks of forest-induced moisture flows across the Amazon. For details on the Lagrangian moisture tracking scheme, we refer to Staal et al. (2018)[29].

Monthly precipitation and evapotranspiration data for 2003-2014 on 0.25° resolution were taken from the Global Land Data Assimilation System (GLDAS) version 2.1[61]. For 1974-2003 we used GLDAS2.0 since GLDAS2.1 data does not go back until 1974.

Note that all our simulations are based on hydrological years instead of calendar years due to the hydrological cycle over the Amazon basin.

**Computation of MAP and MCWD.** The mean annual precipitation (MAP) is derived from the monthly precipitation values for each cell. The MCWD index is here defined as the absolute value of the most negative value of cumulative water deficit (CWD) reached over a hydrological year

$$\begin{aligned} \mathrm{CWD}_k &= \mathrm{CWD}_{k-1} + \mathrm{Precipitation}_k - \mathrm{Evaporation}_k \\ \max\left(\mathrm{CWD}_k\right) &= 0 \\ \mathrm{MCWD} &= \mathrm{abs}\left(\min\left\{\mathrm{CWD}_k, \mathrm{CWD}_{k+1}, ..., \mathrm{CWD}_{k+12}\right\}\right), \end{aligned} \tag{1}$$

where $k$ is the number of the month in the hydrological year. We make use of the actual measured regional evaporation values, whereas other studies have chosen a fixed evaporation value of 100 mm in each month to compute MCWD[5,35]. We also resimulated all results with a fixed evaporation of 100 mm/month and find that this leads to a decreased tipping due to MCWD. Thus, the southeastern region is less vulnerable to tipping, but the qualitative results are in agreement (see Supplementary Figs. 10d and 12.).

**Computation of the $\mathcal{Z}$-score** The $\mathcal{Z}$-score is used to find the ranges of future conditions that we are simulating in this work. We simulate ranges from current conditions up to extreme droughts that are 3.5 standard deviations away from the mean (see Fig. 2). The MCWD based $\mathcal{Z}$-score is computed by

$$\mathcal{Z}_{\mathrm{MCWD}} = \frac{\mathrm{MCWD(year)} - \mu_{\mathrm{MCWD}}}{\sigma_{\mathrm{MCWD}}}. \tag{2}$$

Here, $\mu_{\mathrm{MCWD}}$ and $\sigma_{\mathrm{MCWD}}$ are the average and standard deviation of the calibration period from 1974-2003. MCWD(year) is the average MCWD of the specific investigated year (see methods: Computation of MAP and MCWD). For comparison, the $\mathcal{Z}$-score based on MAP is computed (see Eq. 3) and plotted for comparison, but there is no relationship between tipped area and a higher MAP based score visible (see Supplementary Fig. 3):

$$\mathcal{Z}_{\mathrm{MAP}} = \frac{\mathrm{MAP(year)} - \mu_{\mathrm{MAP}}}{\sigma_{\mathrm{MAP}}}. \tag{3}$$

**Adaptation and computation of critical thresholds.** For the purpose of computing local adaptation values, we use a calibration dataset from GLDAS from the hydrological years 1974 to 2003. From there, we compute the 30-year long term mean of MAP and MCWD values together with their standard deviations (see Supplementary Fig. 7). The critical value for MAP and MCWD where a state transition occurs is then computed for each grid cell $i$ as

$$\begin{aligned} \mathrm{MAP}_{\mathrm{crit},i} &= \mu_{\mathrm{MAP},i} - \alpha_i \cdot \sigma_{\mathrm{MAP},i} \\ \mathrm{MCWD}_{\mathrm{crit},i} &= \mu_{\mathrm{MCWD},i} + \alpha_i \cdot \sigma_{\mathrm{MCWD},i}. \end{aligned} \tag{4}$$

$\mu_i$ is the mean, $\sigma_i$ the standard deviation of cell $i$ and $\alpha_i$ an adaptation factor that determines the exact value of the tipping point.

This procedure leads to the effect that regions with a high MAP as for instance in the central Amazon region can only be sustained at higher MAP values compared to other, typically drier regions as for instance in the south of the Amazon basin or close to the Andes region. The same arguments are valid for MCWD, with regional differences to MAP. Furthermore, higher variability, i.e., a higher standard deviation, in a region leads to higher adaptation percentage wise (*training effect*). In contrast to potential landscape methods as used in earlier studies[17,32], this procedure has the advantage that it is able to specifically assess sustained periods of changing MAP and MCWD conditions on a local scale.

*Dependence on adaption values.* With our setting, we can now compute what would happen under sustained conditions that resembles the yearly conditions observed in a particular hydrological year of our study period from 2004 to 2014. In our experiments, we assume that each cell starts with full forest cover (state = 1.0) at $t = 0$. If we are taking, for instance the precipitation, evaporation and moisture recycling network of a certain year, then we will find some cells that are unstable since their MAP or, mostly, their MCWD value is below the critical value which is defined with the timeseries from 1974-2003 (see Supplementary Fig. 8). If this

is the case, this cell transgresses its threshold and becomes forest cover free which then leads to reduced moisture recycling since the moisture transport value is multiplied by the fraction of forest cover. This means that the moisture transport value is set to zero when a forested cell tipped. This can then drive further cells towards or across their tipping point such that cascading events can be expected. In case a cell is only driven towards, but not over its tipping point, the effects on moisture recycling and tree cover are still accounted for assuming that the response of the vegetation is linearly represented by the state, instead of this effect being zero as in threshold-only models[32].

The critical values depend on the level of local adaptation $\alpha_i$ (see Eq. 4). Thus, it can be expected that a higher adaptation factor leads to a lower number of tipped rainforest cells. In a calibration experiment for adaptation factors between 1.0 and 3.0 standard deviations and a constant adaptation factor for all cells $i$ ($\alpha_i = \alpha \ \forall i$), we find that the tipped area indeed goes down with increased adaptation factors (see Supplementary Fig. 9). The difference between experiments where we allow cascading effect (blue) and do not (red) is shown in green. In reality, the true value of adaptation of a certain cell is unknown and might vary from location to location. That is why a new ensemble of simulations with increased robustness is required and the constant adaptation factor hypothesis ($\alpha = \alpha_i \ \forall i$) is dropped in favour of an ensemble approach where $\alpha_i$ is varied locally. Thus, we create an ensemble of 100 members for each year in the study period.

**Construction of ensemble.** Eq. 4 determines the critical values for MAP and MCWD for each $1^\circ$x$1^\circ$ cell separately. The critical value is dependent on the local average value as well as the variability of the 30 years before the study period (GLDAS data from 1974-2003). The exact critical value is determined by the adaptation factor $\alpha$ and must in turn be chosen appropriately. Therefore, we assume that a cell is on average able to remain in the same state under MAP

and MCWD conditions that are two standard deviations away from their mean, i.e., from their "experiences" during the last 30 years. However, the exact value of adaptation is uncertain and might be different in different regions, also due to several factors that we do not model explicitly in this work. But we take this into account by drawing the individual adaptation values $\alpha_i$ for each cell $i$ from a $\beta$-distribution that is centred at 2 standard deviations and ranges from 1 to 3 standard deviations

$$\beta\left(x, a, b\right) = \left(\sigma_{\text{upper}} - \sigma_{\text{lower}}\right) \cdot \frac{x^{a-1}(1-x)^{b-1}}{\int_0^1 t^{a-1}(t-1)^{b-1} dt} + \sigma_{\text{lower}}. \tag{5}$$

Here, we use $\sigma_{\text{upper}} = 3.0$ and $\sigma_{\text{lower}} = 1.0$ for the upper and lower bounds. We choose $a = b = 2.5$ which ensures that, on average, 75% of all values lie between 1.5 to 2.5 standard deviations and 12.5% lie between 1.0 to 1.5 or between 2.5 to 3.0 standard deviations, respectively. This means that 75% lie in the central interval and 25% outside (*75-25-rule*). We have chosen a $\beta$-distribution since it is the analogy of a normal distribution for a fixed interval. With that procedure we construct an ensemble of 100 members of which three examples can be found in Supplementary Fig. 10. If not stated otherwise, all results shown are from the average over the 100 ensemble members.

**Network of coupled nonlinear differential equations.** We use a combination of nonlinear differential equations together with a complex network to describe the state of the rainforest cells and their interactions. We use this approach instead of a threshold approach since we want to be able to account for partial changes in the state and their effects on the network. For instance such changes can be critical for the tipping of cells that are not coupled directly, but via an intermediary cell, where partial changes are decisive for the emergence of a tipping cascade. Indirect effects have been found to account for 10% and more, already in very simple interaction structures in so called motifs[62].

In the differential equation approach in this work, we model the main hydrological parameters and the stability of the rainforest, but no further parameters such as biotic variables. The main hydrological properties are the precipitation (MAP), the MCWD and the moisture recycling. Following the reasoning above, we describe the mathematical details in the remainder of this section.

Each $1^{\circ}$x$1^{\circ}$ cell is represented by a differential equation of the form

$$\frac{dx_i}{dt} = x_i^3 - x_i + \mathcal{F}_{\text{crit}}\left(\text{MAP}_i, \text{MCWD}_i\right), \tag{6}$$

where $x_i$ stands for the state of the rainforest cell and can be interpreted as the fraction of the tree cover. The shape of this function can be see in Supplementary Fig. 11. Furthermore, Eq. 6 has the normal form of a saddle-node bifurcation and is a simple form of a differential equation with two stable states. Such equations have been suggested to model dynamics in various contexts such as economics, ecology or the Earth system[63,64,65]. The two states are stable depending on the value of the critical function $\mathcal{F}_{\text{crit}}$ where +1.0 stands for full tree cover and $-1.0$ for the alternative state without full tree cover. Such an alternative state could be a savanna like state or completely treeless. It is not possible for a cell to have lower tree cover values than 0% or values higher than full forest cover such that the state $x_i$ is limited to the interval $[-1.0, 1.0]$. The advantage of choosing state limits of $-1.0$ and $+1.0$ is that the critical value then remains analytically representable and has the specific value $\mathcal{C}_{\text{crit}} = \sqrt{4/27}$ (see Supplementary Fig. 11). This value is derived from the discriminant of the polynomial of Eq. 6 and more details can be found in literature[64,66]. For other state limits such as between $0.0$ and $1.0$, this would have to be dropped since the parameters in front of the cubic and linear terms of Eq. 6 would be different. Therefore, we decided for prefactors of $1.0$ in front of the cubic and the linear term such that the state limits are $-1.0$ and $+1.0$. As soon as the critical value of $\mathcal{C}_{\text{crit}}$ is reached

by $\mathcal{F}_{\text{crit}}$ a state transition will occur since the upper stable state becomes unstable and only the lower stable state remains stable. For more details on this equation and the critical value, see e.g. Wunderling et al. (2020) or Klose et el. (2020)[62,64].

In our case, the rainforest cells are not independent, but interact via moisture recycling such that Eq. 6 becomes

$$\frac{dx_i}{dt} = x_i^3 - x_i + \mathcal{F}_{\text{crit}}\left(\text{MAP}_i, \text{MCWD}_i\right) + \sum_{\substack{j=1 \\ j \neq i}}^{N} \mathcal{M}_{ji}\left(\Delta\text{MAP}_{ji}, \Delta\text{MCWD}_{ji}\right) \frac{x_j}{2}. \tag{7}$$

Here, the entries of the critical matrix $\mathcal{M}_{ji}\left(\Delta\text{MAP}_{ji}, \Delta\text{MCWD}_{ji}\right)$ represent the strength of the moisture recycling link between two grid cells from $j$ to $i$. The state $x_j$ must be divided by 2 since the distance from minimum to maximum state is 2. Similar forms of the network and the differential equation have already been used in earlier studies in the literature, but in a way more simplified form compared to this work[62,38].

**Computation of the critical function.** While the shape of each cell is represented by Eq. 6, the determination of the critical function with respect to MAP and MCWD remains. The critical function $\mathcal{F}_{\text{crit}}\left(\text{MAP}_i, \text{MCWD}_i\right)$ is computed in two steps. Firstly, for MAP

$$\mathcal{F}_{\text{crit}}\left(\text{MAP}_i\right) = \mathcal{C}_{\text{crit}} \cdot \frac{\text{MAP}_i - \mu_{\text{MAP,i}}}{\text{MAP}_{\text{crit,i}} - \mu_{\text{MAP,i}}}, \tag{8}$$

where $\mu_{\text{MAP,i}}$ is the average value of that specific cell over the course of 30 years from the GLDAS calibration dataset (see Supplemenentary Figs. 6 and 7). The critical value $\text{MAP}_{\text{crit,i}}$ is also computed from this dataset using Eq. 4. $\text{MAP}_i$ is the actual precipitation value in the cell within the evaluation period, for instance the value of the year 2010 in this cell for the case that the (drought) conditions of the year 2010 are investigated. Secondly, for MCWD

$$\mathcal{F}_{\text{crit}}\left(\text{MCWD}_i\right) = \mathcal{C}_{\text{crit}} \cdot \frac{\text{MCWD}_i - \mu_{\text{MCWD,i}}}{\text{MCWD}_{\text{crit,i}} - \mu_{\text{MCWD,i}}}. \tag{9}$$

Although both equations (Eqs. 8 and 9) are in principle not limited, we restrict them to the interval $[0, \mathcal{C}_{\text{crit}}]$ since the critical value for tipping of Eq. 6 is reached at $\mathcal{C}_{\text{crit}}$ such that higher values are not necessary to tip a certain cell.

Then, the critical function $\mathcal{F}_{\text{crit}}\left(\text{MAP}_i, \text{MCWD}_i\right)$ is computed as

$$\begin{aligned}\mathcal{F}_{\text{crit}}\left(\text{MAP}_i, \text{MCWD}_i\right) &= \max\left\{\mathcal{F}_{\text{crit}}\left(\text{MAP}_i\right), \mathcal{F}_{\text{crit}}\left(\text{MCWD}_i\right)\right\} + \\ + \left(1 - \frac{\max\left\{\mathcal{F}_{\text{crit}}\left(\text{MAP}_i\right), \mathcal{F}_{\text{crit}}\left(\text{MCWD}_i\right)\right\}}{\mathcal{C}_{\text{crit}}}\right) &\cdot \min\left\{\mathcal{F}_{\text{crit}}\left(\text{MAP}_i\right), \mathcal{F}_{\text{crit}}\left(\text{MCWD}_i\right)\right\}. \end{aligned} \tag{10}$$

Again, the values of Eq. 10 are restricted to the interval $[0, \mathcal{C}_{\text{crit}}]$ since a state change occurs as soon as the upper value of the interval, i.e. $\mathcal{C}_{\text{crit}}$, is reached. The first term of Eq. 10 is sufficient to determine the critical function $\mathcal{F}_{\text{crit}}\left(\text{MAP}_i, \text{MCWD}_i\right)$ if $\mathcal{F}_{\text{crit}}\left(\text{MAP}_i\right)$ or $\mathcal{F}_{\text{crit}}\left(\text{MCWD}_i\right)$ are smaller than zero or larger than $\mathcal{C}_{\text{crit}}$. In case $\mathcal{F}_{\text{crit}}\left(\text{MAP}_i\right)$ and $\mathcal{F}_{\text{crit}}\left(\text{MCWD}_i\right)$ are larger than zero, but smaller than $\mathcal{C}_{\text{crit}}$, both terms of Eq. 10 are required. The second term takes the additional effect of the smaller of the two factors (from Eqs. 8 and 9) into account such that this is represented in the dynamics of Eq. 10. Then, partial state changes (even without tipping) affect the state of the rainforest cell and with that also the moisture recycling values (see curvature before tipping point in the sketch in Fig. 1a, b). This is an advantage of a fully dynamic model such as this, while threshold-only models would not be capable of doing this.

An example could be that $\mathcal{F}_{\text{crit}}\left(\text{MAP}_1\right) = \mathcal{F}_{\text{crit}}\left(\text{MAP}_2\right) = \frac{1}{2} \cdot \mathcal{C}_{\text{crit}}$ due to respective MAP values for two cells at the same time. Then it makes sense that the state of these two cells that have exactly this critical value with respect to MAP is not the same in case they have a different value with respect to their MCWD values. Let us assume that cell 1 has $\mathcal{F}_{\text{crit}}\left(\text{MCWD}_1\right) = \frac{1}{4} \cdot \mathcal{C}_{\text{crit}}$ and cell 2 has $\mathcal{F}_{\text{crit}}\left(\text{MCWD}_2\right) = \frac{1}{16} \cdot \mathcal{C}_{\text{crit}}$. Then, the second term of Eq. 10 takes these differences between the cells 1 and 2 into account shifting cell 1 a bit closer to its tipping point than cell 2 such that the reduction effect on the respective outgoing moisture recycling links is stronger for cell 1 than for cell 2.

**Computation of the critical matrix.** In analogy to Eqs. 8 and 9, we define the critical matrix for MAP as

$$\mathcal{M}_{ji}\left(\Delta\mathrm{MAP}_{ji}\right) = \mathcal{C}_{\mathrm{crit}} \cdot \frac{\Delta\mathrm{MAP}_{ji}}{\mathrm{MAP}_{\mathrm{crit,i}} - \mu_{\mathrm{MAP,i}}} := \mathcal{M}_{ji,\ \mathrm{MAP}}, \tag{11}$$

where $\Delta\mathrm{MAP}_{ji}$ represents the difference of the mean annual precipitation arising from the moisture recycling link $\delta_{ji}$ from cell $j$ to cell $i$. Thus: $\Delta\mathrm{MAP}_{ji} = \Delta\mathrm{MAP}\left(\delta_{ji}\right) = \delta_{ji,\ \mathrm{MAP}}$.

For MCWD we have

$$\mathcal{M}_{ji}\left(\Delta\mathrm{MCWD}_{ji}\right) = \mathcal{C}_{\mathrm{crit}} \cdot \frac{\Delta\mathrm{MCWD}_{ji}}{\mathrm{MCWD}_{\mathrm{crit,i}} - \mu_{\mathrm{MCWD,i}}} := \mathcal{M}_{ji,\ \mathrm{MCWD}}, \tag{12}$$

where $\Delta\mathrm{MCWD}_{ji} = \Delta\mathrm{MCWD}\left(\delta_{ji,\ \mathrm{MAP}}\right)$ is the potential increase of MCWD in response to the moisture recycling link $\delta_{ji,\ \mathrm{MAP}}$ from cell $j$ to cell $i$. Note that the moisture recycling link $\delta_{ji,\ \mathrm{MAP}}$ can reduce the precipitation, while the evaporation (which also goes into the computation of the MCWD value, see Eq. 1) remains constant.

Then, analogously to Eq. 10, the complete critical matrix is computed as

$$\mathcal{M}_{ji}\left(\Delta\mathrm{MAP}_{ji}, \Delta\mathrm{MCWD}_{ji}\right) = \mathcal{M}_{ji,\ \mathrm{MAP}} + \left(1 - \frac{\mathcal{M}_{ji,\ \mathrm{MAP}}}{\mathcal{C}_{\mathrm{crit}}}\right) \cdot \mathcal{M}_{ji,\ \mathrm{MCWD}} \tag{13}$$

if $\mathcal{F}_{\mathrm{crit}}\left(\mathrm{MAP}_i\right) > \mathcal{F}_{\mathrm{crit}}\left(\mathrm{MCWD}_i\right)$ or

$$\mathcal{M}_{ji}\left(\Delta\mathrm{MAP}_{ji}, \Delta\mathrm{MCWD}_{ji}\right) = \mathcal{M}_{ji,\ \mathrm{MCWD}} + \left(1 - \frac{\mathcal{M}_{ji,\ \mathrm{MCWD}}}{\mathcal{C}_{\mathrm{crit}}}\right) \cdot \mathcal{M}_{ji,\ \mathrm{MAP}} \tag{14}$$

if $\mathcal{F}_{\mathrm{crit}}\left(\mathrm{MAP}_i\right) < \mathcal{F}_{\mathrm{crit}}\left(\mathrm{MCWD}_i\right)$.

**Resolution independence.** To check for robustness of our results, we recomputed our simulations with respect to the finer and coarser resolutions of $0.5^{\circ}$x$0.5^{\circ}$, $1.5^{\circ}$x$1.5^{\circ}$ and $2^{\circ}$x$2^{\circ}$ (see Supplementary Figs. 10 and 12). For that purpose, we scale the minimal moisture recycling

value connecting to rainforest cells with the area of a cell. In case of a resolution of $0.5°$x$0.5°$ we take all moisture recycling values of more than 0.25 mm/yr into account, for $1°$x$1°$ we take all values above 1.0 mm/yr into account, for $1.5°$x$1.5°$ all values above 2.25 mm/yr and for $2°$x$2°$ all values above 4.0 mm/yr. Overall, we find that the vulnerability patterns are at the same location in the southeast (compare Fig. 3a with Supplementary Fig. 12a, b, c). Thus, the qualitative pattern is the same. The absolute values also show a close quantitative match within their standard deviations for resolutions of $1°$x$1°$ or coarser (see Supplementary Fig. 13a, b). The finer the resolution is, the higher the tipped area tendentially is. This is due to the fact that a higher resolution resolves cells to a finer level. These cells are then able to tip individually, whereas on a coarser resolution these cells are subsumed under one cell which is then still stable. Also, the scaling of the moisture recycling connections that we take into account might play a role for the increased tipping when the resolution becomes finer. Further note that we decreased the ensemble size for the resolution of $0.5°$x$0.5°$ from 100 to 10 ensemble members due to computational constraints.

**Notes on colour maps.** This paper makes use of perceptually uniform colour maps developed by F. Crameri[67].

**Data and Code availability.** The data and code that support the findings of this study are available from the corresponding authors upon reasonable request.

# References and Notes

[1] Barlow, J. *et al.* The future of hyperdiverse tropical ecosystems. *Nature* **559**, 517–526 (2018).

[2] Mitchard, E. T. The tropical forest carbon cycle and climate change. *Nature* **559**, 527–534 (2018).

[3] Jenkins, C. N., Pimm, S. L. & Joppa, L. N. Global patterns of terrestrial vertebrate diversity and conservation. *Proceedings of the National Academy of Sciences* **110**, E2602–E2610 (2013).

[4] Nobre, C. A. *et al.* Land-use and climate change risks in the amazon and the need of a novel sustainable development paradigm. *Proceedings of the National Academy of Sciences* **113**, 10759–10768 (2016).

[5] Malhi, Y. *et al.* Exploring the likelihood and mechanism of a climate-change-induced dieback of the amazon rainforest. *Proceedings of the National Academy of Sciences* **106**, 20610–20615 (2009).

[6] Malhi, Y. *et al.* Climate change, deforestation, and the fate of the amazon. *science* **319**, 169–172 (2008).

[7] Salazar, L. F. & Nobre, C. A. Climate change and thresholds of biome shifts in amazonia. *Geophysical Research Letters* **37** (2010).

[8] Oyama, M. D. & Nobre, C. A. A new climate-vegetation equilibrium state for tropical south america. *Geophysical research letters* **30** (2003).

[9] Staver, A. C., Archibald, S. & Levin, S. A. The global extent and determinants of savanna and forest as alternative biome states. *Science* **334**, 230–232 (2011).

443 [10] Hirota, M., Holmgren, M., Van Nes, E. H. & Scheffer, M. Global resilience of tropical
444 forest and savanna to critical transitions. *Science* **334**, 232–235 (2011).

445 [11] Staal, A., Dekker, S. C., Hirota, M. & van Nes, E. H. Synergistic effects of drought
446 and deforestation on the resilience of the south-eastern amazon rainforest. *Ecological*
447 *Complexity* **22**, 65–75 (2015).

448 [12] van Nes, E. H., Hirota, M., Holmgren, M. & Scheffer, M. Tipping points in tropical tree
449 cover: linking theory to data. *Global change biology* **20**, 1016–1021 (2014).

450 [13] Meir, P. *et al.* Threshold responses to soil moisture deficit by trees and soil in tropical rain
451 forests: insights from field experiments. *BioScience* **65**, 882–892 (2015).

452 [14] Lenton, T. M. *et al.* Tipping elements in the earth's climate system. *Proceedings of the*
453 *national Academy of Sciences* **105**, 1786–1793 (2008).

454 [15] Lovejoy, T. E. & Nobre, C. Amazon tipping point: Last chance for action (2019).

455 [16] Lenton, T. M. *et al.* Climate tipping points—too risky to bet against (2019).

456 [17] Ciemer, C. *et al.* Higher resilience to climatic disturbances in tropical vegetation exposed
457 to more variable rainfall. *Nature Geoscience* **12**, 174–179 (2019).

458 [18] Holmgren, M., Hirota, M., Van Nes, E. H. & Scheffer, M. Effects of interannual climate
459 variability on tropical tree cover. *Nature Climate Change* **3**, 755–758 (2013).

460 [19] Fu, R. *et al.* Increased dry-season length over southern amazonia in recent decades and
461 its implication for future climate projection. *Proceedings of the National Academy of*
462 *Sciences* **110**, 18110–18115 (2013).

[20] Dubreuil, V., Debortoli, N., Funatsu, B., Nédélec, V. & Durieux, L. Impact of land-cover change in the southern amazonia climate: a case study for the region of alta floresta, mato grosso, brazil. *Environmental monitoring and assessment* **184**, 877–891 (2012).

[21] Marengo, J. A. *et al.* Changes in climate and land use over the amazon region: current and future variability and trends. *Frontiers in Earth Science* **6**, 228 (2018).

[22] Boisier, J. P., Ciais, P., Ducharne, A. & Guimberteau, M. Projected strengthening of amazonian dry season by constrained climate model simulations. *Nature Climate Change* **5**, 656–660 (2015).

[23] Joetzjer, E., Douville, H., Delire, C. & Ciais, P. Present-day and future amazonian precipitation in global climate models: Cmip5 versus cmip3. *Climate Dynamics* **41**, 2921–2936 (2013).

[24] Sakschewski, B. *et al.* Resilience of amazon forests emerges from plant trait diversity. *Nature Climate Change* **6**, 1032–1036 (2016).

[25] Sakschewski, B. *et al.* Variable tree rooting strategies improve tropical productivity and evapotranspiration in a dynamic global vegetation model. *Biogeosciences Discussions* **in review** (2020).

[26] Choat, B. *et al.* Global convergence in the vulnerability of forests to drought. *Nature* **491**, 752–755 (2012).

[27] Aragão, L. E. Environmental science: The rainforest's water pump. *Nature* **489**, 217–218 (2012).

[28] Eltahir, E. A. & Bras, R. L. Precipitation recycling in the amazon basin. *Quarterly Journal of the Royal Meteorological Society* **120**, 861–880 (1994).

485 [29] Staal, A. *et al.* Forest-rainfall cascades buffer against drought across the amazon. *Nature*
486 *Climate Change* **8**, 539–543 (2018).

487 [30] Staal, A. *et al.* Feedback between drought and deforestation in the amazon. *Environmental*
488 *Research Letters* **15**, 044024 (2020).

489 [31] Zemp, D. *et al.* On the importance of cascading moisture recycling in south america.
490 *Atmospheric Chemistry and Physics* (2014).

491 [32] Zemp, D. C. *et al.* Self-amplified amazon forest loss due to vegetation-atmosphere feed-
492 backs. *Nature Communications* **8**, 1–10 (2017).

493 [33] Boers, N., Marwan, N., Barbosa, H. M. & Kurths, J. A deforestation-induced tipping point
494 for the south american monsoon system. *Scientific reports* **7**, 41489 (2017).

495 [34] Anderson, L. O. *et al.* Vulnerability of amazonian forests to repeated droughts. *Philo-*
496 *sophical Transactions of the Royal Society B: Biological Sciences* **373**, 20170411 (2018).

497 [35] Lewis, S. L., Brando, P. M., Phillips, O. L., van der Heijden, G. M. & Nepstad, D. The
498 2010 amazon drought. *Science* **331**, 554–554 (2011).

499 [36] Duffy, P. B., Brando, P., Asner, G. P. & Field, C. B. Projections of future meteorological
500 drought and wet periods in the amazon. *Proceedings of the National Academy of Sciences*
501 **112**, 13172–13177 (2015).

502 [37] Cox, P. M. *et al.* Increasing risk of amazonian drought due to decreasing aerosol pollution.
503 *Nature* **453**, 212–215 (2008).

504 [38] Krönke, J. *et al.* Dynamics of tipping cascades on complex networks. *Physical Review E*
505 **101**, 042311 (2020).

[39] Marengo, J. A., Tomasella, J., Alves, L. M., Soares, W. R. & Rodriguez, D. A. The drought of 2010 in the context of historical droughts in the amazon region. *Geophysical Research Letters* **38** (2011).

[40] NOAA – Climate Prediction Center – ONI. https://origin.cpc.ncep.noaa.gov/products/analysis_monitoring/ensostuff/ONI_v5.php (2020).

[41] Marengo, J. A. & Espinoza, J. C. Extreme seasonal droughts and floods in amazonia: causes, trends and impacts. *International Journal of Climatology* **36**, 1033–1050 (2016).

[42] Maeda, E. E., Kim, H., Aragão, L. E., Famiglietti, J. S. & Oki, T. Disruption of hydroecological equilibrium in southwest amazon mediated by drought. *Geophysical Research Letters* **42**, 7546–7553 (2015).

[43] Restrepo-Coupe, N. *et al.* What drives the seasonality of photosynthesis across the amazon basin? a cross-site analysis of eddy flux tower measurements from the brasil flux network. *Agricultural and Forest Meteorology* **182**, 128–144 (2013).

[44] Aragao, L. E. *et al.* Environmental change and the carbon balance of a mazonian forests. *Biological Reviews* **89**, 913–931 (2014).

[45] Pereira, E. J. d. A. L., de Santana Ribeiro, L. C., da Silva Freitas, L. F. & de Barros Pereira, H. B. Brazilian policy and agribusiness damage the amazon rainforest. *Land Use Policy* **92**, 104491 (2020).

[46] Davidson, E. A. *et al.* The amazon basin in transition. *Nature* **481**, 321–328 (2012).

[47] Ferrante, L. & Fearnside, P. M. The amazon's road to deforestation. *Science* **369**, 634–634 (2020).

[48] dos Santos Júnior, M. *et al.* Br-319 como propulsora de desmatamento: Simulando o impacto da rodovia manaus-porto velho. *Instituto do Desenvolvimento Sustentável da Amazônia [in portuguese]* (2018).

[49] Pfaff, A. *et al.* Road investments, spatial spillovers, and deforestation in the brazilian amazon. *Journal of regional Science* **47**, 109–123 (2007).

[50] Diele-Viegas, L. M., Pereira, E. J. d. A. L. & Rocha, C. F. D. The new brazilian gold rush: Is amazonia at risk? *Forest Policy and Economics* **119**, 102270 (2020).

[51] Artaxo, P. Working together for amazonia. *Science* **363**, 323 (2019).

[52] Holmgren, M. *et al.* Extreme climatic events shape arid and semiarid ecosystems. *Frontiers in Ecology and the Environment* **4**, 87–95 (2006).

[53] Malhi, Y. & Wright, J. Spatial patterns and recent trends in the climate of tropical rainforest regions. *Philosophical Transactions of the Royal Society of London. Series B: Biological Sciences* **359**, 311–329 (2004).

[54] Cai, W. *et al.* Enso and greenhouse warming. *Nature Climate Change* **5**, 849–859 (2015).

[55] Cai, W. *et al.* Increasing frequency of extreme el niño events due to greenhouse warming. *Nature Climate Change* **4**, 111–116 (2014).

[56] Timmermann, A. *et al.* Increased el niño frequency in a climate model forced by future greenhouse warming. *Nature* **398**, 694–697 (1999).

[57] Duque-Villegas, M., Salazar, J. F. & Rendón, A. M. Tipping the enso into a permanent el niño can trigger state transitions in global terrestrial ecosystems. *Earth System Dynamics* **10** (2019).

548 [58] Collins, M. *et al.* The impact of global warming on the tropical pacific ocean and el niño.
549 *Nature Geoscience* **3**, 391–397 (2010).

550 [59] Chambers, J. Q. & Artaxo, P. Biosphere–atmosphere interactions: Deforestation size
551 influences rainfall. *Nature Climate Change* **7**, 175–176 (2017).

552 [60] D'Almeida, C. *et al.* The effects of deforestation on the hydrological cycle in amazonia:
553 a review on scale and resolution. *International Journal of Climatology: A Journal of the*
554 *Royal Meteorological Society* **27**, 633–647 (2007).

555 [61] Rodell, M. *et al.* The global land data assimilation system. *Bulletin of the American*
556 *Meteorological Society* **85**, 381–394 (2004).

557 [62] Wunderling, N. *et al.* How motifs condition critical thresholds for tipping cascades in
558 complex networks: Linking micro-to macro-scales. *Chaos: An Interdisciplinary Journal*
559 *of Nonlinear Science* **30**, 043129 (2020).

560 [63] Wunderling, N., Donges, F. J., Kurths, J. & Winkelmann, R. Interacting tipping elements
561 increase risk of climate domino effects under global warming. *Earth Syst. Dynam. Discuss.*
562 *(in review)* (2020).

563 [64] Klose, A. K., Karle, V., Winkelmann, R. & Donges, J. F. Emergence of cascading dynam-
564 ics in interacting tipping elements of ecology and climate. *Royal Society Open Science* **7**,
565 200599 (2020).

566 [65] Brummitt, C. D., Barnett, G. & D'Souza, R. M. Coupled catastrophes: sudden shifts
567 cascade and hop among interdependent systems. *Journal of The Royal Society Interface*
568 **12**, 20150712 (2015).

569 [66] Kuznetsov, Y. A. *Elements of Applied Bifurcation Theory, Applied Mathematical Sciences*,
570 vol. 112 (Springer Science & Business Media, New York, 2004).

571 [67] Crameri, F. Geodynamic diagnostics, scientific visualisation and staglab 3.0. *Geoscientific*
572 *Model Development* **11**, 2541–2562 (2018).

**Acknowledgements**

We are thankful to Kirsten Thonicke and Markus Drüke for fruitful discussions. This work has been carried out within the framework of PIK's FutureLab on Earth Resilience in the Anthropocene. N.W. and R.W. acknowledge the financial support of the IRTG 1740/TRP 2015/50122-0 project funded by DFG and FAPESP. N.W. is grateful for a scholarship from the Studienstiftung des deutschen Volkes. N.W., J.F.D. and R.W. are thankful for financial support by the Leibniz Association (project DominoES). A.S. and J.F.D. acknowledge support from the European Research Council Advanced Grant project ERA (Earth Resilience in the Anthropocene, ERC-2016-ADG-743080). A.S. and O.A.T. thank for support from the Bolin Centre for Climate Research. B.S. acknowledges funding from the BMBF- and Belmont Forum-funded project "CLIMAX: Climate services through knowledge co-production: A Euro-South American initiative for strengthening societal adaptation response to extreme events", FKZ 01LP1610A. M.H. is supported by a grant from Instituto Serrapilheira/Serra-1709-18983. O.A.T. acknowledges funding from the Netherlands Organisation for Scientific Research Innovational Research Incentives Schemes VENI (016.171.019). J.F.D. is grateful for financial support by the Stordalen Foundation via the Planetary Boundary Research Network (PB.net) and the Earth League's EarthDoc program. H.B. was supported by research grants 2015/50122-0 and 2016/18866-2, São Paulo Research Foundation (FAPESP); and grant 308682/2017-3, Brazilian National Research Council (CNPq). The authors gratefully acknowledge the European Regional Development Fund (ERDF), the German Federal Ministry of Education and Research and the Land Brandenburg for supporting this project by providing resources on the high performance computer system at the Potsdam Institute for Climate Impact Research.

**Author contributions**

N.W., J.F.D, H.B. and R.W. designed the study. N.W. conducted the model simulation runs

and prepared the figures. N.W. and A.S. led the writing of the manuscript with input from all authors. A.S. and O.A.T. developed the moisture recycling dataset of the Amazon rainforest. H.B. and R.W. jointly supervised this study.

## Additional information

Supplementary information is available in the online version of the paper. Reprints and permissions information are available online at www.nature.com/reprints. Requests for materials should be addressed to N.W.

## Competing interests

The authors declare no competing interests.

# Supplementary information

## Network dynamics of drought-induced tipping cascades in the Amazon rainforest

Wunderling et al.

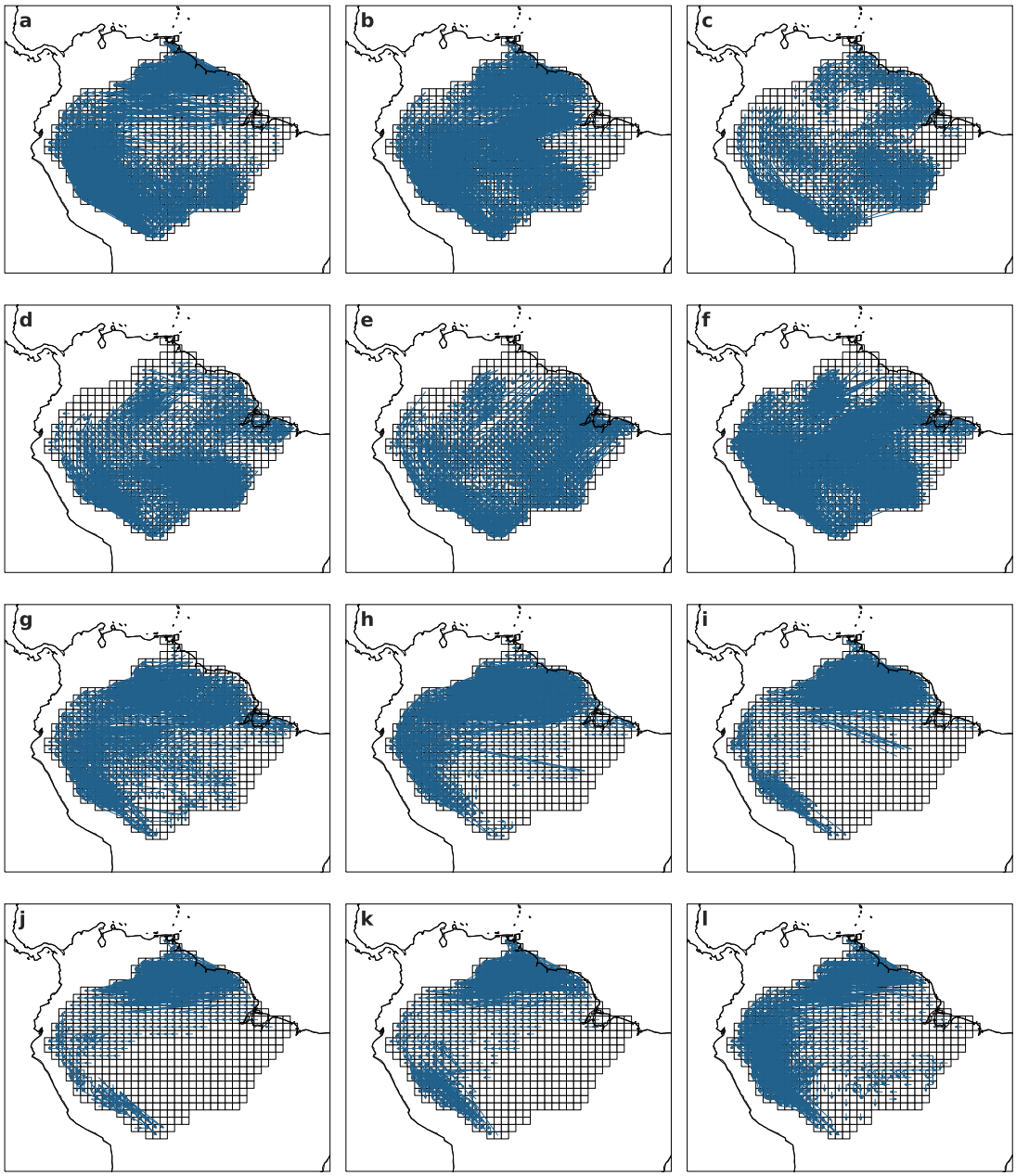


**Supplementary Figure 1 | Moisture recycling network 2014. a–l,** Monthly moisture recycling network links with a strength of 1 mm/month. This threshold has been chosen to preserve visibility. Values are shown for the hydrological year 2014, i.e., from October 2013 (panel **a**) to September 2014 (panel **l**). Compare to drought year 2010 (see Supplementary Fig. 2).

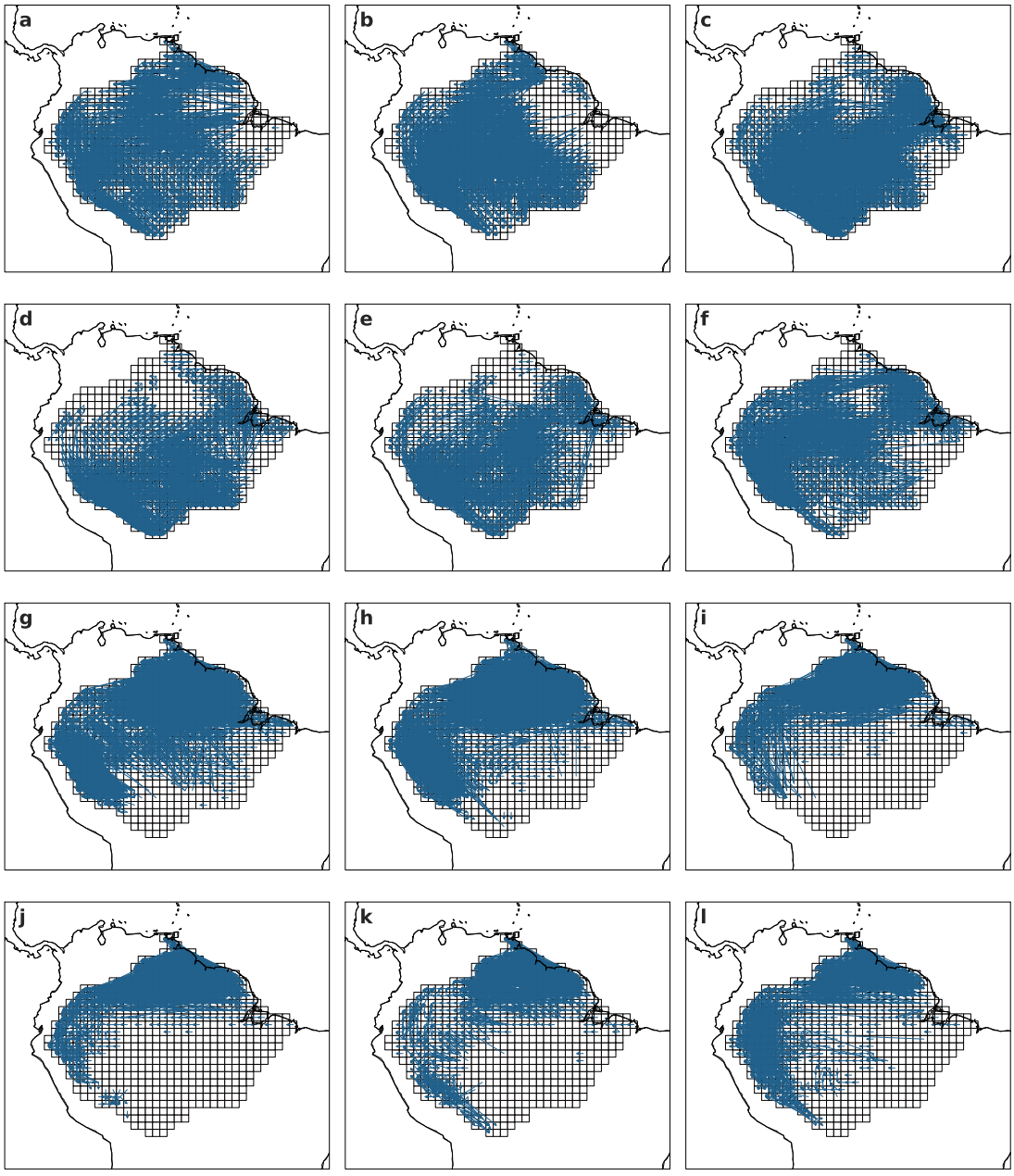


**Supplementary Figure 2 | Moisture recycling network 2010. a–l,** Monthly moisture recycling network links with a strength of 1 mm/month. Values are shown for the drought year 2010. Panel **a** represents October 2009 and panel **l** represents September 2010. Compare with Supplementary Fig. 1 for the year 2014.

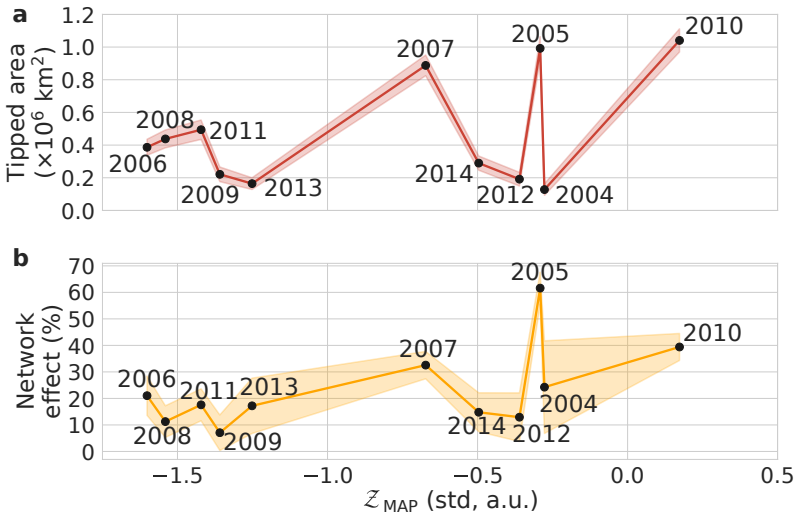


**Supplementary Figure 3 | Vulnerability of the rainforest against a MAP-based $\mathcal{Z}$-score. a,** The total tipped area is shown over the course of the mean annual precipitation based $\mathcal{Z}$-score measured in standard deviations in analogue to the MCWD drought index (see main manuscript's Fig. 2 and Eq. 1). **b,** The additional tipped area due to network effects for each year is shown in percentage of the tipped area in panel **a**. Over the course of the study period, we probe a range from around $-1.5$ to $+0.5$ standard deviations of precipitation (i.e., on average, wetter years than in the calibration period). We do not find a correlation between the MAP based $\mathcal{Z}$-score and the tipped area or the network effects as for the MCWD $\mathcal{Z}$-score.

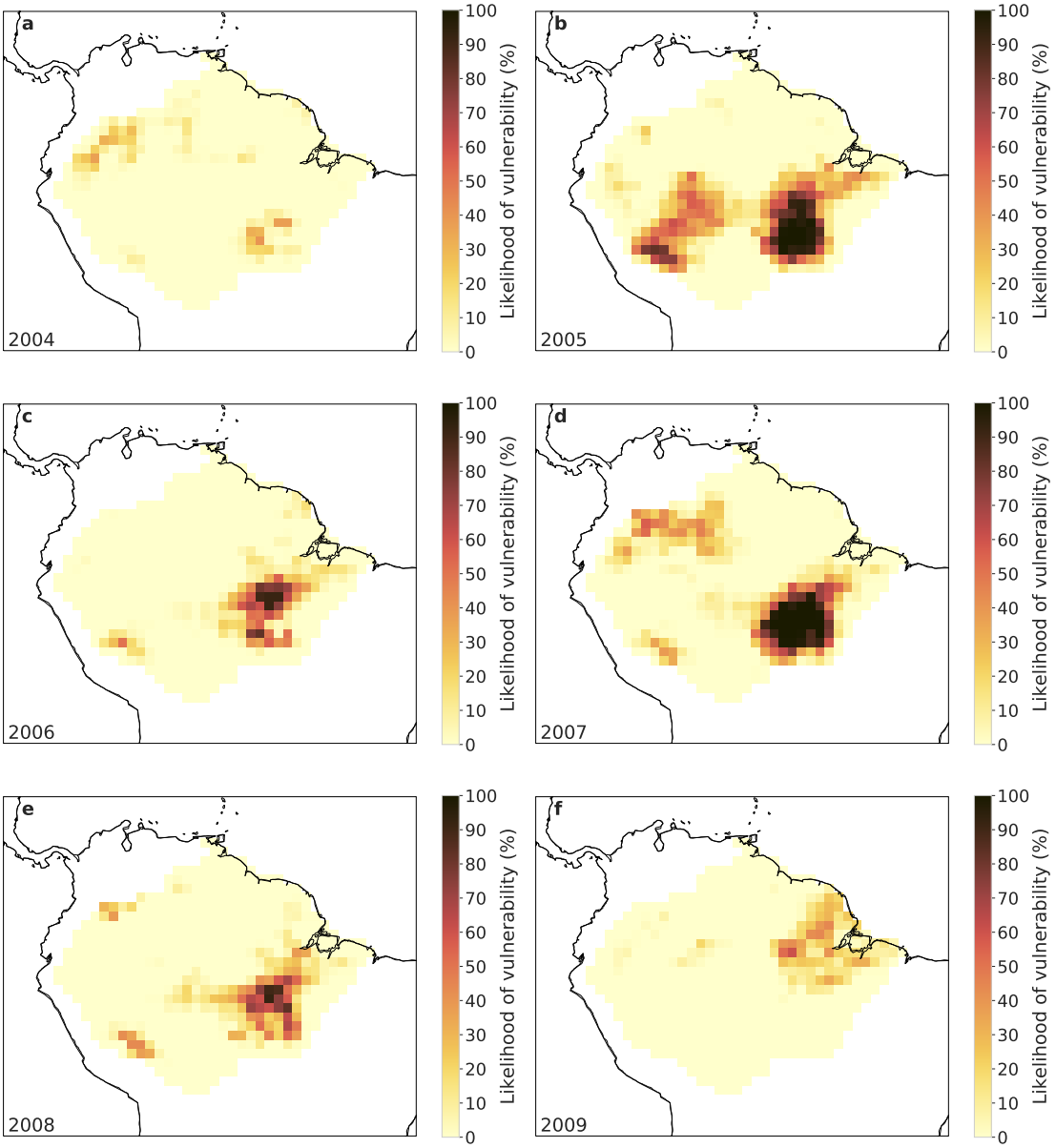
a
2004
b
2005
c
2006
d
2007
e
2008
f
2009
Likelihood of vulnerability (%)
100
90
80
70
60
50
40
30
20
10
0

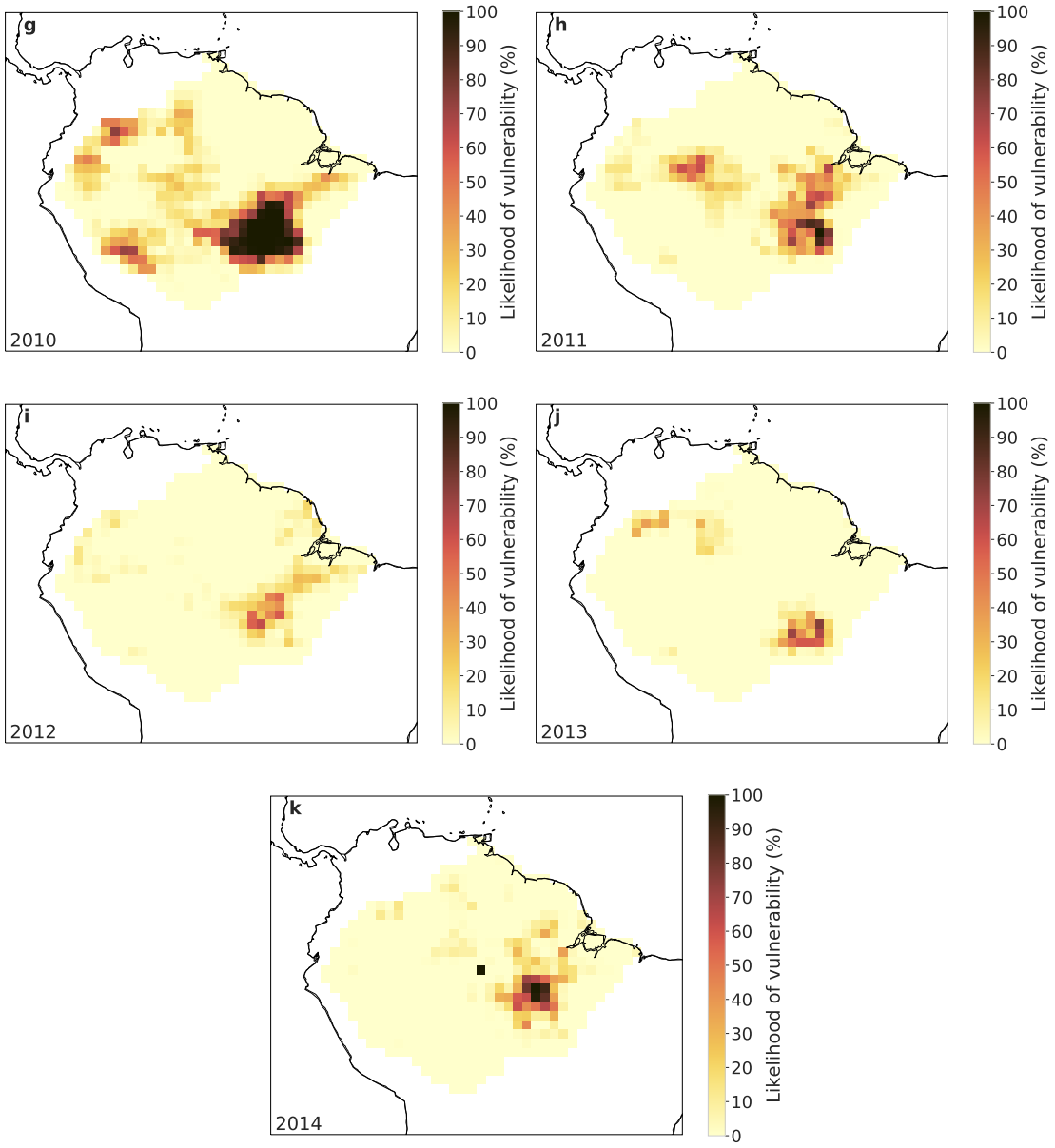


**Supplementary Figure 4 | Endangered regions on a yearly resolution.** Risk maps for the likelihood of instabilities separated for the hydrological years 2004 (panel **a**) to 2014 (panel **k**). The mean of these vulnerability maps is shown in the main manuscript (Fig. 3a).

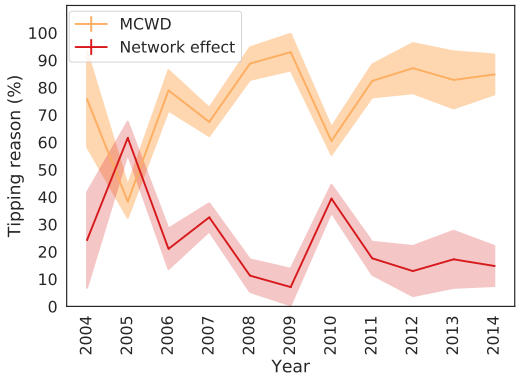


**Supplementary Figure 5 | Tipping reason.** The importance of two possible tipping reasons (MCWD and network effects) is shown versus the study period. Note that tipping cascades (network effects) and direct MCWD induced tipping must add up to 100% since MAP is negligible as a primary tipping reason. Overall, network effects, i.e., cascading effects, account for around 10% to up to 60% of all tipping events. The error bars show the standard deviation over all ensemble members. The mean over all years is shown in the main manuscript in Fig. 3b. MAP as a tipping reason is not shown since it is less than 0.1% overall.

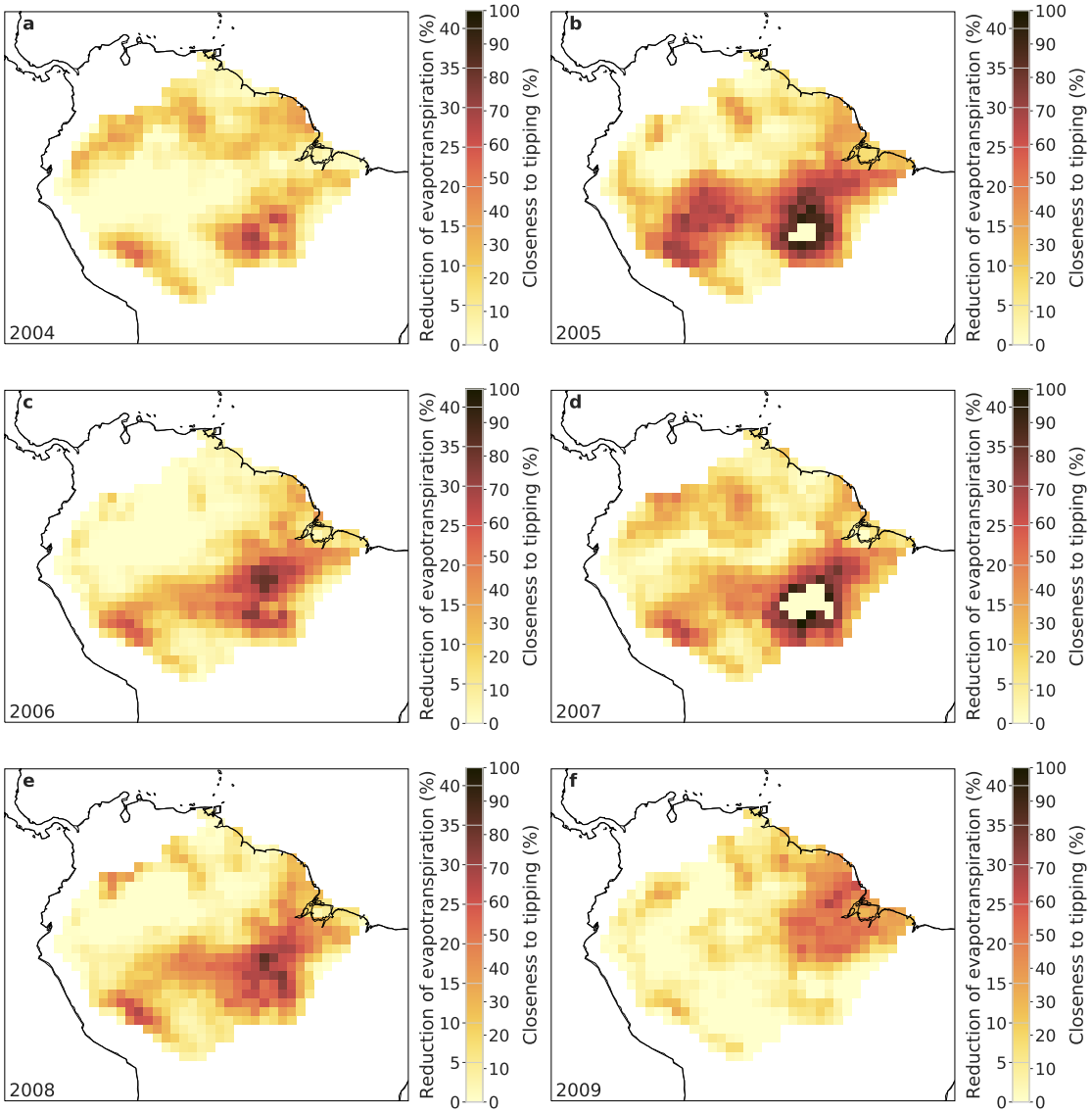
a
2004
b
2005
c
2006
d
2007
e
2008
f
2009
Reduction of evapotranspiration (%)
Closeness to tipping (%)
0
5
10
15
20
25
30
35
40
0
10
20
30
40
50
60
70
80
90
100

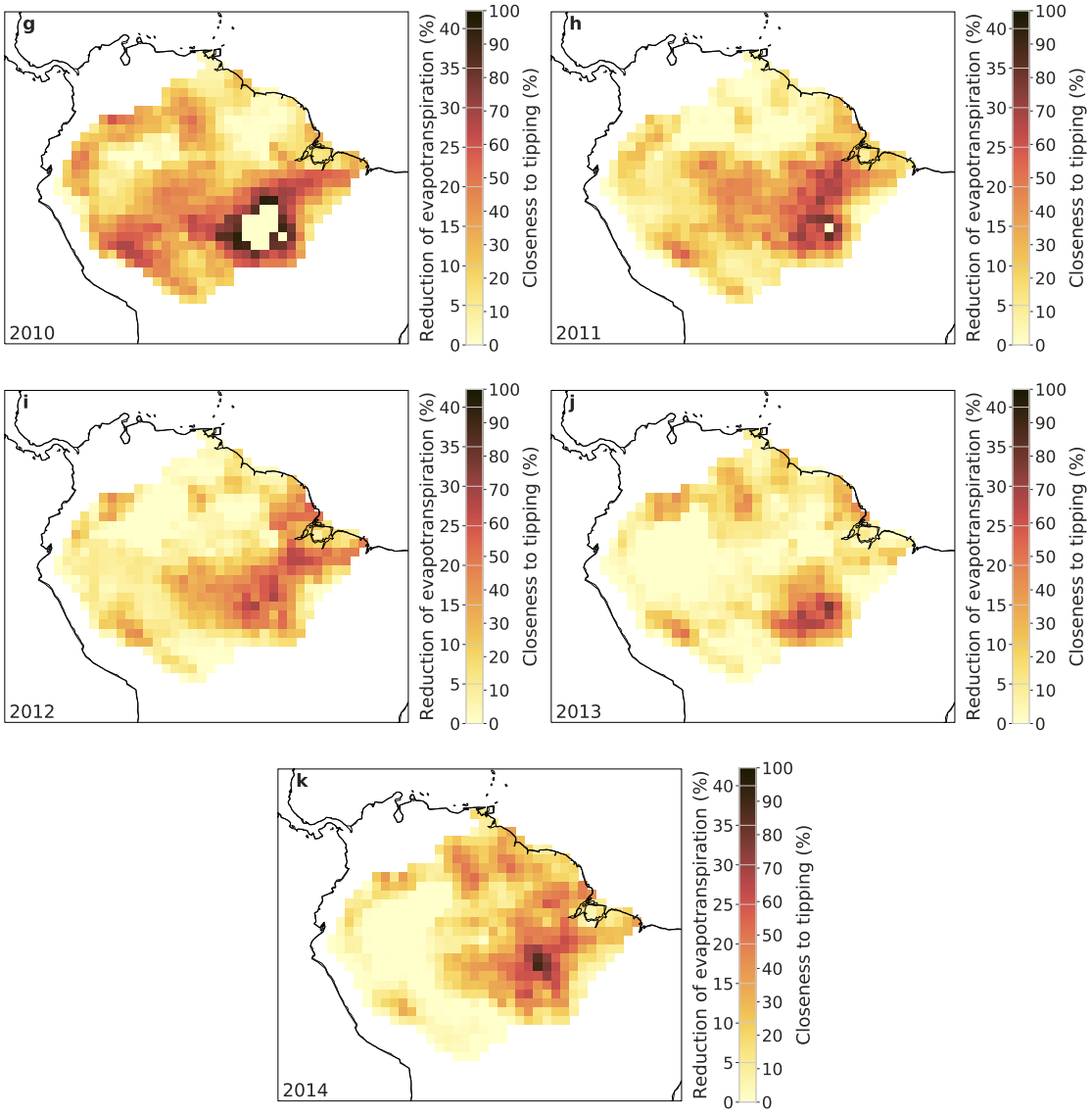


**Supplementary Figure 6 | *Closeness to tipping* on a yearly resolution.** Closeness to tipping separated for the hydrological years 2004 (panel **a**) to 2014 (panel **k**). The plain light beige cells in the middle of dark red regions in the southeastern Amazon reflect that this region is tipped for all 100 ensemble members. At this region, the closeness to tipping cannot be evaluated since the respective cells are already shifted beyond their tipping point, while the closeness to tipping only measures the average shift towards (but not beyond) the tipping point. The summary of these vulnerability maps is shown in the main manuscript (Fig. 4).

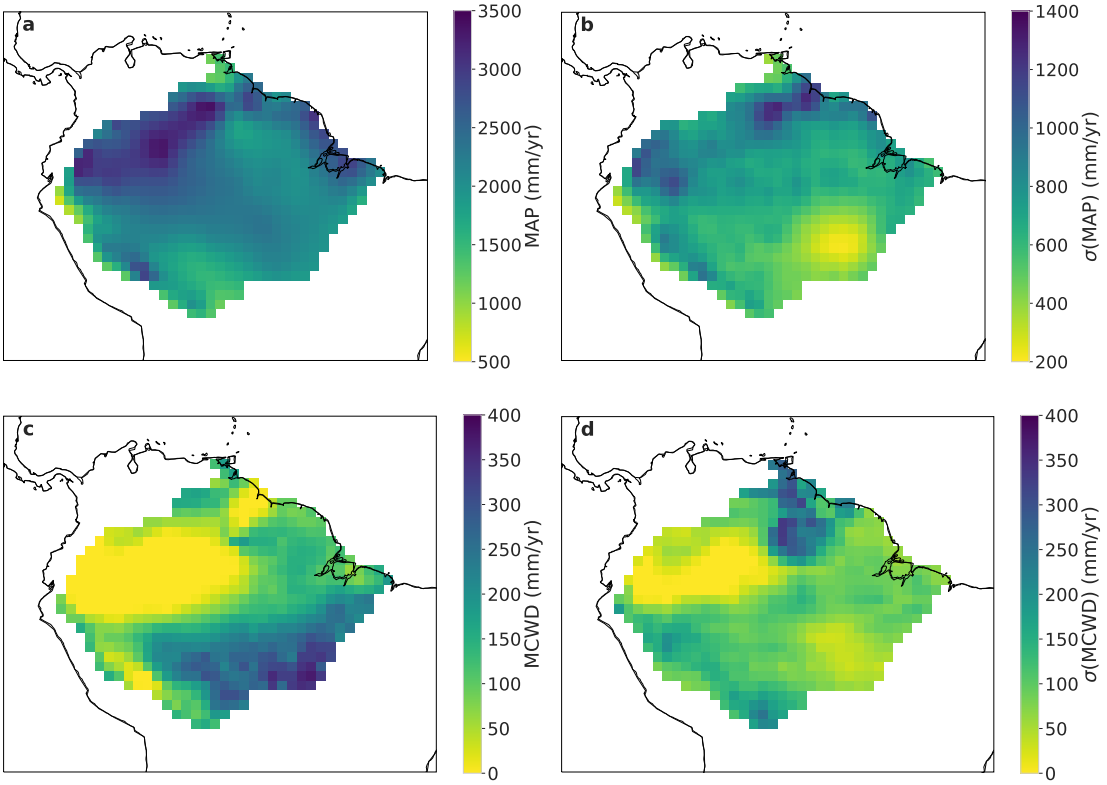


**Supplementary Figure 7 | Determination of the critical values.** **a,** Average mean annual precipitation (MAP), **b,** Standard deviation of MAP, **c,** Average maximum cumulative water deficit (MCWD), **a,** Standard deviation of the average MCWD. All panels show values from the hydrological years 1974 to 2003 derived from GLDAS which are used to compute the critical values of each grid cell located in the Amazon basin.

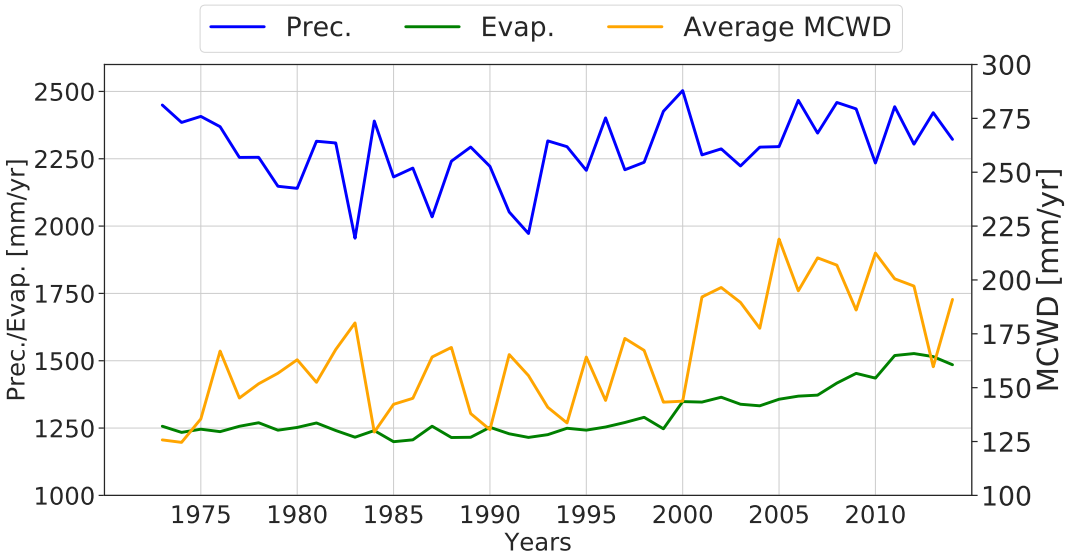


**Supplementary Figure 8 | Average precipitation, evaporation and MCWD from the study period.** Average precipitation (blue) and evaporation (green) for the calibration data set (hydrological years 1974-2003) and the evaluation data set (hydrological years 2004-2014). The data is aggregated on a yearly basis and averaged over the whole Amazon basin. The average MCWD over the study period is plotted in orange (right y-axis).

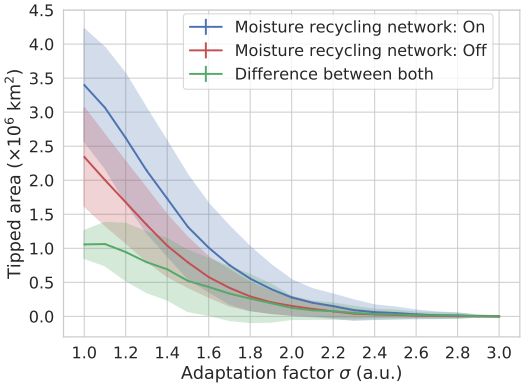


**Supplementary Figure 9 | Dependence on the adaptation factor.** Tipped area versus adaptation factor, where each cell has the same adaptation factor ($\alpha_i = \alpha \; \forall i$). The absolute tipped area is shown for an experiment with the moisture recycling network shut on (blue) and for comparison shut off (red). The absolute difference (green) shows the area that tips due to network effects (tipping cascades). The error bars show the standard deviation that arises from the simulations from the hydrological years 2004 to 2014.

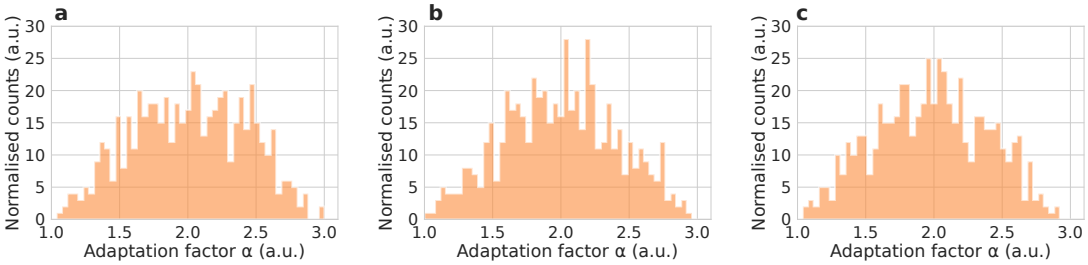


**Supplementary Figure 10 | Ensemble of starting conditions. a–c,** Three examples of initial conditions for the local adaptation factor $\alpha_i$ for the 567 cells in the Amazon rainforest basin at a resolution of 1°x1°. The values are $\beta$-distributed according Eq. 5 in the main manuscript.

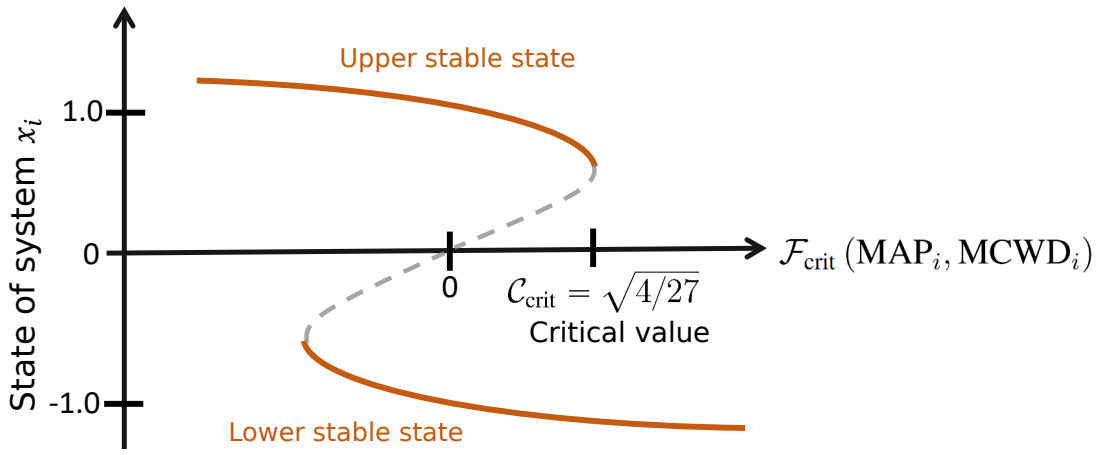


**Supplementary Figure 11 | Bifurcation diagram of a rainforest cell as a tipping element.** Stable states of the tipping element $x_i$ with respect to the critical function $\mathcal{F}_{\text{crit}}\,(\text{MAP}_i, \text{MCWD}_i)$. As soon as the *critical value* is reached, the upper stable branch vanishes and a state transition form the upper to the lower stable state occurs. If the differential equation of the form in Eq. 6 is chosen, the critical value is analytically representable as $\mathcal{C}_{\text{crit}} = \sqrt{4/27}$.

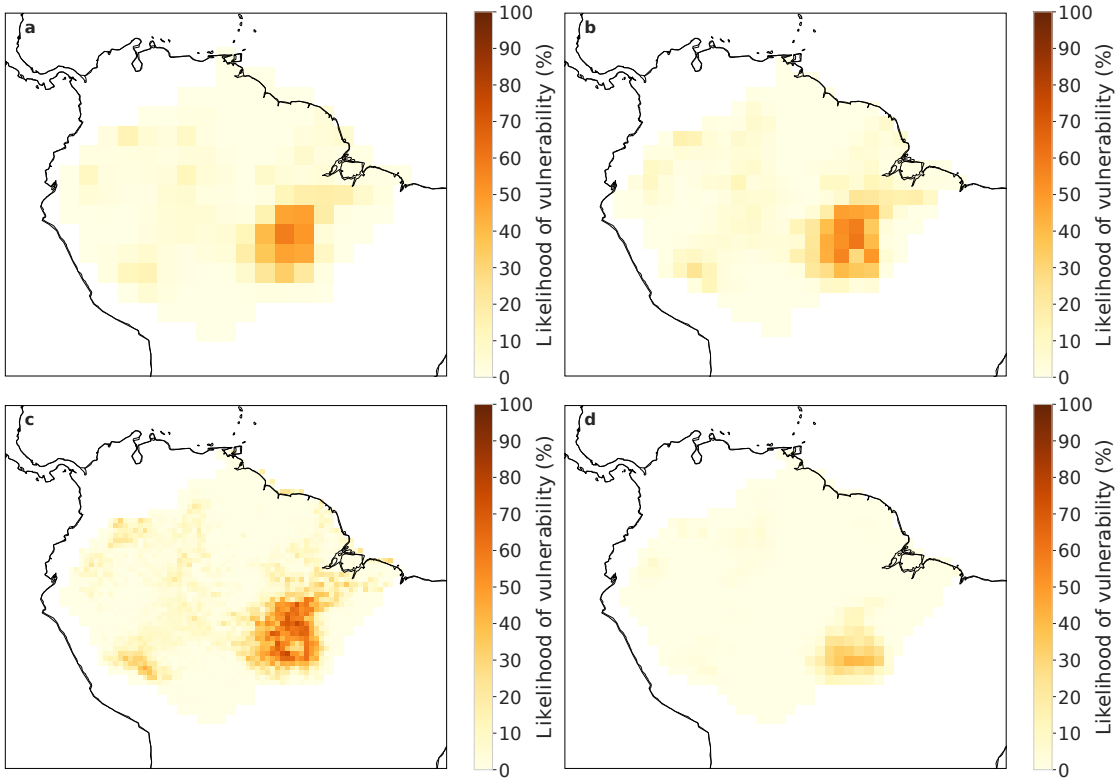


**Supplementary Figure 12 | Regional resolution dependences. a,** Same as Fig. 3 in the main manuscript, but for a resolution of 2°x2°, **b,** for a resolution of 1.5°x1.5° and **c,** for a resolution of 0.5°x0.5°. We find quantitative agreement with the results in Fig. 3a (see also Supplementary Fig. 13). **d,** Same as in Fig. 3 in the main manuscript for a resolution of 1°x1°, but for a constant monthly evaporation of 100 mm/month to compute the MCWD instead of using the observed values. The MCWD has been computed like this earlier in literature[1,2] which is why we want to show a comparison of our results ot this. In the southeast less cells tip compared to Fig. 3a of the main manuscript since the evaporation rate is set constant to 100 mm/month (compare with Supplementary Fig. 13).

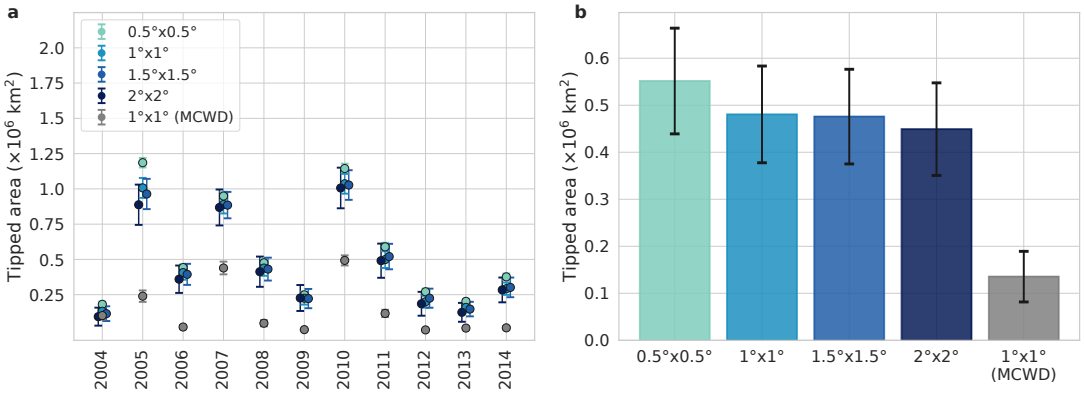


**Supplementary Figure 13 | Absolute resolution dependences. a,** Tipped area over the course of the study period for all investigated resolutions (0.5°x0.5°, 1°x1°, 1.5°x1.5°, 2°x2°) and for constant evaporation of 100 mm/month (1°x1° (MCWD)). Error bars show the standard deviation over the 100 ensemble members. Note that the ensemble for the resolution 0.5°x0.5° consists of only 10 ensemble members instead of 100 due to computational constraints. **b,** Summary of panel **a** over all years. Error bars show the standard deviation over all years in panel **a**.

## References

[1] Malhi, Y. *et al.* Exploring the likelihood and mechanism of a climate-change-induced dieback of the amazon rainforest. *Proceedings of the National Academy of Sciences* **106**, 20610–20615 (2009).

[2] Lewis, S. L., Brando, P. M., Phillips, O. L., van der Heijden, G. M. & Nepstad, D. The 2010 amazon drought. *Science* **331**, 554–554 (2011).

# 2.6 Interacting tipping elements increase risk of climate domino effects under global warming [P6]

**Authors**
Nico Wunderling, Jonathan F. Donges, Jürgen Kurths, Ricarda Winkelmann

**Status**
In Review at *Earth System Dynamics Discussion* (submitted March 2020), doi: 10.5194/esd-2020-18

**Short summary**
In this work, a model of four interacting climate tipping elements is investigated: the Greenland Ice Sheet, the West Antarctic Ice Sheet, the Atlantic Meridional Overturning Circulation (AMOC) and the Amazon rainforest. The established interactions between these four tipping elements from an expert elicitation and the critical temperature ranges of these four tipping elements are used to construct a complex network based on conceptual differential equations representing the climate tipping elements. This approach has been combined with a large-scale Monte Carlo simulation of 3.7 million ensemble members to propagate the many uncertainties linked to the interactions and the critical temperatures. It is found that the reference climate system is destabilised in case the tipping elements are not regarded as isolated entities. Furthermore, the roles of the tipping elements are revealed: the large ice sheets in Greenland and Antarctica act as the initiators of tipping cascades, while the AMOC is a transmittor of cascades and the Amazon rainforest is a follower of cascades. Lastly, it is shown that the main qualitative results remain robust in case the El-Niño Southern Oscillation (ENSO) is taken into account as a fifth tipping element. This shows the structural robustness of these results even under the assumption that the ENSO follows the same dynamical rules as the other four tipping elements.

**Author contributions**
Ricarda Winkelmann and Jonathan Donges conceived the study. Ricarda Winkelmann, Jonathan Donges and Nico Wunderling designed the model experiments. Nico Wunderling conducted the model simulation runs and prepared the figures. Nico Wunderling drafted the first version of the manuscript that was edited and discussed by all authors.

# Interacting tipping elements increase risk of climate domino effects under global warming

Nico Wunderling[1,2,3], Jonathan F. Donges[1,4], Jürgen Kurths[1,5], and Ricarda Winkelmann[1,2]

[1]Earth System Analysis and Complexity Science, Potsdam-Institute for Climate Impact Research (PIK), Member of the Leibniz Association, 14473 Potsdam, Germany
[2]Institute of Physics and Astronomy, University of Potsdam, 14476 Potsdam, Germany
[3]Department of Physics, Humboldt University of Berlin, 12489 Berlin, Germany
[4]Stockholm Resilience Centre, Stockholm University, Stockholm, SE-10691, Sweden
[5]Saratov State University, Saratov, RU-410012, Russia

**Correspondence:** Nico Wunderling (nico.wunderling@pik-potsdam.de), Ricarda Winkelmann (ricarda.winkelmann@pik-potsdam.de)

**Abstract.** With progressing global warming, there is an increased risk that one or several tipping elements in the climate system might cross a critical threshold, resulting in severe consequences for the global climate, ecosystems and human societies. While the underlying processes are fairly well understood, it is unclear how their interactions might impact the overall stability of the Earth's climate system. As of yet, this cannot be fully analysed with state-of-the-art Earth system models due to computational constraints as well as some missing and uncertain process representations of certain tipping elements. Here, we explicitly study the effects of known physical interactions among the Greenland and West Antarctic ice sheets, the Atlantic Meridional Overturning Circulation (AMOC) and the Amazon rainforest using a conceptual network approach. We analyse the risk of domino effects being triggered by each of the individual tipping elements under global warming in equilibrium experiments. In these experiments, we propagate the uncertainties in critical temperature thresholds, interaction strengths and interaction structure via large ensembles of simulations in a Monte-Carlo approach. Overall, we find that the interactions tend to destabilise the network of tipping elements. Furthermore, our analysis reveals the qualitative role of each of the four tipping elements within the network, showing that the polar ice sheets on Greenland and West Antarctica are oftentimes the initiators of tipping cascades, while the AMOC acts as a mediator transmitting cascades. This indicates that the ice sheets, which are already at risk of transgressing their temperature thresholds within the Paris range of 1.5 to 2 °C, are of particular importance for the stability of the climate system as a whole.

## 1 Introduction

### 1.1 Tipping elements in the climate system

The Earth system comprises a number of large-scale subsystems, the so-called *tipping elements*, that can undergo large and possibly irreversible changes in response to environmental or anthropogenic perturbations once a certain critical threshold in

forcing is exceeded (Lenton et al., 2008). Once triggered, the actual tipping process might take several years up to millennia depending on the respective response times of the system (Hughes et al., 2013; Lenton et al., 2008). Among the tipping elements are cryosphere components such as the continental ice sheets on Greenland and Antarctica, biosphere components such as the Amazon rainforest, boreal forests and coral reefs as well as large-scale atmospheric and oceanic circulation patterns such as monsoon systems and the Atlantic Meridional Overturning Circulation (AMOC). With continuing global warming, it becomes more likely that critical thresholds of some tipping elements might be exceeded, possibly within this century, triggering severe consequences for ecosystems, infrastructures and human societies. These critical thresholds can be quantified with respect to the global mean temperature (GMT), resulting in three clusters of tipping elements that are characterised by their critical temperature between 1–3 °C, 3–5 °C, and above 5 °C of warming compared to pre-industrial temperatures, respectively (Schellnhuber et al., 2016). The most vulnerable cluster, which is already at risk between 1–3 °C of warming, includes several cryosphere components, specifically mountain glaciers as well as the Greenland and West Antarctic ice sheets. Recent studies suggest potential early-warning indicators for these tipping elements, showing that some of them are approaching or might have already transgressed a critical threshold (Lenton et al., 2019; Caesar et al., 2018; Nobre et al., 2016; Favier et al., 2014).

### 1.2 Interactions between climate tipping elements

The tipping elements in the Earth system are not isolated systems, but interact on a global scale (Lenton et al., 2019; Kriegler et al., 2009). These interactions could have stabilising or destabilising effects, increasing or decreasing the probability of emerging tipping cascades, and it remains an important problem to understand how this affects the overall stability of the Earth system. Despite the considerable recent progress in global Earth system modelling, current state-of-the-art Earth system models cannot yet comprehensively simulate the nonlinear behaviour and feedbacks between some of the tipping elements due to computational limitations (Wood et al., 2019). Furthermore, the interactions between tipping elements have only partially been described in a framework of more conceptual, but process-based models, and our current understanding of the interaction structure of tipping elements is partly based on expert knowledge. For a subset of five tipping elements, an expert elicitation was conducted synthesising a causal interaction structure and an estimation for the probability of tipping cascades to emerge (Kriegler et al., 2009). These studied tipping elements were the Greenland Ice Sheet, the West Antarctic Ice Sheet, the Atlantic Meridional Overturning Circulation (AMOC), the El-Niño Southern Oscillation (ENSO) and the Amazon rainforest (see Fig. 1 and Fig. S3). Although this network is not complete with respect to the physical interactions between the tipping elements and the actual set of tipping elements themselves (Wang & Hausfather, 2020; Lenton et al., 2019; Steffen et al., 2018), it presented a first step towards synthesising the positive and negative feedbacks between climate tipping elements. To our best knowledge, a systematic update of this assessment or a comparably comprehensive expert assessment has not been undertaken since Kriegler et al. (2009).

Based on the network from this expert elicitation and a Boolean approach based on graph grammars, an earlier study found that the strong positive-negative feedback loop between the Greenland Ice Sheet and the AMOC might act as a stabiliser to the

Earth system (Gaucherel & Moron, 2017). Also, using the interaction network data of Kriegler et al. (2009), it has been shown that large economic damages due to tipping cascades could arise with respect to the social cost of carbon, using a stochastic and dynamic evaluation of tipping points in an integrated assessment model (Cai et al., 2016). Other studies also quantified the economic impacts of single climate tipping events and tipping interactions (Lemoine & Traeger, 2016; Cai et al., 2015). In the light of recent studies that hypothesise a considerable risk of current anthropogenic pressures triggering tipping cascades, up to a potential global cascade (towards a so-called "hothouse state" of the Earth system) (Lenton et al., 2019; Steffen et al., 2018), we here aim at developing a conceptual dynamic network model that can assess whether interactions of tipping elements have an overall stabilising or destabilising effect on the global climate state. As such, we view our approach as an hypotheses generator that produces qualitative scenarios (rather than exact quantifications or projections) that can then be further examined by more process-detailed Earth system models. In this way, the results of this study can lay the foundations and possibly guide towards a more detailed analysis with more complex models or data-based approaches.

### 1.3 Constraints from current observations and paleoclimatic evidence

Observations over the past decades show that several tipping elements are already impacted by progressing global warming (Wang & Hausfather, 2020; Lenton et al., 2019; IPCC, 2014; Levermann et al., 2010). Ice loss from Greenland and West Antarctica has increased and accelerated over the past decades (Shepherd et al., 2018; Khan et al., 2014; Zwally et al., 2011). Recent studies suggest that the Amundsen basin in West Antarctica might in fact have already crossed a tipping point (Favier et al., 2014; Rignot et al., 2014). The grounding lines of glaciers in this region are rapidly retreating, which could induce the Marine Ice Sheet Instability and eventually lead to the disintegration of the entire basin (Mercer, 1978; Weertman, 1974). Paleoclimate records suggest that parts of Antarctica and larger parts of Greenland might already have experienced strong ice retreat in the past, especially during the Pliocene as well as during Marine Isotope Stages 5e and 11 (Dutton et al., 2015).

It has also been shown that the AMOC experienced a significant slow-down since the mid 20th century (Caesar et al., 2018), potentially due to freshening of the North Atlantic ocean by increased meltwater influx from Greenland (Bakker et al., 2016; Böning et al., 2016). An AMOC slow-down has likely also occurred during the last deglaciation in the Heinrich event 1 and Younger Dryas cold periods, as proxies from sea surface and air temperatures as well as climate model simulations suggest (Ritz et al., 2013).

The Amazon rainforest is not only directly impacted by anthropogenic climate change, including the increased risk of extensive drought events or heat waves (Marengo et al., 2015; Brando et al., 2014), but also by deforestation and fire (Thonicke et al., 2020; Malhi et al., 2009). This increases the likelihood that parts of it will shift from a rainforest to a savannah state for instance through diminished moisture recycling (Staal et al., 2018; Zemp et al., 2017). It is suspected that the Amazon rainforest could be close to a critical extent of deforestation which might, together with global warming, suffice to initiate such a critical transition (Nobre et al., 2016). This could put 30–50% of rainforest ecosystems at risk of shifting the rainforest to

tropical savannah or dry forests (Nobre et al., 2016). On a local to regional point of view, the potential for critical transitions in the rainforest is further examined by more recent studies (Staal et al., 2020; Ciemer et al., 2019).

### 1.4 Structure of this work

Following the introduction, in Sect. 2, we provide an overview of the biogeophysical processes governing the individual dynamics and interactions of the four tipping elements considered here, and how these are represented in our conceptual network model. We also describe the construction of the large-scale Monte-Carlo ensemble which enables us to propagate the parameter uncertainties inherent in the modelled tipping elements and their interactions. In Sect. 3, we explore how the critical threshold temperature ranges of the tipping elements change with increasing overall interaction strength. It is also shown which tipping elements initiate and transmit tipping cascades, revealing the characteristic roles of the tipping elements in the Earth system. We also discuss the distinct nature of ENSO as a potential tipping element, and present results of a robustness analysis including this additional tipping element in our network model. Sect. 4 summarises the results and discusses the limitations of our approach. It also outlines possible further lines of research concerning tipping element interactions and risks of emerging tipping cascades with more process-detailed models.

## 2 Methods

In the following, we present our dynamic network approach for modelling tipping interactions and cascades in the Earth system. In Sect. 2.1, we motivate the use of a stylised equation to represent climate tipping elements in a conceptual manner. This equation exhibits a double-fold bifurcation (see Fig. 2)

$$\frac{dx_i}{dt} = \left[-x_i^3 + x_i + c_i\right] \frac{1}{\tau_i}. \tag{1}$$

Here, $x_i$ indicates the state of a certain tipping element, $c_i$ is the critical parameter and $\tau_i$ the typical tipping time scale with $i = \{\text{Greenland Ice Sheet, West Antarctic Ice Sheet, AMOC, Amazon rainforest}\}$. This approach has already been used frequently for qualitatively describing tipping dynamics in different applications and network types and has been applied to systems in climate, ecology, economics and political science (Klose et al., 2020; Krönke et al., 2020; Wunderling et al., 2020a; Dekker et al., 2018; Brummitt et al., 2015; Abraham et al., 1991).

To describe the tipping elements' interactions, we extend Eq. 1 by a linear coupling term (Klose et al., 2020; Krönke et al., 2020; Brummitt et al., 2015) to yield

$$\frac{dx_i}{dt} = \left[ \overbrace{-x_i^3 + x_i + c_i}^{\text{Individual dynamics term}} + \overbrace{\frac{1}{2} \sum_{\substack{j \\ j \neq i}} d_{ij} \left(x_j + 1\right)}^{\text{Coupling term}} \right] \frac{1}{\tau_i}, \tag{2}$$

and describe the physical interpretation of these interactions between the tipping elements in Sect. 2.2. While the first term (*individual dynamics term*) determines the dynamical properties of each individual tipping element, the second term (*coupling*

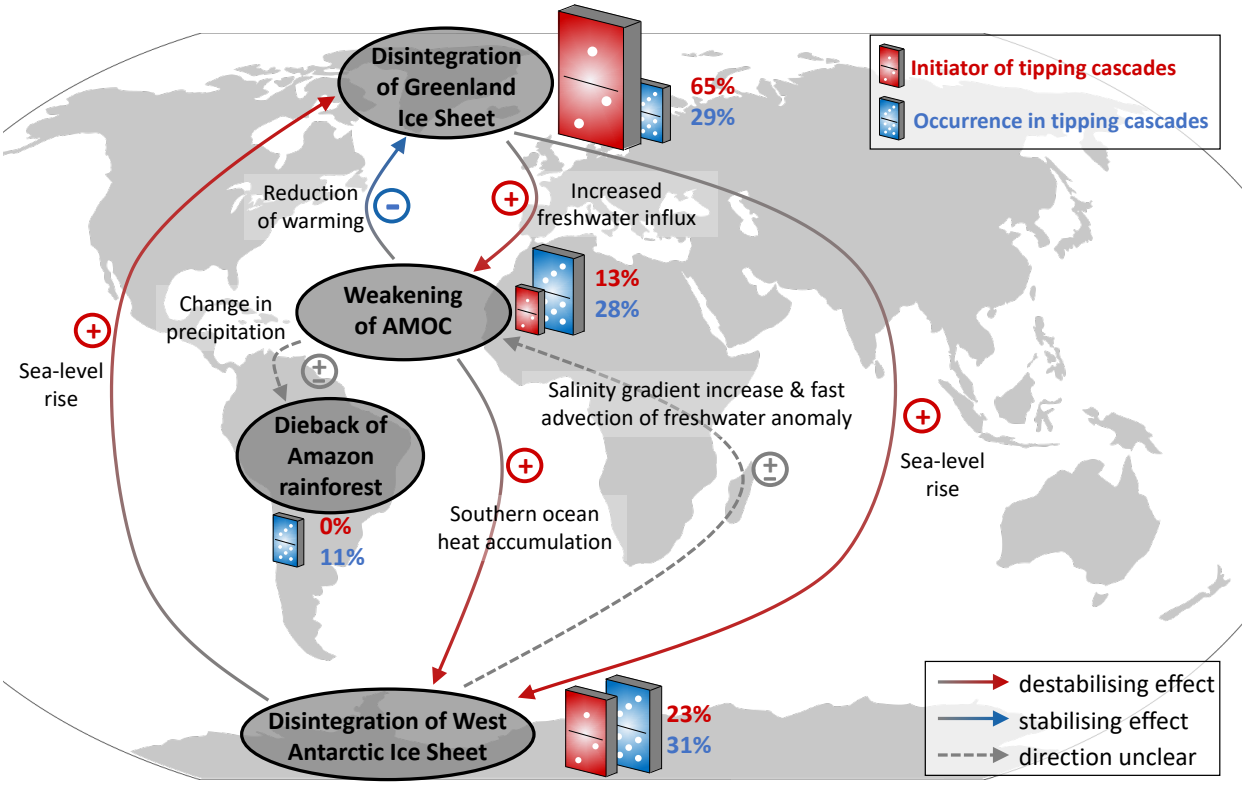


**Figure 1.** Interactions between climate tipping elements and their roles in tipping cascades. The Greenland Ice Sheet, West Antarctic Ice Sheet, Atlantic Meridional Overturning Circulation (AMOC) and the Amazon rainforest are depicted together with their main interactions (Kriegler et al., 2009). The links between the tipping elements are colour-coded, where red arrows depict destabilising and blue arrows depict stabilising interactions. Where the direction is unclear, the link is marked in grey. A more thorough description of each of the tipping elements and the links can be found in Tables 1, 2 and in Sect. 2. Where tipping cascades arise, the relative size of the dominoes illustrates in how many ensemble members the respective climate component initiates (red domino) or occurs in tipping cascades (blue domino). Standard deviations for these values are given in Figs. S1(a) and (b). Generally, the polar ice sheets are found to more frequently take on the role as initiators of cascades than the AMOC and Amazon rainforest.

*term*) describes the effects of interactions between tipping elements. If the prefactors in front of the cubic and the linear term are unity as in Eq. 2 and the additive coupling term is neglected ($d_{ij} = 0$ for all $i$, $j$), the critical threshold values where qualitative state changes occur are $c_{i\ 1,2} = \pm\sqrt{4/27}$ (Klose et al., 2020). The system described by this differential equation is bistable for values of the critical parameter between $c_1$ and $c_2$ and can here be separated into a *transitioned* and a *baseline* state, where $x_i = -1$ denotes the baseline state and $x_i = +1$ the completely transitioned one (see Fig. 2).

Building on these model equations, in Sect. 2.3, we describe the fully parameterised model and its parameters as it is used in this study. Specifications of how tipping cascades are evaluated and time scales are chosen can be found in Sects. 2.4 and 2.5. Lastly, our large scale Monte Carlo ensemble approach for the propagation of parameter and interaction network uncertainties is described in Sect. 2.6.

### 2.1 From conceptual to process-detailed models of climate tipping elements

In the conceptual network model investigated in this study, the main dynamics of each of the tipping elements are condensed to a non-linear differential equation with two stable states representing the current (baseline) state and a possible transitioned state capturing the qualitative dynamics of generalised tipping elements (see Eq. 1). This serves as a stylised representation for the Greenland Ice Sheet, the West Antarctic Ice Sheet, the AMOC and the Amazon rainforest. We here focus on these four out of a larger range of tipping elements in the cryosphere, biosphere and oceanic and atmospheric circulation patterns that have been suggested in the literature (Schellnhuber et al., 2016; Scheffer et al., 2009; Lenton et al., 2008). In this study, we do not consider a possible "backtipping" (or hysteresis behaviour) of climate tipping elements, since the forcing represented by global mean temperature anomalies is only increased, but never decreased in our experiments. It is clear that the representation of a complex climate tipping element with all its interacting processes as well as positive and negative feedbacks in a stylised cusp bifurcation model is a strong simplification. In the following, we elaborate on why such a cusp bifurcation structure (Eq. 1) can nonetheless be assumed to capture the overall stability behaviour for these four tipping elements (Bathiany et al., 2016), before we introduce more mathematical details of our dynamical systems approach in Sect. 2.3.

1. *AMOC*: Early conceptual models introduced in the 1960s showed that the AMOC could exhibit a cusp-like behaviour, using simplified box models based on the so-called salt-advection feedback (Stommel, 1961; Cessi, 1994). Many extensions and updates to this well-known box model approach have been put forward, each confirming the potential multistability of the AMOC (e.g. Wood et al. (2019)). More complex Earth system models including EMICs (e.g., CLIMBER) and AOGCMs (e.g., the FAMOUS and HadGEM3 models) have shown hysteresis behaviour which is qualitatively similar to Eq. 1 (Mecking et al., 2016; Hawkins et al., 2011; Rahmstorf et al., 2005). Furthermore, paleoclimatic evidence suggests a bistability of the AMOC: In paleoclimate records, Dansgaard-Oeschger events (see e.g. Crucifix, 2012) have been associated with large reorganisations of the AMOC (Ditlevsen et al., 2005; Timmermann et al., 2003; Ganopolski & Rahmstorf, 2002), where ice core data links the events to sea-surface temperature increases in the North Atlantic. Even though there are considerable uncertainties, literature estimates suggest the level of global warming sufficient for tipping the AMOC between 3.5–6.0 °C (Schellnhuber et al., 2016; Lenton, 2012; Levermann et al., 2012; Lenton et al.,

2008), with the risk of crossing a critical threshold considerably increasing beyond 4 °C above pre-industrial temperature levels (Kriegler et al., 2009).

2. *Greenland Ice Sheet*: Previous studies have shown that a double fold-like bifurcation structure for the ice sheets can arise from the melt-elevation feedback (Levermann & Winkelmann, 2016) as well as from the Marine Ice Sheet Instability and other positive feedback mechanisms (e.g., DeConto & Pollard, 2016; Schoof, 2007). In particular, dynamic ice sheet model simulations have identified irreversible ice loss once a critical temperature threshold is crossed (Toniazzo et al., 2004), leading to multiple stable states and hysteresis behaviour for the Greenland Ice Sheet (Robinson et al., 2012; Ridley et al., 2010). In Robinson et al. (2012), the critical temperature range for an irreversible disintegration of the Greenland Ice Sheet has been estimated between 0.8–3.2 °C of warming above pre-industrial global mean temperature levels. Paleoclimate evidence further suggests that there have been substantial, potentially self-sustained retreats of the Greenland Ice Sheet in the past. It has, for instance, been simulated that the Greenland Ice Sheet can disintegrate in case warmer ocean conditions from the Pliocene are applied to an initially glaciated Greenland (Koenig et al., 2014). Further, Greenland was nearly ice-free for extended interglacial periods during the Pleistocene (Schaefer et al., 2016). Sea-level reconstructions further suggest that large parts of Greenland could have been ice-free during Marine Isotope Stage 11 and the Pliocene (Dutton et al., 2015).

3. *West Antarctic Ice Sheet*: Compared to the case of the Greenland Ice Sheet, different processes make the West Antarctic Ice Sheet susceptible to tipping dynamics. Since large parts of West Antarctica are grounded in marine basins, changes in the ocean are key in driving the evolution of the ice sheet. The Marine Ice Sheet Instability can trigger self-sustained ice loss where the ice sheet is resting below sea-level on retrograde sloping bedrock (Weertman, 1974; Schoof, 2007). This destabilising mechanism is possibly already underway in the Amundsen Sea region (Favier et al., 2014; Joughin et al., 2014). Once triggered, a single local perturbation via increased sub-shelf melting in the Amundsen region could lead to wide-spread retreat of the West Antarctic Ice Sheet (Feldmann & Levermann, 2015). Further, a recent study shows strong hysteresis behaviour for the whole Antarctic Ice Sheet, identifying two major thresholds which lead to a destabilisation of West Antarctica around 2°C of global warming, and large parts of East Antarctica between 6–9°C of global warming (Garbe et al., 2020). It is likely that the West Antarctic Ice Sheet has experienced brief but dramatic retreats during the past five million years (Pollard & DeConto, 2009). Prior collapses have been suggested from deep-sea-core isotopes and sea-level records (Gasson, 2016; Dutton et al., 2015; Pollard & DeConto, 2005).

4. *Amazon rainforest*: Conceptual models of the Amazon identified multi-stability between rainforest, savannah and treeless states, leading to hysteresis (Staal et al., 2016, 2015; Van Nes et al., 2014). This hysteresis has been found to be shaped by local-scale tipping points of the Amazon rainforest and its resilience might be diminished under climate change until the end of the 21st century (Staal et al., 2020). More complex dynamic vegetation models also found alternative stable states of the Amazon ecosystem (Oyama & Nobre, 2003) and suggest that rainforest dieback might be possible due to drying of the Amazon basin under future climate change scenarios (Nobre et al., 2016; Cox et al., 2004, 2000). Observational data further supports the potential for multi-stability of the Amazon rainforest (Ciemer et al., 2019; Hirota et al., 2011;

Staver et al., 2011). While it remains an open question whether the Amazon has a single system-wide tipping point, the projected increase in droughts and fires (Malhi et al., 2009; Cox et al., 2008) is likely to impact the forest cover on a local to regional scale, which might spread to other parts of the region via moisture-recycling feedbacks (Zemp et al., 2017, 2014; Aragão, 2012). It is important to note that in contrast to the ice sheets and ocean circulation, the rainforest is able to adapt to changing climate conditions to a certain extent (Sakschewski et al., 2016). However, this adaptive capacity might still be outpaced if climate change progresses too rapidly (Wunderling et al., 2020c). A dieback of the Amazon rainforest has been found under a business-as-usual emissions scenario (Cox et al., 2004), which would be equivalent to a global warming of more than 3 °C above pre-industrial levels until 2100 (≈3.5–4.5 °C (see also Schellnhuber et al., 2016)), mainly due to more persistent El-Niño conditions (Betts et al., 2004).

### 2.2 Physical interpretation of tipping element interactions

Based on these conceptual models as well as building on first coupled experiments with a discrete state Boolean model (Gaucherel & Moron, 2017) and economic impact studies (Cai et al., 2016; Lemoine & Traeger, 2016; Cai et al., 2015), we here describe the interactions of the four tipping elements in a network approach using a set of linearly coupled, topologically equivalent differential equations (Kuznetsov, 2004). In the following we go through the different main interactions of the four tipping elements considered here and expand on the underlying physical processes. Overall, the additional literature supports and refines the results from an early expert elicitation (Kriegler et al., 2009).

1. *Greenland Ice Sheet → AMOC*: Increasing freshwater input from enhanced melting of the Greenland Ice Sheet can lead to a weakening of the AMOC, as supported by observations, paleoclimate evidence as well as modelling studies (Caesar et al., 2018; Robson et al., 2014; Driesschaert et al., 2007; Jungclaus et al., 2006; Rahmstorf et al., 2005). Between 1992 and 2018, the Greenland Ice Sheet has lost around 3900±342 Gt of ice (Shepherd et al., 2020). This ice loss has strongly accelerated in recent years (Sasgen et al., 2020), and Greenland has been subject to several extreme melt events in the past decade alone (Tedesco & Fettweis, 2020; Nghiem et al., 2012; Tedesco et al., 2011). At the same time, an AMOC weakening of 15% (3±1 Sv) has been observed since the 1950s (Caesar et al., 2018). This weakening has at least partially been attributed to freshwater influx into the North Atlantic deep water formation regions due to enhanced melting from Greenland. Paleoclimatic records further suggest that the AMOC could exist in multiple stable states, based on observed temperature changes associated with meltwater influx into the North Atlantic (Blunier and Brook, 2001; Dansgaard et al., 1993). Therefore, it is likely that a tipping of the Greenland Ice Sheet would lead to a destabilisation of the AMOC (see Fig. 1).

2. *AMOC → Greenland Ice Sheet*: Conversely, if the AMOC weakens, leading to a decline in its northward surface heat transport, Greenland might experience cooler temperatures (e.g. Jackson et al., 2015; Timmermann et al., 2007; Stouffer et al., 2006), which would have a stabilising effect on the ice sheet. With the global climate model HadGEM3, it has been shown that temperatures in Europe could drop by several degrees if the AMOC collapses, regionally up to 8 °C (Jackson et al., 2015). A cooling trend in sea surface temperatures (SST) over the subpolar gyre, as a result of a weakening AMOC,

has been confirmed by recent reanalysis and observation data (Caesar et al., 2018; Jackson et al., 2016; Frajka-Williams, 2015; Robson et al., 2014). This "fingerprint" translates a reduction in overturning strength by 1.7 Sv per century to 0.44 K SST-cooling per century (Caesar et al., 2018). AMOC regime shifts between weaker and stronger overturning strength during the last glacial period have been associated with large regional temperature changes in Greenland, for example during Dansgaard-Oeschger or Heinrich events (Barker and Knorr, 2016). Moreover, there is paleoclimatic evidence from 3.6 million years ago that a weaker North Atlantic current as part of the AMOC fostered Arctic sea-ice growth which might have preceded continental glaciation in the northern hemisphere at that time (Karas et al., 2020). Based on these findings, we assume that a weakening of the AMOC would have a stabilising effect on the Greenland Ice Sheet (see Fig. 1).

3. *West Antarctic Ice Sheet → AMOC*: It remains unclear whether increased ice loss from the West Antarctic Ice Sheet has a stabilising or destabilising effect on the AMOC (see Fig. 1). Swingedouw et al. (2009) identified different processes based on freshwater hosing experiments into the Southern Ocean, which could be associated with a melting West Antarctic Ice Sheet (Swingedouw et al., 2009). Using the EMIC LOVECLIM1.1, the authors found both enhancing and weakening effects on the AMOC strength:
   First, deep water adjustments are observed. This means that an increase of the North Atlantic Deep Water formation is observed in response to a decrease in Antarctic bottom water production due to the conducted hosing experiment. This mechanism has been termed the so-called bipolar ocean seesaw. Second, salinity anomalies in the Southern Ocean are distributed to the North Atlantic, which dampens the North Atlantic Deep Water formation (compare to Seidov et al., 2005). Third, the North Atlantic Deep Water formation is enhanced by a strengthening of southern hemispheric winds in response to a southern hemispheric cooling. The reason for the stronger winds is the greater meridional temperature gradient between a cooler Antarctic region (due to the hosing experiment) and the equator. This effect has been termed the *Drake Passage effect* (Toggweiler & Samuels, 1995).
   Overall, the first and the third mechanism tend to strengthen the AMOC, while the second process would rather lead to a weakening of the AMOC. The specific time scales and relative strengths of these mechanisms are as of yet unclear (Swingedouw et al., 2009). In a coupled ocean-atmosphere model, a slight weakening of the AMOC was detected for a freshwater input of 1.0 Sv in the Southern Ocean over 100 years (Seidov et al., 2005). However, other studies suggest a stabilisation of the AMOC if influenced by freshwater input from the West Antarctic Ice Sheet due to the effects from the bipolar ocean seesaw by decreasing Antarctic Bottom Water formation as described above (Swingedouw et al., 2008).

4. *AMOC → West Antarctic Ice Sheet*: The interaction from the AMOC to the West Antarctic Ice Sheet is destabilising (see Fig. 1). In case the AMOC shuts down, sea surface temperature anomalies could appear since the northward heat transport is diminished significantly. This could then lead to a warmer south and colder north, as observed in modelling studies (Weijer et al., 2019; Timmermann et al., 2007; Stouffer et al., 2006; Vellinga & Wood, 2002). A model intercomparison study for EMICs and AOGCMs found a sharp decrease of surface air temperatures over the northern hemisphere,

while a slight increase over the southern hemisphere and around the Antarctic Ice Sheet has been observed (Stouffer et al., 2006). In their study (Stouffer et al., 2006), a forcing of 1.0 Sv was applied to the northern part of the North Atlantic Ocean. Therefore, we set this link as destabilising in the interaction network mdoel (see Fig. 1).

5. *Greenland Ice Sheet ↔ West Antarctic Ice Sheet*: The direct interaction between the Greenland and the West Antarctic Ice Sheet via sea level changes can be regarded as mutually destabilising, however with different magnitudes (see Fig. 1). It is a well-known phenomenon from tidal changes that grounding lines of ice sheets are varying (e.g. Sayag & Worster, 2013). Therefore, the Greenland Ice Sheet and the West Antarctic Ice Sheet could influence each other by sea level rise if one or the other cryosphere element would melt. Gravitational, but also elastic and rotational impacts would then enhance the sea level rise in case one of the huge ice sheets would melt first, since then only the other ice sheets exerts strong gravitational forces on ocean waters (Kopp et al., 2010; Mitrovica et al., 2009). The impact of this effect would be larger if Greenland becomes ice-free earlier than West Antarctica, since many marine terminating ice shelves are located in West Antarctica, but the interaction is destabilising in both directions (see Fig. 1).

6. *AMOC → Amazon rainforest*: Lastly, the interaction between the AMOC and the Amazon rainforest is set as unclear (see Fig. 1). It is suspected that the intertropical convergence zone (ITCZ) would be shifted southward in case the AMOC collapses. This could cause large changes in seasonal precipitation on a local scale, and could as such have strong impacts on the Amazon rainforest (Jackson et al., 2015; Parsons, 2014). In the Earth system model ESM2M, it has been found that a strongly suppressed AMOC, through a 1.0 Sv freshwater forcing, leads to drying over many regions of the Amazon rainforest (Parsons, 2014). However, some regions would receive more rainfall than before. On a seasonal level, the wet season precipitation is diminished strongly, while the dry season precipitation is significantly increased (Jackson et al., 2015; Parsons, 2014). This could have consequences for the current vegetation that is adapted to this partially strong seasonal precipitation. But overall, it remains unclear whether the influence from a tipped AMOC on the precipitation in South America has a reducing or increasing influence. Instead, it might differ from locality to locality and is set as unclear in our study (see Fig. 1).

### 2.3 Dynamic network model of interacting tipping elements

In this subsection, we describe the details of the employed dynamic network model, the foundations of which are given by Eqs. 1 and 2. The critical parameter $c_i$ of tipping element $i$ is modelled as a function of global mean temperature, i.e., $c_i = \sqrt{\frac{4}{27}} \cdot \frac{\Delta\text{GMT}}{T_{\text{limit, i}}}$, where $T_{\text{limit, i}}$ is the critical temperature and $\Delta$GMT the increase of the global mean temperature above pre-industrial levels. This parameterization implies that a state change is initiated as soon as the increase of GMT exceeds the critical temperature ($\frac{\Delta\text{GMT}}{T_{\text{limit, i}}} > 1$, see Table 1). In addition, we model the physical interactions between the tipping elements as a linear coupling (first order approach). The coupling term $\frac{1}{2}\sum_j d_{ij}\,(x_j + 1)$ consists of a sum of linear couplings to other elements $x_j$ with $d_{ij} = d \cdot s_{ij}/5$. It is necessary to add $+1$ to $x_j$ such that the direction (sign) of coupling is only determined

by $d_{ij}$ and not by the state $x_j$. Thus, Eq. 2 becomes

$$\frac{dx_i}{dt} = \left[ -x_i^3 + x_i + \sqrt{\frac{4}{27}} \cdot \frac{\Delta\mathrm{GMT}}{T_{\mathrm{limit,\,i}}} + d \cdot \sum_{\substack{j \\ j \neq i}} \frac{s_{ij}}{10} \left(x_j + 1\right) \right] \frac{1}{\tau_i}. \tag{3}$$

Here $d$ is the overall *interaction strength* parameter that we vary in our simulations and $s_{ij}$ is the link strength based on the expert elicitation (Kriegler et al., 2009) (see Table 2 & Sect. 2.6). The prefactor 1/10 sets the coupling term of Eq. 3 to the same scale as the individual dynamics term by normalising $s_{ij}$ when $d$ is varied between 0.0 to 1.0. The geophysical processes behind the interactions between the tipping elements are listed in Table 2 and are described and referenced in Sect. 2.2.

| **Tipping element** | $\mathbf{\Delta T_{limit}}$ **(°C)** |
|---|---|
| Greenland | 0.8 – 3.2 |
| West Antarctica | 0.8 – 5.5 |
| AMOC | 3.5 – 6.0 |
| Amazon rainforest | 3.5 – 4.5 |

**Table 1.** Nodes in the modelled network of interacting tipping elements. For each tipping element in the network (see Fig. 1), a range of critical temperatures $\Delta T_{\mathrm{limit}}$ is known from literature review (Schellnhuber et al., 2016). Within this temperature range, the tipping element is likely to undergo a qualitative state transition.

In this network of tipping elements, very strong interactions exist, as detailed above. For each tipping element, there are two potential reasons for a state transition, either through the increase of GMT or through the coupling to other tipping elements (Fig. 2(a)).

The overall interaction strength $d$ is described as a dimensionless parameter (see Eq. 3) that is varied over a wide range in our simulations, i.e., for $d \in [0; 1]$, to account for the uncertainties in the actual physical interaction strength between the tipping elements. This way a range of different scenarios can be investigated. An interaction strength of 0 implies no coupling between the elements such that only the individual dynamics remain. When the interaction strength reaches high values around 1, the coupling term is of the same order of magnitude as the individual dynamics term. In principle, more complex and data- or model-based interaction terms could be developed. However, while some interactions (e.g. between Greenland Ice Sheet & AMOC) have been established with EMICs such as CLIMBER-2 and Loveclim as well as GCMs (Wood et al., 2019; Sterl et al., 2008; Driesschaert et al., 2007; Jungclaus et al., 2006; Rahmstorf et al., 2005), other interactions are less well understood potentially leading to biased coupling strengths (see also Sect. 2.2). Due to the sparsity of data concerning tipping interactions in the past, it remains challenging to extract the interaction parameters from paleoclimatic evidence. We here therefore attempt to include the full uncertainty ranges concerning the different model parameters and interaction strengths. To this end, we run large ensembles of simulations over long time scales. This is important since the disintegration of the ice sheets for instance

| **Interaction link** | **Maximum link strength $s_{ij}$ (a.u.)** | **Physical process** |
|---|---|---|
| Greenland $\rightarrow$ AMOC | $+10$ | Freshwater influx |
| AMOC $\rightarrow$ Greenland | $-10$ | Reduction of northward heat transport |
| Greenland $\rightarrow$ West Antarctica | $+10$ | Sea-level rise |
| AMOC $\rightarrow$ Amazon rainforest | $\pm 2$ up to $\pm$ 4 | Changes in precipitation patterns |
| West Antarctica $\rightarrow$ AMOC | $\pm 3$ | Increase in meridional salinity gradient ($-$), Fast advection of freshwater anomaly to North Atlantic ($+$) |
| West Antarctica $\rightarrow$ Greenland | $+2$ | Sea-level rise |
| AMOC $\rightarrow$ West Antarctica | $+1.5$ | Heat accumulation in Southern Ocean |

**Table 2.** Interaction links in the network of tipping elements. For each link in the network of Fig. 1, there is a strength and a sign for each interaction of the tipping elements. The sign indicates if the interaction between the tipping elements is increasing or decreasing the danger of tipping cascades. Following Kriegler et al. (2009), the strength $s_{ij}$ gives an estimate in terms of increased or decreased probability of cascading transitions (Kriegler et al., 2009). E.g., if Greenland transgresses its threshold, the probability that the AMOC does as well is increased by a factor of 10 (see entry for Greenland $\rightarrow$ AMOC). Then a random number between $+1$ and $s_{\mathrm{Greenland}\rightarrow\mathrm{AMOC}} = +10$ is drawn for our simulations and used for $s_{ij}$ in Eq. 3. The other way round, the probability that Greenland transgresses its threshold in case the AMOC is in the transitioned state is decreased by a factor of $\frac{1}{10}$. Then a random number between $-1$ and $s_{\mathrm{AMOC}\rightarrow\mathrm{Greenland}} = -10$ is drawn. The main physical processes that connect pairs tipping elements are described in this table and in Sect. 2.2. The link strengths are grouped into strong, intermediate and weak links. Note that in the expert elicitation (Kriegler et al., 2009), there has been an estimation of the maximum increase or decrease of the tipping probability in case the element which starts the interaction is already in the transitioned state. For example, the link between Greenland and AMOC is given as [1; 10] in Kriegler et al. (2009) and is here modelled as a randomly drawn variable between 1 and 10 for $s_{ij}$. An example for an unclear coupling would be the link between West Antarctica and AMOC which is given as [0.3; 3] in Kriegler et al. (2009) which we translate into an $s_{ij}$ between $-3$ and 3. In general, the values are drawn between 1 and the respective maximum value $s_{ij}$ if the interaction between $i$ and $j$ is positive or between $-1$ and the negative maximum value $s_{ij}$ if the interaction between $i$ and $j$ is negative.

would play out over thousands of years (Winkelmann et al., 2015; Robinson et al., 2012). Due to computational constraints, studying such an ensemble of millennial-scale simulations is typically not feasible with more complex Earth System Models. We propagate the considerable uncertainties linked to the parameters of the tipping elements and their interactions with a large-scale Monte-Carlo approach (see Sect. 2.6).

### 2.4 Parameterisation of the tipping elements' intrinsic time scales

The four tipping elements in the coupled system of differential equations form a so-called *fast-slow system* (Kuehn, 2011) describing a dynamical system with slowly varying parameters compared to fast changing states $x_i$. We include the typical transition times $\tau_i$ from the baseline to the transitioned state in Eq. 3 based on literature values (Lenton et al., 2008; Robinson et al., 2012; Winkelmann et al., 2015), setting the tipping time scales for the Greenland Ice Sheet, West Antarctic Ice Sheet, AMOC and the Amazon rainforest to 4900, 2400, 300 and 50 years for a reference warming of 4 °C above pre-industrial GMT, respectively. The tipping time scale is calibrated at this reference temperature in the case of vanishing interaction between the elements. After calibration, the tipping time is allowed to scale freely with changes in the GMT and the interaction strength $d$. We integrate all model simulations to equilibrium, such that the simulation time is at least 20 times larger than the longest assumed tipping timescale of 4900 years. Since the actual *absolute* tipping times derived from our model simulations are difficult to interpret, our results should not be taken as a projection of how long potential tipping cascades would take to unfold. Rather, following our conceptual approach, we are interested in the relative differences (not the absolute values) between the typical tipping times as they can be decisive as to whether a cascade emerges or not. Therefore, the figures below show model years in arbitrary units (see Figs. 2 and 3).

### 2.5 Modelling protocol and evaluation of tipping cascades

In our network model, if the critical temperature threshold of a tipping element is surpassed, it transgresses into the transitioned state (Fig. 2(a)) and can potentially increase the likelihood of further tipping events via its interactions: for instance, the increased freshwater influx from a disintegration of the Greenland Ice Sheet can induce a weakening or even collapse of the AMOC (Fig. 2(b)). In our model simulations, we consider increases of the global mean temperature from 0 up to 8 °C above the pre-industrial average, which could be reached in worst-case scenarios as the extended representative concentration pathway 8.5 (RCP 8.5) by year 2500 (Schellnhuber et al., 2016; IPCC, 2014).

For each tipping element, we start from the *baseline* (non-tipped) state (where $x_i$ is negative). Global warming or interactions with the other parts of the climate system can then cause the element to tip into the *transitioned* state (see Fig. 2). When the critical parameter reaches $\sqrt{\frac{4}{27}}$ from below (i.e., when $\Delta$GMT reaches $T_{\text{limit, i}}$), the stable baseline state $x_i$ reaches $-\frac{1}{\sqrt{3}}$ in case of an autonomous tipping element. Therefore, the threshold for the baseline state is defined as $x_i^- = -\frac{1}{\sqrt{3}}$. If the critical parameter increases above $\sqrt{\frac{4}{27}}$, the state $x_i$ is larger than $x_i^-$, the stability of the lower stable state is lost and a state transition towards the upper stable $x_i^+$ occurs. Correspondingly to the lower stable state $x_i^-$, the stable transitioned state is defined for states $x_i > x_i^+ = +\frac{1}{\sqrt{3}}$.

We identify and define tipping cascades at a fixed interaction strength $d$ and GMT as the number of additionally tipped elements in equilibrium (as defined above) after an incremental GMT increase of 0.1 °C. The tipping element with critical temperature threshold closest to the GMT at this point, is counted as the initiator of the cascade. All tipping elements that appear in a particular cascade are counted as an occurring tipping element in that tipping cascade.

With increasing global mean temperature and interaction strength, generally more tipping cascades occur (Fig. 3). However, the size, the timing and the occurrence of cascades can also depend critically on the specific initial conditions (Wunderling et al., 2020b), which are not varied in the experiments presented here. In an exemplary simulation, we show how in one realisation of our Monte Carlo ensemble at low interaction strength, a global mean temperature increase from 1.5°C to 1.6°C triggers the Greenland Ice Sheet to transition to an ice-free state (Fig. 3(a)). For larger interactions strengths, the West Antarctic Ice Sheet as well as AMOC might then also tip as part of a tipping cascade that was initiated by the Greenland Ice Sheet in this case (Fig. 3(b-c)). The initial conditions and parameters for the specific example of Fig. 3 can be found in supplementary Table S1.

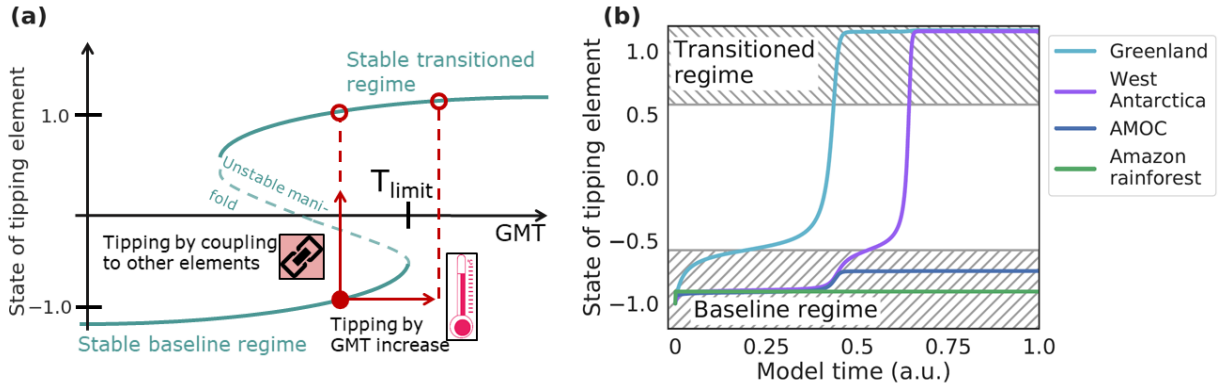


**Figure 2.** Schematic overview of the generalised tipping element and time-series of a tipping cascade. **(a)** Exemplary bifurcation diagram of a tipping element with two stable regimes: The lower state indicates the stable baseline regime, the upper state the stable transitioned regime. In case of the Greenland Ice Sheet, for instance, these correspond to its pre-industrial, almost completely ice-covered state (stable baseline regime) and an almost ice-free state (stable transitioned regime), as can be expected on the long-term for higher warming scenarios (Robinson et al., 2012). There are two ways how a tipping element can transgress its critical threshold (*unstable manifold*) and move into the transitioned state, either by an increase of global mean temperature or via interactions with other climate components. In both cases, the tipping element converges to the stable transitioned regime indicated by the red hollow circles. **(b)** Exemplary time series showing a tipping cascade of two elements. Here, Greenland transgresses its critical temperature ($T_{\text{limit, Greenland}}$) first, i.e., would become ice-free. Through its interaction with the West Antarctic Ice Sheet, the West Antarctic Ice Sheet then transgresses the unstable manifold in vertical direction (following the path of the red upward directed arrow in panel **(a)**). This example is based on a scenario with global mean temperature increase of 1.6 °C above pre-industrial levels and an interaction strength $d = 0.16$ (see also Fig. 3).

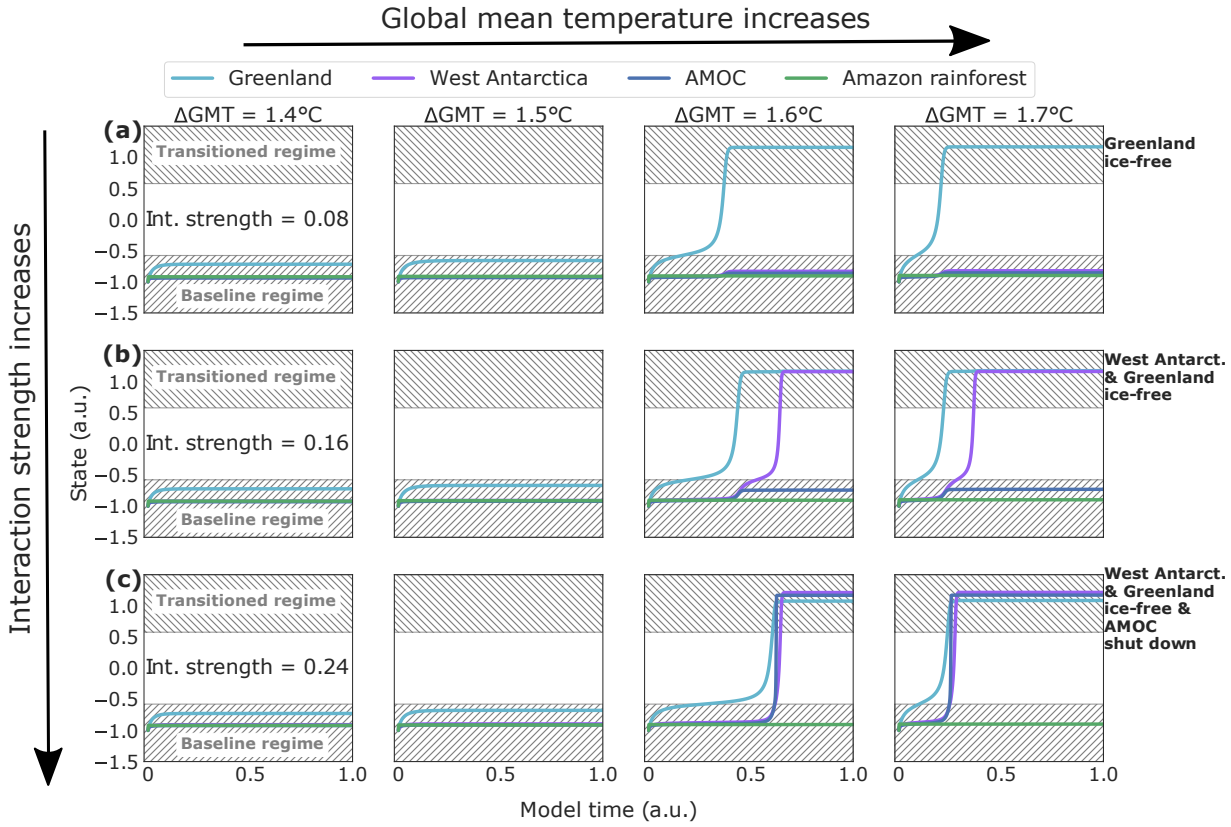


**Figure 3.** Time series of tipping cascades. Exemplary time series of states for each of the four investigated tipping elements, here simulated until equilibrium is reached. For comparability reasons, the parameter settings for the time series are the same (exact parameters can be found in Table S1) and all time series are computed for ΔGMT increases of 1.4, 1.5, 1.6 and 1.7 °C above pre-industrial (columns). Couplings are constant for each row. Tipping cascades as shown here are defined as the number of transitioned elements at a fixed interaction strength and ΔGMT compared to the simulation with a slightly higher ΔGMT (ΔGMT increase by 0.1 °C), but same interaction strength. If, between these two simulations, some of the tipping elements alter their equilibrium state, then a tipping cascade of the respective size occurred and is counted as such. **(a)** Singular tipping event for an interaction strength of 0.08. Tipping occurs at 1.6 °C. **(b)** Tipping cascade of size two for an interaction strength of 0.16. **(c)** Tipping cascade of size three for an interaction strength of 0.24. For other initial conditions, interaction strengths and global mean temperatures (ΔGMT) tipping cascades of size four can occur, too. Additionally, we marked the baseline and the transitioned regime as grey hatched areas. Between the hatched areas, the state is not stable and a critical state transition occurs. In the lower grey area, the element is called to be in the *baseline* regime and in the *transitioned* regime in the upper grey region.

### 2.6 Monte Carlo sampling and propagation of uncertainties

Since the strength of interactions between the tipping elements is highly uncertain, a dimensionless interaction strength is varied over a wide range in our network approach to cover a multitude of possible scenarios. To cope with the uncertainties in the critical threshold temperatures and in the link strengths between pairs of tipping elements (see Eq. 3, Tables 1 and 2), we set up a Monte-Carlo ensemble with approximately 3.7 million members in total.

This Monte Carlo ensemble is generated as follows: for each combination of global mean temperature $\Delta$GMT and overall interaction strength $d$, we create 100 realisations of randomly drawn parameter sets for critical threshold temperatures $T_{\mathrm{limit},i}$ and interaction link strengths $s_{ij}$ based on the uncertainty ranges given above (see Tables 1 and 2). Since our model has 11 parameters with uncertainties (4 critical threshold temperature parameters and 7 interaction link strength parameters), we use a latin-hypercube sampling to construct a set of parameters for each ensemble members such that the multidimensional space of sampled parameters is covered better than with a usual random sample generation (Baudin, 2013).

We also sample all 9 different interaction network structures which arise when we permute all possibilities (negative, zero, positive) arising from the two unclear links between AMOC and Amazon rainforest, and between West Antarctica and the AMOC (see Table 2 and Fig. 1). For each of these 9 network structures, we compute the same 100 starting conditions that we received from our latin-hypercube sampling. Thus, in total, we compute 900 samples for each GMT ($0.0 - 8.0$ °C, step width: 0.1 °C) and interaction strength ($0.0 - 1.0$, step width: 0.02) combination resulting in a large ensemble of 3.7 million members overall.

Our approach is conservative in the sense that there are several destabilising interactions which are not considered here (Lenton et al., 2019; Steffen et al., 2018). Further, by sampling uncertain parameters from a uniform distribution, we are treating lower and higher threshold temperatures as well as strong and weak link interactions equally, potentially resulting in a more balanced ensemble. Additional knowledge about the critical threshold temperatures and interaction link strengths would considerably improve our analysis.

## 3 Results

### 3.1 Shift in effective critical threshold temperatures due to interactions

Owing to the interactions between the tipping elements, their respective critical temperatures (previously identified for each element individually, see Fig. 4(a)) are effectively shifted to lower values (except for Greenland, see Figs. 4(b) and (c)). For West Antarctica and the AMOC, we find a sharp decline for interaction strengths up to 0.2 and an approximately constant critical temperature range afterwards. The effective critical temperature for the Amazon is only marginally reduced due to the interactions within the network, since it is only influenced by the AMOC via an unclear link.

In particular, the ensemble average of the critical temperature at an interaction strength of $d = 1.0$ is lowered by about 1.2 °C (≈40%) for the West Antarctic Ice Sheet, 2.75 °C (≈55%) for the AMOC and 0.5 °C (≈10%) for the Amazon rainforest, respectively (see Fig. S2). This is likely due to the predominantly positive links between these tipping elements (see Fig. 1). In contrast, the critical temperature range for the Greenland Ice Sheet tends in fact to be raised due to the interaction with the other tipping elements, accompanied by a significant increase in overall uncertainty. This can be explained by the strong negative feedback loop between Greenland and the AMOC that is embedded in the assumed interaction network (see Table 2, see also Gaucherel & Moron (2017)). On the one hand, enhanced meltwater influx into the North Atlantic might dampen the AMOC (positive interaction link), while on the other hand, a weakened overturning circulation would lead to a net-cooling effect around Greenland (negative interaction link). Thus, the state of Greenland strongly depends on the specific parameter values in critical threshold temperature and interaction link strength of the respective Monte-Carlo ensemble members. Overall, the interactions are more likely to lead to a destabilisation within the network of climate tipping elements with the exception of the Greenland Ice Sheet.

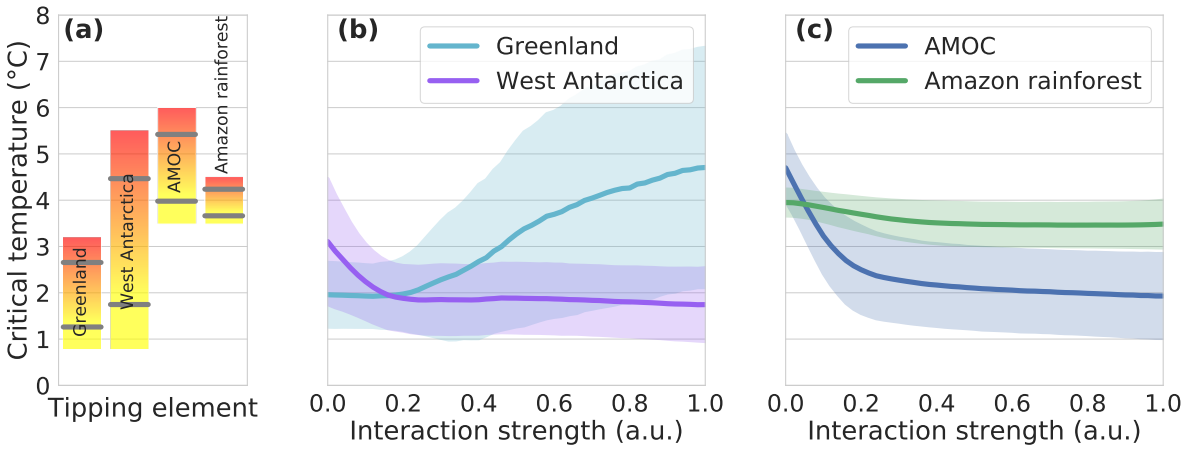


**Figure 4.** Shift of critical temperature ranges due to interactions. **(a)** Critical global mean temperatures for each of the four investigated tipping elements without taking interactions into account (as reproduced from literature; Schellnhuber et al. (2016)). Grey bars indicate the standard deviation arising when drawing from a random uniform distribution between the respective upper and lower temperature limits. These bars correspond to the critical temperature ranges in case of zero interaction strength in panels **(b)** and **(c)**. **(b, c)** Change of critical temperature ranges with increasing interaction strength for the Greenland Ice Sheet and West Antarctic Ice Sheet (panel **(b)**) and the Atlantic Meridional Overturning Circulation (AMOC) and the Amazon rainforest (panel **(c)**). The standard deviation of the critical temperatures for each tipping element within the Monte Carlo ensemble is given as respective colour shading.

### 3.2 Risk of emerging tipping cascades

Tipping cascades occur when two or more tipping elements transgress their critical thresholds for a given temperature level (see Sect. 2.5). We evaluate the associated risk as the share of ensemble simulations in which such tipping cascades are detected. For global warming up to 2.0 °C, tipping occurs in 61% of all simulations (Fig. 5(a)). This comprises the tipping of individual elements (22%) as well as cascades including 2 elements (21%), 3 elements (15%) and 4 elements (3%; see Fig. 5(b)). Since the coupling between the tipping elements is highly uncertain, we introduce an upper limit to the maximum interaction strength and vary it from 0.0 to 1.0 (see Table 3). The highest value of 1.0 implies that the interaction between the elements is as important as the nonlinear threshold behaviour of an individual element (see Eq. 3). For lower values, the interaction plays a less dominant role. We find that the occurrence of tipping events does not depend significantly on the maximum interaction strength – however, the cascade size decreases for lower values.

| **Maximum interaction strength** $d$ | **No tipping (%)** | **Tipping (%)** | **Cascade sizes (%)** | | | |
|---|---|---|---|---|---|---|
| | | | **1** | **2** | **3** | **4** |
| 1.0 | 39 | 61 | 22 | 21 | 15 | 3 |
| 0.75 | 39 | 61 | 26 | 18 | 14 | 2 |
| 0.50 | 39 | 61 | 31 | 15 | 14 | 1 |
| 0.25 | 39 | 61 | 42 | 13 | 6 | 0 |
| 0.10 | 39 | 61 | 56 | 5 | 0 | 0 |

**Table 3.** Share of tipping events in ensemble simulations. For different maximum values of the interaction strength $d$ (first column), the share of ensemble simulations is shown that have a tipping event or cascade (third column) within the Paris limit until the global mean temperature increase reaches 2.0 °C above pre-industrial. This means that 61% of all ensemble members contain a tipping event or cascade, while 39% do not (second column) if all interaction strengths until 1.0 are considered (see Figs. 5(a, b)). Overall, the fraction of tipping events stays the same and does not decrease for lower maximum interaction strengths. However, the distribution of tipping events and cascade sizes changes, i.e., the number of large cascades decreases with lower maximal interaction strength. This is shown in the split last column that displays the share of cascades of size one, two, three and four.

Tipping cascades are first induced at warming levels around 1 °C above pre-industrial GMT, where the lower bound of the critical temperature range for the Greenland Ice Sheet is exceeded. The bulk of tipping cascades, however, is found between 1 and 3 °C GMT increase. This is true for all cascade sizes (see Fig. 5(c, d, e)). For temperatures above 3 °C GMT increase, cascades occur less frequently since most of the tipping elements already transgress their individual threshold before this temperature is reached. The most prevalent tipping cascades of sizes two and three, as simulated in our network approach, consist of cascading transitions between the ice sheets and/or the AMOC, summing up to 80% of all tipping cascades of sizes two or three (Fig. 5(f)).

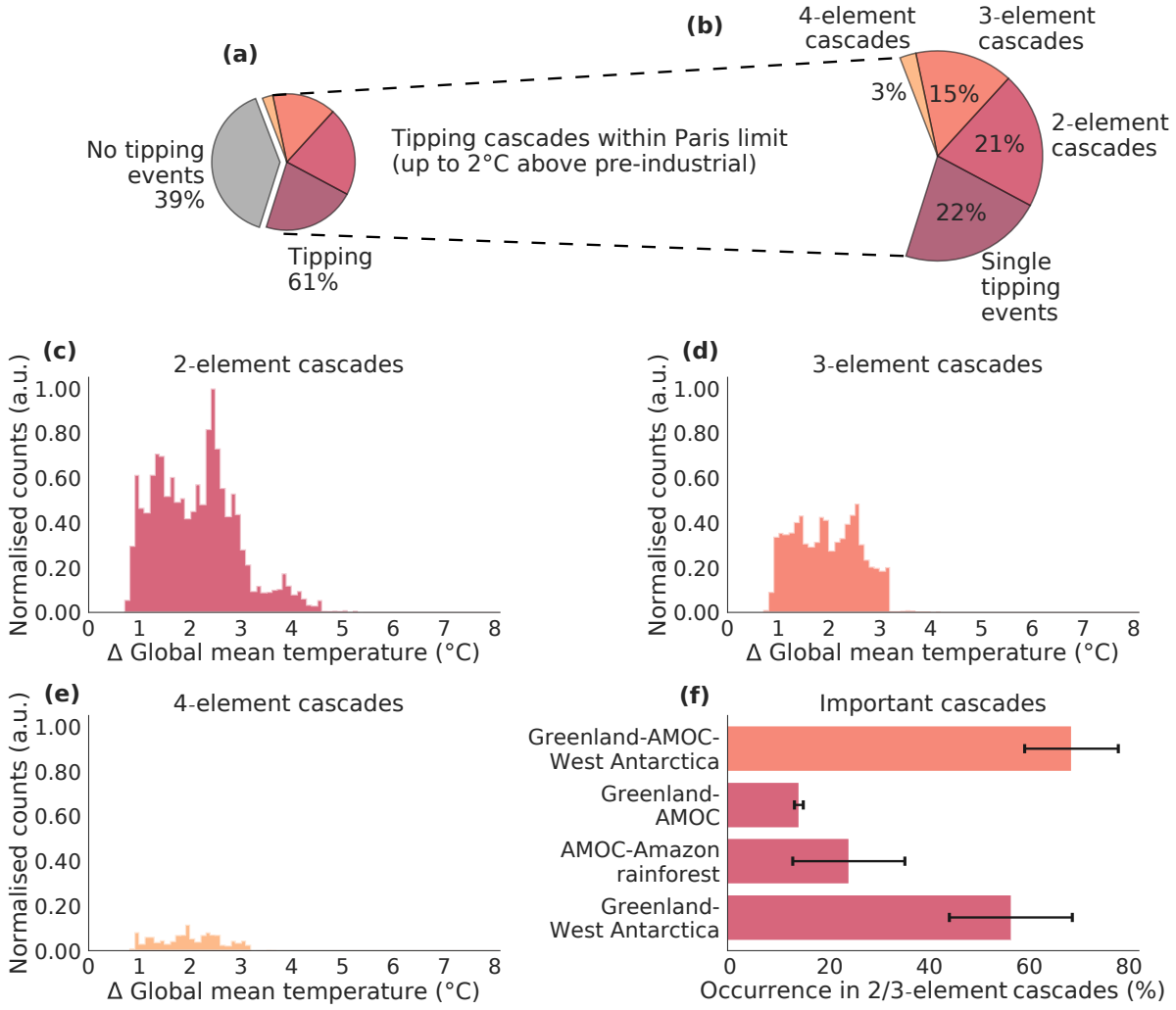


**Figure 5.** Tipping cascades for all interaction strengths between 0.0 and 1.0. **(a, b)** For global warming up to 2.0 °C above pre-industrial levels, the colour shading illustrates the fraction of model representations in the Monte-Carlo ensemble without tipping events (grey), with a singular tipping event (purple) and with cascades including two (red), three (dark orange) and four (light orange) elements. **(c, d, e)** Occurence of tipping cascades of size two, three, and four as a function of global mean temperature increase. The counts are normalised to the highest value of the most frequent tipping cascade (in cascades of size two). **(f)** Dominant cascades of size two and three for temperature increases from $0 - 8$ °C above pre-industrial. Other cascades are not shown, since their relative occurrence is comparatively much smaller. The standard deviation represents the difference between the possible ensemble realisations of the interaction network (see Sect. 2.3). Hence, it tends to be larger for cascades where unclear interaction links are involved, e.g., for the AMOC-Amazon rainforest cascade (compare Fig. 1 and Table 2).

### 3.3 Different roles of tipping elements

For each of the four tipping elements, we systematically assess their role within the network model, generally distinguishing between initiators (triggering a cascade), followers (last element in a tipping chain) and mediators (elements in-between).
We find that in up to 65% of all ensemble simulations, the Greenland Ice Sheet triggers tipping cascades. At the same time, it occurs as frequently in cascades as the other tipping elements (around 29% of all cases, see Fig. 1). Thus, we call Greenland a *dominant initiator* of cascades. Following this argument for Greenland, the West Antarctic Ice Sheet is both an *initiator and mediator* of cascades, since it occurs often in cascades (31%) and, likewise, often acts as the initiator (23%). Although the frequency of occurrence in cascades is very similar for the AMOC as for the two large ice sheets, it is a *dominant mediator* of cascades since it does not initiate many cascades (13%). Lastly, the Amazon rainforest is a *pure follower* in cascades because it is only influenced directly by the AMOC and cannot influence any other tipping element itself in our model due to the given interaction network structure (see Fig. 1). The reason why the ice sheets often act as initiators of tipping cascades in our model is likely because their critical threshold ranges tend to be lower than for the other tipping elements (see Fig. 4a). Many cascades are then passed on to other tipping elements, especially the AMOC. Thus, the role of the AMOC as the main mediator of cascades can be understood from a topological point of view since the AMOC is the most central network element with many connections to the other tipping elements. As such, the AMOC connects the two hemispheres and can be influenced by both the Greenland Ice Sheet and the (West) Antarctic Ice Sheet as is also suggested by literature (Wood et al., 2019; Ivanovic et al., 2018; Hu et al., 2013; Swingedouw et al., 2009; Rahmstorf et al., 2005).

### 3.4 Structural robustness and sensitivity analysis including ENSO

While many tipping elements (including the ice sheets, AMOC and Amazon rainforest) to a first approximation exhibit a transition between two or more alternative stable states, often described by the paradigmatic double-fold bifurcation (Scheffer et al., 2009; Lenton et al., 2008) as discussed above, tipping of the El-Niño Southern Oscillation (ENSO) rather could imply a transition from irregular oscillatory occurrences to a more permanent state of strong El-Niño conditions (Dekker et al., 2018; Lenton et al., 2008; Kriegler et al., 2009). In coupled experiments for AMOC and ENSO with conceptual models, it was found that a changing AMOC could trigger a tipping of ENSO (Dekker et al., 2018; Timmermann et al., 2005). Overall, changes in the frequency of major El-Niño events seem likely, also based on intermediate complexity and conceptual models (Dekker et al., 2018; Timmermann et al., 2005), but whether this poses the possibility of a permanent El-Niño state remains debated. A more frequent occurrence of El-Niño events could have strong impacts on global ecosystems up to a potential dieback of the Amazon rainforest (Duque-Villegas et al., 2019).
While some studies emphasise the uncertainty about future ENSO changes (Kim et al., 2014; Collins et al., 2010), another study found that the frequency of El-Niño events could increase twofold in climate change scenarios in simulations of the CMIP3 and CMIP5 climate model ensembles as well as in perturbed physics experiments (Cai et al., 2014). Also, some ENSO characteristics appear to respond robustly to global warming (Kim et al., 2014; Power et al., 2013; Santoso et al., 2013), such as an intensification of ENSO-driven drying in the western Pacific and rainfall increases in the central and eastern equatorial

Pacific due to nonlinear responses to surface warming (Power et al., 2013). Moreover, from an observational point of view, it was found that the global warming trend since the early 1990s has enhanced the Atlantic capacitor effect which might lead to more favourable conditions for major El-Niño events on a biennial rhythm (Wang et al., 2017). Paleoclimate evidence from the Pliocene (5.3–2.6 Myr before present) with atmospheric $CO_2$ levels comparable to today's conditions suggests that there may have been permanent El-Niño conditions during that epoch (Fedorov et al., 2006; Ravelo et al., 2006; Wara et al., 2005). However, it must be noted that the Pliocene was different in terms of the continental configuration compared to today. Particularly, the Panama gateway was open for at least part of the Pliocene resulting in tropical interactions between Atlantic and Pacific ocean waters (Haug & Tiedemann, 1998).

Given the particular uncertainties regarding ENSO compared to the other tipping elements considered in our analysis, we excluded it and its interactions with the other tipping elements in the main analysis above. However, we performed a comprehensive structural robustness and sensitivity analysis including ENSO as a tipping element (see also Supplementary Figs. S3 – S8): For this purpose, we choose to represent ENSO in the same way as the other tipping elements, although the use of Eq. 1 is not entirely appropriate for ENSO. Rather, the potential tipping behaviour could be conceptualised by a Hopf-bifurcation (i.e., a transition from a limit cycle leading to oscillating behaviour to a stable fixed point attractor) instead of a fold bifurcation (Dekker et al., 2018; Timmermann et al., 2003; Zebiak & Cane, 1987).

A typical transition time of 300 years is chosen, the critical temperature threshold lies between 3.5–7.0°C above pre-industrial levels (Schellnhuber et al., 2016) and our analysis is based on simulations of 11 million ensemble members arising from the 27 different network combinations from the three unclear links AMOC → Amazon rainforest, West Antarctica → AMOC and Amazon rainforest → ENSO (see Fig. S3). The interactions including ENSO are described in detail in the Supplement (see Tab. S2 and description there).

Our robustness analysis reveals that the roles of the tipping elements remain qualitatively the same: the ice sheets remain strong initiators of tipping cascades (in 40% of cases for the Greenland Ice Sheet, and 28% of cases for the West Antarctic Ice Sheet). The AMOC mainly acts as a mediator and only initiates 5% of all cascades (see Fig. S3). In this extended network of tipping elements, ENSO tends to take on an intermediate role. Since it is strongly coupled to the Amazon rainforest, it initiates many cascades including the Amazon rainforest, especially at temperature levels above 3 °C (see Fig. S4). But apart from that, ENSO also mediates tipping cascades from the AMOC to the West Antarctic Ice Sheet or the Amazon rainforest. Generally, we also find that the interactions destabilise the overall network of tipping elements apart from the Greenland Ice Sheet (Figs. S5 and S6). The change in the critical temperature range for the Amazon rainforest is larger and is shifted more towards lower temperature levels due to the influence from ENSO. Overall, the model results remain robust, also with respect to the occurrence and size of tipping cascades (see Fig. S7), suggesting a certain degree of structural stability of our analysis.

## 4 Discussion and Conclusions

It has been shown previously that the four integral components of the Earth's climate system mainly considered here are at risk of transgressing into undesirable states when critical thresholds are crossed (Schellnhuber et al., 2016; Lenton et al.,

2008). Over the past decades, significant changes have been observed for the polar ice sheets, as well as for the Atlantic Meridional Overturning Circulation (AMOC) and the Amazon rainforest (Lenton et al., 2019). Should these climate tipping elements eventually cross their respective critical temperature thresholds, this may affect the stability of the entire climate system (Steffen et al., 2018).

In this study, we show that this risk increases significantly when considering interactions between these climate tipping elements and that these interactions tend to have an overall destabilising effect. Altogether, with the exception of the Greenland Ice Sheet, interactions effectively push the critical threshold temperatures to lower warming levels, thus reducing the overall stability of the climate system. The domino-like interactions also foster cascading, nonlinear responses. Under these circumstances, our model indicates that cascades are predominantly initiated by the polar ice sheets and mediated by the AMOC. Therefore, our results also imply that the negative feedback loop connecting the Greenland Ice Sheet and the AMOC might not be able to stabilise the climate system as a whole, a possibility that was raised in earlier work using a boolean modelling approach (Gaucherel & Moron, 2017).

While our conceptual model evidently does not represent the full complexity of the climate system and is not intended to simulate the multitude of biogeophysical processes or to make predictions of any kind, it allows us to systematically assess the qualitative role of known interactions of some of the most critical components of the climate system. The large-scale Monte Carlo approach further enables us to systematically take into account and propagate the substantial uncertainties associated with the interaction strengths, interaction directions and the individual temperature thresholds. This comprehensive assessment indicates structurally robust results that allow qualitative conclusions, despite all these uncertainties.

In our Monte Carlo approach employed for propagating parameter uncertainties, we assume that all parameters including critical threshold temperatures and interaction link strengths are statistically independent. However, this is likely not the case in the climate system where for example interaction link strengths associated with the AMOC to Greenland and West Antarctica would be expected to be correlated. Further analyses would have to consider the effects of such interdependencies.

Overall, this work could form the basis of a more detailed investigation using more process-detailed Earth System Models that can represent the full dynamics of each tipping element and their interactions. Major advances have been made in developing coupled Earth System Models, however, computational constraints have so far prohibited a detailed interaction analysis as is presented in this work. In the future, these more complex climate models might be driven with advanced ensemble methods for representing and propagating various types of uncertainties in climate change simulations (Daron & Stainforth, 2013; Stainforth et al., 2007), which would comprise a significant step forward in the current debate on nonlinear interacting processes in the realm of Earth system resilience. Some examples of relevant processes that could be investigated with more complex models are the following: First, the changing precipitation patterns over Amazonia due to a tipped AMOC, i.e., whether rainfall patterns will increase or decrease and whether this would be sufficient to induce a tipping cascade in (parts of) the Amazon rainforest. This would shed more light on the interaction pair AMOC-Amazon rainforest. Second, the influence of the disintegration of the West Antarctic Ice Sheet on the AMOC could be further studied by introducing freshwater input into the Southern Ocean surrounding the West Antarctic Ice Sheet similar to the hosing experiments that have been performed for the Greenland Ice Sheet (Wood et al., 2019; Hawkins et al., 2011; Rahmstorf et al., 2005). Here, some studies suggest that

freshwater input into the Southern Ocean at a modest rate would not impact the AMOC as much as freshwater input into the North Atlantic (Ivanovic et al., 2018; Hu et al., 2013; Swingedouw et al., 2009), while higher melt rates could have more severe impacts on the AMOC (Swingedouw et al., 2009). With carefully calibrated coupled ice-ocean models, including dynamic ice sheets (e.g. Kreuzer et al., 2020), ice-ocean tipping cascades could be studied in more detail.

Further, the timescales for potential tipping dynamics need to be more rigorously explored in contrast to the conceptual approach used here. It is important to note that the transition of one tipping element has a delayed effect on the other elements, especially in the case of the comparatively slowly evolving ice sheets. Their temperature threshold is lower than for the other tipping elements considered here and their disintegration would unfold over the course of centuries up to millennia (Winkelmann et al., 2015; Robinson et al., 2012; Lenton et al., 2008). Therefore, meltwater influx into the ocean and changes in sea level would affect the state of other tipping elements only after a significant amount of time. Our analysis of emerging tipping cascades therefore needs to be understood in terms of committed impacts over long time scales due to anthropogenic interference with the climate system mainly in the 20th and 21st centuries, rather than short-term projections.

Finally, it appears worthwhile to perform an updated expert elicitation along the lines of Kriegler et al. (2009), where additional interactions, tipping elements and a better understanding of the interaction strengths would help to narrow down the space of possible scenarios and uncertainties that have been investigated here.

*Code and data availability.* The data that support the findings of this study are available from the corresponding author upon reasonable request. The code for the Monte Carlo ensemble construction and the conceptual network model that support the findings of this study are freely (3-clause BSD license) available on github under the following doi: 10.5281/zenodo.4153102.

*Author contributions.* R.W. and J.F.D. conceived the study. R.W., J.F.D. and N.W. designed the model experiments. N.W. conducted the model simulation runs and prepared the figures. All authors discussed the results and wrote the manuscript.

*Competing interests.* The authors declare no competing interests.

*Acknowledgements.* This work has been carried out within the framework of the IRTG 1740/TRP 2015/50122-0 funded by DFG and FAPESP. N.W., J.K. and R.W. acknowledge their support. N.W. is grateful for a scholarship from the Studienstiftung des Deutschen Volkes. J.F.D. is grateful for financial support by the Stordalen Foundation via the Planetary Boundary Research Network (PB.net), the Earth League's EarthDoc program, and the European Research Council Advanced Grant project ERA (Earth Resilience in the Anthropocene; grant ERC-2016-ADG-743080). R.W. acknowledges support by the European Union's Horizon 2020 research and innovation programme under grant agreement no. 820575 (TiPACCs). We are thankful for support by the Leibniz Association project DominoES. The authors gratefully acknowledge the European Regional Development Fund (ERDF), the German Federal Ministry of Education and Research and the Land Bran-

denburg for supporting this project by providing resources on the high performance computer system at the Potsdam Institute for Climate Impact Research. We thank Anders Levermann, Marc Wiedermann, Jobst Heitzig, Niklas Kitzmann and Julius Garbe for fruitful discussions. We are also grateful to Jonathan Krönke for support with the software package “pycascades”.

**References**


Abraham, R., Keith, A., Koebbe, M., and Mayer-Kress, G.: Computational Unfolding Of Double-Cusp Models Of Opinion Formation, Int. J. Bifurcat. Chaos, 01, 417–430, 1991.

Aragão, L.E.: Environmental science: The rainforest's water pump, Nature, 489, 217-218, 2012.

Bakker, P., Schmittner, A., Lenaerts, J.T.M., Abe-Ouchi, A., Bi, D., van den Broeke, M.R., Chan, W.L., Hu, A., Beadling, R.L., Marsland, S.J. and Mernild, S.H.: Fate of the Atlantic Meridional Overturning Circulation: Strong decline under continued warming and Greenland melting, Geophysical Research Letters, 43, 2016.

Barker, S. and Knorr, G.: A paleo-perspective on the AMOC as a tipping element. PAGES Magazine, 24, 14-15, 2016.

Bathiany, S., Dijkstra, H., Crucifix, M., Dakos, V., Brovkin, V., Williamson, M.S., Lenton, T.M. and Scheffer, M.: Beyond bifurcation: using complex models to understand and predict abrupt climate change, Dynam. Stat. Clim. Syst., 1, 2016.

Baudin, M.: pyDOE: The experimental design package for python, sofware available under the BSD license (3-Clause) at https://pythonhosted.org/pyDOE/index.html, 2013.

Betts, R.A., Cox, P.M., Collins, M., Harris, P.P., Huntingford, C. and Jones, C.D.: The role of ecosystem-atmosphere interactions in simulated Amazonian precipitation decrease and forest dieback under global climate warming, Theor. Appl. Climatol., 78, 157-175, 2004.

Blunier, T. and Brook, E.J.: Timing of millennial-scale climate change in Antarctica and Greenland during the last glacial period, Science, 291, 109-112, 2001.

Böning, C. W., Behrens, E., Biastoch, A., Getzlaff, K., and Bamber, J. L.: Emerging impact of Greenland meltwater on deepwater formation in the North Atlantic Ocean, Nat. Geosci., 9, 523–527, 2016.

Brando, P.M., Balch, J.K., Nepstad, D.C., Morton, D.C., Putz, F.E., Coe, M.T., Silvério, D., Macedo, M.N., Davidson, E.A., Nóbrega, C.C., and Alencar, A.: Abrupt increases in Amazonian tree mortality due to drought-fire interactions, P. Natl. Acad. Sci. USA, 111, 6347-6352, 2014.

Brummitt, C. D., Barnett, G., and Dsouza, R. M.: Coupled catastrophes: sudden shifts cascade and hop among interdependent systems, J. R. Soc. Interface, 12, 439 20150712, 2015.

Caesar, L., Rahmstorf, S., Robinson, A., Feulner, G., and Saba, V.: Observed fingerprint of a weakening Atlantic Ocean overturning circulation, Nature, 556, 191–196, 2018.

Cai, W., Borlace, S., Lengaigne, M., Van Rensch, P., Collins, M., Vecchi, G., Timmermann, A., Santoso, A., McPhaden, M.J., Wu, L., and England, M.H.: Increasing frequency of extreme El Niño events due to greenhouse warming, Nat. Clim. Change, 4, 111–116, 2014.

Cai, Y., Judd, K.L., Lenton, T.M., Lontzek, T.S. and Narita, D.: Environmental tipping points significantly affect the cost-benefit assessment of climate policies. P. Natl. Acad. USA, 112, 4606-4611, 2015.

Cai, Y., Lenton, T.M. and Lontzek, T.S.: Risk of multiple interacting tipping points should encourage rapid $CO_2$ emission reduction, Nat. Clim. Change, 6, 520-525, 2016.

Cessi, P.: A simple box model of stochastically forced thermohaline flow, J. Phys. Oceanogr., 24, 1911-1920, 1994.

Ciemer, C., Boers, N., Hirota, M., Kurths, J., Müller-Hansen, F., Oliveira, R.S. and Winkelmann, R.: Higher resilience to climatic disturbances in tropical vegetation exposed to more variable rainfall, Nat. Geosci., 12, 174-179, 2019.

Collins, M., An, S.I., Cai, W., Ganachaud, A., Guilyardi, E., Jin, F.F., Jochum, M., Lengaigne, M., Power, S., Timmermann, A. and Vecchi, G.: The impact of global warming on the tropical Pacific Ocean and El Niño, Nat. Geosci., 3, 391-397, 2010.

Cox, P.M., Betts, R.A., Jones, C.D., Spall, S.A. and Totterdell, I.J.: Acceleration of global warming due to carbon-cycle feedbacks in a coupled climate model, Nature, 408, 184-187, 2000.

Cox, P.M., Betts, R.A., Collins, M., Harris, P.P., Huntingford, C. and Jones, C.D.: Amazonian forest dieback under climate-carbon cycle projections for the 21st century, Theor. Appl. Climatol., 78, 137-156, 2004.

Cox, P.M., Harris, P.P., Huntingford, C., Betts, R.A., Collins, M., Jones, C.D., Jupp, T.E., Marengo, J.A. and Nobre, C.A.: Increasing risk of Amazonian drought due to decreasing aerosol pollution, Nature, 453, 212-215, 2008.

Crucifix, M.: Oscillators and relaxation phenomena in Pleistocene climate theory, Philos. Trans. R. Soc. A, 370, 1140-1165, 2012.

Dansgaard, W., Johnsen, S.J., Clausen, H.B., Dahl-Jensen, D., Gundestrup, N.S., Hammer, C.U., Hvidberg, C.S., Steffensen, J.P., Sveinbjörnsdottir, A.E., Jouzel, J. and Bond, G.: Evidence for general instability of past climate from a 250-kyr ice-core record, Nature, 364, 218-220, 1993.

Daron, J.D. and Stainforth, D.A.: On predicting climate under climate change, Environ. Res. Lett., 8, 034021, 2013.

DeConto, R.M. and Pollard, D.: Contribution of Antarctica to past and future sea-level rise, Nature, 531, 591-597, 2016.

Dekker, M. M., Heydt, A. S. V. D., and Dijkstra, H. A.: Cascading transitions in the climate system, Earth Syst. Dynam., 9, 1243–1260, 2018.

Ditlevsen, P.D., Kristensen, M.S. and Andersen, K.K.: The recurrence time of Dansgaard–Oeschger events and limits on the possible periodic component, J. Climate, 18, 2594-2603, 2005.

Driesschaert, E., Fichefet, T., Goosse, H., Huybrechts, P., Janssens, I., Mouchet, A., Munhoven, G., Brovkin, V., and Weber, S.L.: Modeling the influence of Greenland ice sheet melting on the Atlantic meridional overturning circulation during the next millennia, Geophys. Res. Lett., 34, 2007.

Duque-Villegas, M., Salazar, J.F. and Rendón, A.M.: Tipping the ENSO into a permanent El-Niño can trigger state transitions in global terrestrial ecosystems. Earth Syst. Dynam., 10, 2019.

Dutton, A., Carlson, A.E., Long, A., Milne, G.A., Clark, P.U., DeConto, R., Horton, B.P., Rahmstorf, S. and Raymo, M.E.: Sea-level rise due to polar ice-sheet mass loss during past warm periods, Science, 349, aaa4019-aaa4019, 2015.

Favier, L., Durand, G., Cornford, S.L., Gudmundsson, G.H., Gagliardini, O., Gillet-Chaulet, F., Zwinger, T., Payne, A.J. and Le Brocq, A.M.: Retreat of Pine Island Glacier controlled by marine ice-sheet instability, Nat. Clim. Change, 4, 117–121, 2014.

Fedorov, A.V., Dekens, P.S., McCarthy, M., Ravelo, A.C., DeMenocal, P.B., Barreiro, M., Pacanowski, R.C. and Philander, S.G.: The Pliocene paradox (mechanisms for a permanent El Niño), Science, 312, 1485-1489, 2006.

Feldmann, J. and Levermann, A.: Collapse of the West Antarctic Ice Sheet after local destabilization of the Amundsen Basin, Proc. Natil. Acad. Sci., 112, 14191-14196, 2015.

Frajka-Williams, E.: Estimating the Atlantic overturning at 26 N using satellite altimetry and cable measurements, Geophys. Res. Lett., 42, 3458-3464, 2015.

Ganopolski, A. and Rahmstorf, S.: Abrupt glacial climate changes due to stochastic resonance, Phys. Rev. Lett., 88, 038501, 2002.

Garbe, J., Albrecht, T., Levermann, A., Donges, J.F. and Winkelmann, R.: The hysteresis of the Antarctic Ice Sheet, Nature, 585, 538-544, 2020.

Gasson, E., DeConto, R.M., Pollard, D. and Levy, R.H.: Dynamic Antarctic ice sheet during the early to mid-Miocene, Proc. Natl. Acad. Sci., 113, 3459-3464, 2016.

Gaucherel, C. and Moron, V.: Potential stabilizing points to mitigate tipping point interactions in Earths climate, Int. J. Climatol., 37, 399–408, 2016.

615 Haug, G.H. and Tiedemann, R.: Effect of the formation of the Isthmus of Panama on Atlantic Ocean thermohaline circulation, Nature, 393, 673-676, 1998.

Hawkins, E., Smith, R.S., Allison, L.C., Gregory, J.M., Woollings, T.J., Pohlmann, H., and De Cuevas, B.: Bistability of the Atlantic overturning circulation in a global climate model and links to ocean freshwater transport, Geophys. Res. Lett., 38, 2011.

Hirota, M., Holmgren, M., Van Nes, E.H. and Scheffer, M.: Global resilience of tropical forest and savanna to critical transitions. Science,
620 334, 232-235, 2011.

Hu, A., Meehl, G.A., Han, W., Yin, J., Wu, B. and Kimoto, M.: Influence of continental ice retreat on future global climate, J. climate, 26, 3087-3111, 2013.

Hughes, T., Carpenter, S., Rockström, J., Scheffer, M., and Walker, B.: Multiscale regime shifts and planetary boundaries. Trends Ecol. Evol., 28, 389-395, 2013.

625 IPCC: Stocker, T.F., Qin, D., Plattner, G.K., Tignor, M., Allen, S.K., Boschung, J., Nauels, A., Xia, Y., Bex, V. and Midgley, P.M.: Climate change 2013: the physical science basis: Working Group I contribution to the fifth assessment report of the intergovernmental panel on climate change, Cambridge University Press, 2014.

IPCC Special Report: Global Warming of 1.5 °C − an IPCC special report on the impacts of global warming of 1.5 °C above pre-industrial levels and related global greenhouse gas emission pathways, in the context of strengthening the global response to the threat of climate
630 change, sustainable development, and efforts to eradicate poverty, 2018.

Ivanovic, R.F., Gregoire, L.J., Wickert, A.D. and Burke, A.: Climatic effect of Antarctic meltwater overwhelmed by concurrent Northern hemispheric melt, Geophys. Res. Lett., 45, 5681-5689, 2018.

Jackson, L.C., Kahana, R., Graham, T., Ringer, M.A., Woollings, T., Mecking, J.V. and Wood, R.A.: Global and European climate impacts of a slowdown of the AMOC in a high resolution GCM, Clim. Dyn., 45, 3299-3316, 2015.

635 Jackson, L.C., Peterson, K.A., Roberts, C.D. and Wood, R.A.: Recent slowing of Atlantic overturning circulation as a recovery from earlier strengthening, Nat. Geosci., 9, 518-522, 2016.

Joughin, I. and Alley, R.B.: Stability of the West Antarctic ice sheet in a warming world, Nat. Geosci., 4, 506-513, 2011.

Joughin, I., Smith, B.E. and Medley, B.: Marine ice sheet collapse potentially under way for the Thwaites Glacier Basin, West Antarctica, Science, 344, 735-738, 2014.

640 Jungclaus, J. H., Haak, H., Esch, M., Roeckner, E., and Marotzke, J.: Will Greenland melting halt the thermohaline circulation? Geophys. Res. Lett., 33, 17, 2006.

Karas, C., Khélifi, N., Bahr, A., Naafs, B.D.A., Nürnberg, D. and Herrle, J.O.: Did North Atlantic cooling and freshening from 3.65–3.5 Ma precondition Northern Hemisphere ice sheet growth?, Glob. Planet. Change, 185, 103085, 2020.

Kim, S. T., Cai, W., Jin, F. F., Santoso, A., Wu, L., Guilyardi, E., and An, S. I.: Response of El Niño sea surface temperature variability to
645 greenhouse warming, Nat. Clim. Change, 4, 786-790, 2014.

Khan, S.A., Kjær, K.H., Bevis, M., Bamber, J.L., Wahr, J., Kjeldsen, K.K., Bjørk, A.A., Korsgaard, N.J., Stearns, L.A., Van Den Broeke, M.R., and Liu, L.: Sustained mass loss of the northeast Greenland ice sheet triggered by regional warming. Nat. Clim. Change, 4, 292–299, 2014.

Klose, A.K., Karle, V., Winkelmann, R., Donges, J.F.: Emergence of cascading dynamics in interacting tipping elements of ecology and
650 climate, Roy. Soc. Open Sci., 7, 200599, 2020.

Koenig, S.J., DeConto, R.M. and Pollard, D.: Impact of reduced Arctic sea ice on Greenland ice sheet variability in a warmer than present climate, Geophys. Res. Lett., 41, 3933-3942, 2014.

Kopp, R.E., Mitrovica, J.X., Griffies, S.M., Yin, J., Hay, C.C. and Stouffer, R.J.: The impact of Greenland melt on local sea levels: a partially coupled analysis of dynamic and static equilibrium effects in idealized water-hosing experiments, Clim. Change, 103, 619-625, 2010.

Kreuzer, M., Reese, R., Huiskamp, W.N., Petri, S., Albrecht, T., Feulner, G. and Winkelmann, R.: Coupling framework (1.0) for the ice sheet model PISM (1.1. 1) and the ocean model MOM5 (5.1. 0) via the ice-shelf cavity module PICO, Geosci. Model Dev. Discuss. [preprint], in review, 2020.

Kriegler, E., Hall, J.W., Held, H., Dawson, R., and Schellnhuber, H. J.: Imprecise probability assessment of tipping points in the climate system. P. Natl. Acad. Sci. USA, 106, 5041–5046, 2009.

Krönke, J., Wunderling, N., Winkelmann, R., Staal, A., Stumpf, B., Tuinenburg, O.A. and Donges, J.F.: Dynamics of tipping cascades on complex networks, Phys. Rev. E, 101, 042311, 2020.

Kuehn, C. A mathematical framework for critical transitions: Bifurcations, fast–slow systems and stochastic dynamics, Physica D, 240, 1020–1035, 2011.

Kuznetsov, Y. A.: Elements of Applied Bifurcation Theory, Applied Mathematical Sciences, Springer, New York, USA, doi:10.1007/978-1-4757-3978-7, 2004.

Lemoine, D. and Traeger, C.P.: Economics of tipping the climate dominoes. Nat. Clim. Change, 6, 514-519, 2016.

Lenton, T. M., Held, H., Kriegler, E., Hall, J. W., Lucht, W., Rahmstorf, S., and Schellnhuber, H. J.: Tipping elements in the Earths climate system. P. Natl. Acad. Sci. USA, 105, 1786–1793, 2008.

Lenton, T.M.: Arctic climate tipping points. Ambio, 41, 10-22, 2012.

Lenton, T. M., and Williams, H. T.: On the origin of planetary-scale tipping points, Trends Ecol. Evol., 28, 380–382, 2013.

Lenton, T. M., Rockström, J., Gaffney, O., Rahmstorf, S., Richardson, K., Steffen, W., and Schellnhuber, H. J.: Climate tipping points — too risky to bet against. Nature, 575, 592-595, 2019.

Levermann, A., Bamber, J., Drijfhout, S., Ganopolski, A., Haeberli, W., Harris, N.R.P., Huss, M., Lenton, T.M., Lindsay, R.W., Notz, D. and Wadhams, P.: Climatic tipping elements with potential impact on Europe. ETC/ACC Technical Paper, 2010.

Levermann, A., Bamber, J.L., Drijfhout, S., Ganopolski, A., Haeberli, W., Harris, N.R., Huss, M., Krüger, K., Lenton, T.M., Lindsay, R.W. and Notz, D.: Potential climatic transitions with profound impact on Europe, Clim. Change, 110, 845-878, 2012.

Levermann, A., and Winkelmann, R.: A simple equation for the melt elevation feedback of ice sheets, The Cryosphere, 10, 1799–1807, 2016.

Malhi, Y., Aragão, L.E., Galbraith, D., Huntingford, C., Fisher, R., Zelazowski, P., Sitch, S., McSweeney, C., and Meir, P.: Exploring the likelihood and mechanism of a climate-change-induced dieback of the Amazon rainforest, P. Natl. Acad. Sci. USA, 106, 20610–20615, 2009.

Marengo, J. A., and Espinoza, J. C.: Extreme seasonal droughts and floods in Amazonia: causes, trends and impacts. Int. J. Climatol., 36, 1033–1050, 2015.

Mercer, J.H.: West Antarctic ice sheet and CO2 greenhouse effect: a threat of disaster, Nature, 271, 321-325, 1978.

Mecking, J.V., Drijfhout, S.S., Jackson, L.C. and Graham, T.: Stable AMOC off state in an eddy-permitting coupled climate model, Clim. Dyn., 47, 2016.

Mitrovica, J.X., Gomez, N. and Clark, P.U.: The sea-level fingerprint of West Antarctic collapse, Science, 323, 753-753, 2009.

Nghiem, S.V., Hall, D.K., Mote, T.L., Tedesco, M., Albert, M.R., Keegan, K., Shuman, C.A., DiGirolamo, N.E. and Neumann, G.: The extreme melt across the Greenland ice sheet in 2012, Geophys. Res. Lett., 39, 2012.

Nes, E. H. V., Hirota, M., Holmgren, M., and Scheffer, M.: Tipping points in tropical tree cover: linking theory to data, Glob. Change Biol., 20, 1016–1021, 2014.

Nobre, C.A., Sampaio, G., Borma, L.S., Castilla-Rubio, J.C., Silva, J.S., and Cardoso, M.: Land-use and climate change risks in the Amazon and the need of a novel sustainable development paradigm, P. Natl. Acad. Sci., 113, 10759–10768, 2016.

Oyama, M.D. and Nobre, C.A.: A new climate-vegetation equilibrium state for tropical South America, Geophys. Res. Lett., 30, 2003.

Parsons, L.A., Yin, J., Overpeck, J.T., Stouffer, R.J. and Malyshev, S.: Influence of the Atlantic Meridional Overturning Circulation on the monsoon rainfall and carbon balance of the American tropics, Geophys. Res. Lett., 41, 146-151, 2014.

Pollard, D. and DeConto, R.M.: Hysteresis in Cenozoic Antarctic ice-sheet variations, Glob. Planet. Change, 45, 9-21, 2005.

Pollard, D. and DeConto, R.M.: Modelling West Antarctic ice sheet growth and collapse through the past five million years, Nature, 458, 329-332, 2009.

Power, S., Delage, F., Chung, C., Kociuba, G. and Keay, K.: Robust twenty-first-century projections of El Niño and related precipitation variability, Nature, 502, 541-545, 2013.

Rahmstorf, S., Crucifix, M., Ganopolski, A., Goosse, H., Kamenkovich, I., Knutti, R., Lohmann, G., Marsh, R., Mysak, L.A., Wang, Z., and Weaver, A.J.: Thermohaline circulation hysteresis: A model intercomparison, Geophys. Res. Lett., 32, 2005.

Ravelo, A.C., Dekens, P.S. and McCarthy, M.: Evidence for El Niño-like conditions during the Pliocene, Gsa Today, 16, 4, 2006.

Ridley, J., Gregory, J.M., Huybrechts, P. and Lowe, J.. Thresholds for irreversible decline of the Greenland ice sheet, Clim. Dyn., 35, 1049-1057, 2010.

Rignot, E., Mouginot, J., Morlighem, M., Seroussi, H. and Scheuchl, B.. Widespread, rapid grounding line retreat of Pine Island, Thwaites, Smith, and Kohler glaciers, West Antarctica, from 1992 to 2011, Geophys. Res. Lett., 41, 3502-3509, 2014.

Ritz, S., Stocker, T., Grimalt, J., Menviel, L., and Timmermann, A.: Estimated strength of the Atlantic overturning circulation during the last deglaciation, Nat. Geosci., 6, 208-212, 2013.

Robinson, A., Calov, R., and Ganopolski, A.: Multistability and critical thresholds of the Greenland ice sheet, Nat. Clim. Change, 2, 429–432, 2012.

Robson, J., Hodson, D., Hawkins, E. and Sutton, R.: Atlantic overturning in decline?, Nat. Geosci., 7, 2-3, 2014.

Sakschewski, B., Von Bloh, W., Boit, A., Poorter, L., Peña-Claros, M., Heinke, J., Joshi, J. and Thonicke, K.: Resilience of Amazon forests emerges from plant trait diversity, Nat. Clim. Change, 6, 1032-1036, 2016.

Santoso, A., McGregor, S., Jin, F.F., Cai, W., England, M.H., An, S.I., McPhaden, M.J. and Guilyardi, E.: Late-twentieth-century emergence of the El Niño propagation asymmetry and future projections, Nature, 504, 126-130, 2013.

Sasgen, I., Wouters, B., Gardner, A.S., King, M.D., Tedesco, M., Landerer, F.W., Dahle, C., Save, H. and Fettweis, X.: Return to rapid ice loss in Greenland and record loss in 2019 detected by the GRACE-FO satellites, Communs. Earth & Environ., 1, 1-8,2020.

Sayag, R. and Worster, M.G.: Elastic dynamics and tidal migration of grounding lines modify subglacial lubrication and melting, Geophys. Res. Lett., 40, 5877-5881, 2013.

Schaefer, J.M., Finkel, R.C., Balco, G., Alley, R.B., Caffee, M.W., Briner, J.P., Young, N.E., Gow, A.J. and Schwartz, R.: Greenland was nearly ice-free for extended periods during the Pleistocene, Nature, 540, 252-255, 2016.

Scheffer, M., Bascompte, J., Brock, W.A., Brovkin, V., Carpenter, S.R., Dakos, V., Held, H., Van Nes, E.H., Rietkerk, M. and Sugihara, G.: Early-warning signals for critical transitions, Nature, 461, 53-59, 2009.

Schellnhuber, H., Rahmstorf, S., and Winkelmann, R.: Why the right climate target was agreed in Paris. Nat. Clim. Change, 6, 649-653, 2016.

Schoof, C.: Ice sheet grounding line dynamics: Steady states, stability, and hysteresis, J. Geophys. Res.-Earth, 112, 2907.

Seidov, D., Stouffer, R.J. and Haupt, B.J.: Is there a simple bi-polar ocean seesaw?, Global Planet. Change, 49, 19-27, 2005.

Shepherd, A., Ivins, E., Rignot, E., Smith, B., Van Den Broeke, M., Velicogna, I., Whitehouse, P., Briggs, K., Joughin, I., Krinner, G., and Nowicki, S., et al.: Mass balance of the Antarctic Ice Sheet from 1992 to 2017, Nature, 558, 219–222, 2018.

Shepherd, A., Ivins, E., Rignot, E., Smith, B., van Den Broeke, M., Velicogna, I., Whitehouse, P., Briggs, K., Joughin, I., Krinner, G. and Nowicki, S., et al.: Mass balance of the Greenland Ice Sheet from 1992 to 2018, Nature, 579, 233-239, 2020.

Staal, A., Dekker, S. C., Hirota, M., and Nes, E. H. V.: Synergistic effects of drought and deforestation on the resilience of the south-eastern Amazon rainforest, Ecol. Complex., 22, 65–75, 2015

Staal, A., Dekker, S.C., Xu, C. and van Nes, E.H.: Bistability, spatial interaction, and the distribution of tropical forests and savannas, Ecosystems, 19, 1080-1091, 2016.

Staal, A., Tuinenburg, O.A., Bosmans, J.H., Holmgren, M., van Nes, E.H., Scheffer, M., Zemp, D.C., and Dekker, S.C.: Forest-rainfall cascades buffer against drought across the Amazon, Nat. Clim. Change, 8, 539–543, 2018.

Staal, A., Fetzer, I., Wang-Erlandsson, L., Bosmans, J.H., Dekker, S.C., van Nes, E.H., Rockström, J. and Tuinenburg, O.A.: Hysteresis of tropical forests in the 21st century, Nat. Communs., 11, 1-8, 2020.

Stainforth, D.A., Downing, T.E., Washington, R., Lopez, A. and New, M.: Issues in the interpretation of climate model ensembles to inform decisions. Philos. Trans. Royal Soc. A, 365, 2163-2177, 2007.

Staver, A.C., Archibald, S. and Levin, S.A.: The global extent and determinants of savanna and forest as alternative biome states. Science, 334, 230-232, 2011.

Steffen, W., Rockström, J., Richardson, K., Lenton, T.M., Folke, C., Liverman, D., Summerhayes, C.P., Barnosky, A.D., Cornell, S.E., Crucifix, M., Donges, J.F., Fetzer, I., Lade, S.J., Scheffer, M., Winkelmann, R., and Schellnhuber, H.J.: Trajectories of the Earth System in the Anthropocene, P. Natl. Acad. Sci. USA, p.201810141, 2018.

Sterl, A., Severijns, C., Dijkstra, H., Hazeleger, W., van Oldenborgh, G.J., van den Broeke, M., Burgers, G., van den Hurk, B., van Leeuwen, P.J. and van Velthoven, P.: When can we expect extremely high surface temperatures?. Geophys. Res. Lett., 35, 14, 2008.

Stommel, H.: Thermohaline Convection with Two Stable Regimes of Flow, Tellus, 13, 224–230, 1961.

Stouffer, R.J., Yin, J., Gregory, J.M., Dixon, K.W., Spelman, M.J., Hurlin, W., Weaver, A.J., Eby, M., Flato, G.M., Hasumi, H. and Hu, A.: Investigating the causes of the response of the thermohaline circulation to past and future climate changes, J. Climate, 19, 1365-1387, 2006.

Swingedouw, D., Fichefet, T., Huybrechts, P., Goosse, H., Driesschaert, E. and Loutre, M.F.: Antarctic ice-sheet melting provides negative feedbacks on future climate warming, Geophys. Res. Lett., 35, 2008.

Swingedouw, D., Fichefet, T., Goosse, H. and Loutre, M.F.: Impact of transient freshwater releases in the Southern Ocean on the AMOC and climate, Clim. Dyn. 33, 365-381, 2009.

Tedesco, M., Fettweis, X., Van den Broeke, M.R., Van de Wal, R.S.W., Smeets, C.J.P.P., van de Berg, W.J., Serreze, M.C. and Box, J.E.: The role of albedo and accumulation in the 2010 melting record in Greenland, Environ. Res. Lett., 6, 014005, 2011.

Tedesco, M. and Fettweis, X.: Unprecedented atmospheric conditions (1948–2019) drive the 2019 exceptional melting season over the Greenland ice sheet, The Cryosphere, 14, 1209-1223, 2020.

Thonicke, K., Bahn, M., Lavorel, S., Bardgett, R.D., Erb, K., Giamberini, M., Reichstein, M., Vollan, B. and Rammig, A.: Advancing the understanding of adaptive capacity of social-ecological systems to absorb climate extremes, Earths Future, 8, p.e2019EF001221, 2020.

Timmermann, A., Jin, F.-F., and Abshagen, J.: A Nonlinear Theory for El Niño Bursting, J. Atmos. Sci., 60, 152–165, 2003.

Timmermann, A., An, S.I., Krebs, U. and Goosse, H.: ENSO suppression due to weakening of the North Atlantic thermohaline circulation, J. Climate, 18, 3122-3139, 2005.

Timmermann, A., Okumura, Y., An, S.I., Clement, A., Dong, B., Guilyardi, E., Hu, A., Jungclaus, J.H., Renold, M., Stocker, T.F. and Stouffer, R.J.: The influence of a weakening of the Atlantic meridional overturning circulation on ENSO, J. Climate, 20, 4899-4919, 2007.

Toggweiler, J.R. and Samuels, B.: Effect of Drake Passage on the global thermohaline circulation, Deep Sea Res. Part I Oceanogr. Res. Pap., 42, 477-500, 1995.

Toniazzo, T., Gregory, J.M. and Huybrechts, P.: Climatic impact of a Greenland deglaciation and its possible irreversibility, J. Climate, 17, 21-33, 2004.

Van Nes, E.H., Hirota, M., Holmgren, M. and Scheffer, M.: Tipping points in tropical tree cover: linking theory to data, Glob. Change Biol., 20, 1016-1021, 2014.

Vellinga, M. and Wood, R.A.: Global climatic impacts of a collapse of the Atlantic thermohaline circulation, Climatic Change, 54, 251-267, 2002.

Wang, L., Yu, J.Y. and Paek, H.: Enhanced biennial variability in the Pacific due to Atlantic capacitor effect, Nat. Communs., 8, 1-7, 2017

Wang, S. and Hausfather, Z.: ESD Reviews: mechanisms, evidence, and impacts of climate tipping elements, Earth Syst. Dynam. Discuss., https://doi.org/10.5194/esd-2020-16, in review, 2020.

Wara, M.W., Ravelo, A.C. and Delaney, M.L.: Permanent El Niño-like conditions during the Pliocene warm period, Science, 309, 758-761, 2005.

Weertman, J.: Stability of the junction of an ice sheet and an ice shelf, J. Glaciol., 13, 3-11, 1974.

Weijer, W., Cheng, W., Drijfhout, S.S., Fedorov, A.V., Hu, A., Jackson, L.C., Liu, W., McDonagh, E.L., Mecking, J.V. and Zhang, J.: Stability of the Atlantic Meridional Overturning Circulation: A review and synthesis, J. Geophys. Res.-Oceans, 124, 5336-5375, 2019.

Winkelmann, R., Levermann, A., Ridgwell, A., and Caldeira, K.: Combustion of available fossil fuel resources sufficient to eliminate the Antarctic Ice Sheet, Science Advances, 1, 2015.

Wood, R.A., Rodríguez, J.M., Smith, R.S., Jackson, L.C. and Hawkins, E.: Observable, low-order dynamical controls on thresholds of the Atlantic Meridional Overturning Circulation, Clim. Dyn., 53, 6815-6834, 2019.

Wunderling, N., Stumpf, B., Krönke, J., Staal, A., Tuinenburg, O.A., Winkelmann, R. and Donges, J.F.: How motifs condition critical thresholds for tipping cascades in complex networks: Linking micro-to macro-scales, Chaos, 30, 043129, 2020.

Wunderling, N., Staal, A., Sakschewski, B., Hirota, M., Tuinenburg, O., Donges, J., Barbosa, H. and Winkelmann, R.: Network dynamics of drought-induced tipping cascades in the Amazon rainforest, 2020 (in review).

Wunderling, N., Gelbrecht, M., Winkelmann, R., Kurths, J. and Donges, J.F.: Basin stability and limit cycles in a conceptual model for climate tipping cascades, New J. Phys., 22, 2020.

Zebiak, S.E. and Cane, M.A.: A model El Niño–southern oscillation, Mon. Weather Rev., 115, 2262-2278, 1987.

Zemp, D.C., Schleussner, C.F., Barbosa, H.M.J., Van der Ent, R.J., Donges, J.F., Heinke, J., Sampaio, G. and Rammig, A.: On the importance of cascading moisture recycling in South America, Atmospheric Chem. Phys., 14, 13337-13359, 2014.

Zemp, D.C., Schleussner, C.F., Barbosa, H.M., Hirota, M., Montade, V., Sampaio, G., Staal, A., Wang-Erlandsson, L. and Rammig, A.: Self-amplified Amazon forest loss due to vegetation-atmosphere feedbacks, Nat. Commun., 8, 14681, 2017.

Zwally, H.J., Li, J., Brenner, A.C., Beckley, M., Cornejo, H.G., DiMarzio, J., Giovinetto, M.B., Neumann, T.A., Robbins, J., Saba, J.L., and Yi, D.: Greenland ice sheet mass balance: distribution of increased mass loss with climate warming; 2003–07 versus 1992–2002, J. Glaciol., 57, 88–102, 2011.

# Supplementary Material of
# Interacting tipping elements increase risk of climate domino effects under global warming

Nico Wunderling[1,2,3], Jonathan F. Donges[1,4], Jürgen Kurths[1,5], and Ricarda Winkelmann[1,2]

[1]Earth System Analysis and Complexity Science, Potsdam-Institute for Climate Impact, Research (PIK), Member of the Leibniz Association, 14473 Potsdam, Germany
[2]Institute of Physics and Astronomy, University of Potsdam, 14476 Potsdam, Germany
[3]Department of Physics, Humboldt University of Berlin, 12489 Berlin, Germany
[4]Stockholm Resilience Centre, Stockholm University, Stockholm, SE-10691, Sweden
[5]Saratov State University, Saratov, RU-410012, Russia

**Correspondence:** Nico Wunderling (nico.wunderling@pik-potsdam.de), Ricarda Winkelmann (ricarda.winkelmann@pik-potsdam.de)

| Parameter group | Parameter | Initial value |
|---|---|---|
| Critical temperatures (°C) | $T_{\text{limit, Greenland}}$ | 1.6 |
| | $T_{\text{limit, West Antarctica}}$ | 5.0 |
| | $T_{\text{limit, AMOC}}$ | 5.5 |
| | $T_{\text{limit, Amazon rainforest}}$ | 3.8 |
| Strong links (a.u.) | Greenland → AMOC | 0.64 |
| | AMOC → Greenland | −0.57 |
| | Greenland → West Antarctica | 0.77 |
| Intermediate links (a.u.) | AMOC → Amazon rainforest | 0.0 |
| | West Antarctica → AMOC | 0.0 |
| Weak links (a.u.) | West Antarctica → Greenland | 0.13 |
| | AMOC → West Antarctica | 0.12 |

**Table S 1.** Exemplary initial values that have been used to construct the timeseries in Figs. 2 and 3 in the main manuscript. All initial values are random numbers drawn from a uniform distribution with a latin-hypercube sampling algorithm (Baudin, 2013) between their respective limits (see Tabs. 1 and 2). The random numbers for the links have already been multiplied with $1/10 \times s_{ij}$ (see Table 2). The exemplary timelines were computed using a network without considering the uncertain links (AMOC → Amazon rainforest and West Antarctica → AMOC), whose link strengths are set to zero.

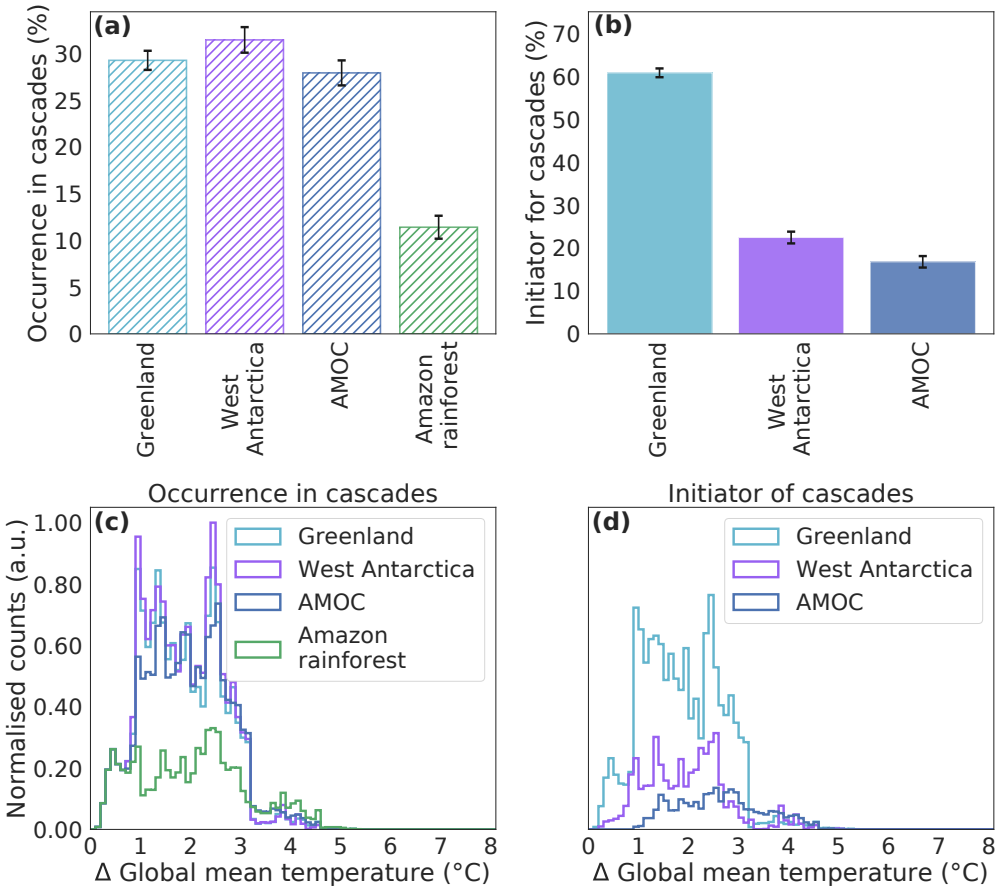


**Figure S 1.** *Role* of tipping elements in cascades. **(a)** Relative frequency in percent of occurrence of a certain tipping element in a tipping cascade (hatched bars). The standard deviation is computed by evaluating the deviation between reasonable network settings (see Sect. 2.7). **(b)** Relative frequency in percent that a certain tipping element causes a tipping cascade (coloured bars). We define that the cause of a cascade is the element, whose critical temperature is closest to the temperature at which the cascade takes place. Again the error bars show the standard deviation between different network settings as in **(a)**. It must be noted that the Amazon rainforest cannot initiate a tipping cascade since it has no outgoing link (see Fig. 1). **(c)** Count versus global mean temperature increase at which a tipping cascade occurs divided into the respective four tipping elements. **(d)** Same as in **(c)**, but for the tipping element which causes the cascade. N.B.: **(c)** and **(d)** are set to the same scale normalised to the highest value in the histogram.

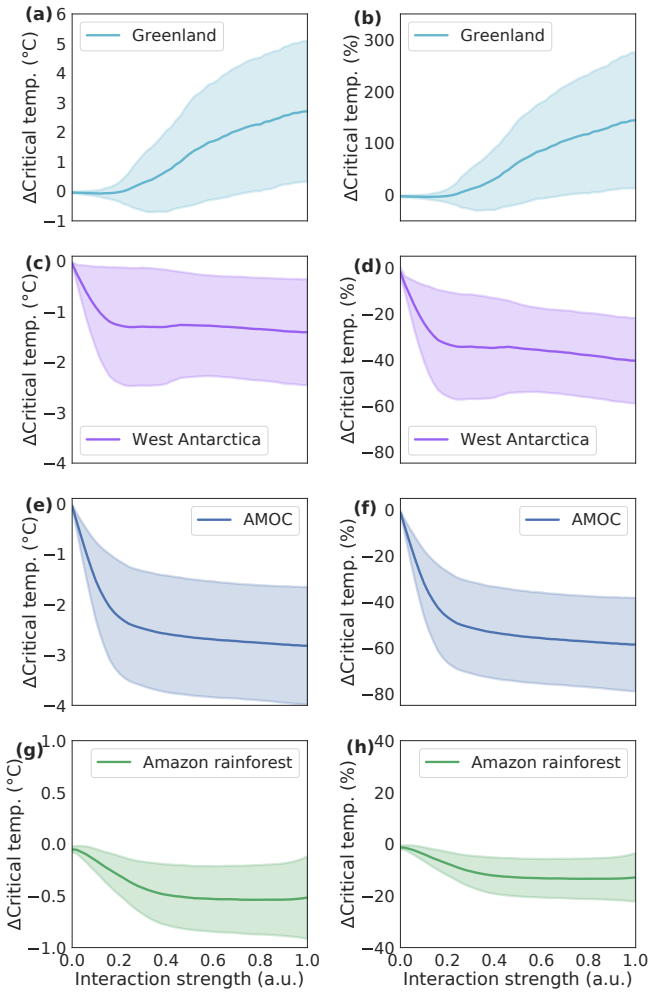


**Figure S 2.** Difference in critical temperatures with respect to the interaction strength. Difference of critical temperatures in °C (left panels) and % (right panels) compared to the respective initially drawn critical temperature for the four investigated tipping elements: **(a, b)** Greenland Ice Sheet, **(c, d)** West Antarctic Ice Sheet, **(e, f)** AMOC and **(g, h)** Amazon rainforest. The standard deviation from the ensemble members is shown as respective colour shading.

**Structural sensitivity analysis including ENSO**

In this section, we perform a structural sensitivity analysis by taking ENSO into account as a tipping element since it is debated whether and to which extent ENSO should be seen as a tipping element (discussion see main manuscript in Sect. 3.4). Below and in Tab. 2, we elaborate on additional references regarding the interactions that include ENSO, equal to the other interactions in the main manuscript (see Sect. 2.2).

1. *AMOC* → *ENSO*: There are two contradicting impacts representing the influence of the AMOC on ENSO: (I) Oceanic Kelvin waves could start from a colder north Atlantic and travel towards the south. In western Africa, Rossby waves could then be produced travelling in northern and southern direction, which are then converted back into Kelvin waves that move into the Pacific sea. This would intensify the Pacific thermocline and thereby dampen the amplitude of ENSO (Timmermann et al., 2005). (II) When the AMOC becomes weaker, the northern tropical Atlantic would become cooler and northerly trade winds would be strengthened over the northeastern tropical Pacific. It has been suggested that this could lead to a southward shift of the ITCZ (Zhang & Delworth , 2005). Simultaneously, it is argued that Rossby waves are sent into the northeast tropical Pacific, which would strengthen ENSO (Dong & Sutton, 2005). Summarised, it is believed that process (II) is more powerful than process (I). Moreover, it has been found in more complex Earth system models that a weakening of the AMOC indeed reinforces the variability of ENSO (Dekker et al., 2018; Sterl et al., 2008). Therefore, this link is set as destabilising (see Fig. S3).

2. *ENSO* → *Amazon rainforest*: It has been proposed that droughts due to climate variabilities (such as ENSO) could harm the Amazon rainforest and its integrity (Holmgren et al., 2013, 2006; Malhi & Wright, 2004). With PlaSim, an Earth system model of intermediate complexity, a permanent El-Niño state would severely threaten major parts of the Amazon basin since the forest might suffer from restricted water access in South America (Duque-Villegas et al., 2019). Therefore, we set this link as destabilising (see Fig. S3).

3. ENSO → West Antarctic Ice Sheet: There is evidence for heating oceanic effects from El-Niño in the Amundsen and Ross Sea region, while La Niña phases would have the opposite oceanic effect. However, the atmosphere could offset the oceanic effect (Bertler et al., 2006). In addition to that, observations have shown that ice shelves gain height, but lose mass during major El-Niño events in the Amundsen and Ross Sea region (Paolo et al., 2018). In particular, a large surface melt event, that was associated with a strong El-Niño event, took place in 2016 (Nicolas et al., 2017). Still, the interaction between ENSO and West Antarctica is one of the interactions with the highest uncertainty (as also noted in Kriegler et al., 2009). Furthermore, some studies suggest that the frequency of El-Niño events increase with ongoing global warming (Cai et al., 2014). Thus, we set this interaction destabilising (see Tab. S2 and Fig. S3).

4. *ENSO* → *AMOC*: It has been argued by evaluating reanalysis data that water vapour transport out of the tropical Atlantic is increased (Schmittner et al., 2000). There is contradicting evidence suggesting that El-Niño conditions might or might not have a strengthening impact the deepwater formation in the north Atlantic and with that the strength of the

AMOC (Spence & Weaver, 2006; Schmittner et al., 2000). This illustrates that this interaction pair is less well understood than others. Therefore, we consider this link as being of low strength, but with a stabilising (negative) sign since there is only evidence for this direction of interaction (see Fig. S3 and Tab. S2).

5. *Amazon rainforest → ENSO*: The moisture recycling feedback would be stopped in case the Amazon rainforest tips to a large portion (Boers et al., 2017; Zemp et al., 2017; Aragão, 2012). Since it is unknown as to whether this would have an impact on the formation of El-Niño events, this link is set as unclear and its uncertainty is propagated in our Monte Carlo ensemble (see Fig. S3). The strength of this interaction is set very weak due to its possibly very limited impact on ENSO (see Tab. S2).

| **Edge** | **Maximal link strength $s_{ij}$ (a.u.)** | **Physical process** |
|---|---|---|
| ENSO → Amazon rainforest | $+10$ | Drying over Amazonia |
| ENSO → West Antarctica | $+5$ | Warming of Ross and Amundsen seas |
| AMOC → ENSO | $+2$ | Cooling of North-East tropical Pacific with thermocline shoaling and weakening of annual cycle in EEP |
| ENSO → AMOC | $-2$ | Enhanced water vapour transport to Pacifics |
| Amazon rainforest → ENSO | $\pm 1.5$ | Changes in tropical moisture supply |

**Table S 2.** Edges in the network of tipping elements that include ENSO. The values are given in analogy to Tab. 2 of the main manuscript.

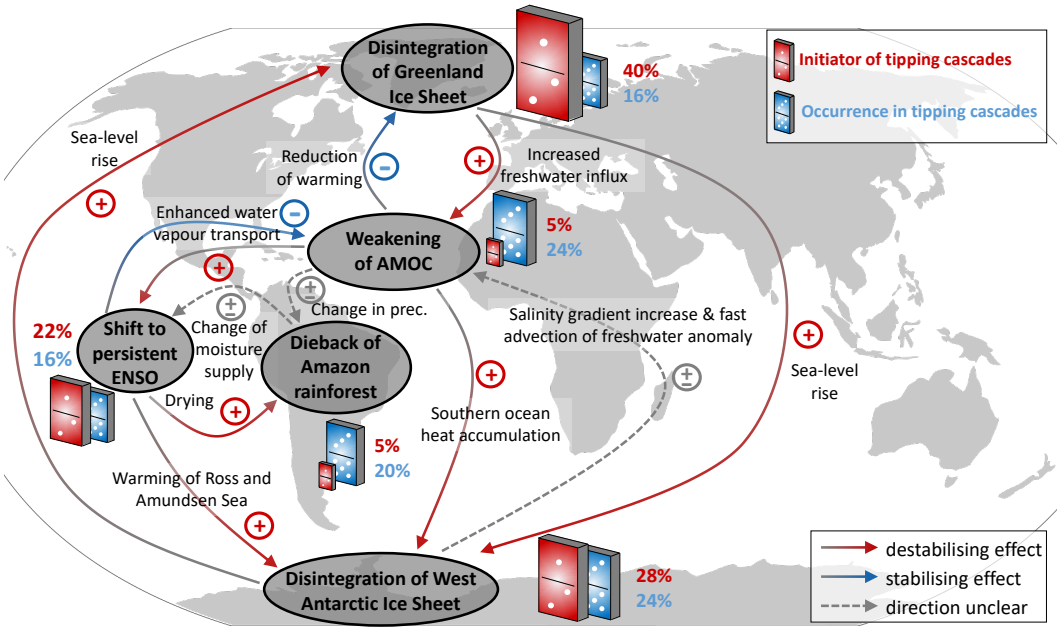


**Figure S 3.** Interactions between climate tipping elements and their roles in tipping cascades. The Greenland Ice Sheet, West Antarctic Ice Sheet, Atlantic Meridional Overturning Circulation (AMOC), El-Niño Southern Oscillation (ENSO) and the Amazon rainforest are depicted together with their main interaction pathways (Kriegler et al., 2009). Same as in Fig. 1 in the main manuscript, but including ENSO as a tipping element.

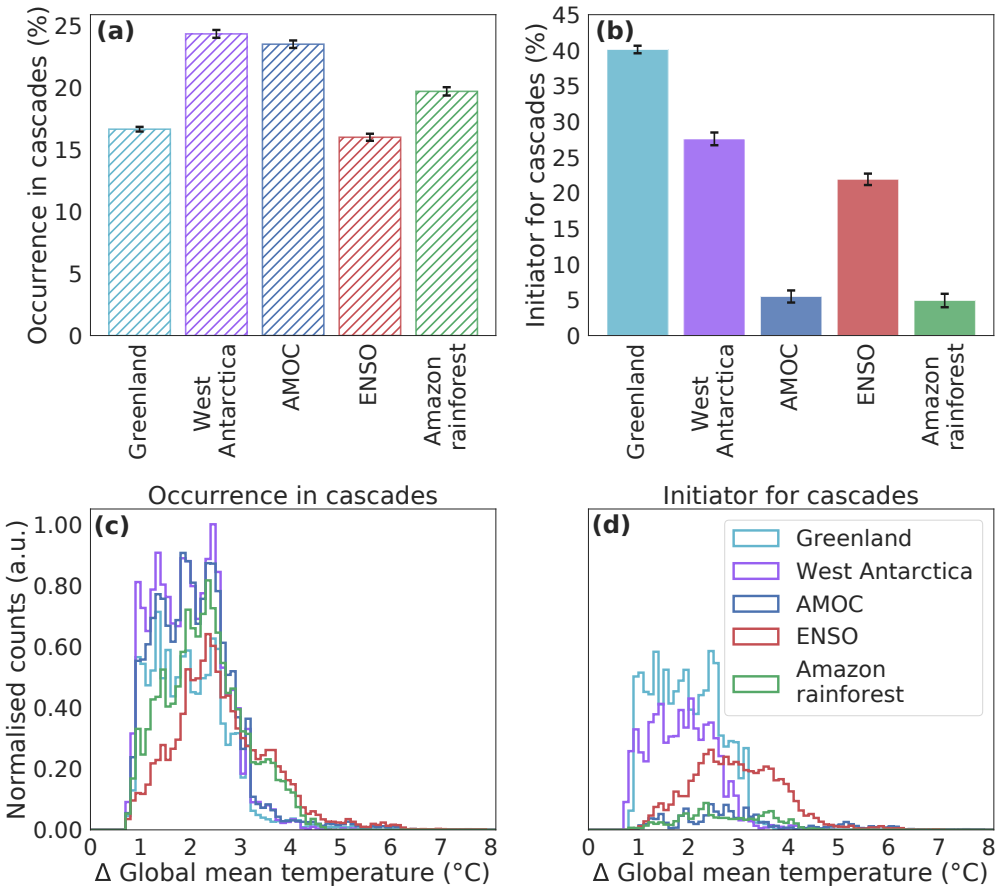


**Figure S 4.** *Role* of the tipping elements including ENSO. The panels **(a,b)** show the same as in Fig. S3, but with error bars (standard deviation). In analogy to the the dominos in Fig. S1 (there without ENSO), the panels **(a,b)** show the frequency of occurrence in a tipping cascade and the frequency in initiating a tipping cascade. The panels **(c,d)** depict the increase of the global mean temperature, at which this cascade occurred or is initiated. The main pattern of the results remains robust, meaning that the large ice sheets are the initiators of cascades, while the AMOC transmits cascades. The role of ENSO is intermediate since it strongly initiates tipping cascades with the Amazon rainforest, but is apart from that less often (than other tipping elements) part of a tipping cascade and also mediates some cascades.

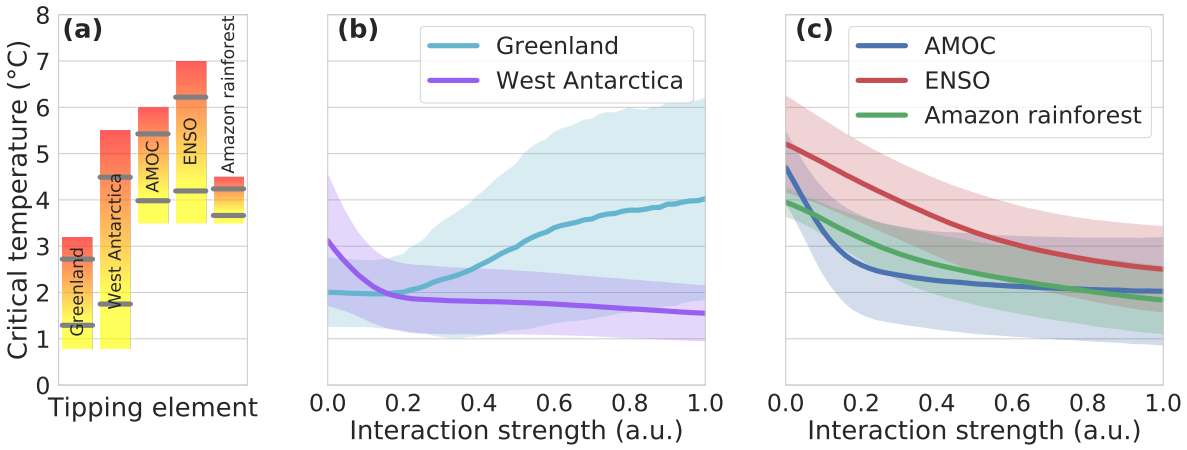


**Figure S 5.** Shift of critical temperature ranges due to interactions with ENSO. The panels are the same as in Fig. 4 of the main manuscript excluding ENSO. With increasing interaction strength, the critical temperatures develop similar as in the case without ENSO for the Greenland Ice Sheet, the West Antarctic Ice Sheet and the AMOC. For the Amazon rainforest, there is now also a strong reduction of its critical temperature since it is strongly connected and influenced by ENSO.

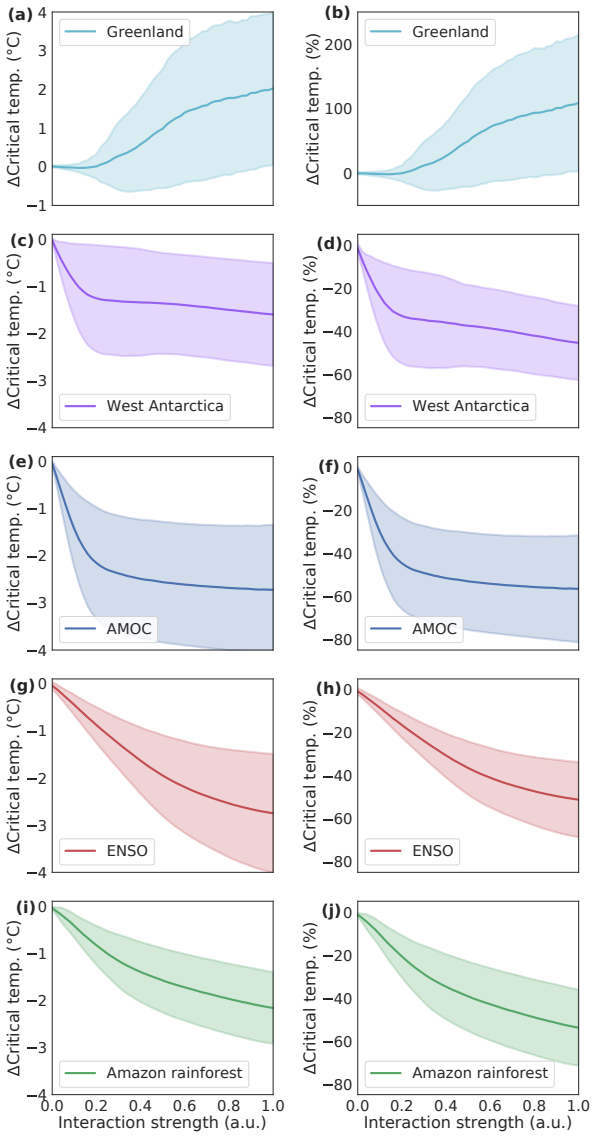


**Figure S 6.** Difference in critical temperatures with respect to the interaction strength including ENSO. The panels show the same as in Fig. S2 without ENSO. The results are similar apart from the Amazon rainforest that shows more reduction in its critical temperature level due to its strong interaction with ENSO.

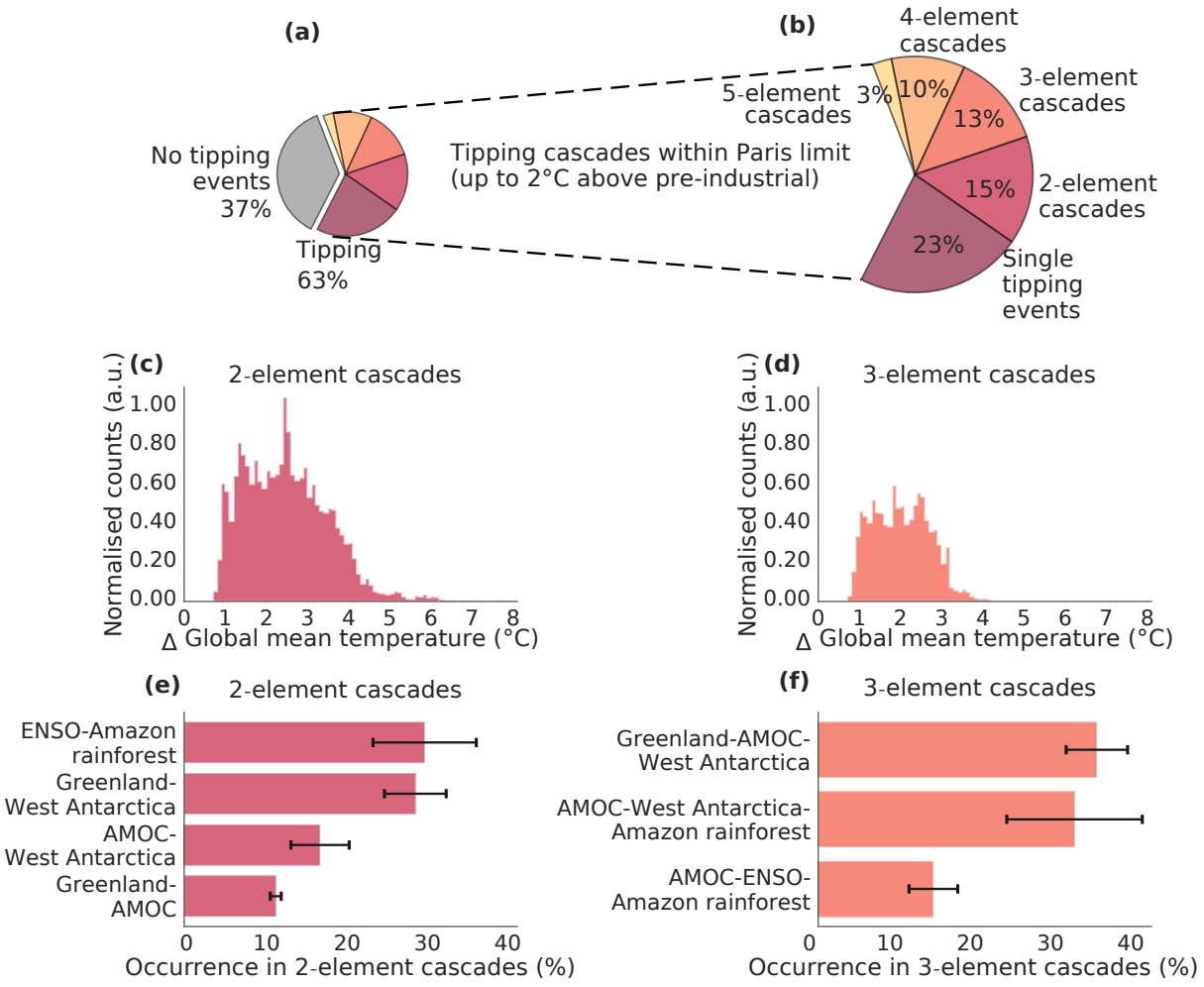


**Figure S 7.** Tipping cascades with ENSO. The results without ENSO are shown in Fig. 5. The warming levels of tipping cascades are very similar to the simulations that exclude ENSO apart from the fact that tipping cascades including ENSO are now possible. One such prominent tipping cascade includes the Amazon rainforest (see panels **(e)** and **(f)**). See Fig. S8 for the distribution of tipping cascades of size four and five expanding the analysis from the panels **(c)** and **(d)**.

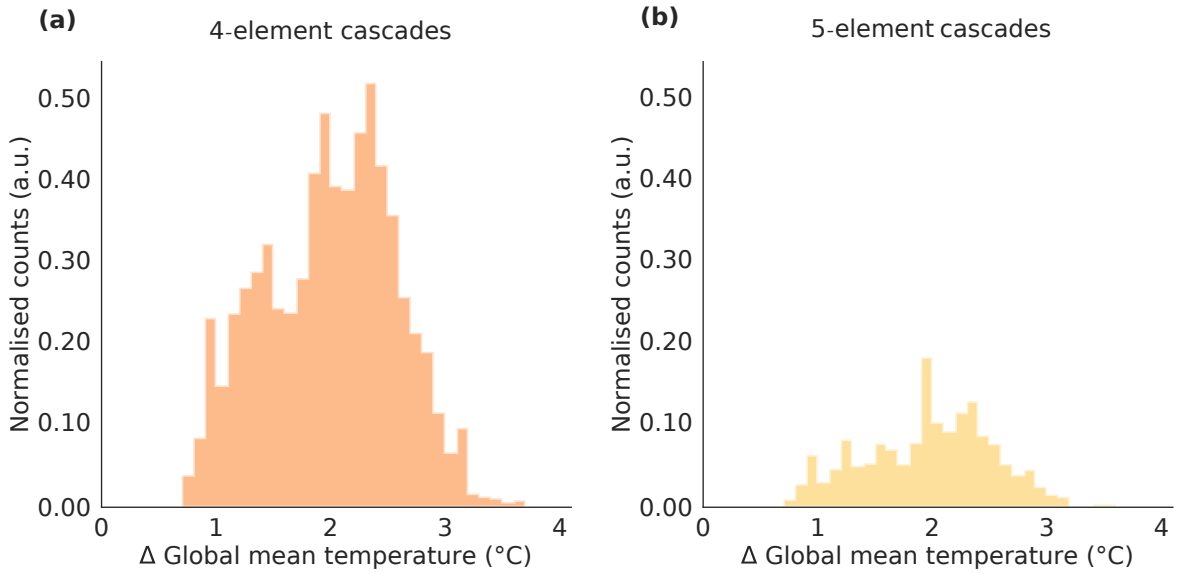


**Figure S 8.** Tipping cascades of size four and five versus temperature increase. **(a)** Tipping cascades of size four, **(b)** Tipping cascades of size five. The scale is the same as in Fig. S7 panels (c) and (d), but here we show a zoom-in in temperature increase and normalised counts to improve visibility.

**References**

Aragão, L.E.: Environmental science: The rainforest's water pump, Nature, 489, 217-218, 2012.

Baudin, M.: pyDOE: The experimental design package for python, sofware available under the BSD license (3-Clause) at https://pythonhosted.org/pyDOE/index.html, 2013.

Bertler, N.A.N., Naish, T.R., Mayewski, P.A. and Barrett, P.J.: Opposing oceanic and atmospheric ENSO influences on the Ross Sea Region, Antarctica, Adv. Geosci., 6, 83-86, 2006.

Boers, N., Marwan, N., Barbosa, H. and Kurths, J.: A deforestation-induced tipping point for the South American monsoon system, Sci. Rep., 7, 41489, 2017.

Cai, W., Borlace, S., Lengaigne, M., Van Rensch, P., Collins, M., Vecchi, G., Timmermann, A., Santoso, A., McPhaden, M.J., Wu, L., and England, M.H.: Increasing frequency of extreme El Niño events due to greenhouse warming, Nat. Clim. Change, 4, 111–116, 2014.

Dekker, M. M., Heydt, A. S. V. D., and Dijkstra, H. A.: Cascading transitions in the climate system, Earth Syst. Dyn., 9, 1243–1260, 2018.

Dong, B. and Sutton, R.T.: Mechanism of interdecadal thermohaline circulation variability in a coupled ocean–atmosphere GCM, J. Climate, 18, 1117-1135, 2005.

Duque-Villegas, M., Salazar, J.F. and Rendón, A.M.: Tipping the ENSO into a permanent El Niño can trigger state transitions in global terrestrial ecosystems, Earth Syst. Dyn., 10, 2019.

Holmgren, M., Stapp, P., Dickman, C.R., Gracia, C., Graham, S., Gutiérrez, J.R., Hice, C., Jaksic, F., Kelt, D.A., Letnic, M. and Lima, M.: Extreme climatic events shape arid and semiarid ecosystems, Front. Ecol. Environ., 4, 87-95, 2006.

Holmgren, M., Hirota, M., Van Nes, E.H. and Scheffer, M.: Effects of interannual climate variability on tropical tree cover, Nat. Clim. Change, 3, 755-758, 2013.

Kriegler, E., Hall, J.W., Held, H., Dawson, R., and Schellnhuber, H. J.: Imprecise probability assessment of tipping points in the climate system, P. Natl. Acad. Sci. USA, 106, 5041–5046, 2009.

Malhi, Y. and Wright, J.: Spatial patterns and recent trends in the climate of tropical rainforest regions, Philos. Trans. R. Soc. B, 359, 311-329, 2004.

Nicolas, J.P., Vogelmann, A.M., Scott, R.C., Wilson, A.B., Cadeddu, M.P., Bromwich, D.H., Verlinde, J., Lubin, D., Russell, L.M., Jenkinson, C. and Powers, H.H.: January 2016 extensive summer melt in West Antarctica favoured by strong El Niño, Nat. Communs, 8, 15799, 2017.

Paolo, F.S., Padman, L., Fricker, H.A., Adusumilli, S., Howard, S. and Siegfried, M.R.: Response of Pacific-sector Antarctic ice shelves to the El-Niño/Southern oscillation, Nat. Geosci, 11, 121-126, 2018.

Schmittner, A., Appenzeller, C. and Stocker, T.F.: Enhanced Atlantic freshwater export during El Niño, Geophys. Res. Lett., 27, 1163-1166, 2000.

Spence, J.P. and Weaver, A.J.: The impact of tropical Atlantic freshwater fluxes on the North Atlantic meridional overturning circulation, J. Climate, 19, 4592-4604, 2006.

Sterl, A., Severijns, C., Dijkstra, H., Hazeleger, W., van Oldenborgh, G.J., van den Broeke, M., Burgers, G., van den Hurk, B., van Leeuwen, P.J. and van Velthoven, P.: When can we expect extremely high surface temperatures?. Geophys. Res. Lett., 35, 14, 2008.

Timmermann, A., An, S.I., Krebs, U. and Goosse, H.: ENSO suppression due to weakening of the North Atlantic thermohaline circulation, J. Climate, 18, 3122-3139, 2005.

Zemp, D.C., Schleussner, C.F., Barbosa, H.M., Hirota, M., Montade, V., Sampaio, G., Staal, A., Wang-Erlandsson, L. and Rammig, A.: Self-amplified Amazon forest loss due to vegetation-atmosphere feedbacks, Nat. Communs., 8, 1-10, 2017.

Zhang, R. and Delworth, T.L.: Simulated tropical response to a substantial weakening of the Atlantic thermohaline circulation, J. Climate, 18, 1853-1860, 2005.

# 2.7 Basin stability and limit cycles in a conceptual model for climate tipping cascades [P7]

**Authors**
Nico Wunderling, Maximilian Gelbrecht, Ricarda Winkelmann, Jürgen Kurths, Jonathan F. Donges

**Status**
Published in *New Journal of Physics* (December 2020), doi: 10.1088/1367-2630/abc98a

**Short summary**
In this manuscript, the dynamical properties of a system of five interacting tipping elements are studied in detail: the Greenland Ice Sheet, the West Antarctic Ice Sheet, the AMOC, the Amazon rainforest and the ENSO. Based on an expert elicitation and a study on the critical temperature ranges of these five tipping elements, uncertainties in interactions and critical temperature thresholds are propagated in a huge-scale Monte Carlo ensemble with approximately 3.6 billion ensemble members. Exploiting the concept of basin stability, regimes of increased basin stability are found for states that include tipped ice sheets on Greenland and West Antarctica implying that the ice sheets seem to be of special relevance for the stability of the climate system. Additionally, limit cycle oscillations through Hopf-bifurcations are detected for rare parameter combinations using a Monte Carlo Basin Bifurcation method (MCBB). Such oscillations especially occur between the strongly interacting Greenland Ice Sheet and AMOC, hinting at possibly dangerous internal modes of variability of the Earth's climate system.

**Author contributions**
Nico Wunderling, Ricarda Winkelmann and Jonathan Donges designed the study. Nico Wunderling conducted the model simulation runs and prepared the figures for the part on basin stability. Maximilian Gelbrecht conducted the simulation runs and prepared the figures for the part on oscillatory states. All authors discussed the results of the paper. Nico Wunderling led the writing of this work with input from all authors.

New Journal of Physics
The open access journal at the forefront of physics

Deutsche Physikalische Gesellschaft DPG IOP Institute of Physics

PAPER • OPEN ACCESS

# Basin stability and limit cycles in a conceptual model for climate tipping cascades

To cite this article: Nico Wunderling *et al* 2020 *New J. Phys.* **22** 123031

IOP Publishing New J. Phys. 22 (2020) 123031 https://doi.org/10.1088/1367-2630/abc98a

New Journal of Physics
The open access journal at the forefront of physics

Deutsche Physikalische Gesellschaft DPG
IOP Institute of Physics

Published in partnership with: Deutsche Physikalische Gesellschaft and the Institute of Physics

OPEN ACCESS

RECEIVED
14 September 2020

REVISED
5 November 2020

ACCEPTED FOR PUBLICATION
11 November 2020

PUBLISHED
21 December 2020



PAPER

# Basin stability and limit cycles in a conceptual model for climate tipping cascades

Nico Wunderling[1,2,3,*], Maximilian Gelbrecht[3,4], Ricarda Winkelmann[1,2], Jürgen Kurths[3,4,5] and Jonathan F Donges[1,6,*]

[1] Earth System Analysis, Potsdam Institute for Climate Impact Research (PIK), Member of the Leibniz Association, 14473 Potsdam, Germany
[2] Institute of Physics and Astronomy, University of Potsdam, 14476 Potsdam, Germany
[3] Department of Physics, Humboldt University of Berlin, 12489 Berlin, Germany
[4] Complexity Science, Potsdam Institute for Climate Impact Research (PIK), Member of the Leibniz Association, 14473 Potsdam, Germany
[5] Lobachevsky State University Nizhny Novgorod, Nizhny Novgorod, Russia,
[6] Stockholm Resilience Centre, Stockholm University, Stockholm, SE-10691, Sweden
[*] Authors to whom any correspondence should be addressed.

**E-mail:** nico.wunderling@pik-potsdam.de and jonathan.donges@pik-potsdam.de

**Keywords:** nonlinear dynamics, complex systems, basin stability, climate tipping elements, bifurcation, nonlinear processes in the earth

## Abstract

Tipping elements in the climate system are large-scale subregions of the Earth that might possess threshold behavior under global warming with large potential impacts on human societies. Here, we study a subset of five tipping elements and their interactions in a conceptual and easily extendable framework: the Greenland Ice Sheets (GIS) and West Antarctic Ice Sheets, the Atlantic meridional overturning circulation (AMOC), the El–Niño Southern Oscillation and the Amazon rainforest. In this nonlinear and multistable system, we perform a basin stability analysis to detect its stable states and their associated Earth system resilience. By combining these two methodologies with a large-scale Monte Carlo approach, we are able to propagate the many uncertainties associated with the critical temperature thresholds and the interaction strengths of the tipping elements. Using this approach, we perform a system-wide and comprehensive robustness analysis with more than 3.5 billion ensemble members. Further, we investigate dynamic regimes where some of the states lose stability and oscillations appear using a newly developed basin bifurcation analysis methodology. Our results reveal that the state of four or five tipped elements has the largest basin volume for large levels of global warming beyond 4 °C above pre-industrial climate conditions, representing a highly undesired state where a majority of the tipping elements reside in the transitioned regime. For lower levels of warming, states including disintegrated ice sheets on west Antarctica and Greenland have higher basin volume than other state configurations. Therefore in our model, we find that the large ice sheets are of particular importance for Earth system resilience. We also detect the emergence of limit cycles for 0.6% of all ensemble members at rare parameter combinations. Such limit cycle oscillations mainly occur between the GIS and AMOC (86%), due to their negative feedback coupling. These limit cycles point to possibly dangerous internal modes of variability in the climate system that could have played a role in paleoclimatic dynamics such as those unfolding during the Pleistocene ice age cycles.

## 1. Introduction

During the last decades, the field of tipping elements has become a major point of interest in complex systems and network science [1, 2]. They have been used in the description of various fields such as in financial markets, technological progress, ecology or in climate science (e.g., [3–6]). Tipping elements can

IOP Publishing New J. Phys. 22 (2020) 123031 N Wunderling et al

interact across scales in space and time [7] which could potentially lead to catastrophic domino effects [8] or, for instance, lead to a hothouse climate state in the case of climate tipping elements [9].

In the climate system, tipping elements are subregions of the Earth system that can exhibit threshold behavior, where a small forcing perturbation can be sufficient to invoke a strong non-linear response of the system that can qualitatively change the state of the whole region or system due to internal, self-enforcing feedbacks [6]. Climate tipping elements comprise systems from the cryosphere (e.g. Greenland, Antarctic Ice Sheet, Permafrost), the biosphere (e.g. Amazon rainforest (AMAZ), coral reefs) and large-scale circulation systems (e.g. Monsoon systems, AMOC) [6, 10]. Their potential tipping to alternative states would be associated with severe impacts on the biosphere and threaten human societies [11].

It has been suggested that several climate tipping elements are at risk or on the way of transgressing into an undesired state even at global warming levels below the 2.0 °C goal of the Paris agreement [10–12]. Among others, tipping elements that already show warning signals of degradation at present times [11, 12] are: the West Antarctic Ice Sheets (WAIS) where parts in the Amundsen Bay (Pine Island & Thwaites region) are suspected to have been destabilized [13–15], the AMOC which experienced a major slowdown of 15% from 1950 to now [16], the AMAZ which might approach a tipping point due to climate change and deforestation [17]. Critical deforestation ratios might lie between 20% to 40%, where current deforestation is reaching 20% [17, 18]. Furthermore, the GIS loses mass at an accelerating pace [19, 20] and the frequency of major El–Niño events are suggested to increase twofold and strong El–Nino Southern Oscillation (ENSO) effects will occur more often as global warming continues [21, 22]. However, others highlight that large uncertainties are related to future changes of ENSO and whether major El–Niño events will become more frequent or intense under global warming [23, 24].

Furthermore, contradicting a common misunderstanding, tipping elements do not necessarily tip immediately after the crossing of their tipping point, but their tipping time trajectory might take very long and appear smooth [25]. For instance for the large ice sheets, the disintegration time scale could be on the order of several centuries up to millennia as has been suggested by modeling studies [26–28].

For most of the tipping elements, there is a critical temperature range at which they are suspected to leave their current safe state separating the climate tipping elements into three groups [10]. The first group comprises elements that might transgress their state within the limits of the Paris agreement (Paris, 2015) of 2 °C above pre-industrial and with that, these are the most vulnerable climate tipping elements with respect to global warming. This group contains mainly cryosphere elements (Arctic summer sea ice, WAIS, GIS and Alpine glaciers) as well as the Coral reefs that are likely to be lost even when global warming is restricted to 2 °C above pre-industrial. The second group might tip at temperatures above 3 °C (for instance the AMAZ, AMOC or ENSO) and the most resilient group only at temperatures around 5 °C above pre-industrial or higher (e.g., parts of the Antarctic ice sheet, permafrost or Arctic winter sea ice).

However, the tipping elements in the climate system are not independent of each other, but connected [11, 29] and the knowledge about the exact interaction structure is sparse and partially based on experts that, for instance, suggested an interaction structure, including sign and strength, for a subset of five tipping elements: the GIS, the WAIS, the AMOC, the AMAZ and the ENSO [29]. Behind each connection between two tipping elements within this subset, there is a physical process or set of processes (see table A.1). For instance the impact of the GIS on the AMOC due to freshwater input from melting ice slows down the AMOC on the one hand and a weakening AMOC on the other hand cools latitudes in the northern hemisphere. Note that this subset network of tipping is neither complete in the number and selection of tipping elements, nor is it comprehensive in the possible connection pathways and their potential strength between the tipping elements. There are also earlier investigations on tipping points [30] and the interaction of tipping points [31, 32] in the context of economic damage and the social cost of carbon using further developed versions of the integrated assessment model DICE [33, 34]. Here, Cai *et al* (2016) [31] explicitly base their findings on the interactions of tipping elements from the expert elicitation in Kriegler *et al* (2009) [29].

Following the elaborations above, in this work we aim at investigating the resilience of various attractors for interacting climate tipping elements and we want to elucidate the role that different tipping cascades have in that regard. The approach put forward here can easily be adapted to more tipping elements and further interaction structures once they are more comprehensively understood (see also [35]).

We explore the stability landscape and the dynamics of a subset of five tipping elements represented by normal form fold bifurcations based on known interactions across scales in time and space between these tipping elements (figure 1) [29]. These five tipping elements are the GIS and WAIS, the AMOC, the ENSO and the AMAZ [29]. We introduce the model of interacting tipping elements in section. We use the concept of basin stability [36] in order to determine the basin sizes of various attractors of this multistable system (see section 2). Based on a large-scale Monte Carlo ensemble, this methodology gives an estimate how stable and resilient various attractors are. It has been applied to many dynamic systems before such as power grids,

178

IOP Publishing New J. Phys. 22 (2020) 123031 N Wunderling et al

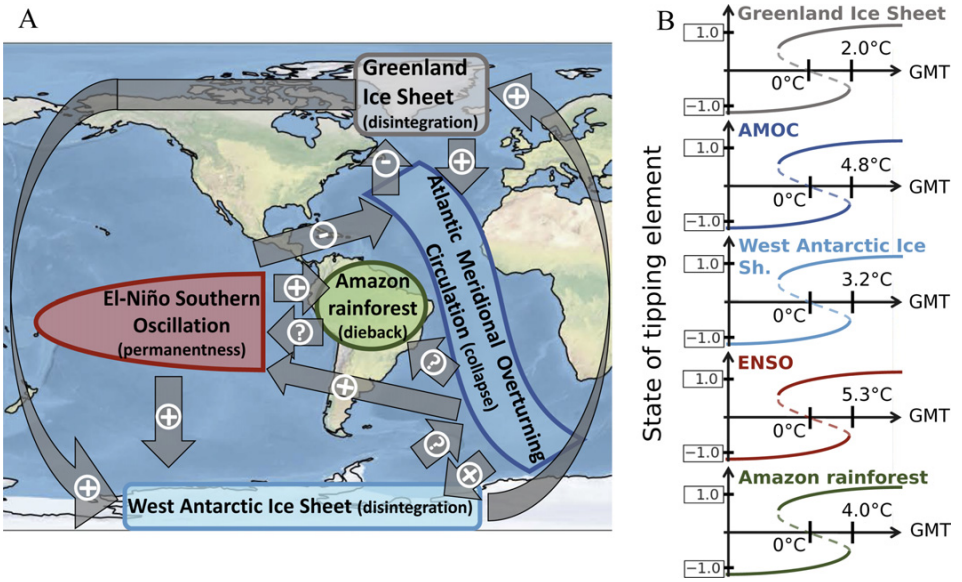


**Figure 1.** (A) World map with connections shown for five tipping elements where the interaction structure is known from an expert elicitation [29, 43]. Each link represents a physical mechanism and has a certain strength (see supplementary table A.1). A positive arrow implies an effect that drives the tipping element closer to its tipping point, a negative arrow drives the tipping element away from its tipping point and a question mark stands for an unclear direction. (B) (Fold) Bifurcation diagram of each of the tipping elements without coupling. On the *x*-axis, the average global warming required for tipping is shown in degrees above pre-industrial global mean temperature levels for the respective tipping element.

neuronal models and further nonlinear systems [37–41]. Furthermore, especially for larger coupling strengths, Hopf bifurcations can occur, thus invoking oscillatory limit-cycle solutions of the model. For the detection and quantification of these types of limit cycle attractors, we apply a newly developed bifurcation algorithm that is able to identify different dynamical properties in complex systems: the Monte Carlo Basin Bifurcation analysis (MCBB) [42].

In the following, we first introduce the methodological approach of this work: the model of interacting tipping elements (section 2.2), the basin stability approach (section 2.3), the construction of the large-scale Monte Carlo ensemble (section 2.4) and the Monte Carlo Basin Bifurcation analysis (section 2.5). Then, we evaluate the basin volume in our model (section 3.1) and quantify the occurrence of limit cycles in our model (section 3.2). Lastly, the results with respect to the climate system are discussed and summarized in sections 4 and 5.

## 2. Methods

For the purpose of investigating the dynamical properties of the subset of five tipping elements, we further developed a conceptual network approach that is fully dynamic and captures the main nonlinear dynamical properties of tipping elements [35, 44, 45]. The actual physical processes behind the tipping elements are not explicitly modeled to maintain an accessible and controllable structure. The modeling of complex systems using conceptual approaches is a popular tool and has been successfully applied to, among others, ecology, social systems or epidemiology [5, 46, 47].

### 2.1. Tipping elements and interactions

Given that, despite major advances, current EMICs (Earth system models of intermediate complexity) and GCMs (global circulation models) are not yet able to fully represent the nonlinear behavior of some Earth system components together with their interactions, but physics based models and equations as well as paleo climate observations suggest the existence of such properties for many tipping elements as for instance the GIS and (West) Antarctic ice sheet [26, 28, 48, 49], the AMOC [50–54], the AMAZ [55–59] or the ENSO [60, 61], the conceptual approach chosen here demonstrates an option how to model interactions between tipping elements. Thus, we put this model forward as a first step towards a more process-detailed assessment of tipping elements and their interactions. This also emphasizes that future research could focus on developing more complex, emulator- or EMIC/GCM-like models of tipping elements to investigate their nonlinear interplay such as has recently been developed for the Antarctic ice sheet [49].

IOP Publishing New J. Phys. 22 (2020) 123031 N Wunderling et al

While we have described why we use a conceptual description of the main dynamics of the tipping elements directly above, we outline the physical mechanisms of there interactions hereafter. Although some interactions between the tipping elements are better understood and evaluated than others, we describe the physical mechanisms of all of them in the following separated into destabilizing (+), stabilizing (−) and unclear links (?) (see figure 1). This description aims to provide a basic physical understanding, but cannot resolve the problem of how strong exactly each of these interactions is. Therefore, the interaction structure is kept as described later in equation (5) with the multiplicative interaction strength factor $d$.

(a) Destabilizing interactions:

1. GIS → AMOC: when the GIS starts to melt, it has a diminishing influence on the overturning strength of the AMOC due to freshwater input into the North Atlantic. This has been observed in modeling studies [16, 51, 62, 63] and in observations [64].
2. AMOC → WAIS: when the AMOC collapses, sea surface temperature anomalies arise due to the collapse of the northward heat transport of the AMOC. This results in a cold north and a warm south of the equator as shown by modeling studies [65–68].
3. GIS → WAIS (and vice versa): the shift of grounding lines due to changing sea level is a well-known phenomenon from tidal changes (e.g. [69]). Thus, if the sea level rises due to global warming, the floating ice shelves could be lifted which is likely to result in grounding line retreat. Furthermore, gravitational changes as well as elastic and rotational effects might then amplify the sea level change if one of the large ice sheets disintegrates first because the gravitational attraction then only emanates from the other, remaining ice sheet [70, 71]. The effect would be stronger if Greenland melts first since the WAIS has more marine terminating glaciers and ice shelves.
4. AMOC → ENSO: there are two opposing effects that have proposed, which describe how the AMOC might influence the ENSO: (i) it has been suggested that oceanic Kelvin waves originate from a colder North Atlantic and travel southward. Then, in western Africa, Rossby waves would be emitted towards the north and the south, which are then translated back into Kelvin waves that travel into the Pacific ocean. This effect would deepen the Pacific thermocline and weaken the amplitude of ENSO [60]. (ii) With a weaker AMOC, the northern tropical Atlantic would in turn become cooler and northerly trade winds would be intensified over the northeastern tropical Pacific. It has been argued that this could result in a southward displacement of the Pacific ITCZ leading to a sea surface temperature anomaly [72]. At the same time, it is argued that Rossby waves are sent into the northeast tropical Pacific [73]. This would intensify ENSO due to wind stress interaction from AMOC. Overall, it is believed that mechanism (ii) is stronger than mechanism (i) [60]. Furthermore, it can be extracted from complex Earth system models that a decrease in AMOC intensity indeed strengthens the variability of ENSO [61, 74].
5. ENSO → AMAZ: literature studies suggest that droughts related to climate variabilities such as the ENSO can affect the stability of the AMAZ [75–77]. Using an EMIC, it has been found that a permanent El–Niño state would endanger substantial portions of the Amazon basin due to a reorganization and reduction of water access in the south American tropics via teleconnections [78].
6. ENSO → WAIS: the interaction between ENSO and the WAIS is one of the least certain interactions as has already been stated in Kriegler *et al* (2009) [29]. Nevertheless, there are hints for warming oceanic effects from El–Niño in the Amundsen and Ross Sea region, while La Niña would cool this region. At the same time, atmospheric effects could have an opposite effect, which would offset the oceanic effect [79]. Besides that, it has been found with satellite observations that ice shelves gain height, but yet lose mass during El–Niño events in the Amundsen and Ross sea region [80]. While the primary driver of melt in west Antarctica is the warm ocean water below ice shelves, an extended period of surface melting has been observed during January 2016, which is likely promoted by the strong El–Niño event in this year [81]. Since it is expected that the frequency of major El–Niño events will increase during climate change [21], we set this interaction positive (see table A.1 and figure 1).

(b) Stabilizing interactions:

1. AMOC → GIS: for a decreasing overturning strength of the AMOC, the northern hemisphere is cooled since the heat transport towards the north Atlantic would be weakened. This has been observed in modeling studies [16, 65, 66, 82].
2. ENSO → AMOC: using reanalysis data, evidence has been found that the transport of water vapor out of the tropical Atlantic is enhanced [83]. Comparing La Niña and El–Niño conditions, it was found in this study that El–Niño conditions lead to a stronger northern AMOC on a multi-decadal timescale. However, another study questions this finding and does not find a strong impact on the

deepwater formation from AMOC [84]. Therefore, this interaction is less well established from literature and therefore considered of low strength, but with a negative sign (see figure 1 and table A.1).

(c) Unclear interaction direction:

1. AMOC → AMAZ: when the AMOC shuts down, the intertropical convergence zone (ITCZ) is likely dislocated southward, leading to large changes in seasonal precipitation on a local to regional degree. This might then impact parts of the AMAZ [68, 82, 85]. Still, it is unknown as to whether this interaction is positive or negative and might differ from region to region. Therefore, this link is set as unclear (see figure 1).
2. WAIS → AMOC: a literature study using a coupled ocean-atmosphere model found a decrease in the AMOC for high freshwater inputs from the WAIS [86]. However, another study detected a stabilization of the AMOC if influenced by freshwater input from west Antarctica. This is ascribed to the effects from the bipolar ocean seesaw due to decreasing Antarctic bottom water formation [87]. With an EMIC, is has been found from using freshwater input experiments into the southern ocean that different processes could enhance or slow down the AMOC [88]: (i) the deep water adjustments via the bipolar ocean seesaw tend to intensify the NADW formation. (ii) The NADW is strengthened by southern hemispheric wind increase representing an ocean-atmosphere interaction. (iii) Salinity anomalies from the southern ocean are distributed to the north Atlantic weakening the NADW (compare to [86]). Overall, the processes (i) and (iii) strengthen the AMOC and process (ii) weakens it. However, the exact time scale and efficiencies of these processes have been rated unknown as of yet [88].
3. AMAZ → ENSO: under a dieback of the AMAZ, the moisture supply to the atmosphere will significantly change, also since the atmospheric moisture recycling feedback over the Amazon basin would break down [89–91]. However, it is unclear whether and to which extent this would then impact ENSO.

### 2.2. Model

In our conceptual model, we divide the dynamics $x_i$ of the considered tipping elements $i$ into their individual dynamics $f_i(x_i)$ and a direct interaction term $g_i(\vec{x}) \equiv g_i(x)$. This yields

$$\tau_i \dot{x}_i = f_i(x_i) + g_i(x), \tag{1}$$

where $\tau_i$ is the typical time that passes when a tipping element undergoes a critical transition from one state to another. We model the individual dynamics of each of the tipping elements with the general tipping approach (CUSP equation [8, 92])

$$f_i(x_i) = -a_i x_i^3 + b_i x_i + c_i \quad a_i, b_i, c_i \in \mathbb{R}, \tag{2}$$

where $a_i > 0$ and $b_i > 0$. Assuming additive separability of the interactions between the tipping elements and linear interactions, the interaction term $g_i(x)$ becomes

$$g_i(x) = \sum_j g_{ij}(x_i, x_j) \underset{\text{interactions}}{\overset{\text{linear}}{=}} \sum_j A_{ij} x_j. \tag{3}$$

Here, $A_{ij}$ is the interaction structure and strength, which is set to zero if there is no connection between the tipping elements $i$ and $j$. Altogether, equation (1) becomes

$$\tau_i \dot{x}_i = -a_i x_i^3 + b_i x_i + c_i + \sum_j A_{ij} x_j. \tag{4}$$

Each tipping element $x_i$ following this equation possesses two fold bifurcations at $\pm\sqrt{(4a_i^3)/(27b_i)}$ and has already been investigated in theoretical works on tipping cascades [92], but also in various contexts where nonlinear behavior is important as for instance in policy, environmental issues, economy or climate [8, 93]. For these equations exist a framework that allows to investigate tipping cascades on larger networks with regard to their interaction structure in the network as well as microstructures that are decisive for finding emergent tipping cascades [44, 45].

In our model, we specify the interaction structure and strength term $A_{ij}$ by setting it equal to a multiplicative factor $d$ times the actual link strength $s_{ij}$ between each pair of tipping elements. Therefore, $A_{ij} = d/10 \cdot s_{ij}$. The link strength values $s_{ij}$ are taken from the expert elicitation [29]. The factor $1/10$ is used for normalization reasons since then $d \in [0, 1]$. If we now additionally set $a = 1, b = 1$ and

181

IOP Publishing New J. Phys. 22 (2020) 123031 N Wunderling et al

$c_i = \left(\sqrt{4/27}/T_{\text{limit, i}}\right) \cdot \Delta\text{GMT}$, the tipping elements are described by the following nonlinear, ordinary differential equation (all parameters of equation (5) are explained in the tables A.1 and A.2)

$$\frac{\mathrm{d}x_i}{\mathrm{d}t} = \left[-x_i^3 + x_i + \frac{\sqrt{4/27}}{T_{\text{limit, i}}} \cdot \Delta\text{GMT} + \frac{d}{10} \cdot \sum_{\substack{j \\ j \neq i}} s_{ij}\left(x_j + 1\right)\right] \frac{1}{\tau_i}. \tag{5}$$

Here, $x_i$ is the state of the tipping element (see figure 1(B)) and $i$ stands for the considered tipping elements $i =$ GIS, WAIS, AMOC, ENSO, AMAZ. We choose these five tipping elements since their interaction structure is known from an expert elicitation [29]. The increase of the global mean temperature above pre-industrial is denoted by $\Delta$GMT, $T_{\text{limit,i}}$ is the critical temperature threshold of the respective element. The last term is the coupling term, where $d$ is a general multiplicator that determines the strength of the interaction term in comparison to the other, individual dynamics terms. The parameter $d$ is varied between 0, meaning no interactions, and 1, where the interactions become as important as the individual dynamics. Following this, one might tend to assume that the individual dynamics of the tipping element influences the tipping element more than the interaction effect. This might make smaller coupling parameters more realistic than higher ones. In equation (5), $s_{ij}$ is the link strength that is based on the expert elicitation [29] and $\tau_i$ is a typical timescale at which a certain tipping element transgresses its state.

This typical tipping time scale ranges from decades for the AMAZ to several millennia for the large ice sheets (see appendix table A.2). Then, our system of differential equations is integrated forward in time using *scipy.odeint* [94] until more than 20 times the GIS's typical transition time scale has passed. This is equal to 100 000 years simulation time. This is the time when equilibrium is reached in the simulations. However, we are not intending to compute an exact time scale for tipping or tipping cascades here, but we are rather interested in the system's attractors and their stability properties. This is why we denote model years in arbitrary units instead of giving an exact time, also since this would be beyond the scope of this conceptual model (see figure 1(A)). Note that we adapted the link from ENSO to AMOC from uncertain to negative compared to the original results of the expert elicitation on tipping element interactions [29] since there is only a dampening process known in literature [43].

There are considerable uncertainties associated with this approach, especially with the critical temperature at which a certain tipping element transgresses its state $T_{\text{limit,i}}$ as well as in the strength of the interactions $s_{ij}$. The uncertainties of these two parameters are shown in the appendix tables A.1 and A.2. Thus, with equation (5), we model tipping events and cascades under certain conditions of global warming (GMT) and the interaction strength ($d$).

### 2.3. Basin stability

We are interested in the stability properties of different attractors within the state space. An appropriate tool to investigate the stability landscape of such states is the so-called *basin stability* [36, 39]. Basin stability is a nonlinear stability measure for the resilience of an attractor to disturbances. Where traditional measures such as the computation of Lyapunov exponents or master stability functions rely on linear approximations in reaction to small perturbations [95, 96], basin stability approaches can also consider large perturbations. Such perturbations can occur in Earth system components such as the large ocean circulations or the AMAZ [36, 97]. The basin stability is an established algorithm focusing on the stability landscape of the entire phase space, while other nonlinear stability measures such as survivability [41], stability threshold [98], constrained basin stability [99] and topology of sustainable management [100] approaches focus on the stability of parts of the state space or desired regimes in it. Therefore, basin stability computations are a first step that aims to quantify the stability of different attracting states, but do not aim to study potential desired regimes as would be required for the other mentioned methods. The concept of basin stability has been applied to many multistable systems. Examples comprise the AMAZ [36], the stability in networks of power grids [37], neuronal models [38] and further nonlinear systems such as in coupled network systems [39], oscillators [101, 102] or chimera states [103]. While basin stability can widely be applied, it has its limitations, for instance in cases where basins become too peculiar, e.g. for riddled basins with holes [40]. Since this is not the case in our model of interacting climate tipping elements, we utilize basin stability in this work.

An attractor $\mathcal{A}$ is defined as the minimal compact invariant set $\mathcal{A} \subseteq X$, where $X$ is the entire state space [104]. $B(\mathcal{A}) \subseteq X$ is the basin of attraction of $\mathcal{A}$ which comprises all states from which the system converges to $\mathcal{A}$. The basin stability or the basin volume $V(\mathcal{A})$ is then quantified as the probability that a system will

182

IOP Publishing New J. Phys. 22 (2020) 123031 N Wunderling et al

return to a certain attractor $\mathcal{A}$ after a perturbation

$$V_B(\mathcal{A}) := \int_R \mathbf{1}_{B(\mathcal{A})} \mathrm{d}\mu \in [0, 1], \tag{6}$$

where $\mathbf{1}_{B(\mathcal{A})}$ is 1 in case $x \in B(\mathcal{A})$ and 0 otherwise. $\mu$ is a measure on the state space $X$ that encodes the relevance of a certain perturbation and our knowledge about the system. The estimation of the integral in equation (6) can be difficult, but in our system it can be assumed that the estimation of the basin volume can be estimated via a Monte Carlo ensemble. The total volume of a basin of attraction is then measured as the fraction of simulations with randomly chosen initial conditions that end up in that certain attractor $N(\mathcal{A})$ over the total number of initial conditions $N(\Omega)$

$$V(\mathcal{A}) = P(\mathcal{A}) = N(\mathcal{A})/N(\Omega). \tag{7}$$

Here, $P(\mathcal{A})$ is the probability that a random initial condition ends up in the basin of attractor $\mathcal{A}$. To assign the basin volume $V(\mathcal{A})$ with the probability $P(\mathcal{A})$, it is required that the space of initial conditions is covered well and uniformly. Therefore in this work, it is necessary to extend the classical concept of basin stability since it is not only required to sample the space of initial conditions sufficiently well, but also to sample over the uncertainties in the model parameters themselves (see tables A.1 and A.2). Thus, we need to set up a very large-scale Monte Carlo ensemble of several billion ensemble members whose construction details can be directly found below.

### 2.4. Monte Carlo ensemble to compute basin stability

In order to apply the concept of basin stability in a meaningful way, the state space must be covered well enough. However, in this application, the parameters of the models have uncertainties themselves in the critical temperature thresholds and the interaction strength and structure. This means, we need a way of covering the many uncertainties in these various parameters as well as the state space itself. Therefore, it is necessary and useful to combine basin stability with a large scale Monte Carlo sample that covers an adequate extent of the phase space and parameter space. This is what explain in the hereafter.

The basic Monte Carlo ensemble without the extension for basin stability is set up as follows: for each pair of global mean temperatures (GMT) and interaction strengths $d$, there is a sample of size 100 constructed with initial conditions from the uncertainty range in $T_{\mathrm{limit,i}}$ and $s_{ij}$ using a latin hypercube algorithm [105] (see tables A.1 and A.2). Latin hypercube sampling is an extension to the usual random sampling and is used to improve the space coverage of initial conditions. Therefore, the space of initial conditions is separated into its dimensions, i.e., the number of different initial parameters (here [17], see tables A.1 and A.2). Then, it is secured that only one sample occurs in each axis hyperplane (compare to the N-rooks problem in mathematics). We apply this sampling procedure for each of the 27 different network setups that arise from the permutation (positive, negative, zero) of the three uncertain links (AMAZ $\rightarrow$ ENSO, AMOC $\rightarrow$ Amazon and WAIS $\rightarrow$ AMOC, see figure 1(A)). This then leads to 2700 samples. These 2700 samples are computed for each global mean temperature increase up to 8 °C above pre-industrial which can be reached in business as usual scenarios RCP8.5 extended from 2100 to 2500 [10] in steps of 0.1 °C and coupling constant $d$ between 0.0 and 1.0 in steps of 0.02 accounting for 864.000 simulation runs.

The extension of the Monte Carlo ensemble, integrating basin stability is detailed below: the basin stability of the system for each of these 864.000 samples is computed by permuting the initial state of each of the five tipping elements within its limit, i.e., between the untipped ($x = -1.0$) and the tipped state ($x = +1.0$). The state variables of the five tipping elements result in a five dimensional state vector

$$\mathrm{vec}_{\text{basin stability, i}} = \{x_{\text{Greenland ice sheet}}(0),\ x_{\mathrm{AMOC}}(0),\ x_{\text{west Antarctic ice sheet}}(0),$$
$$x_{\mathrm{ENSO}}(0),\ x_{\text{Amazon rainforest}}(0)\},$$

where $\mathrm{vec}_{\text{basin stability, i}} \in [-1.0; +1.0]$ for each tipping element. However, $\mathrm{vec}_{\text{basin stability,i}}$ cannot be permuted in a completely random way, but each of its five dimensions needs to be permuted in an independent way since there is a strong nonlinearity at state equal zero for each of the five dimensions. Of course, in principle if there would be infinite computational resources, we would not need to take this nonlinearity into account, but would be able to increase the size of the Monte Carlo ensemble even further. But since this is not the case, we need to 'manually' account for this important nonlinear property. This means that the sign of each state must be equally probable, i.e.:

IOP Publishing New J. Phys. 22 (2020) 123031 N Wunderling et al

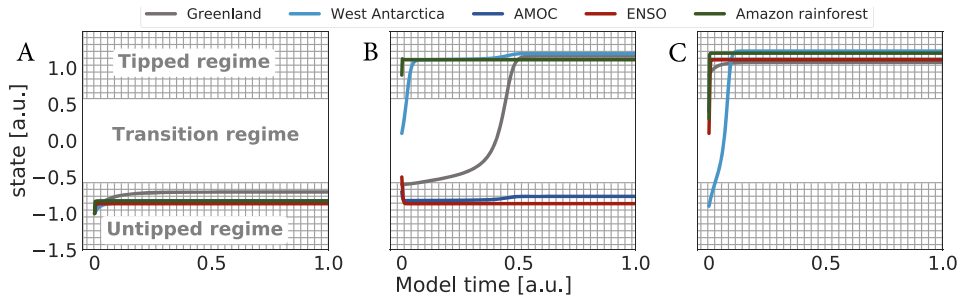


**Figure 2.** (A)–(C) Timelines at GMT = 2.5 °C above pre-industrial levels and $d = 0.15$ with different initial conditions (ICs) as used to probe basin stability. (A) IC = $[-1, -1, -1, -1, -1]$ (today's initial conditions, no element is tipped at $t = 0$), (B) IC = $[-0.6, -0.7, 0.1, -0.5, 0.9]$, (C) IC = $[0.9, 0.4, -0.9, 0.1, 0.3]$.

$$\begin{aligned} P_{\text{sign}} &= P(-,-,-,-,-) = P(+,-,-,-,-) = P(-,+,-,-,-) \\ &= \cdots = P(+,+,+,-,+) = P(+,+,+,+,-) = P(+,+,+,+,+) \\ &= 1/32 = 0.031\,25. \end{aligned} \tag{8}$$

This can be achieved when random starting conditions are drawn from each of the 32 combinations of $P_{\text{sign}}$. Hence, for each of the 32 combinations, we chose 10 different initial conditions ending up with 320 different settings. For the 320 randomly chosen perturbations (i.e., the initial conditions of the tipping elements), we again used a latin hypercube algorithm [105]. That means it fulfils the condition that each of the 32 different possible signs of the initial conditions in their five-dimensional subspace (one dimension for each tipping element) is covered equally often.

Altogether, we employ a very large ensemble of simulations to compute the basin stability of $N_{\text{total}} = 320 \cdot 864.000 = 3.569.184.000 \approx 3.6 \cdot 10^9$ samples. How the final state can depend on the initial conditions is shown exemplary for three timelines in figures 2(A)–(C).

### 2.5. Monte Carlo basin bifurcation analysis

Coupling nonlinear ODEs as in the model described here, invokes the possibility of further types of bifurcations besides fold bifurcations. Here, we utilize Monte Carlo basin bifurcation analysis [42] to uncover system attractors and estimate their basins of attraction finding Hopf-bifurcations and thus oscillating solutions converging to limit cycle attractors. MCBB is a novel, numerical approach to analyze multistable systems, quantify and track their asymptotic states in terms of their basins of attraction by utilizing random sampling and clustering methods. Since MCBB is based on Monte Carlo ensembles and we are interested in a quantitative measure of interesting dynamical properties (here occurring limit cycles, i.e., Hopf-bifurcations), it is a well suited method for our purposes. It has also been applied to other nonlinear systems such as the Dodds–Watts model, the Kuramoto model or Stuart–Landau oscillators [42].

MCBB aims to find classes of attractors that collectively share the largest basins of attractions of the system. Similar attractors, at different parameter values, have to share similar values of invariant measures $\rho$ and the difference of theses measures has to smoothly vanish if the parameter difference goes to zero. If this is the case they are regarded as being part of the same class of attractors. $N_{\text{tr}}$ trajectories of the system, here 140 000, with randomized initial conditions and parameters are integrated. In order to identify the different classes of attractors, suitable statistics $\mathbf{S}_i$ are measured on every system dimension for every trajectory, here, the mean, variance and the Kullbach–Leibler divergence to a normal distribution. Hence, for every statistic $i$, $\mathbf{S}_i$ is a $N_{\text{tr}} \times 5$ matrix. A distance matrix of each trajectory to each other is computed from these statics with

$$D_{ij} = \sum_{k}^{3} w_k \sum_{l}^{5} |\mathbf{S}_{k,il} - \mathbf{S}_{k,jl}| + w_4 |p^{(i)} - p^{(j)}|, \tag{9}$$

where $p^{(i)}$ is the control parameter used to generate the $i$th trajectory and $w_i$ are free parameters of the method, here $[1; 0.5; 0.5; 1]$ which is the default recommendation for these parameters. This distance matrix is used as an input for a density-based clustering algorithm such as DBSCAN which can find if this notion of continuity between different trajectories exists and thus each cluster corresponds to a different class of attractors. For further details on MCBB, refer to [42]. When applying this to the conceptual model for climate tipping points, not only the different possible states of tipped elements are found, but also different classes of oscillating states induced by Hopf-bifurcations are found. For the MCBB analysis, the

IOP Publishing New J. Phys. 22 (2020) 123031 N Wunderling et al

parameter uncertainties were varied randomly within the same bounds as for the previously described basin computations. The initial conditions of five tipping elements were chosen to all start at −1, i.e., not tipped for the results presented in the main text, and at random between −1 and +1 for the results presented in the appendix. The computations are performed with the Julia library MCBB.jl.

## 3. Results

### 3.1. Basin stability

We compute the basin stability of each potential state that could be governed by the network of five tipping elements. The present day state could be considered as some kind of safe state for the Earth system when all five tipping elements are in a negative state. On the other hand there could be a state where all five tipping elements reside in the positive, tipped state. In between there are intermediate scenarios, where some tipping elements already crossed their thresholds and others did not. In figure 3, we show the average basin stability for each of these six possible situations, i.e., with zero, one, two, three, four and five tipped elements. In this experiment, we perturbed the initial conditions of all tipping elements at the same time. The fraction of initial conditions that end up in the respective basin are plotted as the color.

In general, we observe that the size of the basin of attraction for higher global warming levels becomes larger for a higher number of tipped elements as would be expected. For high levels of warming, the basin of five tipped elements dominates.

For increasing interaction strength, the volume of the basins with three or less tipped elements decreases (figures 3(A)–(D)). Contrasting this, the basin volume with four tipped elements increases with increasing interaction strength, while the basin for five tipped elements first increases and then decreases again (figures 3(E) and (F)). The last issue is due to the strong negative feedback loop between the GIS and the AMOC. In such cases of high coupling, the AMOC tips, but safeguards the GIS which reaches the untipped regime for global mean temperature increases above 4 °C and interaction strengths above 0.5. This poses a hypothetical scenario which would only be realistic if the interaction strength between Greenland and AMOC is very high, but this behavior has also been observed in experiments of tipping cascades earlier [35].

For instance, in the basin volume plot of zero, one or two tipped elements, the number of states that equilibrate in this state is very small (figures 3(A)–(C)). For temperature increases above 2 °C the associated basin volume is close to zero for all interaction strengths. At the same time, the size of the basin decreases for higher coupling strengths.

The uncertainties of the basin volumes are quantified as standard deviation in the appendix (figure B.1). We find that uncertainties generally increase for a higher amount of tipped elements as well as for higher interaction strengths. The standard deviation is highest for small temperature increases and high coupling strengths since here, the attractors depend on the initial conditions in terms of the critical temperature thresholds and initial coupling constants (see table A.1). The basin of four and five tipped elements show a regime of increased standard deviation for temperatures around 2 °C–5 °C above pre-industrial and interaction strength parameters of more than 0.2. This is probably due to the fact that in this regime the state of the GIS has a large variation because of its strong negative feedback loop to AMOC. Thus, whether this element tips, also depends a lot on the explicit initial conditions of the state as well as on parameters (see tables A.1 and A.2). Outside and around this regime, the uncertainty is smaller since either Greenland is not tipped with high certainty for lower temperature increases (below 2 °C) or tipped with high certainty at higher temperature increases (above 5 °C).

There exists a narrow range of global mean temperature increases when single tipping elements can transgress their state without triggering a tipping cascade. This range is mostly located below 1 °C above pre-industrial for low coupling strength and well below 1 °C for higher interaction strengths (see figures 3(B) and B.2). If we separate this response into the respective singular tipping elements, we can see that above an interaction strength of 0.2–0.4, the GIS and ENSO cannot tip without causing a cascade due to their strong interactions links to AMOC or the AMAZ, respectively (for more details see appendix B).

Additionally, we investigate some important intermediate states in more detail, where some elements are in the tipped regime, while others are not. It was found that several tipping cascades of size two and three are more frequent than others, for instance a tipping cascade between the GIS and the WAIS is more likely than, for instance, a cascade between the AMOC and the AMAZ [35]. Thus, we investigate the basin volume that corresponds to such cascades.

We find that the ice sheets appear to be of particular importance for the stability of the Earth system in our model because they have a high basin stability in both, when exactly two and exactly three elements are tipped (figures 4 and 5). Although a potential disintegration of the ice sheets can take several centuries up

IOP Publishing New J. Phys. 22 (2020) 123031 N Wunderling et al

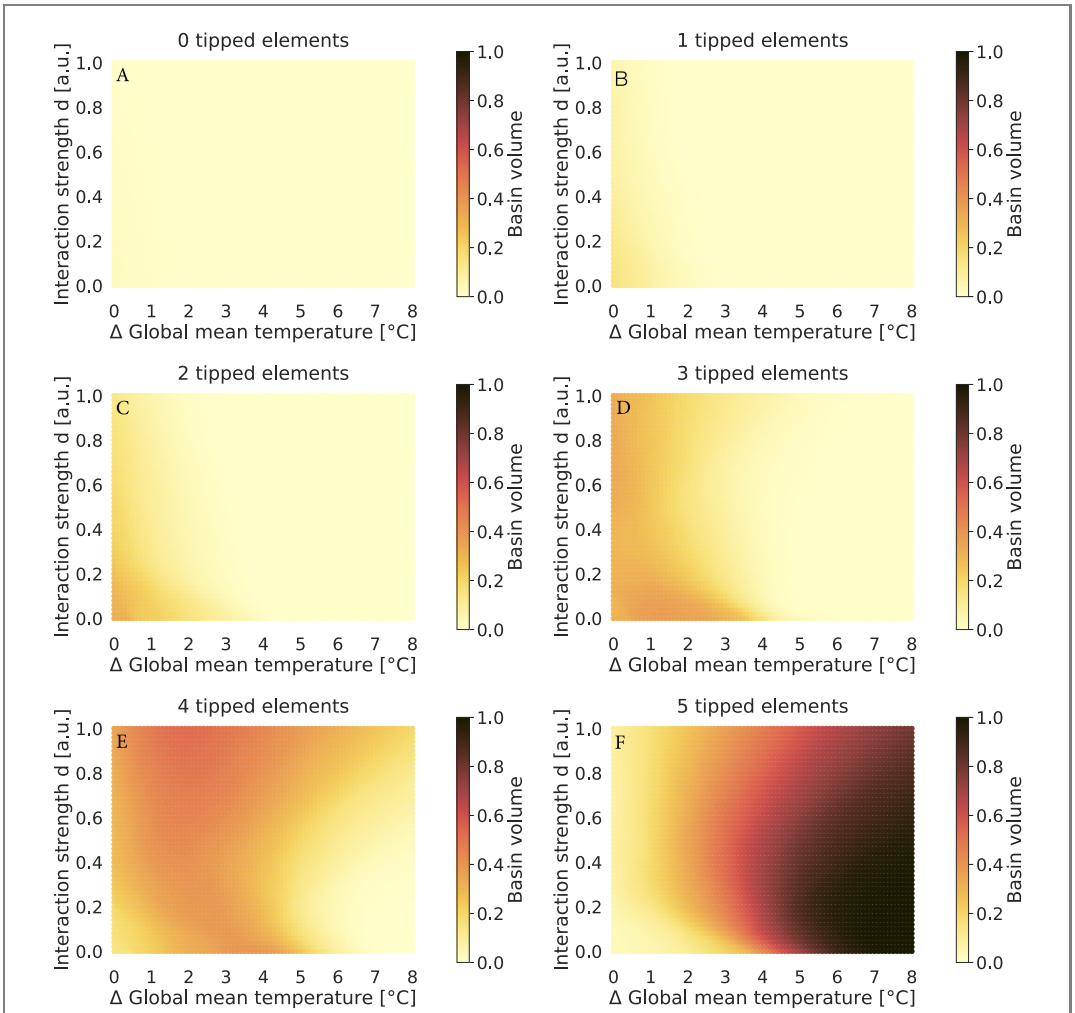


**Figure 3.** Basin volume for each number of tipped elements in dependence of interaction strength and global mean temperature increase. (A)–(F) Basin volume of 0 to 5 tipped elements.

to millennia, states including tipped ice sheets seem to be more stable than states without tipped ice sheets. This is also consistent with the earlier result that the large ice sheets are the initiators of many cascades in the studied model [35].

In case exactly two elements are tipped (figure 4), the basin of the GIS and the WAIS is the only one which has increased basin volume for low interaction strength and global warming levels of 1 °C–3 °C above pre-industrial. This would represent a scenario in which, both, the GIS as well as the WAIS are triggered and become ice free on long time scales without a tipping of the AMOC. This could for example be the case when global warming is higher than necessary to safeguard the large ice sheets, but low enough such that the time of their disintegration is slow enough such that the freshwater input into the AMOC does not stop their functioning.

In parallel, if exactly three elements are tipped, the combinations that include the GIS and the WAIS have a higher basin stability at low interaction strength. Here, global warming levels are up to 4 °C above pre-industrial (figure 5).

We compare the basin volumes of these scenarios, where exactly two or three tipping elements are in the tipped regime and the large ice sheets are among these tipped elements (see figure 6). We observe that the basin volume is highest between 1 °C–4 °C above pre-industrial levels for an interaction strength of 0.1. We find that the basin volume is largest at intermediate interaction strengths $d$ (mainly below 0.2) for a global mean temperature increase of 2 °C above pre-industrial levels. We also reveal that the basin volume for two tipped ice sheets (red curve) is lower than for exactly three tipped elements including the two ice sheets (other curves). Since many basin volumes of exactly two or three tipped elements are very close to zero (see figures 4 and 5) and the basin volumes including tipped ice sheets are different from zero, this emphasizes

186

IOP Publishing New J. Phys. 22 (2020) 123031 N Wunderling et al

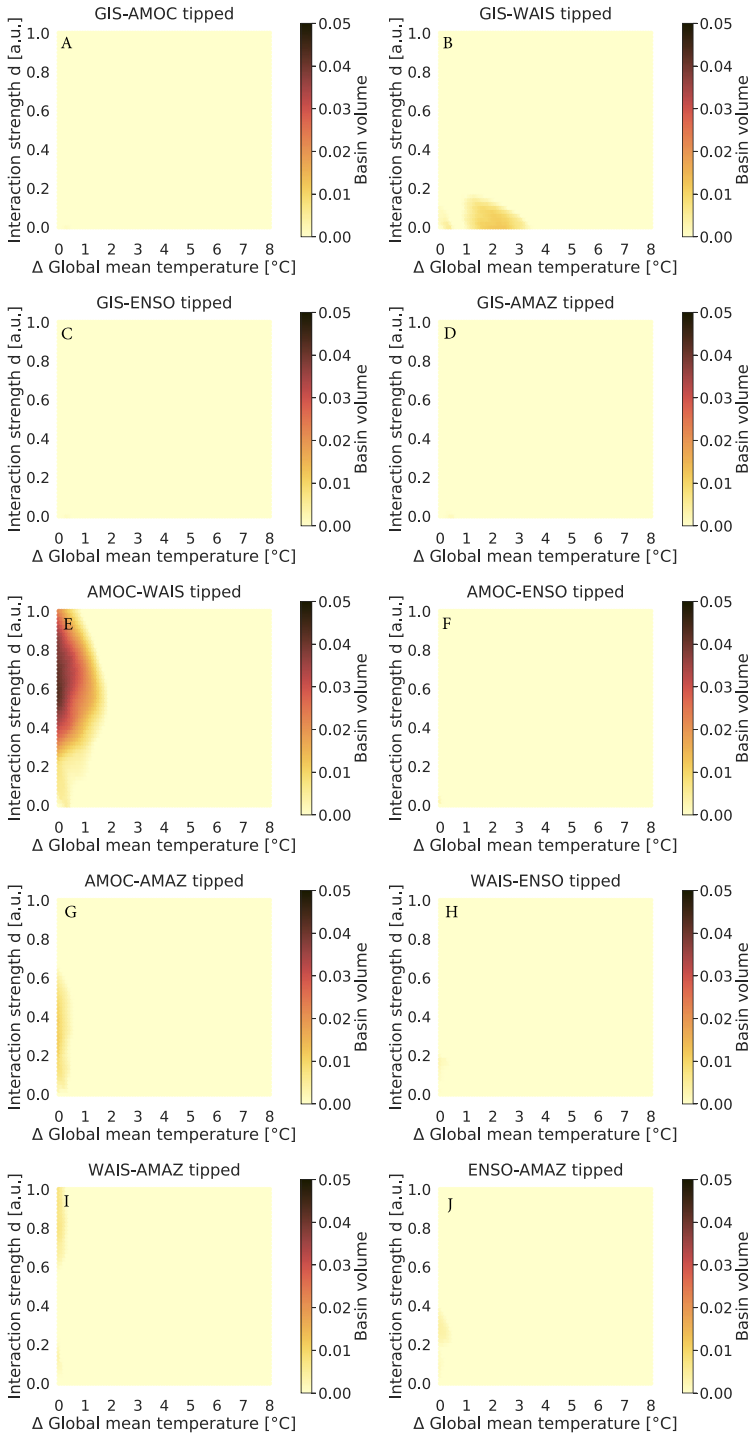


**Figure 4.** Basin stability for exactly two tipped elements for all pairs of tipping elements [panel (A) to (J)]. Most of the basin volumes are very small, but the joint basin of the GIS and the WAIS for low interaction strength and the joint basin of the AMOC and the WAIS for high interaction strength and low temperature is increased. The abbreviations in the title stand for: Greenland Ice Sheet (GIS), West Antarctic Ice Sheet (WAIS), Atlantic Meridional Overturning Circulation (AMOC), El-Niño Southern Oscillation (ENSO) and Amazon rainforest (AMAZ).

again that the ice sheets could be of special interest for the resilience of the Earth system with respect to tipping dynamics.

Furthermore, some basin volumes are increased for low to intermediate levels of global warming and high interaction strengths (above $\approx 0.5$). It is likely that such scenarios are less realistic since, either such a low increase of the global mean temperature is improbable, or such high interaction strength would pose

IOP Publishing New J. Phys. 22 (2020) 123031 N Wunderling et al

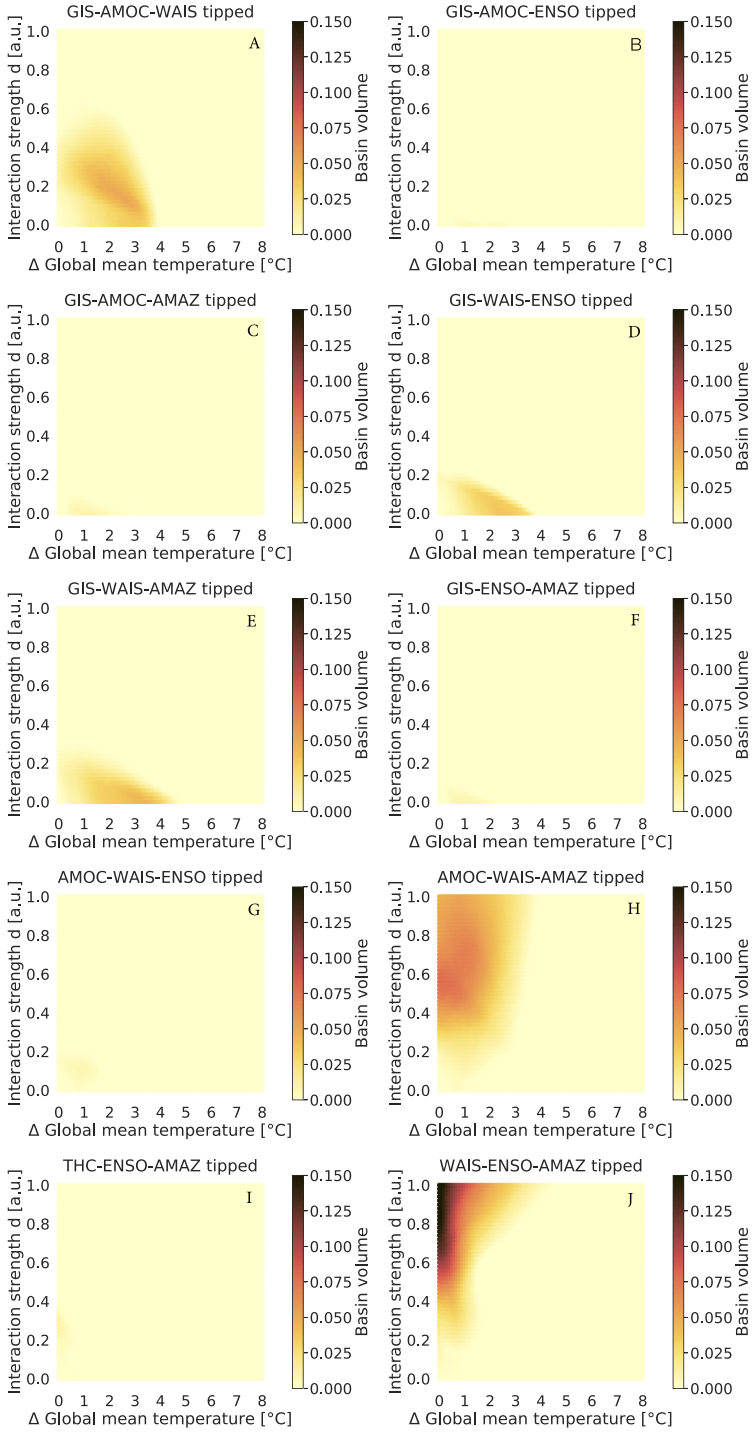


**Figure 5.** Basin stability for exactly three tipped elements [panel (A) to (J)]. The volume of basins is large, where the GIS and the WAIS are included, for low interaction strength and global warming levels of up to 4 °C above pre-industrial.

the unlikely scenario that interactions are as important as the individual dynamics of the tipping elements. This would be the case when the interaction strength $d$ approaches 1.0 (see figures 4 and 5 and compare to equation (5)).

### 3.2. Oscillatory states

188 Furthermore, from the basin stability results we aim to separate off limit cycle attractors in the state space. The results from MCBB [42] identify the parameter regimes where Hopf Bifurcations occur and the tipping

IOP Publishing New J. Phys. 22 (2020) 123031 N Wunderling et al

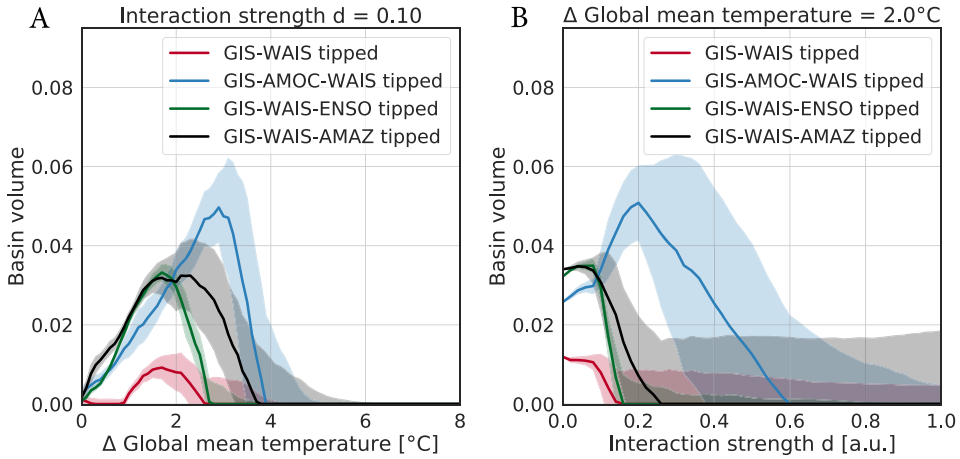


**Figure 6.** Basin volume for selected tipping elements residing in the tipped and untipped regime for (A) an interaction strength of $d = 0.10$ and (B) a global mean temperature increase of 2.0 °C above pre-industrial levels. The shaded colors represent the standard deviation arising from the 27 different network setups due to the structural uncertainties of the network of tipping elements (compare section 2.4 and see figure 1(A)). The standard deviation increases with increasing interaction strength $d$ in panel (B) since the equilibrium state depends on the initial conditions of the respective ensemble member. This equilibrium state is influenced significantly more for higher interaction strengths, but due to stabilizing, destabilizing and unclear links in the network of tipping elements, the change of the equilibrium states fluctuates more and shows a higher uncertainty. Therefore, the standard deviation increases. The same is valid for panel (A) at a region where (parts) the critical temperature ranges $T_{\mathrm{limit,i}}$ are located for many of the tipping elements, that is mainly between 2 °C–4 °C above pre-industrial.

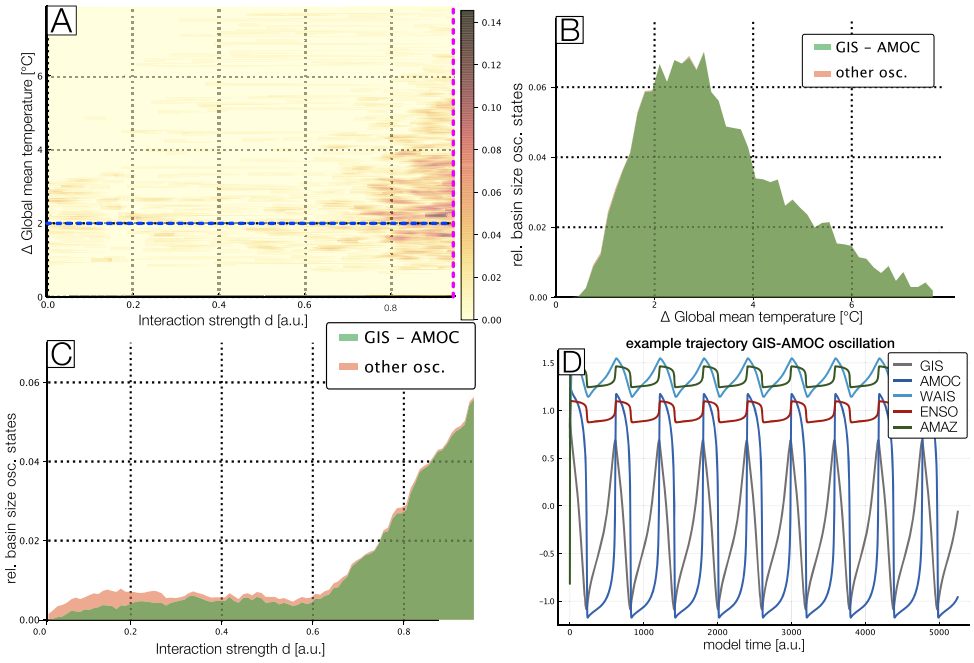


**Figure 7.** Oscillating states in case the initial conditions of all tipping elements are $[-1, -1, -1, -1, -1, -1]$. For random initial conditions, see figure C.1. (A) Occurrence of oscillating states with respect to global warming and interaction strength parameter d. (B) Dependence of limit cycles and their main type on the temperature increase at high interaction strength (dashed magenta line in panel (A). (C) Dependence of limit cycles and their main type on the coupling strength at a temperature increase of 2 °C above pre-industrial (dashed blue line in panel A). (D) Example time series for a limit cycle of AMOC and GIS.

elements start to show Kadyrov oscillations. Such Kadyrov oscillations have already been found in the early literature on dynamical systems of the CUSP type [92]. As shown in figure 7 for initial conditions at −1 for all tipping elements, this is most prominently the case for large interaction strengths and medium temperature increase values. Here, about every tenth solution is oscillating. This is due to the fact that uncertainties are largest in these regimes. For smaller interaction strength values, limit cycles can still occur

IOP Publishing New J. Phys. 22 (2020) 123031 N Wunderling et al

but are much rarer with an occurrence at about 1% of all solutions. Of all these limit cycle oscillations almost all (95%) have a significant amplitude (standard deviation $> 0.1$) in at least one tipping element. The most common limit cycles are simultaneous oscillations of AMOC and GIS as shown in figure 7(D). They make up about 86% of all oscillating states found. The reason for this predominant oscillation is that there is a strong negative feedback loop between the GIS and the AMOC via freshwater input from Greenland that weakens the AMOC, while on the other side a weaker AMOC cools the northern hemisphere (see e.g. [16, 29]). Still, whether such oscillations could indeed exist in the climate system remains speculative, but in principle there is evidence of oscillatory behavior in paleo data of the Earth system [106, 107].

## 4. Discussion

We find that the only dominating stable state in the long term, for large temperature increases around and above 4.0 °C above pre-industrial levels, is the one with four or five tipped elements. Our results emphasize that the ice sheets could be of special importance for the stability of the climate system regarding their increased basin volume in case more than one element is tipped. Based on the known interactions from Kriegler *et al* [29] this makes sense, since the interactions between the ice sheets, especially from Greenland to west Antarctica, are strong due to potentially rising sea level that might cause grounding line retreat [69].

Of course, the ice sheets interact with global modes of ocean variability like the AMOC and reduce its overturning strength, but in our model these interactions are not sufficient to tip the AMOC over in many cases. These states with disintegrated ice sheets are especially relevant exhibiting a high basin volume for intermediate climate warming scenarios consistent with the climate target of the Paris agreement that aims at limiting global warming to well below 2 °C above pre-industrial levels [108]. Limit cycle oscillations between the tipping of some elements have been detected at some rare parameter configurations, mainly between the GIS and the AMOC. Although it remains unclear whether such (Kadyrov) oscillations have occurred in the climate system, they point to possible relevant internal modes of variability in the climate system. In principle such limit cycle behavior could have played a role in paleo climate dynamics such as in the Pleistocene ice age cycles [106, 107]. Further, the individual dynamics are not the sole determinant of the final state of the tipping elements since the network effects can cause additional tipping events. Through this network interaction, it is therefore possible that cascades of tipping events emerge, even before the actual critical temperature threshold for some of the tipping elements is reached [35].

## 5. Conclusion

In this work, we study a conceptual model of five climate tipping elements based on a system of coupled, nonlinear differential equations. We investigate the stability of different dynamical regimes with respect to its stable states applying the concept of basin stability using a very large-scale Monte Carlo simulation of more than 3.5 billion ensemble members. Following that approach, we are able to propagate the numerous uncertainties thoroughly which are associated with the critical temperature thresholds and interaction strengths. With a Monte Carlo basin bifurcation analysis tool, we detected oscillatory states within our system.

We observe that the largest basin volume is that of the basin, where all five tipping elements are in the transgressed state, especially for large levels of global warming. We also detect that the ice sheets are of special importance for the stability of states, where the large cryosphere components reside in the transgressed state, while the other tipping elements do not. We also detect Hopf-bifurcations for few parameter configurations (0.6%), mainly taking place between the GIS and the AMOC (86%).

Our complex dynamical networks approach strongly simplifies the nature of tipping elements as well as their interaction structure. However, it can serve to integrate simplified concepts of tipping elements until coupled, process-based models are developed that can resolve the respective nonlinearities in the Earth system in more detail since current state-of-the-art Earth system models cannot yet model all these nonlinearities due to a lack of comprehensive process-understanding and computational constraints. It is further important to note that some studies have hypothesized that major changes in ENSO are possible [60, 61] based on conceptual models [109, 110], but however, whether this is evidence for a permanent and potentially even irreversibly tipped ENSO remains uncertain and debated. Surely, ENSO exerts strong feedbacks onto the climate system that will increase if major El–Niño events become more frequent, for instance through strong drying trends over Amazonia. Furthermore, in earlier research we found that the main results of our model remain robust under the omission of ENSO such that we decided to investigate the more complex case and included ENSO here, even though the use of equation (5) is only a topologically

IOP Publishing New J. Phys. 22 (2020) 123031 N Wunderling et al

equivalent dynamical equation (for more details see [35]). While some literature studies present ENSO among the list of potential tipping elements [6, 10, 29], it still remains uncertain whether ENSO is a tipping element in a strict sense.

Overall, our network approach can easily be adapted to further tipping elements as soon as their interaction structure would be understood. It is also possible to probe the effect of different structural interaction hypotheses to further tipping elements within the scope of an uncertainty analysis, as has already been performed here for three interaction links. Further, the results of our study motivate that it could be worthwhile to look into the dynamics in more detail using process-detailed Earth system models. Especially the role of the large sheets in the stability landscape and oscillations between climate system components could be of interest. Even though, there is some knowledge about the interaction structure present in literature (see section 2.1), a new expert elicitation might be worthwhile because the knowledge about the interactions between the tipping elements has surely widened since the original expert elicitation from Kriegler *et al* (2009) [29].

## Author contributions

CRediT (contributor roles taxonomy) statement: NW: conceptualization, formal analysis, investigation (basin stability, Monte Carlo), visualization (introduction, methods, basin stability), writing–original draft, writing–review and editing. MG: formal analysis, investigation (MCBB), visualization (oscillatory states), writing–review and editing. RW: conceptualization, writing–review and editing, supervision, funding acquisition. JK: writing–review and editing, funding acquisition. JFD: conceptualization, writing–review and editing, supervision, funding acquisition.

## Note on color maps

This paper makes use of the conceptually uniform colormaps developed by [111].

## Acknowledgments

This work has been carried out within the framework of PIK's FutureLab on Earth Resilience in the Anthropocene. NW, MG, JK and RW acknowledge the financial support by the IRTG 1740/TRP 2015/50122-0 project funded by DFG and FAPESP. NW is grateful for a scholarship from the Studienstiftung des deutschen Volkes. JK acknowledges support by the grant of the Ministry of Education and Science of the Russian Federation Agreement No. 075-15-2020-808. JFD is grateful for financial support by the Stordalen Foundation via the Planetary Boundary Research Network (PB.net), the Earth League's EarthDoc program and the European Research Council Advanced Grant project ERA (Earth Resilience in the Anthropocene, ERC-2016-ADG-743080). We are thankful for financial support by the Leibniz Association (project DominoES). The authors gratefully acknowledge the European Regional Development Fund (ERDF), the German Federal Ministry of Education and Research and the Land Brandenburg for supporting this project by providing resources on the high performance computer system at the Potsdam Institute for Climate Impact Research.

## Appendix A. Parameter uncertainties

In the following tables (tables A.1 and A.2), we list the critical temperatures $T_{\mathrm{limit,i}}$ for the respective tipping element and the interactions between them together with their uncertainties.

## Appendix B. More basin stability results

Here, we show the standard deviation of the basin volume for 0 to 5 tipped elements (figure B.1) and the basin volume for one specific tipped element (figure B.2) to complement the results from figure 3.

## Appendix C. Oscillatory regimes for random initial conditions

Here, we show the results of a MCBB analysis for random initial conditions (figure C.1). We find that limit cycles occur more frequently when the initial conditions are randomly shuffled.

**Table A.1.** Each interaction in the network of figure 1 has a specific link strength range and a specific physical process that is connected to the respective interaction. The link strength ranges are computed from literature values [29, 43] such that they can be used in equation (5). For a more in depth description please be referred to Wunderling *et al* (2020) [35].

| Interaction | Link strength range $s_{ij}$ (a.u.) | Process |
|---|---|---|
| Greenland → AMOC | $[+1; +10]$ | Freshwater inflow |
| AMOC → Greenland | $[-1; -10]$ | AMOC breakdown, Greenland cooling |
| Greenland → west Antarctica | $[+1; +10]$ | Grounding line retreat |
| ENSO → Amazon rainforest | $[+1; +10]$ | Drying over amazonia |
| ENSO → west Antarctica | $[+1; +5]$ | Warming of ross and amundsen seas |
| AMOC → Amazon rainforest | $[\pm 2; \pm 4]$ | Changes in hydrological cycle |
| West Antarctica → AMOC | $[\pm 1; \pm 3]$ | Increase in meridional salinity gradient $(-)$, Fast advection of freshwater anomaly To north atlantic $(+)$ |
| AMOC → ENSO | $[+1; +2]$ | Cooling of north-east tropical pacific with thermo-Cline shoaling and weakening of annual cycle in EEP |
| West Antarctica → Greenland | $[+1; +2]$ | Grounding line retreat |
| ENSO → AMOC | $[-1; -2]$ | Enhanced water vapor transport to pacific |
| AMOC → west Antarctica | $[+1; +1.5]$ | Heat accumulation in southern ocean |
| Amazon rainforest → ENSO | $[\pm 1; \pm 1.5]$ | Changes in tropical moisture supply |

**Table A.2.** Critical temperature range $T_{\mathrm{limit,i}}$ of the five tipping elements as taken from the literature [10], see also equation (5). The typical tipping time scale $\tau_i$ is given in model years (in arbitrary units) since it is beyond the scope of this model to make predictions about the exact tipping times. However, certain differences in tipping times as used here can be decisive whether a tipping event occurs or not. For more information see Wunderling *et al* (2020) [35].

| Tipping element | $T_{\mathrm{limit,i}}$ (°C) | $\tau_i$ [a.u.] |
|---|---|---|
| Greenland | 0.8–3.2 | 4900 |
| West Antarctica | 0.8–5.5 | 2400 |
| AMOC | 3.5–6.0 | 300 |
| ENSO | 3.5–7.0 | 300 |
| Amazon rainforest | 3.5–4.5 | 50 |

IOP Publishing New J. Phys. 22 (2020) 123031 N Wunderling et al

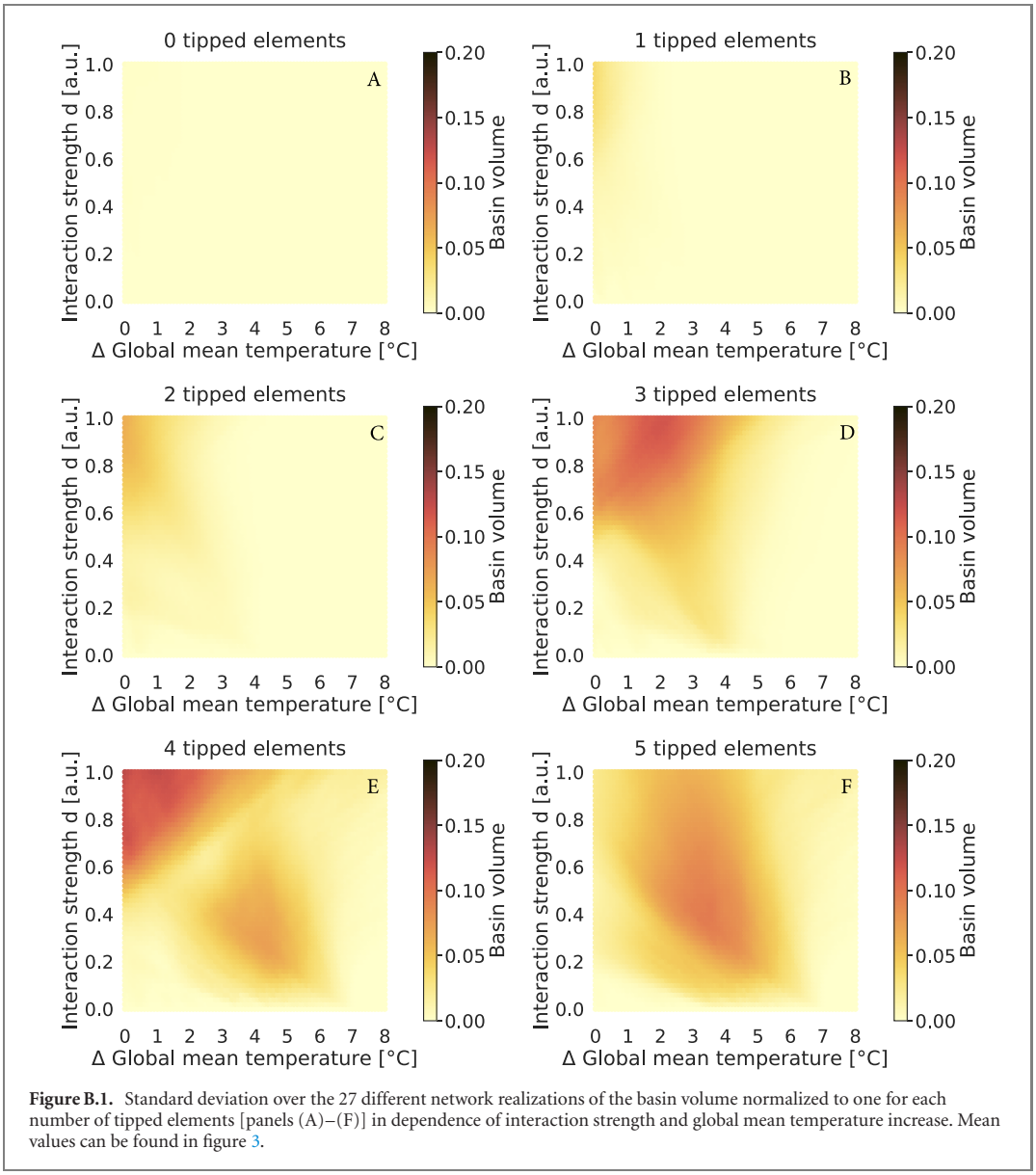


**Figure B.1.** Standard deviation over the 27 different network realizations of the basin volume normalized to one for each number of tipped elements [panels (A)–(F)] in dependence of interaction strength and global mean temperature increase. Mean values can be found in figure 3.

IOP Publishing New J. Phys. 22 (2020) 123031 N Wunderling et al

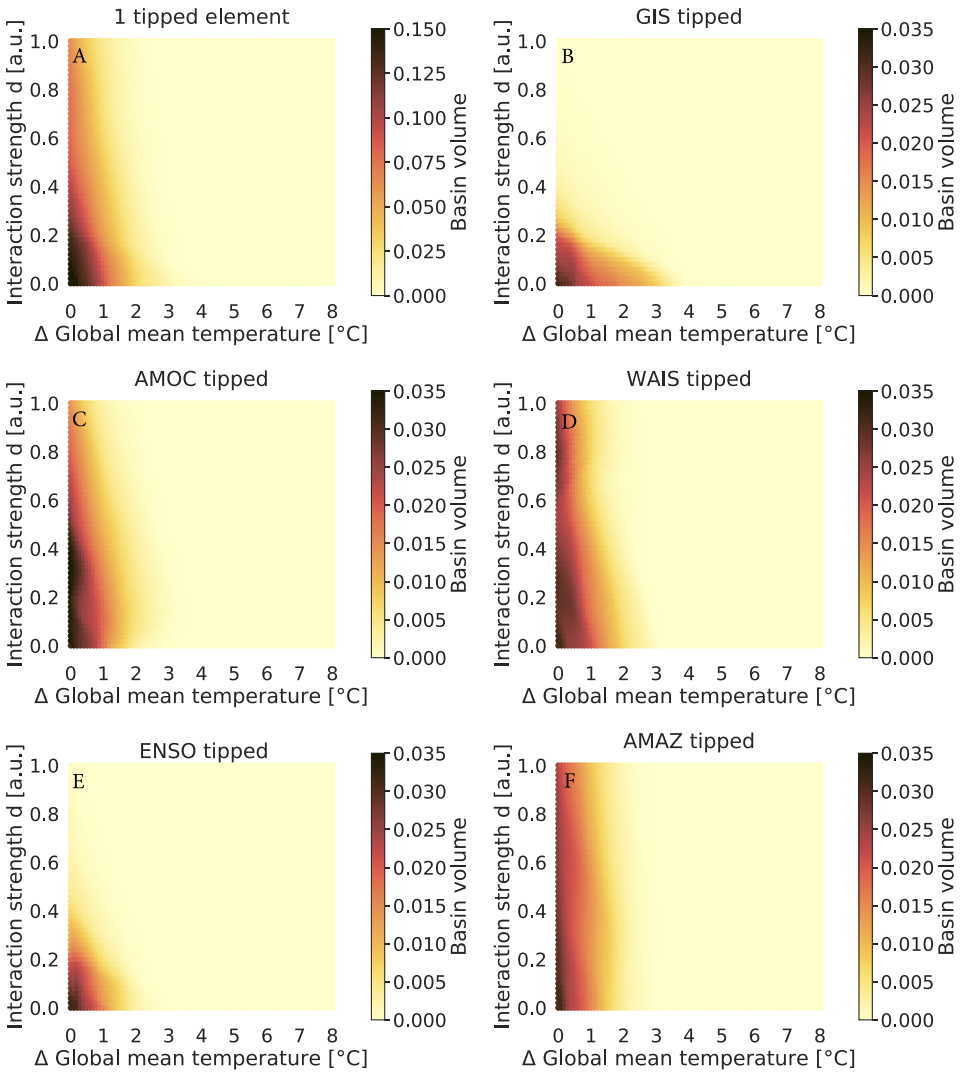


**Figure B.2.** Basin stability for single elements showing that the basin volume for the AMOC, WAIS and AMAZ are qualitatively similar since it is possible that only this particular element tips. However, for ENSO and the GIS this is not the case. It can only very rarely happen that these elements tip on themselves for high interaction strength even at low temperature increases since both of them possess a very strong link to another element that they would draw along into the tipped state. For ENSO, this is the AMAZ and for the GIS it is the AMOC. Note that the color bar is different for panel (A) to improve visibility.

IOP Publishing New J. Phys. 22 (2020) 123031 N Wunderling et al

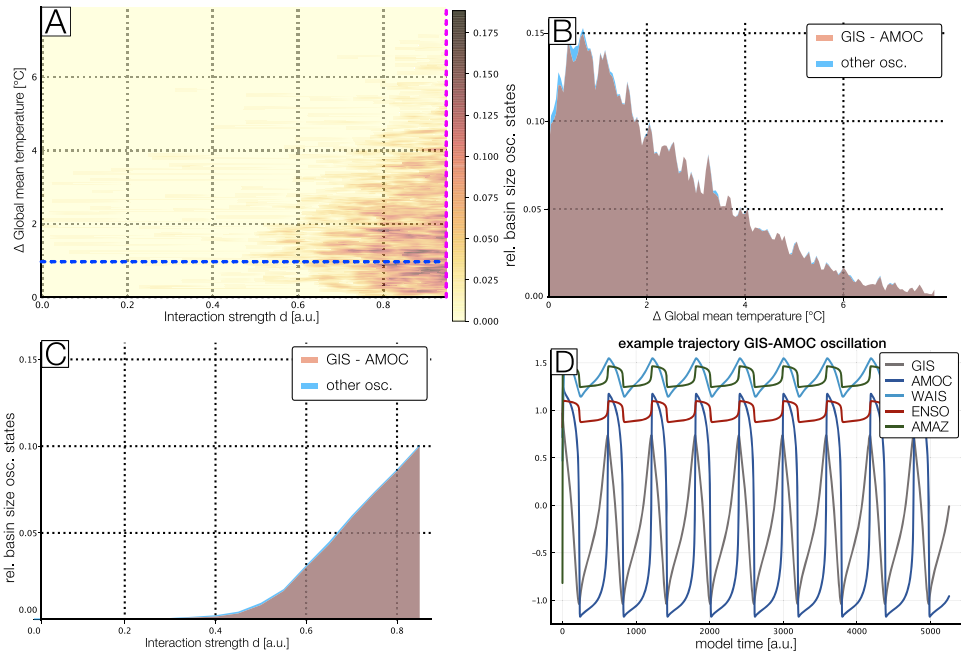


**Figure C.1.** Oscillating states for random initial conditions. Limit cycles occur more often than for initial conditions at −1 for all tipping elements. On the other side, the limit cycle oscillation between the AMOC and the GIS is still dominating.

## ORCID iDs

Nico Wunderling https://orcid.org/0000-0002-3566-323X
Maximilian Gelbrecht https://orcid.org/0000-0002-0729-6671
Ricarda Winkelmann https://orcid.org/0000-0003-1248-3217
Jürgen Kurths https://orcid.org/0000-0002-5926-4276
Jonathan F Donges https://orcid.org/0000-0001-5233-7703

## References

[1] Scheffer M 2009 *Critical Transitions in Nature and Society* vol 16 (Princeton, NJ: Princeton University Press)
[2] Watts D J 2002 *Proc. Natl. Acad. Sci.* **99** 5766–71
[3] May R M, Levin S A and Sugihara G 2008 *Nature* **451** 893–4
[4] Herbig P A 1991 *J. Prod. Innov. Manage.* **8** 127–37
[5] Scheffer M, Carpenter S, Foley J A, Folke C and Walker B 2001 *Nature* **413** 591–6
[6] Lenton T M, Held H, Kriegler E, Hall J W, Lucht W, Rahmstorf S and Schellnhuber H J 2008 *Proc. Natl. Acad. Sci.* **105** 1786–93
[7] Rocha J C, Peterson G, Bodin Ö and Levin S 2018 *Science* **362** 1379–83
[8] Brummitt C D, Barnett G and D'Souza R M 2015 *J. R. Soc. Interface* **12** 20150712
[9] Steffen W *et al* 2018 *Proc. Natl. Acad. Sci.* **115** 8252–9
[10] Donges H J, Rahmstorf S and Winkelmann R 2016 *Nat. Clim. Change* **6** 649
[11] Lenton T M, Rockström J, Gaffney O, Rahmstorf S, Richardson K, Steffen W and Schellnhuber H J 2019 *Nature* **575** 592–5
[12] Wang S and Hausfather Z 2020 *Earth Syst. Dyn. Disc.* https://doi.org/10.5194/esd-2020-16
[13] Joughin I, Smith B E and Medley B 2014 *Science* **344** 735–8
[14] Favier L, Durand G, Cornford S L, Gudmundsson G H, Gagliardini O, Gillet-Chaulet F, Zwinger T, Payne A J and Le Brocq A M 2014 *Nat. Clim. Change* **4** 117–21
[15] Rosier S H, Reese R, Donges J F, Rydt J D, Gudmundsson G H and Winkelmann R 2020 *Cryosphere Disc.* https://doi.org/10.5194/tc-2020-186
[16] Caesar L, Rahmstorf S, Robinson A, Feulner G and Saba V 2018 *Nature* **556** 191–6
[17] Lovejoy T E and Nobre C 2019 *Sci. Adv.* **5** eaax7492
[18] Nobre C A, Sampaio G, Borma L S, Castilla-Rubio J C, Silva J S and Cardoso M 2016 *Proc. Natl. Acad. Sci.* **113** 10759–68
[19] Stocker T F *et al* 2013 *Climate Change 2013: The Physical Science Basis. A Report of Working Group I of the Intergovernmental Panel on Climate Change* (Cambridge: Cambridge University Press)
[20] Zwally H J *et al* 2011 *J. Glaciol.* **57** 88–102
[21] Cai W *et al* 2014 *Nat. Clim. Change* **4** 111–6
[22] England B, Luo X, Yang Y-M, Sun W, Cane M A, Cai W, Yeh S-W and Liu J 2019 *Proc. Natl. Acad. Sci.* **116** 22512–7
[23] Kim S T, Cai W, Jin F-F, Santoso A, Wu L, Guilyardi E and An S-I 2014 *Nat. Clim. Change* **4** 786–90
[24] Collins M *et al* 2010 *Nat. Geosci.* **3** 391–7
[25] Vecchi T P, Carpenter S, Rockström J, Scheffer M and Walker B 2013 *Trends Ecol. Evol.* **28** 389–95

[26] Levermann A and Winkelmann R 2016 *Cryosphere* **10** 1799–807
[27] Winkelmann R, Levermann A, Ridgwell A and Caldeira K 2015 *Sci. Adv.* **1** e1500589
[28] Robinson A, Calov R and Ganopolski A 2012 *Nat. Clim. Change* **2** 429–32
[29] Kriegler E, Hall J W, Held H, Dawson R and Schellnhuber H J 2009 *Proc. Natl. Acad. Sci.* **106** 5041–6
[30] Cai Y, Judd K L, Lenton T M, Lontzek T S and Narita D 2015 *Proc. Natl. Acad. Sci.* **112** 4606–11
[31] Cai Y, Lenton T M and Lontzek T S 2016 *Nat. Clim. Change* **6** 520–5
[32] Lemoine D and Traeger C P 2016 *Nat. Clim. Change* **6** 514–9
[33] Nordhaus W D 2014 *A Question of Balance: Weighing the Options on Global Warming Policies* (New Haven, CT: Yale University Press)
[34] Nordhaus W 2014 *J. Assoc. Environ. Resour. Econ.* **1** 273–312
[35] Wunderling N, Donges F J, Kurths J and Winkelmann R 2020 *Earth Syst. Dyn. Disc.* https://doi.org/10.5194/esd-2020-18
[36] Menck P J, Heitzig J, Marwan N and Kurths J 2013 *Nat. Phys.* **9** 89–92
[37] Schultz P, Heitzig J and Kurths J 2014 *New J. Phys.* **16** 125001
[38] Leng S, Lin W and Kurths J 2016 *Sci. Rep.* **6** 21449
[39] Mitra C, Choudhary A, Sinha S, Kurths J and Donner R V 2017 *Phys. Rev.* E **95** 032317
[40] Schultz P, Menck P J, Heitzig J and Kurths J 2017 *New J. Phys.* **19** 023005
[41] Hellmann F, Schultz P, Grabow C, Heitzig J and Kurths J 2016 *Sci. Rep.* **6** 29654
[42] Gelbrecht M, Kurths J and Hellmann F 2020 *New J. Phys.* **22** 033032
[43] Lenton T M and Williams H T P 2013 *Trends Ecol. Evol.* **28** 380–2
[44] Wunderling N, Stumpf B, Krönke J, Staal A, Tuinenburg O A, Winkelmann R and Donges J F 2020 *Chaos* **30** 043129
[45] Krönke J, Wunderling N, Winkelmann R, Staal A, Stumpf B, Tuinenburg O A and Donges J F 2020 *Phys. Rev.* E **101** 042311
[46] Brockmann D and Helbing D 2013 *Science* **342** 1337–42
[47] Wiedermann M, Smith E K, Heitzig J and Donges J F 2020 *Sci. Rep.* **10** 11202
[48] Ridley J, Gregory J M, Huybrechts P and Lowe J 2010 *Clim. Dyn.* **35** 1049–57
[49] Garbe J, Albrecht T, Levermann A, Donges J F and Winkelmann R 2020 *Nature* **585** 538–44
[50] Stommel H 1961 *Tellus* **13** 224–30
[51] Rahmstorf S *et al* 2005 *Geophys. Res. Lett.* **32** L23605
[52] Hawkins E, Smith R S, Allison L C, Gregory J M, Woollings T J, Pohlmann H and De Cuevas B 2011 *Geophys. Res. Lett.* **38** L10605
[53] Mecking J V, Drijfhout S S, Jackson L C and Graham T 2016 *Clim. Dyn.* **47** 2455–70
[54] Wood R A, Rodríguez J M, Smith R S, Jackson L C and Hawkins E 2019 *Clim. Dyn.* **53** 6815–34
[55] Oyama M D and Nobre C A 2003 *Geophys. Res. Lett.* **30** 2199
[56] Cox P M, Betts R, Collins M, Harris P P, Huntingford C and Jones C 2004 *Theor. Appl. Climatol.* **78** 137–56
[57] Hirota M, Holmgren M, Van Nes E H and Scheffer M 2011 *Science* **334** 232–5
[58] van Nes E H, Hirota M, Holmgren M and Scheffer M 2014 *Global Change Biol.* **20** 1016–21
[59] Staal A, Dekker S C, Hirota M and van Nes E H 2015 *Ecol. Complex.* **22** 65–75
[60] Timmermann A, An S-I, Krebs U and Goosse H 2005 *J. Clim.* **18** 3122–39
[61] Dekker M M, Von Der Heydt A S and Dijkstra H A 2018 *Earth Syst. Dyn.* **9** 1243–60
[62] Jungclaus J, Haak H, Esch M, Roeckner E and Marotzke J 2006 *Geophys. Res. Lett.* **33** L10707
[63] Driesschaert E, Fichefet T, Goosse H, Huybrechts P, Janssens I, Mouchet A, Munhoven G, Brovkin V and Weber S 2007 *Geophys. Res. Lett.* **34** L10707
[64] Robson J, Hodson D, Hawkins E and Sutton R 2014 *Nat. Geosci.* **7** 2–3
[65] Stouffer R J *et al* 2006 *J. Clim.* **19** 1365–87
[66] Hu A *et al* 2007 *J. Clim.* **20** 4899–919
[67] Vellinga M and Wood R A 2002 *Clim. Change* **54** 251–67
[68] Weijer W *et al* 2019 *J. Geophys. Res. Oceans* **124** 5336–75
[69] McDonagh R and Worster M G 2013 *Geophys. Res. Lett.* **40** 5877–81
[70] Mitrovica J X, Gomez N and Clark P U 2009 *Science* **323** 753
[71] Kopp R E, Mitrovica J X, Griffies S M, Yin J, Hay C C and Stouffer R J 2010 *Clim. Change* **103** 619–25
[72] Zhang R and Delworth T L 2005 *J. Clim.* **18** 1853–60
[73] Dong B and Sutton R T 2005 *J. Clim.* **18** 1117–35
[74] Sterl A *et al* 2008 *Geophys. Res. Lett.* **35** L14703
[75] Holmgren M, Hirota M, Van Nes E H and Scheffer M 2013 *Nat. Clim. Change* **3** 755–8
[76] Holmgren M *et al* 2006 *Front. Ecol. Environ.* **4** 87–95
[77] Lima Y and Wright J 2004 *Phil. Trans. R. Soc.* B **359** 311–29
[78] Duque-Villegas M, Salazar J F and Rendón A M 2019 *Earth Syst. Dyn.* **10** 631–50
[79] Bertler N A N, Naish T R, Mayewski P A and Barrett P J 2006 *Adv. Geosci.* **6** 83–6
[80] Paolo F S, Padman L, Fricker H A, Adusumilli S, Howard S and Siegfried M R 2018 *Nat. Geosci.* **11** 121–6
[81] Nicolas J P *et al* 2017 *Nat. Communs.* **8** 15799
[82] Jackson L C, Kahana R, Graham T, Ringer M A, Woollings T, Mecking J V and Wood R A 2015 *Clim. Dyn.* **45** 3299–316
[83] Schmittner A, Appenzeller C and Stocker T F 2000 *Geophys. Res. Lett.* **27** 1163–6
[84] Spence J P and Weaver A J 2006 *J. Clim.* **19** 4592–604
[85] Parsons L A, Yin J, Overpeck J T, Stouffer R J and Malyshev S 2014 *Geophys. Res. Lett.* **41** 146–51
[86] Seidov D, Stouffer R J and Haupt B J 2005 *Global Planet. Change* **49** 19–27
[87] Swingedouw D, Fichefet T, Huybrechts P, Goosse H, Driesschaert E and Loutre M F 2008 *Geophys. Res. Lett.* **35** L17705
[88] Swingedouw D, Fichefet T, Goosse H and Loutre M F 2009 *Clim. Dyn.* **33** 365–81
[89] Aragão L E 2012 *Nature* **489** 217–8
[90] Boers N, Marwan N, Barbosa H M and Kurths J 2017 *Sci. Rep.* **7** 41489
[91] Zemp D C, Schleussner C F, Barbosa H M, Hirota M, Montade V, Sampaio G, Staal A, Wang-Erlandsson L and Rammig A 2017 *Nat. Commun.* **8** 14681
[92] Abraham R, Keith A, Koebbe M and Mayer-Kress G 1991 *Int. J. Bifurcation Chaos Appl. Sci. Eng.* **01** 417–30
[93] Klose A K, Karle V, Winkelmann R and Donges J F 2020 *R. Soc. Open Sci.* **7** 200599
[94] Virtanen P *et al* 2020 *Nat. Methods* **17** 261–72

[95] Bright T and Motter A E 2006 *Phys. Rev.* E **73** 065106
[96] Pecora L M and Carroll T L 1998 *Phys. Rev. Lett.* **80** 2109
[97] Dijkstra H A 2005 *Nonlinear Physical Oceanography: A Dynamical Systems Approach to the Large Scale Ocean Circulation and El Nino* vol 28 (Berlin: Springer)
[98] Klinshov V V, Nekorkin V I and Kurths J 2015 *New J. Phys.* **18** 013004
[99] van Kan A, Jegminat J, Donges J F and Kurths J 2016 *Phys. Rev.* E **93** 042205
[100] Heitzig J, Kittel T, Donges J F and Molkenthin N 2016 *Earth Syst. Dyn.* **7** 21–50
[101] Rakshit S, Bera B K, Majhi S, Hens C and Ghosh D 2017 *Sci. Rep.* **7** 45909
[102] Majhi S, Ghosh D and Kurths J 2019 *Phys. Rev.* E **99** 012308
[103] Rakshit S, Bera B K, Perc M and Ghosh D 2017 *Sci. Rep.* **7** 2412
[104] Milnor J 1985 *Commun. Math. Phys.* **99** 177–95
[105] Baudin M 2013 pyDOE: The experimental design package for python, software available under the BSD license (3-clause) https://pythonhosted.org/pyDOE/index.html Accessed: 2020-06-08
[106] Ditlevsen P, Mitsui T and Crucifix M 2020 *Clim. Dyn.* **54** 1801–18
[107] Crucifix M 2012 *Phil. Trans. R. Soc.* A **370** 1140–65
[108] United Nations/Famework Convention on Climate Change 2015 *Adoption of the Paris Agreement, 21st Conf. of the Parties* (Paris, United Nations) URL https://treaties.un.org/pages/ViewDetails.aspx?src=TREATY\&mtdsg_no=XXVII-7-d\&chapter=27\&clang=_en
[109] Timmermann A, Jin F-F and Abshagen J 2003 *J. Atmos. Sci.* **60** 152–65
[110] Zebiak S E and Cane M A 1987 *Mon. Weather Rev.* **115** 2262–78
[111] Crameri F 2018 *Geosci. Model Dev.* **11** 2541–62

# Chapter 3

# Results

*The world is reaching the tipping point beyond which climate change may become irreversible. If this happens, we risk denying present and future generations the right to a healthy and sustainable planet – the whole humanity stands to lose.*

*Kofi Annan*

In my dissertation, I have extensively used and developed complex systems' methods to apply them to questions relevant for nonlinear processes in Earth system science. The scope of this thesis is to improve the understanding of tipping elements and their interactions by methodological advances. It also aims at addressing specifically the research question as to whether interactions between tipping elements in the climate system might drive the tipping elements towards potentially dangerous tipping events or cascades. Therefore, my dissertation is divided into two major parts: *Theory & Methodologies* and *Climate tipping elements* (see Fig. 1.4). The main developments and results from my dissertation can be found in the following list and will be detailed in the paragraphs and sections thereafter (see Sects. 3.1 and 3.2). Finally, the results will be summarised and an answer to the research questions will be given (see Sect. 3.3).

[P1–P3] The Python based model PyCascades has been developed facilitating future studies on interacting tipping elements in complex networks. This model is publicly available under the doi: 10.5281/zenodo.4153102. With this model, properties of tipping cascades have been determined, ranging from the robustness of the entire network conditioned by micro-scale motifs to the conditions of the emergence of global cascades and phase transitions (see Sect. 3.1).

[P4] The temperature feedback from large cryosphere elements such as the Arctic summer sea ice, the mountain glaciers, and the Greenland and West Antarctic Ice Sheet have a magnitude of around half a degree (0.39–0.46 °C) of additional global warming. Local additional warming patterns can exceed 5 °C over Greenland and West Antarctica (see Sect. 3.2.1).

[P5] Drought-induced tipping events in the Amazon rainforest can be evoked by potentially drier future conditions due to climate change, especially in the southeast of the Amazon basin. Thereby, tipping cascades through atmospheric moisture recycling, connecting different parts of the Amazon rainforest, are an important amplifier of such tipping events, outpacing the adaptation of the Amazon rainforest to current and past environmental conditions (see Sect. 3.2.2).

[P6, P7] The role of the climate tipping elements in cascading transitions has been revealed. While the large ice sheets act as the initiators of tipping cascades, the AMOC is the transmitter. From

this point of view, but also from a basin stability perspective, the large ice sheets are of special importance for the stability of the climate system in general (see Sect. 3.2.3).

[AP1–AP4] Further results, structured in four additional working packages, are briefly listed in the following and elaborated in the Appendix (see chapter 5). [AP1]: Emergence of cooperativity in interacting tipping cascades with noise. [AP2]: Distinction between three different types of tipping cascades (two phase cascade, domino cascade, joint cascade). [AP3]: Hysteresis in the Amazon rainforest in a global dynamic vegetation model. [AP4]: Definition of social tipping processes and differences between natural and social tipping phenomena.

## 3.1 Theory & Methodologies

In the **first major part** of my dissertation, I have laid the theoretical and methodological ground for the investigation of tipping events and cascades in the Earth system and one of its subcomponents, the Amazon rainforest.

During recent years and decades, a focus of research has shifted towards tipping points as they occur in many different systems (Gladwell, 2006; van Nes et al., 2016; Milkoreit et al., 2018). Examples can be found in ecology, economy, the Earth's climate system or social systems (Lenton et al., 2008; May et al., 2008; Tàbara et al., 2018). The interest in modelling interacting tipping elements with models motivated from complex systems research has increased recently (Brummitt et al., 2015; Eom, 2018; Klose et al., 2020). In this work, we fill the gap of these two newly arising research strands (interactions and tipping elements) and bring them together in an easily extendable and flexible software package PyCascades (see Sect. 2.1 [P1]). PyCascades is a modelling package written in Python that is able to simulate the dynamics of interacting tipping elements on complex networks. Two different types of tipping elements are pre-implemented, a tipping element with a Hopf-bifurcation normal form and a tipping element with a Cusp-bifurcation normal form. Tipping elements can be put on arbitrarily defined network structures, but there are also three paradigmatic network types explicitly pre-implemented that can be used out of the box. These are Erdős-Rényi, Barabási-Albert and Watts-Strogatz networks (Erdös and Rényi, 1959; Watts and Strogatz, 1998; Barabási and Albert, 1999). Motivated by numerous prominent examples where noise-induced tipping can occur (Kondepudi et al., 1986; Gammaitoni et al., 1998; Thompson and Sieber, 2011; Ashwin et al., 2012, 2017), it is possible to simulate tipping events and cascades by adding noise to the normal form of the tipping elements. For that purpose, PyCascades has been linked to the open source software package *sdeint* (Aburn and Ram, 2017). While only additive noise is implemented in the current version of PyCascades, we leave the decision of which type of noise (based on respective SciPy functions (Virtanen et al., 2020)) should be used to the modeller: Gaussian, Lévy and Cauchy based noise are possible. Besides these stylised models, three concrete applications are showcased in this piece of work. First, tipping events in the Earth's climate system are investigated. Second, in the Amazon rainforest, tipping cascades are caused by cascading effects that are transported further by atmospheric moisture recycling. Since these two examples are only briefly outlined and exemplified in this paper, please be referred to Sect. 3.2 and Sects. 2.5–2.7 [P5–P7], where these applications are discussed and elaborated in much more detail. The third application of PyCascades deals with tipping cascades in a model of an international supply chain based on the EORA multi-regional input-output database (Lenzen et al., 2012).

As noted above, dynamical systems from various backgrounds possess two different, distinguishable

states that are connected via a bifurcation (see e.g. Brummitt et al., 2015). Using Pycascades and its pre-defined function for the Cusp-bifurcation normal form, such tipping elements can be described by Eq. 1.1 by neglecting the noise term. While it has been argued that the resilience of such networks of tipping elements depends on the topology of networks (Eom, 2018), the conditions for the emergence of *global* tipping cascades have not been extensively studied. Using networks of tipping elements, we address questions around this problem in detail in three pieces of work (see Sect. 2.2 [P2], Sect. 2.3 [P3] and Sect. 5.1 [AP1]).

To investigate different network types, directed versions of the Barabási-Albert and the Watts-Strogatz network have been developed in [P2]. We also included a spatially embedded network of atmospheric moisture flows within the Amazon rainforest. The Amazon rainforest is an ecological system, which can be represented as a network of tipping elements (Hirota et al., 2011; Staver et al., 2011; Zemp et al., 2017). While the individual cells (here on a $2^\circ$x$2^\circ$ grid) represent forest covered or non-forest covered states such as a savannah or a treeless state, the interactions arise from the atmospheric moisture recycling values, that have been quantified in literature (Staal et al., 2018). Therefore, the Amazon rainforest is modelled here as a network of tipping elements that interacts via the moisture recycling network. In [P2], we found that clustering and spatial organisation are indicators for increased network fragility to tipping cascades. Under such very common conditions in real-world networks, e.g. in the moisture recycling network of the Amazon rainforest, tipping cascades can develop under much weaker coupling strengths $d$ than in random networks. This observation has been confirmed by a directed stochastic block model and a configuration model, with which it is possible to isolate the effects on tipping cascades that degree sequence and community structure have. The models for the stochastic block model and the configuration model have been taken from literature (Holland et al., 1983; Newman et al., 2001; Newman and Girvan, 2004). However, for all network types, the aforementioned differences between the network types vanish as soon as the network is not sparsely connected, but more densely. Under such circumstances, the tipping behaviour converges to the same dynamical behaviour for many network types as long as there do not exist isolated parts of the network. This work emphasises that a study using the actual moisture recycling values and better elaborated critical values in the Amazon rainforest might be worthwhile to detect the potential for tipping cascades within the Amazon basin. Therefore, this study lais the motivation for [P5] (see Sect. 2.5).

In [P2] (and [AP1]), mainly global properties of networks of tipping elements are discussed. However, there are certain micro-structures (the so-called *motifs*) within a network that condition the emergence of global cascades by boosting tipping cascades from a local scale to the entire global network (see Sect. 2.3 [P3]). Two decades ago, motifs have been introduced as the building blocks of complex networks (Milo et al., 2002). Among others, they have been identified to be of important functional relevance in food webs, transcriptional biological networks, but also in tumour suppression (Shen-Orr et al., 2002; Lahav et al., 2004; Alon, 2007; Stouffer et al., 2012). It has been observed that one crucial motif is the so-called *feed forward loop* motif, which is found to be significantly over-expressed in real-world networks compared to Erdős-Rényi networks (Milo et al., 2002). In this work, we identify motifs as some of the most important entry points for initiating tipping cascades in a network of tipping elements. Especially, the so-called feed forward loop motif can strongly reduce the critical coupling strength that is necessary to initiate a tipping cascade from 0.183 to 0.162, a reduction of more than 10%. Furthermore, we derive analytic expressions for the likelihood that a certain motif can be found at a randomly chosen node in Erdős-Rényi networks. Exemplary, for the feed forward

loop motif, this likelihood is

$$\mathcal{P}_{\text{feed forward loop}} = 1 - \left(1 - \frac{\langle k \rangle}{N-1}\right)^{\langle k \rangle (\langle k \rangle - 1)}, \tag{3.1}$$

with the network size $N$ and the average degree $\langle k \rangle$. The necessary coupling strength $d$ to initiate a tipping cascade is reduced by more than 90% for dense networks. This can be attributed to multiply coupled feed forward loop motifs. Lastly, the occurrence of motifs in the moisture recycling network of the Amazon rainforest is quantified, revealing three regions of increased motif occurrence: (i) the southern Amazon basin, (ii) close to the Andes region and (iii) the north of the Amazon basin. This hints at regions where very strong network effects are apparent and a higher number of tipping cascades can be expected. Together with a clustering coefficient that is about a magnitude higher than in Erdős-Rényi networks, which can explain why tipping cascades occur at much lower coupling strengths in the Amazon rainforest moisture recycling network than in random networks.

## 3.2 Climate tipping elements

The **second major part** of my dissertation deals with tipping elements in the climate system. This section is divided into three parts, where I would like to start from the cryosphere, through the Amazon rainforest up to a system of interacting climate tipping elements. Thus in the first part, I will discuss how large specific temperature feedbacks are. The second part discusses tipping cascades in a particular subsystem of the Earth that can be modelled as a set of interacting smaller tipping elements on a complex network structure: the Amazon rainforest. And the third part aims to shed light on the interactions of large-scale climate tipping elements and the risk of cascading tipping. In the last results section, it will also be discussed as to whether the additional temperature feedback from the cryosphere elements might induce additional tipping events and diminish the overall stability of the Earth system (see Sect. 3.3).

### 3.2.1 Feedbacks from the cryosphere tipping elements

If tipping elements transgress into the tipped state, this can for some tipping elements lead to self-enforcing temperature feedbacks, which could then drive other tipping elements closer to their critical threshold. In turn, this could, under unmitigated global warming, ultimately lead to a potential large scale tipping cascade in several Earth system components (Steffen et al., 2018). For some tipping elements such as the Amazon rainforest or the Permafrost, the reinforcing temperature feedbacks have been listed in Steffen et al. (2018). The temperature feedback from the large cryosphere elements, however, is not quantified there. Therefore, we conducted a comprehensive quantification of the temperature feedbacks for the large cryosphere elements in case they would disintegrate under future climate change scenarios (see Sect. 2.4 [P4]). The elements that are investigated are the Greenland Ice Sheet, the West Antarctic Ice Sheet, the mountain glaciers and the Arctic summer sea ice, plus the entire Antarctic Ice Sheet in the supplementary information. The recent developments on Greenland, Antarctica, the Arctic summer ice and the mountain glaciers over the last years and decades reveal that such a scenario is not necessarily implausible (Shepherd et al., 2020, 2018; Gardner et al., 2013; Stroeve et al., 2012; Zwally et al., 2011, for more details see Sect. 2.4). While these four regions are at risk, their disintegration would take place on very different timescales. The large ice sheets on Greenland and Antarctica could take centuries to millennia to become ice-free (Robinson et al., 2012; Winkelmann et al., 2015), but the Arctic summer sea ice might be free of ice from mid century onwards (Notz et al., 2013; Niederdrenk and Notz, 2018; SIMIP-Community, 2020). Using the EMIC

CLIMBER-2 (Petoukhov et al., 2000; Ganopolski et al., 2001), we quantify the temperature increase due to the disintegration of the large cryosphere elements to $0.39 - 0.46$ °C ($0.43$ °C) at a background atmospheric $CO_2$ concentration of 400 ppm in CLIMBER-2, equalling 1.5–2 °C of global warming. The interval $0.39 - 0.46$ °C represents the 90% interquartile ranges of the ensemble and the value in brackets is the median of the ensemble. This value is the global average of the additional global warming, but regional warming levels differ largely. While over the regions of the removed ice over Greenland and West Antarctica local warming levels exceed 5 °C, the additional warming at lower equatorial latitudes is on the order of 0.1–0.3 °C. Furthermore, in this study, a separation into the reasons for warming (fast climate feedbacks) is computed. These feedbacks are the albedo, the lapse rate, the water vapour feedback and the clouds feedback. For a background warming of 1.5–2 °C of global warming, the main driver of additional warming is the albedo feedback, which is responsible for 55% of the additional warming. This makes sense since the ice over Greenland and Antarctica as well as the mountain glaciers and the Arctic summer sea ice is artificially removed or masked out, even though afterwards, the ground is allowed to freely evolve into any types of vegetation (snow cover, bare soil, etc.). 40% of the additional warming are due to changes in the lapse rate and the water vapour, while the last 15% of the additional warming are due to the clouds feedback. In the last results section, we elaborate on whether these additional temperature feedbacks impact the number of observed tipping elements (see Sect. 3.3 & Donges and Wunderling et al. (2021, in prep.)).

### 3.2.2 Amazon rainforest

Not only the climate tipping elements compile a (small) network of interacting tipping elements (see Sects. 2.6 and 2.7 [P6, P7]), but also certain sub-elements can, on a finer level, be understood as nonlinear entities that are connected via network structures. The Amazon rainforest is among these tipping elements that have been viewed as a network of tipping elements in the literature (e.g. Zemp et al., 2017). The nodes of the network are local scale rainforest patches that are vulnerable to changing environmental conditions such as, among others, mean annual precipitation or the drought severity. If a critical value of some environmental condition is undercut, then a certain vegetation patch might not be able to exist as rainforest anymore, but only as savannah or completely treeless under such conditions (Hirota et al., 2011; Staver et al., 2011). Moreover, it has been found that the regions of bistability between savannah and rainforest might increase in the Amazon rainforest region under ongoing climate change (Staal et al., 2020a). At the same time, the edges in such a network represent the transport of atmospheric moisture transport that arises through transpiration and evaporation at one site and is transported further by wind to other sites. This atmospheric moisture recycling mechanism is vital for the Amazon rainforest as up to 50% of the moisture is recycled and transported further up to six times (Eltahir and Bras, 1994; Zemp et al., 2014; Staal et al., 2018, 2020b). Furthermore, it has been projected that major droughts might become more frequent under climate change and occur in nine out of ten years by 2060 (Cox et al., 2008; Duffy et al., 2015). Such a significant increase in drought frequency, especially in the southern part of the Amazon basin, is confirmed by state-of-the-art CMIP6 simulations (Cook et al., 2020; Parsons, 2020).
This might then outpace the adaptive capacity of the rainforest and initiate drought-induced tipping events and cascades. In our work (see Sect. 2.5 [P5]), the potential for tipping cascades is quantified under a whole range of possible future climatic scenarios based on realistic drought patterns from the hydrological years 2004–2014. It is found that the vulnerability increases nonlinearily as soon as a certain threshold in the drought intensity as the control parameter, here measured as Maximum Cumulative Water Deficit (MCWD), is exceeded. This threshold lies between 2.5 to 3.0 standard deviations away from the long term average of the drought conditions meaning that for higher drought indices, the tipped area increases strongly and is up to six times higher than for more modest

drought conditions. At the same time, the frequency of tipping cascades increases significantly and approaches 50% of all tipping events when drought conditions surpass 3.0 standard deviations beyond the long term average. Surprisingly, the reasons why certain tipping events are observed, is distributed unevenly between the mean annual precipitation (MAP) as a first control parameter and the drought intensity as the second control parameter (MCWD index). Over the whole ensemble in our study, MAP induced tipping is rarely observed (less than 0.1%), whereas MCWD induced tipping is responsible for the majority of the tipping events (mean$\pm$s.d.: 76.3$\pm$8.5%). Tipping cascades through atmospheric moisture recycling effects are also important: 23.6$\pm$8.5% of all tipping events are due to cascading effects. Lastly, the region that seems most affected by drought-induced tipping is located in the southeast of the Amazon basin. This is a region that already nowadays suffers from large-scale land-use change such as deforestation ("arc of deforestation"), ranching or agriculture (Davidson et al., 2012; Pereira et al., 2020).

Besides viewing the Amazon rainforest as a network of interacting tipping elements on a local to regional scale, another study researches the tropical rainforest systems after further nonlinear properties by using the state-of-the-art dynamic global vegetation model LPJmL5.1 (see Appendix. 5.3 [AP3]). This is a valuable step into the direction of using more complex Earth system models coupled to dynamic vegetation models since, apart from very few studies using more complex vegetation models (e.g. Oyama and Nobre, 2003; Cox et al., 2004), most tipping point studies in the Amazon rainforest rely on conceptual models (e.g. van Nes et al., 2014; Boers et al., 2017; Zemp et al., 2017).

### 3.2.3 Global Earth system

In the introduction of this thesis (see Sect. 1), it has been noted that some climate tipping elements are at risk of transgressing their critical thresholds if the levels of global warming exceed current values (see Fig. 1.2). To investigate the potential risk for tipping events and tipping cascades, we applied a widely extended version of the software framework PyCascades to a set of interacting climate tipping elements (see Sect. 2.6 and 2.7 [P6, P7]). Overall, a subset of four to five interacting climate tipping elements has been investigated: the Greenland Ice Sheet, the West Antarctic Ice Sheet, the AMOC, the Amazon rainforest and the ENSO. The dynamics of these tipping elements are based on topologically equivalent representations of their main dynamical properties (Kuznetsov, 2013; Staal et al., 2015; Levermann and Winkelmann, 2016; Wood et al., 2019). This might be seen as straightforward for the large cryosphere elements, the AMOC and Amazon rainforest, while such a dynamical behaviour is less clear for the ENSO that would also be better represented by a Hopf bifurcation (Timmermann et al., 2003). For ENSO, it is even debated whether it should be regarded as a tipping element in a strict sense under global warming. Some literature sources state that ENSO effects will occur more frequently under climate change (Cai et al., 2014; Wang et al., 2019), while others highlight their uncertainties as to whether ENSO event will become more frequent or intense under global warming (Collins et al., 2010; Kim et al., 2014). For an in-depth discussion see [P6] (see Sect. 2.6). The interactions between tipping elements have been motivated by an expert elicitation (Kriegler et al., 2009), but they can also be motivated by more complex models, where such existing interactions between these Earth system regions have been observed (e.g. Rahmstorf et al., 2005; Seidov et al., 2005; Swingedouw et al., 2008; Mitrovica et al., 2009; Caesar et al., 2018; Weijer et al., 2019) (see [P6, P7]). Furthermore, all structural uncertainties in the critical temperatures and the interaction strengths are propagated using a large-scale Monte Carlo simulation based on a sophisticated latin-hypercube sampling method to randomise the starting conditions of the parameters such that the space of initial conditions is covered well (Baudin, 2013). For further details on the exact mathematical implementation of the tipping elements and their interactions please be

referred to Sect. 2.6 and 2.7 [P6, P7].

In [P6] (see Sect. 2.6), we find that the reference climate is destabilised with increasing interaction strength for the West Antarctic Ice Sheet, the AMOC and the Amazon rainforest. In detail, this means that the critical temperature ranges are decreased by 10% in the case of the Amazon rainforest, 40% for the West Antarctic Ice Sheet and up to 60% for the AMOC when the interactions are of the same importance as the individual dynamics. Further, the critical temperature increases for the Greenland Ice Sheet is, on average about 100%. But at the same time its standard deviation increases largely, too. This is due to the strong negative feedback loop between Greenland and the AMOC, where freshwater input weakens the AMOC on the one hand and a weaker AMOC cools the northern hemisphere on the other hand. However, this is not sufficient to safeguard the reference climate, a possibility that has been raised earlier (Gaucherel and Moron, 2017). Furthermore, we also reveal the roles of the tipping elements in tipping cascades. While the Greenland Ice Sheet and the West Antarctic Ice Sheet are initiators of tipping cascades, starting 65% and 23% of all cascades respectively, the AMOC is a mediator of cascades starting less than 13% of all cascades. Since the Amazon rainforest has no outgoing links in this reduced network, it can only follow the states of the other tipping elements. However, in case ENSO is included in our analysis and a structural robustness analysis is performed, the main qualitative results remain the same. Therefore, most of the tipping cascades occur at global mean temperature increases between 1–3 °C above pre-industrial levels whether ENSO is taking into account as a tipping element or not. Even though the disintegration of some tipping elements can require several centuries up to millennia as for instance for the large cryosphere elements, this emphasises the importance that temperature thresholds should not be surpassed for an extended period of time.

In a further study [P7] (see Sect. 2.7), we use the concept of basin stability (Menck et al., 2013; Mitra et al., 2017) to determine the stability of all possible different states in terms of the number of tipped elements in a huge-scale Monte Carlo simulation of around 3.6 billion ensemble members. Here, it is found that for high levels of global warming of about 3–4 °C above pre-industrial or higher, only the states with four or five tipped elements have a significant proportion of the basin volume. Therefore, in our model, only the states with a high amount of tipped elements are stable. Furthermore, the basin volume of several intermediate states is investigated, where only a certain number of elements is tipped. This can reveal important intermediary states, where some elements reside in the tipped regime, while others could be seen as normally functioning in the sense that they are not tipped. Investigating such intermediary states, it is observed that states including tipped cryosphere elements on Greenland and West Antarctica have a higher basin volume at considerably lower temperature increases (1–3 °C above pre-industrial) and potentially more realistic low interaction strengths of about 0.2 or smaller[1]. This is an interesting result as it reveals the possibility that on the very long term, states without proper ice sheets on Greenland and West Antarctica could be stable configurations of the Earth's climate tipping elements. These are configurations that might also have existed (partially) during paleoclimatic times such as the Marine Isotope Stages MIS 5e, MIS 11 or the Pliocene (Dutton et al., 2015; Tierney et al., 2020). Lastly, in this study, we also detect the emergence of limit cycles (Hopf-bifurcations) under some rare initial conditions: 0.6% of all ensemble members show oscillations. Especially for intermediate temperature increases between 1–4 °C above pre-industrial such oscillating behaviour can be observed. The principal components that oscillate against each other are

[1] Note that an interaction strength of 1.0 approximately means that the interaction is as important as the individual dynamics of a specific tipping element. Therefore, lower interaction strength on the order of 0.2 could be more realistic since there the individual dynamics of the respective tipping element would still be dominant.

the Greenland Ice Sheet and the AMOC: 86% of all oscillations are between these two elements. The reason is their strong negative feedback loop, where the Greenland Ice Sheet weakens the AMOC via freshwater influx, while a weaker AMOC cools the region around Greenland potentially safeguarding the Greenland Ice Sheet. The existence of such limit cycles remains hypothetical, but in principle there is paleoclimatic evidence of oscillatory behaviour in the Earth's climate system (Crucifix, 2012; Ditlevsen et al., 2020).

## 3.3 Conclusion and answer to the research questions

In this section, an answer to the research questions will conclude the results part of my dissertation. In addition, the results will be classified according to their contributions to the respective field of research.

### Interactions of nonlinear dynamical systems

With the software model PyCascades, a contribution could be made to the field of interacting tipping elements from a complex dynamical systems perspective. The software PyCascades has been developed, which is able to simulate the dynamics of tipping elements on various types of complex networks. The investigated types of networks range from Erdős-Rényi, Barabási-Albert, Watts-Strogatz networks to spatially embedded ones. By applying this software framework to these networks of tipping elements, research question RQ1 could be answered (see Sect. 1.4):

**A1:** The critical interaction strength above which tipping cascades emerge depend on global network parameters such as clustering and spatial organisation. If clustering and spatial organisation are higher, the vulnerability of a network of tipping elements increases. Furthermore, certain important micro-structures (*motifs*) indeed decrease the critical coupling strength that is necessary to initiate a tipping cascade. Therefore, tipping events that occur on a micro level are translated into the macro scale or even into global cascades by the facilitation of tipping cascades through local motifs. Lastly, in the large-system limit, global phase transitions and cooperativity emerge if the connectivity is large enough. This means that a set of different, stochastic tipping elements behaves like one large aggregated tipping element, comparable to tipping on different scales, i.e., different aggregation levels.

### Temperature feedbacks from the cryosphere as quantified by an EMIC

As noted in the Sect. 1.4, feedbacks can play an important role in stabilising the transgressed state of the tipping elements once a state transition has begun. By the means of the EMIC CLIMBER-2, the temperature feedbacks has been studied that a disintegration of cryosphere elements would have on a regional to global scale (RQ2).

**A2:** The temperature feedbacks on a global scale are on the order of half a degree of additional warming. More exactly, the temperature feedback is 0.43 °C (interquartile range: 0.39–0.46 °C). The regional levels of additional warming can exceed 5 °C over Greenland and West Antarctica, and 1.5 °C over the Arctic region if only the Arctic summer sea ice disappears. The disappearance of the Arctic summer sea ice poses a realistic scenario until the mid of the 21st century as shown by CMIP5 and CMIP6 models (Notz et al., 2013; Niederdrenk and Notz, 2018; SIMIP-Community, 2020), while other cryosphere elements such as the large ice sheets take centuries to millennia to disintegrate (Robinson et al., 2012; Winkelmann et al., 2015).

### Interactions of climate tipping elements

Using and extending the developed software framework PyCascades, a response to the research questions on the stability of components of the Earth system against tipping events and cascades has been formulated. In particular, the potential for tipping events and cascades in the Amazon rainforest has been investigated since it can well be represented as a networked system. While the nodes represent local scale tipping elements, parts of the Amazon rainforest are connected via the mechanism of atmospheric moisture recycling. Research question RQ3 for the Amazon rainforest is answered under the assumption that the rainforest is vulnerable to diminished rainfall, more severe drought conditions and under the assumption that it is adapted to past environmental conditions.

**A3:** *Amazon rainforest part:* Tipping events are increasing sharply if future drought conditions surpass 2.5–3 standard deviations of past environmental conditions with respect to the MCWD drought index. On the other side, tipping events are only rarely caused by too less mean annual precipitation. Remarkably, while the overall mean annual precipitation does not seem to be an issue, the regional distribution of precipitation and droughts are. Still, the mean annual precipitation is very important, but the fluctuations of annual rainfall are small compared to the fluctuations in dry season intensity (MCWD) in our data. Therefore, very few tipping events triggered by to less mean annual precipitation are observed. Tipping cascades also have a significant potential to intensify regional rainforest dieback, especially in the southeast of the Amazon rainforest. Depending on the exact drought conditions, the potential for tipping cascades can surpass 50% of all tipping events for severe drought conditions. On average, tipping cascades account for approximately a fourth of all tipping events.

The answer to RQ3 with respect to a set of interacting climate tipping elements is:

**A3:** *Climate tipping elements part:* Tipping events in the Earth system most likely start at a global warming of 1–3 °C above pre-industrial levels. At the same increase of the global mean temperature, uncertainties as to whether tipping elements will experience a critical transition are highest. Beyond these levels of global warming, it is likely that many tipping elements will reside in the tipped state on the long term. Therefore, the committed damage under these scenarios would be large since only the states with many tipped elements are stable. Furthermore, the roles of the tipping elements in cascading tipping events are revealed. While the large ice sheets on Greenland and West Antarctica act as the initiators of cascades and are of special importance for the stability of the climate system, the AMOC is a transmitter of cascades. Overall, tipping cascades are possible even for intermediate global warming levels between 1–2 °C above pre-industrial levels. In our model, 39% of all investigated ensemble members show such tipping cascades, averaged over the entire large-scale ensemble.

Overall, the answers A2 & A3 impact the resilience of the Earth system with respect to nonlinear transitions in the climate system or parts of it.
Lastly, the question remains (see Sect. 3.2, RQ3) as to whether these temperature feedbacks indeed affect the occurrence of tipping events. This question is not answered comprehensively in the current publications comprising my dissertation, but is dealt with in a paper that is in preparation (Donges and Wunderling et al., 2021, in prep.). Therefore, we append a short paragraph to answer this question here without an explanation of the employed model, which has been described in detail in the publications [P6] and [P7] (see Sect. 2.6 and Sect. 2.7). The model of four interacting climate tipping elements (Greenland and West Antarctic Ice Sheet, AMOC and Amazon rainforest) of [P6] and [P7] has been extended with respect to inbuilt temperature feedbacks as they have been quantified in [P4] (see Sect. 2.4) for a global warming scenario of 1.5–2 °C above pre-industrial

levels. Explicitly, we implemented the temperature feedbacks for the Greenland Ice Sheet and the West Antarctic Ice Sheet. On top of that, for the Amazon rainforest, a conservative estimation of the temperature feedback until 2100 has been performed in Steffen et al. (2018). Answering the second part of RQ3, we find that the likelihood for additional tipping events is slightly increased, taking into account the temperature feedbacks of the Greenland Ice Sheet, the West Antarctic Ice Sheet and the Amazon rainforest, compared to the case without these temperature feedbacks (see Fig. 3.1a). In case, temperature feedbacks for the Arctic summer sea ice and the mountain glaciers from [P4] are implemented as well, the difference between a scenario with and without temperature feedbacks is larger (see Fig. 3.1b). However, in both cases, the difference between the two scenarios is insignificant compared to the large associated uncertainties, leading to the conclusion that it will be necessary to deepen the understanding of particular components of the Earth system as well as their interactions and feedbacks. This would help to reduce the uncertainties (see shaded colours in Fig. 3.1) raised by the various unknowns in interaction strengths, interaction directions and critical temperature thresholds.

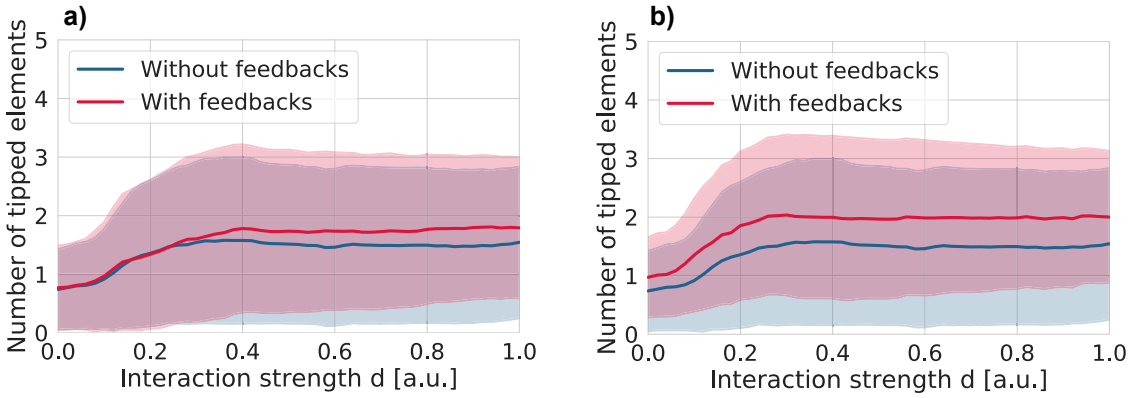


**Figure 3.1:** Number of tipped elements for a scenario of 1.5–2 °C above pre-industrial levels depending on the interaction strength (Donges and Wunderling et al., 2021, in prep.). The same conceptual model with four interacting climate tipping elements as in [P6] has been used, i.e., the Greenland and West Antarctic Ice Sheet, the AMOC and the Amazon rainforest. For further details, see [P6] (Sect. 2.6). A scenario including temperature feedbacks (red) is compared to a scenario without temperature feedbacks (blue) using a Monte Carlo ensemble approach to correctly propagate all uncertainties, equal to the approach used in [P6] and [P7]. **a)** The temperature feedbacks used in this study are taken from [P4] (see Sect. 2.4) for the Greenland Ice Sheet (mean: 0.13 °C; uncertainty range: 0.12-0.14 °C) and the West Antarctic Ice Sheet (mean: 0.05 °C; uncertainty range: 0.04-0.06 °C). The temperature feedback for the Amazon rainforest (mean: 0.05 °C; uncertainty range: 0.03-0.11 °C) has been taken from Steffen et al. (2018). Therefore, in panel **a)** only dynamic feedbacks of simulated dynamics of tipping elements are employed. In panel **b)**, the additional temperature feedbacks from the Arctic summer sea ice (mean: 0.19 °C; uncertainty range: 0.16-0.22 °C) and the mountain glaciers (mean: 0.08 °C; uncertainty range: 0.07-0.09 °C) are also integrated, again taken from [P4].

Overall, my dissertation gave satisfactory answers to the research question posed in Sect. 1.4. Nevertheless, some aspects can be further consolidated with additional experiments or more detailed process-based models. Moreover, several new questions arose from the presented results (see chapter 4).

# Chapter 4

# Discussion & Outlook

*Keep in mind that it is hubris to think that we know how to save the Earth: our planet looks after itself. All we can do is try to save ourselves.*

*James Lovelock*

In my dissertation, I worked on essential compartments of the Earth system that have an inherently nonlinear behaviour, the climate tipping elements. For this purpose, I used two classes of Earth system models, (i) the newly developed conceptual model PyCascades and (ii) the EMIC CLIMBER-2. Both approaches, EMICs and conceptual models, are located on the left hand side of Fig. 1.1, i.e., the model classes that have a higher level of process integration in comparatively fewer equations than typical GCMs.
This brings us back to the bigger picture and the question how my work contributes to Earth system analysis. As mentioned in the introduction, Schellnhuber raised several Hilbertian questions for Earth system science in the 21st century (Schellnhuber et al., 2004, page 9). This dissertation can contribute to the progress on three of these questions:

(HI) What are the major dynamical patterns, teleconnections, and feedback loops in the planetary machinery?

(HII) Is it possible to describe the Earth system as a composition of weakly coupled organs and regions, and to reconstruct the planetary machinery from these parts?

(HIII) What are the principles for constructing 'macroscopes', i.e., representations of the Earth system that aggregate away the details while retaining all systems-order items?

With the study on climate tipping elements, I embedded the available knowledge on critical elements[1] in the Earth system (e.g. Kriegler et al., 2009; Schellnhuber et al., 2016) into a coupled and easily extendable model (see Sects. 2.1–2.3 [P1–P3]). Building on this conceptual model, I revealed important dynamical patterns in terms of the climate change that is necessary to trigger tipping events or cascading transitions for a set of interacting climate tipping elements and the Amazon rainforest (see Sects. 2.5–2.7 [P5–P7]). Further, I determined the temperature feedbacks and fast climate feedbacks from the disintegration of the cryosphere elements (see Sect. 2.4 [P4]).
Taken together, the studies [P4–P7] contribute to the answer of (HI), i.e. to what the vital patterns on the planetary scale are. At the same time, this dissertation aims to be a starting point for the

[1] The question "What are critical elements (thresholds, bottlenecks, switches) in the Earth system?" is actually also a Hilbertian question. I do not try to work out more details on "what" the critical elements are, but I use the knowledge that has already been gained from earlier research.

discussion to (HII). Although the developed model of interacting tipping elements is far from being comprehensive in many ways, it serves as a possible representation of modelling the *(weakly) coupled organs and regions [...] to reconstruct the planetary machinery* (Schellnhuber, 1999, page 9; see also Sects. 2.6 [P6] and 2.7 [P7]). Lastly, (HIII) is not answered directly, but it has in contrast been one of the guiding principles during my dissertation. By the use of complex, but conceptual dynamical systems many details have been *aggregated away*, while the main dynamical properties were kept.

### Limitations & Outlook

Many of the new insights presented in my dissertation rely on results from strongly conceptualised models of tipping elements. While it is possible to represent the main dynamics of interacting tipping elements with such models, the mathematical representation of them remains simplified and neglects their process-detailed physics as of yet. Thus, it would be highly desirable to use fully coupled complex state-of-the-art Earth system models (such as from the CMIP-family or an EMIC) for all the studies, but this notoriously remains an open challenge due to a partially incomplete understanding of some nonlinear properties as well as due to computational constraints (see e.g. Wood et al., 2019). This means that the dynamics of interacting tipping elements are yet difficult to capture in fully complex models. However, for some tipping elements there exist yet simplified, but fully dynamic and process-based (i.e. physics based) models in isolated forms. For instance, these are models for Arctic ice caps (North, 1984; Herald et al., 2013), the Greenland Ice Sheet (Levermann and Winkelmann, 2016), the AMOC (Stommel, 1961; Cessi, 1994; Wood et al., 2019), the Amazon rainforest (Cox, 2001; van Nes et al., 2014; Staal et al., 2015), the ENSO (Zebiak and Cane, 1987; Timmermann et al., 2003) or the Indian summer monsoon (Zickfeld et al., 2005). However, there does not yet exist an interacting model of such conceptual, but process-based tipping elements apart from a coupled model between two tipping elements, the AMOC and ENSO (Dekker et al., 2018).

In my dissertation, I induced critical transitions of the climate tipping elements by keeping the global mean temperature (GMT) increase constant for conditions of 0–8 °C GMT increase above pre-industrial levels. After the GMT value is chosen, the experiment has been run into equilibrium for long simulation times. This excludes the possibility that the critical temperature threshold is surpassed only for some time. But this would open a whole new field of interesting research since it seems likely that humanity will transgress the critical temperature of some of the tipping elements at least for some time. This could especially the case for the cryosphere tipping elements (Schellnhuber et al., 2016). For instance, the critical temperature threshold for the Greenland Ice Sheet might be as low as 0.8 °C above pre-industrial levels (Robinson et al., 2012), while the global warming comparing 1850–1900 with 2006–2015 lies at 0.9 °C (Masson-Delmotte et al., 2018) and the Paris Agreement aims at limiting the warming levels to 1.5-2 °C (Paris Agreement, 2015). Such scenarios, where the critical temperature is surpassed for some amount of time, are called *temperature overshoots*. Further, the rate and persistence of *extreme events* such as heat waves are suspected to increase under climate change, not only over the Greenland Ice Sheet, but also worldwide (Coumou and Rahmstorf, 2012; Coumou et al., 2013; Mann et al., 2018). The effect of both, extreme events (Serdukova et al., 2017; Tesfay et al., 2020) and overshoots (Alkhayuon et al., 2019; Ritchie et al., 2019, 2020), has been investigated in conceptual and isolated climate tipping element models, but to the best of my knowledge not yet to an interacting set of tipping elements. Thus, the study of the stability under such conditions remains an interesting open field for future research in several dimensions, from a theoretical modelling perspective, but also from the climate tipping elements perspective.

Furthermore, it might be of interest to investigate tipping element interactions in more depth since

parts of my studies relied explicitly on an expert elicitation (Kriegler et al., 2009) from the year 2006. Therefore, an update of this expert elicitation could be worthwhile as well as an investigation of the explicit modelling of interactions between tipping elements with EMICs or data based-approaches such as causal effect networks (Runge et al., 2015; Kretschmer et al., 2016). Lastly, a social component could be added to the model of natural tipping elements, creating a model informed from social modelling and climate tipping element aspects, e.g., combining [P6] (see Sect. 2.6) and the study from Wiedermann et al. (2020).

### Final remarks

In the larger context, my dissertation aims at improving the modelling of interacting nonlinear systems and applying those models to matters of topical interest within the realm of tipping elements in the Earth system. Since the knowledge on tipping elements is still fragmentary, further progress in research on tipping elements is clearly desirable. This can be done at the level of complex Earth system models, in data-based research or, as in this thesis, with conceptual and EMIC modelling approaches. All these strands of research contribute to the insights on tipping elements and can therefore make important contributions to a better understanding of some of the most crucial components in the Earth system.

# Chapter 5

# Appendix

*Science never solves a problem without creating ten more.*

*George Bernard Shaw*

In the Appendix, four additional contributions to this thesis are shown as indicated in Sect. 1.4 (see Fig. 5.1). Of these additional four contributions, one is in review, one is submitted and two are in preparation in a close-to-final version.

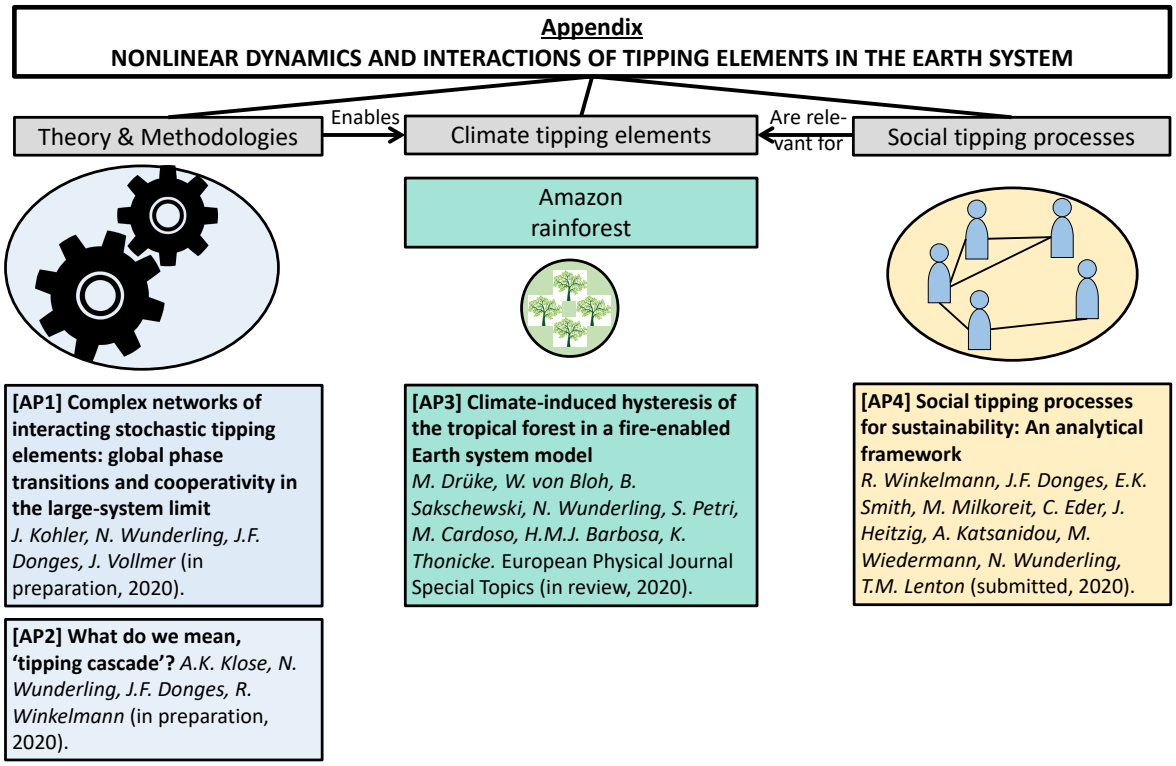


**Figure 5.1:** Overview of the additional contributions in my dissertation, also separated into parts on *Theory & Methodologies*, *Climate tipping elements* and as an outlook on *Social tipping processes*.

# 5.1 Complex networks of interacting stochastic tipping elements: global phase transitions and cooperativity in the large-system limit [AP1]

**Authors**
Jan Kohler, Nico Wunderling, Jonathan F. Donges, Jürgen Vollmer

**Status**
In Preparation

**Short summary**
In this study, the dynamics of conceptualised tipping elements with noise are investigated for the case that the tipping elements are located in the unstable equilibrium at the start of the simulation. It is shown that the network of interacting tipping elements can be boiled down to the behaviour of one aggregated and overarching tipping element. The conditions under which this cooperative behaviour emerges is that the connectivity within the network of tipping elements is sufficiently large. The connectivity is defined as a measure, which is proportional to the number of nodes in the network, the average degree and the likelihood of a connection between two nodes. Then, the remaining differential equation of the aggregated tipping element can be solved analytically and compared to simulations for different network types (Erdős-Rényi, Barabási-Albert, Watts-Strogatz networks). Further, it is found that the connectivity can also explain a random number of initial displacements (i.e. shifts to the tipped state of an arbitrary number of tipping elements) analytically by adding an additional term to the critical parameter. Overall, we conclude that a system of interacting tipping elements, which initially reside at an unstable equilibrium, converge to an initially stable aggregated system.

**Author contributions**
Jan Kohler, Nico Wunderling and Jürgen Vollmer designed the study. Jan Kohler conducted the simulation runs. Nico Wunderling prepared the figures. Jan Kohler drafted the manuscript that was extended by Nico Wunderling and Jürgen Vollmer. All authors discussed the results and further edited this work. This paper is the partially based on the results of the bachelor thesis of Jan Kohler, who was (co-)supervised by Nico Wunderling.

# Complex networks of interacting stochastic tipping elements: global phase transitions and cooperativity in the large-system limit

Jan Kohler,[1, 2, *] Nico Wunderling,[2, 3, 4, †] Jonathan F. Donges,[2, 5] and Jürgen Vollmer[1 ‡]
[1] *Institut für theoretische Physik, University of Leipzig, 04103 Leipzig, Germany, EU*
[2] *Earth System Analysis, Potsdam Institute for Climate Impact Research, Member of the Leibniz Association, 14473 Potsdam, Germany, EU*
[3] *Institute of Physics and Astronomy, University of Potsdam, 14476 Potsdam, Germany, EU*
[4] *Department of Physics, Humboldt University of Berlin, 12489 Berlin, Germany, EU*
[5] *Stockholm Resilience Centre, Stockholm University, 10691 Stockholm, Sweden, EU*

Tipping elements in the Earth System received increased scientific attention over the last years due to their non-linear behavior and the risks of fundamental changes adversely affecting nature and humankind. While being stable over a large range of its parameter space, a tipping element can undergo a drastic shift in its state upon an additional small parameter change when close to its tipping point. Recently, the focus of research shifted towards interactions between tipping elements, in order to explore the effect of tipping events through a network of tipping elements up to potential global tipping cascades. Here, we analyze the dynamics of a network of coupled conceptualized tipping elements with stochasticity and study the response of a system that initially resides in an unstable equilibrium to the perturbation of a single node. We derive an analytic solution for small noise levels using a normalization and mean field approach. With that, we reveal that a system of connected tipping elements can be decoupled and behaves like a single aggregated tipping element in the case of small noise levels. This result is robust for a range of different paradigmatic network types such as Erdös-Rényi, Barabási-Albert and Watts-Strogatz networks. From this approach, we find that the here newly defined measure of the connectivity consisting of the average degree and coupling strength, is a central parameter of the system that determines the time scale of tipping. We demonstrate that shifting the initial position of the tipping elements can be described as an additive term to the critical parameter. Furthermore, in the limit of large connectivity, the behavior of an initially unstable system converges to that of an initially stable system. Thus, this study can contribute to a better understanding of the collective behavior of connected tipping elements across various disciplines which could have implications for tipping elements in climate science, ecology or economy.

## I. INTRODUCTION

Hysteresis is a hallmark of first-order phase transitions. For thermodynamic systems it leads to supercooling and superheating with subsequent explosive phase change. These rapid phase changes are well-understood for common thermodynamic phase transition. However, they still pose challenges for systems with non-standard interaction rules, like Achlioptas Process (da Costa *et al.*, 2010; D'Souza and Mitzenmacher, 2010; D'Souza and Nagler, 2015; Grassberger *et al.*, 2011; Riordan and Warnke, 2011), or topography, like processes on networks, where hysteresis leads to cascading failure (Buldyrev *et al.*, 2010; Motter and Timme, 2018; Watts, 2002). Tipping processes are also prevalent among many ecological systems. It has been shown that the Greenland Ice Sheet (Robinson *et al.*, 2012), shallow lakes (Scheffer, 1989), and the Amazon rainforest can be modelled as a network of tipping elements (Krönke *et al.*, 2020; Wunderling *et al.*, 2020; Zemp *et al.*, 2017). Further applications are in finance, economics and politics (Brummitt *et al.*, 2015).

Current models of climate change are also formulated in terms of networks of interacting tipping elements (Hughes *et al.*, 2013; Lenton *et al.*, 2019; Lenton and Williams, 2013; Rocha *et al.*, 2018; Steffen *et al.*, 2018). The interactions provide long-lived metastable states and rapid cooperative transitions between the states. Often such a stabilization and cooperation in a tipping event is caused by positive feedback effects. A popular example of such an effect in the Earth System is the surface albedo of sea ice. A decrease in the surface area covered with ice due to an increase in global mean temperature decreases the surface albedo which in turn increases the temperature and causes higher rates of melting (Curry *et al.*, 1995). The intereaction between these elements leads to *cascading* behavior when the abrupt state shift of an element causes the tipping of another (Kriegler *et al.*, 2009), thus increasing the risk of possible

* corresponding author: kohler@pik-potsdam.de
† corresponding author: wunderling@pik-potsdam.de
‡ ORCID: 0000-0002-8135-1544

global cascades(Lenton *et al.*, 2019; Lenton and Williams, 2013; Steffen *et al.*, 2018). The resulting rapid nonlinear changes of the climate have been predicted almost 40 years ago (Watson and Lovelock, 1983), and they are currently considered to be one of the greatest risks in the climate debate (Lenton *et al.*, 2019; Schellnhuber, 2009).

The present paper adds to the ongoing research on the dynamic behavior of coupled tipping elements by identifying universal behavior in the tipping of large scale systems. We thus attempt to identify trajectories of large networks when the cascading process has started.

## II. THEORY & METHODS

### A. Model

To model tipping cascades interacting tipping elements are placed in different paradigmatic network types (Erdös-Renyi, Barabasi-Albert, Watts-Strogatz) and are coupled linearly. The system's response to an initial perturbation is studied. These tipping elements are described by a system of differential equations adapted from (Krönke *et al.*, 2020; Wunderling *et al.*, 2020). A Gaussian white noise is applied to the tipping elements to model stochastic fluctuations[1].

Many natural systems show tipping paired with hysteresis-like behavior (Brummitt *et al.*, 2015). The behavior of such a tipping element is commonly modelled by differential equations of the form (Klose *et al.*, 2020; Krönke *et al.*, 2020; Wunderling *et al.*, 2020)

$$\dot{x} = -a(x - x_0)^3 + b(x - x_0) + r \tag{1}$$

with $a \cdot b > 0$, the offset $x_0$ and the critical parameter $r$.

We will show in the following that the dynamics of a tipping element described by Equation (1) is locally topologically equivalent to a saddle-node bifurcation. As a first step, the parameters $a$ and $b$ are subsumed into a rescaled variable $\tilde{x}$ to effectively simplify the system of equations. We divide Equation (1) by the constant parameter $b$, and introduce the new time variable $\tau = bt$. After dividing by $\sqrt{\frac{a}{b}}$ and introducing $\tilde{x} = \sqrt{\frac{a}{b}}x$, the rescaled offset $\tilde{x}_0 = \sqrt{\frac{a}{b}}x_0$ as well as $\tilde{r} = \sqrt{\frac{a}{b^3}}r$ we find

$$\frac{d\tilde{x}}{d\tau} = -(\tilde{x} - \tilde{x}_0)^3 + (\tilde{x} - \tilde{x}_0) + \tilde{r}.$$

As a next step we substitute $\chi = \tilde{x} - \tilde{x}_0$ and rename the variables to $x$, $t$, $r$ yielding a simplified model description

$$\frac{dx}{dt} = -x^3 + x + r. \tag{2}$$

We expect that upon variation of the parameter $r$ one stable and one unstable fixed point will vanish in a saddle-node bifurcation leaving the system with only a single stable fixed point. This can be demonstrated by a Taylor expansion around the extrema at $x = \pm\sqrt{\frac{1}{3}}$.

The expansion around $x = -\sqrt{\frac{1}{3}}$ yields

$$\dot{x} = \big(r - \frac{2}{3\sqrt{3}}\big) + \sqrt{3}\big(x + \frac{1}{\sqrt{3}}\big)^2 + \mathcal{O}(x^3)\,.$$

Upon division by $\sqrt{3}$ this can be written as

$$\frac{d\tilde{x}}{d\tilde{t}} = \tilde{x}^2 + \tilde{r} + \mathcal{O}(\tilde{x}^3)$$

with the rescaled variables and parameters $\tilde{x} = \big(x + \frac{1}{\sqrt{3}}\big)$, $\tilde{t} = \sqrt{3}t$ and $\tilde{r} = \big(\frac{r}{\sqrt{3}} - \frac{2}{9}\big)$.

We can proceed analogously for the expansion around $x = \sqrt{\frac{1}{3}}$. This shows that the dynamics of the system is indeed locally topologically equivalent to a saddle-node bifurcation and upon variation of the parameter $r$, there are two saddle-node bifurcations at different critical values $r^*$ in which two fixed points vanish. The bifurcation diagram of a single node including noise can be seen in Figure 1a.

However, tipping elements are oftentimes not isolated, but interdependent. We model this by interacting tipping elements in paradigmatic network types. For simplification, we restrict ourselves at first to Erdös-Rényi networks. Each node $k$ of the network represents a tipping subsystem and is linearly coupled to another node $l \neq k$ from the network with coupling probability $p$ and coupling strength $d_{kl}$ (see Figure 1b).

Krönke *et al.* (2020) considered the dynamics of $N$ coupled tipping elements $k \in [1, \ldots, N]$ described by

$$\dot{x}_k \equiv \frac{dx_k}{dt} = -a(x_k - x_0)^3 + b(x_k - x_0)r_k + d\sum_{l,l\neq k} a_{kl}x_l,$$

where $d > 0$ denotes a constant coupling strength and $a_{ij}$ are elements of the adjacency matrix. This model is slightly altered here by considering an additive Gaussian white noise to simulate fluctuations in the parameter $r_k$ and allowing $d$ to take different values for different edges, such that

$$\frac{dx_k}{dt} = -a(x_k - x_0)^3 + b(x_k - x_0) + r_k + d_{kl}x_l + \sigma\frac{dW_k}{dt} \tag{3}$$

where $d_{kl} > 0$ are drawn randomly from a uniform distribution over a given interval with probability $p$. Einstein

[1] Note that a Gaussian distribution does not necessarily describe fluctuations of all parameters in the real world nor are real-world fluctuations necessarily uncorrelated.

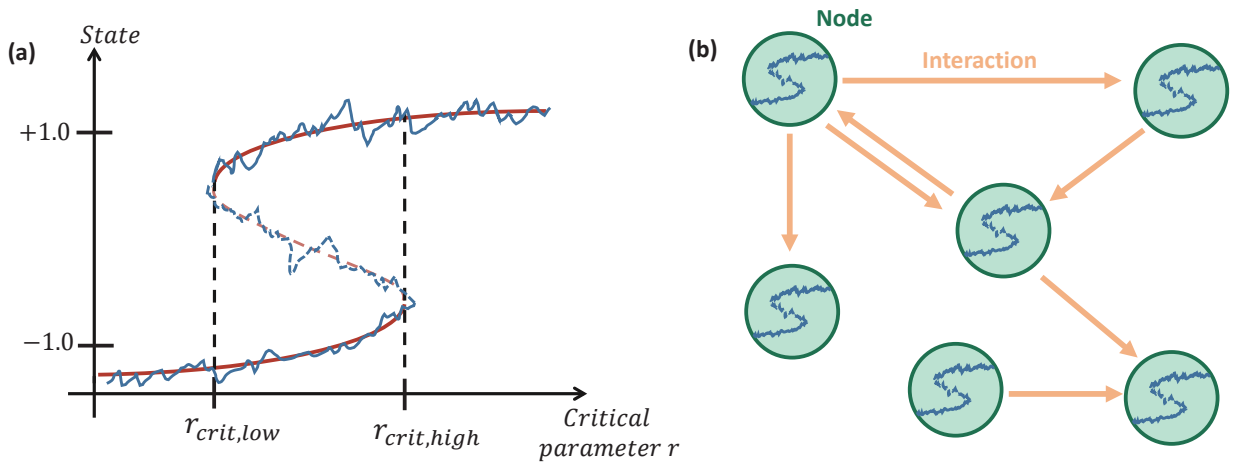


FIG. 1 *Dynamics of the nodes in a network of tipping elements.* **(a)** Bifurcation diagram of Eq. (2) with two stable states between $c_{\text{crit, low}}$ and $c_{\text{crit, high}}$. The red solid line shows the stable states that are connected via a saddle-node bifurcation as soon as the critical parameter $c$ surpasses a certain critical value. The red dashed indicates the unstable equilibrium in between the two stable stated. The trembling blue line displays the stochastic fluctuations around the stable state that we are using here, see Eq. (3). **(b)** Nodes in an exemplary network interacting network of stochastic tipping elements (see Eq. (3)), where each node is of the form that is shown in panel (a).

notation is used here and in the following, i.e. summation over any repeated index variable is implied. We assume spatial homogeneity in this paper meaning that all nodes follow the same dynamics and have the same critical parameter value above which they tip into the other state. Moreover, the parameters are assumed to change slowly compared to the states variables (fast-slow systems) (Kuehn, 2011).

Applying the steps introduced above for an individual tipping element to obtain Equation (2) from Equation (1), it is straightforward to see that the system in Equation (3) can be written as

$$\frac{d\chi_k}{d\tau} = -\chi_k^3 + \chi_k + \tilde{r}_k + \tilde{d}_{kl}(\chi_l + \chi_0) + \tilde{\sigma}\frac{dW_k}{d\tau}$$

where $\chi_k = \sqrt{\frac{a}{b}}(x_k - x_0)$, $\tilde{d}_{kl} = \frac{d_{kl}}{b}$, $\tilde{\sigma} = \sqrt{\frac{a}{b}}\sigma$. Upon renaming all variables and parameters we find the normal form of the system

$$\begin{aligned}\dot{x}_k &= -x_k^3 + x_k + d_{kl}(x_l + x_0) + r_k + \sigma\frac{dW_k}{dt} \\ &:= -x_k^3 + x_k + r_{\text{eff},k} + \sigma\frac{dW_k}{dt}. \end{aligned} \tag{4}$$

Note that the effect of coupling can be understood as an additional term shifting the critical parameter of the system: $r_{\text{eff},k} = r_k + d_{kl}(x_l + x_0)$ . The parameter $r_k$ can be described as an external driving force applied to the elements of the system.

For most parts of this paper we focus on the effects of coupling and therefore will set the critical value $r_k = 0\ \forall k$. In the beginning of the analysis, we will also set $x_0 = 0$ to simplify the calculations before assessing the effect of non-zero $x_0$.

By setting $x_0 = 0$ the position $x = 0$ corresponds to an unstable fixed point. In the simulation runs for this paper all nodes are initially placed at $x = 0$ before one node is perturbed to start a cascade. Therefore, by setting $x_0 = 0$ all nodes are initially at an unstable fixed point. This means that we concentrate on the transient behavior of tipping elements.

The focus of this paper lies on the dynamics of systems while tipping. We therefore study cases where the coupling of the system is strong enough such that all nodes follow the initial displacement of the displaced node.

Setting $x_0 = 0$ and $r_k = 0$, $\forall k$, we can write Equation (4) in vector notation in a simplified way by considering the linear term in the equation as a self-coupling and subsuming it in a modified coupling matrix $D$ with $d_{kk} = 1\ \forall k$, $d_{kl} = 0\ \forall k \neq l$ with probability $1 - p$ and with probability $p$ drawn randomly from a uniform distribution over a given interval, $d_{kl} \in [0, 2d]$, $\forall k \neq l$. Here $d = \langle d_{kl} \rangle$ is the average coupling value and a system parameter.

$$\dot{\vec{x}} = -\vec{x}^3 + D \cdot \vec{x} + \sigma\frac{d\vec{W}}{dt} \tag{5}$$

Krönke *et al.* (2020) developed the python package *PyCascades* to model tipping cascades. We extended

PyCascades for stochastic differential equations (SDEs) based on the package sdeint (Aburn, 2017). This package has been used here to simulate the dynamics of the present model. To this end, a system of coupled tipping elements is modelled by creating a directed network using the python *networkx2.3* package (Hagberg *et al.*, 2008). If not stated otherwise the system has been integrated up to $t = 100$ using a step size of $\Delta t = 0.01$.

## III. RESULTS

### A. Asymptotic Behavior

In this section the behavior of the system described by Equation (5) will be analyzed near its initial and final state. We make the essential assumption that in this region all nodes are in approximately the same state, i.e.,

$$x_i \approx x_j \equiv x \ \forall i,j \text{ if } \begin{cases} x_i \approx 0 \ \forall i \\ x_i \approx 1 \ \forall i \end{cases} . \tag{6}$$

This collectivity assumption yields $\vec{x} = x \begin{pmatrix} 1 \\ \vdots \\ 1 \end{pmatrix} \equiv x\vec{1}$.

Since $D$ is a random matrix with entries of value $d_{kl}$ randomly distributed on the off-diagonals with probability p, we can approximate $D$ for large enough systems as having entries $dp$ on each of its off-diagonal elements, where $d = \langle d_{kl} \rangle$ is the average value of all coupling strengths. We thus replace the specific coupling by an averaged coupling of all nodes to all nodes. This can be interpreted as using a mean-field approach.

We can then rewrite the second term in Equation (5) by splitting $D$ into $D = dp \cdot A + (1 - dp) \cdot I_N$ where $A$ is a matrix with the value 1 on each entry and $I_N$ is the N-dimensional unit matrix. It can easily be seen that $\vec{1}$ is an eigenvector of $A$ with eigenvalue $N$, i.e., $A \cdot \vec{1} = N\vec{1}$. The vector $\vec{1}$ is obviously also an eigenvector to the N-dimensional unit matrix with eigenvalue 1.

$$\begin{aligned} D \cdot \vec{1} &\approx (dpA \cdot \vec{1} + (1 - dp) I_N \cdot \vec{1}) \\ &= \big[Ndp + (1 - dp)\big]\vec{1} = \big[(N - 1)dp + 1\big]\vec{1} \\ &\coloneqq \lambda_d \vec{1} \end{aligned}$$

By using the assumption stated in Equation 6 and assuming a sufficiently large network, the problem has been changed to an eigenvalue problem and the modified coupling matrix can be replaced by its dominant eigenvalue

$$\lambda_d = (N - 1)pd = \langle k \rangle d \tag{7}$$

with $\langle k \rangle = (N - 1)p$ the average degree. This allows the decoupling of the system of differential equations near its asymptotic values. It can be seen easily that $\lambda_d$ describes the average accumulated coupling a node in the network experiences, it is thus a measure of the connectivity of the network. This supports the findings of Wunderling *et al.* (2020) that for systems with high average degree low coupling strengths are already sufficient to initiate a tipping cascade.
The decoupled system can thus be described by

$$\dot{x}_k = -x_k^3 + \lambda_d x_k + \sigma \frac{dW_k}{dt}, \ \forall k. \tag{8}$$

For the moment we consider systems in which the deterministic dynamics dominates over the stochasticity and can therefore approximate the Gaussian white noise to cancel out for large times $\tau$. At large times, the noise-free system is expected to equilibrate, i.e., $\dot{x}_k = 0$, thus

$$0 = -x_{eq}^3 + \lambda_d x_{eq}. \tag{9}$$

We thus find an unstable fixed point at $x^* = 0$ as well as the non-trivial fixed points $x^* = \pm\sqrt{\lambda_d}$. This result can be compared to the solution for a single tipping element with stable equilibria at $x^* = \pm 1$. We see that network size and coupling increase the absolute value of the position of these stable fixed points since $\lambda_d > 1$ for $d > 0$ as considered here. Intuitively, this makes sense when keeping in mind the shape of the bifurcation diagram in Figure 1. Coupling, dependent on average degree and coupling strength, increases the value of the effective parameter $r_{\text{eff}}$ and, following the bifurcation diagram in Figure 1, shifts the position of the stable equilibrium. Simulation runs for different network sizes verify the equilibrium position as can be seen in Figure 2.

We used the asymptotic value obtained in this section to normalize the system. Introducing the dimensionless variables $\tau = \lambda_d t, \ \chi = \frac{x}{\sqrt{\lambda_d}}$, Equation 8 becomes

$$\dot{\chi}_k \coloneqq \frac{d\chi_k}{d\tau} = -\chi_k^3 + \chi_k + \frac{\sigma}{\sqrt{\lambda_d}} \frac{dW_k}{d\tau}. \tag{10}$$

The dimensionless variable $\tau$ is the characteristic time scale of the tipping process. The dependence on $\lambda_d$ shows, in addition to what Eom (2018) has shown with respect to the critical parameter, that an increase in average degree and coupling strength causes a more abrupt tipping in terms of the time scale.

### B. Analytic Solution

In the following an analytic solution for small noise levels $\frac{\sigma}{\sqrt{\lambda_d}} \ll 1$ is developed. In that case the coupled dynamics of the system dominate over the stochastic behavior. We expect that in this deterministic limit the collectivity assumption given by Equation 6 holds not only near the start and final values but for the whole trajectory. The system of equations can then again be decoupled as seen in the previous section and we can find an analytic solution for the whole trajectory.

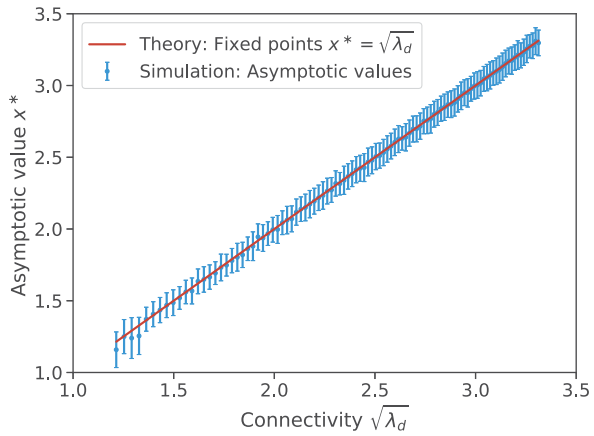


FIG. 2 *Absolute Asymptotic Values vs. Connectivity* $\lambda_d$ Asymptotic values of the mean state of all nodes in an Erdös-Rényi Network of N nodes coupled with $d = 0.1, p = 0.25$ and $\sigma = 0.1$ as a function of $\sqrt{\lambda_d}$. The displayed asymptotic values are the simulated equivalent of the fixed points calculated from Equation 9. $d_{kl}$ are drawn from a uniform distribution $d_{kl} \in [0, 0.2]$. The number of nodes has been varied over $N \in [20, 400]$ yielding the corresponding connectivities $\lambda_d$. Initially, one node has been displaced by $\sqrt{\lambda_d}$ to start the cascade. The error bars represent the standard deviation of the mean values over 50 realizations of $D$ and $\vec{W}$. For small networks and large noise the system occasionally tips into the direction opposite to the perturbation. Hence, we have used the absolute values of the nodes' states.

The deterministic version of Equation 10

$$\dot{\chi}_k = -\chi_k^3 + \chi_k$$

has the solution,

$$\chi_k = \frac{1}{\sqrt{1 + ce^{-2\tau}}} \tag{11}$$

where the constant

$$c = 3e^{2\tau_c} \tag{12}$$

characterizes the critical tipping time $\tau_c$, i.e., the time $\tau = \tau_c$ where $\chi_k = 0.5$.

In the case that coupling dominates the noise, all nodes in all systems can thus be approximately described in the same way shifted by a critical time $\tau_c$.

Figure 3 displays a low-noise tipping system in good agreement with the given theoretical approach in Equation (11). To evaluate the deviation from the theoretical curve the ratio of the simulated and the theoretical data is plotted. As we found in our simulations, there is a good agreement of the mean values for times larger than $\tau \approx 0.5$. This suggests that due to the initial displacement of one node violating the collectivity assumption there is a time shift $\Delta\tau$ needed to organize the system into a collective state. However, upon starting of the cascade at $\tau \approx 0.5$ the system follows the theoretical predictions. The obtained fit parameter $c = 2.6 \cdot 10^4$ is very close to the expected value from Equation (11) for $\tau = 0$ when the time shift $\Delta\tau \approx 0.5$ is considered.
This theoretical behavior holds for different paradigmatic network topologies such as for Barabási-Albert or Watts-Strogatz networks. In this paper, directed Barabási-Albert and Watts-Strogatz networks as they have been adapted and developed in the PyCascades framework are used here(Krönke *et al.*, 2020). Barabási-Albert networks (Barabási and Albert, 1999) are used to model networks with a number of highly-connected elements. In addition to the number of nodes $N$, they are characterized by the parameter $m$ indicating the average degree of the network. The degree distribution decays like a power-law and therefore shows a more pronounced tail than Erdös-Rényi networks. Watts-Strogatz (Watts and Strogatz, 1998) networks show a large clustering coefficient and are therefore used to simulate networks that resemble the small-world phenomenon. Watts-Strogatz networks with $N$ nodes are characterized by the parameters $k$ and $\beta$ indicating the average degree and the rewiring probability, respectively. Therefore, both of these network types have properties making them more realistic in the real world than an Erdös-Rényi network. Tipping behavior on those networks has been analysed more thoroughly by Krönke *et al.* (2020). In Figure 4 the trajectory of different randomly generated networks is displayed against their respective fitted theoretical curve. It can be seen that in addition to Erdös-Rényi networks, trajectories of both Barabási-Albert and Watts-Strogatz networks also follow the expected behavior as derived above. Interestingly, Barabási-Albert networks show a smaller tipping time $\tau_c$, suggesting that the existence of hubs, nodes with a degree greatly exceeding the average, increases the tendency to tip. The ratio of the fitted theoretical curve and the simulated data show a strong consensus of theory and data for all network types (see Figure 4).

Thus, an analytic solution for coupled networks subject to small noise levels has been found that proves its validity for different paradigmatic network types. The collective behavior of the nodes can be decoupled if the connectivity dominates the noise. The collective dynamics can then be described as a single aggregated tipping element, greatly simplifying the problem. This supports the findings of Brummitt *et al.* (2015) that increasing coupling strength entails synchronous behavior of tipping elements for a larger set of initial conditions. In analogy, Hughes *et al.* (2013) have elaborated on how human interactions increase the connectivity of different elements in the Earth System. Consequently, looking at strongly coupled systems is a meaningful and relevant perspective.

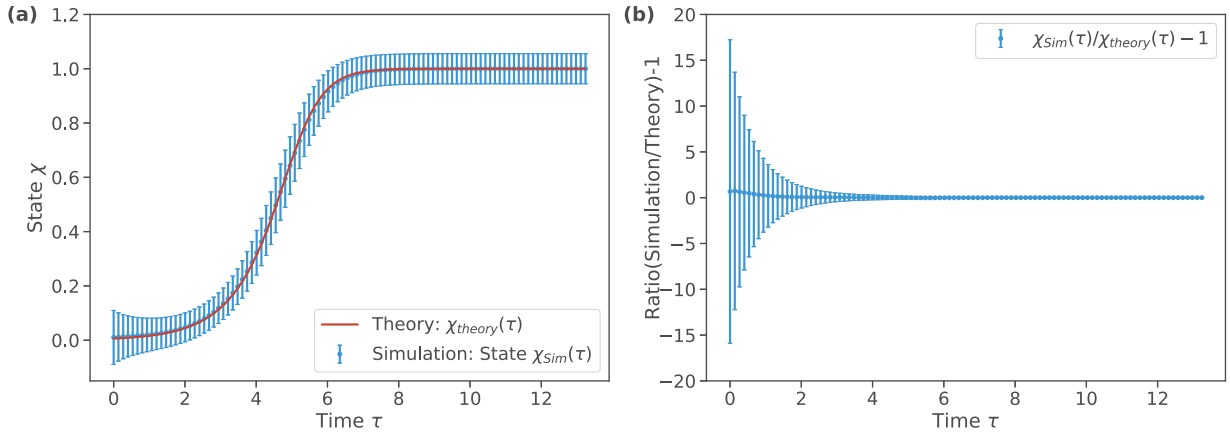


FIG. 3 *Total Fit with Low Noise.* Mean behavior in an Erdös-Rényi Network of 100 nodes coupled with $d = 0.5$, $p = 0.25$ and $\sigma = 0.1$. $d_{kl}$ are drawn from a uniform distribution $d_{kl} \in [0, 1]$. Initially, one node has been displaced by $\chi = 1$ to start the cascade. The error bars represent the standard deviation over all nodes and 50 realizations of $D$ and $\vec{W}$. (a) The theoretical trajectory (red) and the mean trajectory of the nodes (blue) are plotted. The value of $c$ has been obtained as a fit parameter from scipy.curvefit as $c = 2.6 \cdot 10^4$. (b) The ratio of the theoretical and the empirical trajectory is plotted over time $\tau$ using Equation (11). If this ratio gives the value 0, no discrepancy between theory and simulations is obtained.

### C. Influence of Initial Displacement

For the analysis in the previous sections one node has been perturbed and set to $\chi_k = 1$ initially. In this section the effect of the size of the initial displacement relative to the number of nodes $N$ in the network is analyzed.

Assuming that initially $\nu$ nodes are tipped, i.e., displaced to their equilibrium position $\chi_{eq} = 1$, we can find an expression for $c$ and the critical time $\tau_c = \tau(\chi = 0.5)$. Summing over all initial displacements at $\tau = 0$ yields

$$\frac{N}{\sqrt{1+c}} = \nu$$

where $N$ represents the number of nodes in the network. Therefore

$$c = \left(\frac{N}{\nu}\right)^2 - 1. \tag{13}$$

Inserting this into the definition of the critical time $\tau_c$ in Equation (12) yields

$$\tau_c = -\frac{1}{2}\ln\left(\frac{3}{c}\right) = -\frac{1}{2}\ln\left(\frac{3}{\frac{N^2}{\nu^2} - 1}\right) \approx \ln\left(\frac{N}{\nu}\right) - \frac{1}{2}\ln(3)\,.$$

Including the discussed shift of $\tau \approx 0.5$ needed to organize the initial condition into a collective state as has been discussed above, the formula for the tipping time yields

$$\tau_c \approx \ln\left(\frac{N}{\nu}\right) - \frac{1}{2}\ln(3) + 0.5. \tag{14}$$

The effect of the initial displacement on the critical time $\tau_c$ suggests that the initial displacement shifts the trajectory along the $\tau$–axis by $\tau_c$. This suggestion is verified by Figure 5 showing trajectories for different values of $\frac{N}{\nu}$ shifted by the respective critical time $\tau_c$ obtained as a fit parameter from Equation (11). Those trajectories and the critical time follow the theoretical description of Equation (11) and Equation (14) as can be seen in Figure 6.

We have thus found a valid description of the effect of a relative initial displacement $\frac{N}{\nu}$ on the average trajectory of the nodes in the network.

### D. Influence of Shift in the Initial Position

Up to now only the case of $x_0 = 0$ in Equation (4) has been considered as discussed in Section II.A. We will now focus on the influence of finite $x_0$ on the tipping dynamics. This section also contains an analysis of the effect of $x_0$ on the critical point of the system.

To analyze the effect of $x_0$ we consider Equation (4):

$$\dot{x}_k = -x_k^3 + x_k + d_{kl}(x_l + x_0) + r_k + \sigma\frac{dW_k}{dt}.$$

If, like in the previous sections, it is assumed that the system can be decoupled, i.e., the collectivity assumption Equation 6 holds, we can write this as

$$\dot{x}_k = -x_k^3 + \lambda_d x_k + (\lambda_d - 1)x_0 + r_k + \sigma\frac{dW_k}{dt}$$

based on the distributive law of matrix multiplication.

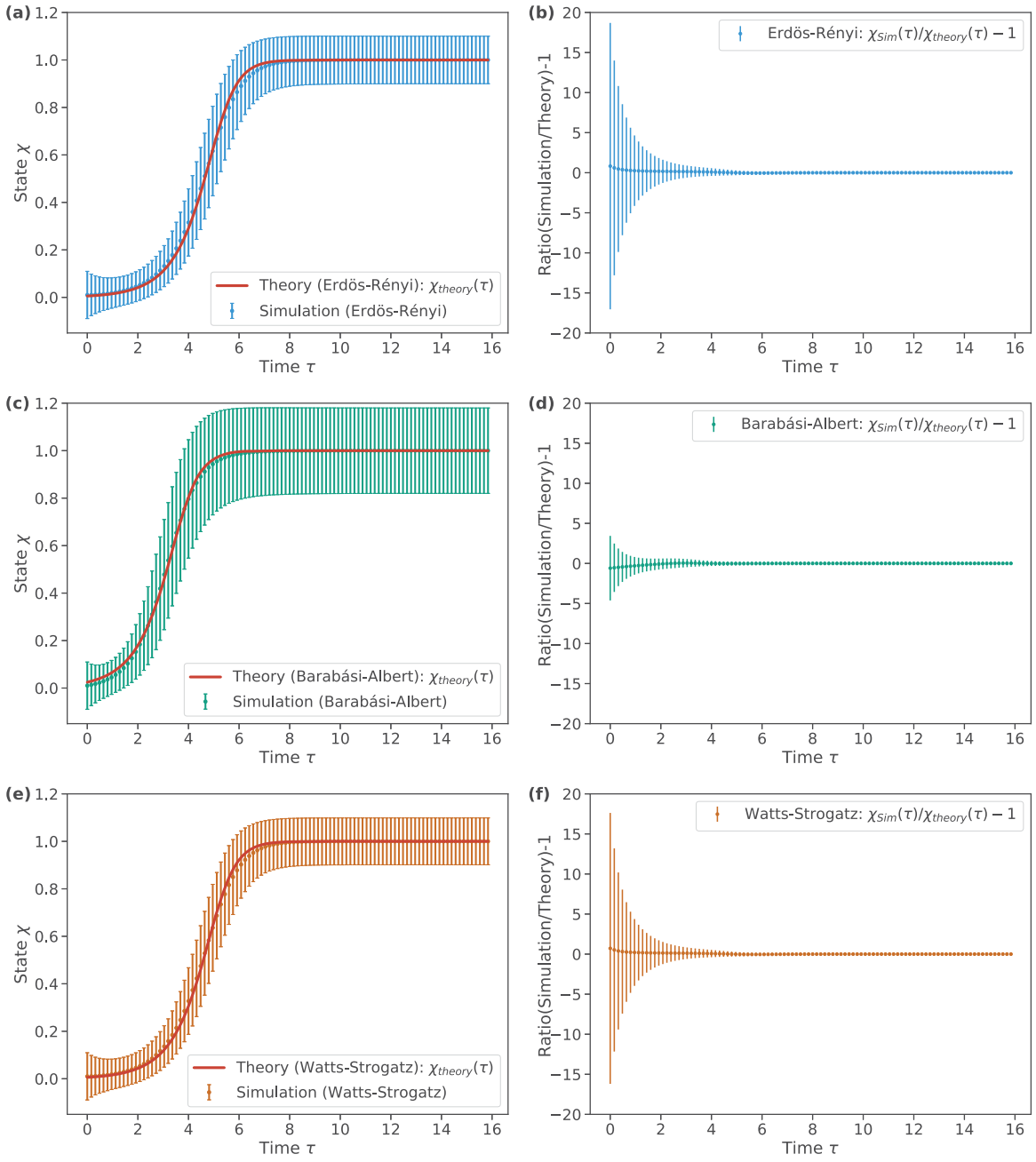


FIG. 4 *Different Network Types.* To obtain the displayed trajectories simulations have been run for 100 nodes in Erdös-Rényi, Barabási-Albert and Watts-Strogatz networks of average degree $\langle k \rangle = 10$. AB and WS networks have been adapted to directed networks using the PyCascades package (Krönke *et al.*, 2020). Parameters: $N = 100$, $\lambda_d = 16$, $d = \frac{\lambda_d - 1}{(N-1)p} \approx 1.5$, $\sigma = 0.1$. The couplings $d_{kl}$ are drawn from a uniform distribution $d_{kl} \in [0, 3]$. AB: $m = 10$. WS: $k = 10$, $\beta = 0.8$. ER: $p = 0.1$. The error bars represent the standard deviation over 50 realizations of $D$ and $\vec{W}$. (a) The theoretical trajectory and the mean trajectory of the nodes are plotted. The value of $c$ has been obtained as a fit parameter from scipy.curvefit as $c_{WS} = 2.9 \cdot 10^4$, $c_{AB} = 1.6 \cdot 10^4$, $c_{ER} = 3.2 \cdot 10^4$. (b) The ratio of the the theoretical and the empirical trajectory is plotted over time $\tau$ using Equation (11). If this ratio gives the value 0, no discrepancy between theory and simulations is obtained.

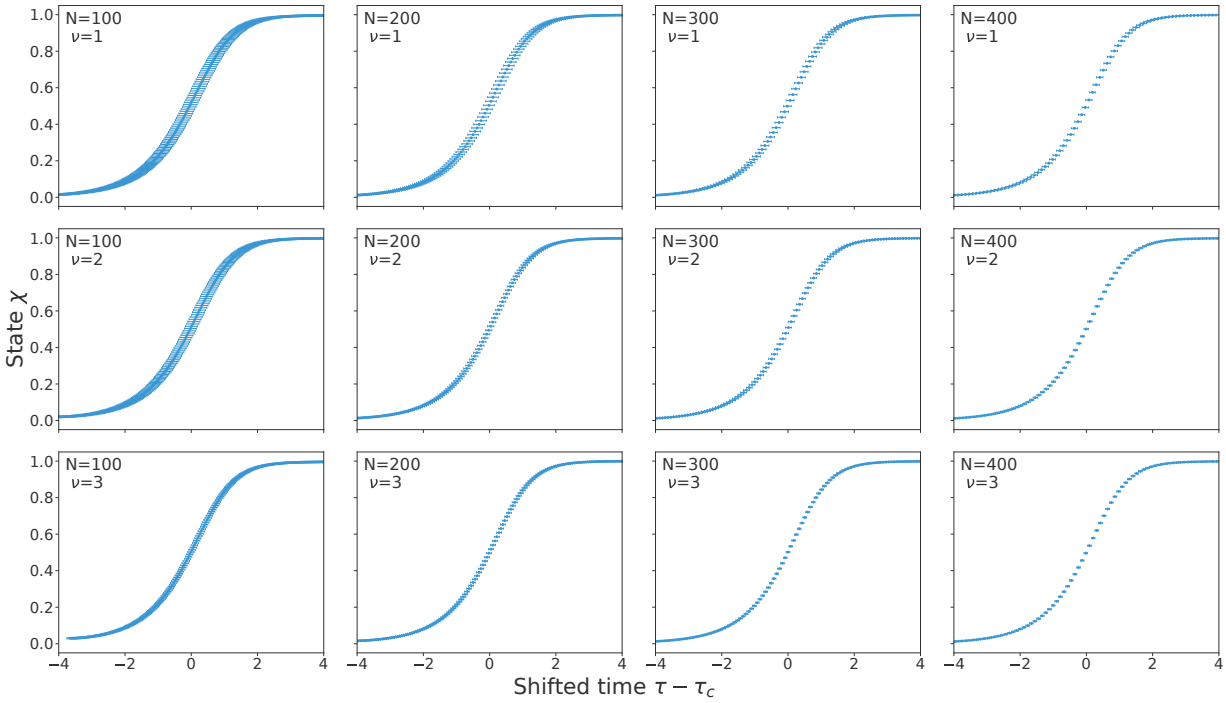


FIG. 5 *Trajectories for Different* $\frac{N}{\nu}$. Calculations have been conducted with $d = 0.1$, $p = 0.25$, $\sigma = 0.1, N \in \{100, 200, 300, 400\}$, $\nu \in \{1, 2, 3\}$. The couplings $d_{kl}$ are drawn from a uniform distribution $d_{kl} \in [0, 0.2]$. The error bars represent the error of $\tau_c$ over 50 realizations of $D$ and $\vec{W}$. Trajectories show different values of the relative initial displacement $\frac{N}{\nu}$ shifted by their respective critical time $\tau_c$ given by Equation (14).

If again, as in Section III.A, the rescaled variables $\chi = \frac{x}{\sqrt{\lambda_d}}$ and $\tau = \lambda_d t$ are introduced, this becomes

$$\frac{d\chi_k}{d\tau} = -\chi_k^3 + \chi_k + \frac{(\lambda_d - 1)}{\lambda_d}\frac{x_0}{\sqrt{\lambda_d}} + \tilde{r}_k + \frac{\sigma}{\sqrt{\lambda_d}}\frac{dW_k}{d\tau} \quad (15)$$

with $\tilde{r}_k = \frac{r_k}{\lambda_d\sqrt{\lambda_d}}$. This $\lambda_d$–dependence in the critical parameter causes a more pronounced bistable regime, i.e. increased global stability, for high connectivities in agreement with the findings of Dunne *et al.* (2002). We will denote this rescaled parameter by $r_k$ in the following. We can see that a finite $x_0$ amounts to a constant shift in the effective parameter $r_{\text{eff}}$ of the differential equation of each node. After the rescaling we introduced in the previous sections the $x_0$-term shows a $\frac{1}{\sqrt{\lambda_d}}$–dependence. For large $\lambda_d$, therefore, this term becomes negligible and the system's behavior can approximately be described as derived above.

This result is interesting, as it implies that for large connectivity $\lambda_d$ the behavior of a system starting with all nodes at a stable equilibrium, i.e., $x_0 = 1$, approaches the behavior of a system starting at the unstable fixed point $x_0 = 0$.

In the previous sections we have seen that the system of coupled tipping elements described by Equation (4) can be decoupled for noises negligible compared to the connectivity of the system. This suggests that from the decoupled description in Equation (15) the critical points of the system should be obtainable by variation of the parameter $r_k$. It can be seen that the general solution for critical points of a bifurcation of the form used here is $r_{\text{crit}} = \pm\sqrt{\frac{4}{27}}$ (cf. Klose *et al.*, 2020). The noise term in Equation 10 can cause the system to cross the critical point even though the critical parameter value $r_{\text{crit}}$ is not yet reached.

Considering non-zero $x_0$ in Equation (4), we can see that in the general case

$$r_{\text{crit}} = \pm\sqrt{\frac{4}{27}} - \frac{\lambda_d - 1}{\sqrt{\lambda_d^3}}x_0. \quad (16)$$

Equation (16) shows that that a non-zero $x_0$ changes the system behavior like an additional term to the effective parameter $r_{\text{eff}}$ of the system. This effect is supported by the fit displayed in Figure 7. The critical points have been obtained for different $x_0$ for systems of tipping elements with $\lambda_d = 16$. The obtained fit clearly shows the expected linear relation and is in good agreement with the expected values.

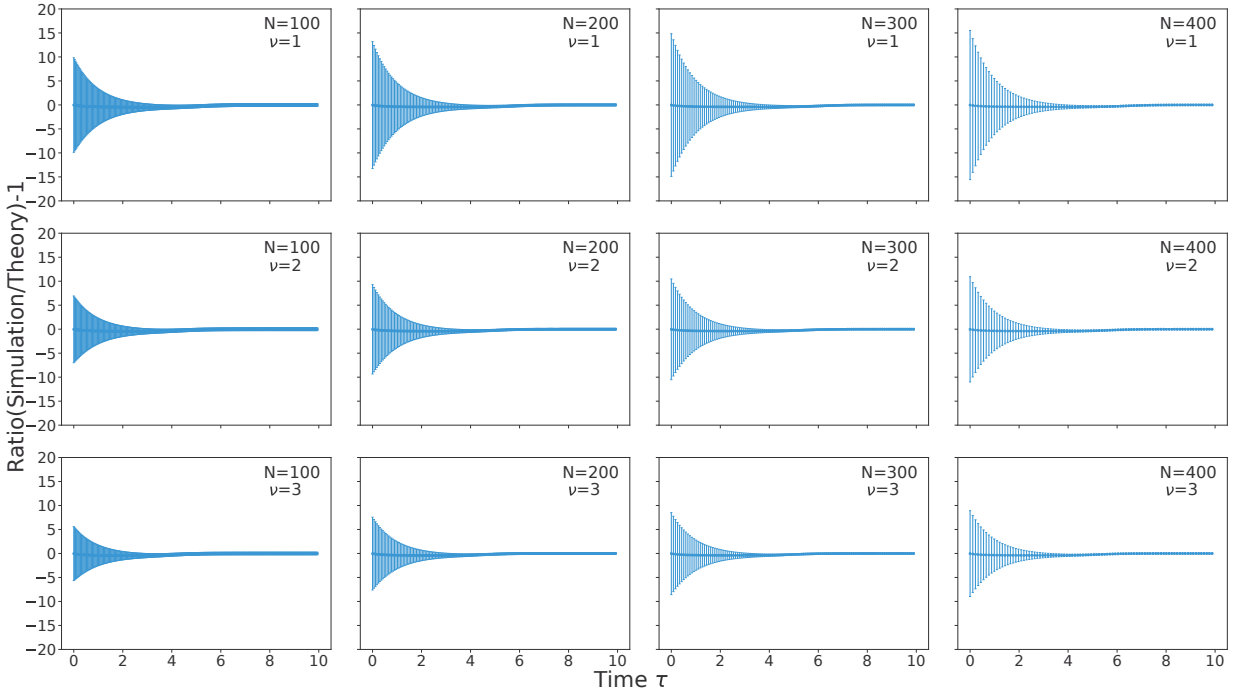


FIG. 6 *Ratio for Different* $\frac{N}{\nu}$. Calculations have been conducted with $d = 0.1$, $p = 0.25$, $\sigma = 0.1, N \in \{100, 200, 300, 400\}$, $\nu \in \{1, 2, 3\}$. The couplings $d_{kl}$ are drawn from a uniform distribution $d_{kl} \in [0, 0.2]$. The ratio of the trajectory of the different systems with respect to the theoretical curve obtained by Equation (11) with $\tau_c$ given by Equation (14) is plotted. If this ratio gives the value 0, no discrepancy between theory and simulations is obtained.

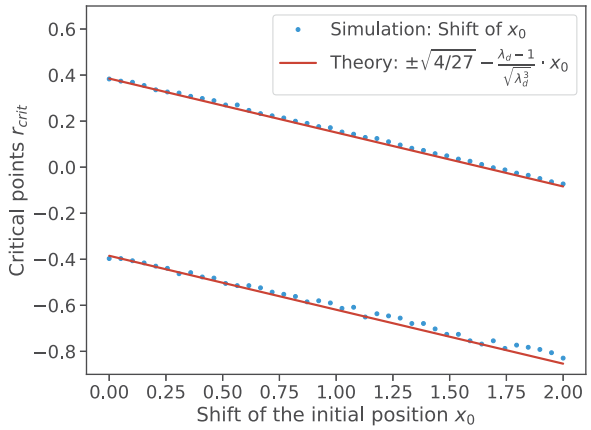


FIG. 7 *Critical Points for Different* $x_0$. Calculations have been conducted with $\lambda_d = 16$, $p = 0.25$, $\sigma = 0.1$, $N = 100$, $d = \frac{\lambda_d - 1}{(N-1)p} \approx 0.6$ and $x_0 \in [0, 2]$ The couplings $d_{kl}$ are drawn from a uniform distribution $d_{kl} \in [0, 1.2]$. The critical points have been obtained from bifurcation diagrams of 50 realizations of $D$ and $\vec{W}$ for each value of $x_0$. The fit values have been obtained using numpy.polyfit in correspondence to Equation (16).

We conclude that the influence of non-zero $x_0$ on the trajectory of the system is negligible for strongly coupled systems. A strongly coupled system initially located at a stable equilibrium reacts like a system located at an unstable equilibrium reacts to a perturbation of one of its nodes. It has also been shown that $x_0$ can be interpreted as an additive term to an effective parameter $r_{\text{eff}}$ of the system and the critical points of a coupled system of tipping points are identical to the critical points of the aggregated tipping element.

## IV. DISCUSSION AND CONCLUSION

In this paper a system of coupled tipping elements has been initially placed at an unstable equilibrium, and the system's response to the perturbation of one tipping element has been studied.

It has been shown that the multidimensional system of coupled tipping elements on a network can be decoupled if the coupling of the nodes dominates over the noise in the system. The trajectory of the tipping elements can then be described using a mean-field approach, thus reducing the number of degrees of freedom to one. The rescaled state coordinate depends on a measure for the connectivity of the system developed in the decoupling

process. This measure of connectivity also determines the characteristic time scale of the tipping process of the system and is therefore of great relevance to cascading behavior on coupled networks.

However, simplifications have to be kept in mind when evaluating the findings of this paper. The influence of global drivers has mostly been ignored in focusing on what Eom (2018) call "internal stress" on the network. This would allow for statements on the effect of coupling on the network dynamics and is based on the assumption that many global drivers change on a larger time scale than the state variables (Brummitt *et al.*, 2015; Kuehn, 2011). Non-stationary parameters can cause a fundamentally different system behavior (cf. Vollmer *et al.*, 2014).

The results of this paper suggest that the inclusion of negative couplings will not qualitatively alter the system behavior as long as the average coupling strength remains positive, contradicting a possibility that was raised earlier in the findings of Gaucherel and Moron (2017) regarding climate tipping elements. Still, nonlinear couplings could change the results and are therefore beyond the scope of this paper.

Nevertheless, the decoupling approach put forward in this work allows an effective analysis of cascading behavior on strongly coupled networks, for which we have provided a comprehensive analytical description that is in excellent agreement with numerical simulations. Hence, the present paper adds to the understanding of cascading behavior by providing a justification to treat coupled systems of tipping elements like one aggregated tipping element.

## ACKNOWLEDGMENTS

N.W. acknowledges support from the the IRTG 1740/TRP 2015/50122-0 funded by DFG and FAPESP. N.W. is grateful for a scholarship from the Studienstiftung des deutschen Volkes. J.F.D. is thankful for support by the Leibniz Association (project DominoES). J.F.D. acknowledges support from the European Research Council project Earth Resilience in the Anthropocene (743080 ERA). The authors gratefully acknowledge the European Regional Development Fund (ERDF), the German Federal Ministry of Education and Research, and the Land Brandenburg for supporting this project by providing resources on the high performance computer system at the Potsdam Institute for Climate Impact Research.

## REFERENCES

Aburn, Matthew J (2017), "sdeint: Numerical integration of stochastic differential equations (SDE), software available under GNU general public license," `https://pypi.org/project/sdeint/`, accessed: 2020-07-18.

Barabási, Albert-László, and Réka Albert (1999), "Emergence of scaling in random networks," Science **286** (5439), 509–512.

Barnosky, Anthony D, Elizabeth A. Hadly, Jordi Bascompte, Eric L. Berlow, James H. Brown, Mikael Fortelius, Wayne M. Getz, John Harte, Alan Hastings, Pablo A Marquet, *et al.* (2012), "Approaching a state shift in earth's biosphere," Nature **486**, 52–58.

Brummitt, Charles D, George Barnett, and Raissa M. D'Souza (2015), "Coupled catastrophes: sudden shifts cascade and hop among interdependent systems," Journal of the Royal Society Interface **12** (112), 20150712.

Buldyrev, Sergey V, Roni Parshani, Gerald Paul, H. Eugene Stanley, and Shlomo Havlin (2010), "Catastrophic cascade of failures in interdependent networks," Nature **464**, 1025–1028.

da Costa, R A, S. N. Dorogovtsev, A. V. Goltsev, and J. F. F. Mendes (2010), "Explosive percolation transition is actually continuous," Phys. Rev. Lett. **105**, 255701.

Curry, Judith A, Julie L. Schramm, and Elizabeth E. Ebert (1995), "Sea ice-albedo climate feedback mechanism," Journal of Climate **8** (2), 240–247.

D'Souza, Raissa M, and Michael Mitzenmacher (2010), "Local cluster aggregation models of explosive percolation," Phys. Rev. Lett. **104**, 195702.

Dunne, Jennifer A, Richard J. Williams, and Neo D. Martinez (2002), "Network structure and biodiversity loss in food webs: robustness increases with connectance," Ecology Letters **5** (4), 558–567.

D'Souza, Raissa M, and Jan Nagler (2015), "Anomalous critical and supercritical phenomena in explosive percolation," Nature Physics **11**, 531–538.

Eom, Young-Ho (2018), "Resilience of networks to environmental stress: From regular to random networks," Physical Review E **97** (4), 042313.

Gaucherel, Cedric, and Vincent Moron (2017), "Potential stabilizing points to mitigate tipping point interactions in earth's climate," International Journal of Climatology **37** (1), 399–408.

Grassberger, Peter, Claire Christensen, Golnoosh Bizhani, Seung-Woo Son, and Maya Paczuski (2011), "Explosive percolation is continuous, but with unusual finite size behavior," Phys. Rev. Lett. **106**, 225701.

Hagberg, Aric, Pieter Swart, and Daniel S Chult (2008), *Exploring network structure, dynamics, and function using NetworkX*, Tech. Rep. (Los Alamos National Lab.(LANL), Los Alamos, NM (United States)).

Hughes, Terry P, Stephen Carpenter, Johan Rockström, Marten Scheffer, and Brian Walker (2013), "Multiscale regime shifts and planetary boundaries," Trends in ecology & evolution **28** (7), 389–395.

Klose, Ann Kristin, Volker Karle, Ricarda Winkelmann, and Jonathan F Donges (2020), "Emergence of cascading dynamics in interacting tipping elements of ecology and climate," Royal Society Open Science **7** (6), 200599.

Kriegler, Elmar, Jim W Hall, Hermann Held, Richard Dawson, and Hans Joachim Schellnhuber (2009), "Imprecise probability assessment of tipping points in the climate system," Proceedings of the national Academy of Sciences **106** (13), 5041–5046.

Krönke, Jonathan, Nico Wunderling, Ricarda Winkelmann, Arie Staal, Benedikt Stumpf, Obbe A. Tuinenburg, and Jonathan F. Donges (2020), "Dynamics of tipping cascades on complex networks," Phys. Rev. E **101**, 042311.

Kuehn, Christian (2011), "A mathematical framework for critical transitions: Bifurcations, fast–slow systems and stochastic dynamics," Physica D: Nonlinear Phenomena **240** (12), 1020–1035.

Lenton, Timothy M, Hermann Held, Elmar Kriegler, Jim W. Hall, Wolfgang Lucht, Stefan Rahmstorf, and Hans J. Schellnhuber (2008), "Tipping elements in the earth's climate system," Proceedings of the national Academy of Sciences **105** (6), 1786–1793.

Lenton, Timothy M, Johan Rockström, Owen Gaffney, Stefan Rahmstorf, Katherine Richardson, Will Steffen, and Hans Joachim Schellnhuber (2019), "Climate tipping points—too risky to bet against," Nature **575**, 592–595.

Lenton, Timothy M, and Hywel T.P. Williams (2013), "On the origin of planetary-scale tipping points," Trends in Ecology & Evolution **28** (7), 380–382.

Motter, Adilson E, and Marc Timme (2018), "Antagonistic phenomena in network dynamics," Annual Review of Condensed Matter Physics **9**, 463–484.

Rahmstorf, Stefan, Michel Crucifix, Andrey Ganopolski, Hugues Goosse, Igor Kamenkovich, Reto Knutti, Gerrit Lohmann, Robert Marsh, Lawrence A Mysak, Zhaomin Wang, *et al.* (2005), "Thermohaline circulation hysteresis: A model intercomparison," Geophysical Research Letters **32** (23).

Riordan, Oliver, and Lutz Warnke (2011), "Explosive percolation is continuous," Science **333** (6040), 322–324.

Robinson, Alexander, Reinhard Calov, and Andrey Ganopolski (2012), "Multistability and critical thresholds of the greenland ice sheet," Nature Climate Change **2** (6), 429–432.

Rocha, Juan C, Garry Peterson, Örjan Bodin, and Simon Levin (2018), "Cascading regime shifts within and across scales," Science **362** (6421), 1379–1383.

Scheffer, Marten (1989), "Alternative stable states in eutrophic, shallow freshwater systems: a minimal model," Hydrobiological Bulletin **23** (1), 73–83.

Schellnhuber, Hans Joachim (2009), "Tipping elements in the earth system," Proceedings of the National Academy of Sciences **106** (49), 20561–20563.

Steffen, Will, Johan Rockström, Katherine Richardson, Timothy M Lenton, Carl Folke, Diana Liverman, Colin P Summerhayes, Anthony D Barnosky, Sarah E Cornell, Michel Crucifix, *et al.* (2018), "Trajectories of the earth system in the anthropocene," Proceedings of the National Academy of Sciences **115** (33), 8252–8259.

Vollmer, Jürgen, Ariane Papke, and Martin Rohloff (2014), "Ripening and focusing of aggregate size distributions with overall volume growth," Frontiers in Physics **2**, 18.

Watson, Andrew J, and James E. Lovelock (1983), "Biological homeostasis of the global environment: the parable of daisyworld," Tellus **35B**, 284–289.

Watts, DJ (2002), "A simple model of global cascades on random networks," Proceedings of the National Academy of Sciences of the United States of America **99** (9), 5766–5771.

Watts, Duncan J, and Steven H. Strogatz (1998), "Collective dynamics of 'small-world' networks," Nature **393** (6684), 440–442.

Wunderling, Nico, Benedikt Stumpf, Jonathan Krönke, Arie Staal, Obbe A Tuinenburg, Ricarda Winkelmann, and Jonathan F Donges (2020), "How motifs condition critical thresholds for tipping cascades in complex networks: Linking micro-to macro-scales," Chaos: An Interdisciplinary Journal of Nonlinear Science **30** (4), 043129.

Zemp, Delphine Clara, Carl-Friedrich Schleussner, Henrique MJ Barbosa, Marina Hirota, Vincent Montade, Gilvan Sampaio, Arie Staal, Lan Wang-Erlandsson, and Anja Rammig (2017), "Self-amplified amazon forest loss due to vegetation-atmosphere feedbacks," Nature communications **8** (1), 1–10.

## 5.2 What do we mean, 'tipping cascade'? [AP2]

**Authors**
Ann Kristin Klose, Nico Wunderling, Ricarda Winkelmann, Jonathan F. Donges

**Status**
In Preparation

**Short summary**
With this manuscript, an ambiguity in the current description of tipping cascades is revealed. Different structural patterns of multiple tipping events are depicted using a system of idealised interacting tipping elements. Three different patterns of multiple tipping with three different dynamic properties in the phase space are distinguished: a two-phase cascade, a domino cascade and a joint cascade. Further, it is found for the following (i.e. influenced) tipping element that early warning signals such as a variance increase and a lag-1 autocorrelation increase is observed for the two phase cascade, but is not observed for the domino cascade. This finding reveals that mitigation and anticipation strategies based on the use of typical early warning signals may not indicate the tipping of the following element and therefore fail.

**Author contributions**
All authors designed this study. Ann Kristin Klose performed the simulations for this work. Nico Wunderling prepared the figures of the main part of the manuscript. Ann Kristin Klose prepared the figures for the supplement. Ann Kristin Klose led the writing of this paper. Nico Wunderling revised the first version of the manuscript. All authors gave input to the manuscript and revised it accordingly.

# What do we mean, 'tipping cascade'?

**Ann Kristin Klose[1,2], Nico Wunderling[1,3,4] and Ricarda Winkelmann[1,3], Jonathan F Donges[1,5]**

[1] Earth System Analysis, Potsdam Institute for Climate Impact, Research (PIK), Member of the Leibniz Association, 14473 Potsdam, Germany
[2] Carl von Ossietzky University Oldenburg, Oldenburg, Germany
[3] Institute of Physics and Astronomy, University of Potsdam, 14476 Potsdam, Germany
[4] Department of Physics, Humboldt University of Berlin, 12489 Berlin, Germany
[5] Stockholm Resilience Centre, Stockholm University, Stockholm, SE-10691, Sweden

E-mail: donges@pik-potsdam.de, akklose@pik-potsdam.de

November 2020

**Abstract.** Based on suggested interactions of possible tipping elements in the climate system, tipping cascades as potential dynamics are increasingly discussed and studied as their activation may take the Earth system into a hothouse climate state and, thereby, would impose a considerable risk on human societies and biosphere integrity. However, there is an ambiguity in the description of tipping cascades within the literature. Here we study a proposed system of idealized interacting tipping elements to illustrate how different patterns of multiple tipping emerge from a very simple coupling of two tipping elements. In particular, we distinguish between a two phase cascade, a domino cascade and a joint cascade. While a mitigation of a two phase cascade may be possible and common early warning indicators show some degree of vulnerability to upcoming critical transitions, the domino cascade may hardly be stopped once initiated and critical slowing down based indicators fail to indicate tipping of the following element. These different possibilities on mitigation and anticipation across the patterns of multiple tipping should be seen as a call to be precise in future discussions on dynamics arising from tipping element interactions in the Earth system.

*Keywords*: tipping cascade, domino effect, tipping interactions, cascading regime shifts

## 1. Introduction

### *1.1. The idea of tipping cascades*

Human-induced impacts on the Earth system increasingly endanger the integrity of the Earth's climate system and some of its most vulnerable components and processes,

the so-called tipping elements [1]. Lately, it has been argued that the risk of potential tipping events or even cascading transitions up to a global cascade is rising under ongoing anthropogenic global warming [2, 3]. While this is the case, there is considerable debate about the nature and description of tipping cascades within the scientific community itself.

The term cascade is used in various fields to describe a certain class of dynamics possibly exhibited by interacting (sub-)systems. It describes the sequential occurrence of similar events (event A is followed by event B), which does not necessarily have to be causal opposed to when event A directly causes event B. The notion of a domino effect is sometimes used synonymously to the term cascade. Examples comprise cascading failures leading to the collapse of power grids as relevant physical infrastructure networks [4, 5, 6, 7, 8]. Such a cascade may occur as an initial failure increasing the likelihood of subsequent failures [4], but it emerge with an initial failure directly leading to the failure of dependent nodes [5].

Similarly, cascading tipping events or regime shifts are increasingly discussed following the rising awareness of a highly interconnected world [9]. Tipping elements possibly undergoing a transition into a qualitatively different state after the crossing of some critical threshold were identified e.g. in ecology and the Earth system [1, 10, 11]. Furthermore, in the Earth system, several interactions between tipping elements were proposed [12, 13, 14, 15, 16, 17]. For example, the Atlantic Meridional Overturning Circulation may slow down due to meltwater originating from the Greenland Ice Sheet [13, 14]. Other examples comprise potential drying over the Amazon rainforest basin, which is influenced by the Atlantic Meridional Overturning Circulation [16] on the one hand and the El–Niño Southern Oscillation on the other hand [17]. Motivated by these and further suggested tipping element interactions, cascading effects arising as potential dynamics are discussed [2, 3, 18, 19, 20, 21, 22] as a mechanism for creating a potential planetary-scale tipping point (of the biosphere) [19, 20, 23, 24]. [3] stated that we may approach a global cascade of tipping points via the progressive activation of tipping point clusters [25] through the increase of the global mean temperature. This could potentially lead to a new, less habitable hothouse climate state [2]. However, it remains unclear whether a cascade-like behavior within the Earth system is promoted by the direction and strength of the existing feedbacks. Recently, first conceptual steps [26, 27] have been undertaken to determine whether the network of Earth system tipping elements is capable to produce global tipping cascades [28, 29]. Using still conceptual, but process-based models, [30] demonstrated a sequence of tipping events in a coupled system of the Atlantic Meridional Overturning Circulation and El–Niño Southern Oscillation. Cost of future climate damages caused by carbon emissions originating from domino effects of interacting tipping elements were studied in an integrated assessment model [31, 32]. Earlier, the propagation of critical transitions in lake chains as an ecological example was analyzed, coupling established models of shallow lakes by a unidirectional stream or diffusion processes [33, 34]. Further examples beyond the biogeophysical Earth system possibly giving rise to the propagation of critical transitions were proposed such as

coupled subsystems in the fields of economics and finance [26].

### *1.2. Descriptions of tipping cascades vary across the literature*

However, tipping cascades or, more generally, patterns of multiple tipping discussed to arise from the interaction of tipping elements are often loosely described suffering a similar fate as its ancestral 'tipping point' concept [35]. We encountered important differences across the definitions of tipping cascades in the recent literature. These differences result in particular from the specification of whether causality is a necessary ingredient for a cascade or not. For example, the event where tipping of one system causes the tipping of another system is called domino dynamics or tipping cascade by [18]. The emergence of such a mechanism for the propagation of regime shifts is underpinned and termed a cascade by [26]. By comparison, the term cascading tipping is used for a sequence of abrupt transitions in [30] that may not necessarily be causal. Furthermore, and not restricted to causal events, an effect of one regime shift on the occurrence of another regime shift is suggested as cascading in [22].

In the following, we relate these varying descriptions of tipping cascades to different patterns of multiple tipping which emerge from the (linear) coupling of two idealized tipping elements (Figure 1). Each tipping element depends on its control parameter (or driver), the variation of which may induce a critical transition from a normal to an alternative state. In addition, the behavior of each tipping element in terms of its state influences the control parameter of a coupled tipping element linearly.

## 2. Patterns of multiple tipping in a model of idealized interacting tipping elements

The patterns of multiple tipping described below and illustrated in Figure 2 originate from different specific pathways through the control parameter space of both tipping elements. During the evolution in the control parameter space, the control parameter $c_2$ of subsystem $X_2$ as *following* tipping element is kept constant at distinct levels (Figure 2, going from top to bottom), while the control parameter $c_1$ of subsystem $X_1$ as *evolving* tipping element is increased (Figure 2, going from left to right) sufficiently slowly such that the system can follow its (moving) equilibrium. In other words, by a separation of the intrinsic system time scale and the time scale of the forcing, the system can be regarded as a fast-slow system [36], where the change in the forcing of the system is slow compared to the intrinsic system time scale.

### *2.1. Two phase cascade (Figure 2A)*

An increase of the control parameter $c_1$ across its threshold and the resulting critical transition of subsystem $X_1$ is not sufficient to trigger a critical transition in subsystem $X_2$. The system converges intermediately to a stable fixed point (as seen in the phase space portraits) and only a further increase of the control parameter $c_1$ can

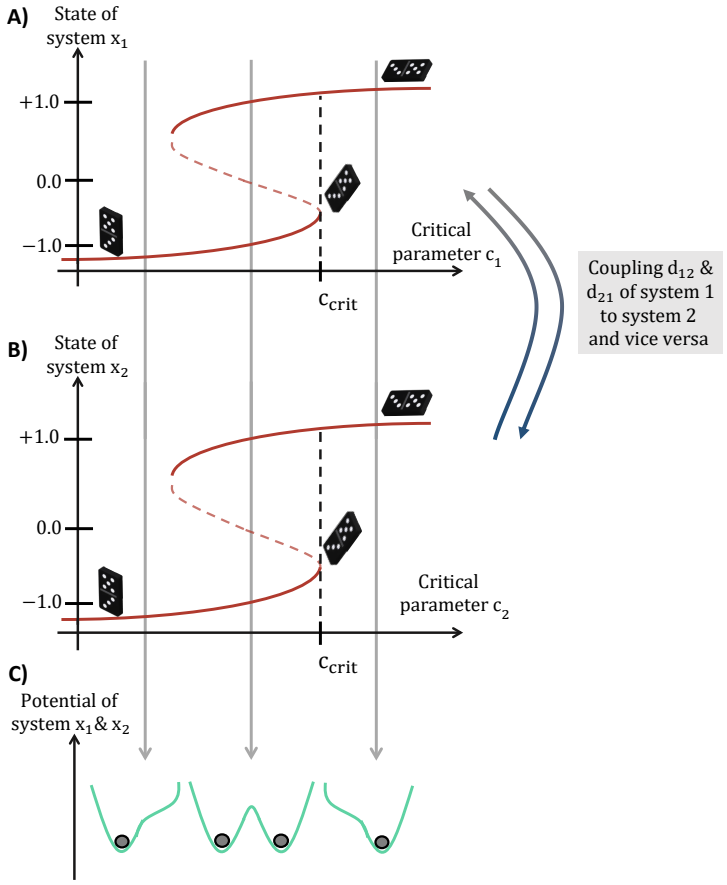


**Figure 1.** A & B: Bifurcation diagram of the idealized tipping elements $X_1$ (A) and $X_2$ (B). The respective differential equation is of the form $\frac{\mathrm{d}x_1}{\mathrm{d}t} = -x_1^3+x_1+c_1+\frac{1}{2}d_{21}(x_2+1)$ for subsystem $X_1$ and $\frac{\mathrm{d}x_2}{\mathrm{d}t} = -x_2^3+x_2+c_2+\frac{1}{2}d_{12}(x_1+1)$ for subsystem $X_2$. Note that for determining the bifurcation diagram of the idealized tipping elements $X_1$ and $X_2$ the coupling term is not taken into account, i.e. the uncoupled case with $d_{21} = 0$ and $d_{12} = 0$ is shown here. Below the critical threshold $c_{i_{\mathrm{crit}}}$, $i = 1, 2$, there exist two stable fixed points. As soon as the control parameter $c_i$ transgresses its critical value $c_{i_{\mathrm{crit}}}$, a fold-bifurcation occurs and the system tips from the lower (normal) state $x^*_{i-}$ to the upper (alternative) state $x^*_{i+}$. C) Sketch of the potential of the two subsystems in case they do not interact shown as a ball–and–cup diagram.

initiate the critical transition in subsystem $X_2$ by the loss of the intermediately occupied stable fixed point. Thus, with a limitation of the increase in the control parameter $c_1$, a full two phase cascade can be mitigated. We can identify the two phase cascade with the cascade described and simulated in [30]. Within the climate system, a stepwise change in the oxygen isotopic ratio at the Eocene-Oligocene transition may be interpreted as a two phase cascade of the Atlantic Meridional Overturning Circulation as the evolving tipping element and the Antarctic Ice Sheet as the following tipping element [30, 37].

An increasingly slower recovery from perturbations and thus an increase in common

statistical indicators such as autocorrelation and variance are observed for subsystem $X_1$ on the approach of the two phase cascade in a *pre–tipping time span* before the critical transition of subsystem $X_1$ (Supplementary Material Figure S1–S3). In contrast, for subsystem $X_2$, an increasingly slower recovery from perturbations as well as increasing autocorrelation and variance can not be detected prior to the critical transition of subsystem $X_1$ in the pre–tipping time span (Supplementary Material, Figure S1–S3). However, given the intermediate convergence to a stable fixed point after the critical transition of subsystem $X_1$ and prior to the critical transition of subsystem $X_2$, an *intermediate time span* offers the possibility to indicate the upcoming critical transition of subsystem $X_2$ in the two phase cascade. A jump to a higher level of the statistical indicators of subsystem $X_2$ compared to the respective level in the pre–tipping time span is observed (Supplementary Material, Figure S2–S3). Accompanied by the determined rotation of the eigenvectors and the change in the eigenvalue magnitude, it becomes apparent that the jump height in the statistical indicators varies with the level of the constant control parameter $c_2$ as a consequence of an increasingly slower recovery from perturbations in the intermediate time span. Apparently, no threshold, i.e. a jump height above which this following tipping occurs, exists but it rather is a continuous and relative quantity. Thus, to use this jump height to clearly indicate an upcoming following transition may be difficult in practice.

*2.2. Domino cascade (Figure 2B)*

In this case, the increase of the control parameter $c_1$ across its threshold and the corresponding critical transition of subsystem $X_1$ towards its alternative state is sufficient to trigger a critical transition of subsystem $X_2$. Note that, in contrast to the two phase cascade, no further increase of the control parameter $c_1$ is necessary to observe the domino cascade, but the tipping of one subsystem (the evolving tipping element) directly causes the tipping of another (the following tipping element). This corresponds to the description of a tipping cascade given in [18] and [26] and the general notion of a domino effect including causality [38]. A notable feature is the expected path of the system in the phase space. Even though the intermediately occupied stable fixed point involved in the two phase cascade is absent, it still influences the dynamics (see phase space, Figure 2B) as a 'ghost' (e.g. [39, 40, 41, 42]). As demonstrated recently in a conceptual model, domino cascades may propagate through tipping elements in the Earth system, for instance between the large ice sheets on Greenland and West Antarctica and the Atlantic Meridional Overturning Circulation [28].

Such a domino cascade may not be preceded clearly by the increase of the common early warning indicators and relying on these indicators may lead to an unexpected following critical transition of the following tipping element. While an increasingly slower recovery from perturbations and thus increasing autocorrelation and variance as common statistical indicators are observed for subsystem $X_1$ on the approach of the domino cascade in the pre–tipping time span (Supplementary Material, Figure S1–S3),

the statistical indicators for subsystem $X_2$ remain constant though on a higher level than for the two phase cascade in the pre–tipping time span (Supplementary Material, Figure S1–S3). However, no clear intermediate time span prior to the critical transition of subsystem $X_2$ exists allowing for an additional detection of early warning signals as for the two phase cascades.

*2.3. Joint cascade (Figure 2C)*

Subsystem $X_1$ and subsystem $X_2$ may tip jointly with a possible trajectory evolving close to the phase space diagonal for an increase of the control parameter $c_1$ across its threshold in contrast to the other two tipping cascade types. The critical transitions of the respective subsystems cannot be distinguished with regard to their order of tipping. Though the case of a joint cascades has not been treated explicitly in the recent literature on interacting tipping elements, a similar behaviour may be observed in spatially extended bistable ecosystems subject to regime shifts as explored by [43, 34].

For both subsystems, a slower recovery from perturbations is expected prior to their joint tipping (Supplementary Material, Figure S1–S2). While for subsystem $X_1$ autocorrelation and variance increase on the approach of the joint cascade, subsystem $X_2$ exhibits a relatively high constant level of these statistical indicators prior to the joint cascade indicating the vulnerability of subsystem $X_2$ (Supplementary Material, Figure S3).

## 3. Discussion

Studying a system of idealized interacting tipping elements [26, 27], different patterns of multiple tipping were identified as a two phase cascade, a domino cascade and a joint cascade.

The various patterns of multiple tipping originating from a model of idealized interacting tipping elements are related to different, though simplified and specific pathways through the control parameter space. In the end, the control parameter evolution determines the emergence of the specific system behavior which may be a domino cascade, a two phase cascade or a joint cascade. The control parameter evolution, i.e., the evolution of the forcing, can therefore determine the architecture of multiple tipping that is observed. Of course, other factors such as the strength and the sign of coupling are as well decisive for the emergence of tipping cascades. Moreover, in more complex systems, control parameters can not be treated separately for each tipping element and drivers may be shared [22].

The different patterns of multiple tipping may have implications for the mitigation of tipping by controlling their respective drivers. A limitation of the forcing can prevent the two phase cascade since a critical transition is not sufficient for the spread of a tipping event to a following subsystem. Instead, the critical transition needs to be followed by a further evolution of the respective subsystem's state before a following

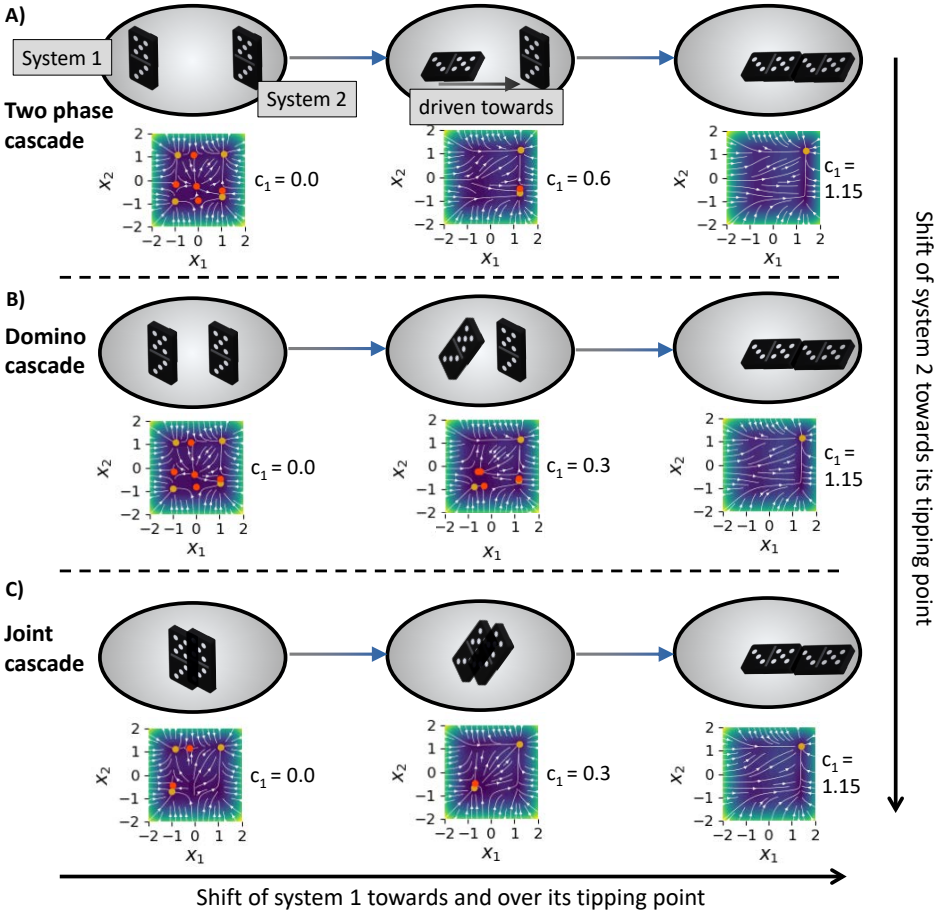


**Figure 2.** Three different types of tipping cascades depicted as three different situations. From left to right, the critical parameter $c_1$ of subsystem $X_1$ is driven closer to and over its tipping point (compare to Figure 1). From top to bottom, the critical parameter $c_2$ of subsystem $X_2$ is also driven closer to, but not across, its tipping point. In this setting, three different patterns of multiple tipping or cascades can occur. A) Two phase cascade: the first subsystem $X_1$ tips, is then shifted closer towards subsystem $X_2$ by an increase of the control parameter $c_1$. Then subsystem $X_2$ tips as well. B) Domino cascade: The subsystems $X_1$ and $X_2$ are closer together than in the two phase cascade such that a tipping of subsystem $X_1$ (middle panel) is sufficient to trigger a critical transition in subsystem $X_2$. C) Joint cascade: The two subsystems are very close to each other such that the beginning of a tipping event in subsystem $X_1$ immediately causes the tipping of the second subsystem $X_2$ and the tipping events cannot be distinguished. The respective stable fixed point attractors and phase diagrams are shown below the domino sketches. Orange dots represent stable fixed points, while unstable fixed points are given by red dots. The white arrows show the trajectories in between. The background colour indicates the normalized speed $v = \sqrt{\dot{x}_1^2 + \dot{x}_2^2}/v_{max}$ going from close to zero (purple) to fast (yellow–green).

critical transition is initiated. However, in a domino cascade an initial critical transition of the evolving tipping element is sufficient to trigger a slightly delayed but inevitable following critical transition.

In addition, the potential success of anticipating the emergence of tipping cascades through early warning indicators based on critical slowing down [44, 45, 46] was assessed and demonstrated to differ across the patterns of multiple tipping. Using insights of [47] and [48] on critical slowing down in multi–component systems in relation to the eigenvector orientation, it is shown how critical slowing down and common statistical indicators for the anticipation of critical transitions may emerge from the rotation of eigenvectors and the change in the eigenvalues' magnitude (see Supplementary Material). Thereby, the analysis of statistical properties of the two phase cascade in [30] is expanded. We found that these common statistical indicators based on critical slowing down may fail for upcoming domino cascades in a system of idealized interacting tipping elements. While increasing autocorrelation and variance are observed for the evolving tipping element on the approach of the domino cascade, constant levels of these statistical indicators were determined for the following tipping element. In the case of a two phase cascade or a joint cascade, the critical slowing down based indicators indicate some degree of vulnerability (or resilience) in the system of interacting tipping elements. However, their application may be unfeasible in practice. In particular, for the two phase cascade, the critical transition of the evolving tipping elements is preceded by increasing autocorrelation and variance of the respective subsystem, while a jump towards a higher level of the statistical indicators in the intermediate time span is found for the following tipping element. The joint cascade may be conceivable with a raised but constant level of autocorrelation and variance for the following tipping element accompanied by an increase of statistical indicators for the evolving tipping element. With the slower recovery from perturbations for both tipping elements, correlations between the subsystems' time series comparable to the application of spatial early warning signals [49, 43, 50, 51, 52] may unfold.

As the very specific and simple scenarios of the control parameter evolution demonstrate that an increase of autocorrelation and variance prior to multiple tipping events cannot necessarily be expected, these common early warning indicators should not be relied on as the only way of anticipating critical transitions in systems of interacting tipping elements. Additionally taking into account often referenced limitations, false alarms and false positives in the application of critical slowing down based indicators to individual tipping elements and their critical transitions [53, 54, 55], it seems to be necessary to invoke a combination of process–based modelling accompanied by monitoring the system under investigation resulting in predictions as well as data–driven techniques [54, 55, 56] to detect upcoming multiple transitions and, in particular, the domino cascade.

Note that the presented discussion is restricted to bifurcation-induced tipping, is purely deterministic and a sufficiently slow change of the tipping element driver is assumed. Hence, our examination of tipping cascades excludes noise or rate–induced

effects which will further influence the presented patterns of multiple tipping. In a related stochastic system, similar patterns were demonstrated as fast and slow domino effects [57]. The patterns of multiple tipping are expected to change in response to a fast change of the tipping element driver which cannot be ruled out given the current unprecedented anthropogenic forcing of the biogeophysical Earth system [58, 59]. In addition, superimposed rate-induced transitions may occur [60, 61] as observed for the Atlantic Meridional Overturning Circulation [62, 63], predator–prey systems [64, 65, 66] and in the form of the compost–bomb instability [61, 67]. Heterogeneity across the response of tipping elements to the same control parameter level [24] was neglected but may influence the overall tipping behaviour of the coupled system [68].

Finally, it is assumed that the long–term behaviour of many real–world systems in terms of the system's state such as the overturning strength of the Atlantic Meridional Overturning Circulation [69, 70], the ice volume of the Greenland Ice Sheet [71] and the algae density in shallow lakes [72, 73] can be qualitatively captured by the studied idealized tipping elements featuring a fold bifurcation as tipping mechanism. However, biogeophysical and biogeochemical processes involved in the behaviour of these real–world systems and included in some more complex climate models may either give rise to further types of cascading tipping or may dampen the overall tipping behavior.

## 4. Conclusion

Different patterns of multiple tipping have been identified in this work. These multiple tipping patterns may emerge as illustrated in a system of idealized interacting tipping elements and include the cases of joint cascades, domino cascades and two phase cascades. As described in [18] and [26] as well as corresponding to the general notion of a domino effect [38], tipping of one subsystem causes or triggers the tipping of another subsystem in a domino cascade. In addition, we find a two phase cascade corresponding to the tipping pattern presented in [30]. While we reveal that it may be possible to find critical slowing down based early warning indicators for the two phase cascade, such indicators can fail in the case of a domino cascade.

However, our results are limited by the conceptual nature of the systems investigated here. In particular, it remains uncertain whether more complex and process–detailed models of tipping elements might smear out the respective nonlinear properties due to processes such as noise, interactions to other system components or further biogeophysical processes that are not modelled here.

Since literature descriptions of cascading tipping dynamics have been ambiguous in the past and the presented patterns of multiple tipping differ in their possibilities of mitigation and anticipation, we propose to be precise in future discussions on potential dynamics arising from the interaction of tipping elements and, in particular, on tipping cascades. In the future, a quantitative assessment of interacting tipping elements with an ongoing improvement of their representation in complex (climate) models e.g. by including interactive evolving ice sheets into Earth system models as well as

the additional use of paleoclimate data [74] may help to reduce uncertainties on the emergence of tipping cascades and possible early warning indicators based on process-understanding. To the end, this may contribute to reflections on the boundaries of the safe-operating space for humanity, also in terms of the Earth system resilience in general.

## References


[1] Lenton T M, Held H, Kriegler E, Hall J W, Lucht W, Rahmstorf S and Schellnhuber H J 2008 *Proceedings of the National Academy of Sciences* **105** 1786–1793

[2] Steffen W, Rockström J, Richardson K, Lenton T M, Folke C, Liverman D, Summerhayes C P, Barnosky A D, Cornell S E, Crucifix M, Donges J F, Fetzer I, Lade S J, Scheffer M, Winkelmann R and Schellnhuber H J 2018 *Proceedings of the National Academy of Sciences* **115** 8252–8259

[3] Lenton T M, Rockström J, Gaffney O, Rahmstorf S, Richardson K, Steffen W and Schellnhuber H J 2019 *Nature* **575** 592–595

[4] Watts D J 2002 *Proceedings of the National Academy of Sciences* **99** 5766–5771

[5] Buldyrev S, Parshani R, Paul G, Staley H and Havlin S 2010 *Nature Letters* **464** 1025–1028

[6] Gao J, Buldyrev S, Havlin S and Stanley H 2011 *Physical Review Letter* **107** 195701

[7] Gao J, Buldyrev S, Stabley H and Havlin S 2012 *Nature Physics* **8** 40–48

[8] Hu Y, Ksherim B, Cohen R and Havlin S 2011 *Physical Review E* **84** 066116

[9] Helbing D 2013 *Nature* **497** 51–59

[10] Scheffer M and Carpenter S R 2003 *Trends in Ecology & Evolution* **18** 648–656

[11] Scheffer M, Carpenter S, Foley J A, Folke C and Walker B 2001 *Nature* **413** 591–596

[12] Kriegler E, Hall J W, Held H, Dawson R and Schellnhuber H J 2009 *Proceedings of the National Academy of Sciences* **106** 5041–5046

[13] Caesar L, Rahmstorf S, Robinson A, Feulner G and Saba V 2018 *Nature* **556** 191–196

[14] Rahmstorf S, Box J E, Feulner G, Mann M E, Robinson A, Rutherford S and Schaffernicht E J 2015 *Nature Climate Change* **5** 475–480

[15] Swingedouw D, Fichefet T, Huybrechts P, Goosse H, Driesschaert E and Loutre M F 2008 *Geophysical Research Letters* **35** L17705

[16] Parsons L, Yin J, Overpeck J, Stouffer R and Malyshev S 2019 *Geophysical Research Letters* **41** 146–151

[17] Duque-Villegas M, Salazar J F and Rendón A M 2019 *Earth System Dynamics* **10** 631—-650

[18] Lenton T M 2020 *Philosophical Transactions of the Royal Society B: Biological Sciences* **375** 20190123

[19] Lenton T M and Williams H T P 2013 *Trends in Ecology & Evolution* **28** 380–382

[20] Hughes T P, Carpenter S, Rockström J, Scheffer M and Walker B 2013 *Trends in Ecology & Evolution* **28** 389–395

[21] Rocha J C, Peterson G D and Biggs R 2015 *PloS One* **10** e0134639

[22] Rocha J C, Peterson G, Bodin Ö and Levin S 2018 *Science* **362** 1379–1383

[23] Barnosky A D, Hadly E A, Bascompte J, Berlow E L, Brown J H, Fortelius M, Getz W M, Harte J, Hastings A, Marquet P A, Martinez N D, Mooers A, Roopnarine P, Vermeij G, Williams J W, Gillespie R, Kitzes J, Marshall C, Matzke N, Mindell D P, Revilla E and Smith A B 2012 *Nature* **486** 52–58

[24] Brook B W, Ellis E C, Perring M P, Mackay A W and Blomqvist L 2013 *Trends in Ecology & Evolution* **28** 396–401

[25] Schellnhuber H J, Rahmstorf S and Winkelmann R 2016 *Nature Climate Change* **6** 649–653

[26] Brummitt C D, Barnett G and D'Souza R M 2015 *Journal of The Royal Society Interface* **12** 20150712

[27] Abraham R, Keith A, Koebbe M and Mayer-Kress G 1991 *International Journal of Bifurcation and Chaos* **1** 417–430

[28] Wunderling N, Donges J F, Kurths J and Winkelmann R 2020 *Earth System Dynamics Discussions* 1–21

[29] Gaucherel C and Moron V 2017 *International Journal of Climatology* **37** 399–408

[30] Dekker M M, Heydt A S and Dijkstra H A 2018 *Earth System Dynamics* **9** 1243–1260

[31] Lemoine D and Traeger C P 2016 *Nature Climate Change* **6** 514–519

[32] Cai Y, Lenton T M and Lontzek T S 2016 *Nature Climate Change* **6** 520–525

[33] Hilt S, Köhler J, Kozerski H P, Van Nes E and Scheffer M 2011 *Oikos* **120** 766–775

[34] van Nes E and Scheffer M 2005 *Ecology* **86** 1797–1807

[35] van Nes E H, Arani B M S, Staal A, van der Bolt B, Flores B M, Bathiany S and Scheffer M 2016 *Trends in Ecology & Evolution* **31** 902–904

[36] Kuehn C 2011 *Physica D: Nonlinear Phenomena* **240** 1020–1035

[37] Tigchelaar M, von der Heydt A S and Dijkstra H A 2011 *Climate of the Past* **7** 235—-247

[38] Hornby A S 2015 *Oxford advanced learner's dictionary of current English* ninth ed (Oxford: Oxford University Press)

[39] Strogatz S H and Westervelt R M 1989 *Physical Review B* **40** 10501

[40] Sardanyés J and Solé R V 2006 *International Journal of Bifurcation and Chaos* **16** 2761–2765

[41] Sardanyés J 2009 *Chaos, Solitons & Fractals* **39** 92–100

[42] Duarte J, Januário C, Martins N and Sardanyés J 2012 *Nonlinear Analysis: Real World Applications* **13** 1647–1661

[43] Dakos V, van Nes E H, Donangelo R, Fort H and Scheffer M 2010 *Theoretical Ecology* **3** 163–174

[44] Wissel C 1984 *Oecologia* **65** 101–107

[45] Scheffer M 2009 *Critical transitions in nature and society* (Princeton / Oxford: Princeton University Press)

[46] Lenton T M 2011 *Nature Climate Change* **1** 201–209

[47] Boerlijst M C, Oudman T and de Roos A M 2013 *PloS One* **8** e62033

[48] Dakos V 2018 *Ecological Indicators* **94** 494–502

[49] Dakos V, Kéfi S, Rietkerk M, Van Nes E H and Scheffer M 2011 *The American Naturalist* **177** E153–E166

[50] Donangelo R, Fort H, Dakos V, Scheffer M and Van Nes E H 2010 *International Journal of Bifurcation and Chaos* **20** 315–321

[51] Guttal V and Jayaprakash C 2009 *Theoretical Ecology* **2** 3–12

[52] Kéfi S, Guttal V, Brock W A, Carpenter S R, Ellison A M, Livina V N, Seekell D A, Scheffer M, van Nes E H and Dakos V 2014 *PloS One* **9** e92097

[53] Boettiger C, Ross N and Hastings A 2013 *Theoretical Ecology* **6** 255–264

[54] Dakos V, Carpenter S R, van Nes E H and Scheffer M 2015 *Philosophical Transactions of the Royal Society B: Biological Sciences* **370** 20130263

[55] Ditlevsen P D and Johnsen S J 2010 *Geophysical Research Letters* **37** L19703

[56] Dakos V, Carpenter S R, Brock W A, Ellison A M, Guttal V, Ives A R, Kéfi S, Livina V, Seekell D A, van Nes E H and Scheffer M 2012 *PloS One* **7** e41010

[57] Ashwin P, Creaser J and Tsaneva-Atanasova K 2017 *Physical Review E* **96** 052309

[58] Joos F and Spahni R 2008 *Proceedings of the National Academy of Sciences* **105** 1425–1430

[59] Zeebe R E, Ridgwell A and Zachos J C 2015 *Nature Geoscience* **9** 325–329

[60] Ashwin P, Wieczorek S, Vitolo R and Cox P 2012 *Philosophical Transactions of the Royal Society A: Mathematical, Physical and Engineering Sciences* **370** 1166–1184

[61] Wieczorek S, Ashwin P, Luke C M and Cox P M 2011 *Proceedings of the Royal Society A: Mathematical, Physical and Engineering Sciences* **467** 1243–1269

[62] Alkhayuon H, Ashwin P, Jackson L C, Quinn C and Wood R A 2019 *Proceedings of the A: Mathematical, Physical and Engineering Sciences* **475** 20190051

[63] Stocker T F and Schmittner A 1997 *Nature* **388** 862–865

[64] O'Keeffe P E and Wieczorek S 2019 Tipping Phenomena and Points of No Return in Ecosystems: Beyond Classical Bifurcations arXiv:1902.01796
[65] Scheffer M, Van Nes E H, Holmgren M and Hughes T 2008 *Ecosystems* **11** 226–237
[66] Siteur K, Eppinga M B, Doelman A, Siero E and Rietkerk M 2016 *Oikos* **125** 1689–1699
[67] Luke C M and Cox P M 2011 *European Journal of Soil Science* **62** 5–12
[68] Scheffer M, Carpenter S R, Lenton T M, Bascompte J, Brock W, Dakos V, van de Koppel J, van de Leemput I A, Levin S A, van Nes E H, Pascual M and Vandermeer J 2012 *Science* **338** 344–348
[69] Stommel H 1961 *Tellus* **13** 224–230
[70] Cessi P 1994 *Journal of Physical oOeanography* **24** 1911–1920
[71] Levermann A and Winkelmann R 2016 *The Cryosphere* **10** 1799–1807
[72] Scheffer M 1989 *Hydrobiological Bulletin* **23** 73–83
[73] Scheffer M, Hosper S H, Meijer M L, Moss B and Jeppesen E 1993 *Trends in Ecology & Evolution* **8** 275–279
[74] Thomas Z A, Jones R T, Turney C S M, Golledge N, Fogwill C, Bradshaw C J A, Menviel L, McKay N P, Bird M, Palmer J, Kershaw P, Wilmshurst J and Muscheler R 2020 *Quaternary Science Reviews* **233** 106222

**Acknowledgments**

This work has been performed in the context of the FutureLab on EarthResilience in the Anthropocene at the Potsdam Institute for Climate Impact Research. N.W. acknowledges support from the IRTG 1740/TRP 2015/50122-0 funded by DFG and FAPESP. N.W. is grateful for a scholarship from the Studienstiftung des Deutschen Volkes. J.F.D. is grateful for financial support by the Stordalen Foundation via the Planetary Boundary Research Network (PB.net), the Earth League's Earth Doc program, and the European Research Council Advanced Grant project ERA (Earth Resilience in the Anthropocene). R.W. acknowledges support by the European Union's Horizon 2020 research and innovation programme under grant agreement no. 820575 (TiPACCs). We are thankful for support by the Leibniz Association project DominoES. Furthermore, we are thankful to xx for discussions on this project.

# What do we mean, 'tipping cascade'? Supplementary Material

**Ann Kristin Klose[1,2], Nico Wunderling[1,3,4] and Ricarda Winkelmann[1,3], Jonathan F Donges[1,5]**

[1] Earth System Analysis, Potsdam Institute for Climate Impact, Research (PIK), Member of the Leibniz Association, 14473 Potsdam, Germany
[2] Carl von Ossietzky University Oldenburg, Oldenburg, Germany
[3] Institute of Physics and Astronomy, University of Potsdam, 14476 Potsdam, Germany
[4] Department of Physics, Humboldt University of Berlin, 12489 Berlin, Germany
[5] Stockholm Resilience Centre, Stockholm University, Stockholm, SE-10691, Sweden

E-mail: donges@pik-potsdam.de, akklose@pik-potsdam.de

November 2020

## 1. Methods

The assessment of possible early warning of critical transitions in a system of interacting tipping elements is based on the model of idealized interacting tipping elements. For simplicity, the analysis is restricted to the simple case of two interacting tipping element ($n = 2$) as given by:

$$x_1(t) = a_1 x_1(t) - b_1 x_1^3(t) + c_1 + \frac{1}{2} d_{21}(x_2(t) + 1) \tag{1}$$

$$x_2(t) = a_2 x_2(t) - b_2 x_2^3(t) + c_2 + \frac{1}{2} d_{12}(x_1(t) + 1) \tag{2}$$

We focus on small coupling strength where the respective coupling terms are kept smaller compared to the intrinsic tipping element's dynamic.

We derive insights on critical slowing down in the above system of interacting tipping elements by the assessment of eigenvectors and eigenvalues based on the main conclusion of [1] and [2]: It was found that critical slowing down occurs in the direction of the eigenvector corresponding to the dominant eigenvalue. The system component closest to the dominant eigenvector exhibits the slowest exponential recovery rate compared to the other components.

The eigenvalues for the system of two interacting idealized tipping element arise from the Jacobian $J$ of the system which is given as

$$J = (a_1 - 3b_1 x_1^2, \frac{1}{2} d_{21}; \frac{1}{2} d_{12}, a_2 - 3b_2 x_2^2) \tag{3}$$

where $a_i, b_i = 1$, $i = 1, 2$ in the following. We analyse the orientation of the eigenvectors $v_i$, $i = 1, 2$ and the magnitude of the corresponding eigenvalues $\lambda_i$, $i = 1, 2$

for the stable fixed point ($x^*_{1-}$, $x^*_{2-}$) at the boundary of its stability area in Section 2. The stability area of the stable fixed point ($x^*_{1-}$, $x^*_{2-}$) is the area in the control parameter space ($c_1$,$c_2$), where this fixed point ($x^*_{1-}$, $x^*_{2-}$) exists and is denoted as $A_{(x^*_{1-},x^*_{2-})}$ in the following. Thereby, we aim to obtain a first indication for critical slowing down immediately prior to leaving its stability area $A_{(x^*_{1-},x^*_{2-})}$. In addition, in Section 3 we assess the eigenvector rotation for the fixed point ($x^*_{1-}$, $x^*_{2-}$) during the evolution in the control parameter space as the system approaches the stability area boundary and the corresponding change in the eigenvalue magnitude. Corresponding to the different patterns of multiple tipping, a simplified scenario of the control parameter evolution is used with an (infinitely) slow increase of the control parameter $c_1$ of subsystem $X_1$ from $c_100$ while keeping the control parameter $c_2$ of subsystem $X_2$ constant ($c_2$ = const.). The eigenvector rotation and the change in the magnitude of the eigenvalues are in addition determined for the stable fixed point ($x^*_{1+}$, $x^*_{2-}$) which is involved in the two phase cascade (compare Figure 2A in main manuscript).

The eigenvector orientation is quantified by the angle $\alpha_i$ between the positive $x_1$–axis and the upper part of the eigenvector $v_i$, $i = 1, 2$ after a shift of the fixed point to the origin. The angle $\alpha_i$ then varies in the range [0°, 180°], where for $\alpha_i = 0°$ and $\alpha_i = 180°$ the eigenvector points to the positive and direction of the $x_1$—axis, respectively. With $\alpha_i = 90°$ the eigenvector points to the direction of the $x_2$-–axis.

Finally, to relate the insights on critical slowing down gained by the assessment of the eigenvectors and eigenvalues to the statistical properties of the different multiple tipping patterns, we estimate autocorrelation and variance as prominent statistical indicators from time series generated by the simulation of the system of interacting tipping elements in Section 4. In the simulations the system approaches the boundary of the stability area $A_{(x^*_{1-},x^*_{2-})}$ and evolves further by a slow linear increase of the control parameter $c_1$ of subsystem $X_1$ from $c_1 = 0$ with the ramping rate $r_{c_1} = 0.01$ while keeping the control parameter $c_2$ of subsystem $X_2$ constant ($c_2$ = const.). Different levels of the control parameter $c_2$ = const. resembling certain patterns of (multiple) tipping are chosen. An ensemble of 100 members is simulated for each pattern of multiple tipping with a time step $\Delta t = 0.1$.

The time spans which include the tipping processes of one or both subsystems are disregarded. As a consequence, statistical indicators are determined for the pre—tipping time span before the tipping of subsystem $X_1$ (and $X_2$ for the domino cascades and a joint tipping of the subsystems $X_1$ and $X_2$) and, in the case of the two phase cascades, for the intermediate time span between the tipping of subsystem $X_1$ and the tipping of subsystem $X_2$. A Gaussian filter with fixed standard deviation is applied to the resulting separated time series which is chosen such that the long–term trend is removed while overfitting is avoided [3, 4]. Autocorrelation and variance are determined in a sliding window approach within a window of a length of half the size of the data set [5, 3]. For the resulting time series of the statistical indicators, Kendall's $\tau$ coefficient is calculated to quantify the increase of the early warning indicators [5]. Although not carried out here, a sensitivity analysis varying the standard deviation of the Gaussian filter and the

length of the sliding window should follow to test the robustness of the results to these data processing parameters of the time series [5] as performed by [3, 4] Boulton et al. (2014) and Thomas et al. (2015).

## 2. Eigenvector orientation at stability area boundary

Different patterns of multiple tipping arise by leaving the stability area $A_{(x^*_{1-},x^*_{2-})}$. Proceeding along the stability area boundary results in a change of the eigenvalue magnitude (Figure S1(a) and (b)) and the eigenvector direction (Figure S1(c)) for the stable fixed point ($x^*_{1-}$, $x^*_{2-}$). In other words, the eigenvalue magnitude and the eigenvector orientation prior to the emergence of (multiple) tipping vary depending on the position along the stability area boundary.

For lower parts of the stability area boundary with low levels of the control parameter $c_2$, the dominant eigenvector $v_2$ with $\lambda_2$ close to zero is mainly orientated in $x_1$–direction with $\alpha_2 \approx 0°$ (Figure S1(c)). Subsystem $X_1$ is much closer to the dominant eigenvector than subsystem $X_2$. Is is therefore expected to show the relatively slower recovery rate for perturbations in the direction of this dominant eigenvector $v_2$ than subsystem $X_2$ prior to leaving the stability area $A_{(x^*_{1-},x^*_{2-})}$. The other eigenvector $v_1$ with $\lambda_1 \approx -2$ is mainly orientated in $x_2$—-direction with $\alpha_1 \approx 90°$ (Figure S1(c)).

Proceeding upwards along the boundary of the stability area $A_{(x^*_{1-},x^*_{2-})}$ with increasing level of the control parameter $c_2$, the dominant eigenvector $v_2$ shows minor changes in its orientation with a slight increase in $\alpha_2$ (Figure S1(c), case A and B corresponding to two phase cascade and domino cascade). Subsystem $X_1$ remains closer to the dominant eigenvector $v_2$. It is therefore expected to show a relatively slower recovery rate to perturbations in the direction of the eigenvector $v_2$ than subsystem $X_2$ prior to leaving the stability area $A_{(x^*_{1-},x^*_{2-})}$. The other eigenvector $v_1$ shows minor changes in its orientation with a slight increase in $\alpha_1$ while the corresponding eigenvalue $\lambda_1$ increases slightly towards zero (Figure S1(c), case A and B corresponding to two phase cascade and domino cascade).

For both the two phase cascade (corresponding to the previously presented case A) and the domino cascade (corresponding to the previously presented case B) a slower recovery from perturbations in subsystem $X_2$ cannot be expected prior to the tipping of subsystem $X_1$. However, given that the system intermediately converges to the stable fixed point ($x^*_{1+}$, $x^*_{2-}$) in the two phase cascade (corresponding to case A) after leaving the stability area $A_{(x^*_{1-},x^*_{2-})}$ and the corresponding loss of the stable fixed point ($x^*_{1-}$, $x^*_{2-}$) (compare Figure 2A in main manuscript), eigenvalues and eigenvectors for this stable fixed point may indicate critical slowing down. These are explored in the following Section 3. On the contrary, for the domino cascade (corresponding to case B) and regions of the stability area boundary towards a joint tipping of both subsystems, a possible dead zone (Figure S1(c), case B until case C is reached in terms of the control parameter $c_2$) for the anticipation of tipping cascades is identified. Note that there is no stable fixed point that the system may intermediately occupy in the domino cascade

(compare Figure 2B in main manuscript).

Reaching the upper parts of the stability area boundary with an elevated level of the control parameter $c_2$, the orientation of the dominant eigenvector $v_2$ changes within a small range of the control parameter $c_2$ until $\alpha_2 \approx 45°$ at the upper corner of the stability area $A_{(x^*_{1-},x^*_{2-})}$ is reached (Figure S1(c), going to case C corresponding to joint cascade). Subsystem $X_1$ and $X_2$ get equally close to the dominant eigenvector $v_2$. A similar recovery rate in subsystem $X_1$ and $X_2$ is therefore expected for perturbations in the direction of the dominant eigenvector $v_2$ prior to leaving the stability area $A_{(x^*_{1-},x^*_{2-})}$. The orientation of the other eigenvector $v_1$ shows major changes within a small range of the control parameter $c_2$ until $\alpha = 135°$ is reached at the upper corner of the stability area $A_{(x^*_{1-},x^*_{2-})}$. In addition, the corresponding eigenvalue $\lambda_1$ increases until zero is almost reached (Figure S1(c)).

Based on the expected slow recovery rates for both subsystems $X_1$ and $X_2$ the anticipation of the critical transitions of both subsystems in the joint cascade (corresponding to the previously presented case B) may be possible.

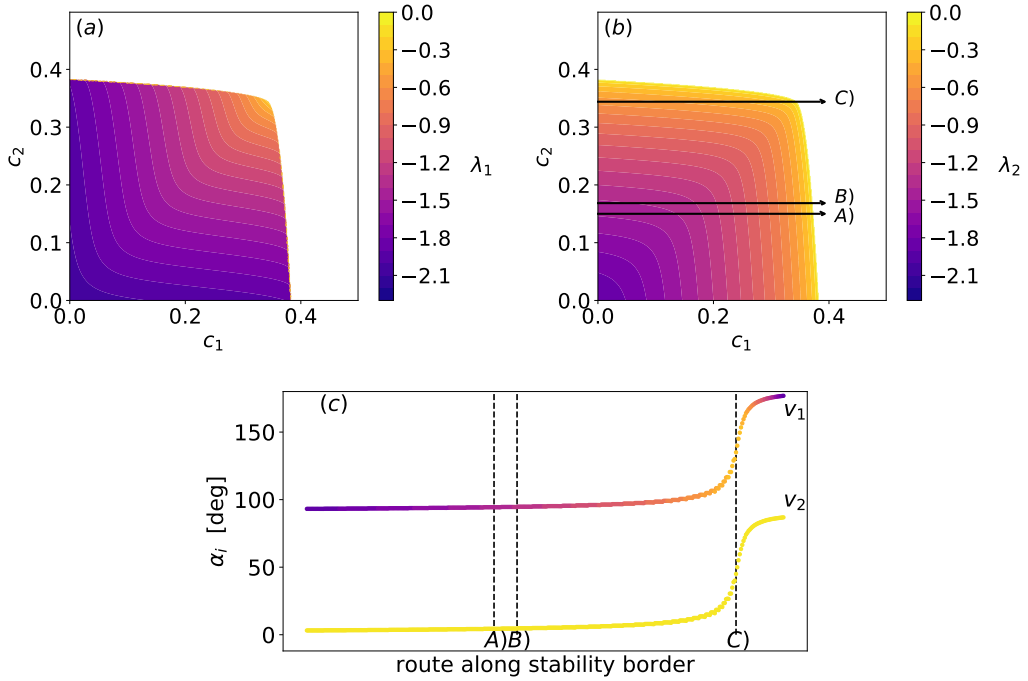


**Figure 1.** Eigenvalues and eigenvectors of the fixed point $(x^*_{1-}, x^*_{2-})$ for two bidirectionally coupled tipping elements given by 2 with $d_{21} = 0.2 > 0$ and $d_{12} = 0.2 > 0$. (a) & (b): Eigenvalues $\lambda_1$ (a) and $\lambda_2$ (b) for the fixed point $(x^*_{1-}, x^*_{2-})$ depending on the control parameters $c_1$ and $c_2$. (c): Angle $\alpha_i$, $i = 1, 2$ giving the direction of the corresponding eigenvectors $v_i$ with $i = 1, 2$ for the fixed point $(x^*_{1-}, x^*_{2-})$ when moving along the boundary of the stability area $A_{(x^*_{1-},x^*_{2-})}$. The colouring represents the magnitude of the corresponding eigenvalue $\lambda_i$, $i = 1, 2$.

**3. Eigenvector rotation and statistical indicators during evolution in the control parameter space**

For a full assessment of the development of critical slowing down and the corresponding evolution of statistical indicators during an approach of the boundary of the stability area $A_{(x^*_{1-},x^*_{2-})}$ it is not sufficient to consider the magnitude of the eigenvalue and the direction of the corresponding (dominant) eigenvector at the point of leaving the stability area $A_{(x^*_{1-},x^*_{2-})}$. The change in the eigenvalue magnitude and the rotation of the corresponding eigenvector along the path in the control parameter space need to be analysed.

The eigenvector rotation of the stable fixed point $(x^*_{1-}, x^*_{2-})$ during the evolution in the control parameter space with $c_2 = \text{const.}$ and an increasing control parameter $c_1$ from $c_1 = 0$ towards the boundary of the stability area $A_{(x^*_{1-},x^*_{2-})}$ follows a general pattern, which can be separated into two distinct phases I and II (Figure S2, left panel). The relative length of the phases depends on the level of the control parameter $c_2 = \text{const.}$ Note that at the lower and upper bounds of the stability area $A_{(x^*_{1-},x^*_{2-})}$, e.g. for $c_2 = 0.344$ (Figure S2C, left panel) only one of the phases can be observed.

In the beginning of phase I, the dominant eigenvector $v_2$ is predominantly orientated in $x_2$–direction. The exact eigenvector orientation quantified by $\alpha_2$ varies with the level of the control parameter $c_2 = \text{const.}$ (Figure S2, left panel, comparing A to C). With increasing control parameter $c_1$, the dominant eigenvector $v_2$ rotates towards $\alpha_2 \approx 45°$. The corresponding eigenvalue $\lambda_2$ increases slightly towards zero but shows only minor changes overall (Figure S2, left panel). Hence, starting from an orientation where the dominant eigenvector is closer to subsystem $X_2$, subsystem $X_1$ and $X_2$ get more equally close to the dominant eigenvector $v_2$ with increasing control parameter $c_1$. In the beginning of phase I, subsystem $X_2$ is thus expected to show a relatively slower recovery from perturbations in the direction of the dominant eigenvector $v_2$ determined by the eigenvalue magnitude. To the end of phase I, a similar recovery in subsystems $X_1$ and $X_2$ is expected from perturbations in the direction of the dominant eigenvector $v_2$ based on the eigenvector orientation. The other eigenvector $v_1$ is predominantly orientated in $x_1$–direction in the beginning of phase I. The exact eigenvector orientation quantified by $\alpha_1$ varies with the level of the control parameter $c_2 = \text{const.}$ (Figure S2, left panel, comparing B to C). With increasing control parameter $c_1$, this eigenvector rotates towards $\alpha_1 = 135°$ with the corresponding eigenvalue $\lambda_1$ being more negative than the dominant eigenvalue $\lambda_2$ with $\lambda_1 < \lambda_2$ (Figure S2).

During phase II, the dominant eigenvector $v_2$ rotates from $\alpha_2 = 45°$ towards $\alpha_2 = 0°$ so that the dominant eigenvector $v_2$ is finally orientated towards the $x_1$–axis before the stability area $A_{(x^*_{1-},x^*_{2-})}$ is left. Note that the final orientation of the dominant eigenvector $v_2$ at the stability area boundary varies with the level of the control parameter $c_2 = \text{const.}$ (Figure S2, left panel, comparing A to C). The corresponding eigenvalue $\lambda_2$ increases with increasing control parameter $c_1$ until it is very close to zero (Figure S2, left panel). Hence, starting from an orientation where

the dominant eigenvector is equally close to subsystem $X_1$ and $X_2$, subsystem $X_1$ gets closer to the dominant eigenvector with increasing control parameter $c_1$. In the beginning of phase II, subsystems $X_1$ and $X_2$ are thus expected to show a similar recovery from perturbations in the direction of the dominant eigenvector $v_2$ determined by the magnitude of the corresponding eigenvalue $\lambda_2$. With a further increasing control parameter $c_1$, a relatively slower recovery determined by the increased eigenvalue $\lambda_2$ is expected in subsystem $X_1$ compared to subsystem $X_2$ from perturbations in the direction of the dominant eigenvector $v_2$. The other eigenvector $v_1$ rotates from $\alpha_1 = 135°$ in the beginning of phase II towards $\alpha_1 \approx 120-100°$ at the stability area boundary (Figure S2, left panel). This eigenvector $v_1$ gets predominantly orientated in $x_2$—direction with increasing control parameter $c_1$. The corresponding eigenvalue $\lambda_1$ increases slightly.

The system may converge intermediately to the stable fixed point $(x^*_{1+},\ x^*_{2-})$ after leaving the stability area $A_{(x^*_{1-},x^*_{2-})}$ and prior to the following critical transition in subsystem $X_2$ in the case of a two phase cascade (compare Figure 2A in main manuscript). The eigenvector rotation and the change of the corresponding eigenvalue magnitude for this stable fixed point $(x^*_{1+},\ x^*_{2-})$ during the evolution in the control parameter space (Figure S2A, right panel) may therefore point to critical slowing down in subsystem $X_2$. The dominant eigenvector $v_2$ points in $x_2$–direction with $\alpha_2 \approx 90°$ throughout an increasing control parameter $c_1$ (Figure S2A, right panel), so that subsystem $X_2$ is closest to this dominant eigenvector $v_2$. The corresponding eigenvalue $\lambda_2$ is close to zero. As a result, a relatively slower recovery from perturbations in the direction of the dominant eigenvector $v_2$ is expected for subsystem $X_2$. The other eigenvector $v_1$ mainly points in $x_1$–direction with $\alpha_1 \approx 180°$ and the corresponding eigenvalue $\lambda_1$ decreases with increasing control parameter $c_1$ (Figure S2A, right panel).

## 4. Evolution of statistical indicators

The evolution of autocorrelation and variance in the *pre—tipping* time span as well as in the *intermediate* time span (for the two phase cascade) are related to the described eigenvector rotation and the change in the eigenvalue magnitude. For the pre—-tipping time span, the evolution of autocorrelation and variance may be determined by the eigenvector rotation and changes in the eigenvalue magnitude of the stable fixed point $(x^*_{1-},\ x^*_{2-})$ when approaching the stability area $A_{(x^*_{1-},x^*_{2-})}$ (Figure S2, left column). The eigenvector rotation and change in the eigenvalue magnitude of the stable fixed point $(x^*_{1+},\ x^*_{2-})$ needs to be taken into account for the evolution of autocorrelation and variance in the intermediate time span of the two phase cascade (Figure S2, right column).

In the pre-–tipping time span prior to leaving the stability area $A_{(x^*_{1-},x^*_{2-})}$, an increase of autocorrelation and variance can be observed for subsystem $X_1$ for all levels of a constant control parameter $c_1$ with subsystem $X_1$ getting closer to the (rotating) dominant eigenvector (Figure S3). Regarding subsystem $X_2$, a relatively constant level of autocorrelation and variance is detected (Figure S3). This level of autocorrelation and

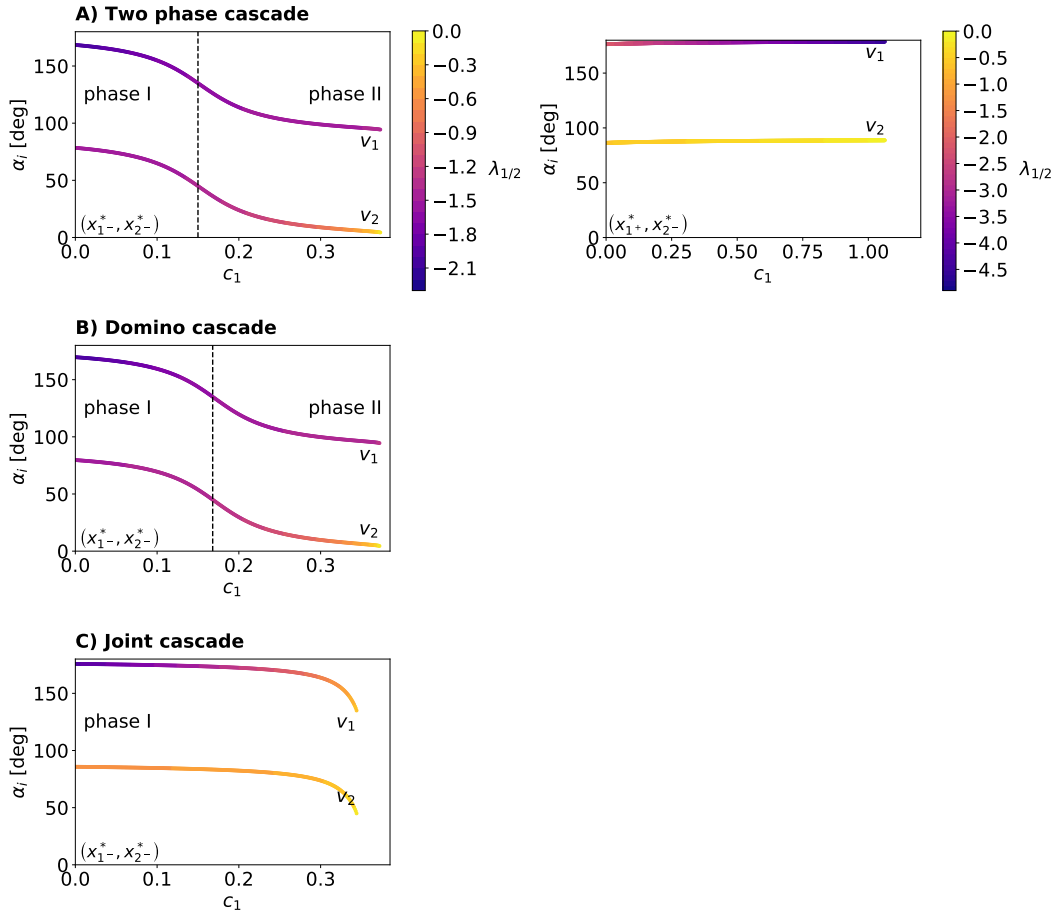


**Figure 2.** Evolution of the angel $\alpha_i$ with $i = 1, 2$ giving the direction of the eigenvectors $v_1$ and $v_2$ for the fixed points $(x_{1-}^*, x_{2-}^*)$ (left column) and $(x_{1+}^*, x_{2-}^*)$ (right column) along different paths within the control parameter space for two bidirectionally coupled tipping elements given by 2 with $d_{21} = 0.2 > 0$ and $d_{12} = 0.2 > 0$. The different pathways within the control parameter space correspond to the types of multiple tipping emerging from an infinitely slowly increase of the control parameter $c_1$ of subsystem $X_1$ while keeping the control parameter $c_2$ of subsystem $X_2$ constant $c_2 = \text{const.}$ (with A: $c_2 = 0.15$, B: $c_2 = 0.16849$, C: $c_2 = 0.344$).

variance increases with increasing level of the constant control parameter $c_2$ (Figure S3, going from A to C) corresponding to the increasing magnitude of the eigenvalues with an increasing level of the constant control parameter $c_2$ (compare Figure S2, left column). It is therefore aligned to the different patterns of multiple tipping. While a high level of autocorrelation and variance in subsystem $X_2$ can be observed for a joint tipping with subsystem $X_1$ (Figure S3C), the level of autocorrelation and variance in subsystem $X_2$ is relatively lower for the domino cascade (Figure S3B) and the two phase cascade (Figure S3A).

In the case of a two–phase cascade, autocorrelation and variance are determined in

an intermediate time span which results from the intermediate residence in the stable fixed point $(x^*_{1+}, x^*_{2-})$ prior to the critical transition in subsystem $X_2$ (Figure S3A). Compared to the pre—tipping time span, a decreasing autocorrelation and variance can be observed for subsystem $X_1$ after its critical transition. For the autocorrelation and variance in subsystem $X_2$ a jump to a higher level of the statistical indicators compared to the level of the statistical indicators in the pre—tipping time span can be observed (Figure S3A). Resembling the results of [6] the ratio of the autocorrelation and variance levels in the intermediate time span to the levels in the pre—tipping time span is higher for a two phase cascade (Figure S3A) than for a single tipping event in subsystem $X_1$ related to the increased magnitude of the corresponding eigenvalue.

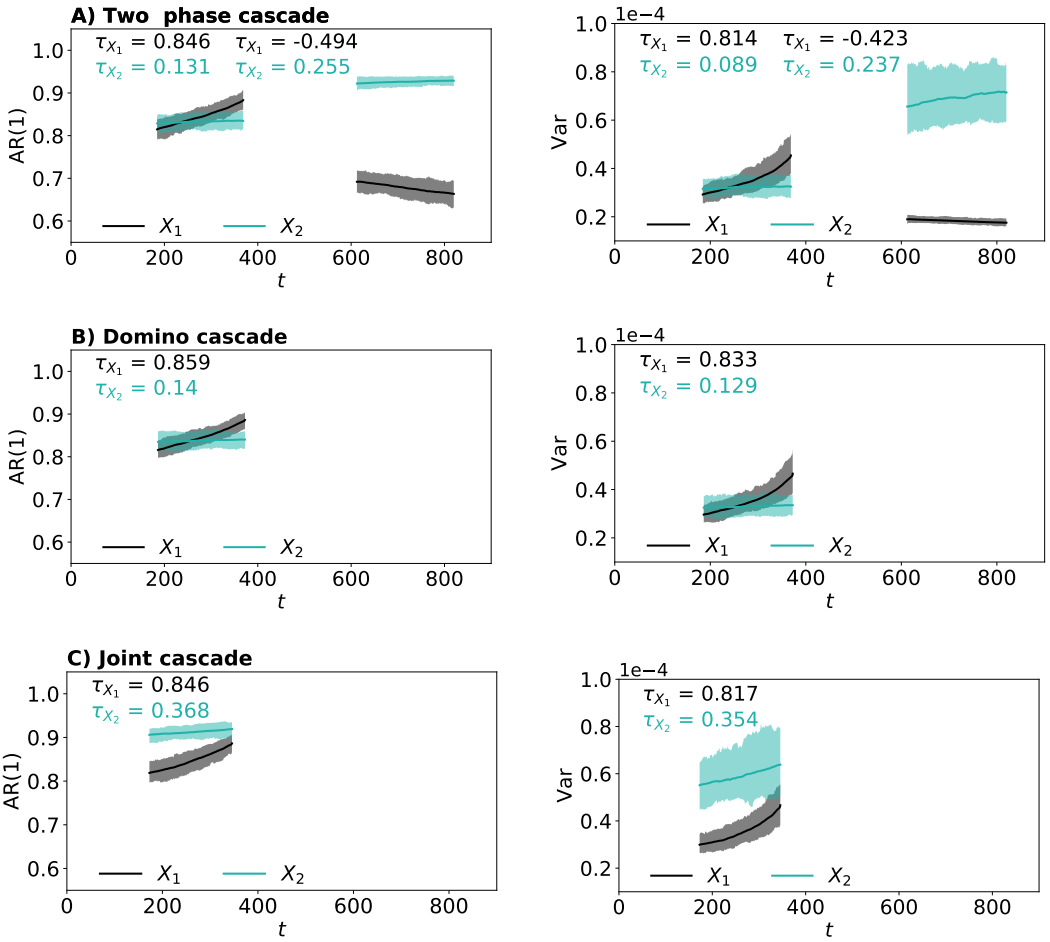


**Figure 3.** Evolution of autocorrelation (left column) and variance (right column) along different paths within the control parameter space for two bidirectionally coupled tipping elements given by 2 with $d_{21} = 0.2 > 0$ and $d_{12} = 0.2 > 0$. The different pathways within the control parameter space correspond to the types of multiple tipping emerging by a slow linear increase of the control parameter $c_1$ of subsystem $X_1$ from $c_1 = 0$ while keeping the control parameter $c_2$ of subsystem $X_2$ constant ($c_2 = \text{const.}$) (with A: $c_2 = 0.15$, B: $c_2 = 0.16846$, C: $c_2 = 0.344$).

## References

[1] Boerlijst M C, Oudman T and de Roos A M 2013 *PloS One* **8** e62033
[2] Dakos V 2018 *Ecological Indicators* **94** 494–502
[3] Dakos V, Scheffer M, van Nes E H, Brovkin V, Petoukhov V and Held H 2008 *Proceedings of the National Academy of Sciences* **105** 14308–14312
[4] Lenton T M, Livina V N, Dakos V, Van Nes E H and Scheffer M 2012 *Philosophical Transactions of the Royal Society A: Mathematical, Physical and Engineering Sciences* **370** 1185–1204
[5] Dakos V, Carpenter S R, Brock W A, Ellison A M, Guttal V, Ives A R, Kéfi S, Livina V, Seekell D A, van Nes E H and Scheffer M 2012 *PloS One* **7** e41010
[6] Dekker M M, Heydt A S and Dijkstra H A 2018 *Earth System Dynamics* **9** 1243–1260

## 5.3 Climate-induced hysteresis of the tropical forest in a fire-enabled Earth system model [AP3]

**Authors**

Markus Drüke, Werner von Bloh, Boris Sakschewski, Nico Wunderling, Stefan Petri, Manoel Cardoso, Henrique M.J. Barbosa, Kirsten Thonicke

**Status**

In Review at *European Physical Journal Special Topics* (submitted October 2020)

**Short summary**

In this study, a climate-change induced hysteresis is investigated in tropical rainforests using the state-of-the-art dynamic global vegetation model LPJmL5.1 that is coupled to the Earth system model CM2Mc. By experiments, where the concentration of atmospheric $CO_2$ is increased (impact phase) and afterwards decreased (recovery phase) over 900 simulation years in total, a hysteresis in vegetation cover and biomass is detected. For both, a simulation with enabled and disabled wildfires, this hysteresis reveals that the tropical rainforest systems do not recover immediately into their original state after the $CO_2$ forcing has ceased, i.e., after the impact and the recovery phase. Further, it is shown that the strength of the hysteresis is strongly spatially heterogeneous. Although no system wide tipping has been found, this study represents an important step forward in investigating hysteretic behaviour in tropical forests with a state-of-the-art dynamic global vegetation model.

**Author contributions**

Markus Drüke designed the study with input from Kirsten Thonicke, Boris Sakschewski, Werner von Bloh and Nico Wunderling. Markus Drüke conducted the simulations and prepared the figures. Markus Drüke wrote the initial version of the manuscript with input from all authors. Nico Wunderling revised the part about nonlinear dynamics and hysteretic behaviour of the Amazon rainforest in detail.

**EPJ manuscript No.**
(will be inserted by the editor)

# Climate-induced hysteresis of the tropical forest in a fire-enabled Earth system model

Markus Drüke[1,2,a], Werner von Bloh[1], Boris Sakschewski[1], Nico Wunderling[1,2,3], Stefan Petri[1], Manoel Cardoso[4], Henrique M. J. Barbosa[5], and Kirsten Thonicke[1]

[1] Potsdam-Institute for Climate Impact Research, Member of the Leibniz Association, P.O. Box 60 12 03, 14412 Potsdam, Germany
[2] Humboldt Universität zu Berlin, Unter den Linden 6, 10099 Berlin, Germany
[3] Institute of Physics and Astronomy, University of Potsdam, 14476 Potsdam, Germany
[4] Instituto Nacional de Pesquisas Espaciais, Av. dos Astronautas, 1.758 - Jardim da Granja, São José dos Campos - SP, 12227-010, Brazil
[5] Physics Institute, University of Sao Paulo (USP), R. do Matão, 1371, Cidade Universitária, Sao Paulo, Brazil

**Abstract.** Tropical rainforests are recognized as one of the terrestrial tipping elements which could have profound impacts on the global climate, once their vegetation has transitioned into savanna or grassland states. While several studies investigated the savannization of, e.g., the Amazon rainforest, few studies considered the influence of fire. Fire is expected to potentially shift the savanna-forest boundary and hence impact the dynamical equilibrium between these two possible vegetation states under changing climate. To investigate the climate-induced hysteresis in pan-tropical forests and the impact of fire under future climate conditions, we employed the Earth system model CM2Mc, which is biophysically coupled to the fire-enabled state-of-the-art dynamic global vegetation model LPJmL. We conducted several simulation experiments where atmospheric $CO_2$ concentrations increased (impact phase) and decreased from the new state (recovery phase), each with and without enabling wildfires. We find a hysteresis of the biomass and vegetation cover in tropical forest systems, with a strong regional heterogeneity. After biomass loss along increasing atmospheric $CO_2$ concentrations and accompanied mean surface temperature increase of about 4°C (impact phase), the system does not recover completely into its original state on its return path, even though atmospheric $CO_2$ concentrations return to their original state. While not detecting large-scale tipping points, our results show a climate-induced hysteresis in tropical forest and lagged responses in forest recovery after the climate has returned to its original state. Wildfires slightly widen the climate-induced hysteresis in tropical forests and lead to a lagged response in forest recovery by ca. 30 years.

## 1 Introduction

Tropical forests play a key role in the Earth's climate system and provide important ecosystem services [1]. Being one of the most productive biomes and largest terrestrial carbon stores, they stabilize global climate and thus the Earth system. By recycling 25-50 % of total rainfall, Amazon rainforests are a huge atmospheric moisture pump, thereby regulating regional climate by evaporative cooling and conserving soil and water in South America [2]. Furthermore, tropical forests provide timber, fiber, fuel wood and non-timber forest products thus ensuring not only local livelihoods [3]. Tropical forests are also the largest global reserve of biodiversity [4, 5]. Today this crucial functionality is at risk as land use change (LUC) and climate change (CC) pose an ever growing threat to tropical forests. Logging, slash and burn practises, drought and temperature stress, as well as increasing fire regimes threaten the survival of large areas of tropical forests [6, 7, 8, 9, 10].

In particular the interaction between fire, vegetation and climate plays a key role for the geographic distribution of tropical forests and might lead to a vast transition from forest to non-forest states, such as savannas and grasslands [11, 12]. In a dense forest, the closed canopy favors a moist and relatively cool micro-climate, which prevents fire and stabilizes the forest state [13]. However, increasing fire regimes, through LUC and CC, degrade forests and decrease canopy closure specifically at the forest perimeter [14]. As a consequence, fuel at the forest floor dries out more and grass cover increases, which in turn increases fire frequency due to easily ignitable fine fuels. In addition, a grassy environment leads to a dry, hot and windy microclimate, further increasing fire regimes. Frequent fires are thought to prevent the establishment of new trees and stabilizing the grassland state [13, 14]. Fire and deforestation can change vegetation-climate feedbacks in tropical forests in such a way that multiple stable states are possible implying a hysteresis in the impact and recovery phase of the system [15, 16]. For example, a disturbance by elevated atmospheric $CO_2$ levels and hence, higher temperatures, could increase tree mortality, enhance grass growth and push the system towards a less vegetated state. With fires burning more frequently in grassland and savanna ecosystems, tree recovery could be prevented under decreasing temperatures and atmospheric $CO_2$ concentrations, thus leading to a lock-in effect and bistable states [13]. Similar mechanisms were found for atmospheric moisture recycling [17] and deforestation [18].

Such system hysteresis is often accompanied by the existence of tipping points, where relatively small disturbances can cause a transition from one system state to another. Several previous studies indicate the presence of such tipping points and stable states in tropical forests [13, 16, 18, 19, 20, 21, 22]. Bistability between grassland and trees has been investigated by e.g. Baudena et al. [20], using a simple conceptual model. They found a possible coexistence between grassland and trees. While fire widens the parameter range for the coexistence it also induces a bistability between forest and grasslands. Especially in the transition zones between grasslands and forests fire-sensitive tipping points exists. This has be shown by Lasslop et al. [13], using a fire-enabled dynamic global vegetation model (DGVM). Another study identified three stable states (forest, savanna and grassland) by analyzing remote sensing data (Hirota et al. [16]). They also found that deforestation to the threshold of 60% tree cover might lead to a self-propagating shift to an open savanna state. Recently, several tipping points of tropical forests for different regions and climatic conditions were found by Staal et al. [21]. Using integrated remote sensing data, a hydrological model and atmosphere moisture tracking simulations, they emphasized the importance of moisture recycling in forests for the spatial extent of tropical forests.

[a] e-mail: drueke@pik-potsdam.de

Most of these studies rely on conceptual models, uncoupled simulations or remote sensing data - hardly ever on Earth system models. However, neither conceptual models nor standalone DGVMs (not coupled to an Earth system model) can account for multiple feedbacks between vegetation and climate, and using historical data doesn't allow to investigate various scenarios and processes separately. Nevertheless, investigating the tropical hysteresis by using a fire-enabled and state-of-the-art DGVM coupled to an Earth system model (ESM) still remains a challenge, because of the complexity of such a models and computational demands.
In this study, we aimed to investigate the potential for a climate-induced hysteresis and multiple stable states using the fire-enabled DGVM LPJmL, coupled to the ESM CM2Mc. Starting from a pre-industrial potential natural vegetation state (vegetation that establishes under climate and soil conditions in a particular area or grid cell in the absence of human influence such as land use), we investigated the response of tropical forests to a linear increase of atmospheric $CO_2$ over a 350-year time span. In order to study the recovery of the tropical forests, i.e. potential hysteresis and bistability, we decreased atmospheric $CO_2$ afterwards by the same amount and over the same time span. The aim of these idealized climate change scenarios was not to represent a realistic historic or future atmospheric greenhouse gas concentration but to investigate the response of the model to an extreme warming scenario. In addition, to disentangle the impact of fire on tree mortality and recovery, we performed simulation experiments with and without fire. The impact of changing climate, forced by atmospheric $CO_2$, and thus fire on vegetation was quantified by changes in the time series of average tropical biomass and by evaluating spatial differences between the different experiments.

## 2 Methods

### 2.1 CM2Mc-LPJmL

We used the coupled Earth system model CM2Mc-LPJmL v.1.0 (see Fig. 1), which combines the fast but coarse-grained atmosphere and ocean model CM2Mc [23] with the state-of-the-art DGVM LPJmL5.0-FMS [24, 25], using the process-based fire model SPITFIRE [26] which was recently optimized for South America [27]. An upcoming publication will give the technical details of the biophysical coupling between CM2Mc and LPJmL and availability of the code to the scientific community [1].

#### 2.1.1 CM2Mc

CM2Mc is a configuration of the Climate Model 2 (CM2) [28] model framework of the Geophysical Fluid Dynamics Laboratory (GFDL), which is coupled to the Modular Ocean Model 5 (MOM5) at a coarse spatial resolution of 3°x3.75° latitude-longitude [23]. The original configuration of the model includes the global atmosphere and land model AM2-LM2 [29] with static vegetation. In the configuration of CM2Mc-LPJmL, the land model LM2 is replaced by the dynamic global vegetation model LPJmL, while keeping MOM5 dynamically coupled. The model components are connected via GFDL's Flexible Modeling System (FMS), which is a software framework to support the efficient software development, coupling and application of its land, atmosphere and ocean components [30].

[1] submitted to Geoscientific Model Development

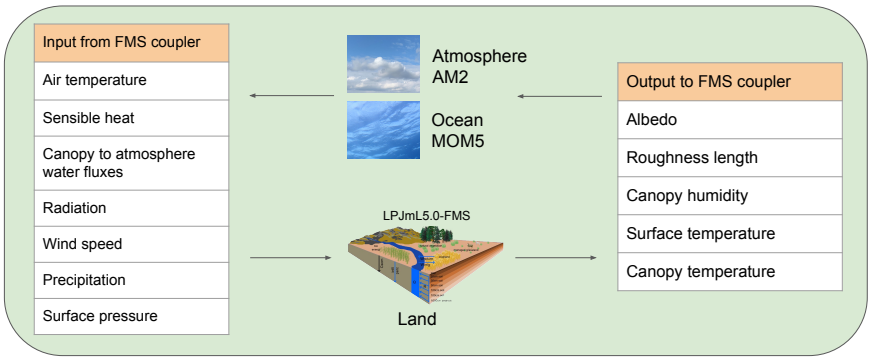


**Fig. 1.** Schematic overview of the coupling and the model components in CM2Mc-LPJmL.

### 2.1.2 LPJmL

The Lund-Potsdam-Jena managed Land version model (LPJmL5.0-FMS, based on LPJmL4.0 [24, 31] and LPJmL5.0 [25]) is a well established and validated process-based DGVM, which globally simulates the surface energy balance, water fluxes, carbon fluxes and stocks for natural and managed vegetation forced by climate and soil input data. LPJmL simulates the establishment, growth, competition and mortality of plant functional types (PFT) in natural vegetation and crop functional types (CFT) on managed land. Vegetation composition results from changes in foliar projective cover (FPC) of competing PFTs. The establishment and survival of different PFTs is regulated through bioclimatic limits and effects of heat, productivity and fire on plant mortality. These processes enable LPJmL to investigate feedbacks, for example, between vegetation and fire. LPJmL simulates water balance [32], impacts of agriculture [33], wildfires in natural vegetation (SPITFIRE) [26], permafrost [34] and specified multiple climate drivers on phenology [35]. Recently, by using an optimization approach, several important parameters in LPJmL have been newly estimated [36] and the fire model has been improved by developing a new fire danger index, in order to obtain a more realistic fire representation [27]. We applied the optimized and improved SPITFIRE in this study.

### 2.1.3 Coupling interface

The biophysical coupling of LPJmL in CM2Mc consists of canopy humidity, soil and canopy temperature, roughness length and albedo, that interact with the atmosphere in a temporal resolution of one hour. These variables are calculated within LPJmL and then passed to the coupling software FMS. The coupler provides LPJmL with the necessary climatic input as i.e. radiation and precipitation (Fig. 1). The spatial resolution of the atmosphere and ocean is 3° x 3.75° latitude-longitude, while LPJmL uses its native resolution of a 0.5° x 0.5° latitude-longitude grid. The FMS interpolates the variables exchanged in both directions, guaranteeing conservation of all scalar and

vector fields. Thus, the atmospheric input in one grid cell is distributed over several biosphere grid cells.
In order to couple LPJmL with CM2Mc, several adjustments in LPJmL had to be implemented, including the use of the Penman Monteith scheme [37] for the calculation of potential evapotranspiration and the modeling of canopy humidity. We furthermore included the calculation of surface temperature by employing a simple energy balance parameterization. Roughness lengths and albedo have been calculated as in stand-alone LPJmL [24]. To counteract a large negative temperature bias in the northern latitudes we added a more detailed parameterization of the sublimation [38]. In order to make the LPJmL grid compatible with the FMS grid, a small wrapper library for the data exchange between LPJmL and the FMS domain was developed.
The detailed description of the coupling between CM2Mc and LPJmL and a thorough evaluation of the model will be published soon.

### 2.2 Experimental setup

To ensure our simulation experiments start from an equilibrium of long-term soil and ocean carbon pools, we used a 5000 years stand-alone LPJmL spin up and restart files from CM2Mc. This first model spin-up was followed by a second spin-up by running the fully coupled model for 750 simulation years under pre-industrial conditions without land use, but with fire disturbance enabled. This second spin-up ensured a consistent equilibrium between soil, vegetation and climate.
In order to investigate the existence of a climate-induced hysteresis in tropical forests, we conducted a set of simulation experiments based on the following protocol which included 3 phases:

1. Impact phase: Linear increase of atmospheric $CO_2$ level by 1% (from 284 ppm) per year, starting from pre-industrial conditions at 284 ppm over 350 years, reaching a final $CO_2$ level of 1280 ppm.
2. Recovery phase: Subsequent linear $CO_2$ decrease, according to the impact phase, reaching 284 ppm after 350 simulation years.
3. Post-recovery phase: 350 additional years with constant $CO_2$ at 284 ppm to establish the experiment closer to an equilibrium state.

In order to investigate the contribution of fire, we repeated the spin-up and the 3 phases in another set of simulation experiments but with fire disabled (no-fire). The 1% $CO_2$ concentration increase is an accepted method to force idealised climate change scenarios [39]. To focus on the main drivers of the climate-induced hysteresis in an already complex ecosystem, we turned land use off in order to have an undisturbed potential natural vegetation (since SPITFIRE does not work on managed land, the inclusion of land use would skew the results), and disabled $CO_2$-fertilization and the nitrogen cycle within LPJmL. Aerosols, greenhouse gases besides $CO_2$, ozone and solar irradiance were set to pre-industrial values from 1860, which allowed to isolate the impact of increasing $CO_2$ and fire on natural vegetation. The experiments were performed globally, but we analysed simulation results covering the tropical latitudes 30°S to 30°N only.

## 3 Results and Discussion

### 3.1 Trajectories of tropical biomass and temperature

In the impact phase of the experiments, where atmospheric $CO_2$ increased from 284 ppm to 1280 ppm over a period of 350 years, average tropical surface temperature

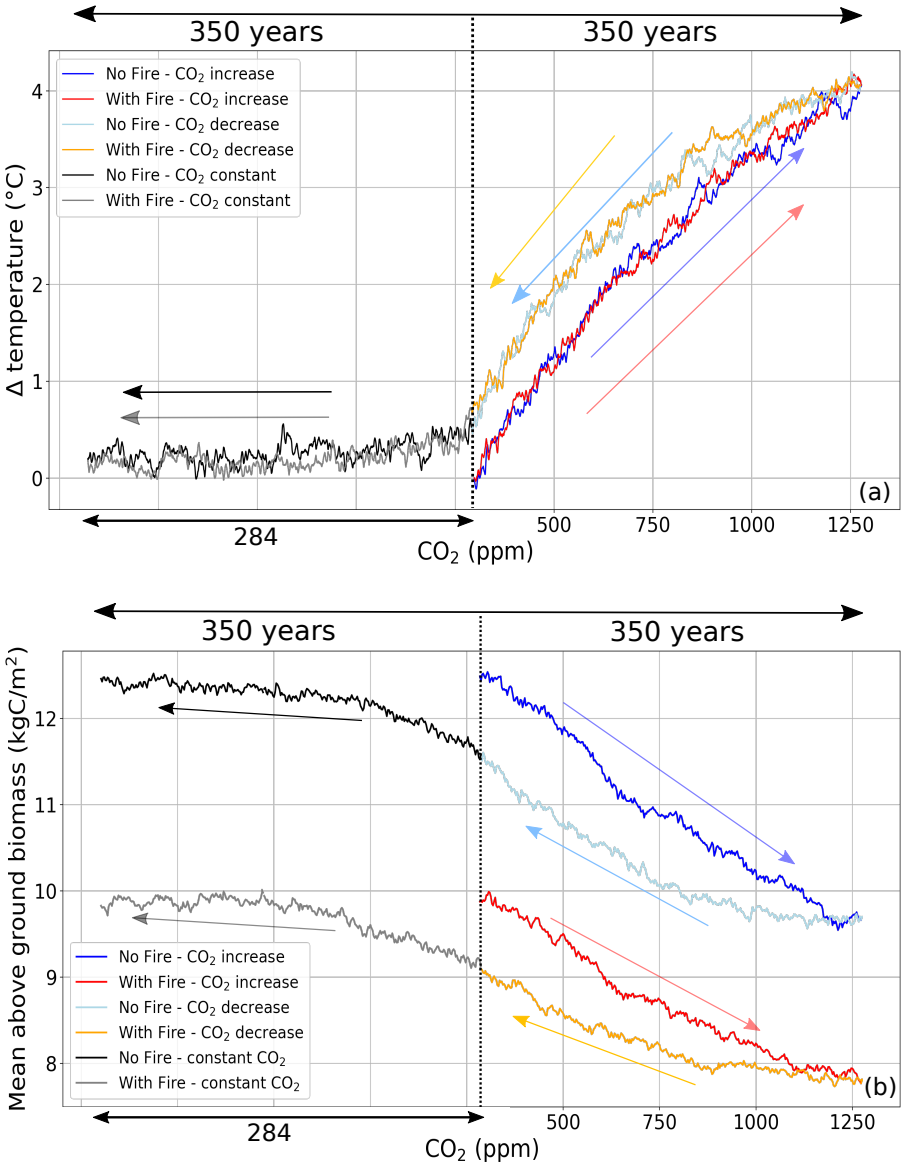


**Fig. 2.** (a) Overview of tropical mean land surface temperature for the simulation experiments. Atmospheric $CO_2$ is increasing from 284 ppm to 1280 ppm in 350 years, leading to warming of 4.1°C in the no-fire (blue line) as well as fire-enabled (red line) experiments, respectively. In the recovery phase experiments, $CO_2$, and hence tropical surface temperature, decreases again for another 350 simulation years (fire-enabled - orange line; no-fire - light-blue line). Each experiment is then continued for another 350 simulation years under pre-industrial conditions marking the post-recovery phase (fire-enabled - light grey line; no-fire - dark grey line). (b) Overview of tropical mean above-ground biomass for the simulation experiments. Atmospheric $CO_2$ is increasing from 284 ppm to 1280 ppm in 350 years, leading to a decrease in biomass of ca. 20% in the no-fire (blue line) and fire-enabled (red line) experiments, respectively. In the reverse experiments, $CO_2$ decreases again for another 350 simulation years, followed by an increase in biomass (fire-enabled - orange line; no-fire - light blue line). Each experiment is then continued for another 350 simulation years under pre-industrial conditions (fire-enabled - light grey line; no-fire - dark grey line).

(called temperature, hereafter) increased by ca. 4.1 ℃ with and without fire (Fig. 2a). Alongside the temperature increase in the impact phase, the modelled biomass decreased by ca. 20% for both experiments (Fig. 2b). Previous studies suggest temperature stress on the vegetation as the cause for this large reduction [40]. Without fire, the total biomass was ca 25% larger, due to missing combustion and fire-related tree mortality [41].
In the recovery phase, atmospheric $CO_2$ decreased over another 350 years, until the starting value of 284 ppm was reached. In the first years of climate recovery, the temperature decrease was rather small, due to a delay in the response of the surface to the new $CO_2$ values. After ca. 100 years, the temperature decreased faster and finally reached a value of ca. 0.7 ℃ above the starting value of the impact phase for both experiments.
This temperature offset occurs for two reasons: 1) The temperature was not yet in a radiative equilibrium with the new $CO_2$ values, which takes a few years, given no other interactions between temperature and vegetation [42]. 2) At the end of the recovery phase the vegetation was in a different state compared to the beginning. Average vegetation carbon (orange and light blue lines in Fig. 2b) were still ca. 10% lower than at the beginning of the impact phase. Here, a lower biomass showed less evaporative cooling, leading to a higher temperature. Both effects, higher temperature and less biomass, are highly connected and strengthen this offset [43].
In the post-recovery phase of the experiments, atmospheric $CO_2$ was kept constant at 284 ppm for 350 years, to investigate lagged effects of the reverse trajectory in the climate-induced hysteresis in tropical forests. In both experiments, the temperature decreased rapidly over the first 10-20 years, reaching the radiative equilibrium at the lower $CO_2$ value of 284 ppm. In the remaining ca. 330 years, the temperature decreased much slower from ca. 0.3–0.4 ℃ to 0.1–0.2 ℃ above the starting value in the first experiment. Even at the end of the post-recovery phase, the temperature was still slightly elevated and did not reach its original state yet. Biomass continued to recover slowly (by ca. 10%) in this last phase. To estimate the rate of recovery, we subtracted the standard deviation of the last 100 years (where biomass was relatively stable) from the mean of this period. The resulting value has been reached by the fire enabled experiment (light grey line, Fig. 2b) after ca. 160 years of the post-recovery phase and by the no-fire experiment (black line, Fig. 2b) after ca. 130 years. Hence, the experiment without fire recovered slightly faster than the experiment with fire disturbance enabled. After 200 years of the post-recovery phase the biomass was relatively stable for both experiments and approximately as large as in the initial state.

### 3.2 Spatial heterogeneity

The response of vegetation and climate in the conducted experiments had a strong regional variation. Here, we discuss the spatial heterogeneity of how tropical biomass, vegetation cover type and precipitation responded to the different $CO_2$ trajectories (fire disturbance included) across the tropics.
In the fire-enabled experiment, temperature was still slightly elevated but average biomass had recovered after ca. 200 years of the post-recovery phase. This behaviour can be explained by nonlinear effects in the vegetation-climate interaction in combination with regionally different biomass changes (Fig. 3). Fig. 3a shows the distribution of biomass in the state before the impact phase. Here, highest values (25-35 $kgC/m^2$) were found close to the equator. Savanna areas, as the Cerrado in Brazil or the Sahel zone, had biomass values of ca. 10-20 $kgC/m^2$. Panels b-d of Fig. 3 show the absolute difference in biomass comparing the 3 phases, thus areas with a large biomass exhibited the largest magnitude of change. These most affected areas lost almost half of

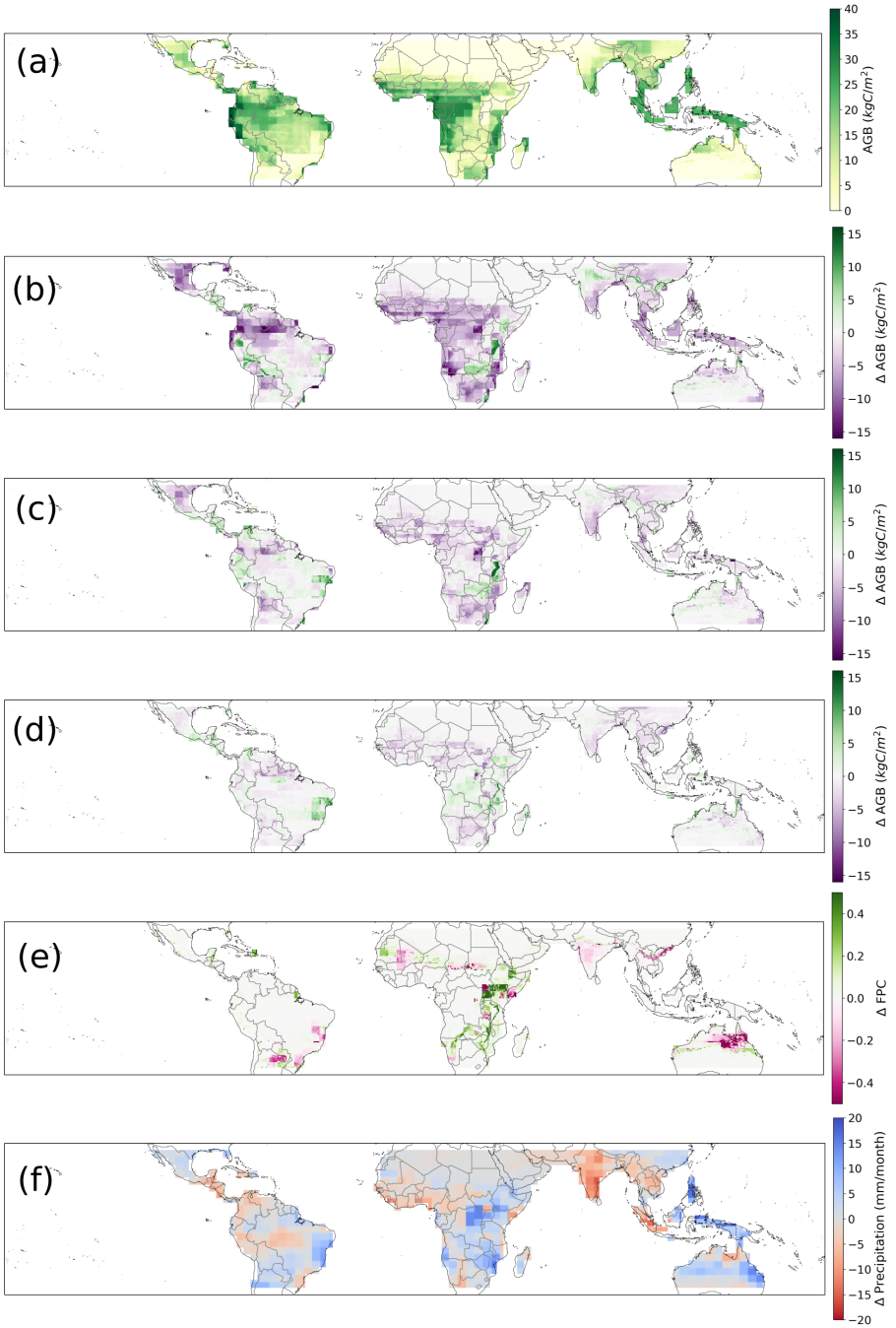


**Fig. 3.** (a) Simulated above-ground biomass (AGB) at the beginning of the experiments at 284 ppm with fire activated. (b) Difference between (a) and the end of the impact phase after the first 350 years reaching 1280 ppm. (c) Difference between (a) and the end of the recovery phase after another 350 years reaching 284 ppm again. (d) Difference between (a) and after 200 years of the post-recovery phase, after simulating another 200 years under constant $CO_2$ of 284 ppm. (e) Difference of foliar projective cover (FPC) of tropical trees between the beginning of impact phase and the state after 200 years of the post-recovery phase. (f) Difference of global precipitation between the beginning of impact phase and the state after 200 years of the post-recovery phase.

their respective biomass (10-15 kgC/m$^2$) throughout the impact phase (e.g. Amazon and African rainforests), but still maintained biomass levels higher than is usually found in tropical grassland areas of ca. 2-3 kgC/m$^2$. Only a few, cooler regions offered better growing conditions in a 4 ℃ warmer climate, mostly mountain ranges, such as the Andes. These biomass increases are supported by earlier studies showing that higher temperatures could lead to a greening of mountainous regions [44]. At the end of the recovery phase, much of the biomass recovered (Fig. 3c), except northern Amazon and northern Central-African forests where biomass was still ca. 3-5 kg/m$^2$ lower. Biomass loss affected also African savannas (Fig. 3 b and c). Regions that gained biomass from elevated temperatures, continued this trend (Fig. 3c).
After atmospheric $CO_2$ levels returned to the pre-impact state, biomass recovery still required 200 years of the post-recovery phase to reach its original state in most regions (Fig. 3d). Even after these additional 200 years, vulnerable regions, such as the northern Amazon and savannas in northern Africa, still did not fully recover. Conversely, regions such as the Caatinga in north-eastern Brazil, showed an even larger biomass compared to the beginning of the impact phase. This is due to a slightly wetter climate, caused by temperature changes, impacting the Atlantic ocean and hence, the precipitation in northeastern Brazil (Fig. 3f). Similarly, biomass increased along increasing precipitation in eastern Africa. On the contrary, biomass decreased in India and China, which is connected to a decrease in precipitation (Fig. 3f). Comparing Fig. 3 and Fig. 2b shows, that even with almost completely restored average biomass after 200 years of the post-recovery phase, regional differences still remained and the original state was not completely restored.
While biomass was changed throughout the different phases of the experiment, also the vegetation composition reacted to the impact of changing $CO_2$ concentrations (Fig. 3e). For some small regions in, e.g., the Brazilian Cerrado and northern Australia, the fraction of tropical trees decreased by ca. 0.1 and 0.3 between the start of the impact phase and the state after 200 years of the post-recovery phase. Hence, the vegetation cover switched to a more grassy environment. In some mountainous areas in eastern Africa, the fraction increased by 0.2-0.3, indicating a shift towards forest. These changes correspond quite well to the differences in biomass (Fig. 3d) and precipitation (Fig. 3f).

### 3.3 The hysteresis of the tropical forest

We clearly observed in our study a hysteresis in time between the impact and recovery phases of the tropical forests. After completing the recovery phase, tropical average biomass was still decreased by ca. 10% compared to the original value and needed 200 more years at constant $CO_2$ to reach the value it had at the beginning of the impact phase.
Various regions showed a different response to our experiment ranging from an overall increase of biomass to an incomplete recovery (decrease) after 200 years of the post-recovery phase. A transition to another stable state of vegetation cover was, however, only detected in small regions, which were sparsely vegetated at the beginning. This was the case for a transition to a more grassy and less woody environment in, e.g., the Cerrado or northern Australia and for a transition to a more woody environment in, e.g., eastern Africa. These shifts went along with changes in the precipitation patterns, as well as increased average tropical surface temperature after 200 years of the post-recovery phase.
While part of the observed hysteresis was due to the normal recovery time of the vegetation after a disturbance, a large part can be ascribed to dynamic changes in the vegetation-climate interactions: Some regions, as e.g. the northern Amazon, showed a

very tight vegetation-climate interaction by a strong response to higher temperatures and a slow recovery. Mountainous regions were able to establish more trees in warmer climate, which led to more precipitation and stabilized the new vegetation cover. Our results show, that an impact through elevated atmospheric $CO_2$ concentrations disturbs climate-vegetation interactions and their co-evolution over centuries.

We find, however, that biophysical interactions between climate and vegetation, including fire, cannot push complete biomes, such as the entire Amazon rainforest, to a point beyond recovery. Other perturbations such as deforestation or factors such as biogeochemical coupling, incl. respective fire effects, might increase the probability of such tipping events. For example, Lasslop et al. [13], Hirota et al. [16] Baudena et al. [20] and Staal et al. [21] found tipping points and bistability in the tropical forests by using different methods. While we used a biophysically fully coupled, fire-enabled Earth system model for this study and investigated the climate-induced hysteresis, these studies focused on land use change scenarios alongside climate change using simpler model approaches, remote sensing data or conceptional models. CM2Mc-LPJmL employs a state-of-the-art DGVM, which is fully biophysically coupled to an atmosphere. Hence we have included several positive and negative feedback processes, including i) the impact of evaporation on the temperature and precipitation, ii) the impact of roughness lengths, albedo and wind on the temperature, iii) the impact of shifting PFTs on the water cycle [45] and iv) fire dynamics [26].

Incorporating further important model features would improve our process understanding of the climate-induced hysteresis in tropical forests. For instance, accounting for the fertilizing effect of elevated atmospheric $CO_2$ concentration on vegetation growth would most likely lead to overall higher biomass accumulation as anticipated in this study. We decided to neglect this effect in this study, since $CO_2$-fertilization can be limited by other factors such as nutrient availability [46] or leaf cooling [47], which are not accounted for in this model version either. Including related processes such as the nitrogen cycle [25] and implementing the calculation of explicit leaf temperatures is in the scope of further studies. Furthermore, accounting for natural plant trait diversity, e.g. a continuum of tree rooting strategies, could reduce simulated drought stress and thus increase biomass resilience under changing climate [45]. The inclusion of a realistic land use pattern in the modeling experiments would lead to less fire and a lower mean biomass at the beginning of the experiments. Since the parameters chosen to simulate crop growth in LPJmL are similar to the respective physiological parameters for natural plant types, crop biomass would also decline with increasing heat stress.

In the experiments of this study, fire had a strong influence on biomass stocks, leading to about 25% lower biomass throughout all phases of the experiment (Fig. 2b). This effect of fire has also been shown by Lasslop et al. [41]. Nonetheless, the impact of fire on the decrease and increase biomass was small in the impact and recovery phase. Only towards the end of the recovery phase and the first half of the post-recovery phase, fire slightly delayed the increase of biomass, hence the system needed more time to reach a near-equilibrium (Fig. 2b). The temperature recovery was however very similar for both experiments (Fig. 2a). The described hysteresis of vegetation cover was observed in both experiments with and without fire disturbance. Hence, the hysteresis does not depend on weather fire is activated or not in the model CM2Mc-LPJmL. This effect might be due to an imprecise modelling of fire feedbacks in the model or due to the much larger impact of rapidly increasing heat stress on tropical biomass, superimposing a smaller fire impact. If a future climate or land use change leads to a shift of wet tropical rainforest to a grassland state, the rapidly burning grass could increase the impact of fire.

## 4 Conclusion

In this study we present an important step in quantifying the climate-induced hysteresis of tropical forests by investigating changes in biomass, following an atmospheric $CO_2$ perturbation and recovery over the course of 1050 years. We applied the state-of-the-art fire-enabled dynamic global vegetation model LPJmL, biophysically coupled to the Earth system model CM2Mc, and simulated the response of potential natural vegetation and fire to changes in climate feedbacks due to elevated atmospheric $CO_2$. Our results show a delayed recovery of biomass and temperature due to fire-vegetation-climate feedbacks, after an impact and recovery phase of 350 years, respectively. It took another 200 years (post-recovery phase) at constant $CO_2$ level of 284 ppm, to reach pre-impact temperature and biomass levels. The system response was spatially heterogeneous, with some regions in the tropics showing an even slower recovery, while other regions exhibited a larger biomass after 200 years of the post-recovery phase. Fire generally had a large impact on vegetation stocks and led to a slightly slower recovery in our experiments.

Biophysical coupling between climate, fire and vegetation, while not considering land use changes, did not lead to large-scale tipping of tropical forests or alternative stable states in vegetation cover. Analyzing the climate-induced hysteresis, only a few smaller regions shifted to a more grassy environment (e.g. Brazilian Cerrado), while other regions increased their tree cover (e.g. eastern Africa). Smaller regions in the tropical forests showed a very strong response to $CO_2$ changes and a very slow recovery after several centuries (e.g. the northern Amazon).

By using an Earth system model that accounts for complex vegetation processes, fire and climate-induced feedbacks the presented study is an important step in evaluating hysteresis in tropical forests and in quantifying the impact of fire-vegetation-climate interactions.

## 5 Acknowledgements

This paper was developed within the scope of the IRTG 1740/TRP 2015/50122-0, funded by the DFG/FAPESP (MD, NW and KT). MC acknowledges the support from the projects FAPESP 2015/50122-0 (São Paulo Research Foundation), and CNPq 314016/2009-0 (Brazilian National Council for Scientific and Technological Development). KT and BS acknowledge funding from the BMBF- and Belmont Forum-funded project "CLIMAX: Climate Services Through Knowledge Co-Production: A Euro-South American Initiative For Strengthening Societal Adaptation Response to Extreme Events", Grant no. 01LP1610A. NW is grateful for a scholarship from the Studienstiftung des deutschen Volkes. The authors gratefully acknowledge the European Regional Development Fund (ERDF), the German Federal Ministry of Education and Research and the Land Brandenburg for supporting this project by providing resources on the high performance computer system at the Potsdam Institute for Climate Impact Research.

## 6 Code and data availability

The model code of LPJmL4 is publicly available through PIK's gitlab server [2]. LPJmL5.0 is publicly available under the GNU AGPL version 3 license [3]. MOM5 code and example configurations are public available via the project homepage[4]. Further information about the CM2Mc setup and BLING is available at the Integrated Earth System Dynamics Laboratory[5]. Code, input data, and model output of the coupled system are stored in PIK's long-term archive and will be made available to interested parties upon request. It is planned to publish the coupling interface as open source.

## 7 Author contribution statement

MD designed the study with input from KT, BS, WvB and NW. MD conducted the simulations and prepared the figures. MD wrote the initial version of the manuscript with input from all authors.

[2] https://gitlab.pik-potsdam.de/lpjml/LPJmL
[3] https://doi.org/10.5880/pik.2018.011
[4] https://mom-ocean.github.io/
[5] https://earthsystemdynamics.org/models/bling/

## References


1. Brovkin, V., Raddatz, T., Reick, C. H., Claussen, M. & Gayler, V. Global biogeophysical interactions between forest and climate. *Geophysical Research Letters* **36** (2009).
2. Zemp, D. C. *et al.* Self-amplified Amazon forest loss due to vegetation-atmosphere feedbacks. *Nature Communications* **8**, 1–10 (2017).
3. Importance of Tropical Forests. In *Tropical Forest Ecology*, 1–17 (Springer-Verlag, 2005). URL `https://link.springer.com/chapter/10.1007/3-540-27244-5_1`.
4. Lahsen, M., Bustamante, M. M. C. & Dalla-Nora, E. L. Undervaluing and Overexploiting the Brazilian Cerrado at Our Peril. *Environment: Science and Policy for Sustainable Development* **58**, 4–15 (2016).
5. Barlow, J. *et al.* The future of hyperdiverse tropical ecosystems (2018).
6. Cochrane, M. A. & Laurance, W. F. Synergisms among Fire, Land Use, and Climate Change in the Amazon. *Ambio* **37**, 522–527 (2008).
7. Beuchle, R. *et al.* Land cover changes in the Brazilian Cerrado and Caatinga biomes from 1990 to 2010 based on a systematic remote sensing sampling approach. *Appl. Geogr.* **58**, 116–127 (2015).
8. Malhi, Y. *et al.* Climate change, deforestation, and the fate of the Amazon (2008).
9. Davidson, E. A. *et al.* The Amazon basin in transition (2012).
10. Nobre, C. A. *et al.* Land-use and climate change risks in the amazon and the need of a novel sustainable development paradigm. *Proceedings of the National Academy of Sciences of the United States of America* **113**, 10759–10768 (2016).
11. Silverio, D. V. *et al.* Testing the Amazon savannization hypothesis: fire effects on invasion of a neotropical forest by native cerrado and exotic pasture grasses. *Philosophical Transactions of the Royal Society B: Biological Sciences* (2013).
12. Gomes, L., Miranda, H. S. & Bustamante, M. M. d. C. How can we advance the knowledge on the behavior and effects of fire in the Cerrado biome? *Forest Ecology and Management* **417**, 281–290 (2018).
13. Lasslop, G., Brovkin, V., Reick, C. H., Bathiany, S. & Kloster, S. Multiple stable states of tree cover in a global land surface model due to a fire-vegetation feedback. *Geophys. Res. Lett.* **43**, 6324–6331 (2016).
14. Brando, P. M. *et al.* The gathering firestorm in southern Amazonia. *Science Advances* **6**, eaay1632 (2020).
15. Higgins, S. I. & Scheiter, S. Atmospheric CO2 forces abrupt vegetation shifts locally, but not globally. *Nature* **488**, 209–212 (2012).
16. Hirota, M., Holmgren, M., Van Nes, E. H. & Scheffer, M. Global resilience of tropical forest and savanna to critical transitions. *Science* **334**, 232–235 (2011).
17. Zemp, D. C., Schleussner, C. F., Barbosa, H. M. J. & Rammig, A. Deforestation effects on Amazon forest resilience. *Geophysical Research Letters* **44**, 6182–6190 (2017).
18. Boers, N., Marwan, N., Barbosa, H. M. & Kurths, J. A deforestation-induced tipping point for the South American monsoon system. *Scientific Reports* **7**, 1–9 (2017).
19. Lenton, T. M. *et al.* Tipping elements in the Earth's climate system (2008).
20. Baudena, M., D'Andrea, F. & Provenzale, A. An idealized model for tree-grass coexistence in savannas: the role of life stage structure and fire disturbances. *Journal of Ecology* **98**, 74–80 (2010).
21. Staal, A. *et al.* Hysteresis of tropical forests in the 21st century. *Nature Communications* **11**, 4978 (2020).
22. Staver, A. C., Archibald, S. & Levin, S. A. The global extent and determinants of savanna and forest as alternative biome states. *Science* **334**, 230–232 (2011).

23. Galbraith, E. D. *et al.* Climate variability and radiocarbon in the CM2Mc earth system model. *Journal of Climate* **24**, 4230–4254 (2011).
24. Schaphoff, S. *et al.* LPJmL4 - a dynamic global vegetation model with managed land - Part 1: Model description. *Geoscientific Model Development* **11**, 1343–1375 (2018).
25. Von Bloh, W. *et al.* Implementing the nitrogen cycle into the dynamic global vegetation, hydrology, and crop growth model LPJmL (version 5.0). *Geoscientific Model Development* **11**, 2789–2812 (2018).
26. Thonicke, K. *et al.* The influence of vegetation, fire spread and fire behaviour on biomass burning and trace gas emissions: results from a process-based model. *Biogeosciences* **7**, 1991–2011 (2010).
27. Drüke, M. *et al.* Improving the LPJmL4-SPITFIRE vegetation–fire model for South America using satellite data. *Geoscientific Model Development* **12**, 5029–5054 (2019).
28. Milly, P. C. & Shmakin, A. B. Global modeling of land water and energy balances. Part I: The land dynamics (LaD) model. *Journal of Hydrometeorology* **3**, 283–299 (2002).
29. Anderson, J. L. *et al.* The new GFDL global atmosphere and land model AM2-LM2: Evaluation with prescribed SST simulations. *Journal of Climate* **17**, 4641–4673 (2004).
30. Balaji, V. The FMS Manual: A developer ' s guide to the GFDL Flexible Modeling System (2002). URL `http://www.gfdl.noaa.gov/~vb/FMSManual/FMSManual.html`.
31. Schaphoff, S. *et al.* LPJmL4 - a dynamic global vegetation model with managed land: Part 2: Model evaluation. *Geoscientific Model Development* **11**, 1377–1403 (2018).
32. Gerten, D., Schaphoff, S., Haberlandt, U., Lucht, W. & Sitch, S. Terrestrial vegetation and water balance - hydrological evaluation of a dynamic global vegetation model. *J. Hydrol.* **286**, 249–270 (2004).
33. Bondeau, A. *et al.* Modelling the role of agriculture for the 20th century global terrestrial carbon balance. *Global Change Biol.* **13**, 679–706 (2007).
34. Schaphoff, S. *et al.* Contribution of permafrost soils to the global carbon budget. *Environ. Res. Lett.* **8**, 14026 (2013).
35. Forkel, M. *et al.* Identifying environmental controls on vegetation greenness phenology through model-data integration. *Biogeosciences* **11**, 7025–7050 (2014).
36. Forkel, M. *et al.* Constraining modelled global vegetation dynamics and carbon turnover using multiple satellite observations. *Scientific Reports* **9** (2019).
37. Monteith, J. L. Rothamsted Repository Download. *Symposia of the Society for Experimental Biology* 205–234 (1965).
38. Gelfan, A. N., Pomeroy, J. W. & Kuchment, L. S. Modeling forest cover influences on snow accumulation, sublimation, and melt. *Journal of Hydrometeorology* **5**, 785–803 (2004).
39. Chapter 10: Global Climate Projections - AR4 WGI. URL `https://archive.ipcc.ch/publications_and_data/ar4/wg1/en/ch10.html`.
40. Clark, D. A., Clark, D. B. & Oberbauer, S. F. Field-quantified responses of tropical rainforest aboveground productivity to increasing CO2 and climatic stress, 1997-2009. *Journal of Geophysical Research: Biogeosciences* **118**, 783–794 (2013).
41. Lasslop, G. *et al.* Global ecosystems and fire: Multi-model assessment of fire-induced tree-cover and carbon storage reduction. *Global Change Biology* **26**, 5027–5041 (2020).
42. Yokohata, T. *et al.* Comparison of equilibrium and transient responses to CO2 increase in eight state-of-the-art climate models. In *Tellus, Series A: Dynamic Meteorology and Oceanography*, vol. 60, 946–961 (2008).

43. Bonan, G. B. Forests and climate change: Forcings, feedbacks, and the climate benefits of forests. *Science* **320**, 1444–1449 (2008).
44. Callaway, R. M., DeLucia, E. H. & Schlesinger, W. H. Biomass Allocation of Montane and Desert Ponderosa Pine: An Analog for Response to Climate Change. *Ecology* **75**, 1474–1481 (1994).
45. Sakschewski, B. *et al.* Variable tree rooting strategies improve tropical productivity and evapotranspiration in a dynamic global vegetation model. *Biogeosciences Discussions* 1–35 (2020).
46. Davies-Barnard, T. *et al.* Nitrogen cycling in CMIP6 land surface models: progress and limitations. *Biogeosciences* **17**, 5129–5148 (2020). URL `https://bg.copernicus.org/articles/17/5129/2020/`.
47. Medlyn, B. E. *et al.* Temperature response of parameters of a biochemically based model of photosynthesis. II. A review of experimental data. *Plant, Cell and Environment* **25**, 1167–1179 (2002).

## 5.4 Social tipping processes for sustainability: An analytical framework [AP4]

**Authors**
Ricarda Winkelmann, Jonathan F. Donges, E. Keith Smith, Manjana Milkoreit, Christina Eder, Jobst Heitzig, Alexia Katsanidou, Marc Wiedermann, Nico Wunderling, Timothy M. Lenton

**Status**
Submitted (December, 2020). Pre-print available in the arXiv under: arXiv:2010.04488

**Short summary**
Societal transformations towards a sustainable future of the Earth are required to limit global warming, the loss of biodiversity around the world and to achieve the UN sustainable development goals. This work develops a framework to identify and characterise social tipping processes for sustainability. Building on an expert elicitation and a comprehensive literature research, it is found that the main characteristics of social tipping processes are human agency, socio-institutional network structures as well as different temporal and spatial scales. This also separates social tipping from ecological or climate tipping. In this paper, a formal definition is suggested for social tipping processes decisive for sustainability in the Anthropocene. The developed framework is exemplified in relevant social processes for sustainability: the FridaysForFuture movement and changes in the willingness among the population to vote for the Green party in Germany.

**Author contributions**
Drawing upon the concepts developed in the expert elicitation workshop, Ricarda Winkelmann, Jonathan Donges, Keith Smith, Manjana Milkoreit and Timothy Lenton structured the conceptualisation into the resultant framework and wrote the paper with the support of all co-authors. All co-authors contributed to the discussion of the manuscript. Marc Wiedermann analysed data and created Fig. 1. Ricarda Winkelmann and Keith Smith created Fig. 2. Keith Smith analysed data and created Fig. 3. Jobst Heitzig derived the mathematical definition of social tipping processes (Sect. S1). Nico Wunderling drafted the initial version of the introduction of the paper.

**Social tipping processes for sustainability: An analytical framework**

**Authors**

*Ricarda Winkelmann[1,2]*†, Jonathan F. Donges[1,3]*†, E. Keith Smith[4,5]*†, Manjana Milkoreit[6]†, Christina Eder[4], Jobst Heitzig[7], Alexia Katsanidou[4,8], Marc Wiedermann[7], Nico Wunderling[1,2,9], Timothy M. Lenton[10]*

**Affiliations**

(1) FutureLab on Earth Resilience in the Anthropocene, Earth System Analysis, Potsdam Institute for Climate Impact Research, Member of the Leibniz Association, Telegrafenberg A31, 14473 Potsdam, Germany
(2) Institute of Physics and Astronomy, University of Potsdam, Potsdam, Germany
(3) Stockholm Resilience Centre, Stockholm University, Kräftriket 2B, 114 19 Stockholm, Sweden
(4) GESIS – Leibniz Institute for the Social Sciences, Unter Sachsenhausen 6-8, 50667 Cologne, Germany
(5) International Political Economy and Environmental Politics, ETH Zurich, Switzerland
(6) Department of Political Science, Purdue University, 100N University Street, West Lafayette, IN 47906, United States of America
(7) FutureLab on Game Theory and Networks of Interacting Agents, Complexity Science, Potsdam Institute for Climate Impact Research, Member of the Leibniz Association, Telegrafenberg A31, 14473 Potsdam, Germany
(8) Institute of Sociology and Social Psychology, University of Cologne, Cologne, Germany
(9) Department of Physics, Humboldt University of Berlin, Berlin, Germany
(10) Global Systems Institute, University of Exeter, Exeter, EX4 4QE, United Kingdom
** Corresponding authors: ricarda.winkelmann@pik-potsdam.de, jonathan.donges@pik-potsdam.de, keith.smith@gess.ethz.ch*
† *shared lead authorship*

**Abstract**

Societal transformations are necessary to address critical global challenges, such as mitigation of anthropogenic climate change and reaching UN sustainable development goals. Recently, social tipping processes have received increased attention, as they present a form of social change whereby a small change can shift a sensitive social system into a qualitatively different state due to strongly self-amplifying (mathematically positive) feedback mechanisms. Social tipping processes have been suggested as key drivers of sustainability transitions emerging in the fields of technological and energy systems, political mobilization, financial markets and sociocultural norms and behaviors.

Drawing from expert elicitation and comprehensive literature review, we develop a framework to identify and characterize social tipping processes critical to facilitating rapid social transformations. We find that social tipping processes are distinguishable from those of already more widely studied climate and ecological tipping dynamics. In particular, we identify human agency, social-institutional network structures, different spatial and temporal scales and increased complexity as key distinctive features underlying social tipping processes. Building on these characteristics, we propose a formal definition for social tipping processes and filtering criteria for those processes that could be decisive for future trajectories to global sustainability in the Anthropocene. We illustrate this definition with the European political system as an example of potential social tipping processes, highlighting the potential role of the FridaysForFuture movement.

Accordingly, this analytical framework for social tipping processes can be utilized to illuminate mechanisms for necessary transformative climate change mitigation policies and actions.

**Keywords**

Social tipping dynamics, social change, sustainability, critical states, network structures, FridaysForFuture

**MAIN TEXT**

## 1. Introduction

There is growing concern that global climate change is reaching a point where parts of the Earth System are starting to pass damaging climate tipping points (*1*): In particular, part of the West Antarctic Ice Sheet (WAIS) appears to already be collapsing because of irreversible retreat of grounding lines (*2*, *3*) which in turn is expected to trigger loss of the rest of the WAIS (*4*). Other tipping points may be close: A recent systematic scan of Earth system model projections has detected a cluster of abrupt shifts between 1.5 and 2.0°C of global warming (*5*), including a collapse of Labrador Sea convection with far-reaching impacts on human societies. The abrupt degradation of tropical coral reefs is projected to be almost complete if warming reaches 2.0°C (*6*, *7*). The possibility of the global climate tipping to a 'hothouse Earth' state has even been posited (*8*).

Against this backdrop, there is a growing consensus that avoiding crossing undesired climate tipping points requires rapid transformational social change, which may be propelled (intentionally or unintentionally) by triggering social tipping processes (*9*, *10*) or "sensitive intervention points" (*11*, *12*). Examples for such proposed social tipping dynamics include divestment from fossil fuels in financial markets, political mobilization and social norm change, socio-technical innovation (*9–11*, *13*, *14*). Equally, if human societies do not act collectively and decisively, climate change could conceivably trigger undesirable social tipping processes, such as international migration bursts, food system collapse or political revolutions (*15*). Social tipping processes have received recent attention, as they encompass this sort of rapid, transformational system change (*9*, *10*, *13*, *15*).

Here we develop an analytical framework for social tipping processes. Drawing upon expert elicitation and a comprehensive literature review, we find that the mechanisms underlying social tipping processes are categorically different from other forms of tipping, as they uniquely have the capacity for agency, they operate on networked social structures, have different spatial and temporal scales, and a higher degree of complexity. Following these distinctions, we present a definitional framework for identifying social tipping processes for sustainability, where under critical conditions, a small perturbation can induce non-linear systemic change, driven by positive feedback mechanisms and cascading network effects. We adopt this framework to understand potential social tipping dynamics in the European political system, where the *FridaysForFuture* movement (*16*) pushes the system towards criticality, generating the conditions for shifting climate policy regimes into a qualitatively different state.

The proposed framework aims to establish a common terminology to avoid misconceptions, including the notions of agency, criticality as well as the manifestation and intervention time horizons in the context of social tipping. In this way, the framework can serve to connect literatures and science communities working on social tipping, social change, complex contagion dynamics and evidence from behavioral experiments (e.g. *14*, *17*).

## 2. Background

### *2.1. Tipping points as social-ecological systems features*

We start by reviewing the characterization of tipping points across the natural and social sciences. Over the last 150 years, a suite of concepts and theories describing small changes with large systemic effects has been developed at the intersection of natural and social sciences. More recently, the concepts of tipping points and tipping elements have been broadly adopted by both natural and social scientists working within the field of climate change.

While the concept of 'tipping' originated in the natural sciences (*18*, *19*), social scientists made extensive use of the idea in the 20th century, often without using the terminology of tipping.

Famously, Schelling (*20*), following Grodzins (*21*), developed a theory of tipping processes to explain racial segregation in US neighbourhoods. Granovetter (*22*) modeled collective behavior as a tipping process that depends on passing individual thresholds for participation in riots or strikes. Kuran (*23*) described political revolution in terms of tipping dynamics, while Gould and Eldridge (*24*) distinguish phases of policy change and stability in terms of 'punctuated equilibrium'. Gladwell (*25*) popularised the concept of 'tipping points', exploring contagion effects ("fads and fashions"), sometimes triggered by specific events.

Several recent studies have examined tipping processes within contemporary social systems. Homer-Dixon (*26*) and Battison (*27*) explored the 2008 financial crisis as a tipping phenomenon. Nyborg (*14*, *28*) discussed shifts in norms and attitudes, for example regarding smoking behaviors. Centola (*17*) associated tipping points with the "critical mass phenomenon", wherein 20–30% of a population becoming engaged in an activity can be sufficient to tip the whole society. Similarly, Rockström et al. (*29*) highlighted this so-called Pareto effect in the context of decarbonization transitions. Kopp et al. (*15*) distinguished different social tipping elements within the realm of policy, new technologies, migration and civil conflict that are sensitive to "climate-economic shocks". Here, a tipping element is a system or subsystem that may undergo a tipping process.

Since the mid 1990s, ecologists and social-ecological systems (SES) researchers have also developed an extensive body of research on tipping processes using the terminology of 'regime shifts' and 'critical transitions' (e.g. *30–32*). Recognizing the impacts of human development on various ecosystems, this body of work often models ecological regime shifts as a consequence of social drivers. Less attention, however, has been paid to sudden changes in social systems triggered by ecosystem changes.

There is a rich literature on the collapse of past civilizations (e.g. *33*, *34*) and the potential role of tipping points in that (*35*). Recently, Cumming and Peterson (*36*) brought this together with work on ecological regime shifts, proposing a "unifying social-ecological framework" for understanding resilience and collapse. Further, Rocha et al. (*37*) noted that tipping dynamics can be produced by the interactions between climatic, ecological and social regime shifts.

The concept of climate tipping elements introduced by Lenton et al. (*1*) and Schellnhuber (*38*), has been increasingly adopted within Earth and climate sciences. Climate tipping elements are defined as at least sub-continental-scale components of the climate system that can undergo a qualitative change once a critical threshold in a control variable, e.g., global mean temperature, is crossed. Positive feedback mechanisms at the critical threshold drive the system's transition from a previously stable to a qualitatively different state (*1*). Other scholars, e.g., Levermann et al. (*39*), suggest a somewhat narrower definition of climate tipping elements by introducing additional characteristics, such as (limited) reversibility or abruptness. The tipping elements identified so far include biosphere components such as the Amazon rainforest (*40–42*) and coral reefs (*6*, *7*), cryosphere components such as the ice-sheets on Greenland and Antarctica (*43*), and large-scale atmospheric or oceanic circulation systems including the Atlantic meridional overturning circulation (*44*, *45*). Their tipping would have far-reaching impacts on the global climate, ecosystems and human societies (e.g. *8*, *46*).

### *2.2. Social Tipping*

In response to the concept of climate tipping points, social scientists are re-engaging with this concept yet again, creating an additional layer of tipping scholarship with an emphasis on the need for and possibility of deliberate tipping of social systems onto novel development pathways towards sustainability (e.g. *11*, *47*). Scholars argue in particular that the rapid, non-linear change of social tipping dynamics might be necessary to speed up societies' responses to climate change, and to achieve the goals of the Paris Agreement. It is this element of acceleration, propelled by positive feedbacks, that makes the concept of tipping particularly interesting. For example, Otto and Donges et al. (*9*) reported expert elicitations identifying social tipping elements relevant for driving rapid

decarbonization by 2050. Rapid-paced changes are a distinctive feature potentially differentiating tipping dynamics from many other forms of social change, including incremental (policy or institutional) changes, or more radical (socio-technical) transitions or societal transformations.

Over the last decade, the literature on deliberate transitions and transformations towards sustainability has expanded significantly, exploring the dynamics that lead to the reorganization of social, economic or political systems (e.g. *48*, *49*). In many ways, this literature and the emerging work on social tipping are interested in very similar phenomena: fundamental shifts in the organization of social or social-ecological systems - a movement from one stable state to another - including a change in power relations, resource flows, as well as actor identities, norms and other meanings (*48*). Transformations can be fast, but speed is generally not one of their defining characteristics.

This temporal feature of social tipping points - rapidity of change compared to the system's normal background rate of change - combined with the fact that tipping processes can be triggered by a relatively small disturbance of the system is motivating scholarship on leverage or 'sensitive intervention points', e.g. Farmer et al. (*12*), who identified such potentially high-impact intervention opportunities, e.g., financial disclosure, choosing investments in technology and political mobilization that may be key for triggering decarbonization transitions.

Based on a bibliometric and qualitative review of these various bodies of literature across the natural and social sciences, Milkoreit et al. (*10*) proposed the following general definition of (social) tipping: "the point or threshold at which small quantitative changes in the system trigger a non-linear change process that is driven by system-internal feedback mechanisms and inevitably leads to a qualitatively different state of the system, which is often irreversible." Milkoreit et al. (*10*) further noted there is a need to recognize and identify potential differences between climatic (or ecological) and social tipping processes to gain a deeper understanding of these phenomena.

**3. Methods and analytical structure**

Given this diverse and nascent field, there is a clear need for consensus as to what defines social tipping processes, as well as an understanding of how these processes are similar and diverge from dynamics in other non-social systems. Further, there are currently limited examples of social tipping elements in the context of sustainability transitions presented within the broader literature (*9*, *12*, *13*, *15*).

Here we explore the characterization of tipping processes within the natural and social sciences, examining how social and climate tipping processes are differently conceptualized. We draw upon a mixed qualitative methodological approach to illuminate these differences and key distinctions. Initially, core differences were identified and discussed via expert elicitation (*50*). A selected group of 25 experts from across the climate and social sciences were invited to take part in an expert elicitation workshop, that focused on identifying a common definition for social tipping processes, as well as the characterization of their dynamics. This workshop was convened in June 2018 in Cologne, Germany. The workshop participants were split into cross-disciplinary breakout groups, to independently identify the dynamics of social tipping processes. Then, each of these groups reported their findings to the broader plenary, for discussion, consolidation, reconciliation and clarification. The process was then repeated for further clarification within the breakout groups. Through this iterative inductive and deductive process, several unique themes and characteristics were identified from the broader set of codes, resulting in the key differences in and definition of social tipping processes presented below.

Drawing upon the differences identified in the expert elicitation workshop, we then review and synthesize the emerging field of social tipping processes, particularly in comparison to the related climate and ecological tipping dynamics. We then draw upon these unique characteristics to develop

a common definition for social tipping processes, which we explore using the example of the *FridaysForFuture* student movement.

## 4. Results

### *4.1. Key differences between social and climate tipping processes*

Social and climate systems' tipping processes exhibit several broad, fundamental differences in their structure and underlying mechanisms: (i) agency is a main causal driver of social tipping processes, (ii) the quality of social networks and associated information exchange provides for specific social change mechanisms not available in non-human systems, (iii) climate and social tipping processes occur at different spatial and temporal scales, and (iv) social tipping dynamics exhibit significantly more complexity than climatic ones.

**Agency:** The most important characteristic differentiating social from climate tipping processes is the *presence of agency*. While a significant body of work (e.g. *51*), including Latour's actor-network theory (*52*), addresses different forms and effects of non-human or more-than-human agency, here, we focus on a more narrow understanding of agency that is based on consciousness and cognitive processes such as foresight, planning, normative-principled and strategic thinking, that allow human beings to purposefully affect their environment on multiple temporal and spatial scales. While humans have a generally poor track record of utilizing their agentic capacities especially with regard to shaping the future (e.g. *53–55*), they appear unique in their capacity to transcend current realities with their decisions.

Agency in this more narrow sense can be understood as the human capacity to exercise free will, to make decisions and consciously chart a path of action (individually or collectively) that shapes future life events and the environment (*56*). The notion of intentionality inherent in the idea of agency implies that human actors are not only able to adapt to changes in their environment, but also deliberately create such changes. Non-human life forms can also be engaged in deliberate changes of their environment (e.g., beavers building dams), but the cognitive quality of these actions differs from those of humans, which can be based on different forms of knowledge and meaning about the world, moral norms and principles, or ideas about desirable futures. Agency allows individuals and societies to be proactive rather than merely responsive in their relationships with other humans or the environment through planning, goal setting and strategic decision-making, which links decisions and behaviors in the present with consequences and realities in the (distant) future (*57*).

Governance scholars address this social-cognitive capacity for forethought and goal-pursuit in terms of anticipation (*58*) and imagination (*10*), which can be tied to a set of futuring methods (*59*, *60*). The ability to anticipate and imagine futures enables humans and their societies (*53*, *54*) – as opposed to animal communities or ecosystems – to transcend the present and shape the future according to our values and goals (*61*), possibly increasing the prospects for human survival in times of fast and significant environmental change (*56*, *62*). Although this ability has been underutilized in the past, especially in the context of responding to climate change (*63*), it is a crucial dimension of the human repertoire of tools to create change and to ensure its long-term well-being.

Agency interacts with many of the additional differentiating characteristics we identify below in important ways. For example, agency plays a role in the creation of social networks, institutions and meaning, i.e., the production of the structures of social systems. These network structures in turn enable and constrain agency (e.g. *64*, *65*).

Physical climate tipping elements, such as ice sheets or ocean circulations, lack that ability to intentionally act and adapt. However, the adaptive capacity of ecosystems can be interpreted as a form of non-human agency and learning mechanism (*66*), see also Supplementary Information S2. While scholarship on non-human agency, including that of animals, inanimate objects, landscape

features or ecosystems (e.g. *67*, *68*) might expand our understanding of agency, the cognitive abilities that characterize human agency, especially long-term and strategic thinking, do not exist in the non-human or inanimate worlds.

**Social networks:** Understanding the *nature of social networks* is crucial for studying social tipping. While both natural (including physical and ecological) and social systems can be structurally characterized as networks and studied using a network science approach (*69*), social systems differ from natural systems in the quality of the networks' nodes and interconnections and the processes and dynamics facilitated and impacted by these particular network characteristics. Social systems feature additional network levels of information transmission (cultural and symbolic) that are largely restricted to human societies compared to natural systems (*70*).

*Network qualities unique to social systems:*
Networks in social and natural systems share various commonalities such as the existence of fundamental nodes and links (*69*). In contrast to most natural systems, however, social networks have the capacity to intentionally generate new nodes, which include socially constructed entities such as organizations and movements (*71*). New nodes can be created through cultural, political or legal means, as can the rules for their interactions with other existing nodes. Social system nodes are unique in that they have richer cognitive realities, particularly agency and forethought. These nodes often have conflicting vested interests, which may be more short-sighted than future oriented.

Relationships in social networks can consist of shared meanings – especially norms, identities and other ideas – and a vast variety of cultural, economic and political relationships (e.g., employment, citizenship), all of which are not as pronounced or non-existent in less complex human societies and nature. Hence, social network links are more diverse than links in natural systems and enable different kinds of network processes. For example, links between nodes in social networks are not necessarily dependent on physical co-presence, due to technologically enabled connections or the presence of more abstract interrelations such as shared norms, values or interpersonal relationships.

*Network processes*:
Social network dynamics can be of a purely ideational nature (e.g., the subject of the study of opinion and belief dynamics), but also involve material changes (e.g., resource extraction, movement and transformation for economic purpose). Markets are unique social networks, involving both ideational and material network processes. In the Anthropocene, the intensity and speed of socially networked interaction has increased dramatically, largely due to new media, digitalization, more efficient means of transportation, lower travel costs, and overall increased mobility, which is likely to increase spreading rates, while at the same time affecting the stability of the network itself (*72–74*).

Generally, social tipping can either occur on a given network (e.g., through spreading dynamics changing the state of nodes (*75*) or change the network structure itself (see Figure 1). The structural network changes generated by social tipping processes include transitions from centralistic or hierarchical to more polycentric (neuromorphic) structures in urban systems, energy distribution and generation networks (*76*, *77*). Structural changes can manifest on large and small-scale spatial networks across multiple social structure levels. In order to capture these network tipping processes, quantifiers from complex network theory such as modularity, degree distribution, centrality or clustering can be used (*69*).

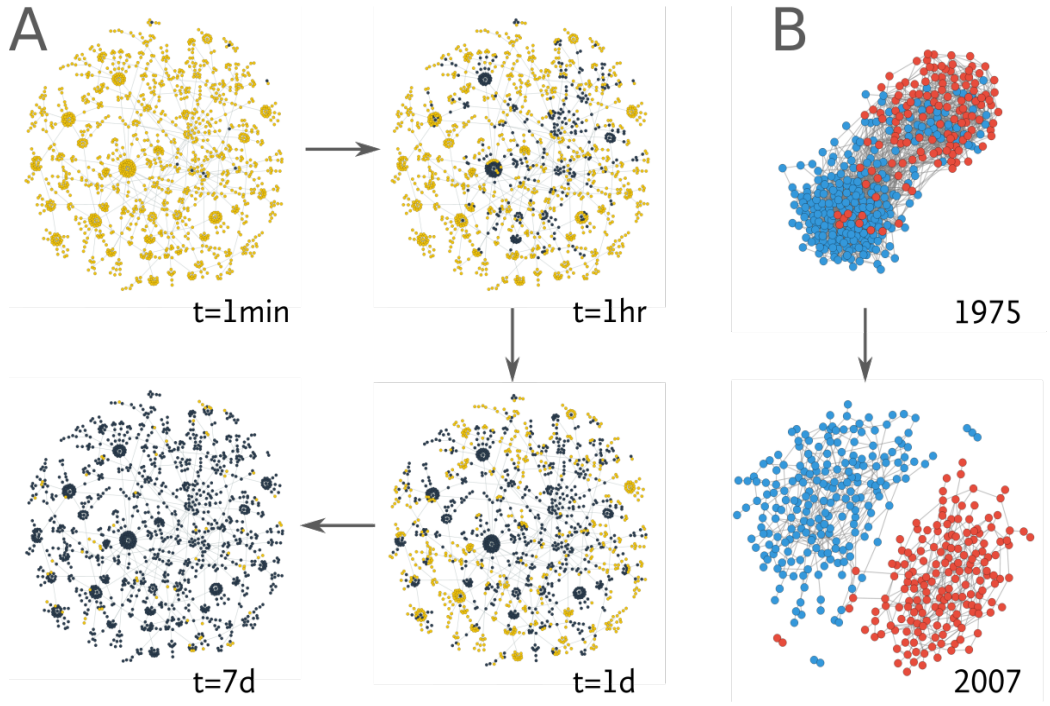


***Figure 1: Two types of social tipping in a complex network.*** *(A) Social tipping can on the one hand be characterized by a contagion process where initially only a few nodes exhibit a certain property that then spreads through a large portion of the network. (B) On the other hand social tipping may also qualitatively alter the entire network structure from, e.g., a state with closely entangled nodes of different states to an almost or full disintegration of the network in smaller disjoint groups. The example in (A) shows the spread of an avatar among users in an online virtual world over the course of one week after it was first introduced by a small number of users* ***(78)****. Nodes represent users and links represent the imitation of the avatar from one user to another. Yellow nodes denote users that have not picked up the avatar, while black nodes indicate those that did. (B) The upper network shows the members of the House of Representatives in the 94th United States Congress (January 3, 1975 to January 3, 1977). Node colors indicate different party membership and links between nodes are drawn if the corresponding members agree on 66% of all votes in the considered two-year period. The lower network shows the same for the 110th United States Congress (January 3, 2007, to January 3, 2009). The transition from a closely entangled to an almost fragmented topology indicates a polarisation between Democratic and Republican Party members over time (16).*

**Temporal and spatial scales:** Scales can differ greatly between social tipping and climate tipping processes and are more ephemeral for social tipping than for climate tipping.

Temporally, tipping in social systems manifests more commonly on the scale of *months to decades*, while for the climate tipping elements range from *years to millennia*. Human actors tend to focus on more short-term consequences or outcomes, as complex issues (such as climate change) with longer timeframes are often harder to assess (*79*). Within social systems, fund manager performance is evaluated quarterly, politicians often think in electoral cycles, business operates with annual or five-year forecasts, while individual practices and dispositions are constantly evaluated and reevaluated (*80–82*). In natural systems, however, it might take decades, centuries or even millennia for outcomes of change processes to become detectable (see Figure 2).

Both social and climate tipping elements can be ordered spatially (*1*, *39*, *83*), although social tipping elements cannot always be precisely located geographically. Social scientists and economists have long grouped systems and processes as existing on the macro-, meso- and micro-levels (or some variation thereof), whereby some social systems (e.g., financial markets, political systems, technologies) consist of interdependent subsystems existing on multiple spatial levels.

Social tipping processes can also display spatial-temporal *ephemerality*. While climate tipping elements have a known spatial extent and dimensionality (with often a comparable extent in latitude and longitude and a generally much smaller extent in altitude) and have persisted in their current stable state for thousands (if not millions) of years, social tipping processes do not have a spatial extent or effective dimensionality that is known ex-ante and they can emerge (move into a critical state) and disappear (move out of a critical state) over time.

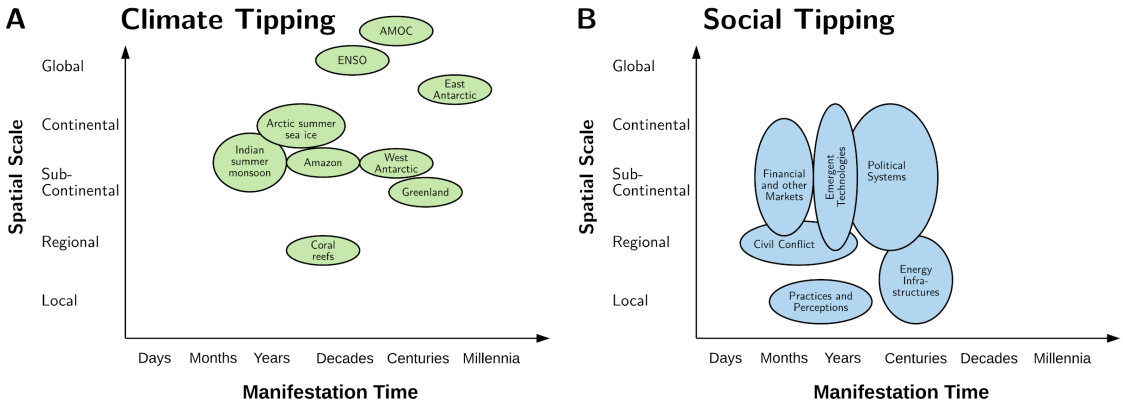


***Figure 2: Examples of spatial and temporal scales for climate and social tipping elements.*** *Example climate tipping elements are broadly compiled from Lenton et al. (1), Levermann et al. (39), and Schellnhuber et al. (83). Social tipping elements are broadly compiled from Kopp et al. (15), Farmer et al. (12), Otto and Donges et al. (9), Hsiang (84), Tabara (11) and Lenton (13).*

**Complexity:** Social tipping processes occur in complex *adaptive* systems (*85–87*) as opposed to the complex but non-adaptive physical climate system. As such they can exhibit comparatively *greater complexity* in the (i) drivers, (ii) mechanisms and (iii) resulting pathways of social tipping processes, as well as the aforementioned ephemerality in their spatial-temporal manifestations, including a potentially fractal and varying dimensionality and a more complex interaction topology (*88*, *89*).

Social tipping processes can rarely be linked to a single common control parameter, such as is the case with global mean temperature in climate tipping dynamics. For most of the climate tipping elements like the ice sheets or the Atlantic meridional overturning circulation, the control variables such as local air temperature, precipitation or ocean heat transport, can often be translated or downscaled into changes in global mean temperature as one common driver (*1*, *38*). However, for social tipping processes, multiple, interrelated factors are often identified as forcing the critical transition. For example, shifts in social norms regarding smoking (*14*) can be linked to several, entwined factors, such as policies, taxation, advertising and communication, social feedbacks (e.g., via normative conformity), or individual preference changes. Centola et al. (*17*) show that tipping in social convention is possibly explained by a single parameter: the size of the committed minority). At larger scales, the collapse of complex civilizations has been linked to multiple interacting causes, and whilst disagreement abounds over the balance of causes in particular cases,

there is general agreement that multiple factors were at play (*33*). This kind of causality – multiple interacting, distributed causes across varying scales – are a key characteristic of complex systems (*90*), contrasting starkly with conventional notions of causality involving bivariate relationships (one cause and one effect).

Further, due to their potential for agency and adaptive plasticity, social systems are open to a larger number of mechanisms that could cause a tipping process and various pathways of change that a tipping process could follow towards a greater number of potentially stable post-tipping states (*91*). Climate tipping processes are often modeled as bi- or multistable, where the directional outcomes of forcing are to some extent known or knowable, e.g., based on paleoclimatic data and process-based Earth system modelling. Given a specific forcing change, one can predict in what state the element will restabilize as well as the "net" effects of the tipping process on larger Earth systems. Based on this understanding, the tipping of climate system elements is generally perceived as undesirable and often as part of pushing the Earth system out of the "safe operating space for humanity" (*92*, *93*).

In contrast, for social systems, it is often unclear what a final stable state of the system will look like, or even whether the changes resulting from a tipping process will be normatively considered "positive" or "negative". As Clark and Harley (*94*) point out, the characteristics of complex-adaptive social systems, including the diversity of actors and elements and the different outcomes generated by local and global interactions, imply that the development pathways of these systems are less predictable. Further, a social tipping process can generate new and destroy existing actor types (e.g., identities, institutions) and their behaviors. Cross-scale dynamics and local differences are important to understand the emergent system structure and change dynamics, but predictive capacities, e.g., regarding the timing of a social tipping point or the boundaries between different stable states, do not yet exist (*94*). Hence, the term 'managing transitions' is less useful than the idea of navigating a transformation pathway.

The political nature of social change processes (*95*) – different actors within a social community pursuing different, sometimes opposing, interests and visions for a reorganization of a social system while bringing to bear different resources and strategies – further exacerbate this situation. Actors can deliberately generate new feedback dynamics that support or slow change, even after a tipping point has been passed, and they can actively work to adjust the direction of change.

### *4.2. Proposed definition of social tipping processes*

From the discussion above, it follows that a definition of social tipping process should take a micro-perspective and incorporate network effects and agency in addition to common tipping characteristics already explored in the review by Milkoreit et al. (*10*). It should also describe the timing aspects sufficiently well to understand possibilities for intervention, similar to what Lenton et al. (*1*) suggested for climate tipping elements. Hence we propose the following definition of the various terms relevant for studying social tipping processes (see Supplementary Material S1 for a more formal mathematical definition suggested for use in simulation modelling and data analysis that is consistent with what we put forward here):

> ***Definitions:*** *A 'social system' can be described as a network consisting of social agents (or subsystems) embedded within a social-ecological 'environment'. Such a social system is called a 'social tipping element' if under certain ('critical') conditions, small changes in the system or its environment can lead to a qualitative (macroscopic) change, typically via cascading network effects such as complex contagion and positive feedback mechanisms. Agency is involved in moving the system towards criticality, creating small disturbances and generating network effects. By this definition, near the critical condition the stability of the*

*social tipping element is low. The resulting change process is called the 'tipping process. The time it takes for this change to manifest is the 'manifestation time'.*[1]

If a tipping element *is* already in a critical condition, where the stability of its current state is low, there may be a time window during which an agential intervention might *prevent* an unwanted tipping process by moving the system into an uncritical condition (see also SI text S1). Alternatively, if a tipping element *is not* already in a critical condition, there may be a time window during which some intervention might move it into a critical condition in order to *bring about* a desired tipping process.

The small change triggering the tipping process could be either (i) a localized modification of the network structure (e.g., a change on the level of single nodes, small groups of nodes or links) or of the state of agents or subsystems, (ii) small changes of macroscopic parameters or properties, or (iii) small external perturbations or shocks. We deliberately do *not* require the trigger to be a *single* driving parameter. This is because we expect that a social tipping process could be triggered by a *combination* of causes rather than a single cause. Furthermore, a social tipping element may be tipped by several *different* combinations of causes. Consequently, for social tipping elements we cannot always expect at this point to identify a common aggregate indicator (such as global mean temperature in the case of climatic tipping elements) and a well-defined 'threshold' for this indicator at which the system will tip (see also the discussion on complexity above).

Note that social tipping as defined here is a unique form of social change, e.g., distinct from climate economic shocks (*15*) and more specific than socio-technical transitions (*96*, *97*). Further, social tipping also denotes a shift to a qualitatively different state, and such, is different from standard business cycles or causes of seasonality. As such, social tipping presents a particular process of social change, where a system undergoes a transformation from one qualitatively different state to another, after being in a more critical state and affected by a potentially small triggering event.

### *4.3. Filtering criteria*

We propose several filtering criteria to focus on social tipping processes (i) that have the potential to be relevant to global sustainability in future Earth system tractories and (ii) where human interventions can occur within a pertinent *intervention time horizon* on the order of decades and will have consequences within a *political/ethical time horizon* on the order of hundreds of years.

(i) Relevance of social tipping for global sustainability

The social tipping process can impact a wide array of social systems, such as technological or energy systems, political mobilization, financial markets and sociocultural norms. We consider social tipping processes to be relevant here that have an impact on the biophysical Earth system or on macro-scale social systems. The qualitative change in a 'relevant' social tipping process significantly affects the future state of the Earth system in the Anthropocene directly or indirectly through interactions with other social tipping processes. Relevance can hence be defined in terms of impacts on biophysical Earth system properties such as global mean temperature, biosphere integrity or other planetary boundary dimensions. For example, tipping dynamics to a political system could result in policy regime changes, affecting substantial reductions in greenhouse gas emissions (*9*, *12*). Furthermore, we consider social tipping processes that have relevant impacts on macro-social systems and can be triggered by changes in the same biophysical Earth systems, for example, mass migration due to climate impacts (*84*, *98*).

[1] This is analogous to the 'transition time' in Lenton et al. (*1*) . We avoid the term 'tipping *point*' in this definition since some of the literature uses it to refer to a point in time while some of the literature uses it to refer to a certain state of the system or its environment.

(ii) Intervention and ethical time horizons

We are interested in potential social tipping processes in which humans have the agency to substantively intervene. For example, such interventions could be via technological or physical capacities of agential or structural actors. This therefore places emphasis on human intervention, such as decreasing the likelihood of extreme weather events via mitigation efforts, or triggering socio-technological changes towards decarbonization. We define intervention and ethical time horizons as follows:

*Intervention time horizon*
Human agency interferes with a social tipping element, such that decisions and actions taken between now and an 'intervention time horizon' could influence whether (or not) the system tips. We suggest to consider only social tipping processes with an intervention time on the order of 10 years (*9*), which arguably presents a practical limit of human forethought (*99*) and of future-oriented political agency. For example, international governance efforts for global sustainability challenges, such as the ozone regime or the Sustainable Development Goals, tend to work with similar time horizons. Similarly, social tipping processes for rapid decarbonization to meet the Paris climate agreement would have to be triggered within the next few years (*9*), with ambitious emissions reduction roadmaps aiming for peak greenhouse gas emissions in 2020 (*29*, *100*). The intervention time horizon is analogous to the 'political time horizon' defined for climate tipping elements in Lenton et al. (*1*).

*Ethical time horizon*
The time to observe these relevant consequences should lie within an 'ethical time horizon'. This recognizes that consequences manifesting too far in the future are not relevant to the current discourse on how contemporary societies impact Earth systems. Such an ethical time horizon could consider only social tipping processes which can have relevant *consequences within the next centuries* at most, corresponding to an upper life expectancy of the next generations of children born.

### *4.4. Example of a potential social tipping process: European Climate Change Policy Dynamics Europe and FridaysForFuture*

Currently, international climate policies, including those of the European Union (EU) are insufficient to meet the +1.5°C or +2°C goals of the Paris Agreement (*101*). While European policy makers presume to lead global mitigation efforts and characterize their actions as ambitious (*102*, *103*), actual policy measures and proposals have been lagging behind this aspiration (*104*). EU countries emit about a tenth of the world's emissions, and a policy change towards more rapid decarbonization would not only have significant direct impacts on the climate system, but likely have indirect effects on the policies of other major emitters. But what kinds of sociopolitical processes can lead to these necessary changes? Could such changes result from social tipping dynamics?

Public opinion is a crucial factor in policy formation, where the public can be understood as a "thermostat" signalling what is politically feasible (*105*, *106*). Shifts in public opinion can punctuate previously stable and 'sticky' institutions, leading to policy change (*107*). Increased activism and public concern regarding climate change can generate new coalitions, or shift the priorities of existing ones (*108*, *109*). Here we examine the European political system as an example of and how social tipping processes could be triggered as a result of large-scale public activism and social movements.

The European political system is composed of networks of agents (i.e., activists, decision-makers and organizations) with a range of social and political ties and is structured in nested and overlapping subsystems (i.e., national group, transnational political coalitions). Viewed through the lens of social tipping, European political dynamics present a 'social system', embedded within the broader international political and climate change governance community 'environment'. Driven

by the *FridaysForFuture* movement (*16*) (among other things), a groundswell of bottom-up support for more proactive climate policies has recently developed among European citizens, resulting in routine mass demonstrations and historical wins for Green parties in the 2019 European Parliamentary Elections, as well as in federal elections in Austria, Belgium and Switzerland. The European political system could be moving towards a critical 'state', creating the conditions for a tipping process towards radical policy change, bringing European climate policy in line with the Paris Agreement. Accordingly, the European political system could constitute a potential 'social tipping element', where as it nears critical conditions, a small change to the system or its broader environment could lead to large-scale macroscopic changes, affected by cascading network dynamics and positive feedback mechanisms. Such transformations could involve establishing more aggressive mitigation strategies that connect goals (such as remaining below +2°C, 50% emissions reductions by 2030, zero carbon emissions by 2050) with measures and pathways that have a reasonable chance to achieve them (i.e., investment in negative emission technologies, increased carbon taxation policies etc.).

The *FridaysForFuture* movement has been pushing the European political system towards criticality, where it becomes more likely that the system will be propelled into a qualitatively different state. The movement was set off and inspired by a single Swedish high school student choosing to protest on the steps of the Riksdag for meaningful climate action. Greta Thunberg's protest quickly spread through the European social-political networks until more than a million students have been participating in weekly protests. This growing bottom-up pressure on the European climate policy-makers (*16*, *110*) has created an opening for significant policy change.

The European political system consists of embedded subsystems at multiple scales. At the national scale, for example, the German socio-political system responded strongly to the activities of the *FridaysForFuture* movement. Polling throughout 2019 in Germany suggested that the environment was the most important public policy challenge, ahead of other issues, such as the migration and financial crises. Drawing upon survey data collected monthly by the Politbarometer, 40–60% of Germans responded that the environment was an important problem in the Fall of 2019, a rapid increase from roughly 5% in the Fall of 2018 (Figure 3, Panels A and B). Since 2000, rarely more than 10% of Germans have viewed the environment as an important problem – a time period which includes the emergence of other large environmental movements in Germany, such as protests against nuclear energy in response to Fukushima. The specific upward shift in Germans viewing the environment as an important problem appears to coincide with the large-scale protests organized by *FridaysForFuture* in March, May and September of 2019.

Similarly, several national Western European Green Parties received historically strong electoral support in the May 2019 European Parliamentary Elections (such as in Belgium, Germany, Finland, France and Luxembourg). This increased support is also reflected in polling data in Germany, where the Green Party has been effectively equal with the conservative party as the preferred political party of German voters in the latter half of 2019 (Figure 3, Panels C and D). Subsequently, Germany introduced its first ever federal climate change laws, mandating that the country meet its 2030 goals (a ~55% reduction in GHG emissions) and establishing pathways to carbon neutrality by 2050. Currently, only a limited set of countries have enacted national climate change laws, and Germany is one of the largest and most diverse economies to propose such actions. This presents the possibility for policy diffusion and transfer to other states (*111*), particularly considering the influential role Germany plays within the European Union. Climate policy entrepreneurs could build upon momentum to further capitalize on windows of opportunity, pushing climate change proposals prominently into national and supra-national governmental agendas before the ephemeral moment passes (*112*).

The 2020 COVID-19 pandemic has placed new priorities on the policy agenda, also reflected in issue salience of climate change (see also Fig. S1 in Supplementary Materials). As political and behavioral responses to COVID-19 have led already to a significant temporary reduction in greenhouse gas emissions (*113*), this shock could be further leveraged to reinforce climate action –

future economic recovery packages should set European economies on a pathway towards carbon-neutrality, rather than return to the old normal (*114*, *115*). Drawing from this social tipping framework, the European political system may remain near a critical state. It remains unclear whether the COVID-19 shock has supplanted climate change, or whether both remain on the political agenda. For example, discussions of a "Green New Deal" remain at the core of COVID-19 economic recovery plans within the European Union.

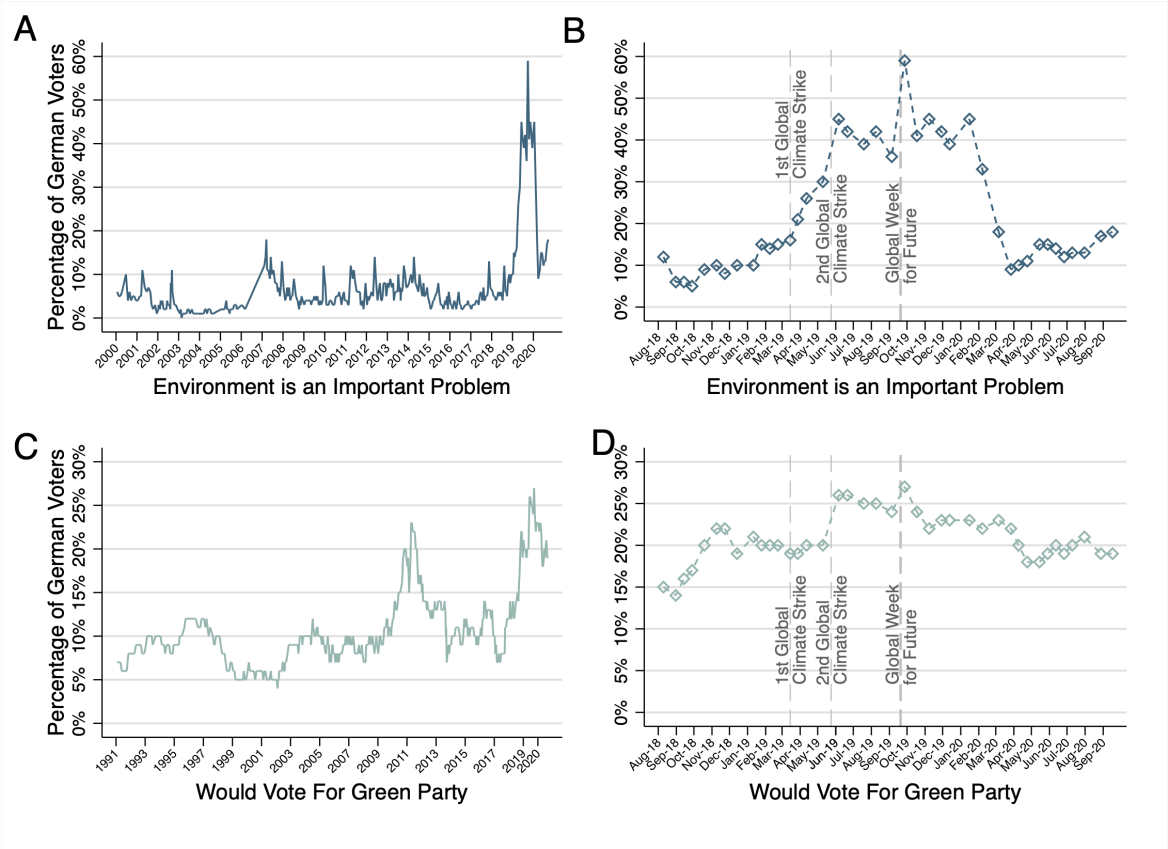


***Figure 3: Environment as an issue and willingness to vote for the Green Party in Germany.*** *Percentages of potential German voters that list the environment as an important issue for the country and willingness to vote for the Green Party (Bündnis 90/Die Grünen) if the election were to be held "today". Panels (A) and (C) present monthly survey data from 2000 to September 2020 Panels (B) and (D) display monthly surveys from August 2018 – September 2020, showing the change since the beginning of Greta Thunberg's protest actions. Dotted grey vertical lines display days of global strikes organized by FridaysForFuture in March, May and September 2019. Data is collected by Forschungsgruppe Wahlen: Politbarometer .*

*Implications for criticality*

The sociopolitical dynamics have likely moved the Germany political subsystem further towards criticality, but it remains largely unknown whether this will result in tipping towards a qualitatively different state, in Germany or in the broader European political system. Rather, these judgements can *likely only be made in hindsight*, observing whether the system remained stable, moved towards criticality or experienced tipping dynamics. Such an analysis in line with the proposed framework requires specific process tracing, identifying the key moments, actors, networks, mechanisms affecting criticality, the triggering event (threshold), and the positive feedback dynamics propelling the system towards qualitative changes. Much attention is often paid to the specific triggering event, but it is rarely one single actor or action which accounts for the entirety of the tipping process.

Rather a full account needs to be made of all of the previous and related processes that have further placed the system towards criticality, allowing for such changes to become more likely. Accordingly, for a tipping process to occur at the scale of the entire European political system, moving it into a state of decarbonization that is aligned with the Paris Agreement, a series of additional social movements and protests, or other shifts within the system or the environment, may be required.

While we identify the role of *FridaysForFuture* in creating critical conditions, or potentially triggering the social transformations required for global sustainability, recent literature has identified further tipping candidates which could have generally "positive" effects on global sustainability. For example, divestment and reinvestment present candidates for rapid decarbonization and processes to achieve climate targets (*9*, *12*). In this case, intervention times range from years to decades, depending on the social structure level (*9*). Previous studies note that the adoption of technologies and behaviors such as rapid uptake of autonomously driven electric vehicles (if socially licensed), rapid change in dietary preferences reducing meat consumption and associated land-use and climate impacts can follow an epidemic-type model of diffusing across social networks (*13*, *15*).

Alternatively, social tipping processes can lead to states of criticality with less desirable outcomes: Recently it has been shown that climate change has contributed to the emergence of infections carried by mosquitoes, like dengue fever or Zika, which could be accelerated further by increased mobility, e.g., through denser air traffic networks (*75*). The thermal minimum for transmission of the Zika virus could in fact give rise to a threshold behaviour (*116*). Changes to the local environment may enact "push" factors, resulting in large scale migrations (*117*, *118*). Further, increased global mean temperature has been suggested to increase the likelihood of civil conflicts (*84*).

These social tipping processes are of great interest to policy makers, as it is desirable to potentially trigger or facilitate "positive" tipping (*11*, *13*), while at the same time, mitigating the effects of potential "negative" outcomes.

## 5. Discussion

Social tipping processes have been recently recognized as potentially key pathways for generating the necessary shifts for sustainability. Drawing upon this emerging field, this paper develops a framework for characterizing social tipping processes. We find that mechanisms underlying social tipping processes are more likely to exhibit the unique characteristics of agency, social-institutional and cultural network structures, they occur across different spatial and temporal scales to climate tipping, and the nature of tipping can be more complex. Social tipping processes thus present qualitatively different characteristics to those shared by climate tipping processes.

Accordingly, this paper develops a common framework for the unique characteristics of social tipping processes. We identify social tipping as a process, resultant of a complex system of drivers, resulting in shifting a system into a more (or less) critical state. It can thus serve to structure and inform future data analysis and process-based modelling exercises (*118*, *119*).

Even so, while there is an emerging focus on social tipping dynamics (*9–13*), there remains great difficulty in pinpointing tipping events and generalizing the emerging dynamics. Drawing from natural tipping dynamics**,** previous work on social tipping has often focused on identifying specific trigger events or critical thresholds in macroscopic system variables in analogy to identifying for instance critical temperature thresholds in the context of climate tipping (*10*). In natural systems the underlying dynamics are more deterministic and often can be directly observed, allowing for the identification of specific thresholds and events. While social systems comprise a much more open and complex system, one that is constantly adapting and where dynamics are often incredibly

complex, interrelated and cannot be directly observed. Accordingly, one could observe the same event across ten similar social systems, and could potentially observe ten unique outcomes. As such, anticipating a specific trigger, making causal inferences, or having generalizability in expected effects are all greatly limited within social systems. Further, social tipping points are sometimes also understood as a point in time, rather than a point in a complex parameter space. Such an approach makes it difficult to identify social tipping processes, as they often do not contain easily observable macroscopic thresholds nor temporal markers for change.

Rather, a complex adaptive systems viewpoint is required, understanding the multitude of interrelated processes and social structures driving change, and not focusing on a single trigger or threshold. Accordingly, our framework proposed here focuses on identifying the processes and mechanisms of such change, and not a single triggering event, where the interplay of micro-level changes embedded within adaptive structural conditions can affect systemic changes.

The notion of a critical state is central within our framework. Changing conditions to the system's environment can cause it to enter more (or less) critical states, such that a single, or multiplicative action, can effect a systemic change. It is these changing conditions, and specifically the processes and dynamics underlying them, that are of analytical importance. Drawing upon the analogy of a tipping coal wagon (*15*), it is not the single, specific piece of coal that caused the wagon to tip, but rather the processes by which the wagon was filled with enough coal that any single piece (placed at a number of different locales) could cause such tipping. Accordingly, the specific triggering event of a social tipping process could be somewhat random or arbitrary, as the conditions are critical enough such that any event with enough magnitude could have triggered these dynamics.

It is therefore key to focus on the processes and mechanisms underlying the nature of such critical states which allow some trigger event to cause contagion dynamics. From social network models, we can deduce which kind of structural features make a system less resilient and thus more prone to social tipping (*119*). One example is polarization, where social network models and social media-based data analyses have shown that in polarized states with nearly disconnected network communities which in themselves are highly connected, contagion processes are more likely to occur (*120–122*). Behavioral experiments and corresponding conceptual modelling approaches suggest that minority groups can initiate social change dynamics in the emergence of new social conventions (*17*, *119*). Furthermore, a rich social science literature has noted an array of factors (i.e. political institutions, technological or behavioral adaptation, environmental, normative and attitudinal) effective in shifting the social conditions surrounding climate change (*14*). A better understanding of critical states as demanded by our framework may help to identify early warning signals that could possibly indicate that a social-ecological system is close to a critical state in specific situations (*30*, *123*).

Social tipping processes present a specific type of social change – characteristized by non-linear shifting states driving by positive feedbacks – which is similar to, but conceptually distinct from, other forms of social change. Similar to how we explore the differences between natural and social tipping processes, further research should engage with social tipping in comparison to other forms of social change (such as historical institutionalist perspectives, social movements, policy feedbacks, complex systems). One of the greatest challenges lies in dealing with multiple, entangled drivers of tipping processes on different scales – temporal, spatial or social structural levels – and different levels of agency and heterogeneous agents and subsystems. In order to further understand the dynamics arising from these various levels of agency, it is crucial to identify examples from different subfields (economics, political science, demographics). A key current limitation in applying our framework is finding and operationalizing empirical data describing actual spreading processes on networks across these different levels, particularly compared to macro-economic data and public opinion polls (*124*), even though first steps in this direction are being made (*125*, *126*). Particularly data on the social structures and networks is notoriously difficult to access. While there have been advances in developing modeling frameworks (*119*, *127*) to simulate social tipping dynamics, linking these theoretical modelling to empirical data and behavioral experiments requires

more attention. Even if predictive modeling (i.e., the kind of deterministic, time-forward modeling we know from Earth System Models for instance) of such social dynamics in the sense of inferring time trajectories is very difficult or even conceptually unfeasible, such process-based modelling of social tipping dynamics can be very crucial to understand the nature of critical states also in real-world social situations. Lastly, we focus here specifically on social tipping processes relevant for mitigating climate change, or sustainability more broadly, fitting within the previous literature. But, such a framework for social tipping dynamics is generalizable to other areas of study and social phenomena (such as the 2020 rapid social movements and public opinion dynamics surrounding racial inequality in the United States).

While we explore one example of social tipping in detail, further inquiry is required to test the distinctiveness of social tipping processes, as well as the utility of the proposed definition to other social tipping processes. Systematizing the types of social tipping processes, and exemplary case studies, would help to further illustrate these forms of change. Research is also warranted into establishing typical timescales of social tipping; understanding how network structures affect social tipping dynamics; identifying typical network structures of systems entering critical states; discerning the temporal aspects of how effects travel through different social network structures; and gaining a better understanding of the origin of spreading processes. Data acquisition, analysis and process-based modelling could all play a role in this research agenda. A wealth of social media data is available to study potential social tipping processes. However, this kind of data has mostly yet to be adopted within the context of Earth System analysis and tipping dynamics.

Social tipping processes could be decisive for the future of the Earth System in the Anthropocene: some rapid shifts in social systems are, in fact, necessary to meet the targets of the Paris Agreement and the Sustainable Development Goals (*8*). While we focus here on processes relevant for future trajectories of the Earth system, we suggest that further analysis could use or adapt our definition to characterize other types of general social tipping processes (i.e. revolutions or rapid transformations). We also recognize that tipping processes within ecosystems present an interesting intermediary case between social and physical climate tipping as they typically incorporate characteristics from both realms. They are also crucial in determining future trajectories of the Earth system (see preliminary discussion in the SI). Understanding, identifying and potentially instigating some social tipping processes is highly relevant for the future of the Anthropocene, particularly with regard to the potential role in triggering rapid transformative change needed for effective Earth system stewardship (*9*, *11–13*).

**References and Notes**


1. T. M. Lenton, H. Held, E. Kriegler, J. W. Hall, W. Lucht, S. Rahmstorf, H. J. Schellnhuber, Tipping elements in the Earth's climate system. *Proc. Natl. Acad. Sci.* **105**, 1786–1793 (2008).
2. L. Favier, G. Durand, S. L. Cornford, G. H. Gudmundsson, O. Gagliardini, F. Gillet-Chaulet, T. Zwinger, A. J. Payne, A. M. Le Brocq, Retreat of Pine Island Glacier controlled by marine ice-sheet instability. *Nat. Clim. Change*. **4**, 117–121 (2014).
3. I. Joughin, B. E. Smith, B. Medley, Marine Ice Sheet Collapse Potentially Under Way for the Thwaites Glacier Basin, West Antarctica. *Science*. **344**, 735–738 (2014).
4. I. Joughin, R. B. Alley, Stability of the West Antarctic ice sheet in a warming world. *Nat. Geosci.* **4**, 506–513 (2011).
5. S. Drijfhout, S. Bathiany, C. Beaulieu, V. Brovkin, M. Claussen, C. Huntingford, M. Scheffer, G. Sgubin, D. Swingedouw, Catalogue of abrupt shifts in Intergovernmental Panel on Climate Change climate models. *Proc. Natl. Acad. Sci.* **112**, E5777–E5786 (2015).
6. K. Frieler, M. Meinshausen, A. Golly, M. Mengel, K. Lebek, S. D. Donner, O. Hoegh-Guldberg, Limiting global warming to 2 °C is unlikely to save most coral reefs. *Nat. Clim. Change*. **3**, 165–170 (2013).
7. T. P. Hughes, M. L. Barnes, D. R. Bellwood, J. E. Cinner, G. S. Cumming, J. B. Jackson, J. Kleypas, I. A. Van De Leemput, J. M. Lough, T. H. Morrison, others, Coral reefs in the Anthropocene. *Nature*. **546**, 82–90 (2017).
8. W. Steffen, J. Rockström, K. Richardson, T. M. Lenton, C. Folke, D. Liverman, C. P. Summerhayes, A. D. Barnosky, S. E. Cornell, M. Crucifix, J. F. Donges, I. Fetzer, S. J. Lade, M. Scheffer, R. Winkelmann, H. J.

Schellnhuber, Trajectories of the Earth System in the Anthropocene. *Proc. Natl. Acad. Sci.* **115**, 8252–8259 (2018).
10. M. Milkoreit, J. Hodbod, J. Baggio, K. Benessaiah, R. Calderón-Contreras, J. F. Donges, J.-D. Mathias, J. C. Rocha, M. Schoon, S. E. Werners, Defining tipping points for social-ecological systems scholarship—an interdisciplinary literature review. *Environ. Res. Lett.* **13**, 033005 (2018).
11. J. D. Tàbara, N. Frantzeskaki, K. Hölscher, S. Pedde, K. Kok, F. Lamperti, J. H. Christensen, J. Jäger, P. Berry, Positive tipping points in a rapidly warming world. *Curr. Opin. Environ. Sustain.* **31**, 120–129 (2018).
12. J. D. Farmer, C. Hepburn, M. C. Ives, T. Hale, T. Wetzer, P. Mealy, R. Rafaty, S. Srivastav, R. Way, Sensitive intervention points in the post-carbon transition. *Science*. **364**, 132–134 (2019).
13. T. M. Lenton, Tipping positive change. *Philos. Trans. R. Soc. B Biol. Sci.* **375**, 20190123 (2020).
14. K. Nyborg, J. M. Anderies, A. Dannenberg, T. Lindahl, C. Schill, M. Schlüter, W. N. Adger, K. J. Arrow, S. Barrett, S. Carpenter, others, Social norms as solutions. *Science*. **354**, 42–43 (2016).
15. R. E. Kopp, R. L. Shwom, G. Wagner, J. Yuan, Tipping elements and climate--economic shocks: Pathways toward integrated assessment. *Earths Future*. **4**, 346–372 (2016).
16. G. Hagedorn, P. Kalmus, M. Mann, S. Vicca, J. V. den Berge, J.-P. van Ypersele, D. Bourg, J. Rotmans, R. Kaaronen, S. Rahmstorf, H. Kromp-Kolb, G. Kirchengast, R. Knutti, S. I. Seneviratne, P. Thalmann, R. Cretney, A. Green, K. Anderson, M. Hedberg, D. Nilsson, A. Kuttner, K. Hayhoe, Concerns of young protesters are justified. *Science*. **364**, 139–140 (2019).
17. D. Centola, J. Becker, D. Brackbill, A. Baronchelli, Experimental evidence for tipping points in social convention. *Science*. **360**, 1116–1119 (2018).
18. J. Hoadley, A tilting water meter for purposes of experiment. *J. Frankl. Inst.* **117**, 273–278 (1884).
19. H. Poincaré, Sur l'équilibre d'une masse fluide animée d'un mouvement de rotation. *Acta Math.* **7**, 259–380 (1885).
20. T. C. Schelling, Dynamic models of segregation. *J. Math. Sociol.* **1**, 143–186 (1971).
21. M. Grodzins, Metropolitan segregation. *Sci. Am.* **197**, 33–41 (1957).
22. M. Granovetter, Threshold models of collective behavior. *Am. J. Sociol.* **83**, 1420–1443 (1978).
23. T. Kuran, Sparks and prairie fires: A theory of unanticipated political revolution. *Public Choice*. **61**, 41–74 (1989).
24. S. J. Gould, N. Eldredge, Punctuated equilibrium comes of age. *Nature*. **366**, 223 (1993).
25. M. Gladwell, *The tipping point: How little things can make a big difference* (Little, Brown and Company, Boston, MA, 2000).
26. T. Homer-Dixon, B. Walker, R. Biggs, A.-S. Crepin, C. Folke, E. F. Lambin, G. Peterson, J. Rockstrom, M. Scheffer, W. Steffen, M. Troell, Synchronous failure: the emerging causal architecture of global crisis. *Ecol. Soc.* (2015), doi:10.5751/ES-07681-200306.
27. S. Battiston, J. D. Farmer, A. Flache, D. Garlaschelli, A. G. Haldane, H. Heesterbeek, C. Hommes, C. Jaeger, R. May, M. Scheffer, Complexity theory and financial regulation. *Science*. **351**, 818–819 (2016).
28. K. Nyborg, M. Rege, On social norms: the evolution of considerate smoking behavior. *J. Econ. Behav. Organ.* **52**, 323–340 (2003).
29. J. Rockström, O. Gaffney, J. Rogelj, M. Meinshausen, N. Nakicenovic, H. J. Schellnhuber, A roadmap for rapid decarbonization. *Science*. **355**, 1269–1271 (2017).
30. M. Scheffer, *Critical transitions in nature and society* (Princeton University Press, 2009), vol. 16.
31. C. Folke, S. Carpenter, B. Walker, M. Scheffer, T. Elmqvist, L. Gunderson, C. S. Holling, Regime Shifts, Resilience, and Biodiversity in Ecosystem Management. *Annu. Rev. Ecol. Evol. Syst.* **35**, 557–581 (2004).
32. B. Walker, J. Meyers, Thresholds in Ecological and Social–Ecological Systems: a Developing Database. *Ecol. Soc.* **9** (2004), doi:10.5751/ES-00664-090203.
33. J. Tainter, *The collapse of complex societies* (Cambridge university press, 1990).
34. K. W. Butzer, Collapse, environment, and society. *Proc. Natl. Acad. Sci.* **109**, 3632–3639 (2012).
35. M. A. Janssen, T. A. Kohler, M. Scheffer, Sunk-cost effects and vulnerability to collapse in ancient societies. *Curr. Anthropol.* **44**, 722–728 (2003).
36. G. S. Cumming, G. D. Peterson, Unifying research on social--ecological resilience and collapse. *Trends Ecol. Evol.* **32**, 695–713 (2017).
37. J. C. Rocha, G. Peterson, Ö. Bodin, S. Levin, Cascading regime shifts within and across scales. *Science*. **362**, 1379–1383 (2018).
38. H. J. Schellnhuber, Tipping elements in the Earth System. *Proc. Natl. Acad. Sci.* **106**, 20561–20563 (2009).
39. A. Levermann, J. L. Bamber, S. Drijfhout, A. Ganopolski, W. Haeberli, N. R. Harris, M. Huss, K. Krüger, T. M. Lenton, R. W. Lindsay, others, Potential climatic transitions with profound impact on Europe. *Clim. Change*. **110**, 845–878 (2012).
40. C. A. Nobre, L. D. S. Borma, 'Tipping points' for the Amazon forest. *Curr. Opin. Environ. Sustain.* **1**, 28–36 (2009).
41. C. A. Nobre, G. Sampaio, L. S. Borma, J. C. Castilla-Rubio, J. S. Silva, M. Cardoso, Land-use and climate change risks in the Amazon and the need of a novel sustainable development paradigm. *Proc. Natl. Acad. Sci.*

**113**, 10759–10768 (2016).
42. M. Hirota, M. Holmgren, E. H. Van Nes, M. Scheffer, Global resilience of tropical forest and savanna to critical transitions. *Science*. **334**, 232–235 (2011).
43. A. Robinson, R. Calov, A. Ganopolski, Multistability and critical thresholds of the Greenland ice sheet. *Nat. Clim. Change*. **2**, 429 (2012).
44. S. Rahmstorf, Ocean circulation and climate during the past 120,000 years. *Nature*. **419**, 207 (2002).
45. L. Caesar, S. Rahmstorf, A. Robinson, G. Feulner, V. Saba, Observed fingerprint of a weakening Atlantic Ocean overturning circulation. *Nature*. **556**, 191 (2018).
46. Y. Cai, T. M. Lenton, T. S. Lontzek, Risk of multiple interacting tipping points should encourage rapid CO 2 emission reduction. *Nat. Clim. Change*. **6**, 520 (2016).
47. F. Westley, P. Olsson, C. Folke, T. Homer-Dixon, H. Vredenburg, D. Loorbach, J. Thompson, M. Nilsson, E. Lambin, J. Sendzimir, others, Tipping toward sustainability: emerging pathways of transformation. *Ambio*. **40**, 762 (2011).
48. M.-L. Moore, O. Tjornbo, E. Enfors, C. Knapp, J. Hodbod, J. A. Baggio, A. Norström, P. Olsson, D. Biggs, Studying the complexity of change: toward an analytical framework for understanding deliberate social-ecological transformations. *Ecol. Soc.* **19** (2014) (available at https://www.jstor.org/stable/26269689).
49. G. Feola, Societal transformation in response to global environmental change: A review of emerging concepts. *Ambio*. **44**, 376–390 (2015).
50. B. Ayyub, *Elicitation of Expert Opinions for Uncertainty and Risks* (CRC Press, Boca Raton, Florida, 2001).
51. L. Nash, The Agency of Nature or the Nature of Agency? *Environ. Hist.* **10**, 67–69 (2005).
52. B. Latour, *Reassembling the Social: An Introduction to Actor-Network-Theory* (Oxford University Press, Oxford, UK, 2005).
53. European Environmental Agency, "Late lessons from early warnings:the precautionary principle 1896–2000," *Environmental Issue Report* (22, European Environmental Agency, Copenhagen, 2001).
54. European Environmental Agency, "Late lessons from early warnings: Science, precaution, innovation," *EEA Report* (1/2013, European Environmental Agency, Copenhagen, 2013).
55. A. Bandura, Toward a Psychology of Human Agency. *Perspect. Psychol. Sci.* **1**, 164–180 (2006).
56. A. Bandura, Human agency in social cognitive theory. *Am. Psychol.* **44**, 1175 (1989).
57. T. M. Lenton, B. Latour, Gaia 2.0. *Science*. **361**, 1066–1068 (2018).
58. E. Boyd, B. Nykvist, S. Borgström, I. A. Stacewicz, Anticipatory governance for social-ecological resilience. *AMBIO*. **44**, 149–161 (2015).
59. A. Hebinck, J. Vervoort, P. Hebinck, L. Rutting, F. Galli, Imagining transformative futures: participatory foresight for food systems change. *Ecol. Soc.* **23** (2018), doi:10.5751/ES-10054-230216.
60. L. Pereira, T. Hichert, M. Hamann, R. Preiser, R. Biggs, *Ecol. Soc.*, in press, doi:10.5751/ES-09907-230119.
61. T. Urdan, F. Pajares, *Selfefficacy beliefs of adolescents* (IAP, 2006).
62. M. Milkoreit, *Mindmade politics: The cognitive roots of international climate governance* (MIT Press, 2017).
63. M. Milkoreit, in *Reimagining Climate Change*, P. Wapner, H. Elver, Eds. (Routledge, New York, 2016), pp. 171–191.
64. A. Giddens, *The consequences of modernity* (Stanford University Press, Stanford, CA, 1990).
65. P. Bourdieu, L. J. Wacquant, *An invitation to reflexive sociology* (University of Chicago press, 1992).
66. R. A. Watson, E. Szathmáry, How Can Evolution Learn? *Trends Ecol. Evol.* **31**, 147–157 (2016).
67. C. Knappett, L. Malafouris, *Material Agency: Towards a Non-Anthropocentric Approach* (Springer, New York, 2008).
68. L. A. Brown, W. H. Walker, Prologue: Archaeology, Animism and Non-Human Agents. *J. Archaeol. Method Theory*. **15**, 297–299 (2008).
69. M. Newman, *Networks* (Oxford University Press, Oxford, UK, 2nd Edition., 2018).
70. E. Jablonka, M. Lamb, *Inheritance Systems and the Extended Synthesis* (Cambridge University Press, New York, 2020).
71. C. Castellano, S. Fortunato, V. Loreto, Statistical physics of social dynamics. *Rev. Mod. Phys.* **81**, 591–646 (2009).
72. M. Castells, G. Cardoso, others, *The network society: From knowledge to policy* (Johns Hopkins Center for Transatlantic Relations Washington, DC, 2006).
73. A. Giddens, *Runaway world: How globalization is reshaping our lives* (Taylor & Francis, 2003).
74. D. Harvey, *The condition of postmodernity* (Blackwell Oxford, 1989), vol. 14.
75. D. Brockmann, D. Helbing, The Hidden Geometry of Complex, Network-Driven Contagion Phenomena. *Science*. **342**, 1337–1342 (2013).
76. E. Ostrom, Polycentric systems for coping with collective action and global environmental change. *Glob. Environ. Change*. **20**, 550–557 (2010).
77. F. Kraas, C. Leggewie, P. Lemke, E. Matthies, D. Messner, N. Nakicenovic, H. J. Schellnhuber, S. Schlacke, U. Schneidewind, C. Brandi, C. Butsch, S. Busch, F. Hanusch, R. Haum, M. Jaeger-Erben, M. Köster, M. Kroll, C. Loose, A. Ley, D. Martens, I. Paulini, B. Pilardeaux, T. Schlüter, G. Schöneberg, A. Schulz, A.

Schwachula, B. Soete, B. Stephan, J. Sutter, K. Vinke, M. Wanner, *Humanity on the move: Unlocking the transformative power of cities* (WBGU - German Advisory Council on Global Change, Berlin, 2016; http://www.wbgu.de/en/flagship-reports/fr-2016-urbanization/).
78. J. Jankowski, R. Michalski, P. Bródka, A multilayer network dataset of interaction and influence spreading in a virtual world. *Sci. Data*. **4**, 170144 (2017).
79. D. M. Kahan, 'Ordinary science intelligence': a science-comprehension measure for study of risk and science communication, with notes on evolution and climate change. *J. Risk Res.* **20**, 995–1016 (2017).
80. W. D. Nordhaus, The Political Business Cycle. *Rev. Econ. Stud.* **42**, 169–190 (1975).
81. E. Dubois, Political business cycles 40 years after Nordhaus. *Public Choice*. **166**, 235–259 (2016).
82. A. Alesina, G. D. Cohen, N. Roubini, Electoral business cycle in industrial democracies. *Eur. J. Polit. Econ.* **9**, 1–23 (1993).
83. H. J. Schellnhuber, S. Rahmstorf, R. Winkelmann, Why the right climate target was agreed in Paris. *Nat. Clim. Change*. **6**, 649 (2016).
84. S. M. Hsiang, M. Burke, E. Miguel, Quantifying the Influence of Climate on Human Conflict. *Science*. **341** (2013), doi:10.1126/science.1235367.
85. S. Levin, T. Xepapadeas, A.-S. Crépin, J. Norberg, A. de Zeeuw, C. Folke, T. Hughes, K. Arrow, S. Barrett, G. Daily, P. Ehrlich, N. Kautsky, K.-G. Mäler, S. Polasky, M. Troell, J. R. Vincent, B. Walker, Social-ecological systems as complex adaptive systems: modeling and policy implications. *Environ. Dev. Econ.* **18**, 111–132 (2013).
86. C. S. Holling, Understanding the Complexity of Economic, Ecological, and Social Systems. *Ecosystems*. **4**, 390–405 (2001).
87. J. Miller, S. Page, *Adaptive Systems: An Introduction to Computational Models of Social Life* (Princeton University Press, Princeton, NJ, 2007).
88. C. Song, S. Havlin, H. A. Makse, Self-similarity of complex networks. *Nature*. **433**, 392–395 (2005).
89. C. Song, S. Havlin, H. A. Makse, Origins of fractality in the growth of complex networks. *Nat. Phys.* **2**, 275–281 (2006).
90. S. Thurner, R. Hanel, P. Klimek, *Introduction to the theory of complex system* (Oxford University Press, New York, 2018).
91. J.-D. Mathias, J. M. Anderies, J. Baggio, J. Hodbod, S. Huet, M. A. Janssen, M. Milkoreit, M. Schoon, Exploring non-linear transition pathways in social-ecological systems. *Sci. Rep.* **10**, 1–12 (2020).
92. J. Rockström, W. Steffen, K. Noone, Å. Persson, F. S. Chapin III, E. F. Lambin, T. M. Lenton, M. Scheffer, C. Folke, H. J. Schellnhuber, others, A safe operating space for humanity. *nature*. **461**, 472 (2009).
93. W. Steffen, K. Richardson, J. Rockström, S. E. Cornell, I. Fetzer, E. M. Bennett, R. Biggs, S. R. Carpenter, W. de Vries, C. A. de Wit, C. Folke, D. Gerten, J. Heinke, G. M. Mace, L. M. Persson, V. Ramanathan, B. Reyers, S. Sörlin, Planetary boundaries: Guiding human development on a changing planet. *Science*. **347**, 1259855 (2015).
94. W. C. Clark, A. G. Harley, "Sustainability Science: Towards a Synthesis," *Sustainability Science Program* (Working Paper 2019-01, John F. Kennedy School of Government, Harvard University, Cambridge, MA).
95. J. Patterson, K. Schulz, J. Vervoort, S. van der Hel, O. Widerberg, C. Adler, M. Hurlbert, K. Anderton, M. Sethi, A. Barau, Exploring the governance and politics of transformations towards sustainability. *Environ. Innov. Soc. Transit.* **24**, 1–16 (2017).
96. F. W. Geels, Ontologies, socio-technical transitions (to sustainability), and the multi-level perspective. *Res. Policy*. **39**, 495–510 (2010).
97. F. W. Geels, The multi-level perspective on sustainability transitions: Responses to seven criticisms. *Environ. Innov. Soc. Transit.* **1**, 24–40 (2011).
98. M. Burke, S. M. Hsiang, E. Miguel, Climate and Conflict. *Annu. Rev. Econ.* **7**, 577–617 (2015).
99. B. Tonn, A. Hemrick, F. Conrad, Cognitive representations of the future: Survey results. *Futures*. **38**, 810–829 (2006).
100. C. Figueres, H. J. Schellnhuber, G. Whiteman, J. Rockström, A. Hobley, S. Rahmstorf, Three years to safeguard our climate. *Nat. News*. **546**, 593 (2017).
101. J. Rogelj, M. den Elzen, N. Höhne, T. Fransen, H. Fekete, H. Winkler, R. Schaeffer, F. Sha, K. Riahi, M. Meinshausen, Paris Agreement climate proposals need a boost to keep warming well below 2 °C. *Nature*. **534**, 631–639 (2016).
102. T. Rayner, A. Jordan, in *Climate Change Policy in the European Union: Confronting the Dilemmas of Mitigation and Adaptation?* (Cambridge University Press, Cambridge, UK, 2010), pp. 145–166.
103. C. F. Parker, C. Karlsson, M. Hjerpe, Assessing the European Union's global climate change leadership: from Copenhagen to the Paris Agreement. *J. Eur. Integr.* **39**, 239–252 (2017).
104. O. Geden, The Paris Agreement and the inherent inconsistency of climate policymaking. *Wiley Interdiscip. Rev. Clim. Change*. **7**, 790–797 (2016).
105. C. Wlezien, The Public as Thermostat: Dynamics of Preferences for Spending. *Am. J. Polit. Sci.* **39**, 981–1000 (1995).

106. S. N. Soroka, C. Wlezien, *Degrees of Democracy: Politics, Public Opinion and Policy* (Cambridge University Press, New York, 2010).
107. F. R. Baumgartner, B. D. Jones, *Agendas and instability in American politics* (University of Chicago Press, Chicago, 2010).
108. P. A. Sabatier, An advocacy coalition framework of policy change and the role of policy-oriented learning therein. *Policy Sci.* **21**, 129–168 (1988).
109. C. Weible, P. A. Sabatier, *Theories of the Policy Process* (Westview Press, New York, ed. 4th, 2017).
110. D. Evensen, The rhetorical limitations of the #FridaysForFuture movement. *Nat. Clim. Change*. **9**, 428–430 (2019).
111. C. R. Shipan, C. Volden, The Mechanisms of Policy Diffusion. *Am. J. Polit. Sci.* **52**, 840–857 (2008).
112. J. W. Kingdon, *Agendas, alternatives, and public policies* (HarperCollins College Publishers, New York, 1995).
113. C. Le Quéré, R. B. Jackson, M. W. Jones, A. J. P. Smith, S. Abernethy, R. M. Andrew, A. J. De-Gol, D. R. Willis, Y. Shan, J. G. Canadell, P. Friedlingstein, F. Creutzig, G. P. Peters, Temporary reduction in daily global CO 2 emissions during the COVID-19 forced confinement. *Nat. Clim. Change*. **10**, 647–653 (2020).
114. R. Hanna, Y. Xu, D. G. Victor, After COVID-19, green investment must deliver jobs to get political traction. *Nature*. **582**, 178–180 (2020).
115. D. Rosenbloom, J. Markard, A COVID-19 recovery for climate. *Science*. **368**, 447–447 (2020).
116. B. Tesla, L. R. Demakovsky, E. A. Mordecai, S. J. Ryan, M. H. Bonds, C. N. Ngonghala, M. A. Brindley, C. C. Murdock, Temperature drives Zika virus transmission: evidence from empirical and mathematical models. *Proc. R. Soc. B Biol. Sci.* **285**, 20180795 (2018).
117. R. McLeman, B. Smit, Migration as an Adaptation to Climate Change. *Clim. Change*. **76**, 31–53 (2006).
118. R. Jennissen, Causality Chains in the International Migration Systems Approach. *Popul. Res. Policy Rev.* **26**, 411–436 (2007).
119. M. Wiedermann, E. K. Smith, J. Heitzig, J. F. Donges, A network-based microfoundation of Granovetter's threshold model for social tipping. *Sci. Rep.* **10**, 11202 (2020).
120. P. Törnberg, Echo chambers and viral misinformation: Modeling fake news as complex contagion. *PLOS ONE*. **13**, e0203958 (2018).
121. V. V. Vasconcelos, S. A. Levin, F. L. Pinheiro, Consensus and polarization in competing complex contagion processes. *J. R. Soc. Interface*. **16**, 20190196 (2019).
122. M. Del Vicario, G. Vivaldo, A. Bessi, F. Zollo, A. Scala, G. Caldarelli, W. Quattrociocchi, Echo Chambers: Emotional Contagion and Group Polarization on Facebook. *Sci. Rep.* **6**, 37825 (2016).
123. C. T. Bauch, R. Sigdel, J. Pharaon, M. Anand, Early warning signals of regime shifts in coupled human–environment systems. *Proc. Natl. Acad. Sci.* **113**, 14560–14567 (2016).
124. D. Helbing, S. Bishop, R. Conte, P. Lukowicz, J. B. McCarthy, FuturICT: Participatory computing to understand and manage our complex world in a more sustainable and resilient way. *Eur. Phys. J. Spec. Top.* **214**, 11–39 (2012).
125. V. Sekara, A. Stopczynski, S. Lehmann, Fundamental structures of dynamic social networks. *Proc. Natl. Acad. Sci.* **113**, 9977–9982 (2016).
126. P. Sapiezynski, A. Stopczynski, D. D. Lassen, S. Lehmann, Interaction data from the Copenhagen Networks Study. *Sci. Data*. **6**, 315 (2019).
127. J. F. Donges, J. Heitzig, W. Barfuss, M. Wiedermann, J. A. Kassel, T. Kittel, J. J. Kolb, T. Kolster, F. Müller-Hansen, I. M. Otto, K. B. Zimmerer, W. Lucht, Earth system modeling with endogenous and dynamic human societies: the copan:CORE open World–Earth modeling framework. *Earth Syst. Dyn.* **11**, 395–413 (2020).
128. B. Schuldt, A. Buras, M. Arend, Y. Vitasse, C. Beierkuhnlein, A. Damm, M. Gharun, T. E. E. Grams, M. Hauck, P. Hajek, H. Hartmann, E. Hiltbrunner, G. Hoch, M. Holloway-Phillips, C. Körner, E. Larysch, T. Lübbe, D. B. Nelson, A. Rammig, A. Rigling, L. Rose, N. K. Ruehr, K. Schumann, F. Weiser, C. Werner, T. Wohlgemuth, C. S. Zang, A. Kahmen, A first assessment of the impact of the extreme 2018 summer drought on Central European forests. *Basic Appl. Ecol.* **45**, 86–103 (2020).

## Acknowledgments

**General**: We are very grateful to William C. Clark, Anne-Sophie Crépin, Niklas Harring, Matthew Ives, J. Doyne Farmer, Wolfgang Lucht, and John Schellnhuber, for providing helpful insights and comments. We thank the participants of two DominoES workshops on social tipping dynamics held at GESIS Leibniz Institute for Social Science, Cologne, in summer 2018 and 2019 for foundational and framing discussions.

**Funding:** This work has been supported by the Leibniz Association (project DominoES), the Stordalen Foundation via the Planetary Boundary Research Network (PB.net), the Earth League's EarthDoc programme, IRTG 1740 funded by DFG and FAPESP, and the European Research Council (ERC advanced grant project ERA: Earth resilience in the Anthropocene, ERC-2016-ADG-743080). T.M.L.'s contribution was supported by the Leverhulme Trust (RPG-2018-046).

**Author Contributions:** Drawing upon the concepts developed in the expert elicitation workshop, R.W., J.F.D., E.K.S., M.M. and T.M.L structured the conceptualization into the resultant framework and wrote the paper with the support of all co-authors. All co-authors contributed to the discussion of the manuscript. M.W. analyzed data and created Fig. 1. R.W. and E.K.S. created Fig. 2. E.K.S. analyzed data and created Fig. 3. J.H. derived the mathematical definition of social tipping processes (Sect. S1).

**Competing Interests**: The authors declare no competing interests.

## Supplementary Materials

### *S1: A mathematical definition of social tipping processes*

In this section, we give a more formal version of the definition of 'social tipping process' given in the main text, as a reference for mathematically inclined readers.

After defining what we mean by a social system and its environment, we first classify their possible states into critical, unmanageable, uncritical, and tippable conditions, and then finally define the notions of prevention time and triggering time.

By a *social system*, $\Sigma$, we mean a set of agents together with a network-like social structure, that interacts in some form with the rest of the world, called the *environment*, $E$, of the system, such that, if no "perturbation" or deliberate "influence" by some decision-maker occurs, $\Sigma$ and $E$ together can only follow certain "quasi-inertial" (or "default") trajectories restricted by the agency of the system's agents. Let $x_{(t)}$ and $y_{(t)}$ denote the *states* that $\Sigma$ and $E$ are actually in at time $t$.

A *critical condition* for the system is a pair of possible system and environment states, $(x^*, y^*)$, such that there exists another possible pair of states, $(x', y')$, with the following properties:

1. The state pair $(x', y')$ is no further away in state space from $(x^*, y^*)$ than a certain "small" distance, $\epsilon$, that represents the possible magnitude of "local" perturbations in $\Sigma$ (affecting only few agents or network links directly) or small changes in $E$ that are considered sufficiently "likely" to care about, with respect to some suitable distance function $d$. In other words, $d((x', y'), (x^*, y^*)) < \epsilon$.
2. If $\Sigma$ and $E$ were in state $(x', y')$ at any time $t'$, there is a quasi-inertial trajectory that would move $\Sigma$ at some later time $t'' > t'$ into some state $x''$ that is "qualitatively" different from $x^*$. This move represents a "global" (i.e., affecting a very large fraction of the agents) and "significant" change in the system (but not necessarily in its environment).

If such a change actually happens, the time point $t'$ (not the state!) at which it starts may be called the *tipping point* or less ambiguously the *triggering time point*, and the system behavior within the time interval from $t'$ to $t''$ is called the corresponding *tipping process*. An *uncritical* condition for $\Sigma$ and $E$ then is any pair of states that is not critical.

A critical condition is *unmanageable* for an actor that may influence $\Sigma$ or $E$ in some way if there exists a possible pair of states, $(x', y')$, with $d((x', y'), (x^*, y^*)) < \epsilon$ and the following property:

- Assume that $\Sigma$ and $E$ were in state $(x', y')$ at any time $t'$ and afterwards the state of $\Sigma$ and $E$ would follow any trajectory $(x(t), y(t))_{t \geq t'}$ that the actor can force it to follow. Then the

resulting trajectory would still move $\Sigma$ at some time $t'' > t'$ into some state $x''$ (which will usually depend on the influence exerted) that is qualitatively different from $x^*$.

Similarly, an uncritical condition, $(x^\circ, y^\circ)$, is *tippable* by a decision maker if there is a possible trajectory $(x(t), y(t))_{t \geq t'}$, starting in $(x^\circ, y^\circ)$ at some time $t'$, that the decision maker can force $\Sigma$ and $E$ to follow, and this trajectory would move $\Sigma$ into some state $x''$ at some time $t'' > t'$ that is qualitatively different from $x^\circ$ (a tippable uncritical state roughly corresponds to what others call a 'sensitive intervention point' ).

At any time at which the system is not in an unmanageable critical state, the *prevention time* is the time interval it takes before some quasi-inertial trajectory has moved it into an unmanageable critical state. In other words, at time zero it is the largest time interval $T$ so that, when no intervention takes place until time $T$, for all $t > 0$ with $t < T$, the system would not be in an unmanageable critical state at time $t$.

Similarly, at any time at which the system is in a tippable uncritical state, the *triggering time* is the time interval it takes before some quasi-inertial trajectory has moved it into an uncritical state that is no longer tippable. In other words, at time zero it is the largest time interval $T$ so that, when no intervention takes place until time $T$, for all $t > 0$ with $t < T$, the system would not be in a tippable uncritical state at time $t$.

We only consider social tipping processes for which the prevention or triggering time is smaller than some *intervention time* *horizon*.

***S2 Ecosystem tipping as intermediary case***

Ecosystem tipping processes share properties of physical climate tipping dynamics in atmosphere, ocean and cryosphere in that they can often be described by a common driver, as well as that of deliberative social tipping elements in that they have adaptive capacity, and can therefore be regarded as intermediate. But, as previously noted, human agential capacity is far greater than those of other species.

Similarly to human social systems, ecosystems are comprised of interacting living organisms, they can be viewed as networks with components that can adapt (e.g., food webs). This is different from physical tipping elements such as the cryosphere elements (e.g., melting of permafrost) which do not typically exhibit the same networked structures. Within the nominally 'climate' tipping elements are some major biomes – notably boreal forests, the Amazon rainforest, and coral reefs – that are composed of living organisms and exhibit ecological network structures. Indeed changing interactions between the living elements of these systems may be key to tipping dynamics – for example epidemic bark beetle infestation of boreal forests triggered by climate warming allowing the beetles to complete two life cycles rather than one within a season (*128*). Thus these biotic tipping elements lie towards smaller scale ecosystems in the continuum, and tend to be more closely related to social systems in spatial and temporal scales compared to the typically much larger and more slowly changing physical climate tipping elements.

These differences give rise to a proposed ordering of tipping elements, ranging from (1) the physical climate tipping elements via (2) ecosystem tipping elements to (3) social tipping elements (Table S1).

***Table S1: Proposed ordering of tipping processes ranging from physical climate tipping processes via ecosystem tipping processes to social tipping processes.***

| Properties | Physical climate tipping processes | Ecological tipping processes | Social tipping processes |
|---|---|---|---|
| Degree of agency | *Low/Absent* | *Intermediate* | *High* |
| Network structure | *Uncommon* | *Common* | *Common* |
| Temporal-spatial scales | *Slower and larger* | *Faster and smaller* | *Faster and smaller* |
| Degree of complexity | *Lower* | *Intermediate* | *High* |

***Figure S1:***

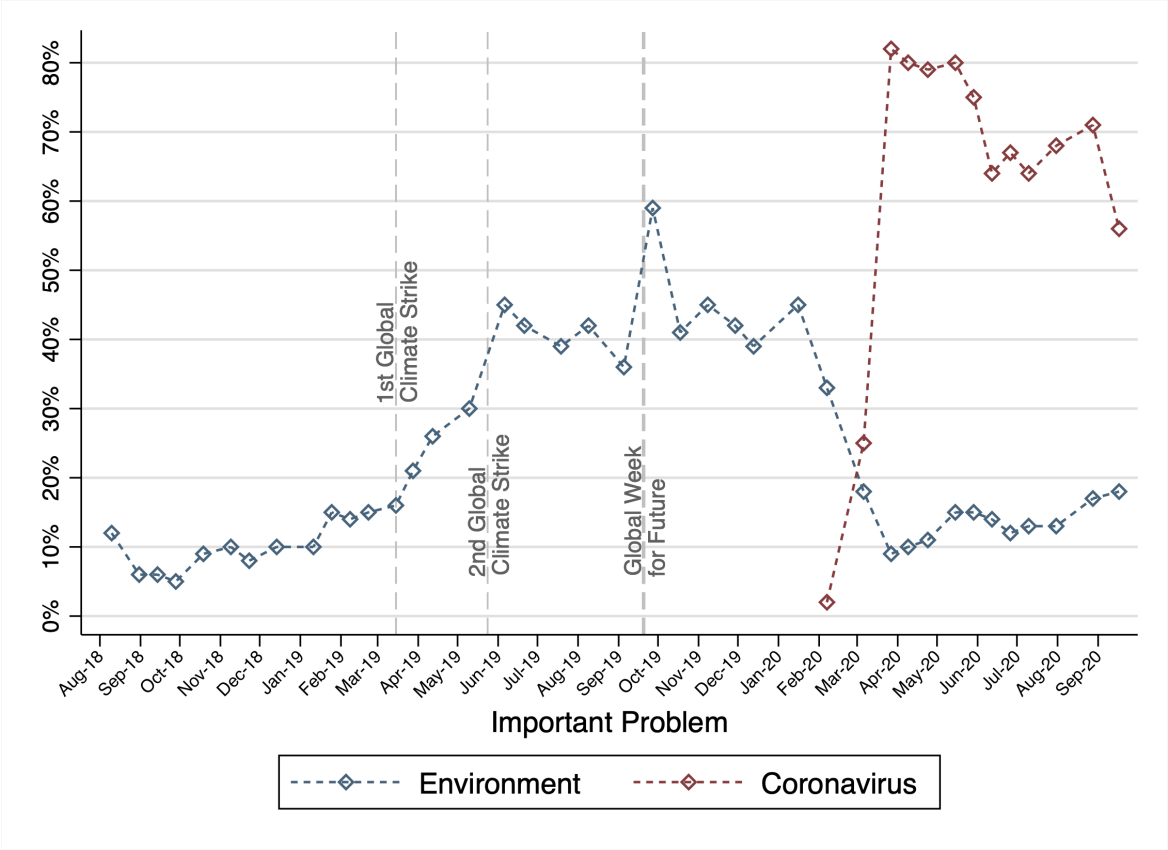


***Figure S1: Environment and Corona as an important issue in Germany.*** *Percentages of potential German voters that list the environment and the Coronavirus as an important issue for the country*

*from August 2018 – September 2020, showing the change since the beginning of Greta Thunberg's protest actions. Dotted grey vertical lines display days of global strikes organized by FridaysForFuture in March, May and September 2019. Data is collected by Forschungsgruppe Wahlen: Politbarometer .*

# References


M. J. Aburn and Y. Ram.
Numerical integration of stochastic differential equations (SDEs), 2017.
URL `https://github.com/mattja/sdeint/`.
Accessed Sep. 23, 2020.

R. Albert and A.-L. Barabási.
Statistical mechanics of complex networks.
*Reviews of Modern Physics*, 74(1):47, 2002.

H. Alkhayuon, P. Ashwin, L. C. Jackson, C. Quinn, and R. A. Wood.
Basin bifurcations, oscillatory instability and rate-induced thresholds for Atlantic Meridional Overturning Circulation in a global oceanic box model.
*Proceedings of the Royal Society A*, 475(2225):20190051, 2019.

H. M. Alkhayuon and P. Ashwin.
Rate-induced tipping from periodic attractors: Partial tipping and connecting orbits.
*Chaos: An Interdisciplinary Journal of Nonlinear Science*, 28(3):033608, 2018.

U. Alon.
Network motifs: theory and experimental approaches.
*Nature Reviews Genetics*, 8(6):450–461, 2007.

L. E. Aragão.
Environmental science: The rainforest's water pump.
*Nature*, 489(7415):217–218, 2012.

P. Ashwin, S. Wieczorek, R. Vitolo, and P. Cox.
Tipping points in open systems: bifurcation, noise-induced and rate-dependent examples in the climate system.
*Philosophical Transactions of the Royal Society A: Mathematical, Physical and Engineering Sciences*, 370(1962):1166–1184, 2012.

P. Ashwin, S. Coombes, and R. Nicks.
Mathematical frameworks for oscillatory network dynamics in neuroscience.
*The Journal of Mathematical Neuroscience*, 6(1):2, 2016.

P. Ashwin, C. Perryman, and S. Wieczorek.
Parameter shifts for nonautonomous systems in low dimension: bifurcation-and rate-induced tipping.
*Nonlinearity*, 30(6):2185, 2017.

A.-L. Barabási and R. Albert.
Emergence of scaling in random networks.
*Science*, 286(5439):509–512, 1999.

M. Baudin.
pydoe: The experimental design package for python, sofware available under the bsd license (3-clause).
`https://pythonhosted.org/pyDOE/index.html`, 2013.
Accessed Jun., 2020.

N. Boers, N. Marwan, H. M. Barbosa, and J. Kurths.
A deforestation-induced tipping point for the south american monsoon system.
*Scientific Reports*, 7:41489, 2017.

P. M. Brando, D. C. Nepstad, E. A. Davidson, S. E. Trumbore, D. Ray, and P. Camargo.
Drought effects on litterfall, wood production and belowground carbon cycling in an Amazon forest: results of a throughfall reduction experiment.
*Philosophical Transactions of the Royal Society B: Biological Sciences*, 363(1498):1839–1848, 2008.

D. Brockmann and D. Helbing.
The hidden geometry of complex, network-driven contagion phenomena.
*Science*, 342(6164):1337–1342, 2013.

E. S. Brondizio, J. Settele, S. Díaz, and H. Ngo.
Global assessment report on biodiversity and ecosystem services of the Intergovernmental Science-Policy Platform on Biodiversity and Ecosystem Services.
*IPBES Secretariat: Bonn, Germany*, 2019.

C. D. Brummitt, G. Barnett, and R. M. D'Souza.
Coupled catastrophes: sudden shifts cascade and hop among interdependent systems.
*Journal of The Royal Society Interface*, 12(112):20150712, 2015.

M. I. Budyko.
The effect of solar radiation variations on the climate of the earth.
*Tellus*, 21(5):611–619, 1969.

L. Caesar, S. Rahmstorf, A. Robinson, G. Feulner, and V. Saba.
Observed fingerprint of a weakening Atlantic Ocean overturning circulation.
*Nature*, 556(7700):191–196, 2018.

W. Cai, S. Borlace, M. Lengaigne, P. Van Rensch, M. Collins, G. Vecchi, A. Timmermann, A. Santoso, M. J. McPhaden, L. Wu, et al.
Increasing frequency of extreme El-Niño events due to greenhouse warming.
*Nature Climate Change*, 4(2):111–116, 2014.

P. Cessi.
A simple box model of stochastically forced thermohaline flow.
*Journal of Physical Oceanography*, 24(9):1911–1920, 1994.

H. Cheng, R. L. Edwards, A. Sinha, C. Spötl, L. Yi, S. Chen, M. Kelly, G. Kathayat, X. Wang, X. Li, et al.
The Asian monsoon over the past 640,000 years and ice age terminations.
*Nature*, 534(7609):640–646, 2016.

M. Claussen, A. Ganopolski, J. Schellnhuber, and W. Cramer.
Earth system models of intermediate complexity.
*Global Change Newsletter*, 41:4–6, 2000.

M. Claussen, L. Mysak, A. Weaver, M. Crucifix, T. Fichefet, M.-F. Loutre, S. Weber, J. Alcamo, V. Alexeev, A. Berger, et al.
Earth system models of intermediate complexity: closing the gap in the spectrum of climate system models.
*Climate Dynamics*, 18(7):579–586, 2002.

M. Collins, S.-I. An, W. Cai, A. Ganachaud, E. Guilyardi, F.-F. Jin, M. Jochum, M. Lengaigne, S. Power, A. Timmermann, et al.
The impact of global warming on the tropical Pacific Ocean and El-Niño.
*Nature Geoscience*, 3(6):391–397, 2010.

B. Cook, J. Mankin, K. Marvel, A. Williams, J. Smerdon, and K. Anchukaitis.
Twenty-first century drought projections in the CMIP6 forcing scenarios.
*Earth's Future*, 8(6):e2019EF001461, 2020.

D. Coumou and S. Rahmstorf.
A decade of weather extremes.
*Nature Climate Change*, 2(7):491–496, 2012.

D. Coumou, A. Robinson, and S. Rahmstorf.
Global increase in record-breaking monthly-mean temperatures.
*Climatic Change*, 118(3-4):771–782, 2013.

P. M. Cox.
Description of the "TRIFFID" dynamic global vegetation model.
*Hadley Centre Technical Note 24*, 2001.

P. M. Cox, R. Betts, M. Collins, P. P. Harris, C. Huntingford, and C. Jones.
Amazonian forest dieback under climate-carbon cycle projections for the 21st century.
*Theoretical and Applied Climatology*, 78(1-3):137–156, 2004.

P. M. Cox, P. P. Harris, C. Huntingford, R. A. Betts, M. Collins, C. D. Jones, T. E. Jupp, J. A. Marengo, and C. A. Nobre.
Increasing risk of Amazonian drought due to decreasing aerosol pollution.
*Nature*, 453(7192):212–215, 2008.

M. Crucifix.
Oscillators and relaxation phenomena in pleistocene climate theory.
*Philosophical Transactions of the Royal Society A: Mathematical, Physical and Engineering Sciences*, 370(1962):1140–1165, 2012.

P. J. Crutzen.
Geology of mankind.
*Nature*, 415(23), 2002.

J. D. Daron and D. A. Stainforth.
On predicting climate under climate change.
*Environmental Research Letters*, 8(3):034021, 2013.

E. A. Davidson, A. C. de Araújo, P. Artaxo, J. K. Balch, I. F. Brown, M. M. Bustamante, M. T. Coe, R. S. DeFries, M. Keller, M. Longo, et al.
The Amazon basin in transition.
*Nature*, 481(7381):321–328, 2012.

M. M. Dekker, A. S. Von Der Heydt, and H. A. Dijkstra.
Cascading transitions in the climate system.
*Earth System Dynamics*, 9(4):1243–1260, 2018.

P. Ditlevsen, T. Mitsui, and M. Crucifix.
Crossover and peaks in the pleistocene climate spectrum; understanding from simple ice age models.
*Climate Dynamics*, 54(3):1801–1818, 2020.

J. F. Donges and N. Wunderling et al.
Cascading interactions increase risk of transgressing climate tipping points.
2021, in prep.

J. F. Donges, Y. Zou, N. Marwan, and J. Kurths.
The backbone of the climate network.
*EPL (Europhysics Letters)*, 87(4):48007, 2009.

J. F. Donges, R. Winkelmann, W. Lucht, S. E. Cornell, J. G. Dyke, J. Rockström, J. Heitzig, and H. J. Schellnhuber.
Closing the loop: Reconnecting human dynamics to earth system science.
*The Anthropocene Review*, 4(2):151–157, 2017.

P. B. Duffy, P. Brando, G. P. Asner, and C. B. Field.
Projections of future meteorological drought and wet periods in the Amazon.
*Proceedings of the National Academy of Sciences*, 112(43):13172–13177, 2015.

A. Dutton, A. E. Carlson, A. Long, G. A. Milne, P. U. Clark, R. DeConto, B. P. Horton, S. Rahmstorf, and M. E. Raymo.
Sea-level rise due to polar ice-sheet mass loss during past warm periods.
*Science*, 349(6244), 2015.

M. Eby, A. J. Weaver, K. Alexander, K. Zickfeld, A. Abe-Ouchi, A. Cimatoribus, E. Crespin, S. Drijfhout, N. Edwards, A. Eliseev, et al.
Historical and idealized climate model experiments: an intercomparison of earth system models of intermediate complexity.
*Climate of the Past*, 9:1111–1140, 2013.

E. A. Eltahir and R. L. Bras.
Precipitation recycling in the Amazon basin.
*Quarterly Journal of the Royal Meteorological Society*, 120(518):861–880, 1994.

Y.-H. Eom.
Resilience of networks to environmental stress: From regular to random networks.
*Physical Review E*, 97(4):042313, 2018.

P. Erdös and A. Rényi.
On random graphs, i.
*Publicationes Mathematicae (Debrecen)*, 6:290–297, 1959.

V. Eyring, S. Bony, G. A. Meehl, C. A. Senior, B. Stevens, R. J. Stouffer, and K. E. Taylor.
Overview of the Coupled Model Intercomparison Project Phase 6 (CMIP6) experimental design and organization.
*Geoscientific Model Development*, 9(5):1937–1958, 2016.

J. Fan, J. Meng, J. Ludescher, X. Chen, Y. Ashkenazy, J. Kurths, S. Havlin, and H. J. Schellnhuber.
Statistical physics approaches to the complex earth system.
*Physics Reports*, 2020.

G. M. Flato.
Earth system models: an overview.
*Wiley Interdisciplinary Reviews: Climate Change*, 2(6):783–800, 2011.

L. Gammaitoni, P. Hänggi, P. Jung, and F. Marchesoni.
Stochastic resonance.
*Reviews of Modern Physics*, 70(1):223, 1998.

A. Ganopolski, V. Petoukhov, S. Rahmstorf, V. Brovkin, M. Claussen, A. Eliseev, and C. Kubatzki.
CLIMBER-2: a climate system model of intermediate complexity. Part II: model sensitivity.
*Climate Dynamics*, 17(10):735–751, 2001.

A. Ganopolski, R. Winkelmann, and H. J. Schellnhuber.
Critical insolation–CO2 relation for diagnosing past and future glacial inception.
*Nature*, 529(7585):200–203, 2016.

A. S. Gardner, G. Moholdt, J. G. Cogley, B. Wouters, A. A. Arendt, J. Wahr, E. Berthier, R. Hock, W. T. Pfeffer, G. Kaser, et al.
A reconciled estimate of glacier contributions to sea level rise: 2003 to 2009.
*Science*, 340(6134):852–857, 2013.

C. Gaucherel and V. Moron.
Potential stabilizing points to mitigate tipping point interactions in Earth's climate.
*International Journal of Climatology*, 37(1):399–408, 2017.

M. Gladwell.
*The tipping point: How little things can make a big difference*.
Little, Brown, 2006.

J. Glen.
The mechanical properties of ice I. the plastic properties of ice.
*Advances in Physics*, 7(26):254–265, 1958.

T. Gross, L. Rudolf, S. A. Levin, and U. Dieckmann.
Generalized models reveal stabilizing factors in food webs.
*Science*, 325(5941):747–750, 2009.

L. Halekotte and U. Feudel.
Minimal fatal shocks in multistable complex networks.
*Scientific Reports*, 10(1):1–13, 2020.

C. M. Herald, S. Kurita, and A. S. Telyakovskiy.
Simple climate models to illustrate how bifurcations can alter equilibria and stability.
*Journal of Contemporary Water Research & Education*, 152(1):14–21, 2013.

M. Hirota, M. Holmgren, E. H. Van Nes, and M. Scheffer.
Global resilience of tropical forest and savanna to critical transitions.
*Science*, 334(6053):232–235, 2011.

P. W. Holland, K. B. Laskey, and S. Leinhardt.
Stochastic blockmodels: First steps.
*Social Networks*, 5(2):109–137, 1983.

G. J. Huffman, D. T. Bolvin, E. J. Nelkin, D. B. Wolff, R. F. Adler, G. Gu, Y. Hong, K. P. Bowman, and E. F. Stocker.
The TRMM multisatellite precipitation analysis (TMPA): Quasi-global, multiyear, combined-sensor precipitation estimates at fine scales.
*Journal of hydrometeorology*, 8(1):38–55, 2007.

J. Jouzel, V. Masson-Delmotte, O. Cattani, G. Dreyfus, S. Falourd, G. Hoffmann, B. Minster, J. Nouet, J.-M. Barnola, J. Chappellaz, et al.
Orbital and millennial antarctic climate variability over the past 800,000 years.
*science*, 317(5839):793–796, 2007.

E. Kalnay, M. Kanamitsu, R. Kistler, W. Collins, D. Deaven, L. Gandin, M. Iredell, S. Saha, G. White, J. Woollen, et al.
The ncep/ncar 40-year reanalysis project.
*Bulletin of the American meteorological Society*, 77(3):437–472, 1996.

S. T. Kim, W. Cai, F.-F. Jin, A. Santoso, L. Wu, E. Guilyardi, and S.-I. An.
Response of El-Niño sea surface temperature variability to greenhouse warming.
*Nature Climate Change*, 4(9):786–790, 2014.

A. K. Klose, V. Karle, R. Winkelmann, and J. F. Donges.
Emergence of cascading dynamics in interacting tipping elements of ecology and climate.
*Royal Society Open Science*, 7(6):200599, 2020.

D. Kondepudi, F. Moss, and P. V. McClintock.
Observation of symmetry breaking, state selection and sensitivity in a noisy electronic system.
*Physica D: Nonlinear Phenomena*, 21(2-3):296–306, 1986.

M. Kretschmer, D. Coumou, J. F. Donges, and J. Runge.
Using causal effect networks to analyze different arctic drivers of midlatitude winter circulation.
*Journal of Climate*, 29(11):4069–4081, 2016.

E. Kriegler, J. W. Hall, H. Held, R. Dawson, and H. J. Schellnhuber.
Imprecise probability assessment of tipping points in the climate system.
*Proceedings of the National Academy of Sciences*, 106(13):5041–5046, 2009.

Y. A. Kuznetsov.
*Elements of applied bifurcation theory*, volume 112.
Springer Science & Business Media, 2013.

G. Lahav, N. Rosenfeld, A. Sigal, N. Geva-Zatorsky, A. J. Levine, M. B. Elowitz, and U. Alon.
Dynamics of the p53-mdm2 feedback loop in individual cells.
*Nature Genetics*, 36(2):147–150, 2004.

P. W. Leclercq, J. Oerlemans, and J. G. Cogley.
Estimating the glacier contribution to sea-level rise for the period 1800–2005.
*Surveys in Geophysics*, 32(4-5):519, 2011.

T. M. Lenton, H. Held, E. Kriegler, J. W. Hall, W. Lucht, S. Rahmstorf, and H. J. Schellnhuber.
Tipping elements in the Earth's climate system.
*Proceedings of the National Academy of Sciences*, 105(6):1786–1793, 2008.

T. M. Lenton, J. Rockström, O. Gaffney, S. Rahmstorf, K. Richardson, W. Steffen, and H. J. Schellnhuber.
Climate tipping points—too risky to bet against.
*Nature*, 575:592–595, 2019.

M. Lenzen, K. Kanemoto, D. Moran, and A. Geschke.
Mapping the structure of the world economy.
*Environmental Science & Technology*, 46(15):8374–8381, 2012.

A. Levermann and R. Winkelmann.
A simple equation for the melt elevation feedback of ice sheets.
*The Cryosphere*, 10(4):1799–1807, 2016.

T. E. Lovejoy and C. Nobre.
Amazon tipping point: Last chance for action.
*Science Advances*, 5(12):eaba2949, 2019.

J. E. Lovelock and L. Margulis.
Atmospheric homeostasis by and for the biosphere: the gaia hypothesis.
*Tellus*, 26(1-2):2–10, 1974.

V. Lucarini and T. Bódai.
Transitions across melancholia states in a climate model: Reconciling the deterministic and stochastic points of view.
*Physical Review Letters*, 122(15):158701, 2019.

M. E. Mann, S. Rahmstorf, K. Kornhuber, B. A. Steinman, S. K. Miller, S. Petri, and D. Coumou.
Projected changes in persistent extreme summer weather events: The role of quasi-resonant amplification.
*Science Advances*, 4(10):eaat3272, 2018.

V. Masson-Delmotte, P. Zhai, H.-O. Pörtner, D. Roberts, J. Skea, P. Shukla, A. Pirani, W. Moufouma-Okia, C. Péan, R. Pidcock, et al.
*Global Warming of 1.5 °C: An IPCC Special Report on the Impacts of Global Warming of 1.5 °C Above Pre-industrial Levels and Related Global Greenhouse Gas Emission Pathways, in the Context of Strengthening the Global Response to the Threat of Climate Change, Sustainable Development, and Efforts to Eradicate Poverty*.
World Meteorological Organization Geneva, Switzerland, 2018.

R. M. May, S. A. Levin, and G. Sugihara.
Ecology for bankers.
*Nature*, 451(7181):893–894, 2008.

P. J. Menck, J. Heitzig, N. Marwan, and J. Kurths.
How basin stability complements the linear-stability paradigm.
*Nature Physics*, 9(2):89–92, 2013.

M. Milkoreit, J. Hodbod, J. Baggio, K. Benessaiah, R. Calderón-Contreras, J. F. Donges, J.-D. Mathias, J. C. Rocha, M. Schoon, and S. E. Werners.
Defining tipping points for social-ecological systems scholarship—an interdisciplinary literature review.
*Environmental Research Letters*, 13(3):033005, 2018.

R. Milo, S. Shen-Orr, S. Itzkovitz, N. Kashtan, D. Chklovskii, and U. Alon.
Network motifs: simple building blocks of complex networks.
*Science*, 298(5594):824–827, 2002.

C. Mitra, A. Choudhary, S. Sinha, J. Kurths, and R. V. Donner.
Multiple-node basin stability in complex dynamical networks.
*Physical Review E*, 95(3):032317, 2017.

J. X. Mitrovica, N. Gomez, and P. U. Clark.
The sea-level fingerprint of West Antarctic collapse.
*Science*, 323(5915):753–753, 2009.

M. E. Newman.
The structure and function of complex networks.
*SIAM Review*, 45(2):167–256, 2003.

M. E. Newman and M. Girvan.
Finding and evaluating community structure in networks.
*Physical Review E*, 69(2):026113, 2004.

M. E. Newman, S. H. Strogatz, and D. J. Watts.
Random graphs with arbitrary degree distributions and their applications.
*Physical Review E*, 64(2):026118, 2001.

A. L. Niederdrenk and D. Notz.
Arctic sea ice in a 1.5 °C warmer world.
*Geophysical Research Letters*, 45(4):1963–1971, 2018.

C. A. Nobre, G. Sampaio, L. S. Borma, J. C. Castilla-Rubio, J. S. Silva, and M. Cardoso.
Land-use and climate change risks in the Amazon and the need of a novel sustainable development paradigm.
*Proceedings of the National Academy of Sciences*, 113(39):10759–10768, 2016.

G. R. North.
The small ice cap instability in diffusive climate models.
*Journal of the Atmospheric Sciences*, 41(23):3390–3395, 1984.

D. Notz, F. A. Haumann, H. Haak, J. H. Jungclaus, and J. Marotzke.
Arctic sea-ice evolution as modeled by Max Planck Institute for Meteorology's Earth system model.
*Journal of Advances in Modeling Earth Systems*, 5(2):173–194, 2013.

M. D. Oyama and C. A. Nobre.
A new climate-vegetation equilibrium state for tropical South America.
*Geophysical Research Letters*, 30(23), 2003.

Paris Agreement.
United Nations/Framework Convention on Climate Change (2015), Adoption of the Paris Agreement, 21st Conference of the Parties.
Paris, 2015.

L. Parsons.
Implications of CMIP6 projected drying trends for 21st century Amazonian drought risk.
*Earth's Future*, 8(10):e2020EF001608, 2020.

E. J. d. A. L. Pereira, L. C. de Santana Ribeiro, L. F. da Silva Freitas, and H. B. de Barros Pereira.
Brazilian policy and agribusiness damage the Amazon rainforest.
*Land Use Policy*, 92:104491, 2020.

V. Petoukhov, A. Ganopolski, V. Brovkin, M. Claussen, A. Eliseev, C. Kubatzki, and S. Rahmstorf.
CLIMBER-2: a climate system model of intermediate complexity. Part I: model description and performance for present climate.
*Climate Dynamics*, 16(1):1–17, 2000.

V. Petoukhov, M. Claussen, A. Berger, M. Crucifix, M. Eby, A. Eliseev, T. Fichefet, A. Ganopolski, H. Goosse, I. Kamenkovich, et al.
EMIC Intercomparison Project (EMIP–CO2): comparative analysis of EMIC simulations of climate, and of equilibrium and transient responses to atmospheric CO2 doubling.
*Climate Dynamics*, 25(4):363–385, 2005.

S. Rahmstorf and D. Coumou.
Increase of extreme events in a warming world.
*Proceedings of the National Academy of Sciences*, 108(44):17905–17909, 2011.

S. Rahmstorf, M. Crucifix, A. Ganopolski, H. Goosse, I. Kamenkovich, R. Knutti, G. Lohmann, R. Marsh, L. A. Mysak, Z. Wang, et al.
Thermohaline circulation hysteresis: A model intercomparison.
*Geophysical Research Letters*, 32(23), 2005.

E. Rignot, J. Mouginot, B. Scheuchl, M. van den Broeke, M. J. van Wessem, and M. Morlighem.
Four decades of Antarctic Ice Sheet mass balance from 1979–2017.
*Proceedings of the National Academy of Sciences*, 116(4):1095–1103, 2019.

P. Ritchie and J. Sieber.
Probability of noise-and rate-induced tipping.
*Physical Review E*, 95(5):052209, 2017.

P. Ritchie, Ö. Karabacak, and J. Sieber.
Inverse-square law between time and amplitude for crossing tipping thresholds.
*Proceedings of the Royal Society A*, 475(2222):20180504, 2019.

P. Ritchie, P. Cox, and J. Sieber.
How fast to turn around: preventing tipping after a system has crossed a climate tipping threshold.
In *EGU General Assembly Conference Abstracts*, page 5555, 2020.

A. Robinson, R. Calov, and A. Ganopolski.
Multistability and critical thresholds of the Greenland Ice Sheet.
*Nature Climate Change*, 2(6):429–432, 2012.

J. C. Rocha, G. Peterson, Ö. Bodin, and S. Levin.
Cascading regime shifts within and across scales.
*Science*, 362(6421):1379–1383, 2018.

J. Runge, V. Petoukhov, J. F. Donges, J. Hlinka, N. Jajcay, M. Vejmelka, D. Hartman, N. Marwan, M. Paluš, and J. Kurths.
Identifying causal gateways and mediators in complex spatio-temporal systems.
*Nature Communications*, 6(1):1–10, 2015.

B. Saltzman and K. A. Maasch.
Carbon cycle instability as a cause of the late Pleistocene ice age oscillations: modeling the asymmetric response.
*Global Biogeochemical Cycles*, 2(2):177–185, 1988.

I. Sasgen, B. Wouters, A. S. Gardner, M. D. King, M. Tedesco, F. W. Landerer, C. Dahle, H. Save, and X. Fettweis.
Return to rapid ice loss in Greenland and record loss in 2019 detected by the GRACE-FO satellites.
*Communications Earth & Environment*, 1(1):1–8, 2020.

M. Scheffer, S. Carpenter, J. A. Foley, C. Folke, and B. Walker.
Catastrophic shifts in ecosystems.
*Nature*, 413(6856):591, 2001.

H. J. Schellnhuber.
'Earth system' analysis and the second copernican revolution.
*Nature*, 402(6761):C19–C23, 1999.

H.-J. Schellnhuber, P. J. Crutzen, W. C. Clark, H. Held, M. Claussen, et al.
*Earth system analysis for sustainability*.
MIT Press, Cambridge, Massacusetts, 2004.

H. J. Schellnhuber, S. Rahmstorf, and R. Winkelmann.
Why the right climate target was agreed in Paris.
*Nature Climate Change*, 6(7):649–653, 2016.

C. Schoof.
Ice sheet grounding line dynamics: Steady states, stability, and hysteresis.
*Journal of Geophysical Research: Earth Surface*, 112(F3), 2007.

D. Seidov, R. J. Stouffer, and B. J. Haupt.
Is there a simple bi-polar ocean seesaw?
*Global and Planetary Change*, 49(1-2):19–27, 2005.

W. D. Sellers.
A global climatic model based on the energy balance of the earth-atmosphere system.
*Journal of Applied Meteorology and Climatology*, 8(3):392–400, 1969.

L. Serdukova, Y. Zheng, J. Duan, and J. Kurths.
Metastability for discontinuous dynamical systems under Lévy noise: Case study on Amazonian vegetation.
*Scientific Reports*, 7(1):1–13, 2017.

S. S. Shen-Orr, R. Milo, S. Mangan, and U. Alon.
Network motifs in the transcriptional regulation network of Escherichia coli.
*Nature Genetics*, 31(1):64–68, 2002.

A. Shepherd, E. Ivins, E. Rignot, B. Smith, M. Van Den Broeke, I. Velicogna, P. Whitehouse, K. Briggs, I. Joughin, G. Krinner, et al.
Mass balance of the Antarctic Ice Sheet from 1992 to 2017.
*Nature*, 558:219–222, 2018.

A. Shepherd, E. Ivins, E. Rignot, B. Smith, M. van den Broeke, I. Velicogna, P. Whitehouse, K. Briggs, I. Joughin, G. Krinner, et al.
Mass balance of the Greenland Ice Sheet from 1992 to 2018.
*Nature*, 579(7798):233–239, 2020.

D. V. Silvério, P. M. Brando, J. K. Balch, F. E. Putz, D. C. Nepstad, C. Oliveira-Santos, and M. M. Bustamante.
Testing the Amazon savannization hypothesis: fire effects on invasion of a neotropical forest by native Cerrado and exotic pasture grasses.
*Philosophical Transactions of the Royal Society B: Biological Sciences*, 368(1619):20120427, 2013.

SIMIP-Community.
Arctic sea ice in CMIP6.
*Geophysical Research Letters*, 47(10):e2019GL086749, 2020.

A. Staal, S. C. Dekker, M. Hirota, and E. H. van Nes.
Synergistic effects of drought and deforestation on the resilience of the south-eastern Amazon rainforest.
*Ecological Complexity*, 22:65–75, 2015.

A. Staal, O. A. Tuinenburg, J. H. Bosmans, M. Holmgren, E. H. van Nes, M. Scheffer, D. C. Zemp, S. C. Dekker, et al.
Forest-rainfall cascades buffer against drought across the Amazon.
*Nature Climate Change*, 8(6):539–543, 2018.

A. Staal, I. Fetzer, L. Wang-Erlandsson, J. H. Bosmans, S. C. Dekker, E. H. van Nes, J. Rockström, and O. A. Tuinenburg.
Hysteresis of tropical forests in the 21st century.
*Nature Communications*, 11(4978), 2020a.

A. Staal, B. M. Flores, A. P. D. Aguiar, J. H. Bosmans, I. Fetzer, and O. A. Tuinenburg.
Feedback between drought and deforestation in the Amazon.
*Environmental Research Letters*, 15(4):044024, 2020b.

D. A. Stainforth, T. E. Downing, R. Washington, A. Lopez, and M. New.
Issues in the interpretation of climate model ensembles to inform decisions.

*Philosophical Transactions of the Royal Society A: Mathematical, Physical and Engineering Sciences*, 365(1857):2163–2177, 2007.

A. C. Staver, S. Archibald, and S. A. Levin.
The global extent and determinants of savanna and forest as alternative biome states.
*Science*, 334(6053):230–232, 2011.

W. Steffen, W. Broadgate, L. Deutsch, O. Gaffney, and C. Ludwig.
The trajectory of the Anthropocene: the great acceleration.
*The Anthropocene Review*, 2(1):81–98, 2015.

W. Steffen, J. Rockström, K. Richardson, T. M. Lenton, C. Folke, D. Liverman, C. P. Summerhayes, A. D. Barnosky, S. E. Cornell, M. Crucifix, et al.
Trajectories of the Earth system in the Anthropocene.
*Proceedings of the National Academy of Sciences*, 115(33):8252–8259, 2018.

W. Steffen, K. Richardson, J. Rockström, H. J. Schellnhuber, O. P. Dube, S. Dutreuil, T. M. Lenton, and J. Lubchenco.
The emergence and evolution of earth system science.
*Nature Reviews Earth & Environment*, 1(1):54–63, 2020.

T. F. Stocker, D. Qin, G.-K. Plattner, M. Tignor, S. K. Allen, J. Boschung, A. Nauels, Y. Xia, V. Bex, P. M. Midgley, et al.
Climate change 2013: The physical science basis.
*Contribution of working group I to the fifth assessment report of the intergovernmental panel on climate change*, 1535, 2013.

H. Stommel.
Thermohaline convection with two stable regimes of flow.
*Tellus*, 13(2):224–230, 1961.

D. B. Stouffer, M. Sales-Pardo, M. I. Sirer, and J. Bascompte.
Evolutionary conservation of species' roles in food webs.
*Science*, 335(6075):1489–1492, 2012.

J. C. Stroeve, M. C. Serreze, M. M. Holland, J. E. Kay, J. Malanik, and A. P. Barrett.
The Arctic's rapidly shrinking sea ice cover: a research synthesis.
*Climatic Change*, 110(3-4):1005–1027, 2012.

D. Swingedouw, T. Fichefet, P. Huybrechts, H. Goosse, E. Driesschaert, and M.-F. Loutre.
Antarctic ice-sheet melting provides negative feedbacks on future climate warming.
*Geophysical Research Letters*, 35(17), 2008.

J. D. Tàbara, N. Frantzeskaki, K. Hölscher, S. Pedde, K. Kok, F. Lamperti, J. H. Christensen, J. Jäger, and P. Berry.
Positive tipping points in a rapidly warming world.
*Current Opinion in Environmental Sustainability*, 31:120–129, 2018.

K. E. Taylor, R. J. Stouffer, and G. A. Meehl.
An overview of CMIP5 and the experiment design.
*Bulletin of the American Meteorological Society*, 93(4):485–498, 2012.

D. Tesfay, L. Serdukova, Y. Zheng, P. Wei, J. Duan, and J. Kurths.
Influence of extreme events modeled by Lévy flight on global thermohaline circulation stability.
*Nonlinear Processes in Geophysics Discussions*, pages 1–16, 2020.

J. M. T. Thompson and J. Sieber.
Predicting climate tipping as a noisy bifurcation: a review.
*International Journal of Bifurcation and Chaos*, 21(02):399–423, 2011.

J. E. Tierney, C. J. Poulsen, I. P. Montañez, T. Bhattacharya, R. Feng, H. L. Ford, B. Hönisch, G. N. Inglis, S. V. Petersen, N. Sagoo, et al.
Past climates inform our future.
*Science*, 370(6517), 2020.

A. Timmermann, F.-F. Jin, and J. Abshagen.
A nonlinear theory for El-Niño bursting.
*Journal of the Atmospheric Sciences*, 60(1):152–165, 2003.

E. H. van Nes, M. Hirota, M. Holmgren, and M. Scheffer.
Tipping points in tropical tree cover: linking theory to data.
*Global Change Biology*, 20(3):1016–1021, 2014.

E. H. van Nes, B. M. Arani, A. Staal, B. van der Bolt, B. M. Flores, S. Bathiany, and M. Scheffer.
What do you mean,'tipping point'?
*Trends in Ecology & Evolution*, 31(12):902–904, 2016.

P. Virtanen, R. Gommers, T. E. Oliphant, M. Haberland, T. Reddy, D. Cournapeau, E. Burovski, P. Peterson, W. Weckesser, J. Bright, S. J. van der Walt, M. Brett, J. Wilson, K. J. Millman, N. Mayorov, A. R. J. Nelson, E. Jones, R. Kern, E. Larson, C. J. Carey, İ. Polat, Y. Feng, E. W. Moore, J. VanderPlas, D. Laxalde, J. Perktold, R. Cimrman, I. Henriksen, E. A. Quintero, C. R. Harris, A. M. Archibald, A. H. Ribeiro, F. Pedregosa, P. van Mulbregt, and SciPy 1.0 Contributors.
SciPy 1.0: Fundamental Algorithms for Scientific Computing in Python.
*Nature Methods*, 17:261–272, 2020.
doi: 10.1038/s41592-019-0686-2.

B. Wang, X. Luo, Y.-M. Yang, W. Sun, M. A. Cane, W. Cai, S.-W. Yeh, and J. Liu.
Historical change of El Niño properties sheds light on future changes of extreme El Niño.
*Proceedings of the National Academy of Sciences*, 116(45):22512–22517, 2019.

S. Wang and Z. Hausfather.
ESD Reviews: mechanisms, evidence, and impacts of climate tipping elements.
*Earth System Dynamics Discussions*, pages 1–93, 2020.

D. J. Watts and S. H. Strogatz.
Collective dynamics of 'small-world'networks.
*Nature*, 393(6684):440–442, 1998.

S. L. Weber.
The utility of earth system models of intermediate complexity (EMICs).
*Wiley Interdisciplinary Reviews: Climate Change*, 1(2):243–252, 2010.

W. Weijer, W. Cheng, S. S. Drijfhout, A. V. Fedorov, A. Hu, L. C. Jackson, W. Liu, E. L. McDonagh, J. V. Mecking, and J. Zhang.

Stability of the Atlantic Meridional Overturning Circulation: A review and synthesis.
*Journal of Geophysical Research: Oceans*, 124(8):5336–5375, 2019.

M. Wiedermann, E. K. Smith, J. Heitzig, and J. F. Donges.
A network-based microfoundation of Granovetter's threshold model for social tipping.
*Scientific Reports*, 10(1):1–10, 2020.

M. Willeit, A. Ganopolski, R. Calov, and V. Brovkin.
Mid-pleistocene transition in glacial cycles explained by declining CO2 and regolith removal.
*Science Advances*, 5(4):eaav7337, 2019.

R. Winkelmann, A. Levermann, A. Ridgwell, and K. Caldeira.
Combustion of available fossil fuel resources sufficient to eliminate the Antarctic Ice Sheet.
*Science advances*, 1(8):e1500589, 2015.

R. A. Wood, J. M. Rodríguez, R. S. Smith, L. C. Jackson, and E. Hawkins.
Observable, low-order dynamical controls on thresholds of the Atlantic Meridional Overturning Circulation.
*Climate Dynamics*, 53(11):6815–6834, 2019.

J. Zalasiewicz, C. N. Waters, M. Williams, and C. P. Summerhayes.
*The Anthropocene as a Geological Time Unit: A Guide to the Scientific Evidence and Current Debate*.
Cambridge University Press, 2019.

S. E. Zebiak and M. A. Cane.
A model El-Niño-Southern Oscillation.
*Monthly Weather Review*, 115(10):2262–2278, 1987.

D. Zemp, C.-F. Schleussner, H. Barbosa, R. Van der Ent, J. F. Donges, J. Heinke, G. Sampaio, and A. Rammig.
On the importance of cascading moisture recycling in south america.
*Atmospheric Chemistry and Physics*, 2014.

D. C. Zemp, C.-F. Schleussner, H. M. Barbosa, M. Hirota, V. Montade, G. Sampaio, A. Staal, L. Wang-Erlandsson, and A. Rammig.
Self-amplified Amazon forest loss due to vegetation-atmosphere feedbacks.
*Nature Communications*, 8(1):1–10, 2017.

S. Zhao, N. Pederson, L. D'Orangeville, J. HilleRisLambers, E. Boose, C. Penone, B. Bauer, Y. Jiang, and R. D. Manzanedo.
The International Tree-Ring Data Bank (ITRDB) revisited: Data availability and global ecological representativity.
*Journal of Biogeography*, 46(2):355–368, 2019.

K. Zickfeld, B. Knopf, V. u. Petoukhov, and H. Schellnhuber.
Is the Indian summer monsoon stable against global change?
*Geophysical Research Letters*, 32(15), 2005.

K. Zickfeld, M. Eby, A. J. Weaver, K. Alexander, E. Crespin, N. R. Edwards, A. V. Eliseev, G. Feulner, T. Fichefet, C. E. Forest, et al.
Long-term climate change commitment and reversibility: an EMIC intercomparison.
*Journal of Climate*, 26(16):5782–5809, 2013.

W. Zou, D. Senthilkumar, M. Zhan, and J. Kurths.
Reviving oscillations in coupled nonlinear oscillators.
*Physical Review Letters*, 111(1):014101, 2013.

H. J. Zwally, J. Li, A. C. Brenner, M. Beckley, H. G. Cornejo, J. Di Marzio, M. B. Giovinetto, T. A. Neumann, J. Robbins, J. L. Saba, et al.
Greenland Ice Sheet mass balance: distribution of increased mass loss with climate warming; 2003–07 versus 1992–2002.
*Journal of Glaciology*, 57(201):88–102, 2011.

# Acknowledgements

First and foremost I want to thank my supervisors Professor Ricarda Winkelmann and Dr. Jonathan Donges for offering me the opportunity to perform my Ph.D. at the Potsdam-Institute for Climate Impact Research. Without their support my doctoral studies would not have been such a pleasant and motivating venture. I am very grateful for our meetings, discussions and thoughts on the various projects and I appreciated your questions, advices and thorough reviews of my work. Besides the great supervision, I would like to thank Ricarda Winkelmann and Jonathan Donges for letting me participate in the Dominoes group. It was always a pleasure to thrive into the new fields of social×natural science by collaborating with great people like Jobst Heitzig, Marc Wiedermann, Maria Zeitz, Julius Garbe, Keith Smith, Christina Eder or Alexia Katsanidou. I am also very thankful for the many fruitful discussions and very valuable feedback on the conceptual Earth system model with Professor Jürgen Kurths.

Further, I enjoyed the weekly meetings at the ERA-Lab, the COPAN and the ICE group. In particular, I would like to thank Ronja Reese, Johanna Beckmann, Boris Sakschewski, Wolfram Barfuss, Jakob Kolb, Ilona Otto, Torsten Albrecht and Niklas Kitzmann for their support and valuable feedback during the last three years. I am also very grateful for the exchange and mutual support with Ann Kristin Klose who worked on a similar class of dynamical models.

Importantly, I would also like to emphasise the many fruitful collaborations with Arie Staal, who is a wonderful colleague and whose support I appreciated very much during the many studies we co-authored.

My daily work has also greatly benefited from the support of my colleagues at PIK who were also associated with my research stays in Brazil. I would like to particularly thank Markus Drüke, Frederik Wolf, Maximilian Gelbrecht, Nicolai Friedhoff, Tomaso Rosati and Robert Ronge. Moreover, I would like to thank my supervisor in Brazil, Professor Henrique Barbosa, who supported and supervised me during my time in São Paulo and afterwards. I am also grateful for the collaboration with Professor Marina Hirota, even though my research stay in Brazil was interrupted due to the corona pandemic before I could visit her in Florianopólis.

Também, eu gostaria de agradecer o Carlos Afonso, nosso professor de português, o curso dele eu frequentava durante os últimos três anos. Sem a ajuda dele, a vida no Brasil não teria sido tão fácil para mim.

I am also very grateful to have been part of the scientific Kolleg of the Studienstiftung des deutschen Volkes as a co-supervisor together with Marc Wiedermann, Jobst Heitzig, Jonathan Donges and Professor Jürgen Kurths, where I had the opportunity to be part of a very enthusiastic and motivated group of students over the course of two years.

Furthermore, I would like to thank for the commitment of the students, who I (co-)supervised. Some of the achievements during the last three years would not have been possible without their contributions. Therefore, I would like to thank Jonathan Krönke, Benedikt Stumpf, Jan Kohler,

Hannah Mevenkamp and Valentin Wohlfarth.

My work was financially supported by the IRTG 1740/TRP 2011/50151-0, funded by the DFG/FAPESP and by a Ph.D. scholarship from the Studienstiftung des deutschen Volkes.

Last but not least, I would like to thank my family, friends and partner, who always supported me during the last three years.